THE DEVELOPMENT OF METHODS FOR IMPROVING ACCURACY AND VALIDITY OF MUSCULOSKELETAL MODELLING OF THE LOWER LIMB

VOLUME I

ALLAN CARMAN

A thesis submitted for the degree of

Doctor of Philosophy

at the University of Otago, Dunedin

New Zealand

September, 2000

ABSTRACT

The aim of present study was to address limitations in model design, anatomical data, and implementation of muscle force-length and force velocity relationships for the purpose of improving accuracy and validity of musculoskeletal modelling. To achieve these a comprehensive three dimensional musculoskeletal model of the leg was developed and implemented in the analysis of gait.

The following were achieved:

i) Anatomical data for 48 muscle elements of the lower limb, including skeletal co-ordinate data to define muscle-tendon paths and moment arms throughout joint movements.

ii) Optimisation of muscle model parameters to changes in muscle belly lengths to define an optimal fibre length and force-length relationship.

iii) Equations describing muscle model geometry, force-length and force-velocity relationships to describe muscle model contraction dynamics.

iv) A cost function which minimised the sum of squared normalised muscle forces with soft constraints on maximum and minimum muscle force, which allowed for the unconstrained minimisation of the cost function.

v) An optimisation procedure that combined the equipollence equations, muscle excitation and contraction dynamics and muscle force limits in the minimisation of the cost function.

The limitations identified include:

i) Accuracy of velocity data achieved was not sufficient to determine muscle contraction dynamics which relied on muscle contractile element velocity to determine maximum muscle forces;

ii) Calculation of moment arms from muscle-tendon co-ordinate data was extremely sensitive to errors including :

- accurate location of body-fixed axes from external markers;
- relative motion of muscle point co-ordinates and joint centres;
- the use of straight as opposed to curved-line tendon paths;
- accuracy of three dimension segment location during movement.

iii) The muscle model predicted contractile element velocities larger than those modelled by the present force-velocity equations, indicating a need to scale force-velocity relationships to the maximum contractile element velocities.

iv) The optimisation approach predicted consistent forces for the 48 muscle elements of the lower limb, however limitations were:

- determining initial muscle force estimates in accordance with the equipollence equations;
- minimisation of the cost function did not change muscle forces significantly from their initial estimated values.

Improvements suggested include:

i) Improvements in moment arm prediction by:

- use of pre-trial functional evaluations of predicted centres of rotation to improve location of body fixed axes;
- improved location of muscle point co-ordinates to define muscle lines of action at varying joint angles.

ii) Optimise the muscle model parameters to the range of muscle lengths determined by the end-range of motion instead of the motion within a trial to achieve a more realistic optimal fibre length and force-length relationship by considering the change in fibre lengths as an approximation of the maximum changes in fibre lengths.

iii) Improve the validity of the joint models to:

- determine moments to be balanced by muscular forces.
- improve the optimisation procedure to obtain muscle forces.
- increase accuracy of muscle force prediction.

iv) Review the force-velocity relationship, the dynamic response of the muscle model, and assess the validity of the muscle model in predicting maximum muscle forces;

v) Improved initial muscle force estimates which meet the equipollence equations and achieve convergence to a global minimum.

vi) Apply the optimisation procedures to movements involving higher muscle forces, where accurate prediction of maximum muscle forces, modelling of joint passive forces, and excitation dynamics become more critical.

While the present study succeeds in many respects, its succeeds most in identifying the complexity of the process and proposing methods to achieve greater success.

ACKNOWLEDGEMENTS

The author wish to gratefully acknowledge the following people for their assistance during the cause of this thesis.

To Assoc. Prof. Peter Milburn who as a mentor and friend made this thesis possible. His supervision, guidance and encouragement saw the completion of this thesis. Through a chance meeting in Wollongong has shaped my career ever since, though first a masters and then PhD. Thank you also to Allison Milburn, always enthusiastic and always supportive.

To Dr Michael Albert for his valuable contribution and guidance on mathematical aspects of this thesis.

To Christoph Zinc and Doris Maicher, dear friends who earned their Doctorates in Geology at the University of Otago. Memories and friendships to last a life time. Thank you for introducing me to Kayaking and our travels exploring parts of NZ that I would not have otherwise seen. Not to mention the support and motivation over the three years by mealy by being two friends that were also undertaking a PhD.

To Denise Taylor and Jo Harlick, at the School of Physiotherapy, a little laugh every now and then goes a long way. To Tereise Seufatu and Ngaire Timlin, secretaries at the School of Physiotherapy, for all those small administration things that add up to a lot over the years.

Thank you also goes to:

All those friends I have made though my involvement in athletics as a member of the Leith and Otago Athletics clubs, who have always supported my endeavours in athletics and the many other athletes and friends scattered over New Zealand. Just to mention a few Trevor King, Shareen and Dough Crumpton, Helen Boyd, Wayne Edgeler, Blair Martin, Ed Stevens, Cris Dagg, Bruce Patton and the Remarkable runners, Paul Morrow, Reon Rollo and the Christchurch crew, last but not least Brooke Eddy and Graham from sunny Invercargil.

Fellow students and staff within the School of Physiotherapy, University of Otago for their support and friendship.

To Rebecca and the Pluncket Street crew, and all other friends that I have made during my time in New Zealand.

Finally the deepest appreciation and love goes to my mother Dorothy, father Peter, sister Heather and brother David for their love and support. The time spent away has been long, however my thoughts and love are always with you.

TABLE OF CONTENTS

Page

LIST OF FIGURES

Page

LIST OF TABLES

1 INTRODUCTION

Mathematical modelling of the human musculoskeletal system provides an instrument which enables an understanding of human movement through the measurement of motion and forces. Muscle forces, under the control of the central nervous system, are transferred through bones and ligaments to overcome inertial forces to produce movement. As such individual muscle forces reflect muscle recruitment patterns and movement strategies adopted by the central nervous system. Individual muscle forces also contribute significantly to the loading of skeletal structures. As such a major area of biomechanics involves the prediction of individual muscle forces through mathematical modelling, to gain an insight into the control of movement by the central nervous system, as well as the forces placed on internal structures of the body. To successfully predict individual muscle forces the model must accurately reflect the structure and function of the musculoskeletal system, including that of the body segments, joints, muscle and the strategies employed by the central nervous system.

The following section presents the aims and purpose of this study. Initially the role of mathematical modelling in the clinical setting is presented. Then a brief review of the application of gait analysis and mathematical modelling to hip replacement surgery is presented as a means of introducing methods, assumption and limitations. Limitations in motion analysis and musculo-skeletal modelling to be addressed by the present study are then introduced. This is followed by the aims and purpose of the present study. Finally an outline of the present study is given and how the aims of the present study will met.

1.1 Role of mathematical modelling and gait analysis in the clinical setting

Mathematical modelling provides a means for quantifying human movement. Motion descriptors such as position, velocity, acceleration, force, energy, and work can be calculated for structures comprising the human body, such as rigid segments, joints, ligaments and muscles, or for the whole body. The benefits of this approach include:

a) predicting internal forces acting within the human body from a kinematic description of the motion and measured external forces (inverse dynamics analysis);
b) predicting kinematic responses of the human body from internal and external forces (forward dynamics analysis); or

c) predicting internal forces required to elicit a desired optimal performance criteria (optimisation or forward simulation analysis).

Biomechanical modelling therefore provides a powerful tool for gaining indirect information and insight into human motion that may not otherwise be obtained. Applications include:

i) Quantitative evaluation of movement and muscle pathologies to guide clinicians in the diagnosis and treatment of musculoskeletal disorders. Gait analysis has helped improve outcomes in the correction of cerebral palsy gait by surgical or clinical intervention (Gage, 1991; Gage & Coop, 1995). Analysis of gait has enabled a more precise determination of gait abnormalities and to accurately assess the outcomes of a particular treatment or intervention (Gage & Coop, 1995) thus improving the decision making process and outcomes in the correction of cerebral palsy gait (Gage, 1991).

ii) Providing quantitative information on movement patterns and magnitudes of internal forces to aid in ergonomics, sports and the design of prosthetic devices. Mathematical modelling has helped improved occupation safety through changes to work practices to reduce the risk of injury in manual handling tasks (Chaffin & Andersson, 1991). By assessing movement patterns, loads lifted, frequency of lifting, height of lift, and reach distance, in combination with mathematical modelling and normative strength data, task demands can be established and compared to maximum permissible force limits, thus providing quantitative information for the re-design or remove the task from the workplace.

Davis (1988) listed possible applications of biomechanical gait analysis applied specifically to surgery as (i) quantification of the pre- and post-effects of surgery; (ii) evaluation of the effectiveness of prosthetic joint replacement; (iii) examination of improvements in orthotic and prosthetic design; and (iv) quantification of the effects of changes in prosthetic design.

1.2 Application of mathematical modelling and gait analysis to hip replacement surgery

Studies of gait analysis following hip replacement surgery are presented to provide an introduction to the methods and assumption employed as well as to provide a background to limitations of gait analysis and mathematical modelling. Paul & Berme (1985) defined one of main aims of mathematical modelling in the clinical field as the prediction of load actions in non-standard anthropometry, anatomical structures and activities, or in the prediction of optimal gait for individuals suffering from pathologies restricting their motion. If a biomechanical study is to produce meaningful and valid results, it is therefore essential that the mathematical model be specific to the clinical condition under investigation and accurately represent the underlying structure and function of the musculo-skeletal system. Research presented in this section investigates the relationship between reconstructed hip geometry, muscle function, symmetry of gait, and the forces placed on the hip joint. The potential benefits include assisting in prosthetic design and surgery to decrease post-operative forces on the hip prosthesis and to attaining symmetry of gait with the aim of promote longevity of the prosthesis and mobility of the patient. Variables relevant to the outcome of prosthetic surgery which have been shown to contribute to asymmetrical gait, excessive hip joint forces and prosthetic failure are (Mulier, 1985):

a) Type of hip prosthesis (Moore, Austin-Moore, McKnee-Farrar), including stem length and femoral head diameter.
b) Placement of prosthesis:
    i) location of femoral head in relation to normal centre of rotation;
    ii) location of femoral head in relation to moment arms of force acting on femur;
    iii) orientation of prosthesis (angle of varus or valgus and frontal angle of femoral neck).
c) Muscular reattachment and function of muscles crossing the hip joint.
    i) changes in muscle length;
    ii) changes in moment arms;
    iii) moment generating capacity.
d) Leg length discrepancy.

The general aims of the gait analysis studies presented involve maintaining moment-generating capacity of muscles, decreasing maximum contact forces, promoting optimal direction of the contact force vector between acetabulum and femoral head and reducing torsion loads about the prosthesis.

Inman (1947) investigated functional aspects of the hip abductors, where hip joint centres and moment arms were measured from roentgenograms (x-ray pictures). By assuming the distribution of forces between the iliotibial tract and the abductor muscles was a function of pelvic tilt, and by assuming muscle force distribution between the gluteus medius, gluteus minimus, tensor fasciae latae muscles was in proportion to the respective muscle mass, the author was able to estimate the direction of the resultant bone-on-bone force at the femoral head. This was found to be between 165-170 degrees for changing pelvis orientation, and is consistent with lines of medial trabecular in the femoral neck, and acts to thrust the head of the femur into the acetabulum.

Murry, et al. (1972) conducted gait analysis of 30 patients before and up to six months after total hip replacement surgery. Limited to a two dimensional study, the authors noted a general improvement in gait, however abnormalities remained. As is common to the procedure, a slow return of hip muscle strength particular the abductors was observed. With the authors suspecting that muscle lengths were not significantly altered, the weaker abductor muscles may have resulted from trauma to gluteus maximus or minimus or incision through the tensor facia lata.

Hodge and workers (Andriacchi & Strickland, 1985) investigated outcomes of total hip replacement with the use of x-rays and motion analysis to find that a femur placed in a valgus position promoted normal gait and improved clinical results. This finding confirmed clinical observations, but could not be explained.

Andriacchi & Strickland (1985) demonstrated the complexity of the relationship between femoral head placement, muscle moments and gait. Patients with shortened abductor moment arms relative to the non-operated hip (i.e. valgus hip), produced gait patterns resembling normal. However, patients without shortened abductor moment arms showed a reduced range of motion during walking and increased maximum moments in flexion and extension. Unexpected to the authors, the extent of shortening of the abductor moment arms, relative to

the non-operated hip, showed no significant differences in abductor-adductor moments during gait.

These studies indicate that in order to gain a more complete understanding of surgical and pathological changes in musculoskeletal mechanics following hip replacement surgery, a comprehensive approach is needed, including a three dimensional description of joint geometry and the effects of changing geometry on moment arms, maximum forces and moment generating capacity of muscles. In hip replacement surgery, changes in the hip joint centre, muscle-tendon lengths and moment arms are determined by the placement of the acetabular cup and femoral geometry (neck length, neck-stem angle, and antiversion angle, Andriacchi & Strickland, 1985; Delp & Maloney, 1993; Delp, et al., 1994; Free & Delp, 1996). However, predicting changes in maximum muscle force and moment generating capacity due to muscle-tendon lengthening, resulting from changes in hip geometry, will depend on the ability of the muscle model to accurately represent muscle contraction dynamics and account for possible adaptations to these length changes following surgery.

Delp & Zajac (1992) used a computer model of the lower extremity to investigate the effects of tendon lengthening on the moment generating capacity of the muscle-tendon complex. The authors found a decrease in muscle force due to tendon lengthening. Muscles with larger optimal fibre length, increased tendon elasticity and increased angle of pennation were less sensitive to tendon lengthening. The effect of tendon stretch on the force produced depended on the ratio of tendon length to muscle fibre length. However, few muscle possessed a pennation angle large enough (greater than 20 degrees) to significantly decrease sensitivity. Whether the change in muscle force affected total joint moments depended on physiological cross sectional area (peak force) and moment arm of each muscle.

The previous studies not only demonstrate the inter-relationship of muscle model parameters and that any one parameter cannot be considered in isolation but also the need for valid muscle models in drawing sound conclusions. The following studies also indicate the complexity of investigating changes in hip geometry and functional outcomes as well as the need for valid modelling techniques and limitations that are encountered. In the following four studies, a mathematical model was developed which generated maximum isometric force and moments for 25 modelled muscle elements crossing the hip joint. The first study looked at relationship between displacements in the hip joint centre and alterations in moment generating capacity of

muscles as predicted by the model. The remaining three studies investigated whether the reduced moment generating capacity of a superior displacement of the hip joint centre could be compensated for by changes in femoral neck length and trochanter transfer. The model used has several limitations as discussed by the authors:

a) Only maximal isometric forces and moments were generated and considered, as calculated over a range of joint angles by scaling a generic muscle model;
b) Forces and moments do not represent those generated during movements;
c) The model does not account for muscle adaptation, including:.
    - changes in muscle and muscle fibre length;
    - changes in optimal fibre length;
    - changes in physiological cross sectional area; and
    - changes in force-length curves;
d) Muscle model inputs were kept constant throughout (for example physiological cross sectional area, optimal fibre length, force length relationships, and tendon slack length);
e) Hip internal and external rotators were not considered due to lack of experimental data on these muscles;
f) The muscle model was applicable to a normal individual with nominal musculoskeletal data. Subject variability and pathological conditions would alter the model;
g) Relative changes indicate relative effects rather than the importance of absolute values; and
h) These studies only looked at changing muscular geometry and maximal forces produced by the muscles. Changing geometry will also affect muscular forces required during gait. The authors note that a superior, lateral and posterior displacement of the hip can substantially increase the moments required by the hip abductors. Medial displacement of the hip centre reduces abduction moments required by reducing the distance between the hip joint centre and the body's centre of mass.

Delp & Maloney (1993), investigated the effects of changes in hip joint centre location on the moment-generating capacity of muscles crossing the hip joint. An inferior-medial positioning of the hip joint centre was desirable for maintaining or improving the moment-generating

capacity of the hip abductors, adductors and flexors. A superior displacement decreased moment generating capacity of hip abductors, adductors, and flexors. Medial, lateral, anterior and posterior displacements had lesser effects on moment-generating capacity of muscle groups crossing the hip joint. In this study the femur was displaced as a unit, and the relationship between femoral head, femoral neck and greater trochanter was constant.

Vasavada, et al. (1994) also investigated the effects of changes in hip joint centre on the moment-generating capacity of muscles. Expanding on Delp & Maloney (1993), this study adjusted femoral neck length to keep muscle lengths constant for changes in hip joint centre and as a result only moment arms were altered. In general when the hip centre was moved into a position that shortens the muscle, maintaining muscle length within model produced greater increases or small decreases in moment-generating capacity. Similarly, when the hip centre was moved into a position that lengthens the muscle, allowing the muscle to lengthen within the model produced greater increases or small decreases in moment-generating capacity. This was due to assumptions within the model which predicted greater muscle forces when the muscle length was increased and smaller forces when the muscle was shortened. In terms of preserving abductor muscle strength, the authors concluded that it is advantageous to maintain muscle length when the hip centre is moved superior or medially as maximum abductor force decreased by a smaller amount.

Although it is known that certain locations of the hip joint centre theoretically increase the moment-generating capacities of muscles, the positions are not always practical in terms of acetabular placement (Vasavada, et al., 1994). A superior position may be required to obtain a more stable fixation (Mulier, 1985; Vasavada, et al., 1994), however, there may be an option to compensate for changes in muscle length and moment arms by altering the geometry of the hip.

Delp, et al. (1994) investigated restoring the moment-generating capacity of hip abductors, adductors, flexors, and extensors after superior displacement of the hip centre by altering prosthetic neck length, neck-stem angle and antiversion angle. Using the mathematical model of the hip mentioned previously (Delp & Maloney, 1993; Vasavada, et al., 1994) the authors observed that the moment-generating capacity of all muscle groups decreased with superior placement of the hip joint, with the largest decrease reported for hip abductors. Increasing in neck length was found to restore the moment-generating capacity of the flexors, extensors and

adductors, however abductor moment arms decreased. The authors note that changing geometry may influence other variables not looked at such as, bending moments in the neck, stress and twisting moments at the bone-cement interface.

Free & Delp (1996) investigated whether trochanter transfer could increase the capacity of the abductors to generate moments by increasing moment arms and muscle forces. The three dimensional model mentioned previously was used (Delp & Maloney, 1993; Vasavada, et al., 1994; Delp, et al., 1994), however only the gluteus medius and minimus were modelled, with each muscle comprising three compartments. The effects of other muscle groups were not considered. Neck angle, neck length and antiversion angle were not considered. Maximum isometric force for each muscle compartment was calculated over a range of joint angles. With the hip in the neutral position a slight increase in abduction moment arm occurred with anterior and superior transfers while reductions in moment arm were seen in posterior-medial transfers. As most changes in moment arms were less than five percent, the authors concluded that trochanteric transfer had little biomechanical advantage when the hip joint is in its natural position and femoral geometry is restored. Free & Delp's (1994) study did however support the use of distal (inferior) transfer where the hip joint had been displaced superior to restore abductor moment-generating capacity. This result was due to the muscle model predicting increases in the force generating-capacity of the muscles as a result of muscle elongation increasing passive forces due to stretching of the muscle beyond it's resting length. Moment arms remained below normal.

Critical to the success of the four previously mentioned studies in drawing valid conclusions is the ability of the model to predicting changes in maximum muscle force and hence moment generating capacity due to changes in muscle-tendon length as a result of changes in hip geometry. The muscle model used included both active forces produced by contractile elements and passive forces due to stretch of tendon and muscle connective tissue. For changes in hip joint centre, the model generally predicting an increase in maximum isometric muscle force for an increase in muscle-tendon length due to the increase in passive forces. Similarly, a decrease in maximum isometric muscle force was predicted for a decrease in muscle-tendon length due to a decrease in passive force. Hence, passive forces were modelled as having a significant contribution to changes in maximum muscle forces due to changes in muscle-tendon length resulting from changes in the nominal hip joint centre position. Vrahas, et al. (1990) investigated the contribution of passive forces to moment about the hip joint

from near full extension to 60 degrees flexion at speeds similar to those of walking. The authors concluded that during most of the gait cycle it is reasonable to assume a negligible contribution of passive forces. Inman (1947), as mentioned previously, found that muscle lengths were not altered significantly, however gait asymmetries and weakness in abductor muscle forces were noted. These two studies indicate that passive force would play a minor role in gait asymmetries and weakness in abductor muscles following hip replacement surgery. Results which question the current model in which passive forces significantly influenced moment generating capacity of muscles following changes in muscle-tendon length.

In the model 25 muscle elements crossing the hip were divided into abductors, adductors, extensors, and flexors and moments produced about each axis calculated from within these groups. This approach ignores moments produced by muscle elements about other axes, the relative contributions of which may vary significantly with changing moment arms during movement. Kotzar, et al. (1995) showed a complex relationship between torques about the prosthetic stem and stem directed forces following total hip replacement by using a telemetered hip component. During weight-bearing, a component of the joint contact force is directed along the stem, forcing the stem into contact with the surrounding bone. A second component of joint contact force acts out of plane of the prosthesis contributing to twisting moments about the stem axis and may contribute to stem loosening. While a third component of joint force acts in the plane of the prosthesis but perpendicular to the neck which may contribute to fracture of femoral components (Huiskes, 1985). Modelling joint shear and compressive contact forces requires a knowledge of individual muscle forces and moment arms. Limitations in the number of muscles and degrees of freedom modelled will limit the ability to understand the potentially complex relationship between internal forces, hip joint geometry and symmetry of gait.

In presenting a brief review of methods and assumptions in mathematical modelling applied to predicting outcomes of hip replacement surgery, an insight is gained into limitations that occur and the dependency of valid results and conclusion on the validity of the modelling techniques used. The review demonstrates the need to look at a comprehensive three dimensional mathematical models of the musculo-skeletal system, and at the same time the methods and models used need to be accurate and valid in order to draw sound conclusions.

1.3 Limitations in studies of motion analysis and musculo-skeletal modelling

Limitations in three dimensional modelling of the musculoskeletal system were briefly introduced previously in a review of hip replacement surgery, however the limitations encountered are not specific to this area, and are applicable to all studies which involve the modelling of the musculoskeletal system for the purposes of evaluating forces on internal structures such as muscles, ligament, and joint contact surfaces. The limitations listed are by no means comprehensive to the three dimensional analysis of the musculoskeletal system. The limitation addressed by the present study are:

i) There is limited information on the accuracy and validity of three dimensional modelling, specifically the ability to accurately reconstruct three dimensional motion from externally placed markers and the sensitivity of derived variables to these errors. Studies have reported that the use of three surface markers per segment is insufficient to accurately quantify three dimensional segment location (Miller, et al., 1980; Luchetti, et al., 1998) and that six to ten markers are required to account for motion artefact (Miller, et al., 1980). With limited marker numbers, the ability to discriminate small movements is reduced to the extent that unreliable values can occur about segment axes (Luchetti, et al., 1998). The sensitivity of rotations about body segments axes to errors in reproduced three dimensional location is increased by external markers being placed close to the axes of rotation. Even with six markers on the thigh and shank, Reinschmidt, et al. (1997) found that substantial errors occurred in internal-external rotation about the longitudinal axis and adduction-abduction rotations about the anterior-posterior axis of the knee during running. Therefore, in three dimensional investigation of motion, errors of this nature can reduce the ability to draw conclusive or even valid results as certain motions and derived measures (accelerations, resultant joint moments, moment arms, and muscle forces) may be unreliable.

Segment accelerations, muscle moment arms and muscle force predictions are especially sensitive to errors in three dimensional segment position. Acceleration is derived through double differentiation of position data, which can be considered as consisting of higher frequency noise in addition to the lower frequency displacement. In the differentiation process, the magnitude of the output signal is proportional to the frequency, hence small errors in position data can lead to relatively large errors in acceleration, due to the higher frequency of the errors (Wood, 1980). Muscle moment arms are generally small in magnitude and

dependent on the accuracy of two adjacent segments for accurate reproduction of joint centre and muscle lines of action crossing the joint, and are hence sensitive to errors in positions of individual segments. In addition to the errors in reconstructing segment axes from external markers containing movement artefacts, moment arms are sensitive to errors arising from differences in defining subject segment axes from external landmarks, and the skeletal reference axes from which joint centres and muscle co-ordinate data have been derived. Errors in the alignment of subject and skeletal axes will result in erroneous muscle and joint position data when the skeletal co-ordinate data are scaled to the individual and are used to describe moment arms for a range of joint angles. Muscle force prediction is also sensitive to accurate three dimensional segment location as muscle force is dependent on accurate moment arms. Therefore, small changes in moment arms affect the derived moment-generating capacity and predicted muscle forces.

ii) Studies mentioned previously have shown the need to look at all three dimensions when investigating movements, forces and moments about the hip joint. Ignoring movements and forces in any one plane limits the ability of the study to draw comprehensive or conclusive results (Andriacchi & Strickland, 1985; Delp et al., 1994; Free & Delp, 1996). Muscles may be grouped into functional groups where the muscle may be considered to be producing moments about only one axis, ignoring contributions to other axes of rotation. Muscles, however, produce moments about all three axes of any joint they cross, and the relative moment arms and contributions to resultant joint moments can change significantly with changing joint angle. Insufficient data on muscle attachment sites and lines of action or the presence of sufficient errors or uncertainly in the three dimensional position of segment axes can, lead to some axes of rotation or muscle actions being ignored, thereby placing limits on the study.

iii) There is a lack of data on muscle attachments and deflection points to describe muscle-tendon lengths and moment arms of a comprehensive set of lower limb muscle elements that is also applicable to the range of joint angles at the pelvis, thigh, shank, and foot. The available information often limits studies to simply describing muscle paths only by an origin and insertion for the majority of muscles (Brand, et al., 1982; Dostal & Andrews, 1981). For many of the muscles of the lower limb, an origin and insertion is insufficient to describe muscle paths, lengths, velocities, and moment arms during human movement since muscle-tendon complexes may wrap around joint capsules, bone, retinacula, or other muscles. Pierrynowski

(1995) provides provides comprehensive muscle-tendon co-ordinate data, with up to six points and both straight and curves line segments describing muscle-tendon paths. Moment arms can be calculated experimentally by the tendon travel approach where the muscle-tendon travel past a joint is divided by the change in angle of a joint (Spoor, et al., 1990; Spoor & van Leeuwen, 1992) and is well suited for use in cadavers where the disected muscle-tendon complex's are used and only one joint is manipulated. The tendon travel approach provides valuable information on moment arms to validate muscle-tendon co-ordinate data, and the location of segment axes and joint centres over a range of joint angles. In the analysis of human motion where limited number of points describe muscle-tendon paths, the use of changes in muscle length divided by changes in joint angle to calculate moment arms is questionable. The validity of tendon travel approach is particularly questionable when the muscle-tendon complex is described only by an origin and insertion when it wraps around joint capsules or when applied to muscles that cross more than one joint with motion occuring at both joints.

iv) For the purposes of video-based motion analysis of subjects, there is a need to express the local co-ordinates describing muscle origins, insertions and muscle paths relative to a set of axes that are clearly defined from internal bony landmarks, and can be accurately reconstructed from externally placed markers. For the application of skeletal co-ordinate data to patients, there is also a need to normalise the local co-ordinates describing muscle origins, insertions and paths relative to segment dimensions that can be readily measured on these subjects. For the pelvis axis system, this would involve normalising each co-ordinate to a respective medio-lateral, antero-posterior and superior-inferior anthropometric measure (Seidel, et al., 1995). Normalising dimensions may well be bi-ASIS, mid-PSIS to mid-ASIS, and sitting height of the pelvis respectively, where sitting height of the pelvis is measured as bench-top to iliac crest as an approximation to inferior ramus of the pubis to iliac crest in the skeletal model.

v) Subject specific joint centre and muscle-tendon co-ordinate data as well as muscle model parameters, including mass, pennation angle, fibre length, are required in order to describe individual muscle lengths, moment arms and muscle force-length, force-velocity relationships. Subject specific anatomical data is usually obtained by scaling data from a reference skeletal model to the individual using segment dimensions and circumferences (Pierrynowski and Morrison, 1985b; Seidel, et al., 1995) or total body height and length (Pierrynowski, 1995).

However, defining subject specific anatomical data by scaling skeletal reference data to the individual, is subject to considerable inaccuracies due to individual variations within the musculo-skeletal system (Pierrynowski, 1995). To reduce the inaccuracies in anatomical data, measurements of musculo-skeletal function can be used to optimise segment fixed axes location and muscle model parameters to the subject in order to achieve a satisfactory description of muscle moment arms and muscle excitation contraction dynamics (Audu & Davy, 1985; Herzog, 1985). The inaccuracies in obtaining subject specific anatomical data and the sensitivity of musculo-skeletal modelling to anatomical data, highlights the need for improved scaling methods and further development of optimisation techniques based on subject specific functional measures to adjust co-ordinate data and muscle model parameters to the individual.

vi) Muscle models estimate force output from the instantaneous contractile conditions (muscle length and velocities) and excitation dynamics (activation levels) based on a reference muscle length at which fibre length, pennation angle, physiological cross sectional area, and tendon slack length are known. Optimal fibre length, maximum isometric force and force length and velocity relationships are derived from these measures. Current muscle models do not account for adaptation of muscles through changes in optimal fibre length due to changes in the maximum and minimum (range) of muscle fibre lengths, changes in maximum isometric force due to changes in mass and physiological cross sectional area, or changes in the force-length and force-velocity characteristics of muscles. Muscle models, therefore, predict maximum force output based on an accurate set of model parameters that describe the geometry and contraction dynamics of the muscle, in short-term responses to changes in muscle length, velocity and excitation. An assumption on which these models are based is that the muscle model parameters are constant over this short-term period. Without accounting for muscle adaptation, musculo-skeletal models cannot predict force output over extended periods of time in response to changes in tendon or whole muscle length due to altered musculo-skeletal geometry. Over an extended period of time there is the likelihood of adaptation to the new conditions, resulting in changes to optimal fibre lengths, physiological cross sectional areas, maximum isometric forces, and the force-length, force-velocity relationships.

vii) There is a need for a method that incorporates muscle force-length, force-velocity relationships and excitation dynamics into a muscle model. The muscle model would need to include variables such as fibre length, pennation angle, muscle belly length, and tendon slack

length. The fibre length in turn may include a contractile element and fibre series-elastic component, while tendon elasticity and cross sectional area gives rise to a tendon series elastic component. The resultant model and model parameters defining muscle force over a range of muscle-tendon lengths and velocities in the dynamic analysis of the musculo-skeletal system. Therefore, maximum force in the direction of the tendon is dependent on the velocity of the contractile elements, the maximum isometric force in the direction of the contractile elements at the current fibre length, and the pennation angle also at the current fibre length. Contractile element length is dependent on fibre length and fibre series elastic component length, although fibre series elastic component length is in itself dependent on the force in the direction of the contractile elements. Fibre length and pennation angle are dependent on the muscle length and tendon length. However, tendon length is dependent on the force in the direction of the tendon, which in turn is dependent on the pennation angle. This leads to the formulation of a set of non-linear simultaneously equations which need to be solved.

1.4 Aim

The aim of the present study is to present a comprehensive approach to the three dimensional modelling of the musculoskeletal system of the human lower limb. This modelling includes:

i) Providing comprehensive anatomical data and methods required for the three dimensional modelling of the musculo-skeletal system of the lower limb, including:

- defining a body fixed axis system from external markers for each segment;
- defining rigid body centres of mass and joint centres from the body-fixed axes;
- producing co-ordinate data on muscle origins, insertions and deflection points to define muscle paths in order to calculate muscle lengths and moment arms for a range of joint position for the muscles of the lower limb; and
- expressing the anatomical data presented (muscle co-ordinate data, joint centres and centres of mass) relative to the same body fixed axes system for each segment and normalised to a set of anthropometric measures taken from palpable landmarks which can be accurately measured on live subjects.

ii) An approach for the implementation of a muscle model and the force-length relationship to the musculo-skeletal model used to describe human movement. This involves optimisation of

muscle model parameters, including fibre length and pennation angle, based on the force-length relationship and the range of muscle lengths measured in the movement under investigation. A result of the process is the development of an optimal fibre length and optimal isometric force for each muscle;

iii) Presenting a method for introducing muscle force-length and force-velocity characteristics into a muscle model for the estimation of maximum muscle forces. The muscle model incorporates a contractile element component, fibre series elastic component, fibre length, pennation angle, belly length, and a tendon slack length with tendon elasticity. The model will also need to account for the inter-dependency between variables through the solution of non-linear simultaneous equations;

iv) The introduction of a variation on an existing musculoskeletal cost function, based on minimisation of the sum of muscle stress (Siemienski, 1992) to produce a function that imposes both maximum and minimum soft constraints on muscle forces. The nature of the cost function is to produce more realistic muscle forces near maximum and minimum resultant joint moments. The cost function also allows an unconstrained minimisation of the cost function in order to calculate individual muscle forces with less computational effort;

iv) Presenting an approach for the determination of individual muscle forces involving the estimation of maximum and minimum muscle force values subject to muscle excitation and contraction dynamics and the unconstrained minimisation of the cost function presented earlier. A requirement of the optimisation procedure is an initial estimate of muscle forces which are required to meet the equipollence equations and be a reasonable approximation to the minimum solution. Therefore, an additional aim is to present an approach for obtaining muscle force first estimates for the minimisation procedure, based on an iterative procedure which distributes muscle forces based on moment generating capacity of the muscles;

vi) Incorporating the anatomical data produced and methods developed into a three dimensional video-based analysis of movements of the lower limb. This will incorporate a model consisting of four segments (pelvis, thigh, shank, and foot), 27 segment markers (five pelvic, eight thigh, eight shank, six foot markers) and 48 muscle elements (33 crossing the hip joint, 15 crossing the knee and 13 crossing the ankle), to predict three dimensional segment

kinematics and kinetics as well as muscle lengths, moment arms, fibre lengths, contractile element lengths, and muscle forces for the lower limb during human gait.

1.5 Purpose

In the application of three dimensional human movement analysis and musculo-skeletal modelling to clinical applications, it is necessary to utilise models and procedures which accurately reflect structure and function. Many studies (Inman, 1947; Andriacchi & Strickland, 1985; Delp & Zajac, 1992; Delp & Maloney, 1993; Delp et al., 1994; Vasavada, 1994; Kotzar et al., 1995; Brand & Yack, 1996; Free & Delp, 1996) show the complexity of the relationship between components of this system, but ignore or do not account for certain variables. The assumptions and limitations of this previous research, increases the inaccuracies and decreases the validity of results and the ability to draw sound conclusions.

When the model is required to predict individual muscle forces detailed musculoskeletal models are required which involve accurate predictions of segment position, resultant joint moments, accurate anatomical data (co-ordinate data describing muscle-tendon origin, insertion and path, fibre length, pennation angle, physiological cross sectional area, tendon length, fibre types percentages, optimal fibre length, and joint centres), valid force-length and force-velocity and excitation characteristics, and a physiologically-based criteria for distribution of muscle forces.

The prediction of individual muscle forces is required to determine internal forces that act on the skeletal system including joint compressive and shear forces, and is applied to a variety of applications such as aiding in rehabilitation, surgical intervention, and prosthetic design, and in investigative studies of muscular function. For movement analysis and musculo-skeletal modelling to be used successfully in clinical applications the accuracy and limitations of the data and procedures used must be known.

The present study is to develop a three dimensional model for the analysis of the musculo-skeletal system of the lower limbs, and attempts to address limitations in model design, anatomical data, and the implementation of the force-length and force velocity relationships. In addressing these limitations, anatomical data and procedures will be presented, implemented and discussed for the purpose of improving the accuracy and validity of movement analysis

and musculo-skeletal modelling. Although *in vivo* muscle forces can not be measured in human movements (i.e. the gold standard) to which modelling result can be compared, we can still improve validity of the modelling process by integrating available knowledge to improve musculo-skeletal modelling and muscle force prediction towards what we know or can indirectly measure in human subject. Thus improving methods and at the same time reducing assumptions and limitations that are made within the modelling process. In the case of modelling the dynamics of muscle force production improved validity of the modelling process may be obtained by implementing current models derived from animal studies. Where theories and mathematical descriptions of muscle force production subject to excitation contraction dynamics and muscle pre-activity can be developed, involving more invasive research, and then applied to the human model (Herzog & Leonard, 1991; Hawkins & Bey, 1997; Baratta, et al., 2000). The present study will also provide a basis for further investigation into three dimensional modelling of the musculo-skeletal system including the reconstruction of three dimensional segment location and anatomical data, muscle-tendon modelling techniques, and the optimisation approach to musculoskeletal modelling.

1.6 Outline of the present study

A comprehensive three dimensional mathematical model of the musculoskeletal system will be developed. The process starts by defining rigid body segments and concludes with the prediction of individual muscle forces. During this process the methodologies and protocols will be developed and implemented to address certain limitations in the three dimensional mathematical modelling of the musculoskeletal system. The study will involve:

i) Motion data derived from a video-based motion analysis system, utilising reflective markers to define segment trajectories. The protocol will involve four segments (pelvis, thigh, shank, foot) with 26 external markers placed on the lower limb (five, eight, eight and six markers on each segment respectively). Three walk and three step tasks will be analysed, the later involving stepping up onto a raised platform and returning. Ground reaction force data using a floor mounted force plate will be simultaneously collected;

ii) A rigid body system of axes will be defined from external markers placed on anatomical landmarks of the subject. The axis system corresponds to the skeletal axes system from which

segment centre of mass, joint centres, and muscle origins, insertions, and deflection points are defined;

iii) Three dimensional segment locations will be reproduced and an inverse dynamics approach used to calculate resultant joint moments;

iv) Acceleration of the centre of mass of each segment will be compared across trials and related to the three dimensional segment marker trajectories used to calculate segment location to access the present experimental design in terms of camera numbers and segment marker numbers, and the accuracy of three dimensional segment location;

v) A database will be developed describing the origin, insertion and deflection points of 48 muscle elements of the lower limb. The data suitable for describing muscle lengths and moment arms for a range of joint angles. The co-ordinates are expressed relative to the skeletal co-ordinate axes system for each respective segment and normalised using the same anthropometric measures as used to normalise locations of centre of mass, joint centres, and muscle model parameters of tendon cross sectional area and muscle mass. The skeletal axes location and orientation are the same as that defined from external markers for the video-based motion analysis;

vi) A muscle model will be defined for the 48 muscle elements. The muscle model incorporates muscle fibre length, pennation angle, muscle belly length and tendon slack length. The fibre component, in turn, comprises a fibre contractile element and fibre series elastic component, while tendon elasticity and cross sectional area gives rise to a tendon series-elastic component. Reference muscle model parameters will be obtained from the studies of Pierrynowski & Morrison (1985a, 1985b) and include muscle fibre length and tendon length as percentages of a reference muscle-tendon length, pennation angle, tendon cross sectional area, muscle mass, tendon slack lengths, and fibre type percentages. The reference muscle length at which the reference model data apply will be the standing anatomical position. Muscle-tendon lengths in the standing anatomical position are obtained by reproducing segment positions of the subject while standing and applying the co-ordinate data defining muscle paths. To apply tendon cross-sectional area and muscle mass to individual subjects, these measures will be normalised to segment lengths and lean circumferences. Force-length and force-velocity relationships will be defined using equations and parameters from Pierrynowski & Morrison (1985b);

vii) A method for incorporating the force-length and force-velocity relationship of muscles into the muscle model for determining muscle forces under known muscle-tendon lengths will be introduced. The maximum force produced by a muscle is dependent on fibre length and contractile element velocity. The length and velocity of these components, are in turn dependent on the inter-relationship between fibre series elastic component, tendon series elastic components, fibre length, pennation angle, contractile element length, as well as the forces produced by the contractile elements. To overcome this inter-dependency of muscle model parameters, a procedure is introduced to predict maximum isometric and dynamic muscle forces by the solution of series of non-linear simultaneous equation. The procedures are demonstrated on sample pennate and non-pennate muscle as well as in the optimisation of muscle parameters to muscle range of lengths for the 48 muscle elements in three dimensional analysis of a series of walk and step trials;

viii) From the three dimensional reproduction of segment motion for a given task and the data describing each muscle-tendon path, the range of muscle lengths will be determined for the movement under investigation. With known standard muscle parameters, range of muscle-tendon lengths, and equations describing the force-length relationship, muscle model parameters will be optimised to the range of fibre lengths (change in muscle belly length) throughout the movement. The optimisation procedure also produces an optimal fibre length and optimal isometric force. Muscle model parameter optimisation ensures that the force-length relationship is defined over the range of fibre lengths for the specific movement. An approach to the optimisation of muscle model parameters to the range of motion will be introduced and tested on sample muscles as well as in the three dimensional analysis of movements of the lower limb during the walk and step trials;

ix) Muscle length and moment arms will be calculated over the range of each movement and compared across each trial. This enables assessment of the validity and consistency of the calculations in relation to the accuracy of three dimensional segment location and anatomical data describing origins, insertions and paths. Muscle lengths and moment arms will also be compared to previous research;

x) A cost function and optimisation procedure will be introduced. The cost function involves soft constraints on maximum and minimum forces and is based on the minimisation of sum of muscle stress squared. The optimisation approach utilises a gradient projection algorithm,

given an initial estimate of muscle forces which meet the equipollence equations. A method for obtaining the first estimates of muscle forces as a starting point for the optimisation procedure will be developed. The validity of the cost function and optimisation approach will be tested by predicting muscle forces in a simple two-joint, eight muscle system at various resultant joint moments, as well as in predicting muscle forces in three dimensional movements of the leg;

xi) Forces will be predicted for 48 muscle elements in three dimensional movement trials. Results of muscle forces, fibre length and contractile element length will be compared across trials. Furthermore, muscle force predictions will be compared to electromyogaphic data collected during the trials.

1.7 Limitations

These will be discussed in detail when presenting the musculoskeletal model (Section 2.6)

1.8 Delimitations

The model was applied to only one healthy subject performing a series of motion trials (three walk trials and three step trials). It is expected that the numerical values may change between individuals, but it is anticipated that methods developed within this study for modelling the musculo-skeletal system would be valid and transferable to other healthy individuals performing similar tasks. The current aim is to develop and test methods for the three dimensional analysis of the musculoskeletal system of the lower limb, for improving the accuracy and validity of current modelling techniques. The information gained from the implementation of the model in movement trials, is specific to evaluating the performance outcomes of methods developed within this study, rather than the nature of the movement itself. It is anticipated, that in implementing the model in a series of movement trials, the outcomes and conclusions drawn with respect to the methods developed are valid to the general application of the model. It is acknowledged that in the application of musculoskeletal models to the analysis of pathological conditions the model will have to adapt to specifics of the condition. However, the formulation of any model needs to be based on accurate and valid techniques to draw sound conclusions. In the present study, the accuracy and validity of the methods proposed will be established, which in turn may lead to their future application in musculoskeletal modelling.

2 REVIEW OF LITERATURE

This section presents a review of literature on the three dimensional quantitative analysis of human motion. First, a brief introduction is given on methods for obtaining three dimensional segment locations from external segment markers via a video-based approach. Segment location history is fundamental to the quantification of human motion. Rigid body mechanics is then reviewed, starting with statics describing segment location and progressing to dynamics describing segment motion, inertia, momentum and kinetic energy. Euler equations of motion are introduced along with joint equipolance equations. Mathematical modelling of the human body is introduced, applying rigid body dynamics through link segment models, free body diagrams, estimating joint centres, and the inverse dynamics approach to calculating resultant joint forces and moments. A review is then presented of muscle force prediction from the equipolance equations. The review incluews redundancy and the distribution problem, muscle models, cost functions and the optimisation approach.

2.1 Obtaining segment location

A fundamental requirement in the analysis of human movement is to describe the orientation of limb segments and the relative rotations that are occurring at segmental joints. The complexity of human movement, and the need to make accurate, and at times detailed, assessment of human movement, has led to the use of three dimensional photogrammetric and rigid body techniques to record and quantify the motion of limb segments. The quantitative approach of modelling limb movements provides a large array of variables which describe motion that would not have otherwise been available as well as provides a basis for more complex and powerful dynamic models enabling the prediction of individual muscle forces, optimisation of movement and movement synthesis. The detail to which human movement can be described has enabled an expansion of research involving a wide range of aspects of human movement components.

The biomechanical modelling of limb segments in human motion has predominantly been based on rigid body segments interconnected by joints without friction of varying degrees of freedom (Hatze, 1977; McGee, et al., 1979). This approach lends itself to established methods of rigid body mechanics. A body-fixed right-hand Cartesian co-ordinate system embedded in each body segment is used to describe the location and orientation of that segment. Mass and

inertial characteristics, as well as geometric and structural properties of the segment, are also expressed relative to the body-fixed axis. Knowing the location of the body-fixed axis relative to inertial space and to the body segment is therefore basic to the description of the kinematics, kinetics and energetics of individual segments and of the human body (Marshall, 1985; Enoka, 1988; Winter, 1990).

The location and orientation of a body-fixed reference frame and the associated rigid body segment can be established from at least three non-linear points located on that that segment (Spoor & Veldpaus, 1980). If the three dimensional co-ordinates of the segment markers are known in the inertial reference frame, as well as their local co-ordinates with respect to the segmental fixed axes, then the three translation and three rotational variables needed to specify the location the segment in the inertial frame can be readily obtained (Hussain, 1977; Miller, 1980; Challis, 1995). Hussain (1977) confirmed the validity and repeatability of this approach when applied to the controlled motion of cadaver monkey limb segments by using ten external markers located on a plate which was physically attached to the femur and tibia bones. This approach is seldom possible in analysing the movement of live subjects, and external markers placed on the surface of the segment are used to approximate a body-fixed axes system which in turn approximates the position of the segment. Miller (1980), in the case of live subjects, recommended the placement of between six to ten markers on the surface of the limb segment and a least squares solution was found to improve accuracy which accounted for the varying motion of individual markers produced by the movement of soft tissue.

Stereophotogrammetry involves the reconstruction of three dimensional co-ordinate data from corresponding two dimensional co-ordinate data taken from multiple camera images. Various analytical photogrammetric techniques exist for taking measurement and calculations from camera image data. In the biomechanics literature the, Direct Linear Transformation (DLT) method, developed by Abdel-Aziz and Karara (Shapiro, 1978; Miller, et al., 1980; Cappozzo, 1985) is widely used as a mathematical model for the reconstruction of object space co-ordinates. This technique has several advantages over the more traditional stereometric model based on the colinearity equations. Namely, the DLT equations are linear making mathematical computations easier, the method does not require an exact knowledge of the experimental set-up or of internal camera geometry, and the DLT method removes the inflexibility and laborious set-up procedure required with the use of the traditional colinearity equations. At the same time, it retains the same number of unknowns in the solution and yields a similar

accuracy as the traditional approach (Keating, 1977; Shapiro, 1978; Miller, et al., 1980; Cappozzo, 1985).

The photographic and mathematical techniques that have been used in three dimensional quantification of human movement have developed out of disciplines such as surveying, mathematics, engineering, and medicine. The interdisciplinary nature of biomechanics has partly led to the differences in methodologies and nomenclature seen in the literature describing human movement. Such variations in biomechanical research make the understanding and comparison of both the methodologies and results more difficult. Authors have expressed the need for some uniformity in the form of standardisation in the approach to modelling of human motion. This would greatly facilitate the understanding and comparisons of the modelling techniques and results (Grood & Suntay, 1983; Small, et al., 1992), and has been pursued by the relevant profesional societies (for example, International Society of Biomechanics, Standardisation and Terminology Committee).

2.2 Rigid body statics

A rigid body comprises of a system of particles in which the distance between any two particles does not change regardless of the forces acting. The three dimensional motion of a rigid body can be described by three translation and three rotational parameters taken with respect to a suitable Cartesian axes system fixed in relation to the rigid body. These six parameters coincide with the number of degrees of freedom of a 'free' body. The origin of the body-fixed axes is generally taken as the centre of mass, but may well be taken as a proximal or distal joint centre when considering body segment motion.

In biomechanical literature, various conventions have been used in both the placement of fixed axes system on body segments and in the method used to describe the orientation of the axis system with respect to an inertial axes system. Despite a right-hand axis system being generally placed perpendicular with the longitudinal, transverse and frontal-coronal planes of individual segments, differences lie in defining which axis (**i**, **j**, **k**) is perpendicular to which anatomical plane (Chao, 1980; Hatze, 1980; Grood & Suntay, 1983; Seireg & Avikar, 1989). A number of rotational conventions are used in the literature, including Eulerian two-axis (Z X' Z"), Cardan rotations or Eulerian three-axis (X Y' Z"), and screw axis to describe the orientation of the body-fixed axes. As would be expected, the different conventions produce similar results

(Small, et al., 1992). Whichever rotational convention is used, anatomically meaningful rotations and displacements should be generated to give results which are meaningful to readers of human motion studies. The screw axis method, for example, has no direct relationship with anatomical movements (Small, et al., 1992). Which prompted the development of the floating axis system of Grood & Suntay (1983). The floating axis convention does not use mutually orthogonal axis and therefore is not applicable to established methods of rigid body dynamics, but it does provide a set of axes which are anatomically meaningful in terms of rotations between segments. The same rotations can however, be achieved by appropriately placed orthogonal body-fixed axes and a Cardan rotation sequence at less numerical cost. As previously mentioned, the orthogonal body-fixed axes and Cardan sequence can be used to describe the dynamics of the rigid body.

2.2.1 Co-ordinate transformation

The relationship between two co-ordinate systems, one usually being a body-fixed (non-inertial) co-ordinate system and the other an global space (inertial) co-ordinate system, can be expressed in the form of a matrix transformation. The transformation maps a position vector of a point, with components relative to one co-ordinate system, to a position vector of the same point expressed relative to a second co-ordinate system. The transformation is a function of the linear displacement of the two co-ordinate system origins and the directional cosines between respective axes (Fig. 2.2.1).

In Fig. 2.2.1, a vector **P** in the local co-ordinate system **X,Y,Z** locating point 'p' can be expressed as components (x,y,z) projected along respective unit axes (**i**, **j**, **k**) with α, β, γ being the angles between **P** and the unit axes **i**, **j** and **k** respectively. Alternatively point 'p' can be expressed as a unit vector **n** multiplied by the scalar length 'p'.

$$\begin{aligned} \mathbf{P} &= x\mathbf{i} + y\mathbf{j} + z\mathbf{k} \\ &= p.(\cos\alpha\,\mathbf{i} + \cos\beta\,\mathbf{j} + \cos\gamma\,\mathbf{k}) \\ &= p.\mathbf{n} \end{aligned} \qquad 2.2.1$$

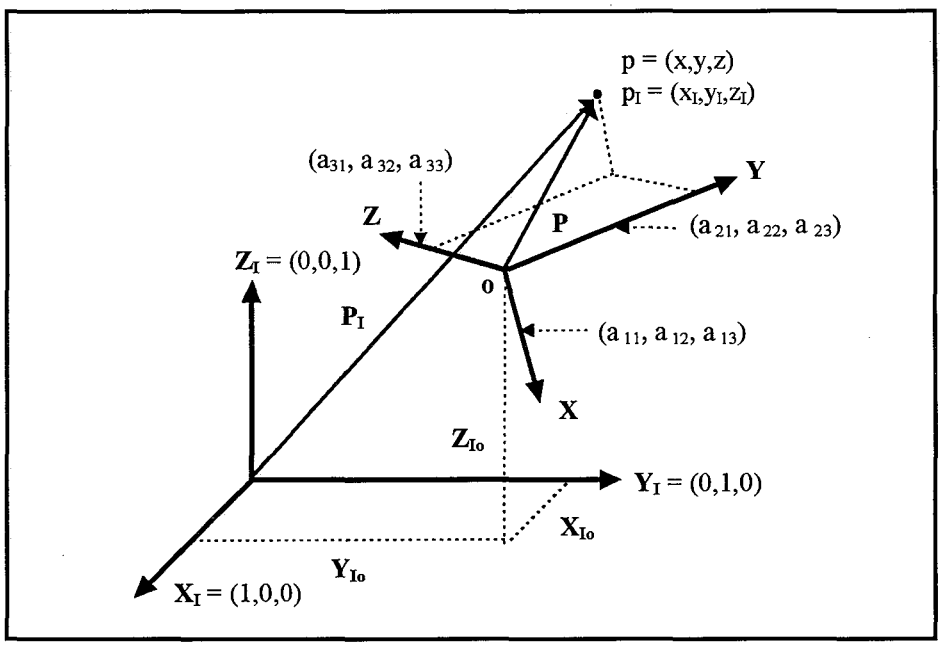

Figure 2.2.1 Location of a point with respect to global and body-fixed axes systems. The global axes are $\mathbf{X}_I$, $\mathbf{Y}_I$, and $\mathbf{Z}_I$ with unit vectors (1,0,0), (0,1,0), and (0,0,1) respectively. The body-fixed axes are given by **X**, **Y**, and **Z** with unit vectors (a_{11},a_{12},a_{13}), (a_{21},a_{22},a_{23}), and (a_{31},a_{32},a_{33}) respectively. The location of point 'p' can be given by the vectors $\mathbf{P}(x,y,z)$ or $\mathbf{P}_I(x_I,y_I,z_I)$ relative to the body-fixed or global axes respectively.

The quantities $\cos\alpha$, $\cos\beta$ and $\cos\gamma$ form the directional cosines of **P** with respect to the unit axes **i**, **j**, and **k**. Similarly, the unit vectors i, **j**, and **k** can be expressed relative to the inertial axes $\mathbf{X}_I$, $\mathbf{Y}_I$, $\mathbf{Z}_I$, by their projections onto these axes:

$$\begin{aligned}
\mathbf{i} &= a_{11}\,\mathbf{i}_I + a_{12}\,\mathbf{j}_I + a_{13}\,\mathbf{k}_I \\
&= \left(\cos\theta_{11}\,\mathbf{i}_I + \cos\theta_{12}\,\mathbf{j}_I + \cos\theta_{13}\,\mathbf{k}_I\right) \\
\mathbf{j} &= a_{21}\,\mathbf{i}_I + a_{22}\,\mathbf{j}_I + a_{23}\,\mathbf{k}_I \\
&= \left(\cos\theta_{21}\,\mathbf{i}_I + \cos\theta_{22}\,\mathbf{j}_I + \cos\theta_{23}\,\mathbf{k}_I\right) \\
\mathbf{k} &= a_{31}\,\mathbf{i}_I + a_{32}\,\mathbf{j}_I + a_{33}\,\mathbf{k}_I \\
&= \left(\cos\theta_{31}\,\mathbf{i}_I + \cos\theta_{32}\,\mathbf{j}_I + \cos\theta_{33}\,\mathbf{k}_I\right)
\end{aligned} \qquad 2.2.2$$

where:

θ_{ij} = angle between axis **i** of local axes and axis **j** of inertial axes.

$\cos\theta_{ij}$ = direction cosines of axes **i**, **j**, **k**.

Substituting (2.2.2) into (2.2.1), a vector **P** in the local co-ordinate system can be expressed relative to the global system by the directional cosines:

$$\begin{aligned}\mathbf{P} = & \left(x.\cos\theta_{11} + y.\cos\theta_{21} + z.\cos\theta_{31}\right)\mathbf{i_I} \\ & + \left(x.\cos\theta_{12} + y.\cos\theta_{22} + z.\cos\theta_{32}\right)\mathbf{j_I} \\ & + \left(x.\cos\theta_{13} + y.\cos\theta_{23} + z.\cos\theta_{33}\right)\mathbf{k_I}\end{aligned} \qquad 2.2.3$$

With the inclusion of the vector locating the origin of the local axes, the inertial co-ordinates of point 'p' can be given by the scalar equations:

$$\begin{aligned}x_I &= X_{Io} + x.\cos\theta_{11} + y.\cos\theta_{21} + z.\cos\theta_{31} \\ y_I &= Y_{Io} + x.\cos\theta_{12} + y.\cos\theta_{22} + z.\cos\theta_{32} \\ z_I &= Z_{Io} + x.\cos\theta_{13} + y.\cos\theta_{23} + z.\cos\theta_{33}\end{aligned} \qquad 2.2.4$$

Since for any two vectors:

$$\mathbf{a.b} = \|a\|.\|b\|.\cos(\theta) \qquad 2.2.5$$

The transformation can be expressed as:

$$\begin{bmatrix}1\\ x_I\\ y_I\\ z_I\end{bmatrix} = \begin{bmatrix}1 & 0 & 0 & 0\\ X_{Io} & \mathbf{i_I.i} & \mathbf{i_I.j} & \mathbf{i_I.k}\\ Y_{Io} & \mathbf{j_I.i} & \mathbf{j_I.j} & \mathbf{j_I.k}\\ Z_{Io} & \mathbf{k_I.i} & \mathbf{k_I.j} & \mathbf{k_I.k}\end{bmatrix} \cdot \begin{bmatrix}1\\ x\\ y\\ z\end{bmatrix} \qquad 2.2.6$$

where:

x, y, z = co-ordinates of point relative to local co-ordinate system
x_I, y_I, z_I = co-ordinates of point relative to inertial co-ordinate system
X_{Io}, Y_{Io}, Z_{Io} = origin of local co-ordinate system relative to inertial system
$\mathbf{i}, \mathbf{j}, \mathbf{k}$ = orthonormal base vectors of local system
$\mathbf{i_I}, \mathbf{j_I}, \mathbf{k_I}$ = orthonormal base vectors of inertial system

Similarly letting α_{11}, α_{12} .... α_{33} represent the directional cosines;

$$\begin{bmatrix} 1 \\ x_I \\ y_I \\ z_I \end{bmatrix} = \begin{bmatrix} 1 & 0 & 0 & 0 \\ X_{Io} & \alpha_{11} & \alpha_{12} & \alpha_{13} \\ Y_{Io} & \alpha_{21} & \alpha_{22} & \alpha_{23} \\ Z_{Io} & \alpha_{31} & \alpha_{32} & \alpha_{33} \end{bmatrix} \cdot \begin{bmatrix} 1 \\ x \\ y \\ z \end{bmatrix} \qquad 2.2.7$$

In the case that the inertial axes system is described by:

$$\begin{aligned} \mathbf{i}_I &= (1,0,0) \\ \mathbf{j}_I &= (0,1,0) \\ \mathbf{k}_I &= (0,0,1) \end{aligned} \qquad 2.2.8$$

Then:

$$\begin{aligned} \mathbf{i}_I.\mathbf{i} &= (1,0,0).(a_{11},a_{12},a_{13}) = a_{11} \\ \mathbf{j}_I.\mathbf{i} &= (0,1,0).(a_{11},a_{12},a_{13}) = a_{12} \\ \mathbf{k}_I.\mathbf{i} &= (0,0,1).(a_{11},a_{12},a_{13}) = a_{13} \\ &\text{etc.} \end{aligned} \qquad 2.2.9$$

With the result that the rotational transformation can be written:

$$\begin{bmatrix} \mathbf{i}_I.\mathbf{i} & \mathbf{i}_I.\mathbf{j} & \mathbf{i}_I.\mathbf{k} \\ \mathbf{j}_I.\mathbf{i} & \mathbf{j}_I.\mathbf{j} & \mathbf{j}_I.\mathbf{k} \\ \mathbf{k}_I.\mathbf{i} & \mathbf{k}_I.\mathbf{j} & \mathbf{k}_I.\mathbf{k} \end{bmatrix} \equiv \begin{bmatrix} a_{11} & a_{21} & a_{31} \\ a_{12} & a_{22} & a_{32} \\ a_{13} & a_{23} & a_{33} \end{bmatrix} \qquad 2.2.10$$

Therefore, if the inertial axes $\mathbf{i}_I$, $\mathbf{j}_I$, $\mathbf{k}_I$ take the form (1,0,0), (0,1,0) and (0,0,1) respectively, then the rotational matrix relating the non-inertial axes system to the inertial axes system, is formed by the column space of the non-inertial unit axes, in this case (a_{11},a_{12},a_{13}), (a_{21},a_{22},a_{23}) and (a_{31},a_{32},a_{33}).

A vector represented in the global system can likewise be expressed relative to the local co-ordinate system.

$$\begin{bmatrix} 1 \\ x \\ y \\ z \end{bmatrix} = \begin{bmatrix} 1 & 0 & 0 & 0 \\ X_o & \mathbf{i}.\mathbf{i}_I & \mathbf{i}.\mathbf{j}_I & \mathbf{i}.\mathbf{k}_I \\ Y_o & \mathbf{j}.\mathbf{i}_I & \mathbf{j}.\mathbf{j}_I & \mathbf{j}.\mathbf{k}_I \\ Z_o & \mathbf{k}.\mathbf{i}_I & \mathbf{k}.\mathbf{j}_I & \mathbf{k}.\mathbf{k}_I \end{bmatrix} \cdot \begin{bmatrix} 1 \\ x_I \\ y_I \\ z_I \end{bmatrix} \qquad 2.2.11$$

where:

X_o, Y_o, Z_o = origin of inertial co-ordinate system relative to local system.

The location vector of the inertial co-ordinate axes origin relative to body-fixed axes being given by:

$$\begin{bmatrix} -X_o \\ -Y_o \\ -Z_o \end{bmatrix} = \begin{bmatrix} \mathbf{i}.\mathbf{i}_I & \mathbf{i}.\mathbf{j}_I & \mathbf{i}.\mathbf{k}_I \\ \mathbf{j}.\mathbf{i}_I & \mathbf{j}.\mathbf{j}_I & \mathbf{j}.\mathbf{k}_I \\ \mathbf{k}.\mathbf{i}_I & \mathbf{k}.\mathbf{j}_I & \mathbf{k}.\mathbf{k}_I \end{bmatrix} \cdot \begin{bmatrix} X_{Io} \\ Y_{Io} \\ Z_{Io} \end{bmatrix} \qquad 2..2.12$$

Similarly, if the inertial axes $\mathbf{i}_I$, $\mathbf{j}_I$, $\mathbf{k}_I$ take the form (1,0,0), (0,1,0) and (0,0,1) respectively, then the rotational matrix relating the inertial axes system to the non-inertial axes system is formed by the row space of the non-inertial unit axes:

$$\begin{bmatrix} \mathbf{i}.\mathbf{i}_I & \mathbf{i}.\mathbf{j}_I & \mathbf{i}.\mathbf{k}_I \\ \mathbf{j}.\mathbf{i}_I & \mathbf{j}.\mathbf{j}_I & \mathbf{j}.\mathbf{k}_I \\ \mathbf{k}.\mathbf{i}_I & \mathbf{k}.\mathbf{j}_I & \mathbf{k}.\mathbf{k}_I \end{bmatrix} \equiv \begin{bmatrix} a_{11} & a_{12} & a_{13} \\ a_{21} & a_{22} & a_{23} \\ a_{31} & a_{32} & a_{33} \end{bmatrix} \qquad 2.2.13$$

2.2.2 Least squares calculation of transformation matrix

In calculating the transformation matrix, the problem is usually one in which the inertial system is the global co-ordinate system describing object space and the location of the body-fixed axes system with respect to the global system is desired. In this situation both the global and local co-ordinates of markers attached to the rigid body are known. With a minimum of three body-fixed markers required to locate the rigid body, a least squares approach uses additional markers to improve the accuracy in calculating the transformation matrix. The transformation matrix described in equation 2.2.6 can be written in terms of its rotational and translation components:

$$\begin{bmatrix} x_G \\ y_G \\ z_G \end{bmatrix} = \begin{bmatrix} \mathbf{i_G}.\mathbf{i} & \mathbf{i_G}.\mathbf{j} & \mathbf{i_G}.\mathbf{k} \\ \mathbf{j_G}.\mathbf{i} & \mathbf{j_G}.\mathbf{j} & \mathbf{j_G}.\mathbf{k} \\ \mathbf{k_G}.\mathbf{i} & \mathbf{k_G}.\mathbf{j} & \mathbf{k_G}.\mathbf{k} \end{bmatrix} . \begin{bmatrix} x \\ y \\ z \end{bmatrix} + \begin{bmatrix} X_{Go} \\ Y_{Go} \\ Z_{Go} \end{bmatrix} \qquad 2.2.14$$

or as vectors:

$$\mathbf{r_G} = [R_{GL}].\mathbf{r} + \mathbf{v_{Go}} \qquad 2.2.15$$

where:

x_G, y_G, z_G = co - ordinates with respect to global system.

$[R_{GL}]$ = rotation matrix relating local to global co - ordinates.

Using a least squares method, the problem of determining $[R_{GL}]$ and $\mathbf{v_{Go}}$ is equivalent to minimising (Challis, 1995):

$$\frac{1}{n}\sum_{i=1}^{n}\left([R_{GL}].\mathbf{r_i} + \mathbf{v_{Go}} - \mathbf{r_{Gi}}\right)^T\left([R_{GL}].\mathbf{r_i} + \mathbf{v_{Go}} - \mathbf{r_{Gi}}\right) \qquad 2.2.16$$

In the method of Challis (1995), the vector $\mathbf{v_{Go}}$ can be eliminated by first considering the mean vectors:

$$\begin{aligned} \bar{\mathbf{r}} &= \frac{1}{2}\sum_{i=1}^{n}\mathbf{r_i} \\ \bar{\mathbf{r}}_G &= \frac{1}{2}\sum_{i=1}^{n}\mathbf{r_{Gi}} \end{aligned} \qquad 2.2.17$$

At a minimum, equation 2.2.15 holds and the following relationship exists:

$$\mathbf{v_{Go}} = \bar{\mathbf{r}}_G - [R_{GL}].\bar{\mathbf{r}} \qquad 2.2.18$$

Substituting equation 2.2.18 into equation 2.2.16 and simplifying the result by letting:

$$\begin{aligned} \mathbf{r_i'} &= \mathbf{r_i} - \bar{\mathbf{r}} \\ \mathbf{r'_{Gi}} &= \mathbf{r_{Gi}} - \bar{\mathbf{r}}_G \end{aligned} \qquad 2.2.19$$

The object to be minimised (equation 2.2.16) becomes:

$$\frac{1}{n}\sum_{i=1}^{n}\left(\mathbf{r}'_{Gi} - [R_{GL}].\mathbf{r}'_i\right)^T\left(\mathbf{r}'_{Gi} - [R_{GL}].\mathbf{r}'_i\right) \qquad 2.2.20$$

On expanding equation 2.2.20 gives (Challis, 1995):

$$\frac{1}{n}\sum_{i=1}^{n}\left[\left(\mathbf{r}'_{Gi}\right)^T.\mathbf{r}'_{Gi} + \left(\mathbf{r}'_i\right)^T.\mathbf{r}'_i - 2.\left(\mathbf{r}'_{Gi}\right)^T.[R_{GL}].\mathbf{r}'_i\right] \qquad 2.2.21$$

Since the first two terms of equation 2.2.21 are the sum of two squares and non-negative, minimising equation 2.2.16, or similarly equation 2.2.21, is equivalent to maximising:

$$\frac{1}{n}\sum_{i=1}^{n}\left[\left(\mathbf{r}'_{Gi}\right)^T.[R_{GL}].\mathbf{r}'_i\right] \qquad 2.2.22$$

On expanding, equation 2.2.22 can be written as (Challis, 1995):

$$\mathrm{tr}\left\{[R_{GL}]^T.\frac{1}{n}\sum_{i=1}^{n}\mathbf{r}'_{Gi}.\mathbf{r}'^T_i\right\} \qquad 2.2.23$$

Letting:

$$\begin{aligned}[C] &= \frac{1}{n}\sum_{i=1}^{n}\mathbf{r}'_{Gi}.\mathbf{r}'^T_i \\ &= \frac{1}{n}\sum_{i=1}^{n}\left(\mathbf{r}_{Gi} - \bar{\mathbf{r}}_G\right).\left(\mathbf{r}_i - \bar{\mathbf{r}}\right)^T\end{aligned} \qquad 2.2.24$$

The object to be maximised can be written as:

$$\mathrm{tr}\left\{[R_{GL}]^T.[C]\right\} \qquad 2.2.25$$

The singular value decomposition of [C] yields:

$$[C] = [U].[W].[V]^T \qquad 2.2.26$$

Where [U] and [V] are orthogonal matrices and [W] is a diagonal matrix which contains the singular values of [C]. Substituting equation 2.2.26 into equation 2.2.25 and introducing matrix [Q] gives:

$$\begin{aligned} tr\left\{[R_{GL}]^T.[C]\right\} &= tr\left\{[R_{GL}]^T.[U].[W].[V]^T\right\} \\ &= tr\left\{[V]^T.[R_{GL}]^T.[U].[W]\right\} \\ &= tr\left\{[Q].[W]\right\} \end{aligned} \qquad 2.2.27$$

With

$$[Q] = [V]^T.[R_{GL}]^T.[U] \qquad 2.2.28$$

Since $[V]^T$, $[R_{GL}]^T$ and [U] are orthogonal, matrix [Q] is also orthogonal with maximal and minimal possible diagonal element values of plus or minus unity respectively. The diagonal elements of [Q] are multiplied by the singular values held in the diagonal matrix [W], which may be positive or negative. Therefore in order to maximise the sum of diagonal elements, as in equation 2.2.27, [R] is a matrix such that the resultant [Q] has maximum values of either plus or minus one on the diagonal elements depending on the signs of the diagonal elements of [W]. Hence the diagonal elements of [Q] and [W] are of the same sign. Therefore [Q] is given by:

$$[Q] = \begin{bmatrix} \frac{w_{11}}{\|w_{11}\|} & 0 & 0 \\ 0 & \frac{w_{22}}{\|w_{22}\|} & 0 \\ 0 & 0 & \frac{w_{33}}{\|w_{33}\|} \end{bmatrix} \qquad 2.2.29$$

and $[R_{GL}]$ is given by:

$$[R_{GL}] = [U].[Q].[V]^T \qquad 2.2.30$$

To calculate $[R_{GL}]$, first matrix [C] is calculated as in (2.2.24). Then a singular value decomposition is performed on [C] to give matrices $[U][W][V]^T$. The elements on the diagonal of [Q] are then set to either +1 if the corresponding element of [W] is greater than one, or to -1 if the corresponding element of [W] is less than one. Matrix $[R_{GL}]$ is then calculated by the product $[U][Q]\,[V]^T$.

To calculate the vector $\mathbf{v}_{G_o}$ equation 2.2.18 is used with known $\bar{\mathbf{r}}$, $\bar{\mathbf{r}}_G$ and $[R_{GL}]$.

2.2.3 Euler and Cardan rotations

Euler and Cardan rotations involve three ordered rotations about the axes of a reference co-ordinate system (inertial) in order to define the orientation of a second axes system (in this case body-fixed axes). Euler rotations take the form of various two-axis or three-axis conventions while Cardan rotations follow a three-axis convention. A rotation sequence about three consecutive axes following the right hand order of an axis system may be referred to as a three-axis Euler or Cardan rotation. In the present discussion, Euler rotations will refer to a two axis rotation sequence about $\mathbf{Z}_I$, $\mathbf{X}'$, and $\mathbf{Z}''$ axes, while Cardan rotations will refer to rotations about $\mathbf{X}_I$, $\mathbf{Y}'$, and $\mathbf{Z}''$ axes. The expanded form of the transformation matrix [T], involving Euler or Cardan angles, depends on the rotational convention used.

2.2.3.1 Euler two axis rotations

Euler two axes rotations can be defined by ordered rotations about three axes, the first and last axes being of common descent. The Euler two-axis rotation of interest involves consecutive rotations about the $\mathbf{Z}_I$ axis, $\mathbf{X}'$ axis and $\mathbf{Z}''$ axis (Fig. 2.2.2). Letting the three rotations be (ϕ, θ, φ), the rotation matrix [R] can be expressed as three separate rotations which relate global to local co-ordinates.

$$\begin{aligned} \mathbf{r} &= [R].\mathbf{r}_I \\ &= [R_\varphi].[R_\theta].[R_\phi].\mathbf{r}_I \end{aligned} \qquad 2.2.31$$

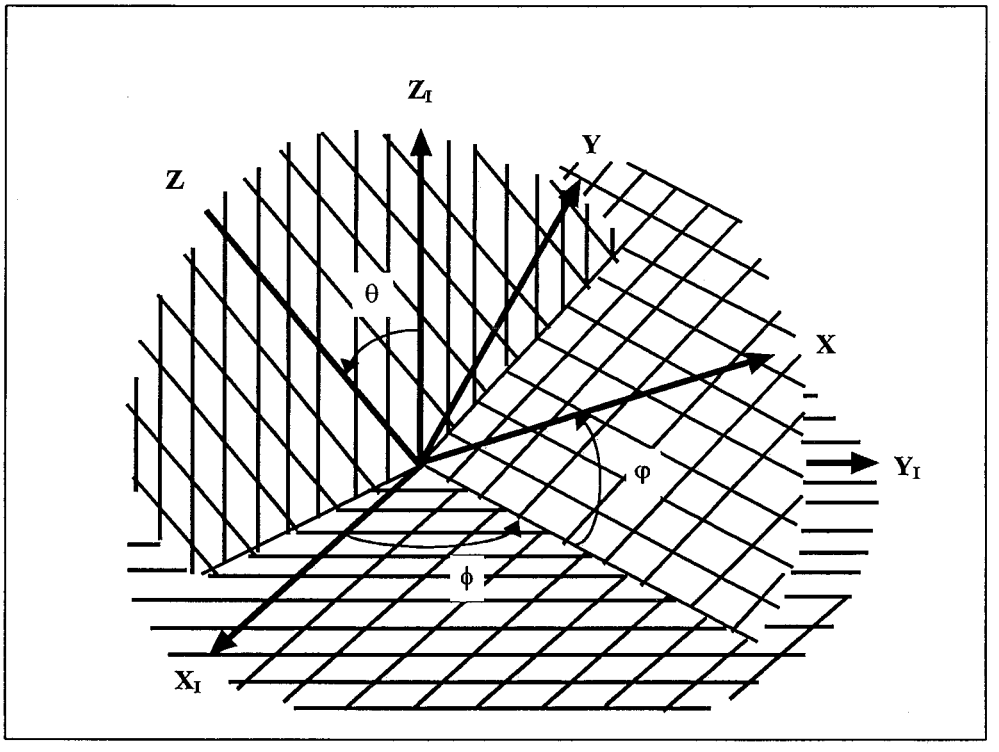

Figure 2.2.2 Euler two-axis rotation. The first rotation is about the $\mathbf{Z}_I$ axis of angle ϕ, the second rotation about the $\mathbf{X}'$ axis of angle θ, and the third rotation about the $\mathbf{Z}''$ axis of angle φ.

The expanded form of the rotation matrix, where the directional cosines are expressed in terms of the three individual rotations (ϕ, θ, φ), can be derived by looking at each rotation in turn. A rotation (ϕ) about the $\mathbf{Z}_I$ axis gives:

$$\begin{aligned} x' &= x_I.\cos\phi + y_I.\sin\phi \\ y' &= -x_I.\sin\phi + y_I.\cos\phi \\ z' &= z_I \end{aligned} \qquad 2.2.32a$$

and

$$[R_\phi] = \begin{bmatrix} \cos\phi & \sin\phi & 0 \\ -\sin\phi & \cos\phi & 0 \\ 0 & 0 & 1 \end{bmatrix} \qquad 2.2.32b$$

A second rotation (θ) about the $\mathbf{X}'$ axis gives:

$$\begin{aligned} x'' &= x' \\ y'' &= y'.\cos\theta + z'.\sin\theta \\ z'' &= -y'.\sin\theta + z'.\cos\theta \end{aligned} \qquad 2.2.33a$$

and

$$[R_\theta] = \begin{bmatrix} 1 & 0 & 0 \\ 0 & \cos\theta & \sin\theta \\ 0 & -\sin\theta & \cos\theta \end{bmatrix} \qquad 2.2.33b$$

A final rotation (φ) about the $\mathbf{Z}''$ axis gives:

$$\begin{aligned} x &= x''.\cos\varphi + y''.\sin\varphi \\ y &= -x''.\sin\varphi + y''.\cos\varphi \\ z &= z'' \end{aligned} \qquad 2.2.34a$$

and

$$[R\varphi] = \begin{bmatrix} \cos\varphi & \sin\varphi & 0 \\ -\sin\varphi & \cos\varphi & 0 \\ 0 & 0 & 1 \end{bmatrix} \qquad 2.3.34b$$

Substituting equation 2.2.32a into equation 2.2.33a and then the resultant into equation 2.2.34a, obtains a rotation transformation equation relating inertial co-ordinates (x_I,y_I,z_I) to local co-ordinates.

$$\begin{aligned} x &= f_1(x_I, y_I, z_I, \phi, \theta, \varphi) \\ y &= f_2(x_I, y_I, z_I, \phi, \theta, \varphi) \\ z &= f_3(x_I, y_I, z_I, \phi, \theta, \varphi) \end{aligned} \qquad 2.2.35$$

The same can be achieved by evaluating equation 2.2.31; that is:

$$[R] = [R_\varphi].[R_\theta].[R_\phi] \qquad 2.2.36$$

Combining the rotational equations 2.2.35 with a translation of the origin between the two co-ordinate systems, the expanded form of the transformation matrix [T] is obtained:

$$[T] = \begin{bmatrix} 1 & 0 & 0 & 0 \\ X_o & \cos\phi.\cos\varphi - \sin\phi.\sin\varphi.\cos\theta & \cos\varphi.\sin\phi + \sin\varphi.\cos\phi.\cos\theta & \sin\theta.\sin\varphi \\ Y_o & -\sin\varphi.\cos\phi - \cos\varphi.\sin\phi.\cos\theta & -\sin\phi.\sin\varphi + \cos\phi.\cos\varphi.\cos\theta & \sin\theta.\cos\varphi \\ Z_o & \sin\theta.\sin\phi & -\sin\theta.\cos\phi & \cos\theta \end{bmatrix} \qquad 2.2.37$$

where:

ϕ = first rotation about $\mathbf{k}_I$.
θ = second rotation about $\mathbf{i}'$.
φ = third rotation about $\mathbf{k}''$.
X_o, Y_o, Z_o = origin of inertial axes, with components taken along body-fixed axes.

The expanded form of the inverse transformation $[R]^{-1}$ relating local co-ordinates (x,y,z) to inertial co-ordinates (x_I, y_I, z_I) can also be derived by looking at each individual rotation in turn. A rotation $(-\varphi)$ about the **Z** axis gives:

$$\begin{aligned} x'' &= x.\cos\varphi - y.\sin\varphi \\ y'' &= x.\sin\varphi + y.\cos\varphi \\ z'' &= z \end{aligned} \qquad 2.2.38a$$

and

$$[R\varphi]^{-1} = \begin{bmatrix} \cos\varphi & -\sin\varphi & 0 \\ \sin\varphi & \cos\varphi & 0 \\ 0 & 0 & 1 \end{bmatrix} \qquad 2.2.38b$$

A second rotation $(-\theta)$ about the $\mathbf{X}''$ axis gives:

$$
\begin{aligned}
x' &= x'' \\
y' &= y''.\cos\theta - z''.\sin\theta \\
z' &= y''.\sin\theta + z''.\cos\theta
\end{aligned}
\qquad 2.2.39a
$$

and

$$
[R_\theta]^{-1} = \begin{bmatrix} 1 & 0 & 0 \\ 0 & \cos\theta & -\sin\theta \\ 0 & \sin\theta & \cos\theta \end{bmatrix}
\qquad 2.2.39b
$$

A final rotation $(-\phi)$ about the $\mathbf{Z}'$ axis gives:

$$
\begin{aligned}
x_I &= x'.\cos\phi - y'.\sin\phi \\
y_I &= x'.\sin\phi + y'.\cos\phi \\
z_I &= z'
\end{aligned}
\qquad 2.2.40a
$$

and

$$
[R_\phi]^{-1} = \begin{bmatrix} \cos\phi & -\sin\phi & 0 \\ \sin\phi & \cos\phi & 0 \\ 0 & 0 & 1 \end{bmatrix}
\qquad 2.2.40b
$$

Substituting equation 2.2.38a into equation 2.2.39a and then the resultant into equation 2.2.40a, obtains a rotation transformation equation relating body co-ordinates (x,y,z) to inertial co-ordinates.

$$
\begin{aligned}
x_I &= f_1(x, y, z, \phi, \theta, \varphi) \\
y_I &= f_2(x, y, z, \phi, \theta, \varphi) \\
z_I &= f_3(x, y, z, \phi, \theta, \varphi)
\end{aligned}
\qquad 2.2.41
$$

The same can be achieved by evaluating:

$$
[R]^{-1} = [R_\phi]^{-1}.[R_\theta]^{-1}.[R_\varphi]^{-1}. \qquad 2.2.42
$$

Combining the rotational equation 2.2.41 with a translation of the origin between the two co-ordinate systems, the expanded form of the transformation matrix $[T]^{-1}$ is obtained:

$$[T]^{-1} = \begin{bmatrix} 1 & 0 & 0 & 0 \\ X_{Io} & \cos\phi.\cos\varphi & -\sin\varphi.\cos\phi & \sin\theta.\sin\phi \\ & -\sin\phi.\sin\varphi.\cos\theta & -\cos\varphi.\sin\phi.\cos\theta & \\ Y_{Io} & \cos\varphi.\sin\phi & -\sin\phi.\sin\varphi & -\sin\theta.\cos\phi \\ & \sin\varphi.\cos\phi.\cos\theta & +\cos\phi.\cos\varphi.\cos\theta & \\ Z_{Io} & \sin\theta.\sin\varphi & \sin\theta.\cos\varphi & \cos\theta \end{bmatrix} \quad 2.2.43$$

where:

ϕ = first rotation about $\mathbf{k}_I$.
θ = second rotation about $\mathbf{i}'$.
φ = third rotation about $\mathbf{k}''$.
X_{Io}, Y_{Io}, Z_{Io} = origin of body axes, with components taken along inertial axes.

From equation 2.2.37 and equation 2.2.43 it can be seen that:

$$[R]^{-1} = [R]^T \quad 2.2.44$$

2.2.3.2 Cardan rotations

Cardan rotation can be defined by a number of different ordered rotations about three different axes. This rotation sequence may also be called Byrant rotation or Euler three-axis rotations. The Cardan rotation of interest involves consecutive rotations about the $\mathbf{X}_I$ axis, $\mathbf{Y}'$ axis and $\mathbf{Z}''$ axis (Fig. 2.2.3). As with Euler rotations, the directional cosines between inertial and body fixed axes can be derived by looking at each rotation in turn.

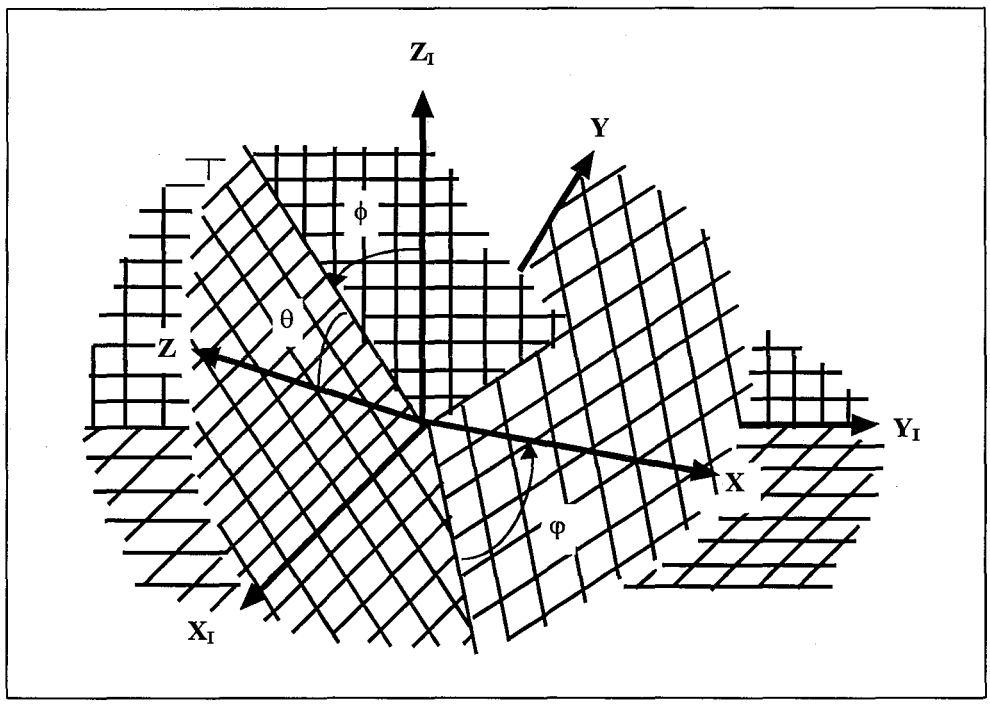

Figure 2.2.3 Cardan three-axis rotation. The first rotation is about the $\mathbf{X_I}$ axis of angle ϕ, the second rotation about the $\mathbf{Y'}$ axis of angle θ, and the third rotation about the $\mathbf{Z''}$ axis of angle φ.

A rotation (ϕ) about the $\mathbf{X_I}$ axis gives:

$$\begin{aligned} x' &= x_I \\ y' &= y_I.\cos\phi + z_I.\sin\phi \\ z' &= -y_I.\sin\phi + z_I.\cos\phi \end{aligned} \qquad 2.2.45a$$

and

$$[R_\phi] = \begin{bmatrix} 1 & 0 & 0 \\ 0 & \cos\phi & \sin\phi \\ 0 & -\sin\phi & \cos\phi \end{bmatrix} \qquad 2.2.45b$$

A second rotation (θ) about the $\mathbf{Y'}$ axis gives:

$$\begin{aligned} x'' &= x'.\cos\theta - z'.\sin\theta \\ y'' &= y' \\ z'' &= x'.\sin\theta + z'.\cos\theta \end{aligned} \qquad 2.2.46a$$

and

$$[R_\theta] = \begin{bmatrix} \cos\theta & 0 & -\sin\theta \\ 0 & 1 & 0 \\ \sin\theta & 0 & \cos\theta \end{bmatrix} \qquad 2.2.46b$$

A third rotation (φ) about the $\mathbf{Z}''$ axis gives:

$$\begin{aligned} x &= x''.\cos\varphi + y''.\sin\varphi \\ y &= -x''.\sin\varphi + y''.\cos\varphi \\ z &= z'' \end{aligned} \qquad 2.2.47a$$

and

$$[R_\varphi] = \begin{bmatrix} \cos\varphi & \sin\varphi & 0 \\ -\sin\varphi & \cos\varphi & 0 \\ 0 & 0 & 1 \end{bmatrix} \qquad 2.2.47b$$

Similarly, combining the three rotations (equations 2.2.45a, 2.2.46a. 2.2.47a), or multiplying the three individual rotations and adding a translation of the origin, the expanded form of the transformation matrix [T] takes the form:

$$[T] = \begin{bmatrix} 1 & 0 & 0 & 0 \\ X_o & \cos\varphi.\cos\theta & \cos\phi.\sin\varphi + \sin\phi.\sin\theta.\cos\varphi & \sin\phi.\sin\varphi - \cos\phi.\sin\theta.\cos\varphi \\ Y_o & -\sin\varphi.\cos\theta & \cos\phi.\cos\varphi - \sin\phi.\sin\varphi.\sin\theta & \sin\phi.\cos\varphi + \cos\phi.\sin\theta.\sin\varphi \\ Z_o & \sin\theta & -\cos\theta.\sin\phi & \cos\theta.\cos\phi \end{bmatrix} \qquad 2.2.48$$

where:

ϕ = first rotation about $\mathbf{i_I}$.

θ = second rotation about $\mathbf{j'}$.

φ = third rotation about $\mathbf{k''}$.

Similarly it can also be shown that:

$$\begin{aligned}[R]^{-1} &= [R_\phi]^{-1}.[R_\theta]^{-1}.[R_\varphi]^{-1} \\ &= [R]^T\end{aligned} \qquad 2.2.49$$

2.2.3.3 Rotational sequence dependency

The net rotational displacement produced by the sequence of rotations about its respective axes is dependent on the order in which they occur. Hence ordered rotations are sequence-dependent. This can be show in the Euler and Cardan rotations by relating the expanded form the directional cosine matrix with the product of the three individual rotations.

$$\begin{aligned}[R] &= [R_\varphi].[R_\theta].[R_\phi] \\ [R] &\neq [R_\theta].[R_\varphi].[R_\phi]\end{aligned} \qquad 2.2.50$$

2.2.3.4 Determining Euler and Cardan angles

The individual Euler and Cardan angles are determined by equating the expanded form of the transformation matrix (equation 2.2.35 and equation 2.2.29) with the unit vector directional cosines (equation 2.2.6). For the Euler two axes convention:

$$\begin{aligned}\cos\theta &= \mathbf{k_I}.\mathbf{k} = \mathbf{k_I}.(a_{31}, a_{32}, a_{33}) \\ \cos\varphi &= \mathbf{k_I}.\mathbf{j}/\sin\theta = \mathbf{k_I}.(a_{21}, a_{22}, a_{23})/\sin\theta \\ \cos\phi &= \mathbf{j_I}.\mathbf{k}/-\sin\theta = \mathbf{j_I}.(a_{31}, a_{32}, a_{33})/-\sin\theta\end{aligned} \qquad 2.2.51$$

For the Cardan convention:

$$\begin{aligned}\sin\theta &= \mathbf{i_I}.\mathbf{k} = \mathbf{i_I}.(a_{31}, a_{32}, a_{33}) \\ \sin\varphi &= \mathbf{i_I}.\mathbf{j}/-\cos\theta = \mathbf{i_I}.(a_{21}, a_{22}, a_{23})/-\cos\theta \\ \sin\phi &= \mathbf{j_I}.\mathbf{k}/-\cos\theta = \mathbf{j_I}.(a_{31}, a_{32}, a_{33})/-\cos\theta\end{aligned} \qquad 2.2.52$$

Euler and Cardan angles can be related by equating directional cosines in equation 2.2.37 and equation 2.2.48, resulting in:

$$\begin{aligned}
\mathbf{i}_I.\mathbf{k} &= \sin\theta_C = \sin\theta_E.\sin\phi_E \\
\mathbf{j}_I.\mathbf{k} &= -\cos\theta_C.\sin\phi_C = -\sin\theta_E.\cos\phi_E \\
\mathbf{k}_I.\mathbf{k} &= \cos\theta_C.\cos\phi_C = \cos\theta_E \\
\mathbf{i}_I.\mathbf{j} &= -\sin\varphi_C.\cos\theta_C = -\sin\varphi_E.\cos\phi_E - \cos\varphi_E.\sin\phi_E.\cos\theta_E
\end{aligned} \qquad 2.2.53$$

2.2.3.5 Physical interpretation of Euler and Cardan angles

The three angles (ϕ, θ, φ) can be visualised by the movement of concentric gimbals attached to the rigid body. The Eulerian two axes rotational sequence is represented in Fig. 2.2.4.

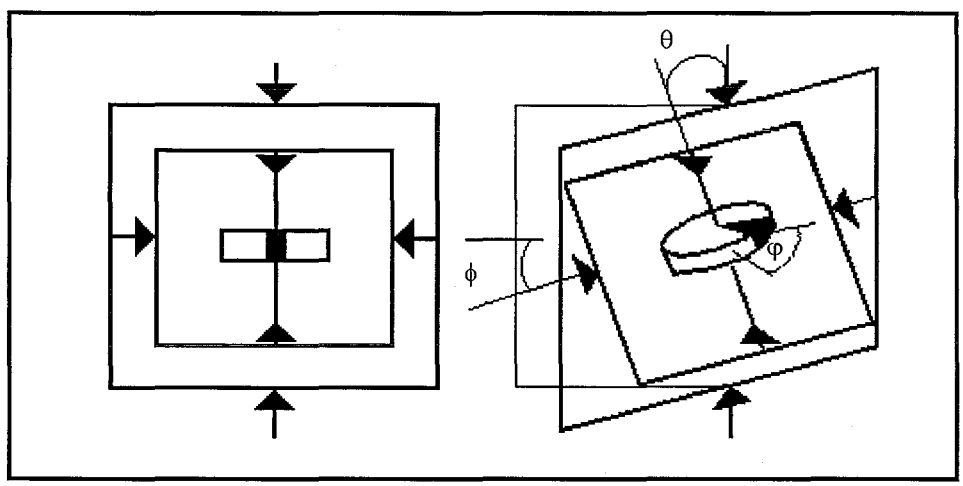

Figure 2.2.4 Euler two-axis sequence and gimbal rotations.

In describing the orientation of a spinning top, the three angles of the Euler two axes convention can be given the notation 'precession', 'nutation', and 'spin' respectively. (Wells, 1967). The Cardan rotational sequence is represented in Fig. 2.2.5.

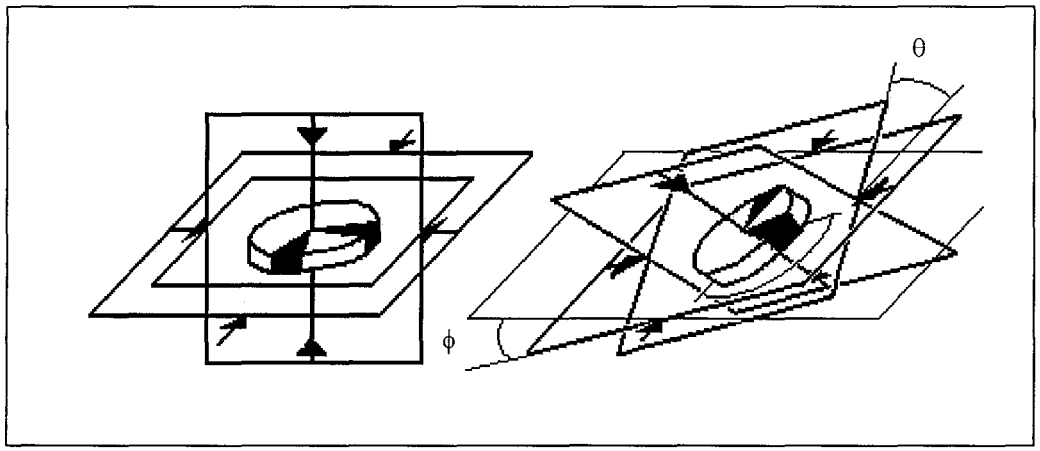

Figure 2.2.5 Cardan sequence and gimbal rotations.

In describing flight mechanics, the three Cardan angles may be given the notation 'pitch', 'yaw' and 'roll', respectively (Small, et el., 1992). In describing whole body orientation the three Cardan angles may be given the notation 'somersault', 'twist' and 'spin', respectively (Yeadon, 1990a).

2.2.3.6 Singularities in Euler and Cardan angles

A point of singularity (gimbal lock) occurs in the Euler two-axis convention (equation 2.2.40) if $\sin\theta = 0$, which occurs when the second rotation $\theta = 0$ or 180 degrees. A point of singularity (gimbal lock) occurs in the Cardan convention (equation 2.2.41) if $\cos\theta = 0$, which occurs when the second rotation $\theta = 90$ or 270 degrees. At the points of singularity more than one combination of ϕ and φ will arrive at the same body fixed axes location. Chao (1980) notes that the solution will also become unstable as a rotational scheme approaches a point of singularity. To overcome singularity problems in rotational based orientation schemes Schiehlen (1984) suggested using alternative schema near a region of instability, such as alternating between Eulerian and Cardan conventions or alternatively adopting other angular measures such as four Euler parameters.

2.3 Rigid body dynamics

The six spatial parameters $(x, y, z, \phi, \theta, \varphi)$ describing the location of a rigid body are fundamental in describing rigid body dynamics. These six spatial parameters and their time derivatives enable the calculation of velocities, acceleration and energies of a rigid body.

2.3.1 Angular velocity of rigid body

The angular velocity of the rigid body with respect to the inertial system is given by the sum of rotations occurring about each axis of the rigid body system.

$$\omega = \omega_x \mathbf{i} + \omega_y \mathbf{j} + \omega_z \mathbf{k} \qquad 2.3.1$$

where:

$\omega_x, \omega_y, \omega_z$ = angular velocity about body-fixed axes

$\mathbf{i}, \mathbf{j}, \mathbf{k}$ = unit vectors in body-fixed x, y, z axes

For the Eulerian two axes rotation (Fig. 2.2.2), the angular velocity along the **i**, **j**, **k** axes are found by the directional cosines between the **i**, **j**, **k** axes and the $\mathbf{Z}_I$, **X'** and **Z''** axes about which the three Euler rotations $\dot{\phi}$, $\dot{\theta}$, $\dot{\varphi}$ are made. The directional cosines being:

	i	**j**	**k**
$\mathbf{Z}_I$	$\sin\theta.\sin\varphi$	$\sin\theta.\cos\varphi$	$\cos\theta$
X'	$\cos\varphi$	$-\sin\varphi$	0
Z''	0	0	1

2.3.2

The components of angular velocity occurring along the axes of the body-fixed system are given by:

$$\begin{aligned} \omega_x &= \dot{\phi}.\ \sin\theta.\sin\varphi + \dot{\theta}.\ \cos\varphi \\ \omega_y &= \dot{\phi}.\ \sin\theta.\cos\varphi - \dot{\theta}.\ \sin\varphi \\ \omega_z &= \dot{\phi}.\ \cos\theta + \dot{\varphi} \end{aligned} \qquad 2.3.3$$

For the Eulerian three-axis rotation (Fig. 2.2.3), the angular velocity along the **i**, **j**, **k** axes are found by the directional cosines between the **i**, **j**, **k** axes and the $\mathbf{X_I}$, **Y'** and **Z''** axes along which the three Euler rotations $\dot{\phi}$, $\dot{\theta}$, $\dot{\varphi}$ are occurring. The directional cosines being:

	i	**j**	**k**
$\mathbf{X_I}$	$\cos\theta.\cos\varphi$	$-\cos\theta.\sin\varphi$	$\sin\theta$
Y'	$\sin\varphi$	$\cos\varphi$	0
Z''	0	0	1

2.3.4

The components of rotation occurring along each axes of the body-fixed system are given by:

$$\begin{aligned} \omega_x &= \dot{\phi}.\cos\theta.\cos\varphi + \dot{\theta}.\sin\varphi \\ \omega_y &= -\dot{\phi}.\cos\theta.\sin\varphi + \dot{\theta}.\cos\varphi \\ \omega_z &= \dot{\phi}.\sin\theta + \dot{\varphi} \end{aligned} \qquad 2.3.5$$

2.3.2 Linear velocity of a point mass

The linear velocity with respect to the inertial system of a point mass **m** located at (a**i**, b**j**, c**k**) in the body-fixed reference frame is given by the components of linear velocity along the instantaneous directions **i**, **j**, **k**.

$$\boldsymbol{v} = v_x\mathbf{i} + v_y\mathbf{j} + v_z\mathbf{k} \qquad 2.3.6$$

where:

v_x, v_y, v_z = linear velocity in body-fixed x, y, z axes

The linear velocity of a point mass located at (a,b,c) resulting from the rotation of the rigid body is given by:

$$\begin{aligned} v_x &= \omega_y.c - \omega_z.b \\ v_y &= \omega_z.a - \omega_x.c \\ v_z &= \omega_x.b - \omega_y.a \end{aligned} \qquad 2.3.7$$

The instantaneous angular velocities about the respective body-fixed axes ω_e, ω_f ω_g are a function of the respective Euler angles $\left(\phi,\ \theta,\ \varphi,\ \dot{\phi},\ \dot{\theta}, \dot{\varphi}\right)$, as in equations (2.3.3) and (2.3.5).

If the body-fixed axis origin has an inertial space linear velocity v_o with components v_{ox}, v_{oy}, v_{oz} along the instantaneous directions of **i**, **j**, **k**, then the linear velocity of a point mass **m** is given by:

$$\begin{aligned} v_x &= v_{ox} + \omega_y.c - \omega_z.b \\ v_y &= v_{oy} + \omega_z.a - \omega_x.c \\ v_z &= v_{oz} + \omega_x.b - \omega_y.a \end{aligned} \qquad 2.3.8$$

where:

v_{ox}, v_{oy}, v_{oz} = linear velocity of body fixed axes origin, in body-fixed x, y, z axes

This can be expressed in matrix form as:

$$\begin{bmatrix} v_x \\ v_y \\ v_z \end{bmatrix} = \begin{bmatrix} v_{ox} \\ v_{oy} \\ v_{oz} \end{bmatrix} + \begin{bmatrix} 0 & -\omega_z & \omega_y \\ \omega_z & 0 & -\omega_x \\ -\omega_y & \omega_x & 0 \end{bmatrix} \cdot \begin{bmatrix} a \\ b \\ c \end{bmatrix} \qquad 2.3.9a$$

or as vectors:

$$\mathbf{v} = \mathbf{v_o} + \omega \times \mathbf{r} \qquad 2.3.9b$$

The velocity of point **m** as seen in the inertial frame and expresses with components along the body-fixed reference frame can be readily expressed with components along the inertial axes by a co-ordinate transformation (equation 2.6).

2.3.3 Linear acceleration of a point mass

The linear acceleration with respect to the inertial system of a point mass **m** located at (a**i**, b**j**, c**k**) in the body-fixed reference frame is given by the components of linear acceleration along the instantaneous directions **i**, **j**, **k**.

$$\boldsymbol{a} = a_x\mathbf{i} + a_y\mathbf{j} + a_z\mathbf{k} \qquad 2.3.10$$

The general expression for the acceleration of a point mass relative to inertial space, and expressed as components taken along the instantaneous directions of body fixed-axes, is given by Wells (1967):

$$a_x = a_{ox} + \ddot{a} - a\left(\omega_y^2 + \omega_z^2\right) + b\left(\omega_y\omega_x - \dot{\omega}_z\right) + c\left(\omega_x\omega_z + \dot{\omega}_y\right) + 2\left(\dot{c}.\omega_y - \dot{b}.\omega_z\right)$$

$$a_y = a_{oy} + \ddot{b} - b\left(\omega_x^2 + \omega_z^2\right) + a\left(\omega_x\omega_y + \dot{\omega}_z\right) + c\left(\omega_y\omega_z - \dot{\omega}_x\right) + 2\left(\dot{a}.\omega_z - \dot{c}.\omega_x\right) \qquad 2.3.11a$$

$$a_z = a_{oz} + \ddot{c} - c\left(\omega_x^2 + \omega_y^2\right) + a\left(\omega_x\omega_z - \dot{\omega}_y\right) + b\left(\omega_y\omega_z + \dot{\omega}_x\right) + 2\left(\dot{b}.\omega_x - \dot{a}.\omega_y\right)$$

where:

a, b, c = coordinates of point relative to body - fixed axes, with components along body fixed axes.

$\dot{a}, \dot{b}, \dot{c}$ = velocity of point relative to body fixed - axes, with components along body fixed axes.

$\ddot{a}, \ddot{b}, \ddot{c}$ = acceleration of point relative to body - fixed axes, with components along body fixed axes.

a_x, a_y, a_z = acceleration of point relative to inertial space, with components along body-fixed axes.

a_{ox}, a_{oy}, a_{oz} = acceleration of body-fixed axes origin relative to inertial space, with components along body-fixed axes.

$\omega_x, \omega_y, \omega_z$ = angular velocity of body-fixed axes relative to inertial space, with components along body-fixed axes.

$\dot{\omega}_x, \dot{\omega}_y, \dot{\omega}_z$ = angular acceleration of body-fixed axes relative to inertial space, with components along body-fixed axes.

The acceleration of a point mass can also be expressed in matrix form:

$$\begin{bmatrix} a_x \\ a_y \\ a_z \end{bmatrix} = \begin{bmatrix} a_{ox} \\ a_{oy} \\ a_{oz} \end{bmatrix} + \begin{bmatrix} \ddot{a} \\ \ddot{b} \\ \ddot{c} \end{bmatrix} + \begin{bmatrix} 0 & -\dot{\omega}_z & \dot{\omega}_y \\ \dot{\omega}_z & 0 & -\dot{\omega}_x \\ -\dot{\omega}_y & \dot{\omega}_x & 0 \end{bmatrix} \cdot \begin{bmatrix} a \\ b \\ c \end{bmatrix}$$
$$+ \begin{bmatrix} 0 & -\omega_z & \omega_y \\ \omega_z & 0 & -\omega_x \\ -\omega_y & \omega_x & 0 \end{bmatrix} \cdot \begin{bmatrix} 0 & -\omega_z & \omega_y \\ \omega_z & 0 & -\omega_x \\ -\omega_y & \omega_x & 0 \end{bmatrix} \cdot \begin{bmatrix} a \\ b \\ c \end{bmatrix} \qquad 2.3.11b$$
$$+ 2. \begin{bmatrix} 0 & -\omega_z & \omega_y \\ \omega_z & 0 & -\omega_x \\ -\omega_y & \omega_x & 0 \end{bmatrix} \cdot \begin{bmatrix} \dot{a} \\ \dot{b} \\ \dot{c} \end{bmatrix}$$

The acceleration of a point mass in vector form is given by (Wells, 1967):

$$\mathbf{a} = \ddot{\mathbf{r}}_o + \mathbf{a}_1 + \dot{\omega} \times \mathbf{r} + \omega \times (\omega \times \mathbf{r}) + 2.\omega \times \mathbf{v} \qquad 2.3.11c$$

where:

$\mathbf{a}$ = acceleration of the point relative to inertial space.

$\ddot{\mathbf{r}}_o$ = double derivative of the position vector of origin of body axes.

$\mathbf{r}$ = position vector of the point relative to body axes.

$\mathbf{v}$ = velocity of the point relative to body axes.

$\mathbf{a}_1$ = acceleration of the point relative to body axes.

ω = angular velocity of body axes.

$\dot{\omega}$ = angular acceleration of body axes.

The instantaneous angular velocities along the body-fixed axes ω_x, ω_y ω_z are a function of the Euler angles $(\phi, \theta, \varphi, \dot{\phi}, \dot{\theta}, \dot{\varphi})$. The instantaneous angular accelerations about the body-fixed axes $(\alpha_e, \alpha_f, \alpha_g)$ or equivalently $(\dot{\omega}_e, \dot{\omega}_f, \dot{\omega}_g)$ are obtained from the time derivative of respective angular velocities.

2.3.3.1 Linear acceleration of rigid body centre of mass

To calculate the acceleration of the centre of mass of a rigid body, (a,b,c) is replaced by $(\bar{a},\bar{b},\bar{c})$ and $\dot{\bar{a}} = \dot{\bar{b}} = \dot{\bar{c}} = 0$. The general formula above (equation 2.3.11a) reduces to:

$$\begin{aligned}
\bar{a}_x &= a_{ox} - \bar{a}\left(\omega_y^2 + \omega_z^2\right) + \bar{b}\left(\omega_y\omega_x - \dot{\omega}_z\right) + \bar{c}\left(\omega_x\omega_z + \dot{\omega}_y\right) \\
\bar{a}_y &= a_{oy} - \bar{b}\left(\omega_x^2 + \omega_z^2\right) + \bar{a}\left(\omega_x\omega_y + \dot{\omega}_z\right) + \bar{c}\left(\omega_y\omega_z - \dot{\omega}_x\right) \qquad 2.3.12a \\
\bar{a}_z &= a_{oz} - \bar{c}\left(\omega_x^2 + \omega_y^2\right) + \bar{a}\left(\omega_x\omega_z - \dot{\omega}_y\right) + \bar{b}\left(\omega_y\omega_z + \dot{\omega}_x\right)
\end{aligned}$$

or in vector form:

$$\mathbf{a} = \ddot{\mathbf{r}}_o + \dot{\boldsymbol{\omega}} \times \mathbf{r} + \boldsymbol{\omega} \times (\boldsymbol{\omega} \times \mathbf{r}) \qquad 2.3.12b$$

2.3.4 Moments of inertia and inertia tensor

The moment of inertia of a particle of mass **m** about an axis is given by the product of the mass and the square of the distance from the axis of rotation. The moment of inertia of a rigid body about an axis can be thought of as the sum of inertia values over a continuous distribution of mass elements comprising the rigid body.

$$\mathbf{I} = \sum m_i . \mathbf{r}_i^2 \qquad 2.3.13$$

For a rigid body with a fixed Cartesian axis system embedded in it, separate rotations about each of the axes are given by the respective moments of inertia. With the position vector of mass element i being:

$$\mathbf{ri} = x_i\mathbf{i} + y_i\mathbf{j} + z_i\mathbf{k} \qquad 2.3.14$$

The moments in inertia are given by:

$$
\begin{aligned}
I_{xx} &= \sum m_i.\left(y_i^2 + z_i^2\right) \\
I_{yy} &= \sum m_i.\left(z_i^2 + x_i^2\right) \\
I_{zz} &= \sum m_i.\left(x_i^2 + y_i^2\right)
\end{aligned}
\qquad 2.3.15
$$

If rotations occur simultaneously about more than one axis, then a point mass element may have components of inertia common to the axes. The common inertia between any two axes is given by the products of inertia.

$$
\begin{aligned}
I_{xy} &= I_{yx} = -\sum m_i.x_i.y_i \\
I_{yz} &= I_{zy} = -\sum m_i.y_i.z_i \\
I_{zx} &= I_{xz} = -\sum m_i.z_i.x_i
\end{aligned}
\qquad 2.3.16
$$

These nine quantities can be represented by an inertia matrix or tensor.

$$
\begin{pmatrix}
I_{xx} & I_{xy} & I_{xz} \\
I_{yx} & I_{yy} & I_{yz} \\
I_{zx} & I_{zy} & I_{zz}
\end{pmatrix}
\qquad 2.3.17
$$

2.3.4.1 Inertia about a line passing through the axis system origin

If the rigid body is rotating about an axis **oa** passing through the origin of the axis system for which the inertia tensor is known (Fig. 2.3.1), and **n** being a unit vector in the direction of **oa** , then the angular velocity can be expressed as:

$$
\omega = \omega\mathbf{n} = \omega\left(\cos\alpha\mathbf{i} + \cos\beta\mathbf{j} + \cos\gamma\mathbf{k}\right) \qquad 2.3.18
$$

where:

$\cos\alpha$, $\cos\beta$, $\cos\gamma$ = directional cosines of **oa** with respect to the **i**, **j**, **k** axes

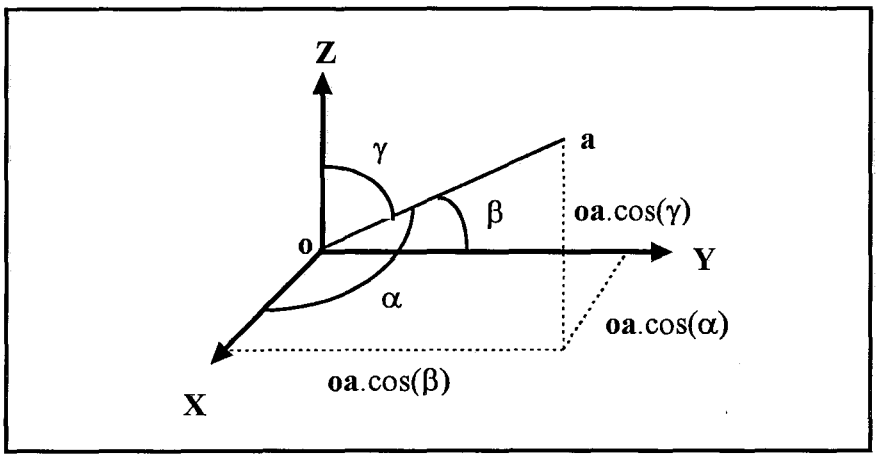

Figure 2.3.1. Directional cosines of a line passing through the axis system origin.

The moment of inertia of the rigid body rotating about an axis **oa** is given by the directional cosines between **oa** and the axes **X**, **Y**, **Z** about which the inertia tensor is given (Wells, 1967):

$$I_{oa} = I_{xx}.\cos^2\alpha + I_{yy}.\cos^2\beta + I_{zz}.\cos^2\gamma - 2.I_{xy}.\cos\alpha.\cos\beta - 2.I_{yz}.\cos\beta.\cos\gamma - 2.I_{xz}.\cos\alpha.\cos\gamma \quad 2.3.19$$

By substituting l,m,n for the three respective directional cosines:

$$I_{oa} = I_{xx}.l^2 + I_{yy}.m^2 + I_{zz}.n^2 - 2.I_{xy}.l.m - 2.I_{yz}.m.n - 2.I_{xz}.l.n \quad 2.3.20$$

2.3.4.2 Inertia tensor for an axis system with a common axes origin

An axis system which has undergone rotation about the origin can be expressed in terms of the inertial axes by directional cosines (equation 2.2.11). Similarly, the inertia tensor for an axis system which has undergone a rotation about the origin can be expressed in terms of a known inertia tensor of the body-fixed axis system by directional cosines (Fig. 2.3.2). By letting αji represent the directional cosine between rotated axis (j) and the known body-fixed axis (i), the inertia tensor for the rotated body axis system is given by (Wells, 1967):

$$I_{rxx} = I_{xx}\alpha_{11}^2 + I_{yy}\alpha_{12}^2 + I_{zz}\alpha_{13}^2 - 2I_{xy}\alpha_{11}\alpha_{12} - 2I_{xz}\alpha_{11}\alpha_{13} - 2I_{yz}\alpha_{12}\alpha_{13}$$

$$I_{ryy} = I_{xx}\alpha_{21}^2 + I_{yy}\alpha_{22}^2 + I_{zz}\alpha_{23}^2 - 2I_{xy}\alpha_{21}\alpha_{22} - 2I_{xz}\alpha_{21}\alpha_{23} - 2I_{yz}\alpha_{22}\alpha_{23}$$

$$I_{rzz} = I_{xx}\alpha_{31}^2 + I_{yy}\alpha_{32}^2 + I_{zz}\alpha_{33}^2 - 2I_{xy}\alpha_{31}\alpha_{32} - 2I_{xz}\alpha_{31}\alpha_{33} - 2I_{yz}\alpha_{32}\alpha_{33}$$

$$I_{rxy} = I_{xy}(\alpha_{11}\alpha_{22} + \alpha_{12}\alpha_{21}) + I_{xz}(\alpha_{11}\alpha_{23} + \alpha_{13}\alpha_{21}) + I_{yz}(\alpha_{12}\alpha_{23} + \alpha_{13}\alpha_{22}) - (\alpha_{11}\alpha_{21}I_{xx} + \alpha_{12}\alpha_{22}I_{yy} + \alpha_{13}\alpha_{23}I_{zz})$$

$$I_{rxz} = I_{xy}(\alpha_{11}\alpha_{32} + \alpha_{12}\alpha_{31}) + I_{xz}(\alpha_{11}\alpha_{33} + \alpha_{13}\alpha_{31}) + I_{yz}(\alpha_{12}\alpha_{33} + \alpha_{32}\alpha_{13}) - (\alpha_{11}\alpha_{31}I_{xx} + \alpha_{12}\alpha_{32}I_{yy} + \alpha_{13}\alpha_{33}I_{zz})$$

$$I_{ryz} = I_{xy}(\alpha_{21}\alpha_{32} + \alpha_{22}\alpha_{31}) + I_{xz}(\alpha_{21}\alpha_{33} + \alpha_{31}\alpha_{23}) + I_{yz}(\alpha_{22}\alpha_{33} + \alpha_{23}\alpha_{32}) - (\alpha_{21}\alpha_{31}I_{xx} + \alpha_{22}\alpha_{32}I_{yy} + \alpha_{23}\alpha_{33}I_{zz})$$

2.3.21

As seen in section 2.2.1, if the directional vectors of the body-fixed axis system (**X**,**Y**,**Z**) are (1,0,0), (0,1,0) and (0,0,1) respectively, then the directional cosines are given by the orthogonal unit vectors $\mathbf{i}_r$, $\mathbf{j}_r$, $\mathbf{k}_r$ of the rotated axes ($\mathbf{X}_r$,$\mathbf{Y}_r$,$\mathbf{Z}_r$). These unit vectors also form the column space of the transformation matrix mapping (**X**,**Y**,**Z**) onto ($\mathbf{X}_r$,$\mathbf{Y}_r$,$\mathbf{Z}_r$).

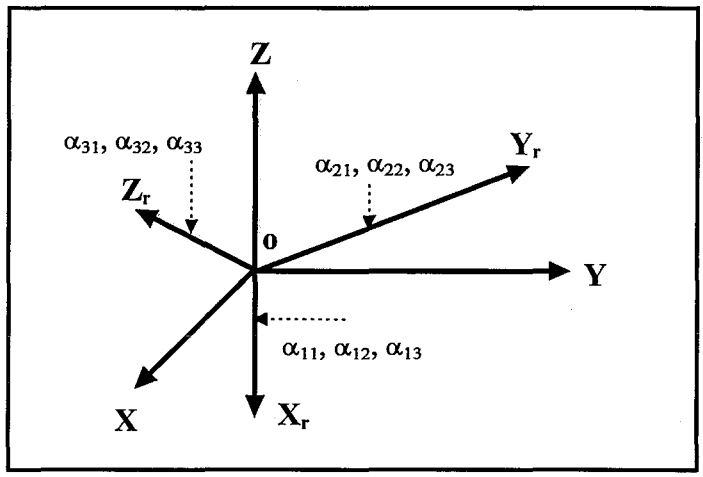

Figure 2.3.2. Directional cosines between two axes systems. (**X**, **Y**, **Z**) represent inertial axes of unit vectors (1,0,0), (0,1,0) and (0,0,1) respectively, and (Xr, Yr, Xr) a second axis with unit vectors and also directional cosines of (α_{11}, α_{12}, α_{13}), (α_{21}, α_{22}, α_{23}), and (α_{31}, α_{32}, α_{33}) respectively.

2.3.4.3 Inertia about a line, from a parallel axis passing through the centre of mass

If the moment of inertia of a given axis is known, and it passes through the centre of mass, then the inertia of any parallel axis can be found by the product of the total mass of the body and the normal distance between the two axes (Fig. 2.3.3).

$$I_{oa} = \bar{I}_{oa} + M.d^2 \qquad 2.3.22$$

The inertia tensor for an axis system can similarly be expressed in terms of the known inertia tensor for a parallel body-fixed axis system with an origin at the centre of mass (Fig. 2.3.3) (Wells, 1967):

$$\begin{aligned} I_{xx} &= \bar{I}_{xx} + M.\left(\bar{y}^2 + \bar{z}^2\right) \\ I_{yy} &= \bar{I}_{yy} + M.\left(\bar{x}^2 + \bar{z}^2\right) \\ I_{zz} &= \bar{I}_{zz} + M.\left(\bar{x}^2 + \bar{y}^2\right) \end{aligned} \qquad 2.3.23a$$

$$I_{xy} = \bar{I}_{xy} + M.(\bar{x}.\bar{y})$$
$$I_{yz} = \bar{I}_{yz} + M.(\bar{y}.\bar{z}) \qquad 2.3.23b$$
$$I_{xz} = \bar{I}_{xz} + M.(\bar{x}.\bar{z})$$

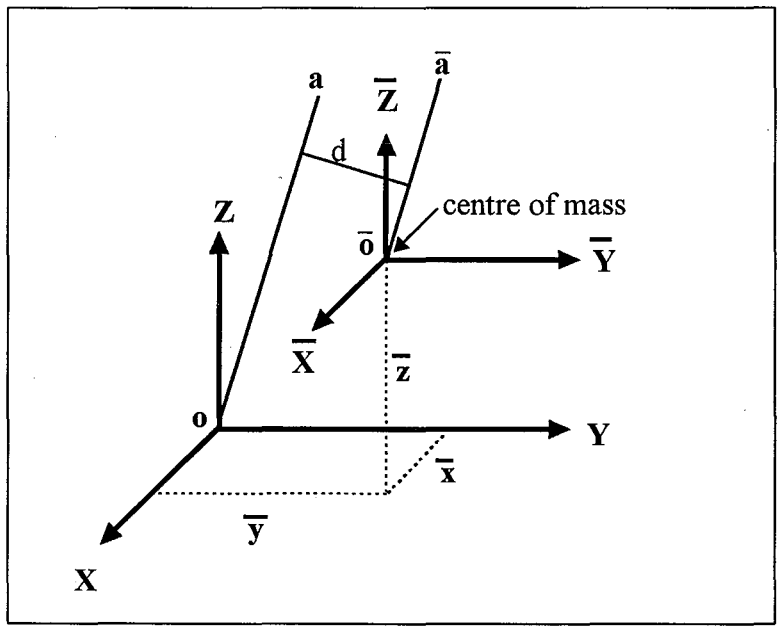

Figure 2.3.3. Parallel axis and parallel axis system. Point $\bar{o}$ indicates the origin of the axis and axes system passing through the centre of mass.

2.3.4.4 Inertia about a line, from an axis passing through the centre of mass

For a known inertia tensor for a given axis system with an origin at the centre of mass, the inertia about any line **oa** can be written in terms of the tensor quantities of the known axis system by combining equations 2.3.20 and 2.3.23 (Wells, 1967):

$$\begin{aligned} I_{oa} = {} & \left[\bar{I}_{xx} + M.\left(\bar{y}^2 + \bar{z}^2\right)\right].l^2 + \left[\bar{I}_{yy} + M.\left(\bar{x}^2 + \bar{z}^2\right)\right].m^2 \\ & + \left[\bar{I}_{zz} + M.\left(\bar{x}^2 + \bar{y}^2\right)\right].n^2 - \left(\bar{I}_{xy} + M.\bar{x}.\bar{y}\right).l.m \\ & - \left(\bar{I}_{yz} + M.\bar{y}.\bar{z}\right).m.n - \left(\bar{I}_{xz} + M.\bar{x}.\bar{z}\right).l.n \end{aligned} \qquad 2.3.24$$

2.3.4.5 Inertia tensor for any parallel axis system

Two parallel axes systems can be expressed in terms of a common parallel axes system located at the centre of mass (equation 2.3.24). The I_{xx} inertial component of the two axes systems takes the form:

$$I_{xx1} = \bar{I}_{xx} + M\left(\bar{y}_1^2 + \bar{z}_1^2\right)$$
$$I_{xx2} = \bar{I}_{xx} + M\left(\bar{y}_2^2 + \bar{z}_2^2\right) \qquad 2.3.25$$

where:

I_{xx1} = I_{xx} inertial component of the first parrallel axis system.
I_{xx2} = I_{xx} inertial component of the second parrallel axis system.
$\bar{I}_{xx}$ = I_{xx} inertial component of the parrallel axis system with origin at the centre of mass.
$\bar{x}_1, \bar{y}_1, \bar{z}_1$ = co-ordinates of centre of mass with respect to first axis system.
$\bar{x}_2, \bar{y}_2, \bar{z}_2$ = co-ordinates of centre of mass with respect to second axis system

Making use of the relation (Fig. 2.3.4):

$$\bar{x}_2 = x_o + \bar{x}_1$$
$$\bar{y}_2 = y_o + \bar{y}_1 \qquad 2.3.26$$
$$\bar{z}_2 = z_o + \bar{z}_1$$

where:

$\bar{x}_1, \bar{y}_1, \bar{z}_1$ = co-ordinates of centre of mass with respect to first axis system.
$\bar{x}_2, \bar{y}_2, \bar{z}_2$ = co-ordinates of centre of mass with respect to second axis system.
x_o, y_o, z_o = co-ordinates of origin of first axis system with respect to second axis system.

The terms involving inertia quantities about a parallel axis system located at the centre of mass can be eliminated, leaving a function involving any two parallel axis systems. For a known inertia tensor for a body-fixed axes (first), the inertia tensor of a second parallel axis system can be written in terms of the tensor quantities of the known axis system (Wells, 1967):

$$
\begin{aligned}
I_{xx2} &= I_{xx1} + M.\left(y_o^{\,2} + z_o^{\,2}\right) + 2.M.\left(y_o.\bar{y}_1 + z_o.\bar{z}_1\right) \\
I_{yy2} &= I_{yy1} + M.\left(x_o^{\,2} + z_o^{\,2}\right) + 2.M.\left(x_o.\bar{x}_1 + z_o.\bar{z}_1\right) \\
I_{zz2} &= I_{zz1} + M.\left(x_o^{\,2} + y_o^{\,2}\right) + 2.M.\left(x_o.\bar{x}_1 + y_o.\bar{y}_1\right) \\
I_{xy2} &= I_{xy1} + M.\left(x_o.y_o\right) + M.\left(x_o.\bar{y}_1 + y_o.\bar{x}_1\right) \\
I_{yz2} &= I_{yz1} + M.\left(y_o.z_o\right) + M.\left(y_o.\bar{z}_1 + z_o.\bar{y}_1\right) \\
I_{xz2} &= I_{xz1} + M.\left(x_o.z_o\right) + M.\left(x_o.\bar{z}_1 + z_o.\bar{x}_1\right)
\end{aligned}
\qquad 2.3.27
$$

where:

x_o, y_o, z_o = origin of first axis system with respect to second axis system

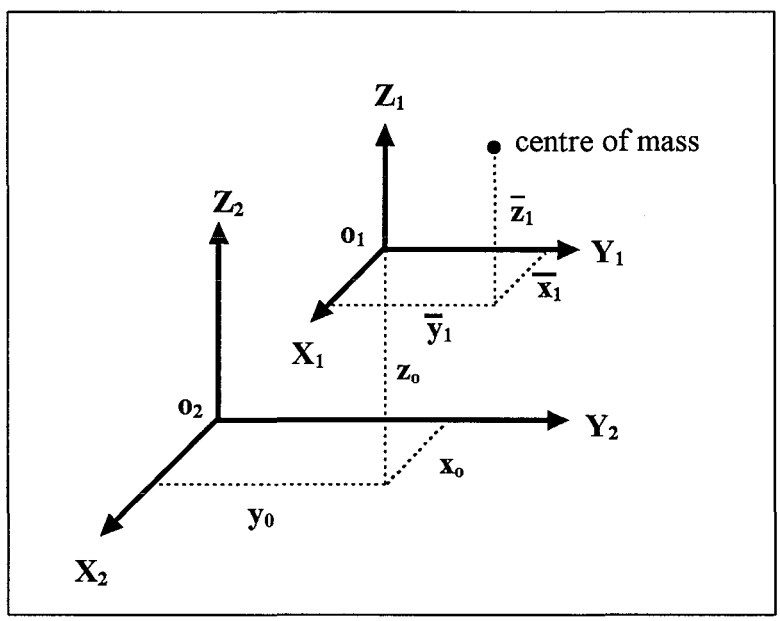

Figure 2.3.4 Co-ordinates relating two axes systems and the centre of mass. The location of the first axis system origin $\mathbf{o}_1$ is given by (x_o,y_o,z_o) with respect to a second axis system with origin $\mathbf{o}_2$. The location of the centre of mass with respect to the first axis system is given by $(\bar{x}_1,\bar{y}_1,\bar{z}_1)$.

2.3.4.6 Principle axis of inertia

If the Cartesian axes system fixed in the body is defined in such a way that the products of inertia are equal to zero, then the three axes are called *principle axes of inertia* for the rigid body. The inertia tensor then takes the form:

$$\begin{pmatrix} I^p_{xx} & 0 & 0 \\ 0 & I^p_{yy} & 0 \\ 0 & 0 & I^p_{zz} \end{pmatrix} \qquad 2.3.28$$

A property of the principal axes of the rigid body is that the mass distribution is symmetrical about the principle axes. If a rigid body rotates about a principle axis the direction of the angular momentum is in the same direction as the angular velocity. Products of inertia result from non-symmetrical mass distribution about the axis of rotation and produce an angular momentum that propagates about the axis of rotation.

It can be seen that if the axis system located at the centre of mass are the principle axes $\left(\bar{I}_{xy} = \bar{I}_{xz} = \bar{I}_{yz} = 0\right)$, a parallel set of axes may contain inertia products given by $I_{xy} = M.\bar{x}.\bar{y}$, etc. (equation 2.3.23). Thus the principle axes through any arbitrary point are in general, not parallel to the principle axes through the centre of mass (Wells, 1967).

Body fixed axes used in modelling body segments usually assume no products of inertia, which implies that the segmental axes are principle axes. Hatze (1980), in defining body fixed axes for a 17 segment whole body model, placed the axes system at the origin of each segment with the unit vectors parallel to the principle moments of inertia about the segment centre of mass. This approach did not assume that axes defined from external markers (longitudinal, anterio-posterior and medio-lateral) were aligned with the principle axes through the segment origin.

2.3.5 External forces and torques

The torque produced by an external force on a rigid-body is given by the sum of torque's acting about the instantaneous positions of the body-fixed axes **i**, **j**, **k**.

$$\boldsymbol{\tau} = \tau_x \mathbf{i} + \tau_y \mathbf{j} + \tau_z \mathbf{k} \qquad 2.3.29$$

With an external force acting at (a**i**, b**j**, c**k**) and given by:

$$\mathbf{F} = f_x \mathbf{i} + f_y \mathbf{j} + f_z \mathbf{k} \qquad 2.3.30$$

The components of torque acting along axes **i**, **j**, **k** are given by (Fig. 2.3.5):

$$\begin{aligned} \tau_x &= f_z.b - f_y.c \\ \tau_y &= f_x.c - f_z.a \\ \tau_z &= f_y.a - f_x.b \end{aligned} \qquad 2.3.31a$$

or as matrices:

$$\begin{bmatrix} \tau_x \\ \tau_y \\ \tau_z \end{bmatrix} = \begin{bmatrix} 0 & f_z & -f_y \\ -f_z & 0 & f_x \\ f_y & -f_x & 0 \end{bmatrix} \cdot \begin{bmatrix} a \\ b \\ c \end{bmatrix} \qquad 2.3.31b$$

The torque produced about any line **oa** (Fig. 2.3.1) can be given by the directional cosines with respect to **i**, **j**, **k** of the body fixed axes.

$$\begin{aligned} \tau_{oa} &= \tau_x.l + \tau_y.m + \tau_z.n \\ \tau_{oa} &= \left(f_z.b - f_y.c\right).l + \left(f_x.c - f_z.a\right).m + \left(f_y.a - f_x.b\right).n \end{aligned} \qquad 2.3.32$$

where:

$l = \cos\alpha$

$m = \cos\beta$

$n = \cos\gamma$

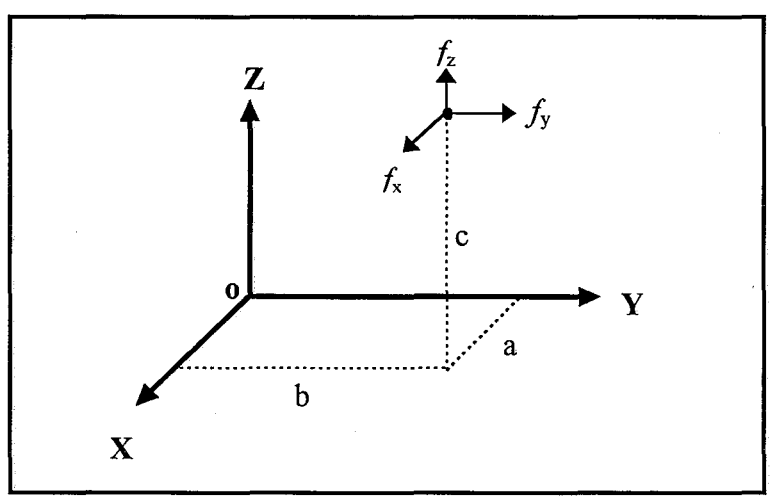

Figure 2.3.5. Co-ordinates of point of application of force.

2.3.6 Angular momentum of rigid body

The angular momentum of a rigid body is given by the product of the inertia of the body about the instantaneous axis of rotation and the angular velocity about this axis.

$$\Omega = I\omega \tag{2.3.33}$$

For a rigid body containing a fixed Cartesian co-ordinate system, angular momentum can be expressed as individual components directed along each axis.

$$\Omega = \Omega_x \mathbf{i} + \Omega_y \mathbf{j} + \Omega_z \mathbf{k} \tag{2.3.34}$$

The components of angular momentum are:

$$\begin{aligned} \Omega_x &= I_{xx}.\omega_x + I_{xy}.\omega_y + I_{xz}.\omega_z \\ \Omega_y &= I_{yx}.\omega_x + I_{yy}.\omega_y + I_{yz}.\omega_z \\ \Omega_z &= I_{zx}.\omega_x + I_{zy}.\omega_y + I_{zz}.\omega_z \end{aligned} \tag{2.3.35a}$$

In matrix form:

$$\begin{pmatrix} \Omega_x \\ \Omega_y \\ \Omega_z \end{pmatrix} = \begin{pmatrix} I_{xx} & I_{xy} & I_{xz} \\ I_{yx} & I_{yy} & I_{yz} \\ I_{zx} & I_{zy} & I_{zz} \end{pmatrix} . \begin{pmatrix} \omega_x \\ \omega_y \\ \omega_z \end{pmatrix} \tag{2.3.35b}$$

The angular velocity of the rigid body about respective body-fixed axes can be given by equation 2.3.3.

2.3.7 Linear momentum of rigid body

The linear momentum of a rigid body is given by the product of the mass of the body and the linear velocity of the centre of mass.

$$\mathbf{P} = m.\bar{v} \tag{2.3.36}$$

For a rigid body containing a fixed Cartesian co-ordinate system, linear momentum can be expressed as individual components directed along each axis.

$$\mathbf{P} = P_x\mathbf{i} + P_y\mathbf{j} + P_z\mathbf{k} \qquad 2.3.37$$

The components of linear momentum are:

$$\begin{aligned} P_x &= m.\bar{v}_x \\ P_y &= m.\bar{v}_y \\ P_z &= m.\bar{v}_z \end{aligned} \qquad 2.3.38a$$

In matrix form:

$$\begin{pmatrix} P_x \\ P_y \\ P_z \end{pmatrix} = \begin{pmatrix} m & 0 & 0 \\ 0 & m & 0 \\ 0 & 0 & m \end{pmatrix} . \begin{pmatrix} \bar{v}_x \\ \bar{v}_y \\ \bar{v}_z \end{pmatrix} \qquad 2.3.38b$$

The linear velocity of the centre of mass can be given by equation 2.3.6.

2.3.8 Kinetic energy of rigid body

The kinetic energy a rigid body is given by the sum of translation kinetic energy and rotational kinetic energy. The translation component is that of the centre of mass and the rotational component is about the instantaneous axis of rotation.

$$T = \frac{1}{2}M\bar{v}^2 + \frac{1}{2}I\omega^2 \qquad 2.3.39$$

The generalised formula of kinetic energy of a rigid body (Wells, 1967) is:

$$
\begin{aligned}
T = & \frac{1}{2}M\left(v_{ox}^2 + v_{oy}^2 + v_{oz}^2\right) \\
& + \frac{1}{2}\left(I_{xx}\omega_x^2 + I_{yy}\omega_y^2 + I_{zz}\omega_z^2 + 2I_{xy}\omega_x\omega_y + 2I_{xz}\omega_x\omega_z + 2I_{yz}\omega_y\omega_z\right) \\
& + M\left[v_{ox}\left(\omega_y\bar{z} - \omega_z\bar{y}\right) + v_{oy}\left(\omega_z\bar{x} - \omega_x\bar{z}\right) + v_{oz}\left(\omega_x\bar{y} - \omega_y\bar{x}\right)\right]
\end{aligned}
\qquad 2.3.40a
$$

Noting:

ω is the angular velocity of the body relative to inertial space and v_o is the linear velocity of the origin of the body-fixed axis system relative to inertial space. ω_x, ω_y, ω_z and v_{ox}, v_{oy}, v_{oz} are the components of ω and v_o respectively along the instantaneous directions of **i**, **j**, **k** of the body-fixed axes. The inertia elements I_{xx}, I_{xy} etc., and the position of the centre of mass $(\bar{x}, \bar{y}, \bar{z})$, are also determined with respect to **i**, **j**, **k** of the body-fixed axes. With **i**, **j**, **k** assumed to be body-fixed axes, the values of the inertia elements I_{xx}, I_{xy} etc., and $\bar{x}$, $\bar{y}$, $\bar{z}$ are constant.

Expressed in matrix form:

$$
\begin{aligned}
T = & \frac{1}{2}M.\begin{bmatrix} v_{ox} \\ v_{oy} \\ v_{oz} \end{bmatrix}^T.\begin{bmatrix} v_{ox} \\ v_{oy} \\ v_{oz} \end{bmatrix} + M.\begin{bmatrix} v_{ox} \\ v_{oy} \\ v_{oz} \end{bmatrix}^T.\begin{bmatrix} 0 & -\omega_z & \omega_y \\ \omega_z & 0 & -\omega_x \\ -\omega_y & \omega_x & 0 \end{bmatrix}.\begin{bmatrix} \bar{x} \\ \bar{y} \\ \bar{z} \end{bmatrix} \\
& + \frac{1}{2}.\begin{bmatrix} 0 & -\omega_z & \omega_y \\ \omega_z & 0 & -\omega_x \\ -\omega_y & \omega_x & 0 \end{bmatrix}.\begin{bmatrix} I_{xx} & I_{xy} & I_{xz} \\ I_{yx} & I_{yy} & I_{yz} \\ I_{zx} & I_{zy} & I_{zz} \end{bmatrix}.\begin{bmatrix} 0 & -\omega_z & \omega_y \\ \omega_z & 0 & -\omega_x \\ -\omega_y & \omega_x & 0 \end{bmatrix}
\end{aligned}
\qquad 2.3.40b
$$

Under certain conditions, which in practice are not always met but are often assumed, the general expression for kinetic energy can be greatly simplified. If the origin of the body-fixed axes is located at the centre of mass, then $\bar{x} = \bar{y} = \bar{z} = 0$. If, in addition, the body-fixed axes were taken along the principle axes at the centre of mass, then the expression for the kinetic energy reduces to:

$$
T = \frac{1}{2}M.\bar{v}^2 + \frac{1}{2}\left(\bar{I}_{xx}.\omega_x^2 + \bar{I}_{yy}.\omega_y^2 + \bar{I}_{zz}.\omega_z^2\right) \qquad 2.3.41
$$

2.4 Euler equations of motion

Euler Equations consist of two fundamental vector quantities which describe the translation and rotational motion of a rigid body (Wells, 1967). When describing three dimensional motion, these two vectors equations are written as three translation equations describing the translation motion of the centre of mass and three rotation equations describing the rotational motion of the body about its instantaneous axis of rotation.

2.4.1 Translation equations of motion

The translation equation of motion relates the sum of external forces acting on a rigid body to the acceleration of the centre of mass of that body, in vector form:

$$\sum \mathbf{F} = M.\bar{\mathbf{a}} \qquad 2.4.1$$

where:

$\sum \mathbf{F}$ = sum of external forces acting on body.

M = mass of body.

$\bar{\mathbf{a}}$ = acceleration of centre of mass relative to inertial space.

Expressing the sum of external forces relative to an orthogonal axes system, three scalar equations of translation motion result:

$$\begin{aligned} \sum F_x &= M.\bar{a}_x \\ \sum F_y &= M.\bar{a}_y \\ \sum F_z &= M.\bar{a}_z \end{aligned} \qquad 2.4.2$$

If the position of body-fixed axis system, with respect to the inertial frame, is given by three translations (X_{IO}, Y_{IO}, Z_{IO}) and three rotations (ϕ, θ, φ) (Fig. 2.4.1), and the origin of the body-fixed axes is located at the centre of mass then, the translation equations of motion can be written (Wells, 1967; Nigg, 1994):

$$\begin{aligned} \sum F_{xI} &= M.\ddot{X}_{Io} \\ \sum F_{yI} &= M.\ddot{Y}_{Io} \\ \sum F_{zI} &= M.\ddot{Z}_{Io} \end{aligned} \qquad 2.4.3$$

where:

$\sum F_{x,y,z,I}$ = sum of forces with respect to the inertial x, y, and z axes

$\ddot{X}_{Io}, \ddot{Y}_{Io}, \ddot{Z}_{Io}$ = acceleration of the body-fixed axes orgin with respect to the inertial axes

In this case the forces are summed with respect to the inertial axis system, and it is with respect to the inertial axes that the velocity of the origin the body-fixed axes are expressed. Making use of a co-ordinate transformation, the forces can equally well be summed with respect to the body-fixed axes:

$$\left[\sum \mathbf{F}\right] = [M].[R].[\ddot{\mathbf{r}}_{Io}] \qquad 2.4.4a$$

or

$$\begin{bmatrix} \sum F_x \\ \sum F_y \\ \sum F_z \end{bmatrix} = \begin{bmatrix} M & 0 & 0 \\ 0 & M & 0 \\ 0 & 0 & M \end{bmatrix} . \begin{bmatrix} \mathbf{i}.\mathbf{i}_I & \mathbf{i}.\mathbf{j}_I & \mathbf{i}.\mathbf{k}_I \\ \mathbf{j}.\mathbf{i}_I & \mathbf{j}.\mathbf{j}_I & \mathbf{j}.\mathbf{k}_I \\ \mathbf{k}.\mathbf{i}_I & \mathbf{k}.\mathbf{j}_I & \mathbf{k}.\mathbf{k}_I \end{bmatrix} . \begin{bmatrix} \ddot{X}_{Io} \\ \ddot{Y}_{Io} \\ \ddot{Z}_{Io} \end{bmatrix} \qquad 2.4.4b$$

where:

$\sum F_{x,y,z}$ = sum of forces in the body-fixed x, y, z axes

$\mathbf{i}, \mathbf{j}, \mathbf{k}$ = unit vectors in the body-fixed x, y, z axes

$\mathbf{i}_I, \mathbf{j}_I, \mathbf{k}_I$ = unit vectors in the inertial x, y, z axes

In the general case where the body-fixed axes are not located at the centre of mass, but the co-ordinates of the centre of mass of the rigid body are given with respect to the local axes by $(\bar{a}, \bar{b}, \bar{c})$, then the general form of the translation equations of motion describing the acceleration of the centre of mass (equation 2.3.12c) can be written:

$$\begin{bmatrix} \sum F_x \\ \sum F_y \\ \sum F_z \end{bmatrix} = \begin{bmatrix} M & 0 & 0 \\ 0 & M & 0 \\ 0 & 0 & M \end{bmatrix} . \begin{bmatrix} \bar{a}_x \\ \bar{a}_y \\ \bar{a}_z \end{bmatrix} \qquad 2.4.5a$$

where:

$\bar{a}_x, \bar{a}_y, \bar{a}_z$ = acceleration of the centre of mass in the body-fixed x, y, z axes

or

$$\begin{bmatrix} \sum F_x \\ \sum F_y \\ \sum F_z \end{bmatrix} = \begin{bmatrix} M & 0 & 0 \\ 0 & M & 0 \\ 0 & 0 & M \end{bmatrix} . \begin{bmatrix} a_{ox} \\ a_{oy} \\ a_{oz} \end{bmatrix} + \begin{bmatrix} M & 0 & 0 \\ 0 & M & 0 \\ 0 & 0 & M \end{bmatrix} . \begin{bmatrix} 0 & -\dot{\omega}_z & \dot{\omega}_y \\ \dot{\omega}_z & 0 & -\dot{\omega}_x \\ -\dot{\omega}_y & \dot{\omega}_x & 0 \end{bmatrix} . \begin{bmatrix} \bar{a} \\ \bar{b} \\ \bar{c} \end{bmatrix}$$
$$+ \begin{bmatrix} M & 0 & 0 \\ 0 & M & 0 \\ 0 & 0 & M \end{bmatrix} . \begin{bmatrix} 0 & -\omega_z & \omega_y \\ \omega_z & 0 & -\omega_x \\ -\omega_y & \omega_x & 0 \end{bmatrix} . \begin{bmatrix} 0 & -\omega_z & \omega_y \\ \omega_z & 0 & -\omega_x \\ -\omega_y & \omega_x & 0 \end{bmatrix} . \begin{bmatrix} \bar{a} \\ \bar{b} \\ \bar{c} \end{bmatrix} \qquad 2.4.5b$$

where:

$\omega_x, \omega_y, \omega_z$ = instantaneous angular velocity about body-fixed axes

$\dot{\omega}_x, \dot{\omega}_y, \dot{\omega}_z$ = instantaneous angular acceleration about body-fixed axes

$\bar{a}, \bar{b}, \bar{c}$ = co-ordinates of centre of mass relative to body fixed axes

a_{ox}, a_{oy}, a_{oz} = acceleration of body-fixed axes origin in the local x, y, z axes

In this case the forces are summed in the instantaneous directions of the body-fixed axes, and it is with respect to the local axes that the co-ordinates of the centre of mass and the instantaneous angular velocities and accelerations are given.

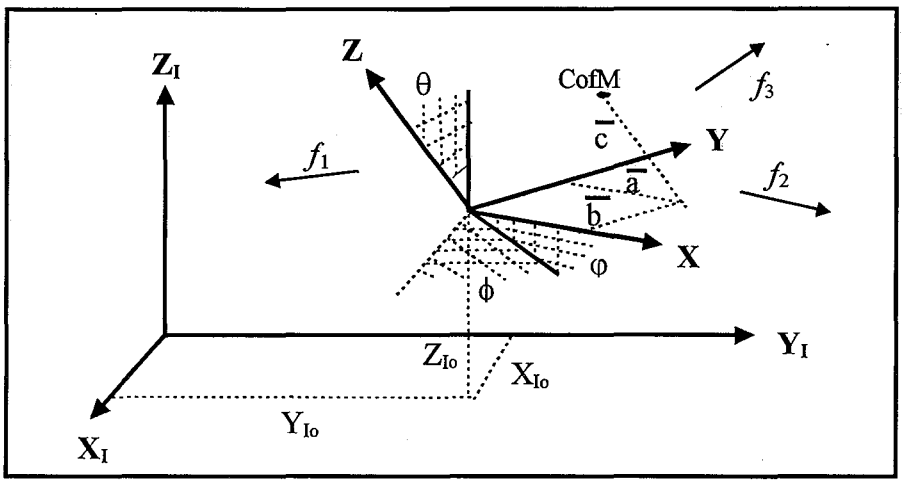

Figure 2.4.1. Location of body-fixed axes in inertial frame. Three translations (X_{IO}, Y_{IO}, Z_{IO}) specify the origin of the body-fixed axes and three rotations (ϕ, θ, φ) specify the orientation of the body-fixed axes. Three forces (f_1, f_2, f_3) are shown to be acting on the rigid body.

2.4.2 Rotational equations of motion

The rotational equation of motion relates the sum of external moments acting on a rigid body to the angular acceleration of that body. In vector form, it can be written:

$$\sum \tau = I.\alpha \qquad 2.4.6$$

The inertia of a rigid body is given by an inertia tensor with respect to the body-fixed axes and the angular acceleration given by the instantaneous angular accelerations along respect body-fixed axes. The general form of the three rotational equations of motion can be written (Wells, 1967):

$$
\begin{aligned}
\sum \tau_x &= I_{xx}.\alpha_x - I_{xy}.\alpha_y - I_{xz}.\alpha_z + \left(I_{zz} - I_{yy}\right)\omega_y.\omega_z \\
&\quad - I_{zx}.\omega_x.\omega_y - I_{zy}.\omega_y.\omega_y + I_{yx}.\omega_x.\omega_z + I_{yz}.\omega_z.\omega_z \\
&\quad + M.\left(a_{oz}.\bar{y} - a_{oy}.\bar{z}\right) \\
\sum \tau_y &= I_{yy}.\alpha_y - I_{yx}.\alpha_x - I_{yz}.\alpha_z + \left(I_{xx} - I_{zz}\right)\omega_x.\omega_z \\
&\quad - I_{xy}.\omega_y.\omega_z - I_{xz}.\omega_z.\omega_z + I_{zx}.\omega_x.\omega_x + I_{zy}.\omega_y.\omega_x \\
&\quad + M.\left(a_{ox}.\bar{z} - a_{oz}.\bar{x}\right) \\
\sum \tau_z &= I_{zz}.\alpha_z - I_{zx}.\alpha_x - I_{zy}.\alpha_y + \left(I_{yy} - I_{xx}\right)\omega_x.\omega_y \\
&\quad - I_{yx}.\omega_x.\omega_x - I_{yz}.\omega_z.\omega_x + I_{xy}.\omega_y.\omega_y + I_{xz}.\omega_z.\omega_y \\
&\quad + M.\left(a_{oy}.\bar{x} - a_{ox}.\bar{y}\right)
\end{aligned}
\qquad 2.4.7a
$$

where:

$\sum \tau_{xyz}$ = resultant moments about the body-fixed axes.

Ixx, Iyy, Izz, Ixy, Ixz, Iyz = principle and products of inertia with respect to the body-fixed axes.

$\bar{x}, \bar{y}, \bar{z}$ = position of center of mass with respect to body-fixed axes.

$\omega_x, \omega_y, \omega_z$ = angular velocity of rigid body about instantaneous directions of body-fixed axes as measured from inertial reference frame.

$\alpha_x, \alpha_y, \alpha_z$ = angular acceleration of rigid body about instantaneous directions of body-fixed axes as measured from inertial reference frame.

a_{ox}, a_{oy}, a_{oz} = linear acceleration of body-fixed axes origin in the body-fixed x, y, x axes

The above rotational equations of motion can be expressed in matrix form (Nigg, 1994)

$$
\begin{aligned}
\begin{bmatrix} \sum \tau_x \\ \sum \tau_y \\ \sum \tau_z \end{bmatrix} &= \begin{bmatrix} I_{xx} & -I_{xy} & -I_{xz} \\ -I_{yx} & I_{yy} & -I_{yx} \\ -I_{zx} & -I_{zy} & I_{zz} \end{bmatrix} . \begin{bmatrix} \alpha_x \\ \alpha_y \\ \alpha_z \end{bmatrix} \\
&\quad + \begin{bmatrix} 0 & -\omega_z & \omega_y \\ \omega_z & 0 & -\omega_x \\ -\omega_y & \omega_x & 0 \end{bmatrix} . \begin{bmatrix} I_{xx} & -I_{xy} & -I_{xz} \\ -I_{yx} & I_{yy} & -I_{yx} \\ -I_{zx} & -I_{zy} & I_{zz} \end{bmatrix} . \begin{bmatrix} \omega_x \\ \omega_y \\ \omega_z \end{bmatrix} \\
&\quad + M. \begin{bmatrix} 0 & a_{oz} & -a_{oy} \\ -a_{oz} & 0 & a_{ox} \\ a_{oy} & -a_{ox} & 0 \end{bmatrix} . \begin{bmatrix} \bar{x} \\ \bar{y} \\ \bar{z} \end{bmatrix}
\end{aligned}
\qquad 2.4.7b
$$

or as vectors (Nigg, 1994):

$$\mathbf{t} = [I].\alpha + [\omega].[I].\omega + M.[a_o].\bar{r} \qquad 2.4.7c$$

If the body-fixed axes are located at the centre of mass and these axes are principal axes, then the rotational equations of motion reduce to (Wells, 1967; Nigg, 1994):

$$\begin{aligned} \sum \tau_x^{cm} &= I_{xx}.\alpha_x + (I_{zz} - I_{yy})\omega_y.\omega_z \\ \sum \tau_y^{cm} &= I_{yy}.\alpha_y + (I_{xx} - I_{zz})\omega_x.\omega_z \\ \sum \tau_z^{cm} &= I_{zz}.\alpha_z + (I_{yy} - I_{xx})\omega_x.\omega_y \end{aligned} \qquad 2.4.8a$$

or in matrix form:

$$\begin{bmatrix} \sum \tau_x \\ \sum \tau_y \\ \sum \tau_z \end{bmatrix} = \begin{bmatrix} I_{xx} & 0 & 0 \\ 0 & I_{yy} & 0 \\ 0 & 0 & I_{zz} \end{bmatrix}.\begin{bmatrix} \alpha_x \\ \alpha_y \\ \alpha_z \end{bmatrix} + \begin{bmatrix} 0 & -\omega_z & \omega_y \\ \omega_z & 0 & -\omega_x \\ -\omega_y & \omega_x & 0 \end{bmatrix}.\begin{bmatrix} I_{xx} & 0 & 0 \\ 0 & I_{yy} & 0 \\ 0 & 0 & I_{zz} \end{bmatrix}.\begin{bmatrix} \omega_x \\ \omega_y \\ \omega_z \end{bmatrix} \qquad 2.4.8.b$$

or as vectors:

$$\mathbf{t}^{cm} = [I].\alpha + [\omega].[I].\omega \qquad 2.4.8.c$$

2.4.3 External forces (non-inertial forces)

The rotational and translation equations describe the motion of a rigid body by equating inertial and non-inertial forces acting on the body. As described, the inertial forces are the product of mass and acceleration and inertial moments are the product of moment of inertia and angular acceleration, and both are relative to inertial space. Schematically, the equation can be represented by:

$$\begin{pmatrix}\text{Summation of}\\ \text{external forces}\end{pmatrix} = \begin{pmatrix}\text{Summation of}\\ \text{inertial forces}\end{pmatrix}$$

$$\begin{pmatrix}\text{Summation of moments}\\ \text{due to external forces}\end{pmatrix} = \begin{pmatrix}\text{Summation of moments}\\ \text{due to inertial forces}\end{pmatrix} \qquad 2.4.9$$

The left hand side of the Euler equations of motion are the sum of all forces and moments that act on the segment. If the forces are given by (Figure 2.10):

$$\mathbf{F} = f_x\mathbf{i} + f_y\mathbf{j} + f_z\mathbf{k} \qquad 2.4.10$$

and act at point (**ai**, **bj**, **ck**) then the left hand side takes the form:

$$\begin{aligned}
\sum F_x &= f_{x1} + f_{x2} + \ldots + f_{xn}\\
\sum F_y &= f_{y1} + f_{y2} + \ldots + f_{yn}\\
\sum F_z &= f_{z1} + f_{z2} + \ldots + f_{zn}\\
\sum \tau_x &= f_{z1}.b_1 - f_{y1}.c_1 + f_{z2}.b_2 - f_{y2}.c_2 + \ldots + f_{zn}.b_n - f_{yn}.c_n\\
\sum \tau_y &= f_{x1}.c_1 - f_{z1}.a_1 + f_{x2}.c_2 - f_{z2}.a_2 + \ldots + f_{xn}.c_n - f_{zn}.a_n\\
\sum \tau_z &= f_{y1}.a_1 - f_{x1}.b_1 + f_{y2}.a_2 - f_{x2}.b_2 + \ldots + f_{yn}.a_n - f_{xn}.b_n
\end{aligned} \qquad 2.4.11$$

where:

$\sum F_{x,y,z}$ = sum of forces in body-fixed x, y, z axes

f_{xi}, f_{yi}, f_{zi} = components of external force in the body-fixed x, y, z axes

$\sum \tau_{x,y,z}$ = sum of torques about body-fixed x, y, z axes

a_i, b_i, c_i = co-ordinates of applied external force relative to body-fixed x, y, z axes

In determining the equations of motion, the co-ordinate system used to evaluate the translation equations with respect to which forces are summated need not be the same as the co-ordinate system used in evaluating the rotational equations about which moments are summed. So long as, in each case, three orthogonal axes are used and accelerations of the body-fixed axes are expressed with respect to the inertia frame of reference.

2.4.4 Joint equipollence equations

In a linked segment system, the external forces acting on a segment can be represented by resultant joint forces and resultant joint moments that act across each joint of a segment. In defining a joint, it is usual to assume it is frictionless and that muscular, ligament and bone contact are the only means by which forces are transmitted across a joint (Herzog & Binding, 1994). A joint centre can be considered as a point in common to all segments that comprise a joint about which rotations occur. The joint centre may be a fixed point defined from anatomical landmarks, or a moving point defined mathematically from the motion of the segments involving the joint (Herzog & Binding, 1994). The later is termed the 'instantaneous joint centre'. It is at the joint centre that the resultant joint force and moment are considered to act.

The joint equipolence equations relate joint muscular, ligament and bone forces to resultant joint forces and resultant joint moments, and take the following form (Herzog & Binding, 1994; Herzog, 1996):

$$\mathbf{R}_{jnt} = \sum_{i=1}^{m} \mathbf{F}_i^M + \sum_{j=1}^{l} \mathbf{F}_j^L + \sum_{k=1}^{b} \mathbf{F}_k^B \qquad 2.4.12a$$

$$\tau_{jnt} = \sum_{i=1}^{m} \left(\mathbf{r}_{\perp i}^M \times \mathbf{F}_i^M \right) + \sum_{j=1}^{l} \left(\mathbf{r}_{\perp j}^L \times \mathbf{F}_j^L \right) + \sum_{k=1}^{b} \left(\mathbf{r}_{\perp k}^B \times \mathbf{F}_k^B \right) \qquad 2.4.12b$$

where:

$\mathbf{R}_{jnt}$ = resultant joint force

τ_{jnt} = resultant joint moment

$\mathbf{F}^{M}$ = muscle force

$\mathbf{F}^{L}$ = ligament force

$\mathbf{F}^{B}$ = bone contact force

$\mathbf{r}_{\perp}^{M}$ = muscle moment arm

$\mathbf{r}_{\perp}^{L}$ = ligament moment arm

$\mathbf{r}_{\perp}^{B}$ = bone contact moment arm

m = number of muscles

l = number of ligaments

b = number of bone contact points

The equations of motion for a segment can now be simplified by the inclusion of resultant joint forces and resultant joint moments instead of individual bone, muscular and ligament forces acting at the joint. This greatly reduces the number of variables appearing in the equations of motion for each segment. With a segment typically having both proximal and distal resultant joint forces and moments, and with the inclusion of a term for any known external forces, the equations of motion can be written:

$$\sum \mathbf{F} = \mathbf{R}_p + \mathbf{R}_d + m.\mathbf{g} + \sum f^{ext}$$

$$\sum \tau = \tau_p + \tau_d + \mathbf{R}_p.\mathbf{r}_p + \mathbf{R}_d.\mathbf{r}_d + m.\mathbf{g}.\bar{\mathbf{r}} + \sum \left(f^{ext}.\mathbf{r}_{ext} \right) \qquad 2.4.13a$$

or as scalar equations:

$$
\begin{aligned}
\sum F_x &= R_{xp} - R_{xd} + m.g_x + \sum f_x^{ext} \\
\sum F_y &= R_{yp} - R_{yd} + m.g_y + \sum f_y^{ext} \\
\sum F_z &= R_{zp} - R_{zd} + m.g_z + \sum f_z^{ext} \\
\sum \tau_x &= \tau_{xp} - \tau_{xd} + R_{zp}.b_p - R_{yp}.c_p + R_{zd}.b_d - R_{yd}.c_d \\
&\quad + m.g_z.\bar{b} - m.g_y.\bar{c} + \sum \left(f_z^{ext}.b_{ext} - f_y^{ext}.c_{ext} \right) \qquad \text{2.4.13.b} \\
\sum \tau_y &= \tau_{yp} - \tau_{yd} + R_{xp}.c_p - R_{zp}.a_p + R_{xd}.c_d - R_{zd}.a_d \\
&\quad + m.g_x.\bar{c} - m.g_z.\bar{a} + \sum \left(f_x^{ext}.c_{ext} - f_z^{ext}.a_{ext} \right) \\
\sum \tau_z &= \tau_{zp} - \tau_{zd} + R_{yp}.a_p - R_{xp}.b_p + R_{yd}.a_d - R_{xd}.b_d \\
&\quad + m.g_y.\bar{a} - m.g_x.\bar{b} + \sum \left(f_y^{ext}.a_{ext} - f_x^{ext}.b_{ext} \right)
\end{aligned}
$$

where:

g_x, g_y, g_z = gravitational acceleration with respect to body-fixed x, y, z axes.

(a_p, b_p, c_p) = co-ordinates of proximal joint with respect to body-fixed x, y, z axes.

(a_d, b_d, c_d) = co-ordinates of distal joint with respect to body-fixed x, y, z axes.

$(\bar{a}, \bar{b}, \bar{c})$ = co-ordinates of center of mass with respect to body-fixed x, y, z axes.

$(a_{ext}, b_{ext}, c_{ext})$ = co-ordinates of applied external force with respect to body-fixed x, y, z axes.

If the body-fixed axes are placed at the proximal or distal joint or the centre of mass, then the location vector of the respective point will be zero and the respective terms will be removed from the sum of moments for the segment.

The components of gravitational acceleration in the instantaneous directions of the body axes are given by a co-ordinate transformation from global (inertial) to body axes. Assuming the global (inertial) Z axis is in the opposite direction of gravitation acceleration, the transformation is:

$$
\begin{bmatrix} g_x \\ g_y \\ g_z \end{bmatrix} = \begin{bmatrix} \mathbf{i}.\mathbf{i}_g & \mathbf{i}.\mathbf{j}_g & \mathbf{i}.\mathbf{k}_g \\ \mathbf{j}.\mathbf{i}_g & \mathbf{j}.\mathbf{j}_g & \mathbf{j}.\mathbf{k}_g \\ \mathbf{k}.\mathbf{i}_g & \mathbf{k}.\mathbf{j}_g & \mathbf{k}.\mathbf{k}_g \end{bmatrix} \begin{bmatrix} 0 \\ 0 \\ -9.81 \end{bmatrix} \qquad \text{2.4.14}
$$

Resultant joint forces and resultant joint moments are the net result of all forces acting across a joint as required to satisfy the equations of motion, and hence to produce the motion as described by position and acceleration data. Resultant forces and moments do not account for co-contraction with agonist and antagonist forces in the three planes for which they are summed whether they be bone, muscular or ligament in nature. As such co-contraction of muscles are not represented in resultant joint forces and moments.

2.5 Mathematical modelling of the human body

The creation of a mathematical representation of the human body allows for the quantification of human movement. Descriptors such as position, velocity, acceleration, force, energy and work for segments or the body as a whole can be calculated for the purpose of:

a) Inverse Dynamics: where internal forces acting within the human body are predicted from known external forces and kinematics of motion.
b) Forward Dynamics (movement synthesis): where kinematic and kinetic responses of the human body are predicted from known internal and external forces.

Kinematic analysis involves the description of motion which includes displacement, velocity and acceleration, without regard for the forces acting to producing the motion, while kinetic analysis includes the description of the forces that produced the motion.

Biomechanical modelling therefore provides a powerful tool for gaining indirect information and insight into human motion that may not be otherwise obtained. As such, it is widely used in ergonomics, biomechanics, medicine, and other related fields. The development of a three dimensional model and the inverse dynamic analysis of the human musculo-skeletal system involves the following steps:

1) The body is represented as a link segment model and a free body diagram established;
2) The equations of motion for the link segment model are developed from Euler equations;

3) The kinematics of motion are introduced and the inverse dynamics modelling approach is used to systematically calculate resultant joint moments and resultant joint forces acting on each segment;
4) Segmental energy, work and power can be calculated for the multi-link model;
5) Muscle insertions and lines of action are included in the model allowing establishment of equipolance equations;
6) Muscle models can be introduced to establish muscle excitation contraction dynamics and impose limits on muscle forces;
7) Individual muscle forces can be predicted from the equipolance moment equations. The indeterminacy problem may be overcome by the use of muscle equivalencies or the introduction of assumptions as to the recruitment strategies. The latter may involve a pre-established method of force-sharing or the use of a criteria (cost function) to determine muscle force-sharing based on optimisation techniques; and
8) Bone-on-bone forces can then be calculated by equating resultant joint forces with individual muscle forces. Bone-on-bone shear and compressive forces can then be calculated.

2.5.1 Link segment model

The human body can be modelled as a series of rigid links (Fig. 2.5.1). which permits rigid body dynamics to be applied to the human body. Required in the formulation of the model are locations of joint centres, as well as segment mass, centre of mass and moments of inertia. In practice, joint centres are approximated from external bone landmarks and previously established criteria are used to locate the joint centres. Segmental mass, centre of mass and inertia values are also estimated from statistical tables or predictive equations based on subject gender, height, weight, and specific anthropometric measurements.

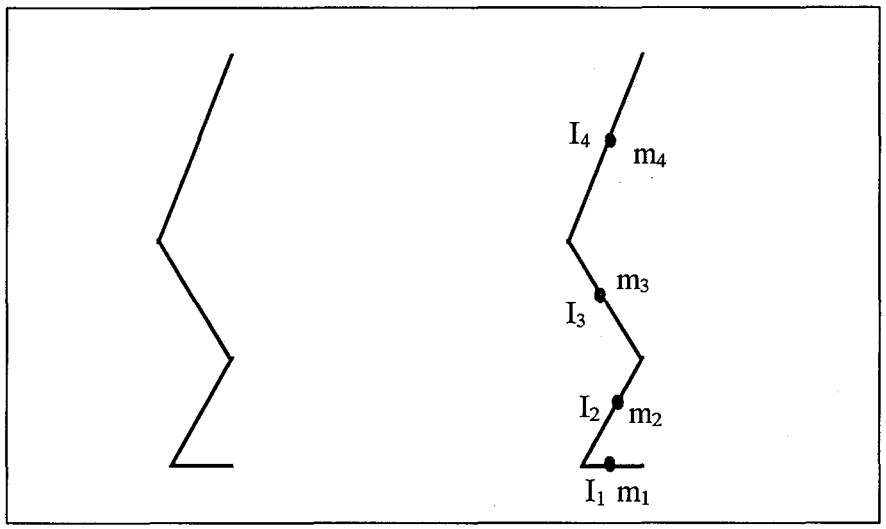

Figure 2.5.1 An anatomical (left) and link-segment model (right) of two dimensional lifting. The joints are represented as pinned joints and the segments by mass mi and moments of inertia **I**i located at each segment's centre of mass.

In representing the human body as coupled link-segments, the following assumptions are made:

1) Each segment is rigid and of fixed mass which is considered a point mass located at it's centre of mass;
2) The location of each segment's centre of mass remains fixed during the movement;
3) The joints between link segments are considered frictionless and pinned;
4) The mass moments of inertia of each segment about it's mass centre or proximal or distal end is constant during the motion;
5) The length of each segment remains constant during the movement; and
6) The mass, centre of mass and inertial properties used are accurate representations of the actual values, so as not to alter the derived measures from their true values.

2.5.2 Muscle path and line of action

The force generated by a muscle is applied to the skeletal system at the muscle-tendon origin, insertion and at points where the muscle-tendon complex is deflected or wraps around underlying tissue. The path of the muscle-tendon will therefore determine the direction of the applied force at both the origin and insertion (line of action), the forces the muscle may exhibit on structures it passes and the length of the muscle. The straight line approach is widely employed for representing paths of muscles in models of the musculoskeletal system (Crowninsheild, et al., 1978; Dostal & Andrews, 1981; Rohrle, et al., 1984; Seireg & Arvikar 1984; Hogfors, et al., 1987). A more accurate representation of muscle paths exists in the centroid line approach but is seldom used due to the added complexity of the method (Jenson & Davy, 1975). With the straight line approach, a muscle may be represented by one or a number of muscle elements depending on the geometry of the muscle. Each muscle element represents a different functional unit; for example, the gluteus medius may be represented by three muscle elements representing anterior, middle and posterior portions of this muscle. A muscle element may also include deflection points where the muscle wraps around other musculoskeletal structures (Fig. 2.5.2). At each deflection point a single muscle element is divided into two sub-elements which possess the same force. The origin, insertion and deflection points are inter-connected by straight lines. The length of the muscle and force generated are determined by the complete muscle, however each sub-element acts as an individual line of force with respective origins and insertions. Therefore to determine forces and moments of each muscle element, the insertion or origin relative to a given segment may well be a deflection point rather than a muscular attachment site (Fig. 2.5.2). For each point of deflection a reaction force is present which impinges on the underlying segment. Therefore, at each deflection point an additional force vector is included in the musculoskeletal model. Deflection points include bony sites, retinacula, and other muscles.

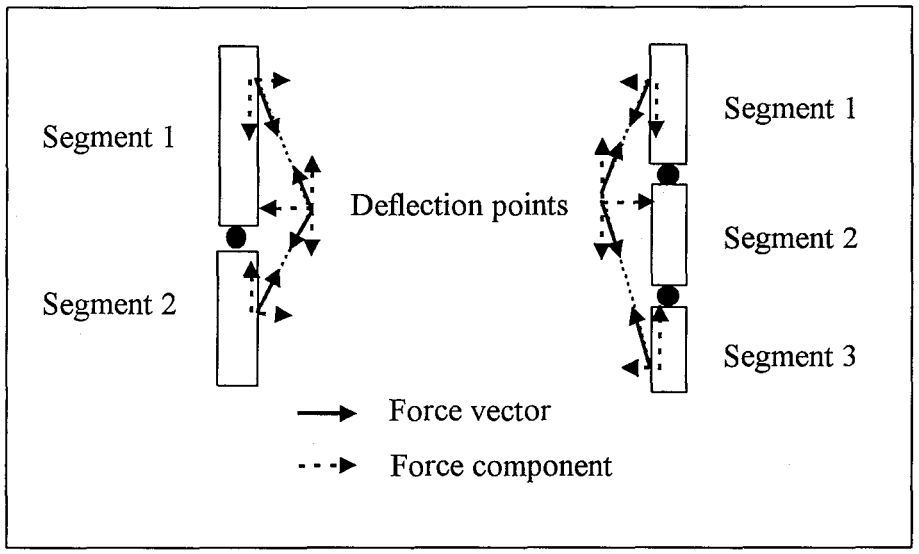

Figure 2.5.2 Muscle represented as two straight line muscle elements and a deflection point.

To illustrate the inclusion of deflection points on the estimation of muscle and internal forces, a simplified model of lower limb extension is presented (Figs. 2.5.3 and 2.5.4). For simplicity, it is assumed that the pelvis, thigh and shank-foot are at rest, the body-fixed axes are all aligned, and the only external force acting is that of gravity. To overcome the force of gravity, it is assumed that the iliopsoas, three vastus muscles, and the rectus femoris generate the required moments. For simplicity, the illioposoas and vastus group are each represented by a single muscle equivalent.

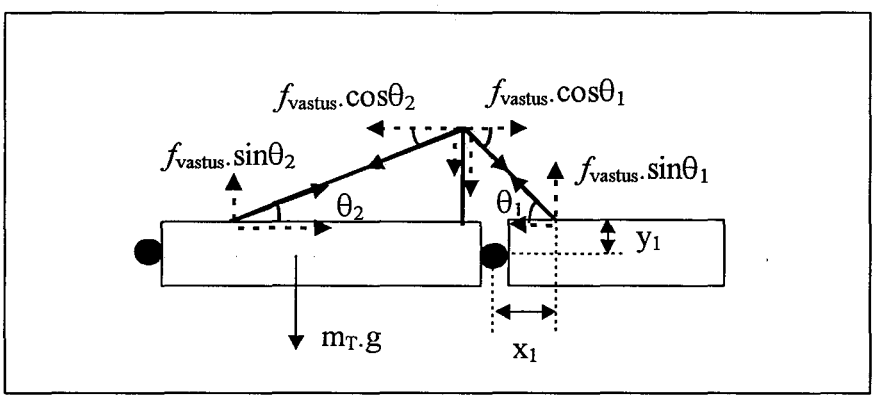

Figure 2.5.3 Deflection point: vastus muscle-tendon element wrapping around patella in the thigh-shank model.

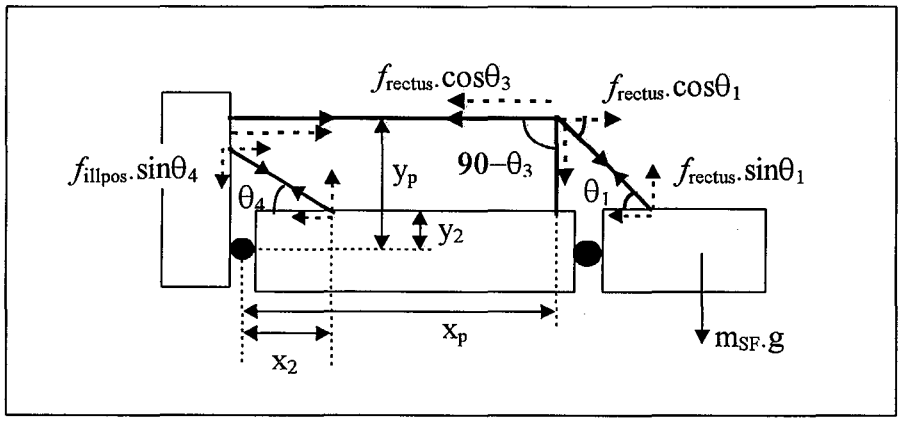

Figure 2.5.4 Deflection point: Rectus femoris muscle-tendon element wrapping around patella in the pelvis-thigh shank-model.

The resultant joint forces and resultant joint moments of the shank/foot and knee respectively, are:

$$\begin{aligned} R_{SFpx} &= m_{SF}.\bar{a}_{SFx} + m_{SF}.g.\sin\theta_{SF} - f_{GRy}.\cos\theta_{SF} - f_{GRz}.\sin\theta_{SF} \\ &= 0 \\ R_{SFpy} &= m_{SF}.\bar{a}_{SFx} + m_{SF}.g.\cos\theta_{SF} + f_{GRy}.\sin\theta_{SF} - f_{GRz}.\cos\theta_{SF} \\ &= -m_{SF}.g \end{aligned} \qquad 2.5.1$$

$$\tau_{Knee} = I_{SF}^{Prox}.\alpha_{SF} - m_{SF}.g.a_{SF}.\cos\theta_{SF} - f_{GRy}.b.\sin\theta_{SF} + f_{GRz}.b.\cos\theta_{SF} \qquad 2.5.2a$$
$$= m_{SF}.g.a_{SF}$$

or

$$\tau_{Knee} = I_{SF}^{CoM}.\alpha_{SF} - R_{SFpy}.a_{SF} - f_{GRy}.c.\sin\theta_{SF} + f_{GRz}.c.\cos\theta_{SF} \qquad 2.5.2b$$
$$= m_{SF}.g.a_{SF}$$

where:

$g = 9.81\ m.s^{-2}$

$\theta_{SF} = 180°$

The resultant joint forces and resultant joint moments of the thigh and hip respectively are:

$$
\begin{aligned}
R_{Tpx} &= m_T.\bar{a}_{Tx} + m_T.g.\sin\theta_T + R_{Tdx} \\
&= 0 \\
R_{Tpy} &= m_T.\bar{a}_{Ty} + m_T.g.\cos\theta_T + R_{Tdy} \\
&= -m_T.g - m_{SF}.g
\end{aligned}
\qquad 2.5.3
$$

$$
\begin{aligned}
\tau_{Hip} &= I_T^{Prox}.\alpha_T - m_T.g.a_T.\cos\theta_T - R_{Tdy}.L_T + \tau_{knee} \\
&= m_T.g.a_T + m_{SF}.g.L_T + m_{SF}.g.a_{SF}
\end{aligned}
\qquad 2.5.4a
$$

or

$$
\begin{aligned}
\tau_{Hip} &= I_T^{CoM}.\alpha_T - R_{Tdy}.(L_T - a_T) - R_{Tpy}.a_T + \tau_{knee} \\
&= m_{SF}.g.(L_T - a_T) + m_T.g.a_T + m_{SF}.g.a_T + m_{SF}.g.a_{SF} \\
&= m_T.g.a_T + m_{SF}.g.L_T + m_{SF}.g.a_{SF}
\end{aligned}
\qquad 2.5.4b
$$

where:

$g = 9.81\ m.s^{-2}$

$\theta_T = 180°$

The equipolance equations for the resultant joint moments at the knee and hip are:

$$
\begin{aligned}
\tau_{Knee} &= f_{vastus}.x_1.\sin\theta_1 + f_{vastus}.y_1.\cos\theta_1 + f_{rectus}.x_1.\sin\theta_1 + f_{rectus}.y_1.\cos\theta_1 \\
&= (f_{vastus} + f_{rectus}).x_1.\sin\theta_1 + (f_{vastus} + f_{rectus}).y_1.\cos\theta_1 \\
\tau_{Hip} &= f_{rectus}.x_p.\sin\theta_3 + f_{rectus}.y_p.\cos\theta_3 + f_{illpos}.x_2.\sin\theta_4 + f_{illpos}.y_2.\cos\theta_4
\end{aligned}
\qquad 2.5.5
$$

The equipolance equations for the resultant joint forces of the thigh and shank are:

$$
\begin{aligned}
R_{SFpx} &= f_{vastus}.\cos\theta_1 + f_{rectus}.\cos\theta_1 + f_{SFpx} \\
R_{SFpy} &= m_{SF}.g - f_{vastus}.\sin\theta_1 - f_{rectus}.\sin\theta_1 + f_{SFpy} \\
R_{Tpx} &= f_{rectus}.\cos\theta_3 + f_{illpos}.\cos\theta_4 + f_{Tpx} \\
R_{Tpy} &= m_T.g - f_{rectus}.\sin\theta_3 - f_{illpos}.\sin\theta_4 + f_{Tpy}
\end{aligned}
\qquad 2.5.6
$$

For any system, the sum of all external force determines the acceleration of the centre of mass of the system, while the sum of all internal forces is equal to zero. Considering the pelvis, thigh and shank-foot as a system, the external forces are those due to gravity acting on the centre of mass of each segment, and an opposing force acting on the pelvis to maintain the static position of the system. Balancing external forces gives the resultant joint moments and resultant joint forces. For the shank-foot segment, the downward force and negative moment created by the weight of the segment is balanced by an upward resultant joint force and positive resultant joint moment at the knee. Similarly for the thigh, downward forces and negative moments created by the weight of the thigh and the resultant force and moment acting at the distant end are balanced by an upward resultant joint force and positive resultant joint moment at the hip. Internal forces resulting from the contraction of illioposoas, vasti and rectus femoris muscles generate the required moments at the hip and knee. All internal forces are balanced due to an equal but opposite forces acting at either end of each straight line muscle element. Bone-on-bone forces at a joint are the sum of forces resulting from internal and external sources. At the knee, the components of bone on bone force are the sum of the components of resultant joint force at the knee and the components of force of all muscle elements that cross the knee joint.

The force that a deflection point impinges on the underlying body segment is found by summing all forces acting on the deflection point. With the patella modelled as a deflection point impinging on the femur, the contact force between the patella and femur (Fig. 2.5.5) is given by the sum of all forces acting on the patella, in this example (Fig. 2.5.5) given by:

$$\begin{aligned} f_{\text{pat x}} &= f_{\text{rectus}} \cdot \cos\theta_3 + f_{\text{vastus}} \cdot \cos\theta_2 - f_{\text{rectus}} \cdot \cos\theta_1 - f_{\text{rectus}} \cdot \cos\theta_1 \\ f_{\text{pat y}} &= f_{\text{rectus}} \cdot \sin\theta_3 + f_{\text{vastus}} \cdot \sin\theta_2 + f_{\text{rectus}} \cdot \sin\theta_1 + f_{\text{vastus}} \cdot \sin\theta_1 \end{aligned} \qquad 2.5.7$$

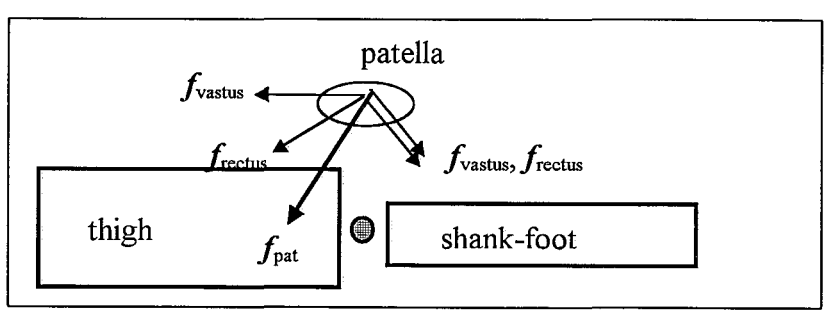

Figure 2.5.5 Deflection point: resultant force on patella (f_{pat}).

2.5.3 Free body diagram

A free-body diagram, drawn as a stick figure, is a simplified representation of a link-segment system in which each segment is isolated from it's surroundings and includes all the forces that act on the segment (Fig. 2.5.6 & Fig. 2.5.7). The lower limb can be represented by four segments - pelvis, thigh, shank, and foot, connected by three joints. Each segment's motion is governed by resultant joint reaction forces, resultant joint moments and a force due to gravity. A multi link segment free body diagram is a collection of the single link-segment diagrams which make up the system. Each link-segment is related to it's adjacent links in terms of forces and torques that act across the link-segments.

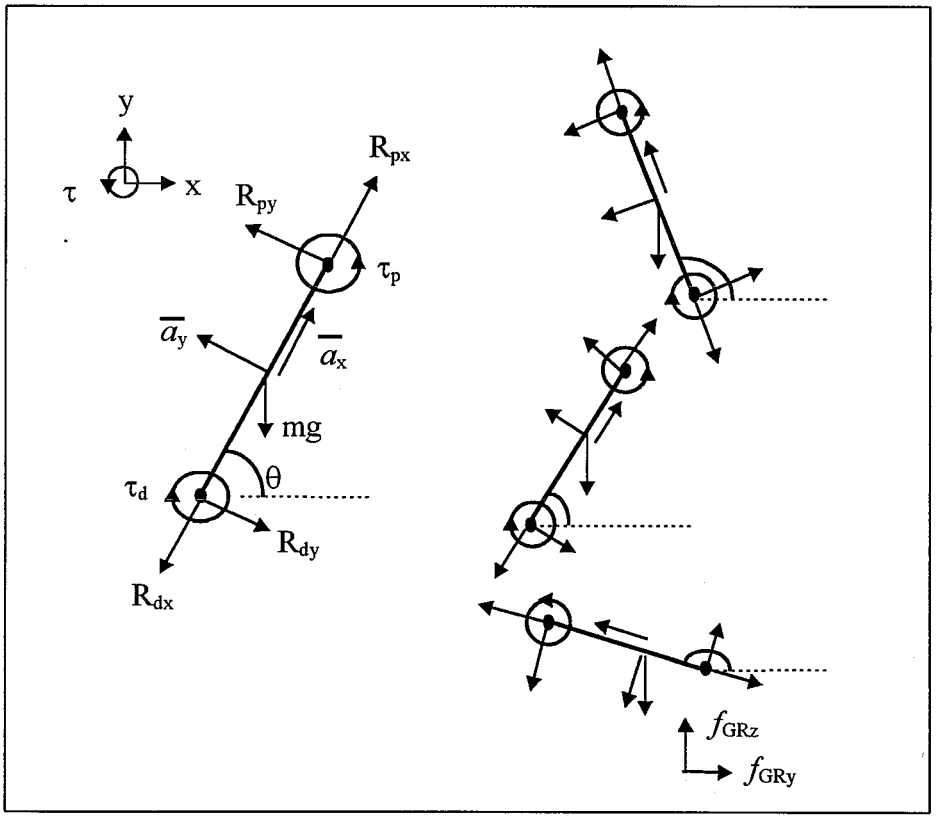

Figure 2.5.6 Two dimensional multi link segment free body diagram. The inertial reference frame is given by vectors **x** and **y**. Rotation is restricted to an axis normal to the plane. The angle of the segment relative to the **x** axis is given by θ, the angular velocity by $\dot{\theta}$ and angular acceleration by $\ddot{\theta}$. The resultant joint reaction forces acting at the proximal and distal ends are represented as $\mathbf{R_{px}}$, $\mathbf{R_{py}}$ and $\mathbf{R_{dx}}$, $\mathbf{R_{dy}}$ respectively. The gravitational force **mg** acts through the centre of mass. The acceleration of the centre of mass is $\boldsymbol{a_x}$, $\boldsymbol{a_y}$. The resultant joint moments are τ_p and τ_d.

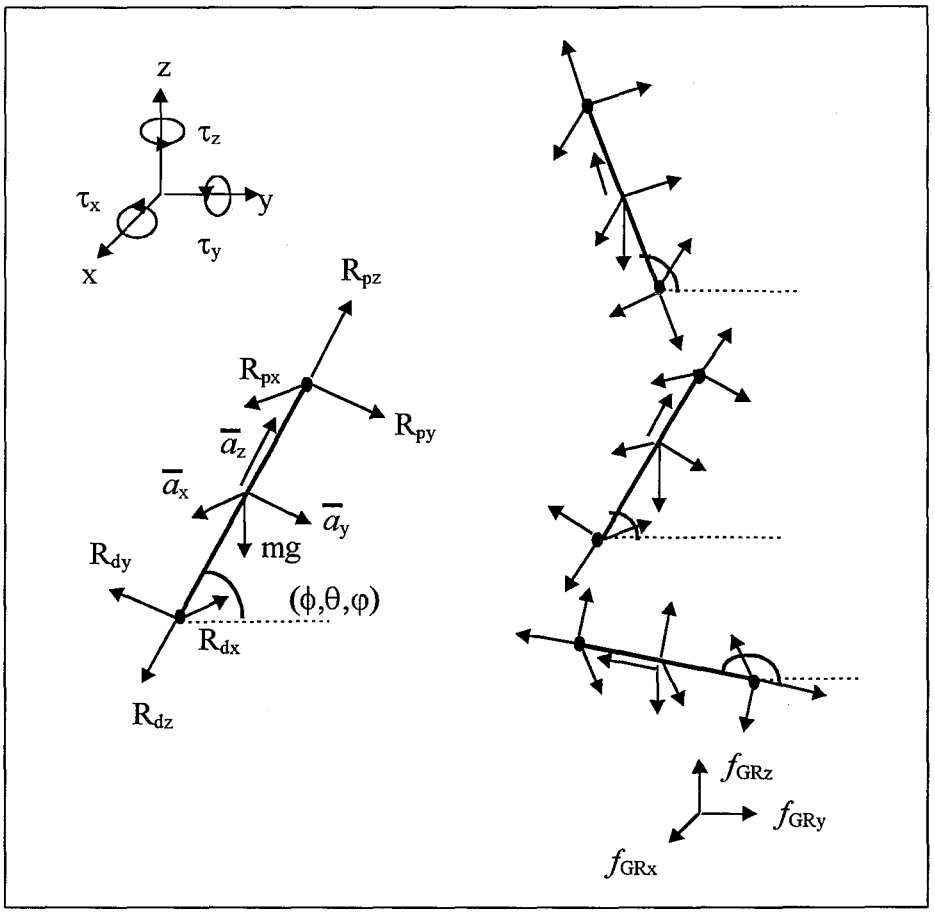

Figure 2.5.7 Three dimensional multi link segment free body diagram. The inertial reference frame is given by the vectors **x**, **y**, **z**. Resultant joint reaction forces acting at the proximal and distal ends are represented as $\mathbf{R_{px}}$, $\mathbf{R_{py}}$, $\mathbf{R_{pz}}$ and $\mathbf{R_{dx}}$, $\mathbf{R_{dy}}$, $\mathbf{R_{dz}}$ respectively. The gravitational force **mg** acts through the centre of mass. The linear acceleration of the centre of mass is $\boldsymbol{a_x}$, $\boldsymbol{a_y}$, $\boldsymbol{a_z}$. The resultant joint moments are τ_{px}, τ_{py}, τ_{pz} and τ_{dx}, τ_{dy}, τ_{dz}. Three angles ϕ, θ, φ define the body-fixed frame with respect to the inertial frame. The angular acceleration is given by $\dot{\omega}_x$, $\dot{\omega}_y$, $\dot{\omega}_z$.

2.5.4 Equations of motion

The equations of motion of the whole system are made up of the equations of motion for each link segment that comprise the system. The equations of motion for each segment are found by equating inertial and non-inertial forces acting on it, as represented in the segment's free body diagram (Hardt & Mann, 1980; Winter, 1990). The translation and rotational equations of motion, involving resultant forces and moments, as well as the translation and rotational

equipolance equations, involving individual muscle forces, can be expressed relative to either the inertial (global) or local body-fixed co-ordinate systems.

2.5.4.1 Equations of motion - resultant forces and resultant moments

For the two dimensional model, forces and moments can equally well be summed relative to the global or inertial axes. However for the three dimensional model, the local co-ordinate system has been chosen for computational efficiency. The reasons for this include:

i) The inertia tensor is known with respect to the local axes system;
ii) The angular velocity and angular acceleration of the rigid body are expressed relative to the instantaneous directions of the body-fixed axes;
iii) The linear velocity of the centre of mass due to rotation of a rigid body about the body-fixed axes is expressed relative to the instantaneous directions of the body-fixed axes;
iv) The co-ordinate of the centre of mass and distal joint centre are known with respect to the local axes system;
v) In most cases, calculated resultant joint forces and moments will be expressed relative to a carefully placed local axis system to give results which are anatomically meaningful;
vi) Potential benefits in computational efficiency by placing body-fixed axes along principle axes of inertia are lost when equating moments relative to global axes, as translating and/or rotating these axes will, in most cases, generate products of inertia; and
vii) The linear velocity of the origin of the local axis system is expressed relative to the global axis system. However, these can be readily expressed relative to the local axis system by a co-ordinate transformation.

The general form of the equations of motion for each two dimensional link segment is of the form (Fig. 2.5.6):

$$\begin{aligned} \sum F_{ix} &= m_i.\bar{a}_{ix} = R_{ipx} - R_{idx} - m_i.g.\sin\theta_i \\ \sum F_{iy} &= m_i.\bar{a}_{iy} = R_{ipy} - R_{idy} - m_i.g.\cos\theta_i \end{aligned} \qquad 2.5.8$$

and

$$\sum \tau_{iz}^{Prox} = I_i^{Prox}.\alpha_i = m_i.g.\bar{y}_i.\sin\theta_i - m_i.g.\bar{x}_i.\cos\theta_i + R_{idx}.y_{id} - R_{idy}.x_{id} + \tau_{ip} - \tau_{id} \quad 2.5.9a$$

or

$$\sum \tau_{iz}^{Dist} = I_i^{Dist}.\alpha_i = m_i.g.\bar{y}_i.\sin\theta_i - m_i.g.\bar{x}_i.\cos\theta_i + R_{ipy}.x_{ip} - R_{ipx}.y_{ip} + \tau_{ip} - \tau_{id} \quad 2.5.9b$$

or

$$\sum \tau_{iz}^{CoM} = I_i^{CoM}.\alpha_i = R_{ipy}.x_{id} - R_{ipx}.y_{ip} - R_{idy}.x_{id} + R_{idx}.y_{id} + \tau_{ip} - \tau_{id} \quad 2.5.9c$$

The equations of motion for the two dimensional link-segment model of the lower limb (Fig. 2.5.6) are:

$$\begin{aligned}
\sum F_{Tx} &= m_T.\bar{a}_{Tx} = R_{Tpx} - R_{Tdx} - m_T.g.\sin\theta_T \\
\sum F_{Ty} &= m_T.\bar{a}_{Ty} = R_{Tpy} - R_{Tdy} - m_T.g.\cos\theta_T \\
\sum F_{Sx} &= m_S.\bar{a}_{Sx} = R_{Spx} - R_{Sdx} - m_S.g.\sin\theta_S \\
\sum F_{Sy} &= m_S.\bar{a}_{Sy} = R_{Spy} - R_{Sdy} - m_S.g.\cos\theta_S \\
\sum F_{Fx} &= m_F.\bar{a}_{Fx} = R_{Fpx} + f_{GRy}.\cos\theta_F + f_{GRz}.\sin\theta_F - m_F.g.\sin\theta_F \\
\sum F_{Fy} &= m_F.\bar{a}_{Fy} = R_{Fpy} - f_{GRy}.\sin\theta_F + f_{GRz}.\cos\theta_F - m_F.g.\cos\theta_F
\end{aligned} \quad 2.5.10$$

and

$$
\begin{aligned}
\sum \tau_{Tz}^{Prox} &= I_T^{Prox}.\alpha_T = m_T.g.\bar{y}_T.\sin\theta_T - m_T.g.\bar{x}_T.\cos\theta_T \\
&\quad + R_{Tdx}.y_{Td} - R_{Tdy}.x_{Td} + \tau_H - \tau_K \\
\sum \tau_{Sz}^{Prox} &= I_S^{Prox}.\alpha_S = m_S.g.\bar{y}_S.\sin\theta_S - m_S.g.\bar{x}_S.\cos\theta_S \\
&\quad + R_{Sdx}.y_{Sd} - R_{Sdy}.x_{Sd} + \tau_K - \tau_A \\
\sum \tau_{Fz}^{Prox} &= I_F^{Prox}.\alpha_F = m_F.g.\bar{y}_F.\sin\theta_F - m_F.g.\bar{x}_F.\cos\theta_F \\
&\quad f_{GRz}.x_{GR}.\cos\theta_F - f_{GRz}.y_{GR}.\sin\theta_F \\
&\quad - f_{GRy}.x_{GR}.\cos\theta_F - f_{GRy}.y_{GR}.\sin\theta_F \\
&\quad + \tau_A
\end{aligned}
\qquad 2.5.11a
$$

or

$$
\begin{aligned}
\sum \tau_{Tz}^{Dist} &= I_T^{Dist}.\alpha_T = m_T.g.\bar{y}_T.\sin\theta_T - m_T.g.\bar{x}_T.\cos\theta_T \\
&\quad + R_{Tpy}.x_{Tp} - R_{Tpx}.y_{Tp} + \tau_H - \tau_K \\
\sum \tau_{Sz}^{Dist} &= I_S^{Dist}.\alpha_S = m_S.g.\bar{y}_S.\sin\theta_S - m_S.g.\bar{x}_S.\cos\theta_S \\
&\quad + R_{Spy}.x_{Sp} - R_{Spx}.y_{Sp} + \tau_K - \tau_A \\
\sum \tau_{Fz}^{Dist} &= I_F^{Dist}.\alpha_F = m_F.g.\bar{y}_F.\sin\theta_F - m_F.g.\bar{x}_F.\cos\theta_F \\
&\quad f_{GRz}.x_{GR}.\cos\theta_F - f_{GRz}.y_{GR}.\sin\theta_F \\
&\quad - f_{GRy}.x_{GR}.\cos\theta_F - f_{GRy}.y_{GR}.\sin\theta_F \\
&\quad + R_{Fpy}.x_{Fp} - R_{Fpx}.y_{Fp} + \tau_A
\end{aligned}
\qquad 2.5.11b
$$

or

$$
\begin{aligned}
\sum \tau_{Tz}^{CoM} &= I_T^{CoM}.\alpha_T = R_{Tpy}.x_{Tp} - R_{Tpx}.y_{Tp} + R_{Tdx}.y_{Td} - R_{Tdy}.x_{Td} \\
&\quad + \tau_H - \tau_K \\
\sum \tau_{Sz}^{CoM} &= I_S^{CoM}.\alpha_S = R_{Spy}.x_{Sp} - R_{Spx}.y_{Sp} + R_{Sdx}.y_{Sd} - R_{Sdy}.x_{Sd} \\
&\quad + \tau_K - \tau_A \\
\sum \tau_{Fz}^{CoM} &= I_F^{CoM}.\alpha_F = R_{Fpy}.x_{Fp} - R_{Fpx}.y_{Fp} + R_{Fdx}.y_{Fd} - R_{Fdy}.x_{Fd} \\
&\quad + f_{GRz}.x_{GRF}.\cos\theta_F - f_{GRz}.y_{GR}.\sin\theta_F \\
&\quad - f_{GRy}.y_{GR}.\cos\theta_F - f_{GRy}.x_{GR}.\sin\theta_F + \tau_A
\end{aligned}
\qquad 2.5.11c
$$

where:

$g = 9.81\ m.s^{-2}$

x,y = local co-ordinates measured from the point about which moments are summed (proximal, centre of mass or distal).

$\bar{x}, \bar{y}$ = local co-ordinates of centre of mass measured from the point about which moments are summed (proximal or distal).

$$\begin{bmatrix} R_{Sdx} \\ R_{Sdy} \end{bmatrix} = [R].\begin{bmatrix} R_{Fpx} \\ R_{Fpy} \end{bmatrix}$$

$$\begin{bmatrix} R_{Tdx} \\ R_{Tdy} \end{bmatrix} = [R].\begin{bmatrix} R_{Spx} \\ R_{Spy} \end{bmatrix}$$

The choice of whether to sum moments about the proximal joint, centre of mass or distal joint depends on individual preferences. If the body-fixed axis system is located at one joint centre and all local co-ordinates are expressed relative to these axes, then it would be efficient to sum moments with respect to this joint centre. However, inertia tensors and local co-ordinates expressed relative to one axis system can always be calculated for another axis system.

The general equations of motion for each three dimensional link-segment model take the form (Figure 2.5.7):

$$\begin{aligned} \sum F_{ix} &= m_i.\bar{a}_{ix} = R_{ipx} - R_{idx} + m_i.g_{ix} \\ \sum F_{iy} &= m_i.\bar{a}_{iy} = R_{ipy} - R_{idy} + m_i.g_{iy} \\ \sum F_{iz} &= m_i.\bar{a}_{iz} = R_{ipz} - R_{idz} + m_i.g_{iz} \end{aligned} \qquad 2.5.12$$

and

$$\begin{aligned} \sum \tau_x^{Prox} &= m.g_z.\bar{y} - m.g_y.\bar{z} - R_{dz}.y_d + R_{dy}.z_d + \tau_{px} - \tau_{dx} \\ \sum \tau_y^{Prox} &= m.g_x.\bar{z} - m.g_z.\bar{x} - R_{dx}.z_d + R_{dz}.x_d + \tau_{py} - \tau_{dy} \\ \sum \tau_z^{Prox} &= m.g_y.\bar{x} - m.g_x.\bar{y} - R_{dy}.x_d + R_{dx}.y_d + \tau_{pz} - \tau_{dz} \end{aligned} \qquad 2.5.13a$$

or

$$\begin{aligned} \sum \tau_x^{CoM} &= R_{pz}.y_p - R_{py}.z_p - R_{dz}.y_d + R_{dy}.z_d + \tau_{px} - \tau_{dx} \\ \sum \tau_y^{CoM} &= R_{px}.z_p - R_{pz}.x_p - R_{dx}.z_d + R_{dz}.x_d + \tau_{py} - \tau_{dy} \\ \sum \tau_z^{CoM} &= R_{py}.x_p - R_{px}.y_p - R_{dy}.x_d + R_{dx}.y_d + \tau_{pz} - \tau_{dz} \end{aligned} \qquad 2.5.13b$$

or

$$\begin{aligned}
\sum \tau_x^{Dist} &= m.g_z.\bar{y} - m.g_y.\bar{z} + R_{pz}.y_p - R_{py}.z_p + \tau_{px} - \tau_{dx} \\
\sum \tau_y^{Dist} &= m.g_x.\bar{z} - m.g_z.\bar{x} + R_{px}.z_p - R_{pz}.x_p + \tau_{py} - \tau_{dy} \\
\sum \tau_z^{Dist} &= m.g_y.\bar{x} - m.g_x.\bar{y} + R_{py}.x_p - R_{px}.y_p + \tau_{pz} - \tau_{dz}
\end{aligned} \qquad 2.5.13c$$

where:

$g = 9.81\ ms^{-2}$

$$[\mathbf{g}_{local}] = [R].[\mathbf{g}_{global}]$$

$$\begin{bmatrix} g_{ix} \\ g_{iy} \\ g_{iz} \end{bmatrix} = \begin{bmatrix} \mathbf{i}.\mathbf{i}_I & \mathbf{i}.\mathbf{j}_I & \mathbf{i}.\mathbf{k}_I \\ \mathbf{j}.\mathbf{i}_I & \mathbf{j}.\mathbf{j}_I & \mathbf{j}.\mathbf{k}_I \\ \mathbf{k}.\mathbf{i}_I & \mathbf{k}.\mathbf{j}_I & \mathbf{k}.\mathbf{k}_I \end{bmatrix} . \begin{bmatrix} 0 \\ 0 \\ -9.81 \end{bmatrix}$$

$$\begin{bmatrix} f_{GRix} \\ f_{GRiy} \\ f_{GRiz} \end{bmatrix} = \begin{bmatrix} \mathbf{i}.\mathbf{i}_I & \mathbf{i}.\mathbf{j}_I & \mathbf{i}.\mathbf{k}_I \\ \mathbf{j}.\mathbf{i}_I & \mathbf{j}.\mathbf{j}_I & \mathbf{j}.\mathbf{k}_I \\ \mathbf{k}.\mathbf{i}_I & \mathbf{k}.\mathbf{j}_I & \mathbf{k}.\mathbf{k}_I \end{bmatrix} . \begin{bmatrix} f_{GRx} \\ f_{GRy} \\ f_{GRz} \end{bmatrix}$$

x, y, z = local co-ordinates measured from the point about which moments are summed (proximal, centre of mass or distal)

$\bar{x}$, $\bar{y}$, $\bar{z}$ = local co-ordinates of centre of mass measured from the point about which moments are summed (proximal or distal)

$f_{GRix}, f_{GRiy}, f_{GRiz}$ = ground reaction force with components along local axes

g_{ix}, g_{iy}, g_{iz} = gravitational acceleration with components along local axes.

The equations of motion for a three dimensional link-segment model of the lower limb (Figure 2.5.7) are:

$$
\begin{aligned}
\sum F_{Tx} &= m_T.\bar{a}_{Tx} = R_{Tpx} - R_{Tdx} + m_T.g_{Tx} \\
\sum F_{Ty} &= m_T.\bar{a}_{Ty} = R_{Tpy} - R_{Tdy} + m_T.g_{Ty} \\
\sum F_{Tz} &= m_T.\bar{a}_{Tz} = R_{Tpz} - R_{Tdz} + m_T.g_{Tz} \\
\sum F_{Sx} &= m_S.\bar{a}_{Sx} = R_{Spx} - R_{Sdx} + m_S.g_{Sx} \\
\sum F_{Sy} &= m_S.\bar{a}_{Sy} = R_{Spy} - R_{Sdy} + m_S.g_{Sy} \\
\sum F_{Sz} &= m_S.\bar{a}_{Sz} = R_{Spz} - R_{Sdz} + m_S.g_{Sz} \\
\sum F_{Fx} &= m_F.\bar{a}_{Fx} = R_{Fpx} + f_{GRFx} + m_F.g_{Fx} \\
\sum F_{Fy} &= m_F.\bar{a}_{Fy} = R_{Fpy} + f_{GRFy} + m_F.g_{Fy} \\
\sum F_{Fz} &= m_F.\bar{a}_{Fz} = R_{Fpz} + f_{GRFz} + m_F.g_{Fz}
\end{aligned}
\qquad 2.5.14
$$

If moments are summed relative to the distal end:

$$
\begin{aligned}
\sum \tau_{Tx}^{Dist} &= m_T.g_{Tz}.\bar{y}_T - m_T.g_{Ty}.\bar{z}_T + R_{Tpz}.y_{Tp} - R_{Tpy}.z_{Tp} + \tau_{Hx} - \tau_{Kx} \\
\sum \tau_{Ty}^{Dist} &= m_T.g_{Tx}.\bar{z}_T - m_T.g_{Tz}.\bar{x}_T + R_{Tpx}.z_{Tp} - R_{Tpz}.x_{Tp} + \tau_{Hy} - \tau_{Ky} \\
\sum \tau_{Tz}^{Dist} &= m_T.g_{Ty}.\bar{x}_T - m_T.g_{Tx}.\bar{y}_T + R_{Tpy}.x_{Tp} - R_{Tpx}.y_{Tp} + \tau_{Hz} - \tau_{Kz}
\end{aligned}
$$

$$
\begin{aligned}
\sum \tau_{Sx}^{Dist} &= m_S.g_{Sz}.\bar{y}_S - m_S.g_{Sy}.\bar{z}_S + R_{Spz}.y_{Sp} - R_{Spy}.z_{Sp} + \tau_{Kx} - \tau_{Ax} \\
\sum \tau_{Sy}^{Dist} &= m_S.g_{Sx}.\bar{z}_S - m_S.g_{Sz}.\bar{x}_S + R_{Spx}.z_{Sp} - R_{Spz}.x_{Sp} + \tau_{Ky} - \tau_{Ay} \\
\sum \tau_{Sz}^{Dist} &= m_S.g_{Sy}.\bar{x}_S - m_S.g_{Sx}.\bar{y}_S + R_{Spy}.x_{Sp} - R_{Spx}.y_{Sp} + \tau_{Kz} - \tau_{Az}
\end{aligned}
$$

$$
\begin{aligned}
\sum \tau_{Fx}^{Dist} &= m_F.g_{Fz}.\bar{y}_F - m_F.g_{Fy}.\bar{z}_F + R_{Fpz}.y_{Fp} - R_{Fpy}.z_{Fp} + \tau_{Ax} \\
&\quad + f_{GRFz}.y_{GRF} - f_{GRFy}.z_{GRF} \\
\sum \tau_{Fy}^{Dist} &= m_F.g_{Fx}.\bar{z}_F - m_F.g_{Fz}.\bar{x}_F + R_{Fpx}.z_{Fp} - R_{Fpz}.x_{Fp} + \tau_{Ay} \\
&\quad + f_{GRFx}.z_{GRF} - f_{GRFz}.x_{GRF} \\
\sum \tau_{Fz}^{Dist} &= m_F.g_{Fy}.\bar{x}_F - m_F.g_{Fx}.\bar{y}_F + R_{Fpy}.x_{Fp} - R_{Fpx}.y_{Fp} + \tau_{Az} \\
&\quad + f_{GRFy}.x_{GRF} - f_{GRFx}.y_{GRF}
\end{aligned}
\qquad 2.5.15
$$

Forces and moments are summed with respect to the body-fixed axes. Resultant forces, moments and co-ordinates are likewise expressed with respect to body-fixed axes.

The expanded form of the left hand side of equations (2.5.14) and (2.5.15) are given in section 2.3.3.1 for the linear acceleration of the centre of mass, section 2.4.1 for the translation equations of motion and section 2.4.2 for the rotation equations of motion.

2.5.4.2 Equipollence equations

The equipollence equations relate resultant joint moments and forces to muscle, bone contact, and ligament forces. In equating moments, the unknown variables are positive scalars in the form of individual muscle forces. Resultant joint moments and forces have previously been calculated along with all muscle elements' lines of action. The choice of axis system in which to express theses equations largely depends on the preferences of the researcher. In the method presented, the equipolance equations are expressed relative to local body-fixed axis systems. Points to be considered in the choice of either a global or local axes system relative to which forces and moments are to be summed, include (Fig. 2.5.8):

i) Information on muscle origins, insertions and deflection points, as well as joint centre locations are expressed relative to local co-ordinate systems;
ii) The position vectors of segment local axes origins are relative to global co-ordinates;
iii) For each segment, two transformations are required to express the joint centre location and resultant moments relative to global axes, while two transformations are required to express the global vector connecting the two local axis systems relative to each local system;
iv) Transformations of vectors locating axis origins, joint centres or components of resultant moments only have to be carried out once for any given instantaneous position;
v) For each muscle, two transformations are required to express the origin and insertion relative to global axes, while two transformations are also required in order to express the opposing origin or insertion relative to each local system;
vi) As a greater number of muscles are modelled than segments, for computational efficiency, the aim would be to minimise the number of transformations involving muscle co-ordinates (i.e. origins, insertions and deflection points) rather than transformations of moments and position vectors of body-fixed axes;
vii) Little difference exists in the number of co-ordinate transformations required in summing moments relative to the global or local systems. The choice of axes maytherefore be for more practical or intuitive reasons;

viii) The directions of compressive and shear bone-on-bone forces are known relative to the local system and may coincide with carefully placed local axes systems; and

ix) Moment arms and muscle lines of action calculated with respect to each local system may be anatomically more meaningful with carefully placed local axes than if these vectors were expressed relate to the global axes.

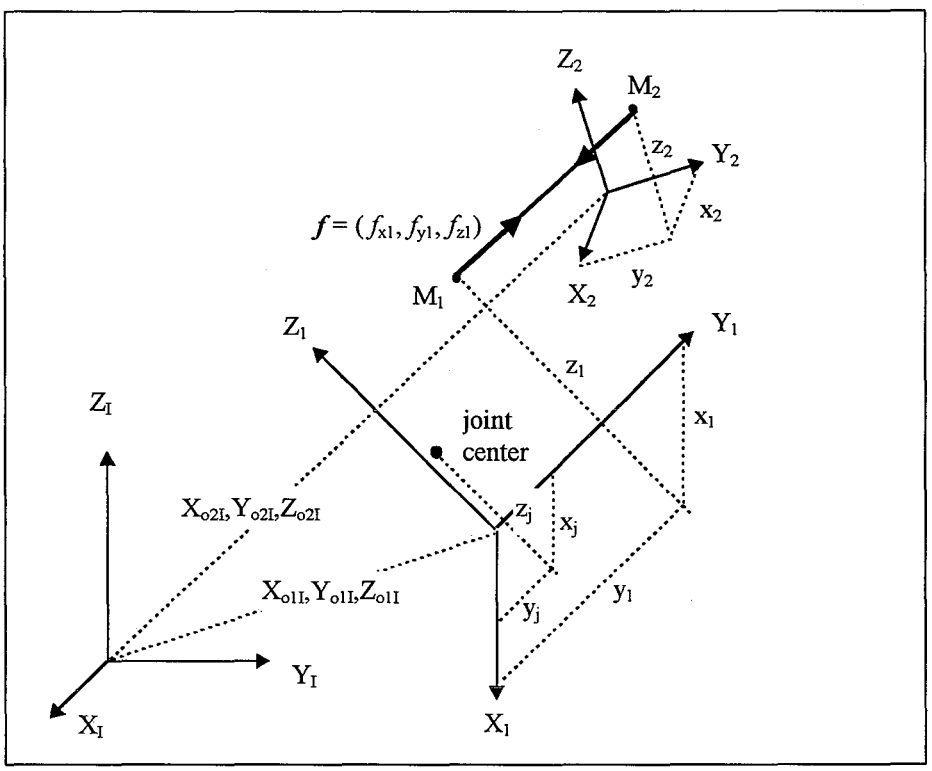

Figure 2.5.8 Body fixed axes related by position in a global axis system. Global axes are given by (X_I, Y_I, Z_I). The origin of two body-fixed axes are given by $(X_{o1I}, Y_{o1I}, Z_{o1I})$ and $(X_{o2I}, Y_{o2I}, Z_{o2I})$. A muscle-tendon element is represented by two points M_1 and M_2 defined in each body-fixed axis system (x_1, y_1, z_1) and (x_2, y_2, z_2) respectively. A co-ordinate transformation is then required to express the muscle origin and insertion in a common axis system and calculate the direction of force (f_{x1}, f_{y1}, f_{z1}).

A global vector relating the origin of the second local system to that of the first is given by (Fig. 2.5.8):

$$\mathbf{r}_{o12\,I} = \mathbf{r}_{o2\,I} - \mathbf{r}_{o1\,I} \qquad 2.5.16a$$

or

$$\begin{bmatrix} X_{o12\,I} \\ Y_{o12\,I} \\ Z_{o12\,I} \end{bmatrix} = \begin{bmatrix} X_{o2\,I} \\ Y_{o2\,I} \\ Z_{o2\,I} \end{bmatrix} - \begin{bmatrix} X_{o1\,I} \\ Y_{o1\,I} \\ Z_{o1\,I} \end{bmatrix} \qquad 2.5.16b$$

The position vector of the origin of the muscle element relative to the first local system, whether it be a point of attachment or deflection in the second axes system, is given by:

$$\mathbf{r}_{\text{muscle origin 1}} = [R_1].\mathbf{r}_{o12\,I} + [R_1].[R_2]^T.\mathbf{r}_2 \qquad 2.5.17a$$

or

$$\begin{bmatrix} x_{mo\,1} \\ y_{mo\,1} \\ z_{mo\,1} \end{bmatrix} = \begin{bmatrix} \mathbf{i}_1.\mathbf{i}_I & \mathbf{i}_1.\mathbf{j}_I & \mathbf{i}_1.\mathbf{k}_I \\ \mathbf{j}_1.\mathbf{i}_I & \mathbf{j}_1.\mathbf{j}_I & \mathbf{j}_1.\mathbf{k}_I \\ \mathbf{k}_1.\mathbf{i}_I & \mathbf{k}_1.\mathbf{j}_I & \mathbf{k}_1.\mathbf{k}_I \end{bmatrix} \begin{bmatrix} X_{o12\,I} \\ Y_{o12\,I} \\ Z_{o12\,I} \end{bmatrix} \qquad 2.5.17b$$

$$+ \begin{bmatrix} \mathbf{i}_1.\mathbf{i}_I & \mathbf{i}_1.\mathbf{j}_I & \mathbf{i}_1.\mathbf{k}_I \\ \mathbf{j}_1.\mathbf{i}_I & \mathbf{j}_1.\mathbf{j}_I & \mathbf{j}_1.\mathbf{k}_I \\ \mathbf{k}_1.\mathbf{i}_I & \mathbf{k}_1.\mathbf{j}_I & \mathbf{k}_1.\mathbf{k}_I \end{bmatrix} \begin{bmatrix} \mathbf{i}_I.\mathbf{i}_2 & \mathbf{i}_I.\mathbf{j}_2 & \mathbf{i}_I.\mathbf{k}_2 \\ \mathbf{j}_I.\mathbf{i}_2 & \mathbf{j}_I.\mathbf{j}_2 & \mathbf{j}_I.\mathbf{k}_2 \\ \mathbf{k}_I.\mathbf{i}_2 & \mathbf{k}_I.\mathbf{j}_2 & \mathbf{k}_I.\mathbf{k}_2 \end{bmatrix} \begin{bmatrix} x_2 \\ y_2 \\ z_2 \end{bmatrix}$$

The force exerted by a muscle may be represented by a vector of appropriate magnitude with components expressed relative to an orthogonal axes system or as a product of magnitude and a unit vector in the direction of the force. Thus, muscle force may be given by:

$$\begin{aligned} f &= \left(f_x\,\mathbf{i}, f_y\,\mathbf{j}, f_z\,\mathbf{k}\right) \\ &= f\left(f_{ux}\,\mathbf{i}, f_{uy}\,\mathbf{j}, f_{uz}\,\mathbf{k}\right) \\ &= f.f_{\text{unit}} \end{aligned} \qquad 2.5.18$$

A unit vector in the direction of the muscle line of action relative to the first local system is given by the origin and insertion of the muscle:

$$f_{\text{unit 1}} = \frac{\mathbf{r}_{\text{muscle origin 1}} - \mathbf{r}_1}{\left\| \mathbf{r}_{\text{muscle origin 1}} - \mathbf{r}_1 \right\|} \qquad 2.5.19$$

The equipolance moment equations for a given joint equate resultant joint moments with the sum of moments produced by each muscle that crosses the joint. Ligaments are assumed not to contribute to the resultant joint moment and only one bone-on-bone force is present which acts through the joint centre. The general form of these equations are:

$$\begin{aligned}
\tau_{jnt\,x} &= \sum_{i=1}^{m} f_i\left(f_{uzi}\cdot(y_i - y_j) - f_{uyi}\cdot(z_i - z_j)\right) \\
\tau_{jnt\,y} &= \sum_{i=1}^{m} f_i\left(f_{uxi}\cdot(z_i - z_j) - f_{uzi}\cdot(x_i - x_j)\right) \\
\tau_{jnt\,z} &= \sum_{i=1}^{m} f_i\left(f_{uyi}\cdot(x_i - x_j) - f_{uxi}\cdot(y_i - y_j)\right)
\end{aligned} \qquad 2.5.20$$

where

τ_{jnt} = resultant joint moment

m = number of muscles crossing the joint

f_i = scalar magnitude of force of muscle i

f_{ux}, f_{uy}, f_{uz} = unit vector in direction of force

x_j, y_j, z_j = coordinates of joint centre

x_i, y_i, z_i = coordinates of insertion of muscle i

If the origin of the body-fixed axes are coincident with the joint centre, then:

$$x_j = y_j = z_j = 0 \qquad 2.5.21$$

For the simplified model of the lower limb, eight muscle groups can be represented (Fig. 2.5.9). In this case the equipolant moment equations are:

$$
\begin{aligned}
\tau_{\text{Hip x}} &= f_1\left(f_{\text{uz1b}} \cdot y_{\text{1b}} - f_{\text{uy1b}} \cdot z_{\text{1b}}\right) + f_2\left(f_{\text{uz2b}} \cdot y_{\text{2b}} - f_{\text{uy2b}} \cdot z_{\text{2b}}\right) \\
&\quad + f_3\left(f_{\text{uz3b}} \cdot y_{\text{3b}} - f_{\text{uy3b}} \cdot z_{\text{3b}}\right) + f_4\left(f_{\text{uz4b}} \cdot y_{\text{4b}} - f_{\text{uy4b}} \cdot z_{\text{4b}}\right) \\
\tau_{\text{Hip y}} &= f_1\left(f_{\text{ux1b}} \cdot z_{\text{1b}} - f_{\text{uz1b}} \cdot x_{\text{1b}}\right) + f_2\left(f_{\text{ux2b}} \cdot z_{\text{2b}} - f_{\text{uz2b}} \cdot x_{\text{2b}}\right) \\
&\quad + f_3\left(f_{\text{ux3b}} \cdot z_{\text{3b}} - f_{\text{uz3b}} \cdot x_{\text{3b}}\right) + f_4\left(f_{\text{ux4b}} \cdot z_{\text{4b}} - f_{\text{uz4b}} \cdot x_{\text{4b}}\right) \\
\tau_{\text{Hip z}} &= f_1\left(f_{\text{uy1b}} \cdot x_{\text{1b}} - f_{\text{ux1b}} \cdot y_{\text{1b}}\right) + f_2\left(f_{\text{uy2b}} \cdot x_{\text{2b}} - f_{\text{ux2b}} \cdot y_{\text{2b}}\right) \\
&\quad + f_3\left(f_{\text{uy3b}} \cdot x_{\text{3b}} - f_{\text{ux3b}} \cdot y_{\text{3b}}\right) + f_4\left(f_{\text{uy4b}} \cdot x_{\text{4b}} - f_{\text{ux4b}} \cdot y_{\text{4b}}\right)
\end{aligned}
\qquad 2.5.22a
$$

$$
\begin{aligned}
\tau_{\text{Knee x}} &= f_3\left(f_{\text{uz3d}} \cdot y_{\text{3d}} - f_{\text{uy3d}} \cdot z_{\text{3d}}\right) + f_4\left(f_{\text{uz4b}} \cdot y_{\text{4b}} - f_{\text{uy4b}} \cdot z_{\text{4b}}\right) \\
&\quad + f_5\left(f_{\text{uz5d}} \cdot y_{\text{5d}} - f_{\text{uy5d}} \cdot z_{\text{5d}}\right) + f_6\left(f_{\text{uz6b}} \cdot y_{\text{6b}} - f_{\text{uy6b}} \cdot z_{\text{6b}}\right) \\
\tau_{\text{Knee y}} &= f_3\left(f_{\text{ux3d}} \cdot z_{\text{3d}} - f_{\text{uz3d}} \cdot x_{\text{3d}}\right) + f_4\left(f_{\text{ux4b}} \cdot z_{\text{4b}} - f_{\text{uz4b}} \cdot x_{\text{4b}}\right) \\
&\quad + f_5\left(f_{\text{ux5d}} \cdot z_{\text{5d}} - f_{\text{uz5d}} \cdot x_{\text{5d}}\right) + f_6\left(f_{\text{ux6b}} \cdot z_{\text{6b}} - f_{\text{uz6b}} \cdot x_{\text{6b}}\right) \\
\tau_{\text{Knee z}} &= f_3\left(f_{\text{uy3d}} \cdot x_{\text{3d}} - f_{\text{ux3d}} \cdot y_{\text{3d}}\right) + f_4\left(f_{\text{uy4b}} \cdot x_{\text{4b}} - f_{\text{ux4b}} \cdot y_{\text{4b}}\right) \\
&\quad + f_5\left(f_{\text{uy5d}} \cdot x_{\text{5d}} - f_{\text{ux5d}} \cdot y_{\text{5d}}\right) + f_6\left(f_{\text{uy6b}} \cdot x_{\text{6b}} - f_{\text{ux6b}} \cdot y_{\text{6b}}\right)
\end{aligned}
\qquad 2.5.22b
$$

$$
\begin{aligned}
\tau_{\text{Ankle x}} &= f_6\left(f_{\text{uz6b}} \cdot y_{\text{6b}} - f_{\text{uy6b}} \cdot z_{\text{6b}}\right) + f_7\left(f_{\text{uz7b}} \cdot y_{\text{7b}} - f_{\text{uy7b}} \cdot z_{\text{7b}}\right) \\
&\quad + f_8\left(f_{\text{uz8b}} \cdot y_{\text{8b}} - f_{\text{uy8b}} \cdot z_{\text{8b}}\right) \\
\tau_{\text{Ankle y}} &= f_6\left(f_{\text{ux6b}} \cdot z_{\text{6b}} - f_{\text{uz6b}} \cdot x_{\text{6b}}\right) + f_7\left(f_{\text{ux7b}} \cdot z_{\text{7b}} - f_{\text{uz7b}} \cdot x_{\text{7b}}\right) \\
&\quad + f_8\left(f_{\text{ux8b}} \cdot z_{\text{8b}} - f_{\text{uz8b}} \cdot x_{\text{8b}}\right) \\
\tau_{\text{Ankle z}} &= f_6\left(f_{\text{uy6b}} \cdot x_{\text{6b}} - f_{\text{ux6b}} \cdot y_{\text{6b}}\right) + f_7\left(f_{\text{uy7b}} \cdot x_{\text{7b}} - f_{\text{ux7b}} \cdot y_{\text{7b}}\right) \\
&\quad + f_8\left(f_{\text{uy8b}} \cdot x_{\text{8b}} - f_{\text{ux8b}} \cdot y_{\text{8b}}\right)
\end{aligned}
\qquad 2.5.22c
$$

Similar expressions can be derived for the resultant joint moments occurring at the distal end of each segment:

$$
\begin{aligned}
-\tau_{\text{Hip x}} &= f_1\left(f_{\text{uz1a}} \cdot y_{\text{1a}} - f_{\text{uy1a}} \cdot z_{\text{1a}}\right) + f_2\left(f_{\text{uz2a}} \cdot y_{\text{2a}} - f_{\text{uy2a}} \cdot z_{\text{2a}}\right) \\
&\quad + f_3\left(f_{\text{uz3a}} \cdot y_{\text{3a}} - f_{\text{uy3a}} \cdot z_{\text{3a}}\right) + f_4\left(f_{\text{uz4a}} \cdot y_{\text{4a}} - f_{\text{uy4a}} \cdot z_{\text{4a}}\right) \\
-\tau_{\text{Hip y}} &= f_1\left(f_{\text{ux1a}} \cdot z_{\text{1a}} - f_{\text{uz1a}} \cdot x_{\text{1a}}\right) + f_2\left(f_{\text{ux2a}} \cdot z_{\text{2a}} - f_{\text{uz2a}} \cdot x_{\text{2a}}\right) \\
&\quad + f_3\left(f_{\text{ux3a}} \cdot z_{\text{3a}} - f_{\text{uz3a}} \cdot x_{\text{3a}}\right) + f_4\left(f_{\text{ux4a}} \cdot z_{\text{4a}} - f_{\text{uz4a}} \cdot x_{\text{4a}}\right) \\
-\tau_{\text{Hip z}} &= f_1\left(f_{\text{uy1a}} \cdot x_{\text{1a}} - f_{\text{ux1a}} \cdot y_{\text{1a}}\right) + f_2\left(f_{\text{uy2a}} \cdot x_{\text{2a}} - f_{\text{ux2a}} \cdot y_{\text{2a}}\right) \\
&\quad + f_3\left(f_{\text{uy3a}} \cdot x_{\text{3a}} - f_{\text{ux3a}} \cdot y_{\text{3a}}\right) + f_4\left(f_{\text{uy4a}} \cdot x_{\text{4a}} - f_{\text{ux4a}} \cdot y_{\text{4a}}\right)
\end{aligned}
\qquad 2.5.23a
$$

$$
\begin{aligned}
-\tau_{\text{Knee x}} &= f_3\left(f_{\text{uz3c}}\cdot y_{3c} - f_{\text{uy3c}}\cdot z_{3c}\right) + f_4\left(f_{\text{uz4a}}\cdot y_{4a} - f_{\text{uy4a}}\cdot z_{4a}\right) \\
&\quad + f_5\left(f_{\text{uz5c}}\cdot y_{5c} - f_{\text{uy5c}}\cdot z_{5c}\right) + f_6\left(f_{\text{uz6a}}\cdot y_{6a} - f_{\text{uy6a}}\cdot z_{6a}\right) \\
-\tau_{\text{Knee y}} &= f_3\left(f_{\text{ux3c}}\cdot z_{3c} - f_{\text{uz3c}}\cdot x_{3c}\right) + f_4\left(f_{\text{ux4a}}\cdot z_{4a} - f_{\text{uz4a}}\cdot x_{4a}\right) \\
&\quad + f_5\left(f_{\text{ux5c}}\cdot z_{5c} - f_{\text{uz5c}}\cdot x_{5c}\right) + f_6\left(f_{\text{ux6a}}\cdot z_{6a} - f_{\text{uz6a}}\cdot x_{6a}\right) \\
-\tau_{\text{Knee z}} &= f_3\left(f_{\text{uy3c}}\cdot x_{3c} - f_{\text{ux3c}}\cdot y_{3c}\right) + f_4\left(f_{\text{uy4a}}\cdot x_{4a} - f_{\text{ux4a}}\cdot y_{4a}\right) \\
&\quad + f_5\left(f_{\text{uy5c}}\cdot x_{5c} - f_{\text{ux5c}}\cdot y_{5c}\right) + f_6\left(f_{\text{uy6a}}\cdot x_{6a} - f_{\text{ux6a}}\cdot y_{6a}\right)
\end{aligned}
\qquad 2.5.23b
$$

$$
\begin{aligned}
-\tau_{\text{Ankle x}} &= f_6\left(f_{\text{uz6a}}\cdot y_{6a} - f_{\text{uy6a}}\cdot z_{6a}\right) + f_7\left(f_{\text{uz7a}}\cdot y_{7a} - f_{\text{uy7a}}\cdot z_{7a}\right) \\
&\quad + f_8\left(f_{\text{uz8a}}\cdot y_{8a} - f_{\text{uy8a}}\cdot z_{8a}\right) \\
-\tau_{\text{Ankle y}} &= f_6\left(f_{\text{ux6a}}\cdot z_{6a} - f_{\text{uz6a}}\cdot x_{6a}\right) + f_7\left(f_{\text{ux7a}}\cdot z_{7a} - f_{\text{uz7a}}\cdot x_{7a}\right) \\
&\quad + f_8\left(f_{\text{ux8a}}\cdot z_{8a} - f_{\text{uz8a}}\cdot x_{8a}\right) \\
-\tau_{\text{Ankle z}} &= f_6\left(f_{\text{uy6a}}\cdot x_{6a} - f_{\text{ux6a}}\cdot y_{6a}\right) + f_7\left(f_{\text{uy7a}}\cdot x_{7a} - f_{\text{ux7a}}\cdot y_{7a}\right) \\
&\quad + f_8\left(f_{\text{uy8a}}\cdot x_{8a} - f_{\text{ux8a}}\cdot y_{8a}\right)
\end{aligned}
\qquad 2.5.23c
$$

The equipolance force equations for a given joint equate resultant joint forces with the sum of forces produced by each muscle that crosses the joint and the bone-on-bone forces produced at the joint. Ligaments are assumed not to contribute to the resultant joint moment and only one bone-on-bone force is present which acts through the joint centre. The general form of these equations are:

$$
\begin{aligned}
R_{px} &= \sum_{i=1}^{m}\left(f_{ix}\right) + f_{px} \\
R_{py} &= \sum_{i=1}^{m}\left(f_{iy}\right) + f_{py} \\
R_{pz} &= \sum_{i=1}^{m}\left(f_{iz}\right) + f_{pz}
\end{aligned}
\qquad 2.5.24
$$

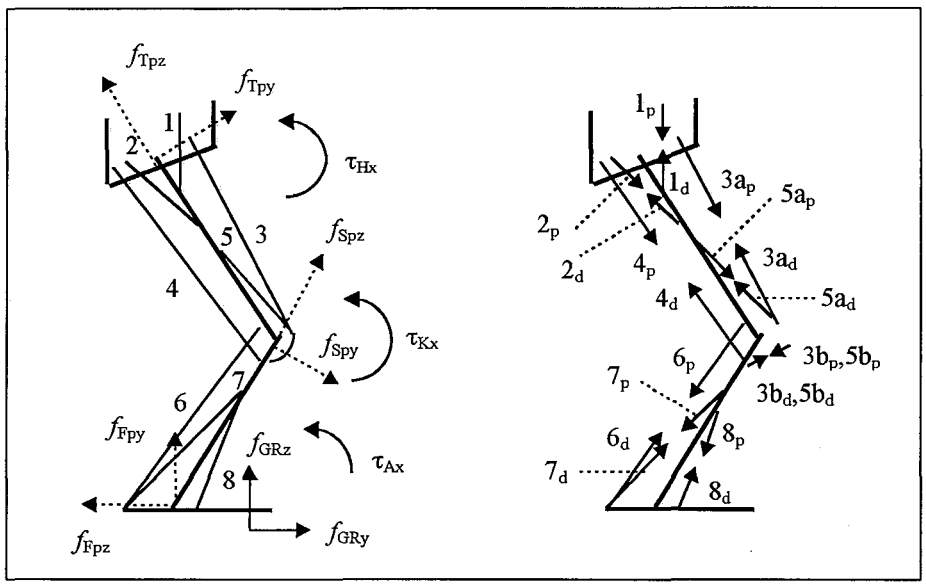

Figure 2.5.9 Free body diagram representing moments and forces of the lower limb. Resultant joint moments of the hip, knee, and ankle are given by τ_{Hx}, τ_{Kx}, and τ_{Ax} respectively. Resultant proximal joint forces of the thigh, shank, and foot are given by (f_{Tpy}, f_{Tpz}), (f_{Spy}, f_{Spz}), and (f_{Fpy}, f_{Fpz}) respectively. Ground reaction force is given by (f_{GRy}, f_{GRz}). Eight muscle-tendon elements are shown.

For the simplified model of the lower limb (Fig. 2.5.9), the equipolant force equations are:

$$
\begin{aligned}
R_{Tpx} &= f_{1bx} + f_{2bx} + f_{3bx} + f_{4bx} + f_{Tpx} \\
R_{Tpy} &= f_{1by} + f_{2by} + f_{3by} + f_{4by} + f_{Tpy} \\
R_{Tpz} &= f_{1bz} + f_{2bz} + f_{3bz} + f_{4bz} + f_{Tpz} \\
\\
R_{Spx} &= f_{3dx} + f_{4bx} + f_{5dx} + f_{6bx} + f_{Spx} \\
R_{Spy} &= f_{3dy} + f_{4by} + f_{5dy} + f_{6by} + f_{Spy} \\
R_{Spz} &= f_{3dz} + f_{4bz} + f_{5dz} + f_{6bz} + f_{Spz} \\
\\
R_{Fpx} &= f_{6bx} + f_{7bx} + f_{8bx} + f_{Fpx} \\
R_{Fpy} &= f_{6by} + f_{7by} + f_{8by} + f_{Fpy} \\
R_{Fpz} &= f_{6bz} + f_{7bz} + f_{8bz} + f_{Fpz}
\end{aligned}
\qquad 2.5.25
$$

Similar expressions can be derived for the resultant joint forces occurring at the distal end of each segment:

$$
\begin{aligned}
-R_{Pdx} &= f_{1ax} + f_{2ax} + f_{3ax} + f_{4ax} + f_{Pdx} \\
-R_{Pdy} &= f_{1ay} + f_{2ay} + f_{3ay} + f_{4ax} + f_{Pdy} \\
-R_{Pdz} &= f_{1az} + f_{2az} + f_{3az} + f_{4ax} + f_{Pdz}
\end{aligned}
$$

$$
\begin{aligned}
-R_{Tdx} &= f_{3cx} + f_{5cx} + f_{4ax} + f_{6ax} + f_{Tdx} \\
-R_{Tdy} &= f_{3cy} + f_{5cy} + f_{4ay} + f_{6ay} + f_{Tdy} \\
-R_{Tdz} &= f_{3cz} + f_{5cz} + f_{4az} + f_{6az} + f_{Tdz}
\end{aligned}
\qquad 2.5.26
$$

$$
\begin{aligned}
-R_{Sdx} &= f_{6ax} + f_{7ax} + f_{8ax} + f_{Sdx} \\
-R_{Sdy} &= f_{6ay} + f_{7ay} + f_{8ay} + f_{Sdy} \\
-R_{Sdz} &= f_{6az} + f_{7az} + f_{8az} + f_{Sdz}
\end{aligned}
$$

with:

$$
\begin{bmatrix} R_{Sdx} \\ R_{Sdy} \\ R_{Sdz} \end{bmatrix} = [R] \begin{bmatrix} R_{Apx} \\ R_{Apx} \\ R_{Apx} \end{bmatrix}
$$

$$
\begin{bmatrix} R_{Tdx} \\ R_{Tdy} \\ R_{Tdz} \end{bmatrix} = [R] \begin{bmatrix} R_{Spx} \\ R_{Spx} \\ R_{Spx} \end{bmatrix}
$$

$$
\begin{bmatrix} R_{Hdx} \\ R_{Hdy} \\ R_{Hdz} \end{bmatrix} = [R] \begin{bmatrix} R_{Tpx} \\ R_{Tpx} \\ R_{Tpx} \end{bmatrix}
$$

Substituting the equipolance force and moment equations for a segment into the equations of motion involving resultant forces and moments results in Euler's translation and rotational equations of motion. Taking the thigh as an example and expanding equations (2.5.14) and (2.5.15):

$$
\begin{aligned}
\sum f_{Tx} &= f_{1bx} + f_{2bx} + f_{3bx} + f_{Tpx} + f_{3cx} + f_{5cx} + f_{6ax} + f_{Tdx} + m_T \cdot g_{Tx} \\
\sum f_{Ty} &= f_{1by} + f_{2by} + f_{3by} + f_{Tpy} + f_{3cy} + f_{5cy} + f_{6ay} + f_{Tdy} + m_T \cdot g_{Ty} \\
\sum f_{Tz} &= f_{1bz} + f_{2bz} + f_{3bz} + f_{Tpz} + f_{3cz} + f_{5cz} + f_{6az} + f_{Tdz} + m_T \cdot g_{Tz}
\end{aligned}
\qquad 2.5.27
$$

$$
\begin{aligned}
\sum \tau_{Tx}^{Dist} &= m_T \cdot g_{Tz} \cdot \bar{y}_T - m_T \cdot g_{Ty} \cdot \bar{z}_T + f_{1bz} \cdot y_{1b} - f_{1by} \cdot z_{1b} + f_{2bz} \cdot y_{2b} \\
&\quad - f_{2by} \cdot z_{2b} + f_{3bz} \cdot y_{3b} - f_{3by} \cdot z_{3b} + f_{4bz} \cdot y_{4b} - f_{4by} \cdot z_{4b} \\
&\quad + f_{3cz} \cdot y_{3c} - f_{3cy} \cdot z_{3c} + f_{4az} \cdot y_{4a} - f_{4ay} \cdot z_{4a} + f_{5cz} \cdot y_{5c} \\
&\quad - f_{5cy} \cdot z_{5c} + f_{6az} \cdot y_{6a} - f_{6ay} \cdot z_{6a} + R_{Tpz} \cdot y_{Tp} - R_{Tpy} \cdot z_{Tp} \\
\sum \tau_{Ty}^{Dist} &= m_T \cdot g_{Tx} \cdot \bar{z}_T - m_T \cdot g_{Tz} \cdot \bar{x}_T + f_{1bx} \cdot z_{1b} - f_{1bz} \cdot x_{1b} + f_{2bx} \cdot z_{2b} \\
&\quad - f_{2bz} \cdot x_{2b} + f_{3bx} \cdot z_{3b} - f_{3bz} \cdot x_{3b} + f_{4bx} \cdot z_{4b} - f_{4bz} \cdot x_{4b} \\
&\quad + f_{3cx} \cdot z_{3c} - f_{3cz} \cdot x_{3c} + f_{4ax} \cdot z_{4a} - f_{4az} \cdot x_{4a} + f_{5cx} \cdot z_{5c} \\
&\quad - f_{5cz} \cdot x_{5c} + f_{6ax} \cdot z_{6a} - f_{6az} \cdot x_{6a} + R_{Tpx} \cdot z_{Tp} - R_{Tpz} \cdot x_{Tp} \\
\sum \tau_{Tz}^{Dist} &= m_T \cdot g_{Ty} \cdot \bar{x}_T - m_T \cdot g_{Tx} \cdot \bar{y}_T + f_{1by} \cdot x_{1b} - f_{1bx} \cdot y_{1b} + f_{2by} \cdot x_{2b} \\
&\quad - f_{2bx} \cdot y_{2b} + f_{3by} \cdot x_{3b} - f_{3bx} \cdot y_{3b} + f_{4by} \cdot x_{4b} - f_{4bx} \cdot y_{4b} \\
&\quad + f_{3cy} \cdot x_{3c} - f_{3cx} \cdot y_{3c} + f_{4ay} \cdot x_{4a} - f_{4ax} \cdot y_{4a} + f_{5cy} \cdot x_{5c} \\
&\quad - f_{5cx} \cdot y_{5c} + f_{6ay} \cdot x_{6a} - f_{6ax} \cdot y_{6a} + R_{Tpy} \cdot x_{Tp} - R_{Tpx} \cdot y_{Tp}
\end{aligned}
\qquad 2.5.28
$$

Note that the moments about the hip, τ_{Hip}, are calculated relative to the proximal joint centre. The vector (x_{Tp}, y_{Tp}, z_{Tp}) is the position of the proximal joint centre relative to the distal joint centre, and the following are equivalent: $f_1 \cdot (f_{ux1a})$ and f_{1ax}.

The unit vectors in the direction of the line of action of individual muscle elements (f_{ux}, f_{uy}, f_{uz}) will depend on each muscle's instantaneous position relative to each segment. The components of bone-on-bone forces directed parallel to the long axis of each segment (f_{Tpz}, f_{Spz}, f_{Fpz}) gives the respective joint compressive forces, while the components of bone-on-bone force perpendicular to the long axis of each segment ($f_{Tpx}, f_{Tpy}, f_{Spx}, f_{Spy}, f_{Fpx}, f_{Fpy}$) give the respective joint shear forces. When interpreting the direction of resultant force, moments or bone-on-bone forces, a positive sign means that it is acting in the same direction as shown on the free body diagram (Fig. 2.5.6, Fig. 2.5.7 and Fig. 2.5.9).

The choice of whether to use equations (2.5.22) and (2.5.25) to sum moments and forces relative to the proximal end, or alternatively using equations (2.5.23) and (2.5.26) to sum moments and forces relative to the distal end of each segment is largely up to personal preference. Further discussion on conventions for placing body-fixed axes is made in Section 3.3. However, if the body-fixed axes are placed at the distal end of each segment, and local co-ordinates of muscle origins and insertions are known relative to these axes, then it would be efficient to use equations (2.5.23) and (2.5.26)

2.5.4.3 Solving for resultant joint moments and resultant joint forces

With an accurate description of the kinematics of the movement, mass and inertial properties of segments and external forces, resultant joint forces and resultant joint moments can be calculated using the equations of motion (Section 2.5.4.1). This is done by starting at a segment where the distal forces acting on the segment are known. In a link-segment system of the human body, the most distal link will not contain resultant forces at a distal joint centre, as in the feet or hands (equations 2.5.10 and 2.5.14). Knowing the mass, acceleration of the centre of mass and all external force acting on the most distal segment, the resultant forces of the proximal joint can be calculated. For the next linked segment, the distal resultant joint forces, mass and acceleration of the centre of mass are now known, and proximal resultant joint forces can be calculated. For the two linked segments, respective distal and proximal resultant joint forces acting across the joint are equal in magnitude. In a similar fashion, resultant joint forces and resultant joint moments can be calculated for the whole linked segment system.

In this progressive manner of calculating resultant force, the trunk should be avoided if possible due to the assumptions that are made in regard to its motion as a rigid link-segment. The trunk's motion is complex where each vertebrae may be thought of as link-segment capable of flexion, extension and rotation. Inherent errors arise in representing the trunk as one or two link-segments. Therefore in a model of the lifting task for example, the forces acting on the arms should be calculated from known loads on the hands rather than from ground reaction forces acting at the feet.

2.5.5 Joint centre

Accurate estimations of joint centre locations are required for the rigid body analysis of motion. In determining resultant joint moments for a rigid body system from the equations of motion, joint centre locations determine points at which forces are transmitted between segments and about which moments are calculated. When determining individual muscle forces, moment arms appear in the constraint equations (equipolance equations which equate muscle forces to resultant joint moments) used in optimisation methods (Herzog, 1987). Moment arms may also appear in the cost function utilised in optimisation methods (Herzog, 1987) or be dependent on the moment arm (Seireg & Arvikar, 1973; Pedotti, 1978;

Crowninshield & Brand, 1987). An exception is the cost function proposed by Dul, et al. (1984a) where the minimum-fatigue criteria is independent of moment arm. In order to calculate an individual muscle's moment arms, the line of action of the muscle-tendon complex and the joint centre need to be defined (Herzog, 1996). An exception to this is determining moment arms by the tendon travel approach of Spoor, et al. (1990).

A joint centre can be defined as a point representing segment contact through which bone-on-bone forces are considered to be transferred. This point represents a mean point of the total contact surface and is not fixed with respect to the two joining segments. Joint centres can be determined using either a functional or predictive approach (Leardini, et al., 1999). In the functional approach a joint centre is taken as the pivot point associated with segment rotations while in the predictive method, regression equations are used to describe normal joint position, usually with respect to bony landmarks.

2.5.5.1 Prediction approach

In the predictive approach, joint centres are commonly described as a fixed point. This assumption reduces the complexity of human joints to simplified geometric structures of fixed centres of rotation. Joint centres would ideally be located through radiographic means, and the location of the joint centres expressed relative to external bony landmarks. In most studies however, direct measurements are not available, and predictive methods are used to locate joint centres based on radiographic and cadaver studies and expressed relative to external bony landmarks (Seidel, et al., 1995; Herzog, 1996; de Leva, 1996; Leardini, et al., 1999). For the lower limb, the following have been used:

Ankle joint centre: In a transverse plane at the level of the inferior tip of the lateral malleolus of the fibula and a point 5 mm (Zatsiorsky, 1998) or 6 mm (de Leva, 1996) inferior to the medial malleoli of the tibia.

Knee joint centre: (Zatsiorsky, 1998) Midpoint of a line joining the centres of the posterior convexities of the femoral condyles, and (de Leva, 1996) in a transverse plane 32 mm or 34 mm superior to the tibiale for females and males respectively.

Hip joint centre : (Seidel, et al., 1995) Pelvic axes placed at mid-ASIS and medio-lateral passing through both ASIS and anterio-superior passing through pubic symphysis. Hip joint centre was located 36% of pelvic width laterally, 34% of pelvic depth posterior, and 79% of pelvic height inferior. Pelvic width is from right to left ASIS, pelvic height is from mid-ASIS to pubic symphysis, and pelvic depth is diagonal distance between contra-lateral ASIS and PSIS.

Hip joint centre : (Leardini, et al., 1999) For the male pelvis, with pelvic axes placed at mid-ASIS and medio-lateral axis passing through both ASIS and the anterio-superior axis passing through mid-PSIS. Hip joint centre was located 39% of pelvic width laterally, 31% of pelvic depth posterior, and 9.6% of leg length inferiorally. Pelvic width is from right to left ASIS, leg length is from ASIS to medial malleolus, and pelvic depth is mid-ASIS to mid-PSIS.

Seidel, et al. (1995) and Leardini, et.al. (1999) found that in the pelvis axis system, the hip joint centre co-ordinates in the medio-lateral, superio-inferior and anterio-posterior directions were best correlated with pelvic width, pelvic or thigh length, and pelvic depth respectively. They concluded that each co-ordinate of hip joint location should be normalised to the corresponding dimension of the pelvis, when applying pelvic co-ordinate data to different subjects. However, pelvic width was found not to be a good predictor of pelvic depth or height, and pelvic depth was not found to be a good predictor of pelvic height.

A disadvantage of the regression approach is the non-specific nature of the prediction, although relative measures are often used that are based on mean joint location and mean segment dimensions. When investigating clinical conditions, greater accuracy is often required, hence the need for subject-specific information on joint centre locations. However, radiographic measures are not always available. It has also been argued that joint axes of rotation and joint centres are not stationary but vary through the range of motion, and may vary widely between subjects (Zatsiorsky, 1998).

2.5.5.2 Functional approach

To improve accuracy, attempts have been made to represent centres of joint rotation and physical joint centres as moving points, which lead to the development of techniques for

calculating instantaneous centres or rotation (ICR) and instantaneous helical axes (IHR) to better describe the rotations occurring at a joint. Physical joint centres have also been estimated by ICR, pivot point of IHA or moving contact point (Herzog, 1996; Zatsiorsky, 1998, Leardini, et al., 1999). Herzog (1996) points out two disadvantages of using a moving contact point for the joint centre: i) the joint centre is hard to determine and ii) the moment produced by the distributed joint contact force cannot be ignored.

2.5.5.2.1 Function approach - planar motion

For planar motion, a finite segment movement can be viewed as a combination of both translation within a plane and rotation about an axes perpendicular to the plane. In the planar case the rotational axes defines the centre of rotation. The centre of rotation is not fixed with respect to the moving segment but migrates with time. As the movement progresses, the changing relative position of the centre of rotation maps out a path called a 'centrode' (Zatsiorsky, 1998). Therefore during any finite change in segment position, the centre of rotation is also changing. In calculating the instantaneous centre of rotation (ICR), the finite difference needs to be sufficiently small so that the changes in finite centre of rotation are also small and approach that of the ICR.

In defining ICR (Zatsiorsky, 1998) as a point about which all points of a segment rotate. This point is not necessarily located on, or fixed in position with respect to the moving segment or any other segment. The movement of the segment with respect to any other point involves translation and rotation. The ICR therefore, does not represent a point of contact between segments or any other physical point.

Methods to locate ICR in the planar case are given by Zatsiorsky (1998).

2.5.5.2.1.1 Reuleaux method

A line connecting two consecutive positions of a single point approximates the direction of the velocity vector of the mid-point. A perpendicular to this vector at the mid-point then represents a radial line passing through the centre of rotation. If the mid-point and perpendiculars of two or more points are found, then the intersection of the radial lines is the mean centre of rotation (ICR) for the change in segment position (Fig. 2.5.10). The

mathematical derivation of the Reuleaux method for calculating ICR is given by Zatsiorsky (1998), where ICR is given by:

$$x_{ICR} = \frac{1}{2} \cdot \frac{(y_4 - y_3)\left(x_2^2 - x_1^2 + y_2^2 - y_1^2\right) + (y_1 - y_2)\left(x_4^2 - x_3^2 + y_4^2 - y_3^2\right)}{(y_4 - y_3)(x_2 - x_1) - (y_2 - y_1)(x_4 - x_3)} \qquad 2.5.29$$

$$y_{ICR} = \frac{1}{2} \cdot \frac{(x_3 - x_4)\left(x_2^2 - x_1^2 + y_2^2 - y_1^2\right) + (x_2 - x_1)\left(x_4^2 - x_3^2 + y_4^2 - y_3^2\right)}{(y_4 - y_3)(x_2 - x_1) - (y_2 - y_1)(x_4 - x_3)} \qquad 2.5.30$$

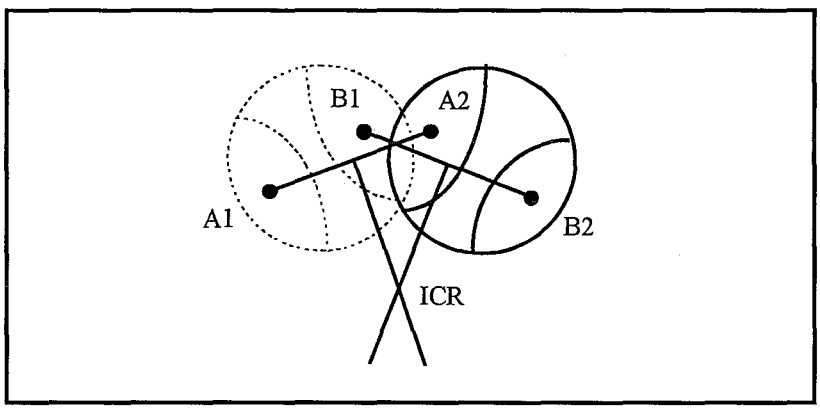

Figure 2.5.10 Reuleaux method for locating an instantaneous centre of rotation.

2.5.5.2.1.2 Point of zero velocity

The general equation relating the inertial velocity and local velocity of a point in a moving frame is:

$$\mathbf{V}_P = \mathbf{V}_L + \omega \times \mathbf{r}_P + \mathbf{v}_P \qquad 2.5.31$$

where

$\mathbf{V}_P$ = velocity of point in global frame
$\mathbf{V}_L$ = velocity of origin of local frame
ω = angular velocity of local frame
$\mathbf{r}_P$ = location vector of point in local frame
$\mathbf{v}_P$ = velocity of point in local frame

The ICR is the instantaneous point on the inertia frame about which all points of the moving frame are instantaneously rotating. Therefore the ICR is at rest with respect to both the inertia and moving frames of reference ($\mathbf{Vc} = \mathbf{vc} = 0$). Therefore,

$$0 = \mathbf{V}_L + \omega \times \mathbf{r}_C \qquad 2.5.32$$

where:
$\mathbf{r}_C$ = position velctor of ICR

For a rigid body ($\mathbf{v}_P = 0$), substituting equation 2.5.32 into equation 2.5.31, yields (Zatsiorsky, 1998);

$$\mathbf{V}_P = \omega \times \mathbf{r}_P - \omega \times \mathbf{r}_C = \omega \times (\mathbf{r}_P - \mathbf{r}_C) \qquad 2.5.33$$

in vector components:

$$\begin{bmatrix} \dot{x} \\ \dot{y} \\ 0 \end{bmatrix} = \begin{bmatrix} 0 & 0 & \omega_z \end{bmatrix} \times \begin{bmatrix} r_{px} \\ r_{py} \\ 0 \end{bmatrix} - \begin{bmatrix} 0 & 0 & \omega_z \end{bmatrix} \times \begin{bmatrix} r_{cx} \\ r_{cy} \\ 0 \end{bmatrix} \qquad 2.5.34$$

expanding gives scalar equations:

$$\begin{aligned} \dot{x} &= r_{cy}.\omega_z - r_{py}.\omega_z \\ \dot{y} &= r_{px}.\omega_z - r_{cx}.\omega_z \end{aligned} \qquad 2.5.35$$

and on rearranging:

$$r_{cy} = r_{py} + \frac{\dot{x}}{\omega_z}$$
$$r_{cx} = r_{px} - \frac{\dot{y}}{\omega_z} \qquad 2.5.36$$

Therefore, in the planar case if the angular velocity of the moving segment is known, in addition to the local co-ordinates and global velocity of a point on the segment, then the ICR can be calculated for the segment.

2.5.5.2.1.3 Kennedy's theorem

When three bodies have planar motion, their instant centres lie on a straight line, called the line of centres. For three linked segments, three ICR exist (C_{12}, C_{13} and C_{23}) where Cij is a point where segment j has zero velocity with respect to segment i (Fig. 2.5.11). The mathematical derivation of Kennedy's theorem for calculating ICR is given by Zatsiorsky (1998), where C_{13} is given by (Fig. 2.5.11):

$$\overline{C_{13}} = \overline{C_{23}} \cdot \left(1 - \frac{\dot{\theta}_1}{\dot{\theta}_2}\right) \qquad 2.5.37$$

where:

C_{12} = instantaneous center of rotation of segment 2 with respect to segment 1.
$\overline{C_{13}}$ = position vector of the instantaneous center of rotation of segment 3. with respect to segement 1, with origin at C_{12}.
$\overline{C_{23}}$ = position vector of the instantaneous center of rotation of segment 3 with respect to segement 2, with origin at C_{12}.
$\dot{\theta}_1$ = angular velocity of the second segment, with respect to the first segment.
$\dot{\theta}_2$ = angular velocity of the third segment, with respect to the first segment.

This states that the position of C_{13} is dependent on the ratio of the angular velocities of the two joints comprising a three segment system. If the angular velocity of the second segment is zero relative to the first segment, then C_{13} is equal to C_{23}. If the angular velocity of the second and third segments are equal, relative to the first segment ($\dot{\theta}_3 = 0$, Fig. 2.5.11), then C_{13} is equal to C_{12}.

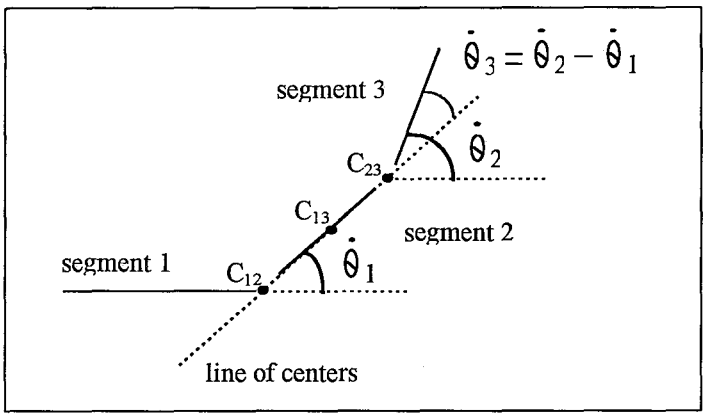

Figure 2.5.11. Instantaneous centres of rotation for three link planar system.

With application to the lower limb comprising foot, shank and thigh, the line of centres joins the ICR of the shank relative to the foot and the ICR of the thigh relative to the shank (Fig. 2.5.12). The ICR of the thigh relative to the foot lies on the line of centres at a position determined by the angular velocities of the shank and thigh relative to the foot.

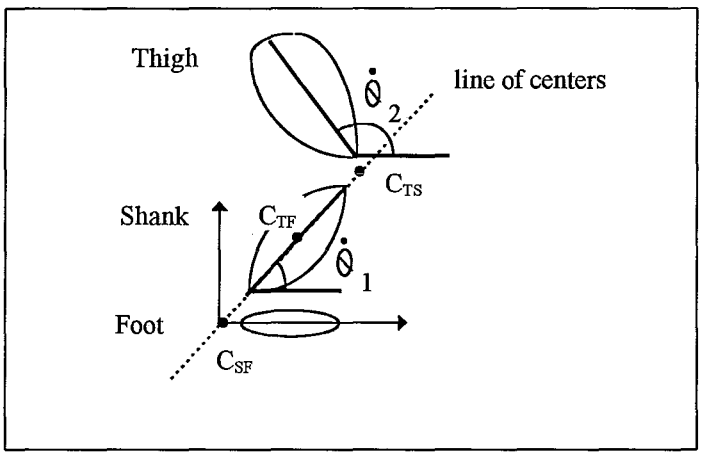

Figure 2.5.12 Instantaneous centres of rotation for three segments of the lower limb.

2.5.5.2.1.4 Measurement error

Planar methods of calculating ICR suffer from measurement errors (Zatsiorsky, 1998). In the two dimensional approach, it is necessary for the movement plane of the segment to be perpendicular to the optical axes viewing the motion (Zatsiorsky, 1998). When this is the case, then pure rotation of the segment or points on the segment will trace out concentric arcs in the

image plane. In practice, the segment movement plane and two dimensional image plane will seldom align for the duration of three dimensional motion. With mal-alignment in image and movement planes, segment rotation will trace out ellipses in the image plane leading to errors in calculating finite joint centres (Zatsiorsky, 1998). Measurement error also results from the accuracy with which locations of points on the segment are measured in the image plane. Measurement error will introduce translations and rotations to the calculated segment position. The time period required to measure changes in segment position needs to be sufficiently large to measure a finite rotation given errors in position data. As proportionally large translation errors and relatively small rotations can result in large errors in centres of rotation and pure translation of the segment an undefined ICR will result.

In summary, the existence of an ICR requires that, at any instant in time the segment rotates about an instantaneous point. This point is not associated with any physical point on the segment. During any finite time period, the ICR is not considered to be fixed but moves in time producing and instant centre pathway. The smaller the period between successive segment positions, the closer a calculated finite centre of rotation approximates the ICR. At the same time if the rotation is small or similarly, the time period is to short, calculating ICR suffers from potentially large inaccuracies due to measurement error (Zatsiorsky, 1998). Zatsiorsky (1998) further states that because of the complexities of motion of may joints (namely the existence of pure rotation), and measurement error, the measurement of finite axes of rotation can be an unreliable estimator of instantaneous centres of rotation. Smoothing successive marker positions prior to calculating ICR may help reduce variability and produce more meaningful results (Zatsiorsky, 1998).

Planar methods are, in general, not suitable for the analysis of joint motion for the following reasons:

i) Joint rotations can seldom be considered as occurring purely in one plane with a constant axis of rotation. Joint movements which may be considered planar may well involve migration of the IAR;
ii) Planar methods are susceptible to measurement errors due to misalignment of image plane (optical axis) and joint movement plane (IAR); and
iii) Joint axes of rotation might not align with anatomic planes or segment body-fixed axes defined from anatomical landmarks.

2.5.5.2.2 Function approach - non-planar motion

In this section, two methods for describing non-planar joint rotation are discussed - namely the instantaneous centre of rotation and the instantaneous helical axis.

2.5.5.2.2.1 Instantaneous centre of rotation

The calculation of instantaneous centre of rotation (ICR) in the planar case as presented in equation 2.5.34, can be expanded to three dimensional motion. On rewriting 2.5.34:

$$\begin{bmatrix} \dot{x} \\ \dot{y} \\ \dot{z} \end{bmatrix} = \begin{bmatrix} \omega_x & \omega_y & \omega_z \end{bmatrix} \times \begin{bmatrix} r_{px} \\ r_{py} \\ r_{pz} \end{bmatrix} - \begin{bmatrix} \omega_x & \omega_y & \omega_z \end{bmatrix} \times \begin{bmatrix} r_{cx} \\ r_{cy} \\ r_{cz} \end{bmatrix} \qquad 2.5.38$$

expanding gives scalar equations:

$$\begin{aligned} \dot{x} &= r_{pz}.\omega_y - r_{py}.\omega_z - r_{cz}.\omega_y + r_{cy}.\omega_z \\ \dot{y} &= r_{px}.\omega_z - r_{pz}.\omega_x + r_{cz}.\omega_x - r_{cx}.\omega_z \\ \dot{z} &= r_{py}.\omega_x - r_{px}.\omega_y - r_{cy}.\omega_x + r_{cx}.\omega_y \end{aligned} \qquad 2.5.39$$

on rearranging:

$$\begin{aligned} r_{cz}.\omega_y - r_{cy}.\omega_z &= r_{pz}.\omega_y - r_{py}.\omega_z - \dot{x} \\ r_{cx}.\omega_z - r_{cz}.\omega_x &= r_{px}.\omega_z - r_{pz}.\omega_x - \dot{y} \\ r_{cy}.\omega_x - r_{cx}.\omega_y &= r_{py}.\omega_x - r_{px}.\omega_y - \dot{z} \end{aligned} \qquad 2.5.40$$

these equation can expressed as matrices and solved by matrix methods.

$$\begin{bmatrix} 0 & -\omega_z & \omega_y \\ \omega_z & 0 & -\omega_x \\ -\omega_y & \omega_x & 0 \end{bmatrix} \begin{bmatrix} r_{cx} \\ r_{cy} \\ r_{cz} \end{bmatrix} = \begin{bmatrix} r_{pz}.\omega_y - r_{py}.\omega_z - \dot{x} \\ r_{px}.\omega_z - r_{pz}.\omega_x - \dot{y} \\ r_{py}.\omega_x - r_{px}.\omega_y - \dot{z} \end{bmatrix} \qquad 2.5.41$$

Leardini, et al. (1999) tested the validity of the centre of rotation as a functional estimation of hip joint centre. In their experiment. four markers were attached to the pelvis and thigh, and their three dimensional position reproduced in hip movements involving flexion/extension and abduction/adduction. The hip joint centre was the centre of the optimal spherical surface that fitted the trajectory of the thigh frame origin. No differences in HJC prediction were found between the two different movements, and the standard deviation for individual subjects in predicted HJC was in the range 2-4 mm. When compared with HJC location obtained from roentgen stero-photogrammetric analysis, the functional method proved an accurate and reliable predictor, with mean differences (functional minus roentgenographic) in medio-lateral, superio-inferior and anterio-posterior co-ordinates of -3.6 mm (std. = 3.5 mm), -1.7 mm (std. = 6.4 mm) and 4.2 mm (std. = 6.7 mm) respectively. Carrying out a paired t-test of the data of Leardini, et al. (1999), the differences in function and roentgenographic HJC superio-inferior and anterio-posterior positions were not significantly different ($p = 0.39$ and 0.06 respectively), however a significant difference was seen in the medio-lateral position ($p = 0.006$).

2.5.5.2.2.2 Helical axis

The three dimensional position of a rigid body can be represented by a translation along and a rotation about an axis, called the helical or screw axis. As with instantaneous axes of rotation, helical axes change position and orientation with time as the three dimensional location of the segment changes. The path of the instantaneous helical axes (IHA) over a period of time is called the axode and the surface produced by the migration of the axis is referred to as the helical axis surface. Unlike Cardan or Euler rotation sequences to describe segment orientation, which are dependent on the direction of the body fixed axes (the respective axes corresponding to longitudinal, sagital and transverse anatomical axis) and rotational order, the screw axis and associated rotation are independent of the criteria used to define body fixed axes with respect to cardinal anatomical planes. Fioretti, et al. (1991) assessed the IHA as a functional tool in analysing joint motion. When applied to a physical joint model of the knee, the authors found that a weighted pivot point (WPP), defined as a point closest to all IHA's in a weighted least squares sense, was a good approximation for the joint centre, with a reported error of 2.3 mm. The mean helical axis (MHA), referred to as an axis passing through the WPP and minimising the mean square distance between an arbitrary point on the axis and the set of all IHA's, was within one degree of the measured axis of rotation. On live subjects, the

WPP of the hip proved to be a repeatable estimate of joint centre (within 0.01 meter of the mean value), although a radiographic based comparison was not available. The authors cautioned that the IHA was unreliable for the knee at slow rotational speeds during stance phase (angular velocity < 2 rad/sec), and that functional use of the IHA for the knee was limited due to measurement error arising from skin motion artefact of segment markers. The experimental protocol involved marker triads taped to the shank and thigh. Blankevoort, et al. (1990) in examining knee flexion, found the helical axis followed two distinct pathways depending on whether an internal or external axial load was applied to the long axis of the tibia during knee flexion. The knee joint, as evidenced by the oblique and varying helical axes, did not exhibit pure flexion with respect to the anatomical planes, but rather a combination of flexion and axial rotation. As cadaver knees were tested, ligament structures were likely to have provided motion constraints and, in doing so, determine the path of the joint and helical axis in response to external axial loading in the absence of neural and muscular responses. However, the natural locking action of the knee when extending to limit axial rotation at full extension, would suggest that similar patterns would be expected in live subjects undergoing knee extension when internal or external torques were applied to the tibia.

For a series of IHA calculated over a period of joint motion, a mean pivot point can be defined as a point of intersection for all IHA's over this period. Given that each axis is defined by an arbitrary point on the axis and a vector in the direction of the axis, then the parametric equation of the axis is (Fig. 2.5.13):

$$\begin{aligned} x &= px + t.a \\ y &= py + t.b \\ z &= pz + t.c \end{aligned} \qquad 2.5.42$$

where:

(x, y, z) = arbitary point on line.
(px, py, pz) = known point on line.
(a, b, c) = vector parallel to line.
t = parameter describing arbitary point.

For any point to lie on the IHA, then a vector from this point to any point located on the axis and a vector parallel to the axis, must also be parallel:

$$(x - px \quad y - py \quad z - pz) \times (a \quad b \quad c) = 0 \qquad 2.5.43$$

on expanding:

$$\begin{aligned} (y - py).c - (z - pz).b &= 0 \\ (z - pz).a - (x - px).c &= 0 \\ (x - px).b - (y - py).a &= 0 \end{aligned} \qquad 2.5.44$$

and rearranging:

$$\begin{aligned} c.y - b.z &= py.c - pz.b \\ a.z - c.x &= pz.a - px.c \\ b.x - a.y &= px.b - py.a \end{aligned} \qquad 2.5.45$$

For a single point to lie at the intersection of a number lines, that is the vectors formed by itself and any point on those lines, must be parallel to each respective vector located on each line, resulting in a series of equations to be solved simultaneously to give a mean pivot point. In matrix form:

$$\begin{bmatrix} 0 & c_1 & -b_1 \\ -c_1 & 0 & a_1 \\ b_1 & -a_1 & 0 \\ \vdots & \vdots & \vdots \\ b_n & -a_n & 0 \end{bmatrix} \cdot \begin{bmatrix} x_{pp} \\ y_{pp} \\ z_{pp} \end{bmatrix} = \begin{bmatrix} py_1.c_1 - pz_1.b_1 \\ pz_1.a_1 - px_1.c_1 \\ px_1.b_1 - py_1.a_1 \\ \vdots \\ px_n.b_n - py_n.a_n \end{bmatrix} \qquad 2.5.46$$

where:

(x_{pp}, y_{pp}, z_{pp}) = co-ordinates of mean pivot point.

If the axes used to describe the foot position are aligned with segment sagittal, transverse and longitudinal planes, a rotation about this joint will result in three distinct Eulerian rotations describing the movement of the foot. Similarly for the knee, if the rotational axes of the joint do not coincide with segment axes, then a pure joint rotation will be measured as three distinct Eularian rotations. Eularian, Cardan or Screw axes can equally be used to describe the dynamics of rigid body motion (Small, et al., 1982). In describing anatomically meaningful rotations, care must therefore be taken when distinguishing between rotations about body-fixed axes (usually defined from anatomical landmarks) and joint axes determined from joint structure. Greene & Heckman (1994) present the rotational order and defined starting points from which rotations are measured for various joints in the clinical setting.

The accuracy and reliability of calculated IHA or ICR and the meaningfulness of centrodes (ICR) or axodes (IHA) paths of human joints are dependent on the accuracy of measured segment location during movement. The motion occurring at a joint, in terms of both translation and rotation, depends on the shape of the joint surfaces and their congruity (Zatsiorsky, 1998). The more the joint surfaces approach simple congruent curved surfaces with similar radii of curvature, such as spheres or cylinders, the more stationary are the axes of rotation and the smaller the translation movements (Zatsiorsky, 1998). For joints with congruent joint surfaces of fixed radii of curvature and coincident centres of rotation (for example, simple hinge and ball and socket joints that do not allow translation within the joint), then the joint centre and ICR describe the same point and the instantaneous helical axis also passes through this point. In human joints, the axes of rotation have been reported to vary through the range of motion and vary widely between individuals (Zatsiorsky, 1998). The extent to which the ICR and pivot point of IHA coincide with the physical joint centre will depend on the magnitude of translation occurring at the joint contact surfaces. The relationship of ICR or mean pivot point derived from IHA to instantaneous joint centres and the influence of joint translation, joint surface and longitudinal rotations on the estimation to joint centres needs to be addressed before making conclusions on the validity and accuracy of functional predictions of physical joint centres.

2.5.5.4 Moment arms - tendon travel approach

Moment arms can be determined from joint morphometry obtained by radiographic images of the joint complex. With the radiographic image plane parallel to the rotational plane, joint

centre position and tendon path can be determined (Spoor, et al., 1990). The moment arm with respect to this axis is the perpendicular distance from the tendon to joint axes in the plane of the rotation. For joints of several rotational degrees of freedom, the moment arm will depend on the rotation chosen and correct alignment of the radiographic image (Spoor, et al., 1990). The accuracy of moment arm measurement is affected by the ability to align optical and joint axes, and to determine joint centres and tendon paths. These are factors are affected by (Spoor, et al., 1990):

i) Changes in rotation axis and joint centre position with changes in joint angle;
ii) Muscle-tendon crossing more than one joint;
iii) Bulging of soft tissue, leading to changes in tendon position, with changes in joint angle; and
iv) The presence of retinaculum and tendon sheaths, making determination of tendon paths more difficult.

An alternative approach to determining moment arms is the tendon travel technique of Spoor, et al. (1990) and Spoor & Leeuwen (1992). For a change in joint angle, the effective moment arm is given by the amount of tendon travel (Fig. 2.5.14).

$$r_{\perp i}^{m} = \frac{\Delta T}{\Delta \theta} \qquad 2.5.47$$

where:

$r_{\perp i}^{m}$ = effective moment arm of muscle - tendon 'i'.
ΔT_i = tendon travel of muscle - tendon 'i'.
$\Delta \theta$ = change in joint angle in radians.

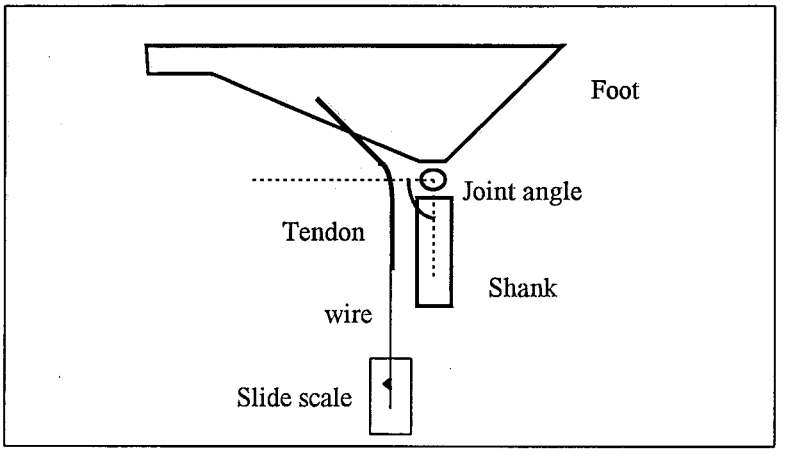

Figure 2.5.14 Tendon travel as a function of joint rotation. Tendon travel is measured on a slide scale for different joint angles.

An advantage of this technique is that it does not require knowledge of joint centre position, however it does require a knowledge of the muscle-tendon pathway and how the muscle tendon length changes with segment rotation. In the approach of Spoor, et al. (1990) and Spoor & Leeuwen (1992), this was achieved in cadaver joints by cutting the muscle-tendon complex in order to leave the insertion closest the joint and passage of the tendon intact. Fine wire attached to a sliding scale was then fixed to the free end of the tendon so that tendon travel as a function of joint angle could be determined. The tendon travel technique is well suited for determining muscle-tendon moments arms in cadaver experiments (Spoor, et al., 1990; Spoor & Leeuwen, 1992), and is preferred over other radiographic techniques (Spoor & Leeuwen, 1992; Herzog, 1996). As the tendon travel approach incorporates the notion of a moving joint centre and moving joint axes (Herzog, 1996), it brings together various structural properties of the tendon-joint complex (Spoor & Leeuwen, 1992). Spoor, et al. (1990) presented moment arms calculated for 13 muscles crossing the ankle, while Spoor & Leeuwen, (1992) presented nine muscle crossing the knee, and in both cases, cadavers and the tendon travel approach were utilised. These studies concluded that accurate moment arms can be attained from smoothed tendon travel versus joint angle data, and that individual muscle-tendon lengths and consequently moment arms cannot be adequately predicted from segment lengths and joint angles alone. It was also concluded that correct moment arms can produce considerable improvement of accuracy in biomechanical models.

Despite the tendon travel approach providing a relatively accurate way of measuring moment arms, the invasive nature of the approach means that at present it is limited to cadaver studies. In applying the technique to live subjects a possibility may lie in surgically fixing radio-opaque markers to the tendon and through medical imaging of the involved limbs at varying joint angles, reproduce the changes in tendon length with changes in joint angle. However, this is purely speculative, but with the possibilities of measuring moment arms *in vivo* the application of the tendon travel approach to live subjects deserves further investigation.

In the three dimensional modelling of human movement, researchers are faced with the task of determining moment arms from known three dimensional segment locations and a limited number of points to describe each muscle-tendon path (Fig. 2.5.15), usually constant relative to respective body-fixed axes. However, the accuracy of using the tendon travel approach in a three dimensional model of the musculo-skeletal system is unknown. If it is assumed that segment locations are accurately known, then tendon travel calculated from a limited number of body-fixed co-ordinates describing tendon path, will not take into account changing structural properties of the joint, or accurately reflect changes in tendon length with changes in joint angles (Fig. 2.5.15). To apply the tendon travel approach to the modelling of human movement improvements in the present methods of representing tendon paths are needed which accurately represent the changes in tendon length with changes in joint angle. Therefore, the tendon travel approach applied to cadaver studies may remain a criteria against which moment arms calculated from estimated jont centres and tendon paths are validated in the modelling of human movement. However, the tendon travel approach can provide valuable information on moment arms for accessing the accuracy of locating segment axes from external markers and the validity of co-ordinate data used to describe joint centres and muscle-tendon paths over a range of joint motions in modelling human movement.

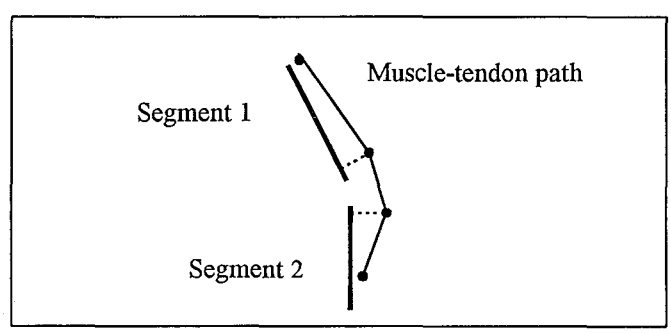

Figure 2.5.15 Muscle-tendon representation in rigid body model. Solid dots represent segment fixed points describing muscle-tendon path.

2.6 Muscle Force Prediction

Muscles are the means by which inertial and external forces are overcome and voluntary movements are produced. A knowledge of the time history of individual muscle forces will give insight into:

i) Forces on the skeletal system, including joint compressive and shear forces; and

ii) The generation of movement by the central nervous system (Herzog, 1996).

Knowledge of the individual muscle forces has application in the clinical study of pathological gait arising from surgical interventions and muscle activation abnormalities (Pierrynowski & Morrison, 1985). Prediction of forces that individual muscles exert in occupation and sport also has applications in efficiency of movement and risk of injury.

2.6.1 Approaches to obtaining muscle forces

Various method exist for the measurement or prediction of individual muscle forces, each with their advantages and disadvantages. Three methods are briefly introduced, consisting of direct measurement, electromyography and modelling. This is then followed by an extensive review of mathematical modelling as a means of predicting individual muscle forces.

2.6.1.1 Direct measurement

The direct measurement of ligament and joint contact forces within the human body is achieved with implanted force transducers, involving sophisticated instrumentation and recording techniques (Bogert, 1994). Due to the invasive nature the application of such techniques have been limited to a few structures, such as Achilles tendon, patella tendon and hip prostheses containing force measuring instruments. Also due to the invasive nature, the direct measurement approach is rarely adopted and is usually limited to case studies conducted under strict medical supervision. The extent to which the invasive techniques used compromise the movement under investigation is not known. However, such studies provide valuable information on internal forces during actual movements and can be used to validate other non-invasive analytical techniques (Bogert, 1994).

2.6.1.2 Electromyography (EMG)

The recording of electrical potentials of muscles by surface (non-invasive) or fine wire (invasive) electrodes provides a means of identifying temporal activation patterns of muscles or motor units. As such, EMG has been widely used in studies of biomechanics, ergonomics and motor control to gain insight into whole muscle and muscle fibre activation patterns in human movement (Basmajian & de Luca, 1985). Despite the appeal of EMG in measuring temporal aspects muscle activity, there is no simple relationship between EMG signal and muscle force. Bogert (1994) summarised two types of models used to estimate muscle forces from EMG signals. The first was a muscle model, typically based on Hill's muscle model, which predicts muscular force output from muscle excitation which intern was estimated from EMG signals (Hof & Berg, 1981). The second model was a regression model relating EMG and kinematics to resultant joint moments (Olney & Winter, 1985). The prediction of individual muscle force from EMG analysis is limited to muscles that are accessible by surface electrodes, do not suffer unduly form cross-talk and, in the calibration procedure, inverse dynamics can provide a good estimate of muscle force (Bogert, 1994).

2.6.1.3 Modelling

Mathematical modelling of the musculo-skeletal system, via an inverse dynamics approach, is the most widely used method of estimating internal forces. As seen in previous sections dealing with rigid body dynamics, this method represents the human body as a set of rigid segments connected by joints of varying degrees of freedom. A mathematical model, in the form of the equations of motion, is used to describe the dynamics of the rigid body segments. From the equations of motion, known external forces, and known inertial properties of the segments, resultant joint forces and resultant joint moments can be calculated. A further mathematical model is developed involving the equipolance equations, and equations describing the dynamics of muscle force generation, transmission of forces through tendons, and passive forces of ligaments. From the equipolance equation, and equations describing muscle force generation and transmission within the musculoskeletal system, individual muscle forces need to be established in an over-determined system. Optimisation methods are typically used to resolve the indeterminacy when modelling individual muscle forces via the use of a criteria (cost function) to assign muscle forces in a manner that reflects the neural process underlying muscle recruitment. Mathematical modelling techniques have seen continual

development as a way of indirectly determining the muscle activation patterns and internal force distribution within the musculo-skeletal system. As modelling and optimisation techniques continues to expand to describe the physiological processes of muscle excitation and contraction dynamics, as well as the neurological processes behind motor unit recruitment, the validity and accuracy of modelling the musculo-skeletal system will continue to increase.

2.6.2 Mathematical modelling

In the following sections, a mathematical approach is presented to obtain muscle forces from the equipolance equations. The redundancy problem is introduced along with reduction and optimisation methods used to solve the equipolance equations. The optimisation approach adopted in the present study is introduced. Several cost functions are introduce along with a 'soft' constrained criteria used in the present study. Limitation and sources of error resulting from the modelling process and choice of cost function are discussed. A mathematical model of the muscle-tendon is then reviewed, including excitation and contraction dynamics. A method for obtaining subject specific muscle model parameters is presented and a method for optimisation of muscle parameters is developed, along with methods for implementing the muscle model. To complete the modelling process techniques used to establish joint centres and moments arms are reviewed. Finally, a gradient projection algorithm is presented for attaining individual muscle forces.

2.6.2.1 Redundancy and the distribution problem

When attempting to determine individual muscle forces, the redundant nature of the musculo-skeletal system has to be overcome (Pierrynowski & Morrison, 1985; Collins, 1995; Buchanan & Shreeve, 1996; Herzog, 1996). The redundant nature is characterised by a large number of muscles crossing a given joint, hence the recruitment of muscles to generate a movement at the joint can be accomplished in more than one way. In the distribution problem we are concerned with predicting muscular recruitment when there are more unknowns in the form of structures transmitting forces across a joint, both muscles and ligaments, than there are degrees of freedom, or equivalently, equations of motion, for the joint. The result is an indeterminate system with a theoretically infinite number of solutions (Collins, 1995; Herzog 1996). A system in which an infinite combination of muscle forces could be derived in order to meet the required resultant joint forces and moments and satisfy the equations of motion, is

described as the distribution or redundancy problem (Herzog, 1996). The distribution problem is described by the joint equipolant equations which relate the resultant joint forces and resultant joint moments to the forces transmitted by individual muscles, ligaments and articular contact surfaces that cross a joint (Herzog & Binding, 1994; Herzog, 1996) (see Section 2.4):

$$\mathbf{R}_{jnt} = \sum_{i=1}^{m} \mathbf{F}_i^M + \sum_{j=1}^{l} \mathbf{F}_j^L + \sum_{k=1}^{b} \mathbf{F}_k^B \qquad 2.6.1a$$

$$\tau_{jnt} = \sum_{i=1}^{m} \left(\mathbf{r}_{\perp i}^M \times \mathbf{F}_i^M \right) + \sum_{j=1}^{l} \left(\mathbf{r}_{\perp j}^L \times \mathbf{F}_j^L \right) + \sum_{k=1}^{b} \left(\mathbf{r}_{\perp k}^B \times \mathbf{F}_k^B \right) \qquad 2.6.1b$$

where the nomenclature is as described previously (Section 2.4.4).

When solving the distribution problem, the aim is to determine muscular, ligament and bony contact forces from known resultant joint forces and moments. The resultant joint moment and joint forces can be determined via the inverse dynamics approach where the kinematics and external forces are measured and resultant kinetics are calculated. Information on the points of application of muscle, ligament and bone contact forces, as well as respective moment arms required in the joint equipolance equations, are also known or approximated from anatomical data. The remaining unknowns in the joint equipolance equations are magnitudes of each muscle and ligament force as well as a vector for each bone contact force. The total number of unknowns is the number of muscles (m) plus the number of ligaments (l) plus three times the number of bone contact points (3b) modelled (Herzog & Binding, 1994).

When solving the distribution problem in practical situations, assumptions are typically made to simplify the equations (Herzog, 1996). It is common to model only one bone contact point (b = 1), and for that point to be located at the joint centre ($\mathbf{r}_{\perp 1}^B = 0$), resulting in bone contact forces not contributing to the resultant moment about the respective joint. It is also common to assume the movement pattern is controlled by voluntary muscular forces and that ligament forces are not involved ($\mathbf{F}_j^L = 0$, for j = 1...L), as opposed to a movement involving a sudden and unanticipated applied external force that may result in ligament forces constraining the

motion of the joints. Under these assumptions, the joint equipolance equations (2.6.1) reduce to (Herzog & Binding, 1994; Herzog, 1996):

$$\mathbf{R}_{jnt} = \sum_{i=1}^{m} \mathbf{F}_i^M + \mathbf{F}^B \qquad 2.6.2a$$

$$\tau_{jnt} = \sum_{i=1}^{m} \left(\mathbf{r}_{\perp i}^M \times \mathbf{F}_i^M \right) \qquad 2.6.2b$$

The equipolance equations involve two vector equations in three dimensional space and therefore give six independent scalar equations. When calculating muscle force, the equation relating moments (2.6.2b) are generally used since the equation equating forces, (2.6.2a) although adding three scalar equations to the description of joint motion, also introduce one vector or three scalar unknowns in the form of bone-on-bone contact forces (Herzog, 1994). When individual muscle forces are known, equation (2.6.2a) can be used to determine joint bone-on-bone contact forces. The resultant joint moments and resultant joint forces of each joint are found experimentally through inverse dynamic analysis. The moment arms of each muscle crossing a joint are also found experimentally from cadaver or medical imaging studies and related to the current limb positions. This can be done by expressing positions of muscle origins and insertions and points defining the muscle path relative to segmental axes and then calculating moment arms from the position of the local axes. As pointed out by Herzog (1996), arriving at relative segmental measures and the position of the body-fixed axes is by no means trivial and has not been solved conclusively. The remaining unknowns in equating moments are the muscle forces which generally exceed in number the three equations for each joint. The reduced equipolance equations (2.6.2), therefore still represent an indeterminate system.

2.6.2.2 Solving the redundancy problem

Two approaches are generally adopted to solve the redundant nature of the musculo-skeletal system when determining individual muscle forces (Pierrynowski & Morrison, 1985; Bogert, 1994; Collins, 1995; Herzog, 1996). These are introduced along with the method adopted for the present study.

2.6.2.2.1 Reduction approach

The reduction approach involves reducing the complexity of the model to make the problem determinable. Strategies adopted include limiting the number of muscles modelled, increasing the constraints on the system, using lines of action representing functional muscle groups, or assigning muscle forces according to set criteria such as cross-sectional area, moment arms or electromyography (EMG) signals. By increasing the assumptions made in the model, the validity of the model is reduced. These studies are typically limited to examinations of single joints, without accounting for the co-contraction of antagonistic muscles or the action of muscle spanning more than one joint. A further approach, called limiting solutions, attempts to overcome some of these limitations and include the optimisation criteria in a reductionism approach. This is done by considering all combinations of a larger over-determined set of modelled muscles by taking a limited set at a time for which the equations of motion can be solved. An appropriate set of results is then selected from the larger set of muscle combinations based on a criterion to be optimised (Collins, 1995).

An example of a reduction approach is the control model used by Pierrynowski & Morrison (1985a). Reference muscle model data describing reference fibre length, reference pennation angle, optimal fibre length, and optimal (maximum) isometric muscle force, along with equations describing the force-length and force-velocity relationship of muscles, can be used to determine the maximum force of a muscle subject to the instantaneous dynamic conditions. In addition, the previous activation state and the maximum force of the muscle at the current instant in time can be used to predict the force generated by a muscle when experiencing a particular level of neural stimulation. The activation state of a muscle is given as the current muscle force divided by the maximum muscle force.

$$q_{cur} = \frac{F^{CE}}{\hat{F}^{CE}} \qquad 2.6.3$$

where:

q_{cur} = activation state.

F^{CE} = current force produced by contracile elements.

$\hat{F}^{CE}$ = maximum force produced by contractile elements due to current fibre length and contractile element velocity.

If the activation state of the muscle at the previous instant in time is known, then the activation state at the current instant can be estimated based on the neural stimulation received by the contractile elements.

$$q_{cur} = q_{pre} + (2S-1).\left[1-\exp\left(-\Delta t/\hat{t}\right)\right].\left(1-q_{pre}\right) \qquad (0.5 < S < 1.0)$$

$$q_{cur} = q_{pre} + (2S-1).\left[1-\exp\left(-\Delta t/\breve{t}\right)\right].\left(1-q_{pre}\right) \qquad (0.0 < S < 0.5) \qquad 2.6.4$$

where:

q_{pre} = activation at previous instant in time
S = neural simulation received by muscle
Δt = change in time
$\hat{t}$ = time constant for rise in activation
$\breve{t}$ = time constant for fall in activation

When the activation level (q) of a muscle at a previous instant in time is known then the maximum and minimum muscle force at the present instant in time can be obtained by letting the neural stimulation (S) equal one or zero respectively.

The control model of Pierrynowski & Morrison (1985a) selects muscle stimuli based on a neurophysiological model of muscle recruitment. In the neurophysiological model, constraints are placed on muscle recruitment. In voluntary muscle contractions, it is thought that muscle units are recruited in order of diminishing fatigue resistance (Pierrynowski & Morrison, 1985a). It has also been suggested that when higher level muscle units are activated, lower level units are not deactivated. There is debate over whether all fibres of a lower level are recruited prior to a higher level fibre activation. Pierrynowski & Morrison (1985a) defined motor unit recruitment as occurring in a fixed order, with all SO fibres recruited first, followed by all FO, and then all FG fibres.

$$SO \rightarrow SO + FO \rightarrow SO + FO + FG \qquad 2.6.5$$

In determining muscle force distribution, the generation of movement patterns is assumed to be done by a relatively autonomous pattern generator. This generator is assumed to operate at the spinal level, the functioning of which is also assumed to occur without supra-spinal control or afferent feedback. The support for such a model is based on observations of animal movement patterns which can be supported without supra-spinal input or afferent feedback. This would suggest that one or more spinal level pattern generators are capable of producing effective movement patterns.

The control model of Pierrynowski & Morrison (1985a) assumes that up to three independent pattern generators exists for each joint - one for each degree of freedom. For each degree of freedom, the signal generated by the respective pattern generator both facilitates the agonists and inhibits the antagonist muscles. The control model also assumes that muscles are recruited in accordance to their ability to produce the resultant joint moments (Pierrynowski & Morrison, 1985a). The ability to generate the required torque can be defined by direction cosines relating the point of force application and direction of force to the axis about which the torque is acting.

The moments about the three axes produced by a force **F** of components f_x, f_y, f_z applied at a point (x,y,z) are given by (Fig. 2.6.1):

$$\begin{aligned} \tau_x &= -f_y \cdot z + f_z \cdot y \\ \tau_y &= f_x \cdot z - f_z \cdot x \\ \tau_z &= -f_x \cdot y + f_y \cdot x \end{aligned} \qquad 2.6.6$$

Using directional cosines the Cartesian co-ordinates of the point (x,y,z) may be expressed in terms of the polar co-ordinates of displacement magnitude r and angles θ and ϕ (Fig. 2.6.1).

$$\begin{aligned} \tau_x &= -f_y \cdot \cos\phi \cdot r + f_z \cdot \sin\phi.\sin\theta \cdot r \\ \tau_y &= f_x \cdot \cos\phi \cdot r - f_z \cdot \sin\phi.\cos\theta \cdot r \\ \tau_z &= -f_x \cdot \sin\phi.\sin\theta \cdot r + f_y \cdot \sin\phi.\cos\theta \cdot r \end{aligned} \qquad 2.6.7$$

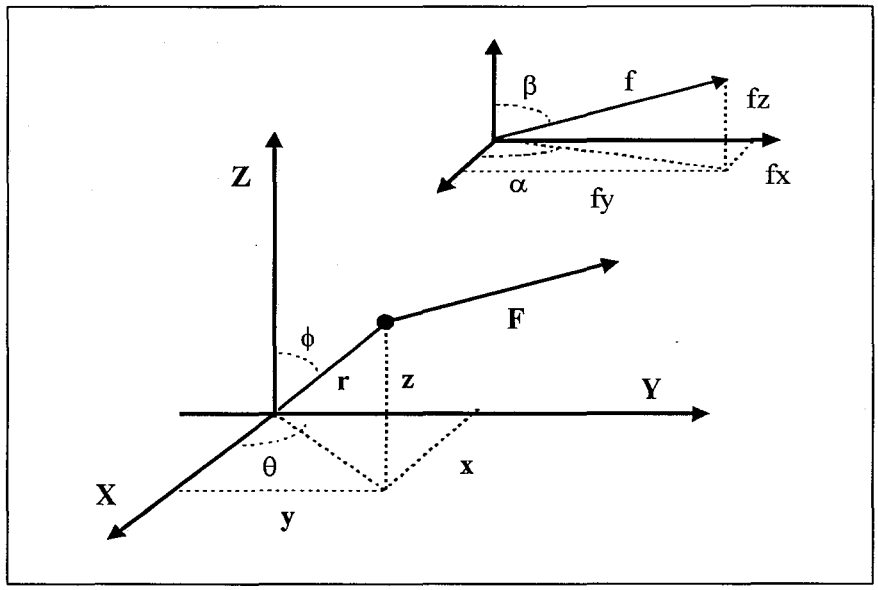

Figure 2.6.1. Force vector expressed as Cartesian and polar co-ordinates. Point of force application is given by Cartesian co-ordinates (x,y,z) or polar co-ordinates (r, θ, ϕ). The force vector is given by Cartesian co-ordinates (fx,fy,fz).

Using directional cosines the Cartesian co-ordinates of the force (fx,fy,fz) may be expressed in terms of the polar co-ordinates of force magnitude f and angles α and β.

$$\begin{aligned} \tau_x &= -\sin\beta.\sin\alpha.\,f.\,\cos\phi\,.\,r + \cos\beta.\,f.\,\sin\phi.\sin\theta\,.\,r \\ \tau_y &= \sin\beta.\cos\alpha.\,f.\,\cos\phi\,.\,r - \cos\beta.\,f.\,\sin\phi.\cos\theta\,.\,r \\ \tau_z &= -\sin\beta.\cos\alpha.\,f.\,\sin\phi.\sin\theta\,.\,r + \sin\beta.\sin\alpha.\,f.\,\sin\phi.\cos\theta\,.\,r \end{aligned} \qquad 2.6.8$$

If the ability to produce the desired torque is considered as a property of the directional cosines, then the two magnitudes can be set to unity. The stimuli received by muscle 'i' from the three possible pattern generators for a joint, whose point of application and direction of force are given by polar co-ordinates, is given by:

$$S_i\,(\text{single joint}) = a_{i,x}PG_x + a_{i,y}PG_y + a_{i,z}PG_z \qquad 2.6.9$$

with:

$$a_{i,x} = \frac{\tau_x}{|\tau_x|}\left[-\sin\beta_i.\sin\alpha_i.\cos\phi_i + \cos\beta_i.\sin\phi_i.\sin\theta_i\right]$$

$$a_{i,y} = \frac{\tau_y}{|\tau_y|}\left[\sin\beta_i.\cos\alpha_i.\cos\phi_i - \cos\beta_i.\sin\phi_i.\cos\theta_i\right] \qquad 2.6.10$$

$$a_{i,z} = \frac{\tau_z}{|\tau_z|}\left[-\sin\beta_i.\cos\alpha_i.\sin\phi_i.\sin\theta_i + \sin\beta_i.\sin\alpha_i.\sin\phi_i.\cos\theta_i\right]$$

where:

S_i (single joint) = stimuli received by muscle 'i' from the three pattern generators associated with a single joint.

$a_{i,x}$ = moment generating capacity of muscle about the x - axis.

PG_x = stimuli from pattern generator associated with the 'x' degree of freedom.

$a_{i,y}$ = moment generating capacity of muscle about the y - axis.

PG_y = stimuli from pattern generator associated with the 'y' degree of freedom.

$a_{i,z}$ = moment generating capacity of muscle about the z - axis.

PG_z = stimuli from pattern generator associated with the 'z' degree of freedom.

τ_x, τ_y, τ_z = resultant moments corresponding to each degree of freedom.

Each coefficient is multiplied by the sign of the torque corresponding to the respective degree of freedom and pattern generator. This is so moments of force that are in the same direction as the resultant moment are facilitated and moments of force in an opposing direction to the resultant torque are inhibited by the pattern generator.

The total muscle stimuli received by a muscle from a multi-joint system is the sum of the stimuli received from each independent pattern generator from each joint.

$$S_i = \sum_{j}^{joints}\left(a_{i,j,x}PG_{j,x} + a_{i,j,y}PG_{j,y} + a_{i,j,z}PG_{j,z}\right) \qquad 2.6.11a$$

or, equivalently:

$$\begin{bmatrix} a_{11x} & a_{11y} & a_{11z} & \cdots & a_{1jx} & a_{1jy} & a_{1jz} \\ a_{21x} & a_{21y} & a_{21z} & & a_{2jx} & a_{2jy} & a_{2jz} \\ \vdots & & & \ddots & & & \vdots \\ a_{m1x} & a_{m1y} & a_{m1z} & \cdots & a_{mjx} & a_{mjy} & a_{mjz} \end{bmatrix} \cdot \begin{bmatrix} PG_{1x} \\ PG_{1y} \\ PG_{1z} \\ \vdots \\ PG_{jx} \\ PG_{jy} \\ PG_{jz} \end{bmatrix} = \begin{bmatrix} S_1 \\ S_2 \\ \vdots \\ S_m \end{bmatrix} \qquad 2.6.11b$$

where:

j = number of joints

m = number of muscles

If a muscle does not cross a given joint, then it will not receive stimuli from the actuators of that joint. Similarly, if the moment arm of a muscle is zero with respect to any degrees of freedom of a joint, then the muscle will receive no stimuli from the respective pattern generator.

For the current instant in time, the moment arms, moment generating capacity (coefficients a_{mj}, Equ. 2.6.11b), and maximum and minimum muscle forces can be calculated. The equipolance equations can now be written in terms of each neural pattern generator stimuli, where muscle force is related to activation level by maximum muscle force (2.6.3), and activation level to muscle stimulation by non-linear equations describing muscle excitation contraction dynamics (2.6.4). Neural stimulation received by individual muscles can be related to each pattern generator by the moment generating capacity of each muscle (2.6.11b). The result is a system of non-linear equations which can be solved for the pattern generator stimuli (Pierrynowski & Morrison, 1985a) in which the number of equations (degrees of freedom) is equal to the number of unknowns (pattern generator stimuli). Knowing each pattern generator stimuli, the neural stimuli received by each muscle can be calculated, along with activation level, and individual muscle force. To solve this system of equations for individual muscle forces, the previous muscle activation levels need to be known (2.6.4). Previous activation levels need to be estimated or ignored for the beginning of a sequence, therefore the initial muscle forces predicted at the beginning of a sequence will be in error and should be ignored (Pierrynowski & Morrison, 1985a).

2.6.2.2.2 Optimisation approach

The most common approach to predicting individual muscle forces is mathematical optimisation. In optimisation, the goal is to assign forces (controls) in such a way as to optimise a performance criterion, while at the same time, meet the equipolance equations and meet any additional constraints imposed on the magnitude of individual muscle forces. (Collins, 1995; Buchanan & Shreeve, 1996). The optimisation approach, therefore, involves a cost function to be minimised (as a function of muscle force in static optimisation or muscle excitation in dynamic optimisation), and constraints in the form of equipolance equations of resultant joint forces or resultant joint moments, and constraints on maximal and minimal muscle forces. The choice of a performance criterion to be optimised is based on physiological principles in order to reflect strategies adopted by the central nervous system in controlling muscle fibre recruitment in the execution of the movement under investigation. Crowninshield & Brand (1981) were amongst the first to emphasis the need to base cost functions on known physiological relationships. The choice of a performance criterion is therefore crucial in that it determines the results of the optimisation procedure and the validity of the model. Unfortunately, not enough is known about the way in which the central nervous system recruits muscles in the execution of movement, and whether or not it follows an optimal control strategy. Thus, although the use of optimisation is mathematically and conceptually appealing, the results are still only approximations.

Optimisation techniques can be grouped into three general categories which reflect the different results obtained in each of the three approaches.

2.6.2.2.2.1 Static optimisation

Optimisation techniques can produces a static solution when predicted individual muscle forces are not constrained by the muscle forces predicted at any previous or future instant in time. In the optimisation procedure, the equipolance equations and cost function are solved independently for each instant in time. The independent nature of the static optimisation procedure at each instant in time means that the control variables are not necessarily continuous from one instant of time to another and may display discontinuities in the time course of individual muscle activation.

2.6.2.2.2.2 Quasti-static optimisation

Quasi-static solutions can be attained by optimisation procedures where muscle activation levels of the previous instant in time are used to constrain muscle forces in the solution of the equipolance equations at the current instant in time. With the inclusion of activation dynamics, this approach models different muscle fibre types and their possible change in activation level under both maximum and minimum neural stimulation, imposing limits on individual muscle forces from one instant in time to the next. A quasi-static solution results, where, as the series of individual optimisations proceed, limits are imposed on the model by the previous excitation levels of the muscles. Herzog (1996) was able to reproduce acceptable force-sharing patterns in the plantar flexors of cats, as shown by direct force measurement, by incorporating basic properties of the muscles in the musculo-skeletal model, which could not be produced via static optimisation. Herzog's model was based on anatomical measurements, force-length and force-velocity relationships, and sinusoidal muscle length changes coupled with sinusoidal changes in activation.

2.6.2.2.2.3 Dynamic optimisation or optimal control

Amongst the first to introduce dynamic optimisation in human dynamic modelling were Davy & Audu (1987), who used it to overcome the problem of discontinuities in individual muscle force prediction that may occur in static optimisation (Herzog, 1996). Dynamic optimisation involves modelling muscle activation levels instead of muscle force, thus allowing each muscle to be represented by a dynamic model in which physiological (activation dynamics) and mechanical (force length and force velocity) properties of muscle are included with the optimisation (Bogert, 1994). Replacing each unknown force in the musculo-skeletal model with an unknown activation level does not reduce the number of unknowns (Bogert, 1994). However, it does reduce the plausible solutions, as the solution has to be consistent with the physiological and mechanical properties of muscle. An optimisation criterion is still required to overcome the problem of indeterminacy and to produce a unique solution, although the cost function usually involves a muscle activation term. Dynamic optimisation currently provides the most comprehensive model of the musculo-skeletal system and, as such, has the potential to obtain the best estimates of muscle forces from an inverse dynamics approach (Bogert, 1994). However dynamic optimisation has not been widely used and few validation studies have been done or comparisons made between dynamic, static and quasi-static optimisation

techniques (Bogert, 1994; Herzog, 1996). A problem that exists with dynamic optimisation is obtaining accurate information on instantaneous contractile conditions and properties of all the muscles included in the model, including muscle lengths, tendon lengths, angles of pennation, PCSA and fibre composition.

2.6.2.2.3 Approach adopted

The approach adopted in the present study is a quasi-static optimisation procedure. A muscle model is adopted that consists of a contractile element and muscle fibre series-elastic element composing a muscle fibre with an angle of pennation contained within a muscle belly. Three different muscle fibre types and an elastic tendon are also included in the muscle model. Muscle excitation and contraction dynamics are modelled, leading to equations describing the force-length, force-velocity and excitation characteristics of each muscle element. From muscle physiological cross sectional area, reference fibre length, reference pennation angle, current length, and velocity of muscle fibres and contractile elements, plus the previous excitation level of the muscle, limits are imposed on the maximum and minimum forces the contractile elements can produce at the current instant in time. The force limits are included in a cost function aimed at minimising sum of squared muscle stresses across all muscles at an instant in time. A solution to the equipolant equation subject to minimising the cost function is achieved via a gradient projection algorithm.

2.6.2.3 Cost function

Several criteria have been proposed for predicting the recruitment strategy and hence force generated by individual muscles. These include the minimisation of the sum of muscle forces, normalised forces, minimal muscle stress, energy expenditure and fatigue, and for a summary see either Dul, et al. (1984a), Pierrynowski & Morrison (1985b), Herzog & Binding (1994), Collins (1995), Buchanan & Shreeve (1996), Herzog & Leonard (1991), Herzog (1996), Glitsch & Baumann (1997), or Prilutsky, et al., (1997). These are outlined below:

$$\text{minimise (force)} \quad \sum_{i=1}^{m} F_i^M \quad \text{(Seireg \& Arvikar, 1973)} \qquad 2.6.12$$

$$\text{minimise energy expenditure} \quad \text{(Hardt, 1978)} \tag{2.6.13}$$

$$\text{minimise (force)}^2 \quad \sum_{i=1}^{m}\left(F_i^M\right)^2 \quad \text{(Pedotti, et al., 1978)} \tag{2.6.14}$$

$$\text{minimise (normal force)}^2 \quad \sum_{i=1}^{m}\left(F_i^M / F_{max,i}^M\right)^2 \quad \text{(Pedotti, et al., 1978)} \tag{2.6.15}$$

$$\text{minimise (stress)}^3 \quad \sum_{i=1}^{m}\left(F_i^M / PCSA_i\right)^3 \quad \text{(Crowninshield \& Brand, 1981)} \tag{2.6.16}$$

$$\text{minimise} \quad \sum_{i=1}^{m}\left(F_i^M / \tau_{max,i}^M\right)^3 \quad \text{(Herzog, 1987)} \tag{2.6.17}$$

$$\text{. (fatigue)} \quad \sum\left(\frac{1}{\text{Muscle endurance time}}\right) \quad \text{(Dul, et al., (1984b)} \tag{2.6.18}$$

where

m = number of muscles.

F_i^M = force of muscle i.

$F_{max,i}^M$ = maximum force of muscle i.

$\tau_{max,i}^M$ = maximum torque generated by muscle i.

$PCSA_i$ = physiological cross sectional area of muscle i.

The different criterion functions used to evaluate muscular forces vary in the physiological parameters that are taken into account (Dul, et al., 1984a; Perrynowski & Morrison, 1985b; Collins, 1995; Siemienski, 1992; Buchanan & Shreeve, 1996). The minimum muscle force takes into account the moment arm of each muscle. The minimisation of muscular stress in addition takes into account physiological cross sectional area (PCSA). The minimisation of normalised force adds the specific tension (α) of the muscles and the minimisation of fatigue includes muscle fibre composition in the function.

The major criticism against using linear criteria such as the sum of muscle force, is that it leads to unreasonably large forces in the most advantageous agonist muscles (Pierrynowski & Morrison, 1985; Collins, 1995), leaving other synergistic muscles inactive (Pierrynowski & Morrison, 1985; Siemienski, 1992; Buchanan & Shreeve, 1996). This generally results in predicted activity in one muscle per degree of freedom (Siemienski, 1992). The study of Yeo (Collins, 1995) found that minimal muscle force predicted fewer active muscles about the elbow than demonstrated by EMG. Attempts have been made to overcome this limitation by imposing limits on the maximum force or maximum stress present in each muscle, and these take the form of inequality constraints. The effect of these constraints on the linear cost function is to allow recruitment of synergistic muscles only after the more advantageous muscles have reach their respective limiting values (Siemienski, 1992). The use of non-linear cost functions is now the dominant method, which has the effect of spreading agonist muscle activity amongst other available synergistic muscles. Non-linear cost functions are based on linear cost functions except the term is raised to an integer power, usually squared or cubed. The reason behind their use is that additional cost is imposed on the solution if all the force is generated by one muscle, hence the minimising solution distributes forces amongst all available synergistic muscles. A non-linear cost function without constraint on maximum individual values will result in a linear relationship between muscle force and increasing joint moment for each muscle, with the more advantageous muscles having a greater proportion of the force (Siemienski, 1992). By imposing limits on maximum individual muscle values, thereby imposing inequality constrains, the relationship becomes piece-wise linear, with discontinuities occurring as each muscle reaches its maximum value (Siemienski, 1992). In the analysis of gait, Collins (1995) compared the effect of minimising the square of muscle force opposed to just muscle force with the former mentioned resulting in a reduced soleus activity and increased activity of the extensors of gastrocnemius and quadriceps. However, it is questionable as to the physiological appropriateness of imposing such constraints on the determination of muscular force (Collins, 1995). In addition, the solution may be dominated by the effects of the constraints instead of the effects of the cost function (Herzog, 1996).

An approach adopted by Siemienski (1992) was to choose the form of the cost function so that the limits on maximum muscle force resulted from the unconstrained optimisation of the cost function. In this way the cost function was said to be 'soft constrained'. This eliminated the need for additional inequality constraints, here called hard 'constraints', to limit maximum

muscle force. By choosing a relative measure and a form that limited the admissible values, Siemienski (1992) produced the following soft contained cost function:

$$-\sum_{i=1}^{M}\left(\sqrt{1-\left(\frac{F_i^m}{F_{max,i}^m}\right)^2}\right) \qquad 2.6.19$$

The result is a non-linear relation between muscle force and joint moment for each muscle, eliminating the piece-wise linear relationships of hard constrained cost functions. This resulted in a more natural distribution of muscle forces over the full range of joint moments, with each muscle reaching its maximum force at the same point (Siemienski, 1992).

Buchanan & Schreeve (1996) question the physiological relevance of any of the non-linear cost functions they evaluated (force, stress, normalised force, and fatigue) where small variations in predicted muscle activation occurred between them, however none adequately described muscle activation of the elbow. Although changes are seen in the solution of muscle forces between different object functions, the authors saw this as less important than the biomechanics of the model. The relative insensitivity of biomechanical models to the cost function used is also supported by Nelson (1983) and Marshall et.al. (1989). In addition, Buchanan & Schreeve (1996) note that it is becoming increasingly clear that muscle control schemes for any task may involve a highly complex process. The schema used may involve training, conditioning, motor learning, and/or psychological attitude. As such, the optimal approach to motor activation prediction may prove to be a difficult task.

2.6.2.4 Sources of error

An inverse dynamic analysis utilising either a reductionism or optimisation approach to predict muscular forces has several areas of inaccuracies or sources of error. These relate to both the inverse dynamics approach to determine resultant joint forces and moments and to the muscle optimisation procedure. Sources of error include:

i) Reproducing the segmental position as opposed to external markers placed on the segment;

ii) Determining segment model parameters such as mass and inertia, joint centres, centre of mass, and muscle origins and insertions;

iii) Determining muscle model parameters, including muscle resting length, tendon length, cross sectional area, pennation, and fibre composition;

iv) The validity of the optimisation criteria. Included in this is the ability to determine synergistic muscle actions and co-contraction of antagonistic muscles, as well as consistency over different tasks; and

v) Solving the equations of motion and muscle optimisation at discrete time intervals through the period of the movement results in a quasi-static solution, in that forces predicted in one instant in time are not necessarily continuous with forces predicted at prior points in time.

Knowing the assumptions and limitations in the modelling process adopted, as well as the errors involved in the output data, is essential in determining the validity and the conclusions that can be drawn from the results. In establishing an expected error for the results of the modelling process, the size of the errors in the input data and the sensitivity of the results to these errors need to be known. This includes the sensitivity of resultant joint forces and moments to errors in position data, mass and inertial parameters, as well as the sensitivity of the optimisation procedure to errors in the muscle model parameters.

2.6.2.4.1 Model design - degrees of freedom

Muscles produce moments in all three axes of a segment which must be balanced either by other active muscles or by passive structures. The relative magnitude of these moment arms may change with changing joint angles. Buchanan & Shreeve (1996) found the results of muscle distribution were strongly dependent on the number of degrees of freedom that were actively balanced in the model of the elbow. One degree of freedom at the elbow resulted in the activation of muscles in a purely flexion or extension role. The inclusion of supination and pronation as a second degree of freedom saw the activation of pronator quadratus to balance a supinating moment produced by the biceps. With the inclusion of varus and valgus as a third degree of freedom, a large shift in the direction of activation was seen to support these moments. Buchanan & Shreeve (1996) found that limiting the degrees of freedom that were actively balanced in the elbow had the effect of ignoring synergistic muscle actions, leading to substantial changes in muscle force prediction.

In modelling muscle forces of the lower limb a protocol that has been used is to only actively balance with muscle forces, degrees of freedom that have significant movement and moment generating capacity (Glitsch & Baumann, 1997). This approach assumes that our control systems does not actively balance degrees of freedom possessing small rotations and moment generating capacity, leaving these moments to be balanced by bone and ligaments forces. Hence, in modelling the lower limb, abduction/adduction and internal/external moments at the knee and ankle joints are effectively ignored in the equipollence equations (Buchanan & Schreeve, 1996; Glitsch & Baumann, 1997). This approach has the advantage of reducing the complexity of the distribution problem, making determination of muscle forces simpler by reducing the degrees of freedom appearing in the equipollence equations.

How biomechanical models are constructed and the role of muscles and ligaments in balancing moments about segment axes and the degrees of freedom that are effectively included in the model, will therefore have a significant effect on the muscle forces predicted.

2.6.2.4.2 Muscle model parameters

Muscle model parameters are central to the cost function and therefore the accuracy of parameters, will readily influence optimisation results. With errors in the order of 30 percent reported in the magnitude of moment arms and PCSA, careful selection of physiological parameters is required (Buchanan & Shreeve, 1996). Buchanan & Shreeve (1996) reported great variations in muscle force prediction due to small changes in muscle parameters of the elbow. Similarly, Brand et.al. (1986) found variations in the order of two to eight in muscle force prediction of the leg in gait when using different reported values for muscle parameters. Siemienski (1992) investigated the influence of different muscle stress limits on the muscle force distribution problem. The analysis involved forces in 17 muscle of the lower limb during running. Changing the stress limit produced slight alterations in muscle forces - a decreased stress limit resulted in a decrease in maximum muscle forces. In addition, a decreased stress limit resulted in a decrease in force for the muscles subject to greatest stresses, and an increase of force in muscles with lower stresses. No muscle reached their maximum force, however a stress limit too low would not allow a solution if the required forces could not be achieved.

2.6.2.4.3 Choice of cost function

Despite knowledge of the neurophysiology of muscle contraction (for example, Sale, 1987; Enoka, 1988; Heckman & Sandercock, 1996; Gottlieb, 1996) the strategy employed by the brain in the recruitment of motor units is still unknown. The strategy behind motor unit recruitment may be a task-dependent act, the resultant of a range of criteria or a universal principle. Consequently, there remains considerable uncertainty and debate over the most appropriate criterion function and which, if any, are physiologically valid when tying to predict individual muscle forces (Pierrynowski & Morrison, 1985; Buchanan & Shreeve, 1996). Due to this uncertainty, the validity of muscle forces obtained via an optimisation procedure need to be established by comparison with other experimental results (Buchanan & Shreeve 1996). These could include other muscle modelling studies, EMG studies and established principles of functional anatomy.

In comparing different criteria Collins (1995) has shown that a number of different combinations of muscular, ligament and joint contact forces can be utilised effectively throughout the gait cycle and keep the limb in agreement with the equilibrium conditions. Conversely, Buchanan & Shreeve (1996) found that amongst several different non-linear cost functions tested, no single function could adequately describe the muscle activation about the elbow. However, improved result were obtained for the wrist, which was nearly a determined system modelled with five muscles and a four directions of movement. As mentioned by Collins (1995), Bogert (1994) and Herzog (1996), many of the previously considered global performance criteria for muscle selection cannot be successfully applied throughout the whole gait cycle. This finding is supported by other researchers who question the global application of minimisation principles to predict the performance of the musculoskeletal system. Furthermore, Collins (1995) suggests it may be unreasonable to suppose that the behaviour of muscular system is governed by a unique performance criteria over the entire gait cycle.

2.6.2.4.4 Co-contraction

A major limitation of current muscle optimisation procedures is the inability to account for co-contraction of antagonistic muscles. This is mainly due to the nature of the performance functions. By minimising the sum of muscular forces, stresses or energy expenditure, the solution favours single joint agonist muscles, as co-contraction of antagonistic muscles would

involve additional costs resulting from an increase activity of both antagonist and agonist muscles. As demonstrated by Collins (1995), optimisation criteria fail to predict quadriceps-hamstring co-contraction in late swing and heel strike during the gait cycle - a phenomenon shown by EMG studies. Despite the absence of co-contraction in the study by Collins (1995), dynamic equilibrium could still be maintained around heel strike. It could be argued that a minimal principle based on the minimisation of muscular force, stress or energy expenditure would be invalid during late swing and early stance. In the study of Collins (1995), the different criteria had excellent agreement between EMG and single joint muscular activity but poorer agreement with double joint muscles. Herzog & Binding (1992) found that the non-linear optimisation involving minimum muscle stress could predict co-contraction under certain circumstances in a multi joint system with single and double joint muscles.

The functional significance of the co-contraction of agonist-antagonist muscle groups is still uncertain. One hypothesis is that co-contraction stabilises one or more joints in the anticipation of externally applied forces (Collins, 1995). In gait, heel strike involves relatively large impact forces occurring over a very small time period (5-25 ms), a time period too small for neuromuscular reflex loops to react to the applied loads. Therefore, the co-activation of hamstrings and quadriceps may be seen as a pre-programmed sequence in order to increase joint stiffness prior to an anticipated load (Collins, 1995). The nature of the quasi-static solution also has implication for predicting muscle forces in anticipation of applied external forces. Current inverse dynamic methodologies and cost functions cannot anticipate loads and therefore may not be able to predict co-contraction involving increasing stiffness prior to an external load.

2.6.2.4.5 Synergistic muscles

Herzog (1996) presents a summary of studies where muscle forces were directly measured in the ankle (soleus, gastrocnemius, plantaris, and tibialis anterior) of cats at different walking speeds. Comparison of experimentally measured muscle forces with theoretically predicted forces revealed limitations in theoretical models. The algorithm predicted a unique relationship between the synergistic soleus and gastrocnemius muscles whereas experimentally, a given force in one muscle can be associated with a wide range of forces in another. The algorithm also predicted a continuously increasing force-sharing relationship between synergistic muscle

with increasing loads. However experimentally the soleus remained relatively constant while the gastrocnemius increased.

2.6.2.5 Muscles

In this section, a mathematical model of a muscle is presented which will describe the force and moment generated by a muscle. The force generated by a muscle is dependent many factors including size, structure, activation, instantaneous contractile conditions, and contractile history. The moment produced by a muscle about a joint is dependent on its moment arm, determined from the line of action of the muscle and a point representing the joint centre. Individual sections that follow address the issues of defining the muscle-tendon path, components of the muscle model, attaining muscle model parameters for an individual subject, modelling muscle excitation and contraction dynamics, muscle model parameter optimisation to changes in muscle belly lengths, implementation of the muscle model, and finishes with an example of the muscle model implementation and optimisation.

2.6.2.5.1 Muscles modelled - lower limb

The number of muscle modelled vary between investigators. Rohrle et.al. (1984) included 38 muscles which were modelled as 42 individual muscle elements. Twenty four muscle elements cross the hip joint, 16 cross the knee, 13 cross the ankle and four cross the metatarsophalangeal joint. Pierrynowski & Morrison (1985) also included 38 muscles which were modelled as 47 individual muscle elements (Table 2.6.1). Twenty nine muscle elements crossed the hip joint, 16 crossed the knee, 13 crossed the ankle and four cross the metatarsophalangeal joint. The difference between these two models was that Gluteus Maximus, Gluteus Medius and Gluteus Minimus were modelled as single elements in the study of Rohrle, et al. (1984), as opposed to two, three and three elements respectively by Pierrynowski & Morrison (1985). Seireg & Arvikar (1989) included fewer muscles (28) which were modelled as 31 individual muscle elements. In their model, 15 muscle elements cross the hip joint, 13 cross the knee, 12 cross the ankle and four cross the metatarsophalangeal joint. Muscles not included in the later study were seven crossing the hip joint (Gremillus Superior, Gremillus Inferior, Obturator Internus, Obturator Externus, Pectinius, Quadratus Femoris, and Piriformus), two crossing the knee joint (Plantaris and Popliteus), and Iliopsoas modelled as one muscle. In more resent study of Glitsch & Baumann (1997), modelled 37 muscle as 47

muscle elements. This was similar to Pierrynowski & Morrison (1985), except the Popliteus and Plantaris were not included, the Gluteus Maximus was modelled as three elements, and the Adductor Brevis was modelled as two elements. These mentioned studies modelled both the Soleus and Psoas as one muscle element respectively. Glitsch & Baumann (1997) concluding that in modelling the musculoskeletal system, including 47 muscle elements was essential in determining three dimensional loading. A reduction in the number of muscles would have caused significant changes in the muscle forces predicted and in calculated joint forces.

Table 2.6.1 Muscles modelled in the lower limb. From Pierrynowski & Morrison (1985).

	Muscle	Joint Involved			
		Hip	Knee	Ankle	MTP
1	Psoas major	*			
2	Iliacus	*			
3	Gemellus Superior	*			
4	Gemellus Inferior	*			
5	Obturator Externus	*			
6	Obturator Internus	*			
7	Piriformis	*			
8	Quadratus Femoris	*			
9	Pectineus	*			
10	Adductor Longus	*			
11	Adductor Magnus (anterior)	*			
12	Adductor Magnus (middle)	*			
13	Adductor Magnus (posterior)	*			
14	Adductor Brevis	*			
15	Gluteus Minimus (anterior)	*			
16	Gluteus Minimus (middle)	*			
17	Gluteus Minimus (posterior)	*			
18	Gluteus Medius (anterior)	*			
19	Gluteus Medius (middle)	*			
20	Gluteus Mmedius (posterior)	*			
21	Gluteus Maximus (deep)	*			
22	Gluteus maximus (superior)	*			
23	Tensor Fasciae Latae	*	*		
24	Semimembranosus	*	*		
25	Semitendinosus	*	*		
26	Gracilis	*	*		
27	Satorius	*	*		
28	Rectus Femorus	*	*		
29	Biceps Femoris (long)	*	*		
30	Biceps Femoris (short)	*	*		
31	Vastus Lateralis	*	*		
32	Vastus Intermedius	*	*		
33	Vastus Medialis	*	*		
34	Popliteus		*		
35	Gastrocnemius (lateral)		*	*	
36	Gastrocnemius (medial)		*	*	
37	Plantaris		*	*	
38	Soleus			*	
39	Tibialis Anterior			*	
40	Tibialis Posterior			*	
41	Peroneus Longus			*	
42	Peroneus Brevis			*	
43	Peroneus Tertius			*	
44	Extensor Digitorum Longus			*	*
45	Extensor Hallucis Longus			*	*
46	Flexor Digitorum Longus			*	*
47	Flexor Hallucis Longus			*	*

2.6.2.5.2 Muscle model: lines of action

Dostal & Andrews (1981) and Brand, et al. (1982) presented comprehensive data on the origin and insertion points for muscles of the lower limb. However, modelling muscle by a straight line approach between origin and insertion is seldom adequate to determine muscle lengths, change in lengths and moment arms in rigid body three dimensional analysis of segments of the lower limb during movement trials.

In modelling 47 muscle elements of the lower limb Pierrynowski & Morrison (1985) defined the origin and insertion plus up to four additional points along which the muscle was constrained to pass. These points were expressed relative to the body-fixed axes of the segment to which the point was considered to belong. The muscle-tendon line of action was then defined by joining its defining points with a combination of either straight or curvilinear lines depending on the path of the muscle. The origin, insertion and deflection point co-ordinate data were not presented.

2.6.2.5.3 Muscle model: structure

Pierrynowski & Morrison (1995b) deemed six parameters to be important in describing muscle structure (Fig. 2.6.2 and Fig. 2.6.3), these being tendon and fibre lengths as a percentage of total muscle length; a muscle shape factor, which is the maximal anatomical cross sectional area divided by its mean anatomical cross sectional area; the cross sectional area of the tendon; the fibre angle of pennation; and the muscle mass.

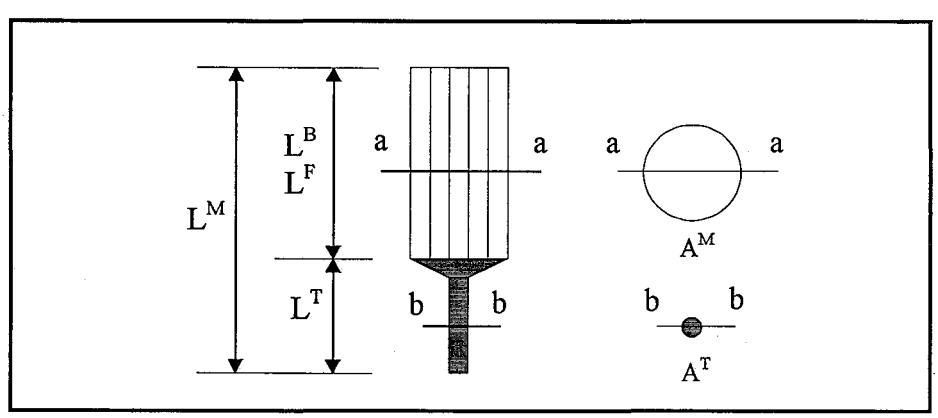

Figure 2.6.2. Muscle structure: parallel fibres. L^M = muscle length, L^T = tendon length, L^B = muscle belly length, L^F = fibre length, A^M = anatomical cross sectional area and A^T = tendon cross sectional area.

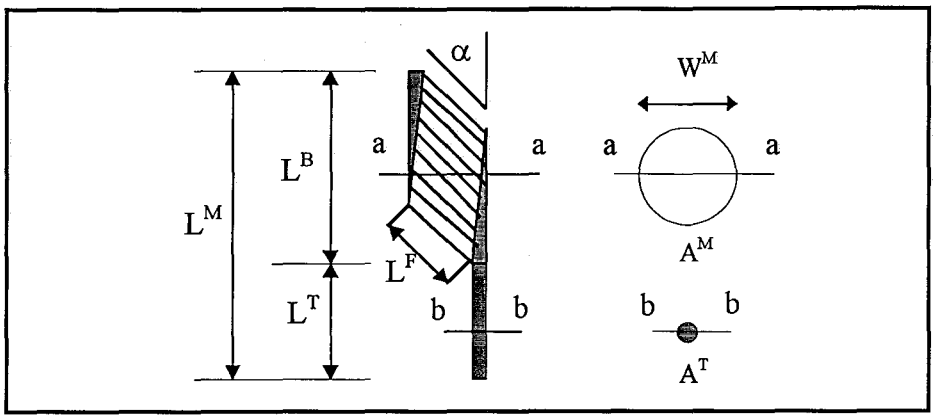

Figure 2.6.3. Muscle structure: pennate fibres. L^M = muscle length, L^T = tendon length, L^B = muscle belly length, L^F = fibre length, α = pennation angle, A^M = anatomical cross sectional area and A^T = tendon cross sectional area, W^M = functional width of muscle.

The muscle model of Pierrynowski & Morrison (1985b) consisted of a series elastic component of the muscle fibre (SEC), the contractile elements (CE) and a series elastic component of the tendon (Fig. 2.6.4 and Fig. 2.6.5). The CE is the only active component in the mechanical model, and its force output depends on its length, velocity and temporal phenomena. The resting lengths of the muscle fibre SEC was defined as being half of the optimal fibre length. It is at this length the muscle fibre can exert its maximum isometric force. The reference CE length is then given by the reference fibre length and the resting muscle fibre SEC. In their model, Pierrynowski & Morrison (1985b) omitted the parallel elastic component (PEC) of muscle fibres due to the small contribution it makes to passive forces in the muscle.

The muscle model used in the current work (Figs 2.6.4 & 2.6.5) assume that cross sectional width of the muscle is constant. This assumption is used to calculate pennation angles and fibre lengths from the changes in muscle belly length relative to a reference pennation angle and muscle belly length. This model represents the function of the whole muscle and importantly the force of the whole muscle in the direction of the tendon subject to the instantaneous pennation angle, fibre length and contractile element velocity of the model. The model does not represent the architecture of individual muscle fibres within the muscle or attempt to model forces perpendicular to the direction of the tendon, and therefore does not address the internal mechanics of fibre architecture and stability perpendicular to the direction of the tendon. In addition as the model uses a single pennation angle and fibre length to represent force in the direction of the tendon a shortening of the belly length resulting in a

pennation of 45 degrees will result in zero force in the direction of the tendon. Hence minimum fibre length that the model can produce is at a pennation angle of 45 degrees and is given by the cosine of the reference pennation angle and reference fibre length. Still shorter belly lengths will result in pennation angles greater than 45 degrees and a negative force predicted by the model in the direction of the tendon.

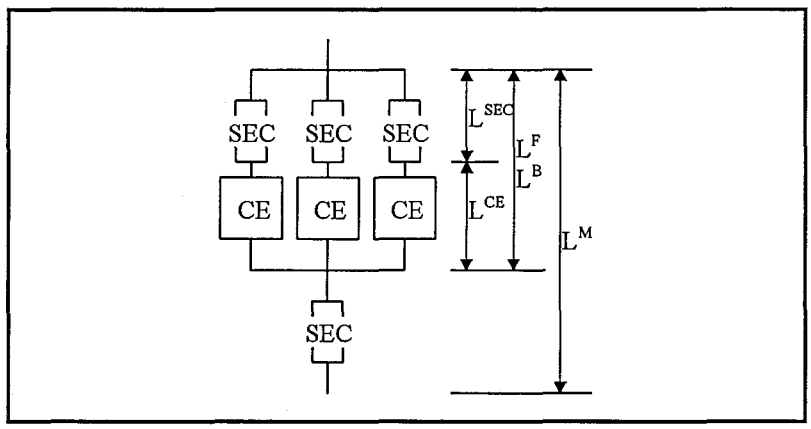

Figure 2.6.4. Series elastic component in parallel fibres. L^{M} = muscle length, L^{B} = muscle belly length, L^{F} = fibre length, α = pennation angle, L^{SEC} muscle fibre series elastic component length, L^{CE} = contractile element length, SEC = series elastic component and CE = contractile element.

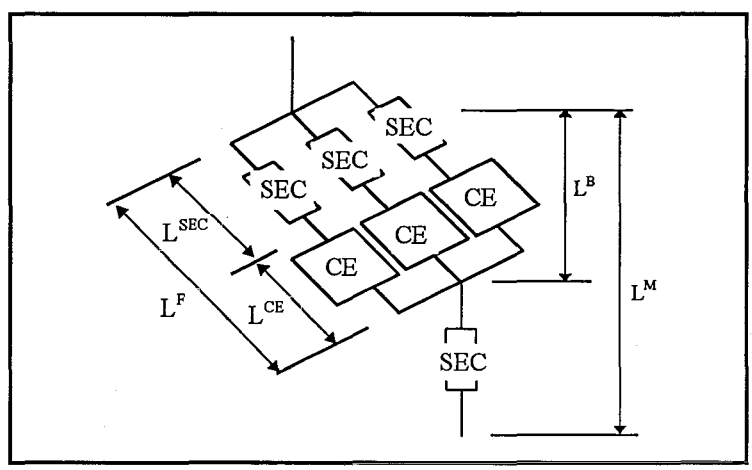

Figure 2.6.5. Series elastic component in pennate fibres. L^{M} = muscle length, L^{B} = muscle belly length, L^{F} = fibre length, L^{SEC} muscle fibre series elastic component length, L^{CE} = contractile element length, SEC = series elastic component and CE = contractile element.

2.6.2.5.4 Muscle model: PCSA

The cross sectional area of a muscle can be measured by taking a cross sectional cut through a muscle perpendicular to the direction of the muscle fibres (Enoka, 1988) and is usually made by cadaver or radio-graphic means. The physiological cross sectional area (PCSA) of a muscle is a measure of cross sectional area that takes into account muscle fibre length and angle of pennation (Enoka, 1988; Herzog, 1986). Although both cross sections indicate cross sectional size of the muscle, the PCSA is thought to be a more appropriate measure of the number of sarcomeres in parallel and the muscle's ability to generate force (Enoka, 1988). The PCSA is calculated from the muscle volume and fibre length, where fibre length is a defined reference length (Pierrynowski & Morrison, 1985b; Enoka, 1988; Herzog, 1996). The PCSA is related to the maximum isometric force of the muscle by the specific tension of the muscle (Enoka, 1988; Herzog, 1986). If the reference pennation angle is also known at the reference fibre length, then the force in the direction of the tendon can be calculated (Herzog, 1996), as well as maximum forces at muscle lengths other than the reference length (Pierrynowski & Morrison, 1985b). These authors also included a muscle shape factor in order to account for the change in size when using the maximum instead of mean PCSA of the muscle. The PCSA as given by Pierrynowski & Morrison (1985b) is:

$$\hat{\bar{A}}^M = \frac{m}{p.\bar{L}^F} . E \qquad 2.6.20$$

Where

$\hat{\bar{A}}^M$ = physiological cross sectional area at the reference fibre length.

m = muscle mass.

p = muscle density (1050 $kg.m^{-3}$).

$\bar{L}^F$ = reference muscle fibre length.

E = muscle shape factor.

$$E = \left[\frac{\text{maximum anatomical cross sectional area}}{\text{mean anatomical cross sectional area}}\right]$$

The PCSA has been calculated from cadaver studies and more recently radiographic techniques on live subjects. However, PCSA from cadaver studies have generally under-estimated the cross sectional areas when compared to those obtained from live subjects (Herzog, 1996). As pointed out by Herzog (1996), most optimisation cost functions use ratios of PCSA when determining force-sharing between muscles, which according to Cutts & Seedhom (1993), were consistent between cadaver and live subjects.

2.6.2.5.5 Muscle model: maximum force

The maximum isometric force developed by a muscle in the direction of its fibres is the product of physiological cross-sectional area (PCSA) and the specific tension (*f*) of the muscle (Pierrynowski & Morrison, 1985b; Enoka, 1988; Herzog, 1996). The specific tension is the maximum force developed by the muscle per unit of physiological cross-sectional area. Values for specific tension vary widely but are generally reported between 16 and 40 N/cm^2 (Enoka, 1988; Herzog, 1996). In the muscle model of Pierrynowski & Morrison (1985) 40 N/cm^2 was used. The maximum isometric force produced is specific to the reference fibre length and reference pennation angle at which the PCSA was determined (see previous section). Hence, in this study the reference maximum isometric force refers to the maximum force calculated for the isometric muscle at a reference fibre length and pennation angle, and is given by:

$$\hat{\bar{F}}^{CE} = \hat{\bar{A}}^{M} . f \qquad 2.6.21$$

where:

$\hat{\bar{F}}^{CE}$ = maximum isometric force in direction of muscle fibres at reference fibre length.

$\hat{\bar{A}}^{M}$ = maximum physiological cross sectional area at reference fibre length.

f = specific tension at reference fibre length.

The component force generated by the fibres in the direction of the muscle's line of action is given by the cosine of the pennate angle (Pierrynowski & Morrison, 1985b; Herzog, 1996). The pennate angle describes the angle between the muscle's line of action and the direction of the muscle fibres.

$$\hat{\bar{F}}^{M} = \hat{\bar{F}}^{CE} \cdot \cos(\bar{\alpha}) \qquad 2.6.22$$

where:

$\hat{\bar{F}}^{M}$ = maximum isometric force in direction of muscle line of action at reference fibre length.

$\hat{\bar{F}}^{CE}$ = maximum isometic force in direction of muscle fibres at reference fibre length.

$\bar{\alpha}$ = reference pennate angle at reference fibre length.

To calculate the maximum force at muscle fibre lengths other than the reference fibre length and at velocities other than the isometric condition, the force-length and force-velocity relationship of the muscle fibres and contractile elements are used. The instantaneous length of the muscle fibres and contractile elements can be calculated, given the length of the muscle, the force exerted and the lengths of muscle fibre and tendon series elastic components. Once the length of muscle contractile elements as a function of time are known, velocities can be calculated, and length and velocity relationships can then be used to modify the maximum force output of muscles.

2.6.2.5.6 Muscle model: fibre length

In a parallel muscle model, the fibre length is equal to the belly length, and if the muscle belly length L^B was to change by an amount 's', then the length of the fibre L^F would also change (Fig. 2.6.2). In a pennate muscle with a change in muscle belly length L^B, the assumption is that the pennate angle will change but the functional width (Fig. 2.6.3) will remain constant (Pierrynowski & Morrison, 1985b). The new pennate angle after a change in muscle belly length (s) can then be calculated from a known reference fibre length and corresponding reference pennate angle.

$$\tan(\alpha) = \frac{\bar{L}^{F} \cdot \sin(\bar{\alpha})}{\bar{L}^{F} \cdot \cos(\bar{\alpha}) + s} \qquad 2.6.23$$

where:

α = pennate angle.

$\bar{L}^F$ = reference fibre length.

$\bar{\alpha}$ = pennate angle at reference fibre length.

s = change in muscle belly length from the reference muscle belly length.

$s = L^B - \bar{L}^B$

- ve for decrease in length.

+ ve for increase in length.

L^B = muscle belly length.

$\bar{L}^B$ = reference muscle belly length.

With a change in muscle belly length the new fibre length of a pennate muscle can be calculated from the reference fibre length, corresponding reference pennate angle and the pennate angle at the new length.

$$L^F = \bar{L}^F . \frac{\sin\bar{\alpha}}{\sin\alpha} \qquad 2.6.24$$

where:

L^F = muscle fibre length.

α = pennate angle.

$\bar{L}^F$ = reference muscle fibre length.

$\bar{\alpha}$ = pennate angle at reference muscle fibre length.

For a pennate muscle, a geometric limit exists on the minimum muscle fibre length defined by the muscle model (Fig. 2.6.3). The minimum model muscle fibre length must be equal to or greater than, the thickness of the muscle fibre, defined by the reference fibre length and the reference pennation angle, assuming that the functional width (Fig. 2.6.3) does not change with changes in fibre length (Pierrynowski & Morrison, 1985b). Therefore:

$$\breve{L}^F_{mod} = \bar{L}^F . \sin(\bar{\alpha}) \qquad 2.6.25$$

where:

$\breve{L}^F_{mod}$ = minimum fibre length defined from muscle model.

$\bar{L}^F$ = reference fibre length.

$\bar{\alpha}$ = reference pennation angle.

2.6.2.5.7 Muscle model: series elastic component

When a muscle is active, the force developed is transferred via the series elastic components of the muscle fibres (SEC) and tendons to the skeleton. The series elastic components do not alter the forces being transmitted through them, however they influence the instantaneous length and velocity of the contractile element (CE) and modify the force (Pierrynowski & Morrison, 1985b). The length of a tendon (L^T) for any force transmitted though it can be calculated from the force, anatomical length, cross-sectional area and modulus of elasticity.

$$L^T = \tilde{L}^T\left(1.0 + \frac{F^M}{1400A^T}\right) \qquad 2.6.26$$

where

L^T = tendon length.

$\tilde{L}^T$ = resting tendon length.

F^M = force generated by contractile elements in direction of tendon.

A^T = cross section area of the tendon.

In Pierrynowski & Morrison (1985b), the resting length of the fibre SEC was defined as half the fibre length at which the muscle fibre can produce maximum force. Using this definition, the resting length of the muscle fibre SEC for this study was defined as half (0.5) of the optimal fibre length, and it is at this length that the muscle fibre can exert its maximum force. With this definition, the muscle fibre SEC will not be longer than the minimum possible modelled fibre length, which in the present study is modelled as 0.58 of the optimal fibre length using the relationship (2.6.33). The reference length of the CE, at zero force, is then defined from the resting length of the fibre SEC, also at zero force, and the reference fibre length.

$$\tilde{\bar{L}}^{SEC} = 0.5 \times \tilde{\bar{L}}^F \qquad 2.6.27$$

$$\bar{L}^{CE} = \bar{L}^F - \tilde{\bar{L}}^{SEC} \qquad 2.6.28$$

where

$\bar{L}^{CE}$ = reference length of contactile element, at zero force.

$\tilde{L}^{SEC}$ = resting length of muscle fibre series elastic component.

$\bar{\bar{L}}^{F}$ = optimal muscle fibre length.

If the contractile elements produce force, the fibre SEC will change length, and in so doing change the length of the contractile elements for a given muscle length. Knowing the instantaneous force of the contractile elements, the length of the fibre SEC can be estimated (Pierrynowski & Morrison, 1985b).

$$L^{SEC} = \tilde{L}^{SEC} + \hat{L}^{F}(Ax + Bx^2 + Cx^3) \qquad 2.6.29$$

where:

L^{SEC} = length of muscle portion of series elastic component.

$\tilde{L}^{SEC}$ = resting length of muscle portion of series elastic component.

$\hat{L}^{F} = 1.8 \times \bar{\bar{L}}^{F}$ = maximum muscle fibre length.

$x = F^{CE} / \hat{\bar{\bar{F}}}_i^{CE}$

$A = 0.21188$

$B = -0.22625$

$C = 0.08438$

F^{CE} = force produced in direction of contractile elements.

$\hat{\bar{\bar{F}}}_i^{CE}$ = maximum isometric force produced at optimal fibre length in direction of contractile elements.

2.6.2.5.8 Muscle model: activation time course

The activation state of a muscle can be used to describe the generation of force by the contractile elements. In Pierrynowski & Morrison (1985b), muscle activation represented the amount of calcium bound to the troponin molecule. In generation of muscle force, this definition includes the number of contractile elements recruited as well as firing frequency. As muscle cannot be activated or relaxed instantaneously, the rise and fall of activation was represented by two exponential equations. Knowing the previous activation level, the rise and fall in activation level can be estimated based on the level of neural stimulation received by the contractile elements (Pierrynowski & Morrison, 1985b).

$$q_{rise} = q_{-\Delta T} + (2S-1).\left[1-\exp\left(-\Delta t/\hat{t}\right)\right].(1-q_{-\Delta T}) \qquad (0.5 < S < 1) \qquad 2.6.30$$

$$q_{fall} = q_{-\Delta T} + (2S-1).\left[1-\exp\left(-\Delta t/\breve{t}\right)\right].(q_{-\Delta T}) \qquad (0 < S < 0.5) \qquad 2.6.31$$

where

$q_{-\Delta T}$ = activation at time t - Δt.

q_{rise} = rise in activation at time t.

q_{fall} = fall in activation a time t.

S = neural stimulation.

$\hat{t}$ = time constant for rise in activation (0.5 < S < 1).

$\breve{t}$ = time constant for fall in activation (0 < S < 0.5).

In the approach adopted by Pierrynowski & Morrison (1985b), muscles produce no force when activation (q) is equal to zero, and produce maximum force when activation (q) is equal to one. At the time period (t) under maximal neural stimulation (S =1), the upper boundary of muscle activation ($\hat{q}$) is given by q rise. At the same time period (t) under no neural stimulation (S=0), the lower boundary of muscle activation ($\breve{q}$) is given by q fall. When the neural stimulation (S) is equal to 0.5 the activation level does not change. In Pierrynowski & Morrison (1985b), the time constant ($\hat{t}$) for the rise in activation (S>0.5) for the three fibre types were estimated at 0.003 second. The time constants ($\breve{t}$) for the fall in activation (S<0.5) for slow-oxidative (SO), fast-oxidative (FO) and fast-glycolytic (FG) fibres were estimated by Pierrynowski & Morrison (1985b) as 0.073, 0.034 and 0.034 seconds respectively.

Due to the varying time constants of SO, FO and FG fibre types within a muscle, the three distinct fibre types are modelled, as opposed to the activation of the muscle as a whole and a single fibre type, and the activation level of each is followed over time. Splitting the muscle model into three contractile elements, each with their own activation level, and three respective fibre SEC, will result in three varying force outputs. As a result of varying forces of the three fibre types, the respective fibre SEC will also vary in length and velocity. It is assumed in the present study that the three fibre types do not vary their length independently, but have a common length and velocity regardless of the force in each of the three fibre types. The model used in this study therefore has one common fibre SEC (Fig. 2.6.6), and the force

of the muscle in the direction of the contractile elements is the sum the force produced by each of the three fibre types. Since the total force determines the length of the tendon, the velocity of the muscle need not correspond to the contractile element velocity due tendon elasticity and the fibe SEC (Enoka, 1988).

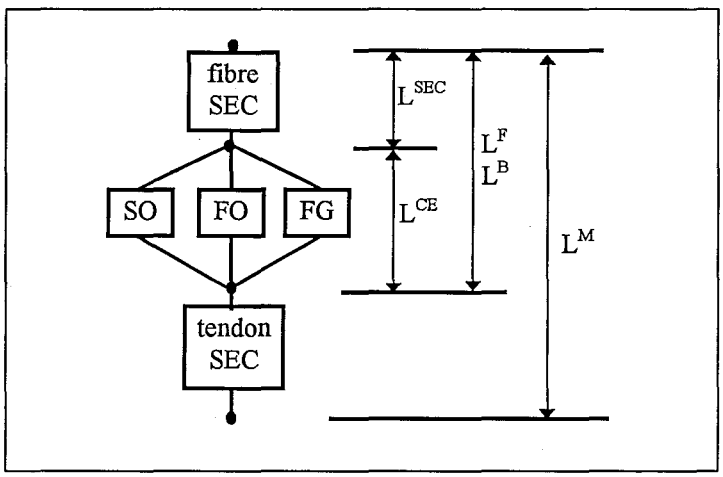

Figure 2.6.6. Parallel muscle with three fibre types. A common fibre series elastic component is assumed, so that the three fibre type have a common length and velocity.

2.6.2.5.9 Muscle model: force-length and force-velocity

The contractile properties of skeletal muscle are described by the force-length and force velocity relationships (Pierrynowski & Morrison, 1995; Herzog, 1996). The force-length relationship describes the maximum isometric force a muscle can exert as a function of its length. Herzog (1996) lists the following problems that arise when incorporating the force-length relationship into a model aimed at predicting muscle force distribution:

i) The force-length properties of most muscles are not known and an estimation must be used;
ii) The force-length relationship is plastic and may adapt to the requirements of every-day life;
iii) The force-length properties for sub-maximal levels of contraction differs vastly from those obtained during maximal levels of contraction;

iv) Force-length properties will differ with differences in the length that is measured and the length that was held isometric during experimentation;

v) In determining force-length properties, artificial stimulation may be used which will introduce properties that are independent of muscle length.

The mechanical properties of a muscle, namely the force-length-velocity relationships, can be estimated for each muscle based on anatomical dimensions (Pierrynowski & Morrison, 1985b). Relating muscle anatomical dimensions to mechanical properties avoids having to perform functional tests on subjects in order to ascertain these relationships. Pierrynowski & Morrison (1985b) used the equation of Hatze (1977) for modelling the force-length relationship for muscle fibre lengths ranging from 0.58 to 1.8 of the optimal fibre length.

$$\frac{\hat{F}_i^{CE}}{\hat{\bar{F}}_i^{CE}} = 0.32 + 0.71.\exp\left[-1.112.\left(L^F/\bar{L}^F - 1.0\right)\right].\sin\left[3.722.\left(L^F/\bar{L}^F - 0.656\right)\right] \qquad 2.6.32$$

where:

$\hat{F}_i^{CE}$ = maximum isometric force in the direction of the contractile elements.

$\hat{\bar{F}}_i^{CE}$ = maximum isometric force at optimal fibre length in the direction of the contractile elements.

L^F = fibre length.

$\bar{L}^F$ = optimal fibre length.

Equation 2.6.32 follows the force-length relationship of the muscle fibre and not of the whole muscle. The above equation results in a predicted maximum isometric force of zero at fibre lengths corresponding to 0.58 and 1.8 of the optimal fibre length (Fig. 2.6.7). These fibre lengths correspond to the maximum and minimum fibre lengths of the length-tension relationship. Therefore, the minimum and maximum muscle fibre lengths possible with equation 2.6.32 are 0.58 and 1.8 of the optimal fibre length, respectively:

$$\check{L}^F_{Abs} = 0.58\,\bar{L}^F \qquad 2.6.33$$

$$\hat{L}^F_{Abs} = 1.8\,\bar{L}^F \qquad 2.6.34$$

where:

$\bar{\bar{L}}^F$ = optimal fibre length.

$\breve{L}^F_{Abs}$ = minimum possible fibre length based on optimal fibre length.

$\hat{L}^F_{Abs}$ = maximum possible fibre length based on optimal fibre length.

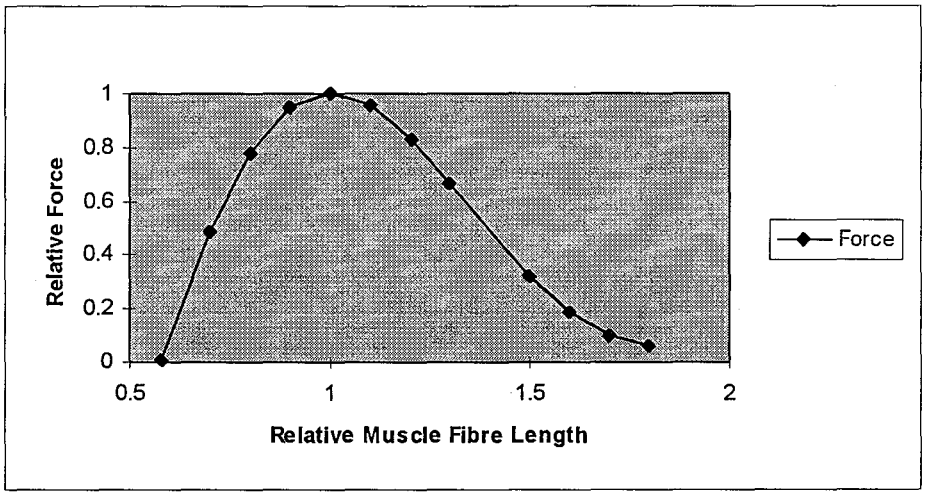

Figure 2.6.7. Force-length relationship for muscle fibre. Fibre length is expressed relative to optimal fibre length and force relative to the maximum isometric force at optimal fibre length. Maximum force of the contractile element occurs at optimal fibre length.

Fibre lengths outside of this range will result in a negative maximum isometric force being predicted by equation 2.6.32. A measure of the functional change in muscle belly length can be obtained from the maximum and minimum muscle lengths produced by the range of motion of the joint system spanned by the muscle. Functional maximum and minimum muscle fibre lengths and pennation angles can be calculated from the reference fibre length and reference pennation angle knowing the changes in muscle belly length. A minimum required optimal fibre length can also be calculated to allow the fibre lengths modelled in equation 2.6.32 to be defined over the range of functionally-measured maximum and minimum muscle fibre lengths. Combining equations 2.6.33 and 2.6.34:

$$\bar{\bar{L}}^F_{Func} = \frac{\hat{L}^F_{Func} - \breve{L}^F_{Func}}{1.22} \qquad 2.6.35$$

where:

$\bar{\bar{L}}^{F}_{Func}$ = minimum optimal fibre length to allow the functional maximum and minimum fibre length to be defined by the force - length relationship.

$\breve{L}^{F}_{Func}$ = functional minimum fibre length.

$\hat{L}^{F}_{Func}$ = functional maximum fibre length.

An optimal fibre length can be calculated which will result in the maximum and minimum possible muscle fibre lengths evenly spanning the measured range of muscle fibre lengths, as calculated from the changes in muscle belly length. Combining equations 2.6.33 and 2.6.34:

$$\bar{\bar{L}}^{F} = \frac{\hat{L}^{F}_{Func} + \breve{L}^{F}_{Func}}{2.38} \qquad 2.6.36$$

The reference data, taken from a skeletal reference and approximated to the subject in the anatomical position (including reference pennate angles, reference PCSA, reference fibre lengths) may well not correspond to the optimal fibre length at which the muscle fibre can produce its maximal contractile force.

The force-velocity relationship describes the maximum force a muscle can exert as a function of contractile speed. Herzog (1996) lists the following problems that arise when incorporating the force-velocity relationship into a model aimed at predicting muscle force distribution:

i) The force-velocity properties of individual human skeletal muscles are virtually unknown and must be estimated;
ii) Stretch related phenomena are also not well understood - for example, the abrupt decrease in muscle force when the muscle is stretched at a constant speed;
iii) The force-velocity relationship appears not to be unique but differs depending on whether the experiment was performed using force or speed control; and
iv) The force-velocity relationship for sub-maximal activation differs substantially from that obtained at maximal activation.

The equation of Hill (1938) is often used to describe the force-velocity relationship for concentric contractions (Pierrynowski & Morrison, 1985b; Herzog, 1996). Hill (1938) suggested that his force-velocity equation, which was determined for optimal fibre lengths,

also holds at other lengths when the maximum isometric force at the fibre length of interest is used instead of the maximum isometric force at optimal fibre length (Herzog, 1996). In this equation for modelling concentric contractions, the velocity is the rate of *shortening* of the contractile elements and is therefore greater than zero ($\dot{L}^{CE} > 0$).

$$\hat{F}^{CE} = \frac{\left(\hat{F}_i^{CE}.b - a.\dot{L}^{CE}\right)}{\dot{L}^{CE} + b} \qquad 2.6.37a$$

which may also be expressed as:

$$\hat{F}^{CE} = \frac{\left(\hat{F}_i^{CE} + a\right)b}{\dot{L}^{CE} + b} - a \qquad 2.6.37b$$

where:

$\hat{F}^{CE}$ = maximum force in the direction of contractile elements relative to velocity of contractile elements and fibre length.

$\hat{F}_i^{CE}$ = maximum isometric force in the direction of contractile elements at specified fibre length.

$\dot{L}^{CE}$ = velocity of shortening of contractile elements.

a,b = thermodynamic constants of units of force and speed, respectively.

To describe the eccentric contraction condition of the force-velocity relationship ($\dot{L}^{CE} < 0$) Pierrynowski and Morrison (1985) used the equation of FitzHugh (1977):

$$\hat{F}^{CE} = \hat{F}_e^{CE} - \frac{D\left(\hat{F}_e^{CE} - \hat{F}_i^{CE}\right)}{D - \dot{L}^{CE}} \qquad 2.6.38$$

where:

$$D = \left[\frac{b\left(\hat{F}_e^{CE} - \hat{F}_i^{CE}\right)}{\hat{F}_i^{CE} + a}\right] \qquad 2.6.39$$

with

$\hat{F}_e^{CE} = 1.25\left(\hat{F}_i^{CE}\right)$.

$\hat{F}^{CE}$ = maximum force in direction of contractile elements relative to velocity of contractile elements and fibre length.

$\hat{F}_i^{CE}$ = maximum isometric force in direction of contractile elements at specified fibre length.

$\hat{F}_e^{CE}$ = maximum eccentric force in direction of contractile elements at a specified fibre length.

$\dot{L}^{CE}$ = velocity of shortening of contractile elements.

a, b = thermodynamic constants of units force and velocity, respectively.

Pierrynowski & Morrison (1985b) assigned the values of $0.20\hat{F}_i^{CE}$, $0.35\hat{F}_i^{CE}$ and $0.35\hat{F}_i^{CE}$ to the constant *a* for the SO, FO and FG fibre types respectively, while the constant *b* was assigned the values $0.40L^F$, $2.25L^F$ and $2.25L^F$ for the three respective fibre groups. Bobbert et al. (1986) gave a value of *a* as $0.41\hat{F}_i^{CE}$ and *b* as $5.2L^F$. Baratta et al. (1995) assign a value for *b* by the relationship:

$$b = a.\frac{\hat{\dot{L}}^{CE}}{\hat{F}_i^{CE}} \qquad 2.6.40$$

where:

$\hat{\dot{L}}^{CE}$ = maximum velocity of shortening.

In addition to the problems in predicting force-length and force-velocity relationships, further problems arise when the two relationships are combined (Herzog, 1996). Substituting the maximum isometric force for varying fibre lengths into the force-velocity relationship results in force-velocity relationship scaled to the maximum isometric force attainable at the length of interest. As noted by Herzog (1996), a consequence of this is that the maximum velocity of shortening, in the unloaded condition, is also scaled, with maximum velocity of shortening occurring at the optimal fibre length, corresponding the maximum isometric force. Herzog (1996) points out that this is not supported by tests of single skeletal fibres where the velocity of unloaded shortening was similar with in a range of muscle fibre lengths. The validity of substituting maximum isometric forces at other fibre lengths may be questionable beyond maximal forces of slow contractile velocity near the optimal fibre length. The precise method for combining force-length and force-velocity relationships is still unknown (Herzog, 1996).

If force-length and force-velocity relationships are known for a muscle, then in order to apply these properties, the instantaneous lengths and rates of change of length of the muscle fibres and contractile elements are required. The instantaneous contractile conditions of the muscle fibres and contractile elements are approximated by a single representative fibre length and contractile element length, along with a representative pennation angle, fibre SEC length and tendon length. The fibre and contractile element lengths represent all muscle fibres included in the muscle model, which in turn, may represent part or all of the muscle. Individual fibres are seldom modelled despite knowledge of factors which effect the number of fibres recruited, order of fibre recruitment, and force generated by fibres individually or as a group, due to a limited knowledge of their interaction and how they should be modelled. Factors to be considered include muscle performance objectives, speed of contraction, fibre type, fatigue as well as the influence of fibre firing frequency and fibre firing synchronisation and how they effect individual fibre recruitment and force production. For this reason, the inclusion of individual muscle fibres and sarcomere length in the muscle model has not been achieved due to a lack of knowledge of how to model individual fibre characteristic.

Attempts to measure in-vivo instantaneous contractile conditions, that is, fibre lengths and rate of change of lengths during muscle activities, have shown to be inconsistent in their findings (Herzog, 1996). Such comparisons show the need for improved methods and a greater understanding of contraction mechanics before information relating to instantaneous contractile condition can be used with confidence (Herzog 1996).

2.6.2.5.10 Muscle model: contractile history

The force developed by a muscle is dependent on the history of its contractile conditions (Forcinito, et al., 1998; Wu & Herzog, 1999). The isometric force developed after stretch is higher than that in the truly isometric case, while isometric force after release is lower (Herzog, 1996). Herzog (1996) found these changes were dependent on the rate of stretch or release, with slow stretches resulting in higher force and slower releases resulting in lower forces. The nature of force enhancement after stretch or decrement after release is not fully understood and as a result is rarely considered in the description of contractile conditions of skeletal muscles (Herzog, 1996). These observation although observed experimentally on muscle tissue preparations are not modelled in classical cross bridge models (Wu & Herzog, 1999), however attempts have been made to incorporate history dependence phenomena into

the classic model (Forcinito, et al., 1998; Wu & Herzog, 1999). However, history dependence of muscle force production have not been included in the present model due to the lack of a clear understanding of mechanisms and accepted mathematical representation of this phenomena. Future research may provide a more precise understanding and appropriate mathematical representation in order to implement history dependence with force-length and force-velocity relationships.

2.6.2.5.11 Muscle model: parameters

Pierrynowski & Morrison (1985b) presented a detailed reference on the geometry of lower limb skeletal musculature. This was achieved by taking measurements from Eycleshymer & Shoemaker's (1970) atlas of cross-section anatomy, in combination with a comprehensive review of scientific literature. The resulting muscle geometry was measured relative to the anatomical length with the following explanations;

i) The Gluteus Minimus and Gluteus Medius were split into three equal sections;
ii) It was assumed that 25% of the Gluteus Maximus fibres inserted into the iliotibial tract;
iii) Some values are of low confidence due to scarcity of relevant literature; and
iv) Little data existed on the distribution of fibre types resulting in many values being estimated.

In the present study, the reference muscle model parameters of Pierrynowski & Morrison (1985b) were used with the following exceptions (Table 2.6.2):

i) Gluteus Maximus was modelled as three equal elements instead of two;
ii) Gluteus Medius was modelled as two equal elements instead of three; and
iii) Soleus was modelled as two equal elements instead of one.

For these three muscles, the mass and tendon cross sectional area were redistributed evenly between elements comprising the muscle. The relative reference fibre length, resting tendon length, reference pennation angle, shape factor, and percentage fibre types remained the same.

Table 2.6.2 Muscle model parameters for 47 muscle elements of the lower limb. From Pierrynowski & Morrison (1985b). See Table 2.6.1 for corresponding muscle names.

Standard Muscle Geometry Data									
Muscle	$\%\overline{L}^F$	$\%\widetilde{L}^T$	$\overline{\alpha}$ (°)	E	$A^T(mm^2)$	Mass (g)	%SO	%FO	%FG
1	0.80	0.20	0.00	2.0	32.0	102.0	0.50	0.20	0.30
2	1.00	0.00	0.00	2.3	0.0	114.0	0.50	0.20	0.30
3	0.90	0.10	0.00	1.5	(15.0)	4.0	0.50	0.20	0.30
4	0.90	0.10	0.00	1.5	(15.0)	6.0	0.50	0.20	0.30
5	0.65	0.35	0.00	2.0	(15.0)	17.0	0.50	0.20	0.30
6	0.40	0.60	0.00	1.2	(15.0)	27.0	0.50	0.20	0.30
7	0.75	0.25	0.00	1.5	(15.0)	23.0	0.50	0.20	0.30
8	1.00	0.00	0.00	1.2	0.00	24.0	0.50	0.20	0.30
9	1.00	0.00	0.00	1.8	0.00	31.0	0.45	0.15	0.40
10	1.00	0.00	0.00	2.6	0.00	107.0	0.65	0.15	0.20
11	1.00	0.00	0.00	1.4	0.00	22.0	0.55	0.15	0.30
12	1.00	0.00	0.00	2.1	0.00	80.0	0.55	0.15	0.30
13	0.75	0.25	0.00	2.1	15.0	248.0	0.55	0.15	0.30
14	1.00	0.00	0.00	1.3	0.0	57.0	0.45	0.15	0.40
15	0.80	0.20	0.00	1.9	19.0	17.0	0.50	0.20	0.30
16	0.80	0.20	0.00	1.9	19.0	17.0	0.50	0.20	0.30
17	0.80	0.20	0.00	1.9	19.0	17.0	0.50	0.20	0.30
18	0.85	0.15	0.00	1.8	13.0	47.0	0.50	0.20	0.30
19	0.85	0.15	0.00	1.8	13.0	47.0	0.50	0.20	0.30
20	0.85	0.15	0.00	1.8	13.0	47.0	0.50	0.20	0.30
21	0.90	0.10	0.00	1.6	69.0	89.0	0.50	0.20	0.30
22	0.30	0.70	0.00	1.6	23.0	265.0	0.50	0.20	0.30
23	0.15	0.85	0.00	1.7	5.0	23.0	0.70	0.10	0.20
24	0.096	0.35	15.0	1.6	24.0	173.0	0.50	0.15	0.35
25	0.60	0.40	0.00	1.9	12.0	102.0	0.50	0.15	0.35
26	0.60	0.40	0.00	1.4	6.0	59.0	0.55	0.15	0.30
27	0.80	0.20	0.00	1.5	24.0	90.0	0.50	0.20	0.30
28	0.102	0.40	15.0	1.7	24.0	105.0	0.45	0.15	0.40
29	0.146	0.45	15.0	1.9	20.0	115.0	0.65	0.10	0.20
30	(0.45)	(0.55)	0.00	1.9	9.0	78.0	0.65	0.10	0.25
31	0.188	0.20	20.0	1.9	89.0	407.0	0.45	0.20	0.35
32	0.177	(0.25)	10.0	1.7	56.0	253.0	0.50	0.15	0.35
33	0.198	0.20	25.0	1.8	32.0	139.0	0.50	0.15	0.35
34	0.80	0.20	0.0	1.9	24.0	(12.0)	0.50	0.15	0.35
35	0.130	0.65	10.0	1.7	(12.0)	53.0	0.55	0.15	0.30
36	0.121	0.65	15.0	1.7	(20.0)	90.0	0.55	0.15	0.30
37	0.20	0.80	5.0	2.0	4.0	6.0	0.45	0.15	0.40
38	0.103	0.80	15.0	1.9	(17.0)	159.0	0.75	0.15	0.10
39	0.208	0.80	10.0	2.2	20.0	63.0	0.70	0.10	0.20
40	0.079	0.60	20.0	2.0	17.0	42.0	0.55	0.25	0.20
41	0.087	0.80	10.0	2.2	21.0	(36.0)	0.60	0.10	0.30
42	0.210	0.90	10.0	2.7	11.0	(20.0)	0.45	0.15	0.40
43	0.200	0.55	(10.0)	1.0	4.0	(10.0)	0.35	0.20	0.45
44	0.120	0.80	15.0	1.9	13.0	34.0	0.40	0.15	0.45
45	0.120	0.85	10.0	2.5	13.0	10.0	0.50	0.20	0.30
46	0.085	0.65	20.0	2.0	12.0	12.0	0.40	0.20	0.40
47	0.090	0.65	20.0	1.8	15.0	30.0	0.50	0.15	0.35

2.6.2.5.12 Muscle model: subject specific anatomical measures

In order to implement the muscle model, subject-specific measures of fibre lengths, pennate angles, resting tendon lengths, and resting SEC lengths are required at a known muscle length. However, if the muscle geometry is known for a skeletal (or reference) specimen in the anatomical position, then these data can be used to approximate the muscle geometry of the subject while also in the anatomical position by scaling reference anatomical data to the subject. With reference fibre lengths and reference tendon lengths of the skeletal specimen being expressed as percentages of the respective muscle-tendon lengths, individual muscle-tendon lengths of the subject are required while also in the anatomical position. Each muscle-tendon path can be specified by a series of co-ordinates derived from a reference skeletal model. The reference co-ordinates define the origin, insertion and points along the muscle-tendon path and are expressed in the local body-fixed axis system of the segment to which the respective points belong. These muscle-tendon co-ordinates, and along with centre of mass and joint centres, can be expressed relative to reference segment dimensions to enable the co-ordinates to be scaled to the dimensions of the subject's respective segments to define muscle-tendon paths and muscle-tendon lengths for the subject. With the subject in the anatomical position, the muscle-tendon lengths, muscle fibre lengths, pennation angles and resting tendon lengths of the subject muscles can be calculated based on reference data (Pierrynowski & Morrison, 1985b). The muscle data derived for the subject is specific to the reference, usually anatomical, position from which it was derived, however muscle geometric and force data can be calculated for other muscle lengths and velocities using the force-length and force-velocity relationships. The reference fibre length ($\overline{L}^F$) and resting tendon length ($\widetilde{L}^T$) of the skeletal specimen are given in Table 2.6.2 as percentages of the reference muscle-tendon length. The pennate angles of Table 2.6.2 are also defined for the reference (or anatomical) position.

To obtain estimates of subject muscle mass (m) and tendon cross sectional area (A^T) it is neccesary to scale the skeletal or standard muscle masses and tendon cross sectional areas to that of the subject. Pierrynowski & Morrison (1985b) used the following method for scaling muscle mass and tendon area data they presented of the lower extremity (Table 2.6.2). Six measurements were taken:

i) Thigh length, L_T (greater tochanter to center of the knee joint);

ii) Shank length, L_S (knee joint center to ankle joint center);

iii) Thigh girth, G_T (at mid thigh length);

iv) Shank girth, G_S (at mid shank length);

v) Thigh skinfold, S_T (at mid shank length); and

vi) Shank skinfold, S_S (at mid shank length).

Two length and two area scaling factors were then defined:

$$\begin{aligned} S_{LT} &= L_T/39.5 \\ S_{LS} &= L_S/45.5 \\ S_{AT} &= (G_T - \pi.S_T)^2/1693 \\ S_{AS} &= (G_S - \pi.S_S)^2/494 \end{aligned} \qquad 2.6.41$$

For muscles contained within the pelvis or thigh, the muscle masses were obtained by the standard mass multiplied by the length and an area scaling factors of the thigh:

$$m_i = m_{si}.S_{LT}.S_{AT} \qquad i = 1, 2 \ldots 33. \qquad 2.6.42$$

For muscles contained within the pelvis or thigh, the tendon cross sectional areas were given by the standard tendon cross sectional area multiplied by an area scaling factor of the thigh:

$$A_i^T = A_{si}^T.S_{AT} \qquad i = 1, 2 \ldots 33. \qquad 2.6.43$$

Simmilarly for muscles contained with in the shank:

$$m_i = m_{si}.S_{LS}.S_{AS} \qquad i = 34, 35 \ldots 47. \qquad 2.6.44$$

$$A_i^T = A_{si}^T.S_{AS} \qquad i = 34, 35 \ldots 47. \qquad 2.6.45$$

Defining subject specific anatomical data by scaling skeletal reference data to the individual, whether it be muscle-tendon co-ordinates or muscle model parameters including muscle mass's, pennation angles and fibre lengths, is subject to considerable inaccuracies due to

individual variations within the musculo-skeletal system (Pierrynowski, 1995). In addition, scaling anatomical data from a reference skeleton produces approximate anatomical data at best as individual differences are not accounted for (Pierrynowski, 1995). Moment arms, defined from muscle-tendon co-ordinate data, and maximum muscle forces subject to muscle contraction dynamics, derived from muscle model parameters are particularly sensitive to errors in scaled anatomical data. As a result of the sensitivity of musculo-skeletal modelling to errors in defining subject specific anatomical data (Pierrynowski, 1995), measurements of musculo-skeletal function have been used to optimise segment fixed axes location and muscle model parameters to the subject in order to achieve a satisfactory description of muscle moment arms and muscle excitation contraction dynamics (Audu & Davy, 1985; Herzog, 1985). Functional measures may include joint centres of rotation and maximum resultant joint moments under isometric and dynamic conditions.

To derive subject specific muscle model parameters Pierrynowski & Morrison (1985a,b) provided individual muscle masses and tendon cross-sectional areas for the lower limb. Sufficient information was also presented to normalise individual muscle masses and tendon cross-sectional areas to the lean circumferences and lengths of the segment to which the muscle belly belonged ($Circ^2$.Length and $Circ^2$, respectively). In a later publication, Pierrynowski (1995) presented a simpler method for normalising these same parameters to either subject total body mass or total body height using allometric scaling with the assumption that length $\propto$ $Mass^4$. Pierrynowski (1995) stating that because of the inaccuracies involved a simpler scaling method will likely give comparable results as a more complex method. However, the use of total body mass and height to scale individual muscle parameters, instead of segment measures, may be contra-indicative of achieving subject specific anatomical data of sufficient accuracy to adequately describe force-length force-velocity relationships in subjects without the need for subject specific functional experiments.

The inaccuracies associated with scaling anatomical data to an individual and the sensitivity of musculo-skeletal modelling to anatomical data, highlights the need for improved methods for deriving subject specific anatomical data. This may involve improved scaling strategies and further development of optimisation techniques based on subject specific functional measures to adjust co-ordinate data and muscle model parameters to the individual.

2.6.2.6 Optimisation - gradient projection algorithm

The optimisation approach assumes that individual muscle are recruited in a manner which minimises a certain mechanical variable. The variable selected, such as muscle stress or energy expenditure, is usually based on physiological principles. Thus, a suitable cost function (objective function) is formulated along with constraints in the form of the equipolance equations as well as constraints on maximum and minimum control variables (muscle force or excitation level). Optimisation techniques are then used to calculate individual muscle forces. Siemienski (1992) points out that although the process is presumably reflective of some aspects of an optimal control pattern, the choice of cost (objective function) to be minimised is often governed by computational convenience rather than the need for reasonable results.

In obtaining a solution, let the unknown variables by given by the vector:

$$\vec{F} = (F_1, F_2 \ldots F_m) \qquad 2.6.46$$

and the cost function to be minimised, by:

$$\text{cost function} = g(\vec{F}) \qquad 2.6.47$$

In addition, the constraints due to the equipolance equations can be represented as:

$$A\vec{F} = \vec{b} \qquad 2.6.48$$

and the constrains due to boundaries:

$$F_{i,min} \leq F_i \leq F_{i,max} \qquad 2.6.49$$

From a current estimate of the unknown variables $(\vec{F}_c)$ at a minimum of the cost function, a new and improved estimate $(\vec{F}_n)$is calculated. The new estimate at the unknown variables is given by:

$$\vec{F}_n = \vec{F}_c + \varsigma.\vec{z} \qquad 2.6.50$$

where:

ς = predetermined step size.

If the vector giving the direction of the step $(\vec{z})$ for the current estimate $(\vec{F}_c)$ can be calculated, then equation 2.6.50 in turn, can be repeated until convergence at the minimum solution. Convergence is given by a criterion based on the size of improvements to the current estimate $(\varsigma.\vec{z})$.

The task is to determine the direction of the step $(\vec{z})$ for each estimate of the unknown variables $(\vec{F}_c)$, since the current and new estimates are required to meet the constraints in the form of the equipolance equations:

$$A.\vec{F}_c = \vec{b} \qquad 2.6.51$$

and

$$A.\vec{F}_n = \vec{b} \qquad 2.6.52$$

therefore:

$$A.\vec{z} = 0 \qquad 2.6.53$$

The quickest descent toward a minimum of the object function is given by the gradient evaluated at the current estimate of the unknown variables. Therefore, the direction of the quickest descent is given by:

$$\vec{w} = (-\nabla\vec{g})(\vec{F}_c) \qquad 2.6.54$$

but generally $\vec{w}$ will not meet the requirements of the equipolance equations:

$$A.\vec{w} \neq 0 \qquad 2.6.55$$

So $\vec{z}$ is found by getting the best approximation to $\vec{w}$ subject to condition 2.6.53. This is achieved by the relationship:

$$\vec{w} - \vec{z} = A^T.\left(A.A^T\right)^{-1}.A.\vec{w} \qquad 2.6.56$$

which can be written:

$$\vec{z} = B.\vec{w} \qquad 2.6.57$$

where:

$$B = I - A^T.\left(A.A^T\right)^{-1}.A \qquad 2.6.58$$

In determining a step size, the cost function used and the magnitude of the variables were considered. In the present example, with the use of the sum of normalised squared muscle forces with maximum and minimum soft constraints, the magnitude of entries in matrix $\vec{z}$ are approximately 1 divided by the result of $F_{i,max}$ minus $F_{i,min}$. With a desired maximum initial correction in variable magnitude of approximately one tenth the initial value, a starting step size was chosen as:

$$\varsigma = \max\left[\left(F_{i,max} - F_{i,min}\right)^2 \times 0.1\right]_{i=1...m} \qquad 2.6.59$$

An initial estimate must first be made for the muscle forces which will meet the equipolance equations and be close to the minimum of the cost function. The closer the initial approximation is the minimum of the cost function, the greater are the chances of convergence to the actual minimum. For the present study, where the cost function involves the minimisation of muscle stresses, a reduction approach was adopted in which muscle forces were directly assigned according to their relative moment-generating capacity. For example, let four muscles cross a joint as described by the equipolance equation relating muscle forces, moments arms, and resultant joint moment:

$$F_1 \times 0.02 + F_2 \times 0.03 + F_3 \times 0.04 + F_4 \times 0.03 = 20\,\text{Nm}. \qquad 2.6.60$$

If the maximum muscle forces for the four muscles are:

$$\begin{aligned} F_{1,max} &= 160\ N \\ F_{2,max} &= 200\ N \\ F_{3,max} &= 200\ N \\ F_{4,max} &= 280\ N \end{aligned} \qquad 2.6.61$$

For the present example, the relative moment-generating capacity (RMGC) of each muscle is given by:

$$RMGC_i = \frac{\left(F_{i,max} \cdot \perp_i\right)}{\left(160 \times 0.02 + 200 \times 0.03 + 200 \times 0.04 + 280 \times 0.03\right)} \qquad 2.6.62$$

For each of the four muscles, the RMGCs are:

$$\begin{aligned} RMGC_1 &= 0.125 \\ RMGC_2 &= 0.234 \\ RMGC_3 &= 0.313 \\ RMGC_4 &= 0.328 \end{aligned} \qquad 2.6.63$$

where:

$$RMGC_1 + RMGC_2 + RMGC_3 + RMGC_4 = 1.000 \qquad 2.6.64$$

For the present example, with a resultant moment of 20 Nm, the initial muscle forces are give by:

$$F_i = \frac{\left(RFGC_i . 20\right)}{\left(\perp_i\right)} \qquad 2.6.65$$

The initial estimations of the four muscle forces are then:

$$\begin{aligned} F_1 &= 125.0\ N \\ F_2 &= 156.0\ N \\ F_3 &= 156.3\ N \\ F_4 &= 218.7\ N \end{aligned} \qquad 2.6.66$$

The solution of the optimisation proceeds as follows:

i) For the current instant in time, matrix A is determined and matrix B derived;

ii) For the current instant in time, a first estimate of muscle forces is obtained which satisfies the equations of motion and these estimates are between any constraints placed on the magnitudes of the forces;

iii) In an iterative procedure,

- For the current muscle force estimates $\vec{w}$ and $\vec{z}$ are calculated;
- The new muscle force estimates are calculated from $\vec{z}$ and a pre-defined step size;
- If the new muscle force estimates are less than zero or greater than the respective maximum value, then the step size is reduced and the iteration repeated; and

iv) The iteration proceeds until a convergence criterion is met.

In the example given earlier of a single joint of one degree of freedom under the control of four muscles, where the cost function is the sum of squared normalised forces with soft constraints on both maximum and minimum muscle forces, the following can be derived:

From the equipolance equations:

$$A = \begin{bmatrix} 0.02 & 0.03 & 0.04 & 0.03 \end{bmatrix} \qquad 2.6.67$$

where:

$$\begin{bmatrix} 0.02 & 0.03 & 0.04 & 0.03 \end{bmatrix} \cdot \begin{bmatrix} F_1 \\ F_2 \\ F_3 \\ F_4 \end{bmatrix} = \begin{bmatrix} \sum \tau \end{bmatrix} \qquad 2.6.68$$

and:

$$B = \begin{bmatrix} 0.8947 & -0.1579 & -0.2105 & -0.1579 \\ -0.1579 & 0.7632 & -0.3158 & -0.2368 \\ -0.2105 & -0.3158 & 0.5789 & -0.3158 \\ -0.1579 & -0.2368 & -0.3158 & 0.7632 \end{bmatrix} \qquad 2.6.69$$

with the cost function:

$$g(\vec{F}) = -\sum_{i=1}^{4}\left(\sqrt{1-\left(\frac{F_i - F_{i,min}}{F_{i,max} - F_{i,min}}\right)^2}\right) \qquad 2.6.70$$

then:

$$\dot{\vec{w}} = (-\nabla\vec{g})(\vec{F}_c) = \left[\frac{-(F_{1,C} - F_{1,min})}{(F_{1,max} - F_{1,min})^2 \cdot \sqrt{1-\left(\frac{F_{1,C} - F_{1,min}}{F_{1,max} - F_{1,min}}\right)^2}}, \ldots\ldots\right.$$

$$\left. \ldots\ldots, \frac{-(F_{4,C} - F_{4,min})}{(F_{4,max} - F_{4,min})^2 \cdot \sqrt{1-\left(\frac{F_{4,C} - F_{4,min}}{F_{4,max} - F_{4,min}}\right)^2}}\right] \qquad 2.6.128$$

With the use of the sum of normalised squared muscle forces with maximum and minimum soft constraints, it can be seen from equation 2.6.65, that in order for the cost function to be defined for the current estimate of the muscle forces:

$$1-\left(\frac{F_{i,C} - F_{i,min}}{F_{i,max} - F_{i,min}}\right)^2 \geq 0.0 \qquad 2.6.71$$

For this to be the case, the initial estimates of muscle forces must be a positive value between $(2.F_{i,min} - F_{i,max})$ and $F_{i,max}$, hence:

$$\breve{F}_i < F_{i,c} < F_{i,max} \qquad 2.6.72$$

where:

$$\breve{F}_i = \begin{cases} 0 & \text{if } \left(2.F_{i,min} - F_{i,max}\right) < 0 \\ 2.F_{i,min} - F_{i,max} & \text{if } \left(2.F_{i,min} - F_{i,max}\right) > 0 \end{cases} \qquad 2.6.73$$

Let the constraints on muscle forces for the current instant in time be:

$$\begin{aligned} F_{1,min} &= 60.0\ \text{N.} \\ F_{2,min} &= 90.0\ \text{N.} \\ F_{3,min} &= 60.0\ \text{N.} \\ F_{4,min} &= 150.0\ \text{N.} \\ F_{1,max} &= 160.0\ \text{N.} \\ F_{2,max} &= 200.0\ \text{N.} \\ F_{3,max} &= 200.0\ \text{N} \\ F_{4,max} &= 280.0\ \text{N.} \end{aligned} \qquad 2.6.74$$

With the cost function and muscle force limits in the present example the range of values that may be used in the initial estimate of muscle forces are:

$$\begin{aligned} 0.0 \le F_{1,C} &\le 160.0\ \text{N.} \\ 0.0 \le F_{2,C} &\le 200.0\ \text{N.} \\ 0.0 \le F_{3,C} &\le 200.0\ \text{N} \\ 20.0 \le F_{4,C} &\le 280.0\ \text{N.} \end{aligned} \qquad 2.6.75$$

The step size chosen was:

$$\varsigma = 5000 \qquad 2.6.76$$

If the sum of moments $\left(\sum \tau\right)$ is equal to 20 Nm for the current instant in time, then an initial approximation to the muscle forces may be:

$$\vec{F}_c = [150.0 \quad 183.33 \quad 127.5 \quad 213.33] \tag{2.6.77}$$

For the first iteration of the unconstrained optimisation:

$$\vec{w} = [-0.02065 \quad -0.01457 \quad -0.00393 \quad -0.00448] \tag{2.6.78}$$

$$\vec{z} = [-0.01464 \quad -0.00556 \quad 0.00809 \quad 0.00453] \tag{2.6.79}$$

$$\vec{F}_n = [76.809 \quad 155.533 \quad 167.939 \quad 236.002] \tag{2.6.80}$$

Should the step result in any of the muscle forces being less then zero or greater than the respective maximum muscle force, then the step size is reduced by an appropriate amount so that the muscle forces remain greater than zero and less than the maximum values and the iteration repeated. Convergence is achieved at:

$$\vec{F} = [97.4 \quad 150.9 \quad 164.8 \quad 231.1] \tag{2.6.81}$$

3 METHODS

This chapter provides a description of the procedures adopted in the present study. Firstly the muscle model parameters required to define the 48 muscle elements of the lower limb are presented. A procedures is then presented to optimise muscle model parameters to the range of muscle belly lengths of the movement analysis to define a force-length relationship for the range of muscle fibre lengths. Procedures are then presented to combine muscle geometric model with force-length and force-velocity relationships to calculate maximum muscle forces accounting for the inter-dependence of muscle model parameters. This is followed by the optimisation procedure, including the analytical approach adopted in implementing maximum dynamic muscle forces and muscle excitation dynamics. Also included in the methods are test examples which implement the methods presented on muscle modelling and optimisation on both a simple one joint and two joint system. The methods used to derive body segment axes from external markers is then given, followed by the derivation of segment mass, inertia, centre of mass and joint centres. A description of the anthropometric measures used to normalise muscle model and segment parameters is also given. The anthropometric measures of the subject are required to scale the standard data presented. This is followed by a brief background on electomyography, as well as the method used in recording and analysing muscle activity in the present study. Finally, the experimental protocol is given, including subject preparation, test set-up, and how the subject trials were conducted.

3.1 Muscle model

In this section, the implementation of the muscle model is given. This involves the derivation of muscle co-ordinate data with respect to segment axes describing each muscle element path, standard muscle model parameters describing model geometry, scaling of the standard muscle data to the dimensions of a subject, optimisation of muscle model parameters to the range of muscle lengths presented in a movement trial, and finally, methods for implementing muscle force-length, force-velocity and excitation characteristics of muscle. This section is concluded with an example of a simple joint system involving both a pennate and non-pennate muscle in which the results of the optimisation procedure and implementation of force-length force-velocity relationships are given.

3.1.1 Muscle model path co-ordinate data

In order to describe muscle-tendon lengths, paths and moment arms during human movement, relative segment co-ordinate data are needed on muscle origins, insertions and deflection points that are applicable to a range of segment positions. In order to gain co-ordinate information on muscle paths a skeletal model was used in which 48 muscle elements of the lower limb were modelled by elastic cords attached to the skeleton at respective origins and insertions as well as passing through deflection points maintained by wire (Fig. 3.1.1, Fig. 3.1.2, Fig. 3.2.3). Deflection points approximated the path of the muscle tendon complex as it was deflected around bone, other muscle, retinacula, and joint capsules. The location of muscle origins, insertions and deflection points were based on standard anatomical text (Romanes, 1972; Agur, et al., 1991; Marieb & Mallett, 1992; Williams & Bannister, 1995). The skeletal model was moved through a range of joint angles (Table 3.1.1) to test the consistency of the deflection points in describing muscle path and moment arms. The number of points used, including origin and insertion, to define the 48 muscle elements in the present study are presented in Table 3.1.2. Descriptions of the pelvis, thigh, shank and foot axes used to describe each segment are given in Section 3.3.1. The measures used to normalise the muscle co-ordinate data were also taken from the skeletal model. The pelvis (x, y, z) co-ordinates were normalised to pelvic width, depth and height respectively, while the thigh, shank and foot (x, y, z) co-ordinates were normalised to segment width, width and length respectively. Descriptions of the segment measurements are given in Section 3.4. The normalised co-ordinates for origin, insertion and deflection points of the 48 muscle elements are presented in Appendix B.

3.1.2 Muscle model parameters

Standard muscle model parameters were required for each muscle element modelled to describe muscle geometry. A single muscle may need to modelled as more than one element to adequately describe the function of that muscle. Standard muscle model parameters were adapted from Pierrynowski & Morrison (1985b), and included percent fibre lengths, percent tendon lengths, pennation angles, shape factors between mean and maximum cross sectional area, tendon cross sctional areas, muscle mass, and percent fibre type of 47 muscle elements of the lower limb. In the study of Pierrynowski & Morrison (1985b) Gluteus Maximus was modelled as two elements, Gluteus Minimus as three and Soleus as one element. In the present

study Gluteus Maximus was modelled as three elements, Gluteus Minimus as two and Soleus as two elements (Table 3.1.3). To adjust the model data of Pierrynowski & Morrison (1985b) the mass and tendon cross-sectional areas of the elements comprising each muscle were summed and divided equally into the required number of elements for that muscle as used in the present study. In this way the three elements of Gluteus Maximus were of equal mass and tendon cross-sectional area, likewise for the two elements of both Gluteus Minimus and Soleus. All other muscle model parameters for Gluteus Maximus, Gluteus Minimus and Soleus remained unchanged. Similarly, all other muscle elements modelled were as in Pierrynowski & Morrison (1985b). Individual muscle element mass and tendon cross-sectional areas in the present study were normalised using thigh and shank length and circumference measurements presented by Pierrynowski and Morrison (1985a). Muscle element masses were normalised by the square of segment lean circumference and segment length, while tendon cross-sectional areas were normalised by the square of segment lean circumference. The normalised muscle element masses and tendon cross sectional areas, along with the non-normalised segment measures used are presented in Appendix B.

Table 3.1.1 Range of motion of skeletal model.

Joint action	Range of motion (degrees)*
Hip flexion	70
Hip extension	25
Hip adduction	30
Hip abduction	35
Hip external rotation	40
Hip internal rotation	25
Knee flexion	90
Knee extension	0
Knee external rotation	10 (at 45° knee flexion)
Knee internal rotation	10 (at 45° knee flexion)
Ankle dorsi-flexion	25
Ankle plantar flexion	40
Ankle eversion	5
Ankle inversion	15

*Neutral or zero position is the standing anatomical position.

Table 3.1.2 Points used to describe muscle element paths.

	Muscle	Number of co-ordinates
1	Psoas Major	4
2	Iliacus	4
3	Gemellus Superior	2
4	Gemellus Inferior	2
5	Obturator Externus	2
6	Obturator Internus	3
7	Piriformis	2
8	Quadratus Femoris	2
9	Pectineus	2
10	Adductor Longus	2
11	Adductor Magnus (anterior)	2
12	Adductor Magnus (middle)	2
13	Adductor Magnus (posterior)	2
14	Adductor Brevis	2
15	Gluteus Minimus (anterior)	2
16	Gluteus Minimus (posterior)	2
17	Gluteus Medius (anterior)	3
18	Gluteus Medius (middle)	3
19	Gluteus Medius (posterior)	3
20	Gluteus Maximus (anterior)	4
21	Gluteus Maximus (middle)	4
22	Gluteus Maximus (posterior)	4
23	Tensor Fasviae Latae	3
24	Semimembranosis	3
25	Semitendinosus	4
26	Gracilis	3
27	Satorius	4
28	Rectus Femorus	4
29	Biceps Femoris (long)	4
30	Biceps Femoris (short)	4
31	Vastus Lateralis	4
32	Vastus Intermedius	4
33	Vastus Medialis	4
34	Popliteus	3
35	Gastrocnemius (lateral)	4
36	Gastrocnemius (medial)	4
37	Plantaris	4
38	Soleus (lateral)	2
39	Soleus (medial)	2
40	Tibialis Anterior	3
41	Tibialis Posterior	4
42	Peroneus Longus	4
43	Peroneus Brevis	3
44	Peroneus Tertius	4
45	Extensor Digitorum Longus	4
46	Extensor Hallucis Longus	4
47	Flexor Digitorum Longus	4
48	Flexor Hallucis Longus	4

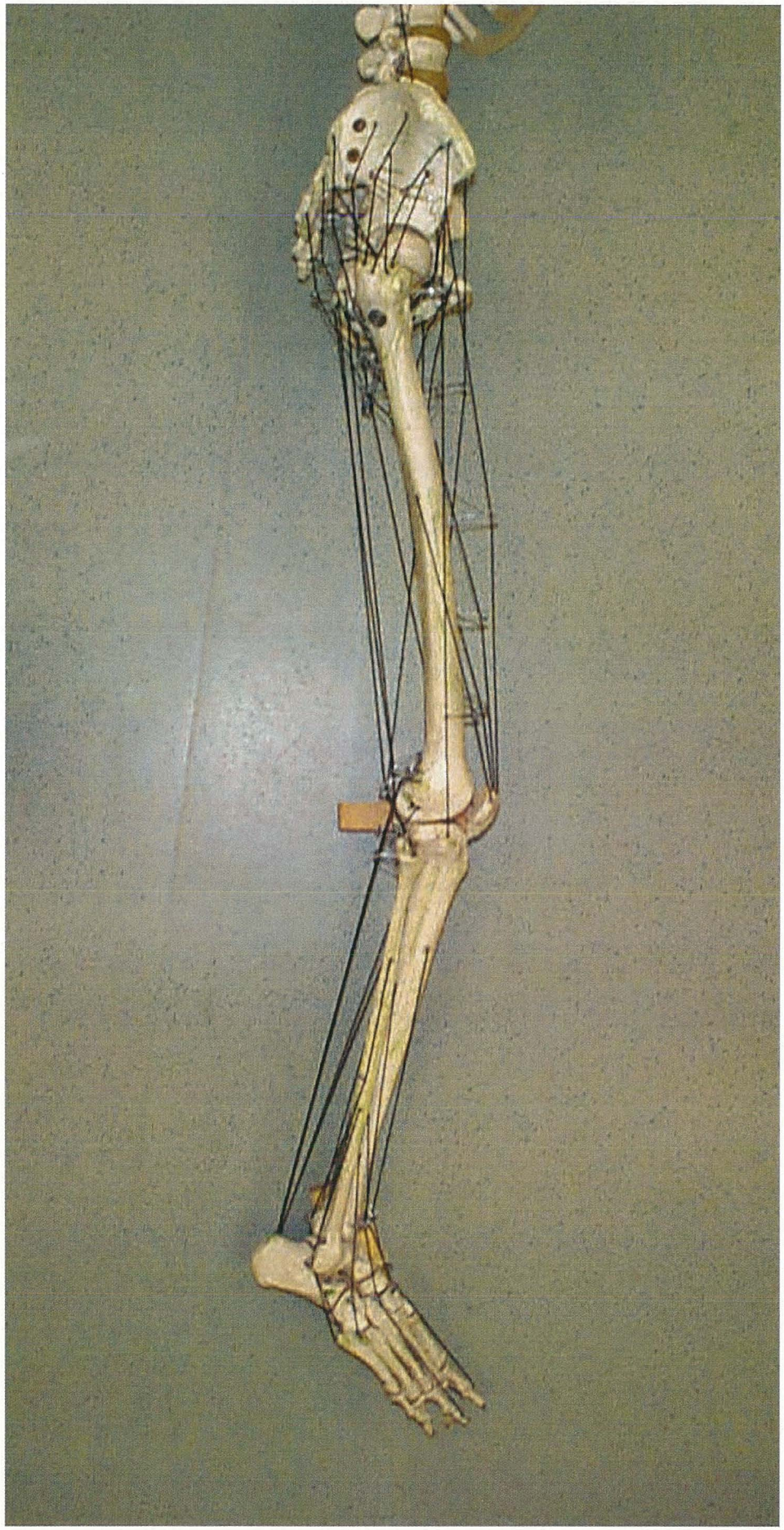

Figure 3.1.1 Skeletal model muscle paths - lateral view.

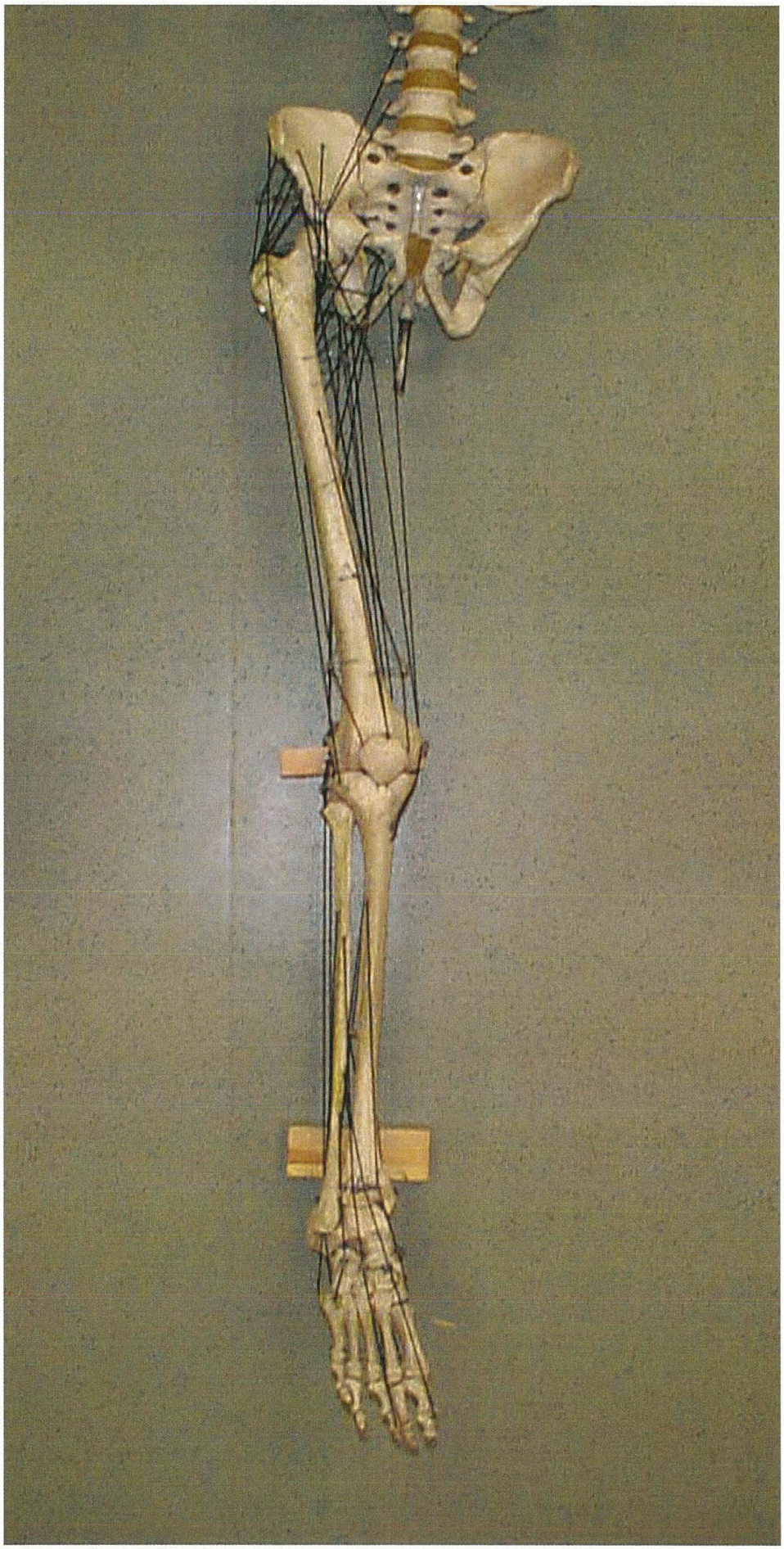

Figure 3.1.2 Skeletal model muscle paths - anterior view.

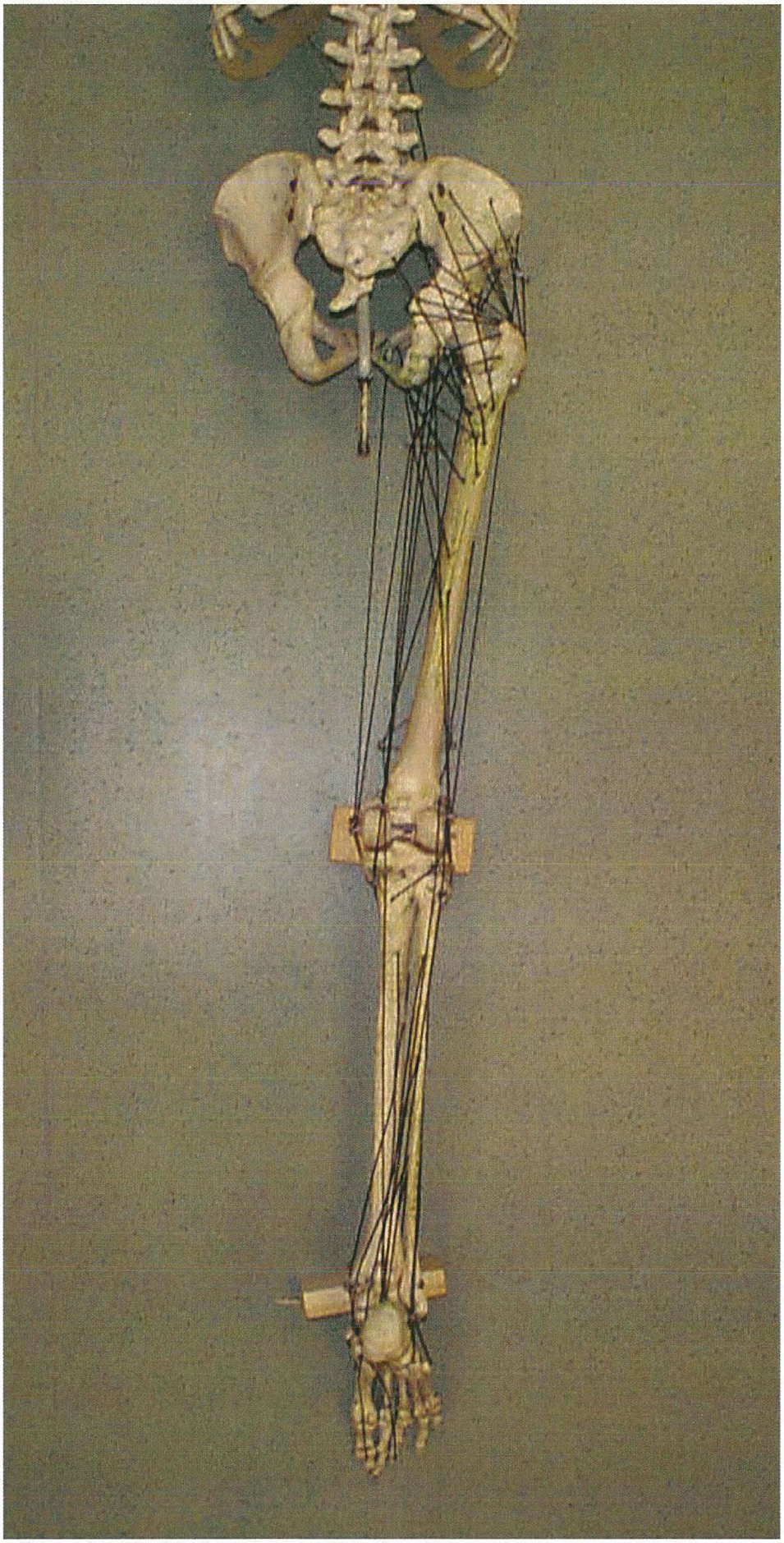

Figure 3.1.3 Skeletal model muscle paths - posterior view.

Table 3.1.3 Muscle model parameters for 48 muscle elements of the lower limb.

Standard Muscle Geometry Data for 48 muscle elements of the lower limb*									
Muscle	$\%\bar{L}^F$	$\%\tilde{L}^T$	$\bar{\alpha}$ (°)	E	$A^T(mm^2)$	Mass (g)	%SO	%FO	%FG
1	0.80	0.20	0.00	2.0	32.0	102.0	0.50	0.20	0.30
2	1.00	0.00	0.00	2.3	0.0	114.0	0.50	0.20	0.30
3	0.90	0.10	0.00	1.5	(15.0)	4.0	0.50	0.20	0.30
4	0.90	0.10	0.00	1.5	(15.0)	6.0	0.50	0.20	0.30
5	0.65	0.35	0.00	2.0	(15.0)	17.0	0.50	0.20	0.30
6	0.40	0.60	0.00	1.2	(15.0)	27.0	0.50	0.20	0.30
7	0.75	0.25	0.00	1.5	(15.0)	23.0	0.50	0.20	0.30
8	1.00	0.00	0.00	1.2	0.00	24.0	0.50	0.20	0.30
9	1.00	0.00	0.00	1.8	0.00	31.0	0.45	0.15	0.40
10	1.00	0.00	0.00	2.6	0.00	107.0	0.65	0.15	0.20
11	1.00	0.00	0.00	1.4	0.00	22.0	0.55	0.15	0.30
12	1.00	0.00	0.00	2.1	0.00	80.0	0.55	0.15	0.30
13	0.75	0.25	0.00	2.1	15.0	248.0	0.55	0.15	0.30
14	1.00	0.00	0.00	1.3	0.0	57.0	0.45	0.15	0.40
15	0.80	0.20	0.00	1.9	29.0	26.0	0.50	0.20	0.30
16	0.80	0.20	0.00	1.9	29.0	26.0	0.50	0.20	0.30
17	0.85	0.15	0.00	1.8	13.0	47.0	0.50	0.20	0.30
18	0.85	0.15	0.00	1.8	13.0	47.0	0.50	0.20	0.30
19	0.85	0.15	0.00	1.8	13.0	47.0	0.50	0.20	0.30
20	0.90	0.10	0.00	1.6	31.0	118.0	0.50	0.20	0.30
21	0.90	0.10	0.00	1.6	31.0	118.0	0.50	0.20	0.30
22	0.90	0.10	0.00	1.6	31.0	118.0	0.50	0.20	0.30
23	0.15	0.85	0.00	1.7	5.0	23.0	0.70	0.10	0.20
24	0.096	0.35	15.0	1.6	24.0	173.0	0.50	0.15	0.35
25	0.60	0.40	0.00	1.9	12.0	102.0	0.50	0.15	0.35
26	0.60	0.40	0.00	1.4	6.0	59.0	0.55	0.15	0.30
27	0.80	0.20	0.00	1.5	24.0	90.0	0.50	0.20	0.30
28	0.102	0.40	15.0	1.7	24.0	105.0	0.45	0.15	0.40
29	0.146	0.45	15.0	1.9	20.0	115.0	0.65	0.10	0.20
30	(0.45)	(0.55)	0.00	1.9	9.0	78.0	0.65	0.10	0.25
31	0.188	0.20	20.0	1.9	89.0	407.0	0.45	0.20	0.35
32	0.177	(0.25)	10.0	1.7	56.0	253.0	0.50	0.15	0.35
33	0.198	0.20	25.0	1.8	32.0	139.0	0.50	0.15	0.35
34	0.80	0.20	0.0	1.9	24.0	(12.0)	0.50	0.15	0.35

(Table continued)

Table 3.1.3 cont. Muscle model parameters for 48 muscle elements of the lower limb.

Standard Muscle Geometry Data for 48 muscle elements of the lower limb*									
Muscle	$\%\overline{L}^F$	$\%\widetilde{L}^T$	$\overline{\alpha}$ (°)	E	A^T (mm^2)	Mass (g)	%SO	%FO	%FG
35	0.130	0.65	10.0	1.7	(12.0)	53.0	0.55	0.15	0.30
36	0.121	0.65	15.0	1.7	(20.0)	90.0	0.55	0.15	0.30
37	0.20	0.80	5.0	2.0	4.0	6.0	0.45	0.15	0.40
38	0.103	0.80	15.0	1.9	(9.0)	80.0	0.75	0.15	0.10
39	0.103	0.80	15.0	1.9	(9.0)	80.0	0.75	0.15	0.10
40	0.208	0.80	10.0	2.2	20.0	63.0	0.70	0.10	0.20
41	0.079	0.60	20.0	2.0	17.0	42.0	0.55	0.25	0.20
42	0.087	0.80	10.0	2.2	21.0	(36.0)	0.60	0.10	0.30
43	0.210	0.90	10.0	2.7	11.0	(20.0)	0.45	0.15	0.40
44	0.200	0.55	(10.0)	1.0	4.0	(10.0)	0.35	0.20	0.45
45	0.120	0.80	15.0	1.9	13.0	34.0	0.40	0.15	0.45
46	0.120	0.85	10.0	2.5	13.0	10.0	0.50	0.20	0.30
47	0.085	0.65	20.0	2.0	12.0	12.0	0.40	0.20	0.40
48	0.090	0.65	20.0	1.8	15.0	30.0	0.50	0.15	0.35

*Adapted from Pierrynowski & Morrison (1985b), where parentheses indicated values of low confidence. See Table 3.1.2 for corresponding muscle names.

$\%\overline{L}^F$ = muscle fibre length relative to reference muscle length.

$\%\widetilde{L}^T$ = tendon slack length relarive to reference muscle length.

$\overline{\alpha}$ (°) = muscle pennation angle in degrees at reference muscle length.

A^T = tendon cross sectional area.

Mass = muscle mass.

%SO = relative distribution of SO muscle fibre type.

%FO= relative distribution of FO muscle fibre type.

%FG= relative distribution of FG muscle fibre type.

3.1.3 Muscle model parameter optimisation

A functional maximum and minimum change in muscle belly length can be obtained from the maximum and minimum muscle lengths produced by the range of motion of the joint system. Limits exist in the range of fibre lengths defined by the force-length relationship when an optimal fibre length is defined. Limits can also be imposed on the pennation angle such that it lies between zero and a maximum angle at the minimum muscle belly length. Knowing the maximum and minimum muscle lengths necessary to produce the desired range of segment motion, reference muscle pennation angles and reference fibre lengths can be adjusted to accommodate the range of motion and pennation angle limits and at the same time derive an optimal fibre length and optimal muscle force for each muscle. The maximum and minimum

muscle-tendon lengths can be found by mathematically modelling each joint at it's full range of motion and applying the skeletal reference co-ordinate data defining each muscle path (Pierrynowski & Morrison, 1985b). Alternatively, maximum and minimum muscle-tendon lengths can be determined for the task under investigation for each segment position recorded, again by using skeletal reference co-ordinate data defining each muscle path. The optimisation in this case is specific to this task and the specific changes in belly length. Optimisation of reference fibre length and reference pennation angle to the maximum and minimum changes in muscle-tendon length, and calculation of an optimal fibre length can be achieved by the solution of simultaneous equations involving changes in muscle belly length and muscle architecture.

The following variables are known from skeletal data fitted to the subject and from subject range of motion:

$\bar{L}^M$ = reference muscle - tendon length, at which reference muscle model data is defined.
$\hat{L}^M$ = maximum muscle - tendon length.
$\check{L}^M$ = minimum muscle - tendon length.
$\hat{L}^T$ = resting tendon length.
$\bar{L}^B$ = reference belly length.

The maximum and minimum changes in muscle belly length relative to the reference belly length are given from the maximum and minimum muscle lengths, resting tendon length, and maximum tendon length. To avoid the mathematical problem of muscles being at their limit of modelled length, as described by the force-length relationship, and unable to produce force at the maximum and minimum range of motion for the movement trial, 15% was arbitrarily added on to the changes in belly length as measured from the range of motion. In effect when the segments were at their limit of recorded range of motion the muscles were not at the limit of their modelled length. This is a practical solution, and the choice of 15% was arbitrarily chosen based on the shape of the muscle fibre force-length curve rather than on physiological rational, in order to ensure the fibre length and pennation angle are such that the change in fibre length will allow movement over a known range of motion and be able to exert force over this range.

The maximum belly length is given by the maximum muscle-tendon length minus the slack (resting) tendon length. The minimum belly length is given by the minimum sum of muscle-tendon length minus tendon length under maximum isometric force at various muscle lengths. As tendon stretch will decrease the belly length and isometric force varies according to muscle fibre length. In the present study, minimum belly length was estimated as the minimum muscle-tendon length minus the maximum tendon length. This is an overestimation of the actual minimum belly length but ensures the range of possible belly lengths is included. The maximum tendon length is calculated from the maximum contractile force of the muscle, being the optimal isometric force at the optimal muscle fibre length. Optimal isometric force for each muscle is calculated within the optimisation procedure from the resulting reference fibre length, pennation angle and optimal fibre length. Hence the maximum stretch of the tendon in the present model is not known until after the parameters have been optimised and optimal muscle force attained, requiring an initial estimate of maximum tendon length to start the optimisation procedure.

As optimal fibre length and optimal force depend on the maximum and minimum belly length used in the optimisation procedure, maximum tendon length and consequently minimum belly length cannot be calculated directly. Instead, an iterative procedure was used with an initial estimation of maximum tendon length. The optimisation procedure was executed and an optimal fibre length and maximum isometric force calculated, and a new maximum tendon length was then calculated. If the change in maximum tendon length was greater than a specified value (say 0.5%) then a new minimum belly length was calculated and the optimisation procedure repeated.

The optimisation procedure began with a minimum and maximum change in muscle belly length, calculated from the muscle lengths of the movement trial and reference tendon and belly lengths, and is given by:

$$\Delta\hat{L}^B = \left(\hat{L}^M - \tilde{L}^T - \bar{L}^B\right) \qquad 3.1.1a$$

$$\Delta\check{L}^B = \left(\check{L}^M - \hat{L}^T - \bar{L}^B\right) \qquad 3.1.1b$$

and

$$\text{ext.}\Delta\hat{L}^B = \left[\left(\Delta\hat{L}^B - \Delta\check{L}^B\right) \times 0.15\right] + \Delta\hat{L}^B \qquad 3.1.2a$$

$$\text{ext.}\Delta\check{L}^B = \Delta\check{L}^B - \left[\left(\Delta\hat{L}^B - \Delta\check{L}^B\right) \times 0.15\right] \qquad 3.1.2b$$

where:

$\Delta\hat{L}^B$ = maximum change in muscle belly length from reference belly length.

$\Delta\check{L}^B$ = minimum change in muscle belly length from reference belly length.

$\hat{L}^M$ = maximum muscle - tendon length.

$\check{L}^M$ = minimum muscle - tendon length.

$\tilde{L}^T$ = resting tendon length.

$\bar{L}^B$ = reference belly length.

$\hat{L}^T$ = maximum length of the tendon, calculated from optimal isometric force.

$\text{ext.}\Delta\hat{L}^B$ = extended maximum change in muscle belly length.

$\text{ext.}\Delta\check{L}^B$ = extended minimum change in muscle belly length.

First reference fibre lengths, reference pennation angles, and optimal fibre lengths are adjusted to the changes in belly length. First, the case of the non-pennate muscle is presented followed by the pennate muscle.

For a non-pennate muscle the relationship between the optimal fibre length, reference fibre length and maximum and minimum changes in belly length are shown in Fig. 3.1.4.

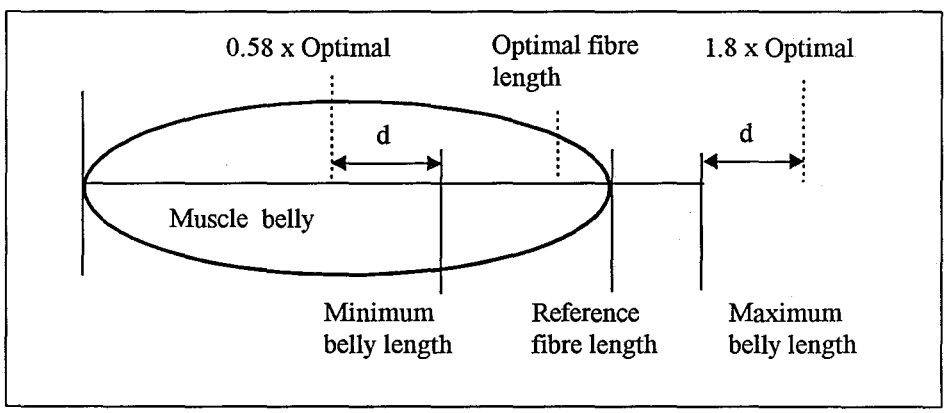

Figure 3.1.4 Relationship between optimal fibre length, reference fibre length and maximum and minimum changes in belly length for a non-pennate muscle. The relationship between maximum and minimum fibre lengths and optimal fibre length are obtained from the force-length relationship of Hatze (1977).

If the optimal muscle fibre length was chosen so that the maximum and minimum possible muscle fibre lengths, as described by the force-length relationship, evenly spanned the changes in muscle belly length, then from Fig. 3.1.4:

$$\hat{L}^F = \overline{L}^F + \text{ext.}\Delta\hat{L}^B = \left(\overline{\overline{L}}^F \times 1.8\right) - d \qquad 3.1.3$$

$$\check{L}^F = \overline{L}^F + \text{ext.}\Delta\check{L}^B = \left(\overline{\overline{L}}^F \times 0.58\right) + d \qquad 3.1.4$$

from which:

$$d = \left(\left(1.8 \times \check{L}^F\right) - \left(0.58 \times \hat{L}^F\right)\right)/2.38 \qquad 3.1.5$$

which also gives the optimal muscle fibre length as:

$$\overline{\overline{L}}^F = \frac{\left(\hat{L}^F + \check{L}^F\right)}{2.38} \qquad 3.1.6$$

However, the minimum optimal fibre length required to span the changes in belly length is:

$$\overline{\overline{L}}^F_{Func} = \frac{\hat{L}^F - \check{L}^F}{1.22} \qquad 3.1.7$$

If the optimal fibre length calculated (equation 3.1.6) should be less than the minimum required (equation 3.1.7) then the optimal fibre length will need to be changed to the minimum value and changes made to the reference belly length and reference muscle lengths in order to accommodate the range of motion. In the case $\left(\overline{\overline{L}}^F < \overline{\overline{L}}^F_{Func}\right)$:

$$\overline{\overline{L}}^F = \overline{\overline{L}}^F_{Func} \qquad 3.1.8$$

$$\hat{L}^F = \left(\overline{\overline{L}}^F \times 1.8\right) \qquad 3.1.9$$

$$\breve{L}^F = \left(\bar{\bar{L}}^F \times 0.58\right) \quad 3.1.10$$

$$\bar{L}^F = \left(\hat{L}^F - \text{ext.}\Delta\hat{L}^B\right) \quad 3.1.11$$

$$\bar{L}^B = \bar{L}^F \quad 3.1.12$$

$$\bar{L}^M = \left(\bar{L}^T - \bar{L}^B\right) \quad 3.1.13$$

To start the procedure for the pennate muscle (equation 3.1.14), maximum and minimum fibre lengths and pennation angles can be calculated from the reference fibre length ($\bar{L}^F$) and reference pennation angle ($\bar{\alpha}$) given the maximum and minimum changes in belly length of the movement trial. If a limit is imposed on the maximum pennation angle and it is exceeded, then the reference pennation angle can be decreased and the reference fibre length increased to reduce the maximum pennation angle at minimum belly length. The procdure is then repeated, where the maximum and minimum muscle fibre lengths and pennation angles can then be recalculated for the same changes in belly length. The optimal fibre length can be calculated from maximum and minimum muscle fibre lengths (equation 2.6.36). A limit exists in the minimum optimal muscle fibre length to accommodate the changes in belly length (equation 2.6.35). If the optimal fibre length falls below this limit then reference fibre length can be increased to increase the optimal fibre length. The procdure is then repeated, where the maximum and minimum muscle fibre lengths and pennation angles can then be recalculated for the same changes in belly length. The minimum possible muscle fibre length can be calculated from the optimal muscle fibre length (equation 2.6.33). However, a geometric limit exists on the minimum modelled fibre length (equation 2.6.25). If the minimum possible muscle fibre length falls below this limit then the reference pennation angle can be decreased and the reference fibre length increased to increase the minimum possible fibre length. The procdure is then repeated, where the maximum and minimum muscle fibre lengths and pennation angles can then be recalculated for the same changes in belly length. The minimum pennation angle corresponding to the minimum possible muscle fibre length can be calculated from the reference muscle fibre length and the reference pennation angle. If a limit is imposed on the

maximum pennation angle and it is exceeded, then the reference pennation angle can be decreased and the reference fibre length increased to reduce the maximum pennation angle at minimum possible muscle fibre length. The procdure is then repeated, where the maximum and minimum muscle fibre lengths and pennation angles can then be recalculated for the same changes in belly length. To achieve a solution the following equations are solved simultaneously by iteration until the maximum and minimum fibre lengths produced by the reference pennation angle, reference fibre length and the changes in belly lengths of the movement trial are included in the maximum and minimum fibre lengths described by the optimal fibre length and force-length relationship.

$$\text{if}\left(\overline{L}^{B} < \overline{L}^{F}.\sin(\overline{\alpha})\right)$$
$$\left\{\overline{L}^{B} = \overline{L}^{F}.\sin(\overline{\alpha});\ \overline{L}^{M} = \overline{L}^{B} + \overline{L}^{T}\right\}$$

$$\hat{\alpha} = f\left(\text{ext.}\Delta\hat{L}^{B},\ \overline{L}^{F},\ \overline{\alpha}\right)$$

$$\check{\alpha} = f\left(\text{ext.}\Delta\check{L}^{B}, \overline{L}^{F},\ \overline{\alpha}\right)$$

$$\hat{L}^{F} = f\left(\hat{\alpha},\ \overline{L}^{F},\ \overline{\alpha}\right)$$

$$\check{L}^{F} = f\left(\check{\alpha},\ \overline{L}^{F},\ \overline{\alpha}\right)$$

$$\text{if}\left(\check{\alpha} > 40°\right)$$
$$\left\{\overline{\alpha}\text{--};\ \overline{L}^{F}\text{++};\ \text{continue;}\right\}$$

$$\overline{\overline{L}}^{F}_{\text{Func}} = \frac{\hat{L}^{F} - \check{L}^{F}}{1.22}$$

$$\overline{\overline{L}}^{F} = \frac{\hat{L}^{F} + \check{L}^{F}}{2.38}$$

$$\text{if}\left(\overline{\overline{L}}^{F} < \overline{\overline{L}}^{F}_{\text{Func}}\right)$$
$$\left\{\overline{L}^{F}\text{++};\ \text{continue;}\right\}$$

$$\check{L}^{F}_{\text{Mod}} = \overline{L}^{F} \times \sin(\overline{\alpha})$$

$$\check{L}^{F}_{\text{Abs}} = \overline{\overline{L}}^{F} \times 0.58$$

$$\text{if}\left(\check{L}^{F}_{\text{Abs}} < \check{L}^{F}_{\text{Mod}}\right)$$
$$\left\{\overline{\alpha}\text{--};\overline{L}^{F}\text{++};\ \text{continue;}\right\}$$

$$\check{\alpha}_{\text{Abs}} = f\left(\check{L}^{F}_{\text{Abs}}, \overline{L}^{F}, \overline{\alpha}\right)$$

$$\text{if}\left(\check{\alpha}_{\text{Abs}} > 40°\right)$$
$$\left\{\overline{\alpha}\text{--};\overline{L}^{F}\text{++};\ \text{continue;}\right\}$$

$$\text{while}\left(\left(\Delta\overline{\alpha}\right)||\left(\Delta\overline{L}^{F}\right)\right)$$

3.1.14

The result for both the pennate or non-pennate muscle is the reference muscle-tendon length, reference pennation angle, reference fibre length optimised to the maximum and minimum changes in muscle belly length, reference belly length, and the optimal muscle fibre length. The following can now be calculated for the reference muscle length:

$$\tilde{L}^{SEC} = 0.5 \times \bar{\bar{L}}^{F} \qquad 3.1.15$$

$$\bar{L}^{CE} = \bar{L}^{F} - \tilde{L}^{SEC} \qquad 3.1.16$$

$$\text{PCSA} = \left(\text{muscle mass} \times \text{shape factor}\right) / \left(\text{muscle density} \times \bar{L}^{F}\right) \qquad 3.1.17$$

$$\hat{\bar{F}}_i^{CE} = \text{PCSA} \times \text{muscle specific tension} \qquad 3.1.18$$

For a pennate muscle at the reference muscle length, if the maximum isometric force was generated, then the resultant tendon length and pennation angle are given by the solution of simultaneous equations. This is due to the dependency of the force generated by the contractile elements in the direction of the tendon on the pennation angle and the dependency of pennation angle on tendon length, which in turn is dependent on the force generated by the contractile elements.

The following are known:

$\bar{L}^{M}$, $\bar{L}^{F}$, $\tilde{L}^{T}$, $\bar{L}^{B}$, $\bar{\alpha}$, $\hat{\bar{F}}_i^{CE}$

With the first approximation:

$$\alpha \approx \bar{\alpha} \qquad 3.1.19$$

The following equations are solved simultaneously by iteration until convergence is achieved in the tendon length (L^{T}) and pennation angle (α);

$$
\begin{aligned}
L^T &= f\left(\tilde{L}^T, \hat{\bar{F}}_i^{CE}, \alpha\right) \\
\Delta L^B &= \left(\bar{L}^M - L^T - \bar{L}^B\right) \\
\alpha &= f\left(\Delta L^B, \bar{L}^F, \bar{\alpha}\right)
\end{aligned}
\quad \Big| \quad \text{while}\left(\left(\Delta L^T\right) \,||\, (\Delta\alpha)\right)
\tag{3.1.20}
$$

In the pennate muscle the fibre length corresponding to the maximum isometric force at the reference muscle-tendon length is then:

$$L^F = \bar{L}^F \times \left(\frac{\sin\bar{\alpha}}{\sin\alpha}\right) \tag{3.1.21}$$

For a non-pennate muscle at the reference muscle-tendon length, if the maximum isometric force was generated, then the resultant tendon length is given directly by:

$$L^T = \tilde{L}^T\left(1.0 + \frac{\hat{\bar{F}}_i^{CE}}{1400A^T}\right) \tag{3.1.22}$$

In the non-pennate muscle the fibre length corresponding to the maximum isometric force at the reference muscle-tendon length is:

$$L^F = \bar{L}^M - L^T \tag{3.1.23}$$

The maximum isometric force at optimal fibre length ($\hat{\bar{F}}_i^{CE}$) is then calculated from the maximum isometric force and corresponding fibre length and pennation angle calculated under this maximum force at the reference muscle length.

$$\hat{\bar{\bar{F}}}_i^{CE} = \frac{\hat{\bar{\bar{F}}}_i^{CE}}{0.32 + 0.71.\exp\left[-1.112.\left(L^F/\bar{\bar{L}}^F - 1.0\right)\right].\sin\left[3.722.\left(L^F/\bar{\bar{L}}^F - 0.656\right)\right]} \qquad 3.1.24$$

The maximum tendon length for the muscle can be calculated knowing the maximum (optimal) isometric force and the optimal muscle fibre length. For a pennate muscle the pennate angle when at the optimal muscle fibre length is:

$$\sin\left(\bar{\bar{\alpha}}\right) = = \sin\left(\bar{\alpha}\right) \times \left(\frac{\bar{L}^F}{\bar{\bar{L}}^F}\right) \qquad 3.1.25$$

where:

$\bar{\bar{\alpha}}$ = pennate angle at optimal muscle fibre length.

For a non-pennate muscle the pennate angle is always zero. The maximum tendon length resulting from the maximum (optimal) isometric force at optimal fibre length is given by:

$$\hat{L}^T = \tilde{L}^T\left(1.0 + \frac{\hat{\bar{\bar{F}}}_i^{CE} \times \cos\left(\bar{\bar{\alpha}}\right)}{1400A^T}\right) \qquad 3.1.26$$

To conclude the optimisation procedure for both pennate and non-pennate muscles the minimum change in belly length is calculated with the new maximum tendon length, equation 3.1.1b. If the minimum change in belly length is less than the extended minimum change in muscle belly length, equation 3.1.2b, then the optimisation procedure is repeated with the new minimum change in belly length, from equation 3.1.1a.

During the optimisation procedure certain geometric constraints have to be met, mainly:

$$\begin{aligned} \bar{L}^B &\geq \bar{L}^F.\cos\left(\bar{\alpha}\right) \\ \bar{L}^M &= \bar{L}^B + \tilde{L}^T \end{aligned} \qquad 3.1.27$$

where:

$\bar{L}^M$ = reference muscle - tendon length.

$\bar{\alpha}$ = reference pennation angle.

$\hat{L}^T$ = resting tendon length.

$\bar{L}^B$ = reference belly length.

$\bar{L}^F$ = reference fibre length.

Should the reference belly length need to be increased to accommodate changes in reference fibre length or reference pennation angle, then the reference muscle-tendon length will also need to be increased, as reference tendon length remains unaltered during the optimisation procedure. An increase in reference muscle-tendon length as a result of the optimisation procedure is stored along with reference muscle data (including, reference fibre length, reference pennation angle, reference belly length, reference fibre SEC length, reference contractile element length and optimal fibre length). Prior to the use of the reference muscle data in the analysis of muscle dynamics of movement for the respective subject, any increase in reference muscle-tendon length is added onto the respective muscle-tendon length every time muscle-tendon length is calculated.

3.1.4 Muscle model maximum force prediction

In the isometric case, knowing the instantaneous length of the muscle-tendon and reference muscle model data allows the maximum isometric force produced and the resultant muscle fibre length and pennation angle to be calculated. To do this however, the isometric force produced by the contractile elements is dependent on the fibre length, while the force produced by the muscle contractile elements in the direction of the tendon will depend on the pennation angle. Both fibre length and pennation angle are dependent on the belly length, which in turn is dependent on the length of the tendon. The length of the tendon is dependent on the force produced by the muscle contractile elements and pennation angle. This dependency can be solved by the solution of simultaneous non-linear equations via an iterative method given a first approximation for the tendon length.

The following are known:

$$L^M, \tilde{L}^T, \bar{L}^B, \bar{\alpha}, \bar{L}^F, \bar{\bar{L}}^F, A^T, \hat{\bar{F}}_i^{CE}$$

Therefore with an approximation for length of the tendon for the first iteration,

$$L^T \approx \tilde{L}^T \qquad 3.1.28$$

For the pennate muscle the following equations are solved simultaneously by iteration until convergence is achieved for the maximum isometric force ($\hat{F}_i^{CE}$):

$$\begin{aligned} \Delta L^B &= \left(L^M - L^T - \bar{L}^B\right) \\ \alpha &= f\left(\Delta L^B\right) \\ L^F &= f(\alpha) \\ \hat{F}_i^{CE} &= f\left(L^F\right) \\ L^T &= f\left(\hat{F}_i^{CE}, \alpha\right) \end{aligned} \Bigg| \; \text{while}\left(\Delta \hat{F}_i^{CE}\right) \qquad 3.1.29$$

For the non-pennate muscle the following equations are solved simultaneously by iteration until convergence is achieved for the maximum isometric force ($\hat{F}_i^{CE}$):

$$\begin{aligned} L^F &= L^M - L^T \\ \hat{F}_i^{CE} &= f\left(L^F\right) \\ L^T &= f\left(\hat{F}_i^{CE}\right) \end{aligned} \Bigg| \; \text{while}\left(\Delta \hat{F}_i^{CE}\right) \qquad 3.1.30$$

The result is the maximum isometric force produced for a given whole muscle-tendon length, as well as the resultant pennation angle, fibre length and tendon length.

In the general case, knowing the instantaneous length and velocity of the muscle fibres and contractile elements allows for the calculation of the maximum force produced by the contractile elements, subject to the muscle model excitation contraction dynamics. In doing this however, the force produced by the muscle contractile elements is dependent on the length of the muscle fibre and velocity of the muscle contractile elements. The length of the contractile elements are dependent on the muscle fibre SEC length and muscle belly length. The muscle belly length is, in turn, dependent on the tendon length. The length of the fibre SEC is dependent on the force in the direction of the muscle fibre, while tendon length is dependent on force in the direction of the tendon. The force in the direction of the tendon will depend on the pennation angle, which, in turn, is dependent on the muscle belly length. Muscle belly length is dependent on the tendon length, which is, in turn, dependent on the force in the contractile elements and pennation angle. This dependency is not solved as readily as in the isometric case due to the need to calculate the velocity of the contractile elements which is dependent on the forces produced in the previous instants in time. However, knowing the previous contractile element length at time $-\Delta T$, the maximum force generated by the contractile elements under the current dynamic conditions can be calculated via the solution of simultaneous non-linear equations. This is achieved via an iterative method given a first approximation for the length of the muscle fibre SEC and tendon.

The following are known,

$$L^{M}, \dot{L}^{M}, \tilde{L}^{SEC}, \tilde{L}^{T}, \overline{L}^{B}, \overline{\alpha}, \overline{L}^{F}, \overline{\overline{L}}^{F}, A^{T}, \hat{\overline{F}}_{i}^{CE}, \%SO, \%FO, \%FG$$

as well as from the previous instant in time:

$$L^{CE}_{-\Delta T} \text{ and } \dot{L}^{CE}_{-\Delta T}$$

and with an approximation for the muscle series elastic component length and tendon length for the first iteration,

$$L^T \approx \tilde{L}^T \qquad 3.1.31$$

$$L^{SEC} \approx \tilde{L}^{SEC} \qquad 3.1.32$$

For the pennate muscle the following equations are solved simultaneously by iteration until convergence is achieved for the maximum force ($\hat{F}^{CE}$):

$$\begin{aligned}
&\Delta L^B = \left(L^M - L^T - \overline{L}^B\right)\\
&\alpha = f\left(\Delta L^B\right)\\
&L^F = f(\alpha)\\
&L^{CE} = L^F - L^{SEC}\\
&\dot{L}^{CE} \approx \frac{\left(L^{CE} - L^{CE}_{-\Delta T}\right)}{\Delta T}\\
&\hat{F}_i^{CE} = f\left(L^F\right)\\
&\hat{F}_i^{SO} = \left(\hat{F}_i^{CE} \times \%SO\right)/100\\
&\hat{F}_i^{FO} = \left(\hat{F}_i^{CE} \times \%FO\right)/100\\
&\hat{F}_i^{FG} = \left(\hat{F}_i^{CE} \times \%FG\right)/100\\
&\hat{F}^{SO} = f\left(\hat{F}_i^{SO}, \dot{L}^{CE}, L^F\right)\\
&\hat{F}^{FO} = f\left(\hat{F}_i^{FO}, \dot{L}^{CE}, L^F\right)\\
&\hat{F}^{FG} = f\left(\hat{F}_i^{FG}, \dot{L}^{CE}, L^F\right)\\
&\hat{F}^{CE} = \hat{F}^{SO} + \hat{F}^{FO} + \hat{F}^{FG}\\
&L^T = f\left(\hat{F}^{CE}, \alpha\right)\\
&L^{SEC} = f\left(\hat{F}^{CE}\right)
\end{aligned}$$

$$\text{while}\left(\left(\Delta\hat{F}^{SO}\right)\|\left(\Delta\hat{F}^{FO}\right)\|\left(\Delta\hat{F}^{FG}\right)\right) \qquad 3.1.33$$

For the non-pennate muscle the following equations are solved simultaneously by iteration until convergence is achieved for the maximum force ($\hat{F}^{CE}$):

$$
\begin{aligned}
L^{F} &= L^{M} - L^{T} \\
L^{CE} &= L^{F} - L^{SEC} \\
\dot{L}^{CE} &\approx \frac{\left(L^{CE} - L^{CE}_{-\Delta T}\right)}{\Delta T} \\
\hat{F}_i^{CE} &= f\left(L^{F}\right) \\
\hat{F}_i^{SO} &= \left(\hat{F}_i^{CE} \times \%SO\right)/100 \\
\hat{F}_i^{FO} &= \left(\hat{F}_i^{CE} \times \%FO\right)/100 \\
\hat{F}_i^{FG} &= \left(\hat{F}_i^{CE} \times \%FG\right)/100 \\
\hat{F}^{SO} &= f\left(\hat{F}_i^{SO}, \dot{L}^{CE}, L^{F}\right) \\
\hat{F}^{FO} &= f\left(\hat{F}_i^{FO}, \dot{L}^{CE}, L^{F}\right) \\
\hat{F}^{FG} &= f\left(\hat{F}_i^{FG}, \dot{L}^{CE}, L^{F}\right) \\
\hat{F}^{CE} &= \hat{F}^{SO} + \hat{F}^{FO} + \hat{F}^{FG} \\
L^{T} &= f\left(\hat{F}^{CE}\right) \\
L^{SEC} &= f\left(\hat{F}^{CE}\right)
\end{aligned}
\qquad \text{while}\left(\left(\Delta\hat{F}^{SO}\right)\|\left(\Delta\hat{F}^{FO}\right)\|\left(\Delta\hat{F}^{FG}\right)\right)
$$

3.1.34

The result of the above iterative procedures (3.1.33 and 3.1.34) is the maximum muscle contractile element force ($\hat{F}^{CE}$) and corresponding maximum force in each fibre component $\left(\hat{F}^{SO}, \hat{F}^{FO}, \hat{F}^{FG}\right)$ for the current instantaneous contractile conditions, and resultant pennation angle, fibre length, muscle fibe SEC length, and tendon length.

The model used to incorporate the SO, FO, and FG fibre types assumes that these fibres act in series as representative functional units within the contractile element component of the muscle model (Fig. 2.6.4, Fig. 2.6.5 and Fig. 3.1.5). This model assumes that the SO, FO, and FG components have the same velocity as the contractile element component, and that the contractile element force, which is the sum of the SO, FO, and FG component forces, acts through one representative muscle fibre series elastic component.

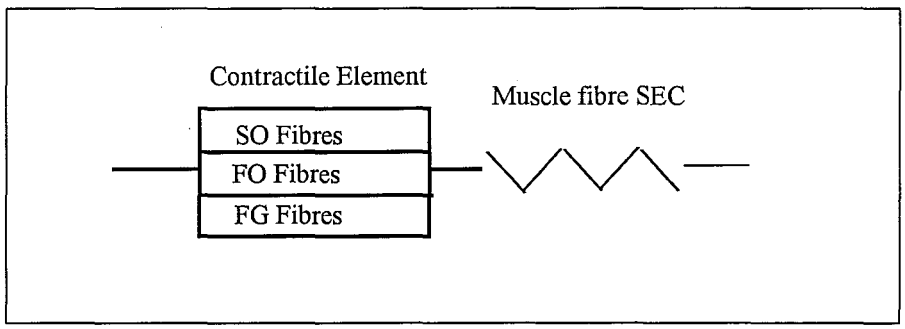

Figure 3.1.5 Muscle Fibre incorporating SO, FO and FG fibre types.

3.1.5 Muscle model excitation and muscle force limits

Muscle excitation dynamics can be included in the muscle model with a knowledge of the individual excitation levels of each fibre type at the previous instant in time. Knowing the time interval to the current frame the maximum and minimum activation states (q rise, q fall) can be calculated (equations 2.6.30 and 2.6.31) using simulation equal to one and simulation equal to zero respectively. For the SO fibre types maximum and minimum activation states are:

$$q_{rise}^{SO} = q_{-\Delta T}^{SO} + \left(1 - \exp\left(-\Delta t/\hat{t}\right)\right).\left(1 - q_{-\Delta T}^{SO}\right) \qquad 3.1.35$$

$$q_{fall}^{SO} = q_{-\Delta T}^{SO} - \left(1 - \exp\left(-\Delta t/\tilde{t}\right)\right).\left(q_{-\Delta T}^{SO}\right) \qquad 3.1.36$$

where:

q_{rise}^{SO} = activation level of SO fibres due to maximum rise in activation from previous activation level.

q_{fall}^{SO} = activation level of SO fibres due to maximum fall in activation from previous activation level.

$q_{-\Delta T}^{SO}$ = activation level of SO fibres at previous instant in time.

$\hat{t}$ = time constant for rise in activation ($0.5 < S < 1.0$).

$\breve{t}$ = time constant for fall in activation ($0 < S < 0.5$).

Δt = time interval.

The muscle contractile element forces limits due to maximum and minimum simulation for the current instant in time are then given by:

$$F_{rise}^{CE} = \left[\left(q_{rise}^{SO} \times \hat{F}^{SO}\right) + \left(q_{rise}^{FO} \times \hat{F}^{FO}\right) + \left(q_{rise}^{FG} \times \hat{F}^{FG}\right)\right] \qquad 3.1.37$$

$$F_{fall}^{CE} = \left[\left(q_{fall}^{SO} \times \hat{F}^{SO}\right) + \left(q_{fall}^{FO} \times \hat{F}^{FO}\right) + \left(q_{fall}^{FG} \times \hat{F}^{FG}\right)\right] \qquad 3.1.38$$

where:

F_{rise}^{CE} = upper limit on contractile element force due maximum rise in activation relative to previous activation level.

F_{fall}^{CE} = lower limit on contractile element force due maximum fall in activation relative to previous activation level.

q_{rise}^{SO} = activation level of SO fibres due to maximum rise in activation from previous activation level.

q_{rise}^{FO} = activation level of FO fibres due to maximum rise in activation from previous activation level.

q_{rise}^{FG} = activation level of FG fibres due to maximum rise in activation from previous activation level.

q_{fall}^{SO} = activation level of SO fibres due to maximum fall in activation from previous activation level.

q_{fall}^{FO} = activation level of FO fibres due to maximum fall in activation from previous activation level.

q_{fall}^{FG} = activation level of FG fibres due to maximum fall in activation from previous activation level.

Knowing the current muscle length and the muscle upper and lower contractile element force limits, due to previous excitation levels, the limits on the force in the direction of the tendon can be calculated. These upper and lower forces in the direction of the tendon form the boundary conditions in solving individual muscle forces from the equipolance equations. For a pennate muscle, the upper limit the force in the direction of the tendon is given by the solution of the following simultaneous equations.

The following are known:

$$L^M, \tilde{L}^T, \overline{L}^B, \overline{\alpha}, \overline{L}^F, A^T, F_{rise}^{CE}$$

Therefore, with an approximation for pennation angle for the first iteration,

$$\alpha_{rise} \approx \overline{\alpha} \qquad 3.1.39$$

For a pennate muscle the following equations are solved simultaneously by iteration until convergence is achieved for the pennation angle:

$$\left.\begin{aligned} L^T &= f\left(F_{rise}^{CE}, \alpha_{rise}\right) \\ \Delta L^B &= \left(L^M - L^T - \overline{L}^B\right) \\ \alpha_{rise} &= f\left(\Delta L^B\right) \end{aligned}\right| \; \text{while}\left(\Delta\alpha_{rise}\right) \qquad 3.1.40$$

From which,

$$F_{rise}^{Tend} = F_{rise}^{CE} \times \cos\left(\alpha_{rise}\right) \qquad 3.1.41$$

Similarly,

$$F_{fall}^{Tend} = F_{fall}^{CE} \times \cos\left(\alpha_{fall}\right) \qquad 3.1.42$$

For the non-pennate muscle the forces in the direction of the tendon are given directly by the contractile element forces as the pennation angle is equal to zero. The result are the maximum and minimum constraint forces in the direction of the tendon as a result of the previous activation levels in each fibre type.

3.1.6 Combining excitation and contraction dynamics with mixed fibre types.

The recruitment of force between the three fibre types (SO, FO, FG) is in order of SO, FO and then FG fibres, which reflects the size principle of motor unit recruitment. At low muscle forces activation of SO fibres would dominate, but with increasing force the activation of FO fibres and then FG fibres would increase. The analytical approach for incorporating mixed fibre types in the present model is as follows.

i) For the previous frame the activation levels in the each of the three fibre types is known $\left(q_{-\Delta T}^{SO},\ q_{-\Delta T}^{FO},\ q_{-\Delta T}^{FG}\right)$. For the current frame the maximum and minimum activation levels for each fibre type is predicted under maximum and minimum simulation (q_{fall}^{SO}, q_{rise}^{SO}, q_{fall}^{FO}, q_{rise}^{FO}, q_{fall}^{FG}, q_{rise}^{FG}, Section 3.1.5, equations 3.1.35 and 3.1.36). Each fibre type having its own activation time cause. For the first frame the activation limits are assumed to be one and zero respectively for each fibre type.

The maximum dynamic muscle force is then calculated subject to the current contraction dynamics. Due to stretch of series elastic component and tendon, steps iii), iv), v) and vi) are solved by iteration until convergence in maximum dynamic contractile element force (Section 3.1.4, equation 3.1.33 for the pennate and 3.1.34 for the non-pennate muscle).

iii) For the current series elastic component and tendon length, pennation angle (α), fibre length $\left(L^F\right)$ and contractile element length $\left(L^{CE}\right)$ and velocity $\left(\dot{L}^{CE}\right)$ are calculated.

iv) For the current frame the maximum isometric force for the contractile elements $\left(\hat{F}_i^{CE}\right)$ can be calculated from the instantaneous fibre length $\left(L^F\right)$.

v) The maximum isometric force in each fibre type $\left(\hat{F}_i^{SO}, \hat{F}_i^{FO}, \hat{F}_i^{FG}\right)$ is given by distributing the maximum isometric force $\left(\hat{F}_i^{CE}\right)$ to each fibre type in proportion to the percentage of each fibre type within the muscle.

vi) For the current frame the maximum dynamic force for each fibre type $\left(\hat{F}^{SO}, \hat{F}^{FO}, \hat{F}^{FG}\right)$ can be calculated from the maximum isometric force $\left(\hat{F}_i^{SO}, \hat{F}_i^{FO}, \hat{F}_i^{FG}\right)$, contractile element velocity $\left(\dot{L}^{CE}\right)$ and force velocity relationship of each fibre type.

vii) The maximum dynamic force of the contractile elements $\left(\hat{F}^{CE}\right)$ is given by the sum of the maximum dynamic forces in each fibre type $\left(\hat{F}^{SO}, \hat{F}^{FO}, \hat{F}^{FG}\right)$.

viii) For the current maximum dynamic force of the contractile elements and pennation angle, the corresponding tendon length $\left(L^T\right)$ and series elastic component $\left(L^{SE}\right)$ are calculated.

The result is maximum dynamic forces in each fibre type $\left(\hat{F}^{SO}, \hat{F}^{FO}, \hat{F}^{FG}\right)$ and of the contractile elements $\left(\hat{F}^{CE}\right)$.

ix) For the current frame the upper and lower force limits for each fibre type $\left(F_{fall}^{SO}, F_{rise}^{SO}, F_{fall}^{FO}, F_{rise}^{FO}, F_{fall}^{FG}, F_{rise}^{FG}\right)$ are calculated from the respective upper and lower activation levels of each fibre type $\left(q_{fall}^{SO}, q_{rise}^{SO}, q_{fall}^{FO}, q_{rise}^{FO}, q_{fall}^{FG}, q_{rise}^{FG}\right)$ and the corresponding maximum dynamic force in each fibre type $\left(\hat{F}^{SO}, \hat{F}^{FO}, \hat{F}^{FG}\right)$. The upper and lower force limits for contractile elements $\left(F_{fall}^{CE}, F_{rise}^{CE}\right)$ are the sum of the forces in each of the three fibre types at either the upper or lower activation levels respectively (Section 3.1.5, equations 3.1.37 and 3.1.38).

x) Knowing the current muscle length and the upper and lower limits of contractile element forces $\left(F_{fall}^{CE}, F_{rise}^{CE}\right)$ the corresponding force limits in the direction of the tendon can be calculated (F_{fall}^{M}, F_{rise}^{M}, Section 3.1.5, equations 3.1.39-42). For a non-pennate muscle this is given directly by the contractile element force.

xi) Optimisation is then carried out subject to maximum and minimum muscle force limits, resultant joint moments and the equipollence equations to determine individual muscle forces (F_i^M, Sections 2.6.2.6 and 3.2).

xii) With known muscle force $\left(F^M\right)$, tendon length $\left(L^T\right)$ can be calculated along with pennation angle and fibre length, series elastic component length $\left(L^{SE}\right)$, contractile element lengths $\left(L^{CE}\right)$ and force in the direction of the contractile elements $\left(F^{CE}\right)$. The velocity of the contractile element for the frame is approximated by:

$$\dot{L}^{CE} \approx \frac{\left(L^{CE} - L^{CE}_{-\Delta T}\right)}{\Delta T} \qquad 3.1.43$$

xi) The current force in each muscle fibre type $\left(F^{SO}, F^{FO}, F^{FG}\right)$ is given by distributing the current predicted contractile element force $\left(F^{CE}\right)$. In the present study this achieved knowing the maximum and minimum force limits in each fibre type $\left(F^{SO}_{fall}, F^{SO}_{rise}, F^{FO}_{fall}, F^{FO}_{rise}, F^{FG}_{fall}, F^{FG}_{rise}\right)$ calculated from the previous excitation levels $\left(q^{SO}_{-\Delta T}, q^{FO}_{-\Delta T}, q^{FG}_{-\Delta T}\right)$. Force distribution was performed preferentially to SO, then FO and lastly FG fibres. Each fibre type was initially given its minimum force limit $\left(F^{SO}_{fall}, F^{FO}_{fall}, F^{FG}_{fall}\right)$ as predicted from previous excitation levels. Any remaining force was then distributed to the SO fibres until they reached there maximum force limit $\left(F^{SO}_{rise}\right)$ as predicted from previous excitation level. Similarly, any remaining force was then distributed to the FO fibre until they reached there maximum force limit $\left(F^{FO}_{rise}\right)$, likewise for FG fibres with any force still remaining.

xii) Knowing the current force in each fibre type $\left(F^{SO}, F^{FO}, F^{FG}\right)$ and the maximum dynamic force possible in each fibre type $\left(\hat{F}^{SO}, \hat{F}^{FO}, \hat{F}^{FG}\right)$ as a result of the instantaneous

contractile conditions, the excitation level of the different fibre types can be calculated for the current frame $\left(q^{SO}, q^{FO}, q^{FG}\right)$.

xiii)The current excitation levels of each muscle fibre type $\left(q^{SO}, q^{FO}, q^{FG}\right)$ are then used to incorporate excitation dynamics at the next instant in time ($q^{SO}_{-\Delta T}$, $q^{FO}_{-\Delta T}$, $q^{FG}_{-\Delta T}$, Section 3.1.5), similarly, the current contractile element length $\left(L^{CE}\right)$ is used when calculating the contractile element velocity and muscle maximum dynamic forces in the next frame($L^{CE}_{-\Delta T}$, Section 3.1.4).

3.1.7 Muscle model test example

In the following example, a single muscle is considered to span a one degree of freedom joint (Fig. 3.1.6). For purpose of comparisons, this muscle is modelled as a pennate and then again as a non pennate muscle with muscle model parameters listed in Table 3.1.4.

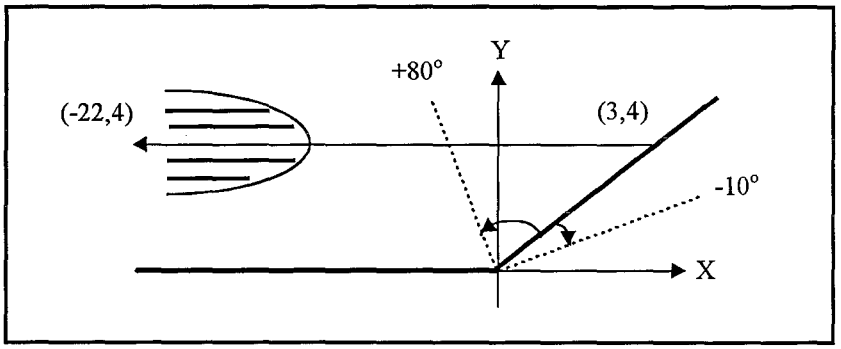

Figure 3.1.6 Single muscle crossing planar joint.

The maximum and minimum muscle model lengths in this example, are given by rotating the joint and hence muscle insertion point to respective limits of the range of motion and calculating respective muscle lengths.

$\hat{L}^M = 0.2566$ m

$\check{L}^M = 0.1859$ m

Optimisation of the muscle model parameters to the changes in muscle belly lengths are given in Table 3.1.5.

Table 3.1.4 Muscle properties for muscle model example.

Measured: subject in reference position	
muscle length in reference position	0.25 m
moment arm in reference position	0.04 m
ROM from reference position	-10° to +80°
Muscle insertion (x,y)	(0.03,0.04)
Muscle origin (x,y)	(-0.22,0.04)
From reference tables:	
Reference %tendon length	0.20
Reference pennate angle (pennate)	0.262 rad
Reference pennate angle (non-pennate)	0.0 rad
Reference %fibre length (pennate)	0.32
Reference %fibre length (non-pennate)	0.80
Shape factor (E)	1.5
Muscle mass (pennate)	0.028 kg
Muscle mass (non-pennate)	0.070 kg
Muscle density	1050 kg/m^2
Muscle specific tension	400,000 N/m^2
Tendon cross sectional area	20 mm^2
Tendon elasticity	1400 N/mm^2
Calculated for reference muscle length	
Reference tendon length	0.05 m
Reference fibre length (pennate)	0.08 m
Reference fibre length (non-pennate)	0.20 m
Reference belly length	0.20 m

The optimised reference fibre length is used to calculate the reference muscle PCSA and maximum reference isometric force. The reference series elastic component length is calculated from the optimal fibre length. The reference series elastic component and the optimised reference fibre lengths are used to calculate the reference contractile element length.

The muscle, belly, tendon and fibre lengths as well as pennation angle following maximum isometric contraction at the reference muscle length are presented in Table 3.1.6. The muscle, belly, tendon and fibre lengths as well as pennation angle following maximum isometric contraction at the optimal fibre length are presented in Table 3.1.7.

Table 3.1.5 Muscle parameters optimised to changes in muscle belly length.

	Pennate	Non-Pennate
Min.change in belly length* ($\Delta\hat{L}^B$)	-0.0758 m	-0.0756 m
Max.change in belly length* ($\Delta\check{L}^B$)	+0.0173 m	+0.0173 m
Optimal fibre length ($\bar{\bar{L}}^F$)	0.0753 m	0.1436 m
Reference muscle length ($\bar{L}^M$)	0.2500 m	0.2500 m
Reference belly length ($\bar{L}^B$)	0.2000 m	0.2000 m
Reference tendon length ($\bar{L}^T$)	0.0500 m	0.0500 m
Reference fibre length ($\bar{L}^F$)	0.1171 m	0.2000 m
Reference pennate angle ($\bar{\alpha}$)	10.94°	0.00°
Reference CE length ($\bar{L}^{CE}$)	0.0795 m	0.1282 m
Reference SEC length ($\bar{L}^{SEC}$)	0.0377 m	0.0718 m
Reference PCSA	0.000342 m^2	0.0005 m^2
Reference Max.Iso.Force ($\hat{\bar{F}}^{CE}$)	136.60 N	200.00 N
Optimal.Iso.Force ($\hat{\bar{\bar{F}}}^{CE}$)	557.42 N	398.28 N
Maximum muscle length** ($\hat{L}^M$)	0.2687 m	0.3084 m
Maximum fibre length** ($\hat{L}^F$)	0.1355 m	0.2584 m
pennate angle** ($\check{\alpha}$)	9.45°	0.00°
Minimum muscle length** ($\check{L}^M$)	0.1726 m	0.1333 m
Minimum fibre length** ($\check{L}^F$)	0.0437 m	0.0833 m
pennate angle** ($\hat{\alpha}$)	30.61°	0.00°

* relative to reference belly length.

** at maximum or minimum model muscle length respectively determined from optimal fibre length.

Table 3.1.6. Muscle parameters following maximum isometric contraction at reference muscle length.

	Pennate	Non-Pennate
Muscle length	0.250 m	0.250 m
Belly length	0.1998 m	0.1996 m
Tendon length	0.0502 m	0.0504 m
Fibre length	0.1169 m	0.1996 m
Pennate angle	10.96 degs	0.00 degs

Table 3.1.7 Muscle parameters following maximum isometric contraction at optimal fibre length.

	Pennate	Non-Pennate
Muscle length	0.2079 m	0.1943 m
Belly length	0.1569 m	0.1436 m
Tendon length	0.0510 m	0.0507 m
Fibre length	0.0753 m	0.1436 m
Pennate angle	17.176 degs	0.000 degs

A graphical representation of the relationship between reference fibre lengths, optimal fibre lengths, maximum and minimum fibre lengths, and range of motion indicated by changes in belly length is presented in Fig. 3.1.7 and Fig. 3.1.8 for the non-pennate and pennate muscle examples respectively.

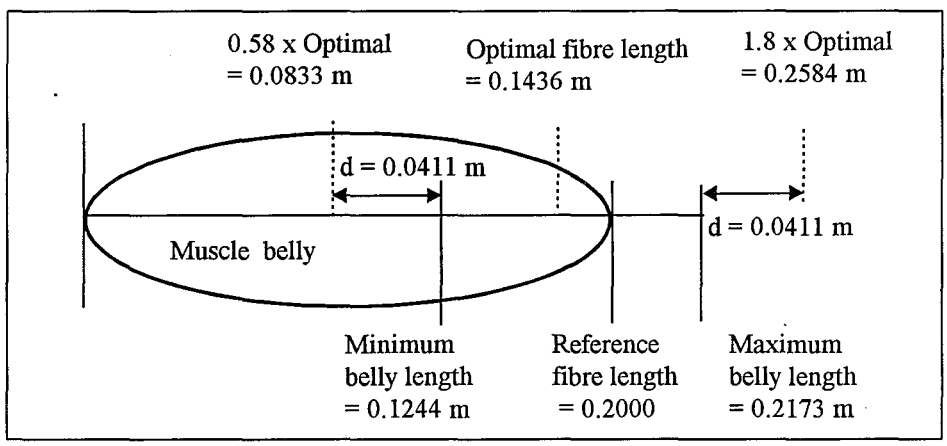

Figure 3.1.7 Relationship between optimal fibre length, reference fibre length and maximum and minimum changes in belly length for non-pennate muscle example.

The force-length relationships, as expressed by equation 2.6.32, for two muscle fibres with optimal lengths of 0.0753 m and 0.1436 m respectively and optimal forces of 557.42 N and 398.28 N respectively, are given in Table 3.1.8, and graphically in Fig. 3.1.9 and Fig. 3.1.10.

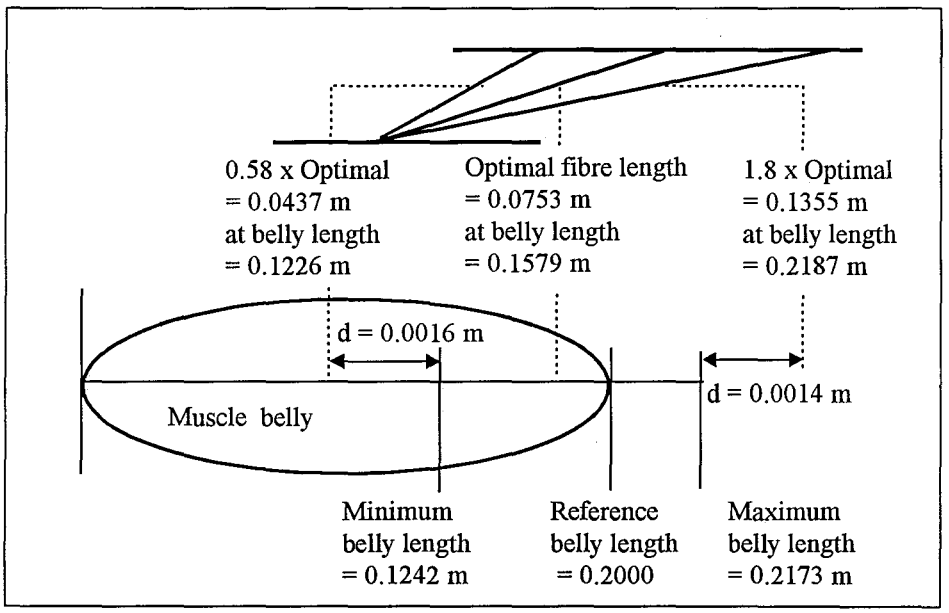

Figure 3.1.8 Relationship between optimal fibre length, reference fibre length and maximum and minimum changes in belly length for pennate muscle example.

Table 3.1.8 Force length relationship for muscle fibres with optimal lengths of 0.0753 m and 0.1436 m optimal forces of 557.42 N and 398.28 N.

	Pennate Muscle		Non-Pennate Muscle	
Relative fibre Length*	Fibre Length (m)	Force CE (N)	Fibre Length (m)	Force CE (N)
0.58	0.0437	002.152	0.0833	001.537
0.7	0.0527	268.452	0.1005	191.809
0.8	0.0602	430.825	0.1149	307.824
0.9	0.0678	527.092	0.1292	376.607
1.0	0.0753	557.424	0.1436	398.279
1.2	0.0904	463.135	0.1723	330.110
1.4	0.1054	270.680	0.2010	193.401
1.6	0.1205	104.563	0.2297	074.710
1.8	0.1355	032.286	0.2584	023.068

* relative to optimal fibre length

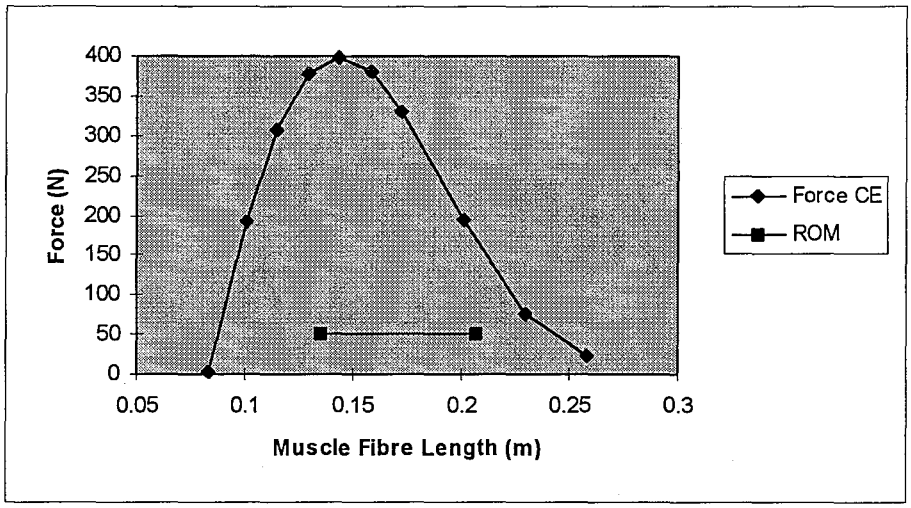

Figure 3.1.9 Force length relationship for muscle fibre with optimal fibre length of 0.1436 m and optimal force of 398.279 N.

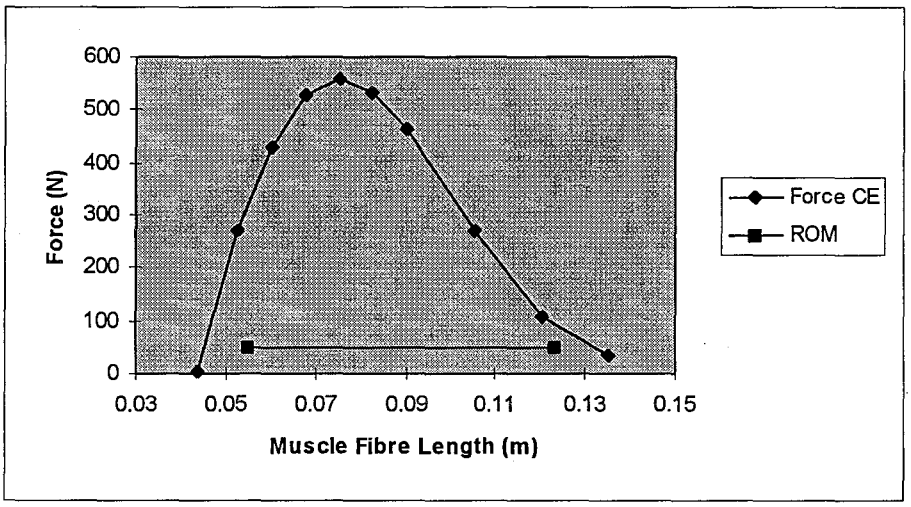

Figure 3.1.10 Force length relationship for muscle fibre with optimal fibre length of 0.0753 m and optimal force of 557.424 N.

The force-length relationship and resulting muscle model parameters over the theoretical range of muscle lengths for the pennate and non-pennate muscle examples are presented in Tables 3.1.9 and 3.1.10 and graphically in Figures 3.1.11 - 3.1.15.

Table 3.1.9 Muscle model parameters for non-pennate muscle during maximum isometric force through range of muscle lengths.

Muscle Length (m)	Muscle parameters under maximum isometric force		
	Force CE (N)	Fibre length (m)	Tendon Length (m)
0.13328	1.4807	0.08327	0.05000
0.15079	191.3484	0.10045	0.05034
0.16831	325.3835	0.11773	0.05058
0.18582	390.9215	0.13513	0.05070
0.20334	390.5237	0.15264	0.05070
0.22086	339.0589	0.17025	0.05061
0.23837	258.3730	0.18791	0.05046
0.25589	171.3157	0.20558	0.05031
0.27341	96.4975	0.22323	0.05017
0.29092	45.7249	0.24084	0.05008
0.30844	23.0499	0.25840	0.05004

Table 3.1.10 Muscle model parameters for pennate muscle during maximum isometric force through range of muscle lengths.

Muscle Length (m)	Muscle parameters under maximum isometric force				
	Force CE (N)	Fibre Length (m)	Pennation (rads)	Belly Length (m)	Tendon Length (m)
0.17259	2.0299	0.04367	0.53423	0.12259	0.05000
0.18220	245.2064	0.05182	0.44352	0.13181	0.05040
0.19181	432.5549	0.06034	0.37741	0.14109	0.05072
0.20142	537.6300	0.06918	0.32721	0.15051	0.05091
0.21103	553.0444	0.07831	0.28791	0.16009	0.05095
0.22064	491.1175	0.08766	0.25645	0.16980	0.05085
0.23026	379.6658	0.09717	0.23087	0.17960	0.05066
0.23987	253.0454	0.10676	0.20980	0.18942	0.05044
0.24948	141.8637	0.11637	0.19226	0.19923	0.05025
0.25909	66.0246	0.12595	0.17747	0.20897	0.05012
0.26870	32.3019	0.13548	0.16487	0.21864	0.05006

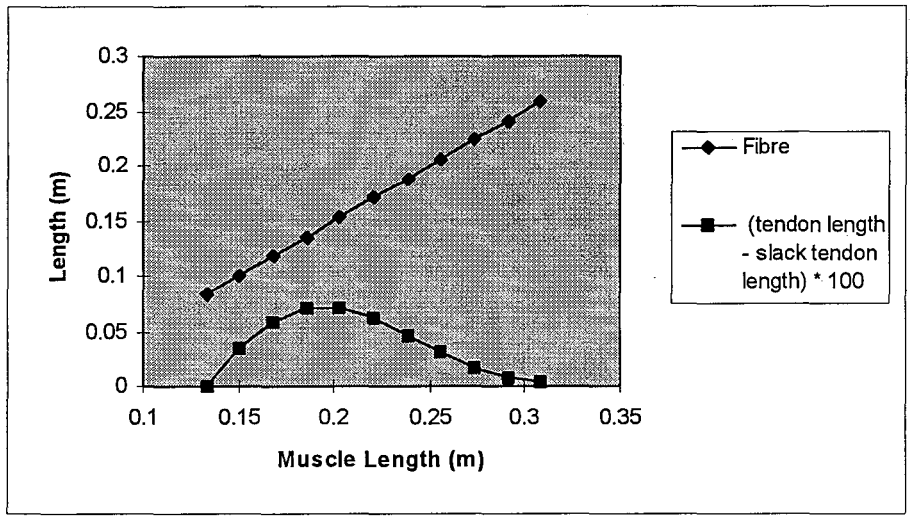

Figure 3.1.11 Fibre length and change in tendon length for non-pennate muscle example during maximum isometric contractions.

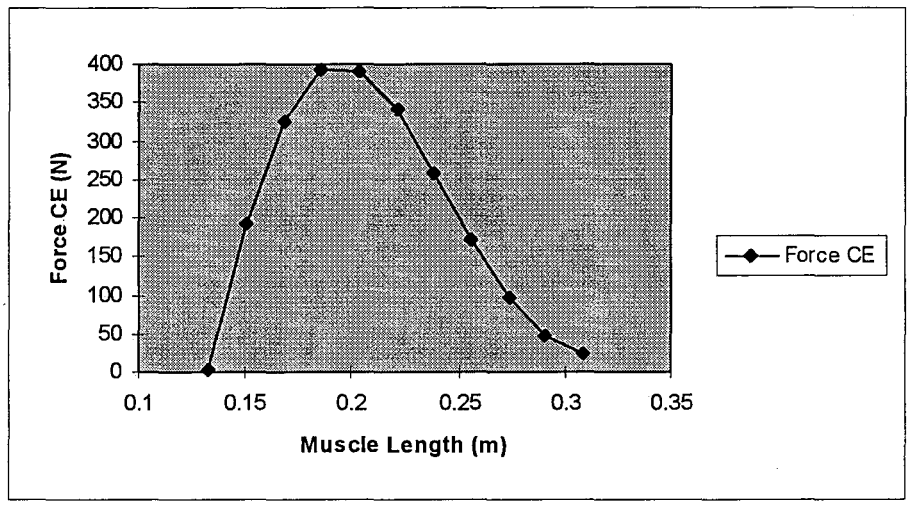

Figure 3.1.12 Contractile element force for non-pennate muscle example during maximum isometric contractions.

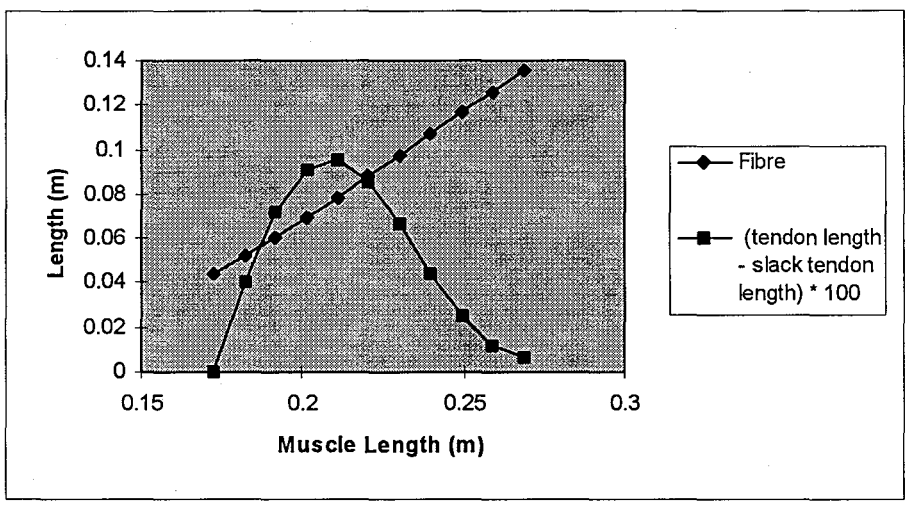

Figure 3.1.13 Fibre length and change in tendon length for pennate muscle example during maximum isometric contractions.

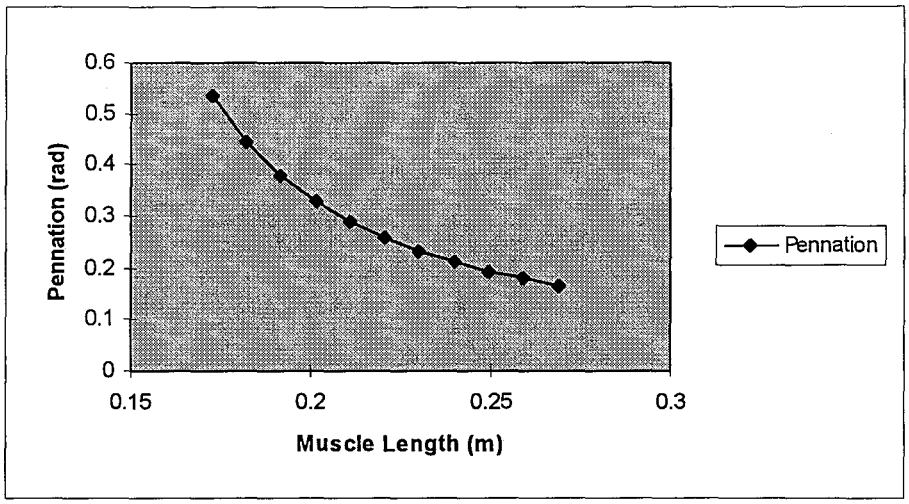

Figure 3.1.14 Pennation angle for pennate muscle example during maximum isometric contractions.

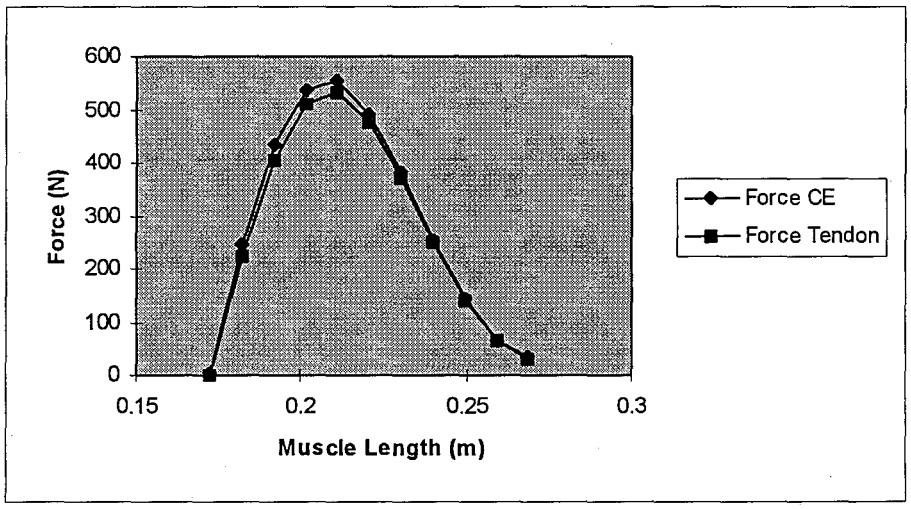

Figure 3.1.15 Contractile element force and tendon force pennate muscle example during maximum isometric contractions.

The force-velocity relationship for both the pennate and non-pennate examples, at muscle lengths of 0.25 m respectively, are presented in Table 3.1.11 and graphically in Figures 3.1.16 and 3.1.17. The muscle fibre compositions represented is 50% slow and 50% fast fibres, and the velocity is that of the contractile element.

Table 3.1.11 Force velocity relationship for pennate and non-pennate muscles examples. Muscle length is 0.25 m, fibre composition is 50% fast and 50% slow fibres, and the velocity is that of the contractile elements.

CE	Pennate Muscle			Non-Pennate Muscle		
velocity (m/s)	SO Fce (N)	FG Fce (N)	TendFce (N)	SO Fce (N)	FG Fce (N)	TendFce (N)
-1.30	0.000	0.000	0.000	0.000	0.000	0.000
-1.26	0.000	0.000	0.000	0.000	0.522	0.522
-1.22	0.000	0.000	0.000	0.000	1.365	1.365
-1.18	0.000	0.000	0.000	0.000	2.250	2.250
-1.14	0.000	0.000	0.000	0.000	3.179	3.179
-1.10	0.000	0.000	0.000	0.000	4.156	4.156
-1.06	0.000	0.000	0.000	0.000	5.186	5.186
-1.02	0.000	0.000	0.000	0.000	6.271	6.271
-0.98	0.000	0.000	0.000	0.000	7.417	7.417
-0.94	0.000	0.000	0.000	0.000	8.630	8.630
-0.90	0.000	0.000	0.000	0.000	9.914	9.914
-0.86	0.000	0.000	0.000	0.000	11.277	11.277
-0.82	0.000	0.000	0.000	0.000	12.726	12.726
-0.78	0.000	0.000	0.000	0.000	14.269	14.269
-0.74	0.000	0.304	0.298	0.000	15.916	15.916
-0.70	0.000	1.293	1.270	0.000	17.678	17.678
-0.66	0.000	2.369	2.326	0.000	19.568	19.568
-0.62	0.000	3.542	3.477	0.000	21.599	21.599
-0.58	0.000	4.827	4.739	0.000	23.788	23.788
-0.54	0.000	6.240	6.126	0.000	26.155	26.155
-0.50	0.000	7.801	7.659	0.000	28.721	28.721
-0.46	0.000	9.536	9.363	0.000	31.514	31.514
-0.42	0.000	11.475	11.266	0.000	34.564	34.564
-0.38	0.000	13.656	13.408	0.857	37.911	38.768
-0.34	0.000	16.128	15.834	2.830	41.599	44.430
-0.30	0.000	18.952	18.607	5.220	45.684	50.904
-0.26	0.000	22.211	21.806	8.173	50.233	58.405
-0.24	0.000	24.035	23.598	9.927	52.706	62.633
-0.22	0.716	26.014	26.243	11.916	55.329	67.245
-0.20	1.867	28.166	29.486	14.190	58.115	72.305
-0.18	3.223	30.514	33.123	16.815	61.080	77.895
-0.16	4.842	33.087	37.239	19.878	64.242	84.120
-0.14	6.809	35.920	41.951	23.501	67.621	91.122
-0.12	9.251	39.053	47.425	27.850	71.242	99.092
-0.10	12.363	42.538	53.901	33.170	75.131	108.302
-0.08	16.461	46.441	61.756	39.826	79.321	119.147
-0.06	22.106	50.842	71.618	48.392	83.851	132.243
-0.04	30.371	55.850	84.649	59.829	88.765	148.594
-0.02	43.633	61.616	103.329	75.871	94.123	169.993
0.00	68.376	68.376	134.255	100.000	100.000	200.000
0.02	80.037	73.504	150.737	113.742	104.932	218.674
0.04	82.344	76.290	155.737	117.792	108.243	226.035
0.06	83.335	78.048	158.435	119.734	110.625	230.359
0.10	84.239	80.144	161.379	121.624	113.827	235.451
0.15	84.735	81.577	163.273	122.715	116.283	238.997

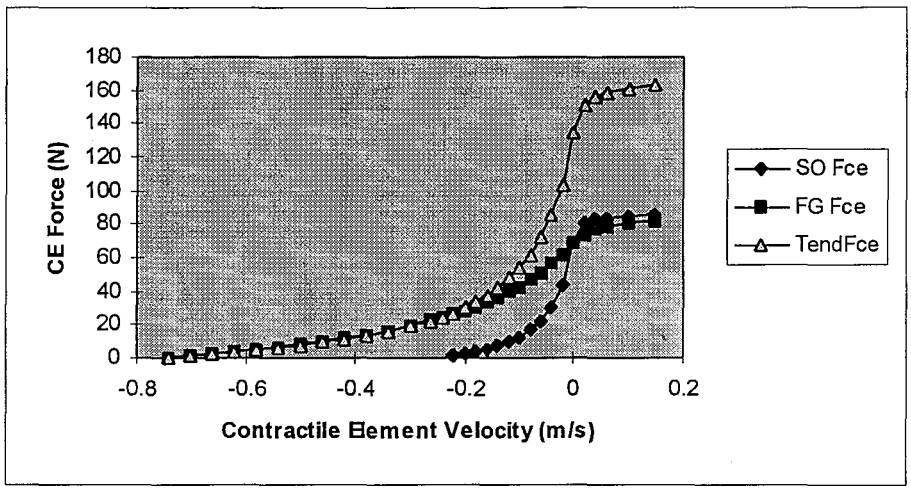

Figure 3.1.16 Force velocity relationship for the pennate muscle example. Muscle length is 0.25m, fibre composition is 50% fast and 50% slow fibres. Force and velocity is that of the contractile element.

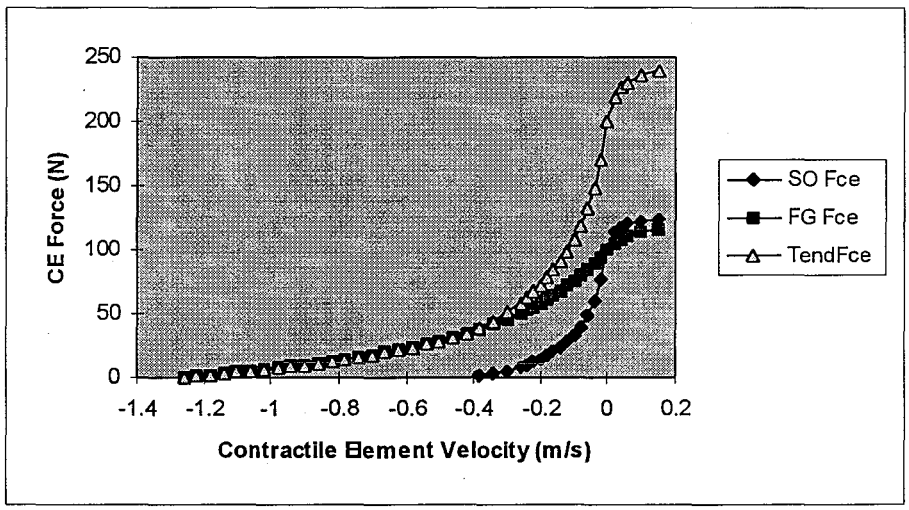

Figure 3.1.17 Force velocity relationship for the non-pennate muscle example. Muscle length of 0.25m. Fibre composition is 50% fast and 50% slow fibres. Force and velocity is that of the contractile element.

The force-velocity relationship with varying fibre composition, for both the pennate and non-pennate muscle examples, at muscle lengths of 0.25m respectively, are presented in Table 3.1.12 and graphically in Figures 3.1.18 and 3.1.19. The muscle fibre compositions being 100% slow, 100% fast and 50% slow, 50% fast fibres. Velocity is that of the contractile element and the force is that experienced by the tendon.

Table 3.1.12 Force-velocity relationship for pennate and non-pennate muscle examples at varying fibre composition. Muscle length is 0.25m, the velocity is that of the contractile elements.

CE velocity (m/s)	Force in Tendon (N)					
	Pennate fibre distribution			Non-Pennate fibre distribution		
	all slow	all fast	50/50	all slow	all fast	50/50
-1.30					0.000	0.000
-1.26					1.043	0.522
-1.22					2.729	1.365
-1.18					4.499	2.250
-1.14					6.357	3.179
-1.10					8.312	4.156
-1.06					10.371	5.186
-1.02					12.543	6.271
-0.98					14.836	7.417
-0.94					17.261	8.630
-0.90					19.831	9.914
-0.86					22.559	11.277
-0.82		0.000	0.000		25.459	12.726
-0.78		0.000	0.000		28.548	14.269
-0.74		0.597	0.298		31.846	15.916
-0.70		2.539	1.270		35.374	17.678
-0.66		4.651	2.326		39.158	19.568
-0.62		6.956	3.477		43.226	21.599
-0.58		9.480	4.739		47.612	23.788
-0.54		12.258	6.126		52.354	26.155
-0.50		15.329	7.659		57.498	28.721
-0.46		18.742	9.363	0.000	63.097	31.514
-0.42		22.558	11.266	0.000	69.214	34.564
-0.38		26.852	13.408	1.723	75.924	38.768
-0.34		31.722	15.834	5.664	83.319	44.430
-0.30		37.290	18.607	10.435	91.509	50.904
-0.26	0.000	43.718	21.806	16.331	100.629	58.405
-0.24	0.000	47.320	23.598	19.834	105.589	62.633
-0.22	1.410	51.224	26.243	23.804	110.848	67.245
-0.20	3.664	55.469	29.486	28.344	116.434	72.305
-0.18	6.318	60.102	33.123	33.584	122.378	77.895
-0.16	9.486	65.180	37.239	39.700	128.716	84.120
-0.14	13.336	70.769	41.951	46.932	135.488	91.122
-0.12	18.113	76.950	47.425	55.616	142.741	99.092
-0.10	24.200	83.825	53.901	66.240	150.527	108.302
-0.08	32.220	91.515	61.756	79.534	158.909	119.147
-0.06	43.269	100.175	71.618	96.651	167.956	132.243
-0.04	59.463	110.003	84.649	119.519	177.753	148.594
-0.02	85.491	121.252	103.329	151.625	188.396	169.993
0.00	134.255	134.255	134.255	200.000	200.000	200.000
0.02	157.279	144.205	150.737	227.573	209.782	218.674
0.04	161.802	149.679	155.737	235.685	216.393	226.035
0.06	163.733	153.143	158.435	239.565	221.160	230.359
0.10	165.484	157.279	161.379	243.333	227.573	235.451
0.15	166.439	160.109	163.273	245.500	232.498	238.997

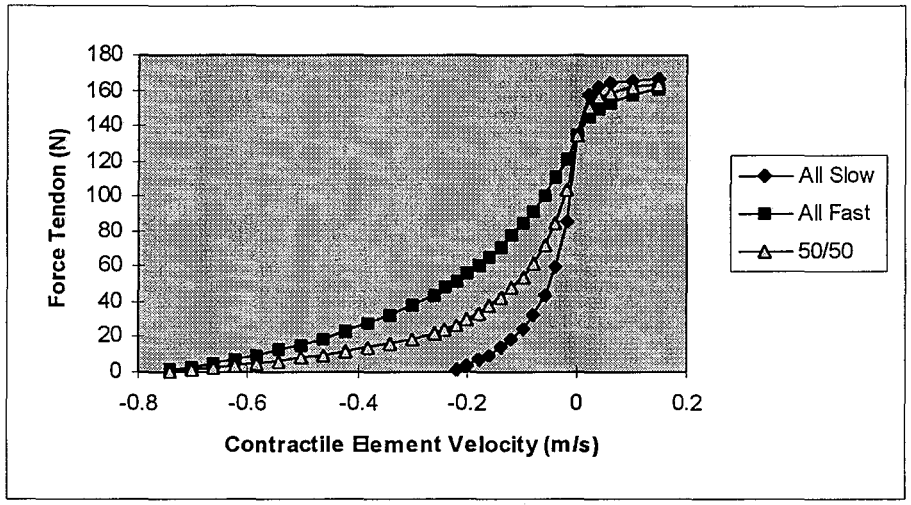

Figure 3.1.18 Force-velocity relationship for the pennate muscle example with varying fibre composition. The muscle length is 0.25m. Three fibre compositions of 100% slow, 100% fast and 50/50 are represented. The velocity is that of the contractile element and the force is that experienced by the tendon.

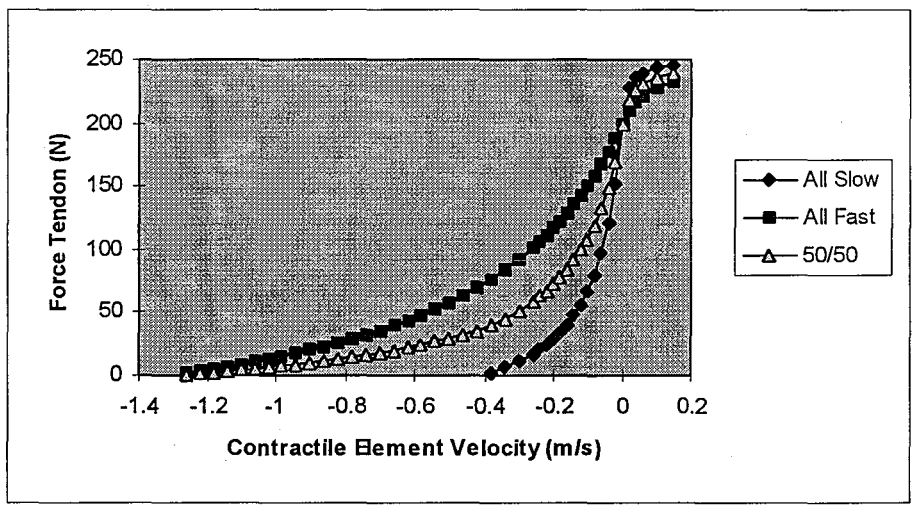

Figure 3.1.19 Force-velocity relationship for the non-pennate muscle example with varying fibre composition. The muscle length is 0.25m. Three fibre compositions of 100% slow, 100% fast and 50/50 are represented. The velocity is that of the contractile element and the force is that experienced by the tendon.

The force-velocity relationship for varying muscle lengths, with a fibre composition of 50/50 fast slow/fibres, for both the pennate and non-pennate examples, are presented in Table 3.1.13 and graphically in Figures 3.1.20 and 3.1.21. The force is that in the tendon and the velocity is that of the contractile element.

Table 3.1.13 Force velocity relationship for pennate and non-pennate muscle examples at varying muscle lengths. The fibre composition is 50/50 slow/fast fibres, and the velocity is that of the contractile elements.

CE velocity	Force in Tendon (N)							
	Pennate Muscle Length (m)				Non-pennate Muscle Length (m)			
(m/s)	0.182	0.208	0.230	0.250	0.151	0.194	0.221	0.250
-1.30								0.000
-1.26								0.522
-1.22								1.365
-1.18								2.250
-1.14								3.179
-1.10							0.000	4.156
-1.06							1.565	5.186
-1.02							3.287	6.271
-0.98							5.110	7.417
-0.94						0.000	7.044	8.630
-0.90						1.569	9.098	9.914
-0.86						3.974	11.285	11.277
-0.82						6.547	13.617	12.726
-0.78				0.000		9.307	16.109	14.269
-0.74				0.298		12.274	18.779	15.916
-0.70				1.270		15.472	21.646	17.678
-0.66			0.000	2.326	0.000	18.930	24.733	19.568
-0.62			0.663	3.477	1.123	22.681	28.067	21.599
-0.58			3.858	4.739	2.865	26.764	31.677	23.788
-0.54			7.390	6.126	4.789	31.224	35.601	26.155
-0.50		0.000	11.317	7.659	6.923	36.117	39.880	28.721
-0.46		4.408	15.708	9.363	9.305	41.509	44.565	31.514
-0.42		11.003	20.649	11.266	11.981	47.480	49.718	34.564
-0.38		18.553	26.253	13.408	15.008	54.129	55.411	38.768
-0.34	0.000	27.284	32.662	15.834	18.459	61.579	61.858	44.430
-0.30	3.414	37.495	40.063	18.607	22.433	69.983	72.599	50.904
-0.26	8.035	49.599	48.706	21.806	27.056	83.082	85.120	58.405
-0.24	10.730	56.533	53.594	23.598	29.663	91.277	92.210	62.633
-0.22	13.741	64.175	58.931	26.243	32.502	100.279	99.971	67.245
-0.20	17.128	72.641	64.780	29.486	35.723	110.231	108.517	72.305
-0.18	20.965	82.071	73.776	33.123	40.892	121.314	117.995	77.895
-0.16	25.350	92.640	84.817	37.239	46.759	133.768	128.598	84.120
-0.14	30.408	108.326	97.543	41.951	53.498	147.914	140.581	91.122
-0.12	36.306	129.442	112.434	47.425	61.350	164.198	154.300	99.092
-0.10	44.064	154.876	130.200	53.901	70.674	183.269	170.260	108.302
-0.08	57.047	186.367	151.960	61.756	82.028	206.114	189.220	119.147
-0.06	74.116	226.938	179.629	71.618	96.360	234.336	212.381	132.243
-0.04	98.135	282.567	216.865	84.649	115.459	270.769	241.791	148.594
-0.02	136.552	367.728	271.959	103.329	143.297	321.042	281.292	169.993
0.00	221.508	532.736	369.682	134.255	191.296	398.407	339.160	200.000
0.02	255.996	609.287	419.083	150.737	215.421	442.056	373.560	218.674
0.04	262.525	627.527	432.692	155.737	222.143	456.711	386.129	226.035
0.06	265.570	636.638	439.811	158.435	225.673	464.880	393.329	230.359
0.10	268.520	645.945	447.371	161.379	229.434	474.060	401.622	235.451
0.15	270.223	651.567	452.104	163.273	231.797	480.143	407.262	238.997

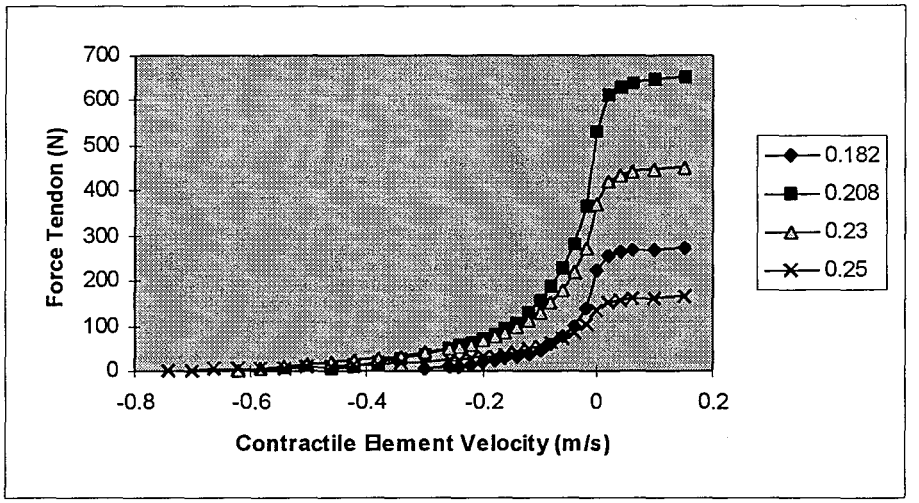

Figure 3.1.20 Force velocity relationship for the pennate muscle example at varying muscle lengths. The fibre composition is 50/50 slow/fast fibres and velocity is that of the contractile element.

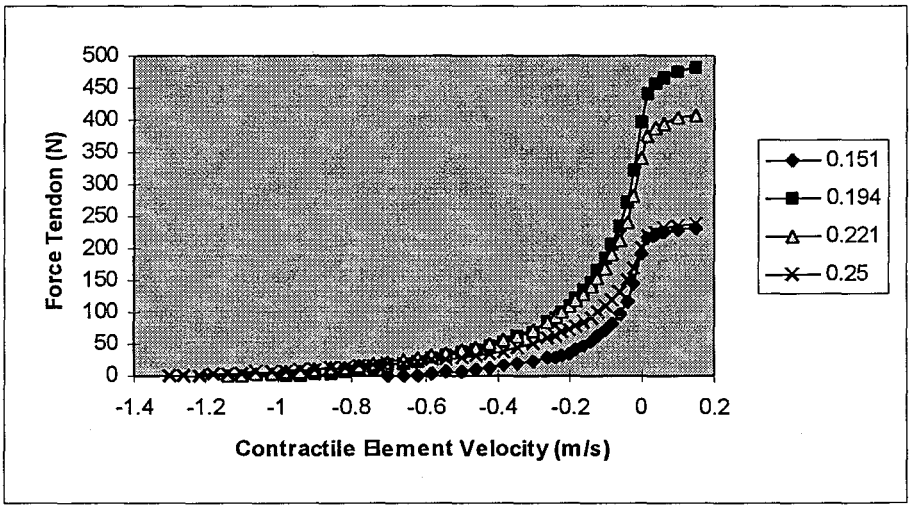

Figure 3.1.21 Force velocity relationship for the non-pennate muscle example at varying muscle lengths. The fibre composition is 50/50 slow/fast fibres and velocity is that of the contractile element.

The maximum shortening velocity at varying muscle lengths for the pennate and non-pennate examples, are presented in Table 3.1.14 and Fig. 3.1.22. The maximum velocity of shortening for each respective muscle length was taken as the point where the force velocity curve extrapolates to zero force. The fibre composition was 50/50 slow/fast fibres, and the velocity is that of the contractile element.

Table 3.1.14 Maximum velocity of shortening at various muscle lengths for the pennate and non-pennate muscle examples. The fibre composition was 50/50 slow/fast fibres. The velocity is that of the contractile element.

Pennate		Non-Pennate	
Muscle Length (m)	Max. Velocity (m/s)	Muscle Length (m)	Max. Velocity (m/s)
0.135*	0.00	0.050*	0.00
0.182	-0.32	0.151	-0.65
0.208	-0.48	0.194	-0.92
0.230	-0.63	0.221	-1.09
0.250	-0.75	0.250	-1.28

* Extrapolated from force-velocity relationship to point of zero force.

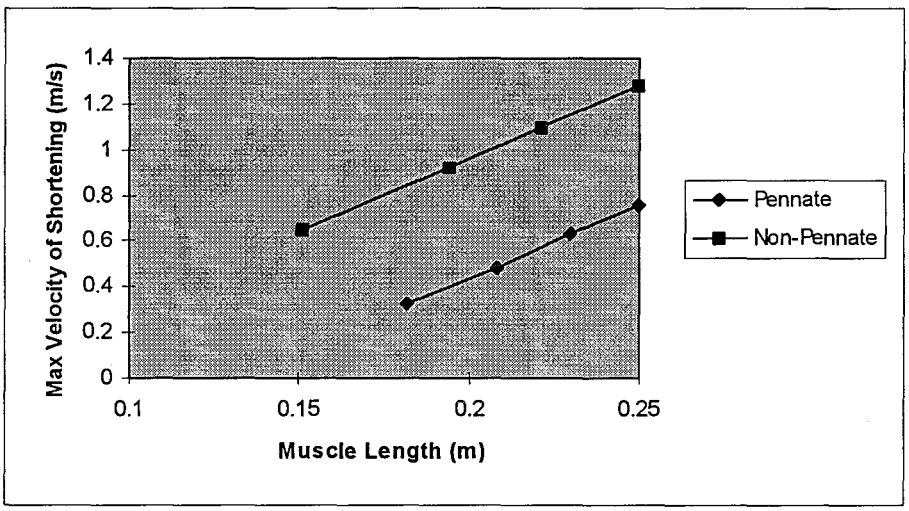

Figure 3.1.22 Maximum velocity of shortening at various muscle lengths for the pennate and non-pennate muscles examples. Fibre composition was 50/50 slow/fast fibres and the velocity is that of the contractile element.

For the non-pennate muscle example, if the reference fibre length (0.200 m) was to reduce to zero, then the reference muscle length (0.250 m) would equal the reference tendon length (0.05 m). This value (0.05 m) corresponds to the value obtained by extrapolating the muscle length versus maximum velocity of shortening data (Table 3.1.14, Fig. 3.1.22) to a muscle length corresponding to zero maximum shortening velocity. Similarly for the pennate muscle, if the cosine of the pennation angle multiplied by the reference fibre length [cos(0.1910) x 0.1171 = 0.1150 m] was to reduce to zero, then the reference muscle length (0.250 m) would

equal the reference tendon length plus the reference belly length minus the portion of fibre length in the direction of the muscle (0.050 + 0.200 - 0.1150 = 0.135 m). This value (0.135 m) corresponds to the value obtained by extrapolating the muscle length versus maximum velocity of shortening data (Table 3.1.14, Figure 3.1.22) to a muscle length corresponding to zero maximum shortening velocity. This observation is of no practical significance since, through optimisation of the muscle model parameters to the range of muscle lengths of the task, the maximum and minimum fibre lengths will not exceed the optimal fibre length times 1.8 or fall bellow the optimal fibre length times 0.58 respectively. In fact the range fibre lengths, for the task to which the muscle parameters were optimised, will fall evenly within the maximum and minimum fibre lengths.

3.2 Optimisation

A cost function is introduced involving the sum of squared normalised muscle forces with soft constraints on maximum and minimum muscle forces. The results of this are tested on a simple joint of varying resultant joint moments balanced by four muscles. The results are also compared to two previous cost functions, sum of squared normalised forces, and sum of squared normalised forces with soft constraints on maximum muscle forces. The analytical approach is introduced which combines estimation of maximum muscle forces, calculation of muscle forces limits, the calculation of muscle force initial estimates subject to resultant joint moments, the optimisation procedure, and the calculation of muscle excitation values based on the predicted muscle forces. A test example is then given on a two-joint, three segment system, involving eight muscles. The muscles used in this model are both single and double joint and of varying moment arms and maximum forces. Individual muscle force prediction is given for a range of resultant joint moments at each joint.

3.2.1 Cost Function

Extending the method of Siemienski (1992), the cost function can also be expressed in a form that will impose soft constraints on both maximum and minimum muscle forces:

$$- \sum_{i=1}^{M} \left(\sqrt{1 - \left(\frac{F_i^m - F_{min,i}^m}{F_{max,i}^m - F_{min,i}^m} \right)^2} \right) \qquad 3.2.1$$

The result is a non-linear relation between muscle forces and joint moment for each muscle, eliminating the hard constraints of minimum muscle forces from equation 2.6.19. If the minimum muscle forces are all zero then equations 2.6.19 and 3.2.1 are equivalent, producing the same muscle forces over the range of joint moments.

For a single muscle the cost function has a minimum of -1 at $F_{i,min}$ and two maxima of zero at $F_{i,max}$ and at $F_{i,min}$ - ($F_{i,max}$ - $F_{i,min}$). The cost function it not defined outside of this range (Fig. 3.2.1).

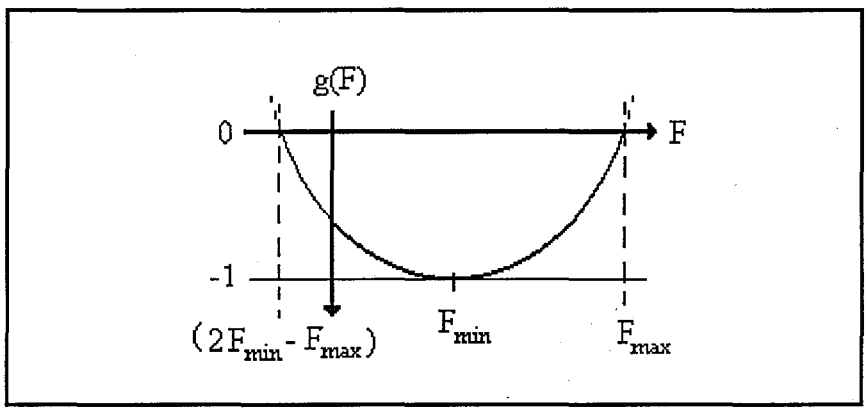

Figure 3.2.1 Cost function of a single muscle - squared normalised muscle force with maximum and minimum soft constraints.

To compare the effects of the form of cost function on the pattern of muscle recruitment, the three functions (2.6.14, 2.6.19 and 3.2.1) which minimise a function involving normalised muscle forces were compared. A single joint of one degree of freedom with four muscle was used, the details are in Table 3.2.1. The results of the optimisations are presented in Tables 3.2.2 - 3.2.4 and graphically in Figures 3.2.2 - 3.2.4. The optimisation method adopted is presented in Section 2.6.2.6 and it's implementation in the following section.

Table 3.2.1 Muscles included in cost function comparison.

	MUSCLE			
	m1	m2	m3	m4
PCSA (cm^2)	4	5	5	7
f (N/cm^2)	40	40	40	40
$r_\perp$ (m)	0.02	0.03	0.04	0.03
min (N)	0	0	0	0
max (N)	160	200	200	280

Table 3.2.2 Muscles forces resulting from minimising the sum of squared normalised muscle force.

Joint Moment (Nm)	Muscle Force (n)				sum of normal forces
	m1	m2	m3	m4	
0	0.0	0.0	0.0	0.0	0
5	14.2	33.2	44.3	64.9	0.71
10	28.3	66.4	88.5	130.0	1.42
15	42.5	99.6	132.8	195.2	2.12
20	56.6	132.8	177.0	260.1	2.83
21.6	60.9	142.6	190.3	279.7	3.04
22.15	63.9	149.7	199.5	280.0	3.15
24.1	85.3	199.8	200.0	280.0	3.53
25.6	160.0	200.0	200.0	280.0	4

Table 3.2.3 Muscles forces resulting from minimising the sum of squared normalised muscle force with soft constrained maximum muscle force.

Joint Moment (Nm)	Muscle Force (n)				sum of normal forces
	m1	m2	m3	m4	
0	0.0	0.0	0.0	0.0	0
2	5.7	13.4	17.8	25.7	0.28
5	14.5	33.6	44.2	64.5	0.71
10	30.6	68.7	87.6	127.3	1.43
15	51.4	107.4	129.4	186.2	2.17
20	83.3	150.6	167.3	237.5	2.96
23	115.3	178.0	186.6	262.9	3.48
25.6	160.0	200.0	200.0	280.0	4

Table 3.2.4 Muscles forces resulting from minimising the sum of squared normalised muscle force with soft constrained maximum and minimum muscle forces. Minimum muscle forces were m1 = 60 N, m2 = 90 N, m3 = 60 N and m4 = 123.33 N, resulting in a minimum joint moment of 10 Nm.

Joint Moment (Nm)	Muscle Force (n)				sum of normal forces
	m1	m2	m3	m4	
0	-	-	-	-	-
5	-	-	-	-	-
10	60.0	90.0	60.0	123.33	1.57
12.5	67.4	103.4	88.6	150.1	1.92
15	75.5	117.6	116.2	177.6	2.28
20	97.4	150.9	164.8	231.1	3.01
23	120.9	176.4	186.9	260.4	3.50
25.6	160.0	200.0	200.0	280.0	4

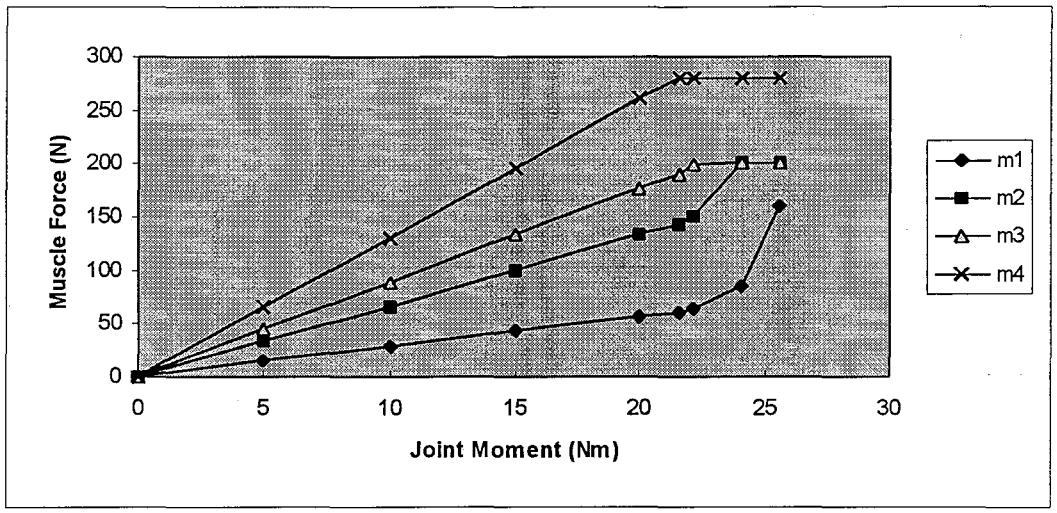

Figure 3.2.2 Distribution of muscle forces over the full range of joint moments predicted from the sum of squared normalised muscle force.

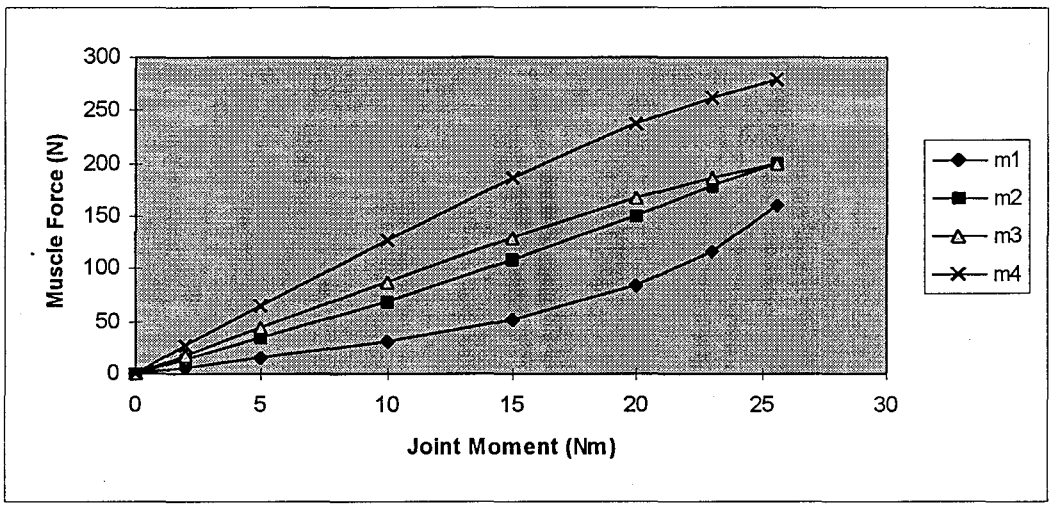

Figure 3.2.3 Distribution of muscle forces over the full range of joint moments predicted from the sum of squared normalised muscle force with soft constrained maximal forces.

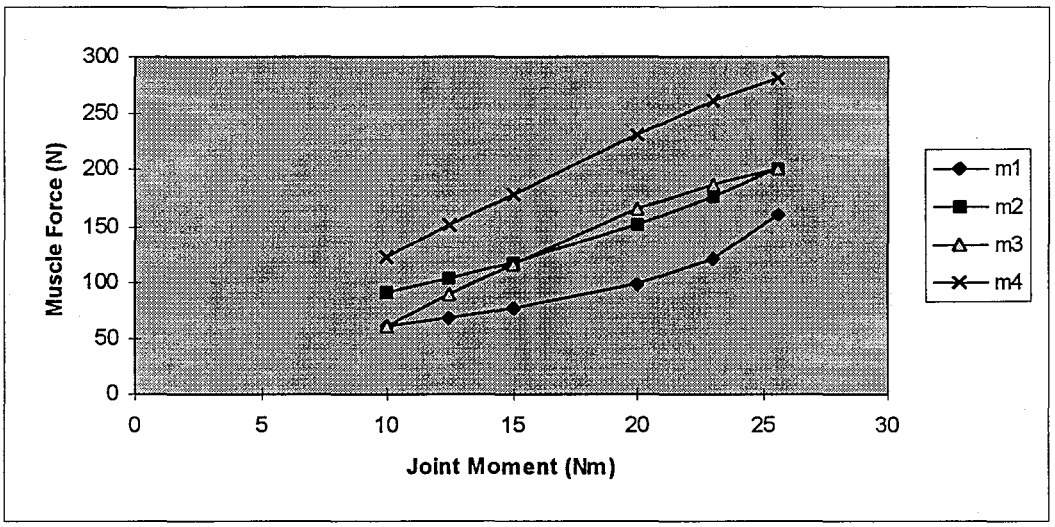

Figure 3.2.4 Distribution of muscle forces over a range of joint moments predicted from the sum of squared normalised force with soft constrained maximal and minimum forces. Minimum forces were m1= 60 N, m2 = 90 N, m3 = 60 N and m4 = 123.33 N.

3.2.2 Muscle force prediction: analytical approach

The analytical approach describes how the separate methods described previously are combined in the estimation of muscle forces. Firstly, at the current instant in time, an estimation of maximum muscle forces is made based on the length and contraction dynamics of the muscle (section 3.1.3). This will give maximum force for each muscle as well as the maximum force of each fibre type (SO, FO, FG). Calculation of muscle forces limits is then made knowing the activation states of each fibre type at a previous instant in time and assuming either maximum or minimum stimulation of the muscle (Section 2.6.2.5.8). The calculation of muscle force initial estimates is then made which will meet the required resultant joint moments. The optimisation procedure is then undertaken to minimise the cost function starting at the initial muscle force estimates. Optimisation involves a gradient projection algorithm (Section 2.6.2.6) where the steepest descent of the cost function is followed at the same time as maintaining the equipolance equations (Section 2.5.4.2). From the predicted muscle forces the forces produced by each fibre type are estimated, and knowing the maximum force of each fibre type, excitation values of each fibre type are then calculated for the current frame.

From video-based motion analysis, three dimensional co-ordinates of the 10 external calibration markers and 27 external segment markers have been reproduced with the subject standing in the anatomical position. Reproduction of each segment local axes allows the local co-ordinates of each segment marker to be calculated. From video-based motion analysis of the subject trail, the three dimensional paths of each of the 27 external segment markers is reconstructed. Segment positions, velocities and accelerations have been derived from three dimensional reproduction of segment location via a least squares routine utilising the markers local co-ordinates. Application of the equations of motion for the pelvis, thigh, shank and foot have given the resultant joint moments for the ankle, knee and hip. A single frame of the subject standing in the anatomical position has been collected, from which segment positions have been reproduced and the muscle origin, insertion and path data used to obtain reference muscle lengths. From reference muscle lengths, reference muscle model data are obtained for muscle fibre length and tendon slack length. Pennation angles and fibre type distribution are obtained directly from reference values, while muscle mass and tendon cross sectional areas are scaled to length and circumference measurements from the respective segments of the subject. For the task under investigation, muscle lengths have been calculated for each frame

using the muscle co-ordinate data, and the muscle model parameters optimised to the range of muscle lengths of the specific task. Optimisation of muscle model parameters also yields an optimal fibre length and optimal isometric force, hence for each muscle the following model parameters are known: reference muscle-tendon length, reference fibre length, reference pennate angle, optimal fibre length, optimal isometric force, muscle specific tension, muscle density, muscle mass, resting tendon length, tendon cross sectional area, tendon modulus of elasticity, ratio between average and maximal muscle cross sectional area, and the percentage of slow oxidative, fast oxidative, and fast glycolytic fibres. For each frame joint centres and muscle moment arms are calculated and equipolance equations have been established.

At each instant in time the goal is to predicted muscle force subject to the excitation and contraction dynamics for that instant in time. The first objective is to establish the maximum force that can be generated by the contractile elements given the instantaneous length and velocity of the muscle fibres and contractile elements respectively (Section 3.1.4). The maximum forces in each fibre type are given in the calculation of maximum contractile force. Then, given the excitation levels of each fibre type for the previous instant in time, the excitation dynamics can be used to establish maximum and minimum force limits of each fibre type. Summing the forces of each fibre type gives the maximum and minimum boundaries for the force of the contractile elements at the current instant in time, from which the upper and lower force limits in the direction of the tendon are calculated (Section 3.1.5). With upper and lower boundaries placed on the force generated by each muscle, and the choice of a cost function, optimisation techniques can be used to assign individual muscle forces (Sections 2.6.2.6 and 3.2.1).

Knowing the muscle force from the optimisation procedure and muscle-tendon length, the current tendon length, fibre length, contractile element force, series elastic component length, contractile element length and velocity for the current instant in time can be calculated (Sections 3.1.5-6). The current force in each muscle fibre type is given by distributing the current predicted contractile element force (Section 3.1.6). Force distribution was then performed preferentially to SO, then FO and lastly FG fibres. Knowing the current force in each fibre type and the maximum forces possible in each fibre type, as a result of the instantaneous contractile conditions, the current excitation level of the different fibre types can be calculated.

The current excitation levels of each muscle fibre type can then be used to incorporate excitation dynamics at the next instant in time (Section 3.1.6), similarly the current contractile element length is used when calculating the contractile element velocity and muscle maximum dynamic forces in the next frame.

3.2.3 Muscle force prediction: test example

In the following example, a planar three segment, two joint system, is spanned by eight muscles (Fig. 3.2.5). In this example the muscles are assumed to be non-pennate with parameters listed in Table 3.2.5. The muscle joint system does not represent any anatomical system but includes various single and double joint muscles of varying moment arms.

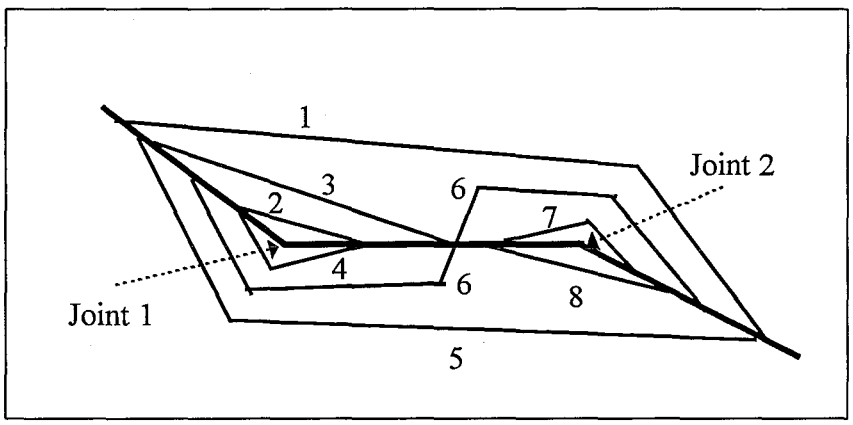

Figure 3.2.5 Eight muscles crossing two planar joints.

Table 3.2.5 Muscle properties for muscle force prediction example. Forces, moment arms and moments are in arbitrary units.

	Maximum	Moment Arms		Maximum Moments		Max. Fibre Force		
Muscle	Force	Joint 1	Joint 2	Joint 1	Joint 2	SO	FO	FG
1	10	+1.0	+0.5	+10.0	+5.0	5	2	3
2	20	+0.3	0.0	+6.0	0.0	10	4	6
3	10	+0.4	0.0	+4.0	0.0	5	2	3
4	15	-0.6	0.0	-9.0	0.0	10	2	3
5	20	-0.2	-0.5	-4.0	-10.0	10	4	6
6	6	-0.4	+0.5	-2.4	+3.0	3	1	2
7	10	0.0	+0.4	0.0	+4.0	5	2	3
8	10	0.0	-0.5	0.0	-5.0	5	2	3

For the purposes of this simplified model, let the required resultant joint moments for the example be +10 Nm for Joint 1 and +12 Nm for Joint 2. Initial muscle force estimates are obtained which meet the resultant joint moments and will act as a starting point and allow the optimisation procedure to converge to a minimum. This is achieved by an iterative procedure assigning muscle forces in accordance to their force generating capacity while reducing the difference between current and required joint moments (Appendix J). The muscle force initial estimates are listed in Table 3.2.6 and the joint moment produced in Table 3.2.7.

Table 3.2.6 Muscle force initial estimates and corresponding fibre type activation levels in muscle force prediction example.

Muscle	Force	Activation levels		
		SO	FO	FG
1	9.88	1.00	1.00	0.96
2	8.38	0.84	0.00	0.00
3	3.62	0.72	0.0	0.0
4	2.35	0.23	0.0	0.0
5	0.0	0.00	0.00	0.00
6	6.0	1.00	1.00	1.00
7	10.0	1.00	1.00	1.00
8	0.0	0.00	0.00	0.00

Table 3.2.7 Joint moments after initial muscle force estimates and following the optimisation procedure.

	Resultant joint moment		
	required	first estimate*	optimisation
Joint 1	10.0	10.04	10.02
Joint 2	12.0	11.94	11.86

* convergence criteria was 0.06.

With the absence of muscle pre-activation levels of each fibre type at a prior instant in time, the initial muscle force estimate will act as muscle pre-activation levels (Table 3.2.6) in the present example. From the pre-activation levels of each fibre type, for a given time period (0.0167 sec. in this example), the maximum and minimum fibre type activation levels and muscle forces can be calculated for the current instant in time (Table 3.2.8).

With the initial muscle force estimates and the muscle force limits, the optimisation routine was carried out to yield an improved muscle force estimate based on a cost function which

minimises muscle stress. The improvements in the cost function for each iteration is presented in Table 3.2.9 and the final muscle force values and activation levels in Table 3.2.10. In the present example the improvement in cost function was obtained by very small changes (< 0.1) in the eight muscle forces.

The activation levels obtained for each fibre type of each muscle then being used as the previous activation levels for the next moment in time.

Muscle force prediction at varying resultant joint moments of the two joints are presented in Tables 3.2.11a - 3.2.11h and Tables 3.2.12a - 3.2.12h and graphically in Figures 3.2.6a - 3.2.6h.

Table 3.2.8 Muscle force limits from pre-activation levels in muscle force prediction example. In the present example the pre-activation levels were taken as the activation level obtained from the initial muscle force estimates (Table 3.2.6).

Muscle		SO	FO	FG	whole muscle
1	max. Activity	1.00	1.00	1.00	1.00
	upper force	5.00	2.00	3.00	10.0
	min. Activity	0.80	0.61	0.59	0.68
	lower force	3.98	1.23	1.77	6.97
2	max. Activity	1.00	1.00	1.00	1.00
	upper force	10.00	4.00	6.00	20.00
	min. Activity	0.67	0.00	0.00	0.33
	lower force	6.68	0.00	0.00	6.68
3	max. Activity	1.00	1.00	1.00	1.00
	upper force	5.00	2.00	3.00	10.00
	min. Activity	0.58	0.00	0.00	0.29
	lower force	2.88	0.00	0.00	2.88
4	max. Activity	1.00	1.00	1.00	1.00
	upper force	10.00	2.00	3.00	15.00
	min. Activity	0.19	0.00	0.00	0.12
	lower force	1.87	0.00	0.00	1.87
5	max. Activity	1.00	1.00	1.00	1.00
	upper force	10.00	4.00	6.00	20.00
	min. Activity	0.00	0.00	0.00	0.00
	lower force	0.00	0.00	0.00	0.00
6	max. Activity	1.00	1.00	1.00	1.00
	upper force	3.00	1.00	2.00	6.00
	min. Activity	0.80	0.61	0.61	0.70
	lower force	2.39	0.61	1.23	4.23
7	max. Activity	1.00	1.00	1.00	1.00
	upper force	5.00	2.00	3.00	10.00
	min. Activity	0.80	0.61	0.61	0.70
	lower force	3.98	1.23	1.84	7.04
8	max. Activity	1.00	1.00	1.00	1.00
	upper force	5.00	2.00	3.00	10.00
	min. Activity	0.00	0.00	0.00	0.00
	lower force	0.00	0.00	0.00	0.00

Table 3.2.9 Improvements in cost function from optimisation procedure in muscle force prediction example.

Iteration	Step size	Cost Function
initial	initial	-5.26
1	0.09	-5.71
2	0.04	-5.80
3	0.01	-5.83

Table 3.2.10 Muscle force estimates and corresponding activation levels in muscle force prediction example.

Muscle	Force	Activation levels		
		SO	FO	FG
1	9.84	1.00	1.00	0.95
2	8.38	0.84	0.00	0.00
3	3.61	0.72	0.0	0.0
4	2.36	0.24	0.0	0.0
5	-0.08	0.00	0.00	0.00
6	5.91	1.00	1.00	0.95
7	9.96	1.00	1.00	0.99
8	-0.09	0.00	0.00	0.00

Table 3.2.11a Muscle forces predicted following optimisation. The resultant moment at Joint 1 is held at +20.0 units while Joint 2 is varied between resultant moments of -15.0 and +12.0 units.

+20.0	Muscle							
Moment 2	1	2	3	4	5	6	7	8
-15	9.93	19.93	9.81	0.00	0.47	0.00	0.00	9.75
-12	9.93	19.93	9.81	0.00	0.42	0.00	0.00	9.75
-8	9.93	19.93	9.81	0.00	0.44	0.00	0.00	9.75
-4	9.93	19.93	9.81	0.00	0.44	0.00	0.00	9.75
0	9.95	19.92	9.79	0.00	0.43	0.00	0.00	9.20
+3	9.96	19.91	9.77	0.00	0.34	0.00	0.02	3.39
+6	9.88	19.91	9.77	0.00	0.00	0.00	3.54	0.56
+9	9.98	19.90	9.75	0.00	0.00	0.16	9.35	0.00
+12	10.00	20.00	10.00	0.00	0.00	0.22	10.00	0.00
max. force	10.0	20.0	10.0	15.0	20.0	6.0	10.0	10.0

Table 3.2.12a Resultant moments and moments produced by predicted muscle forces. The joint moments produced by muscle forces following the first approximation and following the optimisation procedure are shown, as well as any ligament forces required to balance joint moments. The resultant moment at joint one is held at +20.0 units while joint two is varied between resultant moments of -15.0 and +12.0 units.

	Moments				
+20	Resultant	1st estimate	Optimisation	Ligament	difference
Joint 1	+20.0	+19.90	+19.74	0.00	-0.26
Joint 2	-15.0	-0.24	-0.14	-14.86	0.00
Joint 1	+20.0	+19.91	+19.75	0.00	-0.25
Joint 2	-12.0	-0.22	-0.12	-11.88	0.00
Joint 1	+20.0	+19.91	+19.75	0.00	-0.25
Joint 2	-8.0	-0.22	-0.13	-7.87	0.00
Joint 1	+20.0	+19.91	+19.75	0.00	-0.25
Joint 2	-4.0	-0.22	-0.13	-3.87	0.00
Joint 1	+20.0	+19.90	+19.76	0.00	-0.24
Joint 2	0.00	+0.10	+0.16	0.00	+0.16
Joint 1	+20.0	+19.92	+19.78	0.00	-0.22
Joint 2	+3.0	+3.08	+3.12	0.00	+0.12
Joint 1	+20.0	+19.90	+19.76	0.00	-0.24
Joint 2	+6.0	+6.06	+6.08	0.00	+0.08
Joint 1	+20.0	+19.91	+19.79	0.00	-0.21
Joint 2	+9.0	+8.90	+8.81	0.00	-0.19
Joint 1	+20.0	+19.91	+19.91	0.00	-0.09
Joint 2	+12.0	+9.11	+9.11	+2.89	0.00

Table 3.2.11b Muscle forces predicted following optimisation. The resultant moment at Joint 1 is held at +15.0 units while Joint 2 is varied between resultant moments of -15.0 and +12.0 units.

+15.0	Muscle							
Moment 2	1	2	3	4	5	6	7	8
-15	8.90	19.91	9.78	0.00	19.93	0.00	0.00	9.82
-12	8.91	19.91	9.78	0.00	19.93	0.00	0.00	9.82
-8	7.67	19.86	9.67	0.00	13.56	0.00	0.00	9.71
-4	6.20	19.67	9.40	0.00	5.57	0.00	0.00	8.25
0	7.51	16.73	8.15	0.00	4.94	0.00	0.00	2.48
+3	5.84	18.69	8.88	0.00	0.49	0.15	1.71	0.75
+6	6.92	16.50	7.96	0.00	0.00	0.57	5.39	0.00
+9	8.46	14.71	7.09	0.12	0.00	1.52	9.51	0.00
+12	9.94	15.23	7.60	0.59	0.00	5.73	9.91	0.00
max. force	10.0	20.0	10.0	15.0	20.0	6.0	10.0	10.0

Table 3.2.12b Resultant moments and moments produced by predicted muscle forces. The joint moments produced by muscle forces following the first approximation and following the optimisation procedure are shown, as well as any ligament forces required to balance joint moments. The resultant moment at joint one is held at +15.0 units while joint two is varied between resultant moments of -15.0 and +12.0 units.

	Moments				
+15	Resultant	1st estimate	Optimisation	Ligament	difference
Joint 1	+15.0	+14.93	+14.80	0.00	-0.20
Joint 2	-15.0	-10.54	-10.42	-4.58	0.00
Joint 1	+15.0	+14.94	+14.81	0.00	-0.19
Joint 2	-12.0	-10.53	-10.42	-1.58	0.00
Joint 1	+15.0	+14.93	+14.78	0.00	-0.22
Joint 2	-8.0	-7.94	-7.80	0.00	+0.20
Joint 1	+15.0	+14.93	+14.75	0.00	-0.25
Joint 2	-4.0	-3.93	-3.81	0.00	+0.19
Joint 1	+15.0	+14.93	+14.81	0.00	-0.19
Joint 2	0.00	0.00	+0.05	0.00	+0.05
Joint 1	+15.0	+14.94	+14.84	0.00	-0.16
Joint 2	+3.0	+3.06	+3.06	0.00	+0.06
Joint 1	+15.0	+14.93	+14.83	0.00	-0.17
Joint 2	+6.0	+5.95	+5.90	0.00	-0.10
Joint 1	+15.0	+15.06	+15.03	0.00	+0.03
Joint 2	+9.0	+8.93	+8.80	0.00	-0.20
Joint 1	+15.0	+14.93	+14.90	0.00	-0.10
Joint 2	+12.0	+11.93	+11.80	0.00	-0.20

Table 3.2.11c Muscle forces predicted following optimisation. The resultant moment at Joint 1 is held at +10.0 units while Joint 2 is varied between resultant moments of -15.0 and +12.0 units.

+10.0	Muscle							
Moment 2	1	2	3	4	5	6	7	8
-15	3.93	19.89	9.76	0.00	19.94	0.00	0.00	9.82
-12	3.63	19.56	9.59	0.00	17.54	0.00	0.00	9.76
-8	3.41	16.76	8.32	0.00	9.45	0.00	0.00	9.63
-4	3.36	15.22	7.34	0.00	5.07	0.00	0.00	6.01
0	4.99	11.17	5.46	0.00	3.29	0.00	0.00	1.64
+3	4.14	11.85	5.70	0.00	0.00	0.23	2.22	0.09
+6	5.56	9.73	4.64	0.07	0.00	0.75	6.81	0.00
+9	6.83	9.99	4.98	0.88	0.00	3.19	9.62	0.00
+12	9.84	8.38	3.61	2.36	0.00	5.91	9.96	0.00
max. force	10.0	20.0	10.0	15.0	20.0	6.0	10.0	10.0

Table 3.2.12c Resultant moments and moments produced by predicted muscle forces. The joint moments produced by muscle forces following the first approximation and following the optimisation procedure are shown, as well as any ligament forces required to balance joint moments. The resultant moment at joint one is held at +10.0 units while joint two is varied between resultant moments of -15.0 and +12.0 units.

	Moments				
+10	Resultant	1st estimate	Optimisation	Ligament	difference
Joint 1	+10.0	+9.93	+9.81	0.00	-0.19
Joint 2	-15.0	-13.04	-12.92	-2.08	0.00
Joint 1	+10.0	+9.95	+9.83	0.00	-0.17
Joint 2	-12.0	-11.95	-11.84	0.00	+0.16
Joint 1	+10.0	+9.97	+9.87	0.00	-0.13
Joint 2	-8.0	-7.96	-7.84	0.00	+0.16
Joint 1	+10.0	+9.96	+9.84	0.00	-0.16
Joint 2	-4.0	-3.95	-3.86	0.00	+0.14
Joint 1	+10.0	+9.95	+9.87	0.00	-0.13
Joint 2	0.00	0.00	+0.03	0.00	+0.03
Joint 1	+10.0	+9.96	+9.89	0.00	-0.11
Joint 2	+3.0	+3.04	+3.03	0.00	+0.03
Joint 1	+10.0	+10.01	+9.99	0.00	-0.01
Joint 2	+6.0	+5.96	+5.88	0.00	-0.12
Joint 1	+10.0	+10.03	+10.01	0.00	+0.01
Joint 2	+9.0	+8.96	+8.86	0.00	-0.14
Joint 1	+10.0	+10.04	+10.02	0.00	+0.02
Joint 2	+12.0	+11.94	+11.86	0.00	-0.14

Table 3.2.11d Muscle forces predicted following optimisation. The resultant moment at Joint 1 is held at +5.0 units while Joint 2 is varied between resultant moments of -15.0 and +12.0 units.

+5.0	Muscle							
Moment 2	1	2	3	4	5	6	7	8
-15	0.08	17.54	8.71	0.00	19.93	0.00	0.00	9.75
-12	1.98	12.19	6.09	0.00	16.02	0.00	0.00	9.63
-8	1.85	9.61	4.80	0.00	8.66	0.00	0.00	8.97
-4	1.72	8.30	4.09	0.00	4.57	0.00	0.00	5.01
0	2.49	5.59	2.74	0.00	1.64	0.00	0.00	0.81
+3	2.78	4.86	2.31	0.03	0.00	0.36	3.44	0.00
+6	3.78	4.82	2.33	1.03	0.00	1.32	8.35	0.00
+9	5.56	4.98	2.48	2.11	0.0	4.43	9.69	0.00
+12	9.85	0.68	0.00	4.43	0.00	5.91	9.96	0.00
max. force	10.0	20.0	10.0	15.0	20.0	6.0	10.0	10.0

Table 3.2.12d Resultant moments and moments produced by predicted muscle forces. The joint moments produced by muscle forces following the first approximation and following the optimisation procedure are shown, as well as any ligament forces required to balance joint moments. The resultant moment at joint one is held at +5.0 units while joint two is varied between resultant moments of -15.0 and +12.0 units.

	Moments				
+5	Resultant	1st estimate	Optimisation	Ligament	difference
Joint 1	+5.0	+4.93	+4.84	0.00	-0.16
Joint 2	-15.0	-14.93	-14.80	0.00	+0.20
Joint 1	+5.0	+4.95	+4.86	0.00	-0.14
Joint 2	-12.0	-11.95	-11.84	0.00	+0.16
Joint 1	+5.0	+4.97	+4.92	0.00	-0.08
Joint 2	-8.0	-7.96	-7.89	0.00	+0.11
Joint 1	+5.0	+4.98	+4.93	0.00	-0.07
Joint 2	-4.0	-3.98	-3.93	0.00	+0.07
Joint 1	+5.0	+4.98	+4.93	0.00	-0.07
Joint 2	0.00	0.00	+0.02	0.00	+0.02
Joint 1	+5.0	+5.01	+5.00	0.00	0.00
Joint 2	+3.0	+2.98	+2.94	0.00	-0.06
Joint 1	+5.0	+5.03	+5.01	0.00	+0.01
Joint 2	+6.0	+5.97	+5.89	0.00	-0.11
Joint 1	+5.0	+5.02	+5.00	0.00	0.00
Joint 2	+9.0	+8.96	+8.87	0.00	-0.13
Joint 1	+5.0	+5.05	+5.03	0.00	+0.03
Joint 2	+12.0	+11.95	+11.86	0.00	-0.14

Table 3.2.11e Muscle forces predicted following optimisation. The resultant moment at Joint 1 is held at 0.0 units while Joint 2 is varied between resultant moments of -15.0 and +12.0 units.

0.0	Muscle							
Moment 2	1	2	3	4	5	6	7	8
-15	0.03	7.62	3.81	0.00	19.92	0.00	0.00	9.71
-12	1.52	3.21	1.62	0.00	16.04	0.00	0.00	9.14
-8	1.01	2.14	1.07	0.00	10.66	0.00	0.00	6.15
-4	0.51	1.07	0.53	0.00	5.32	0.00	0.00	3.08
0	0.00	0.00	0.00	0.00	0.00	0.00	0.00	0.00
+3	2.49	0.00	0.00	1.86	2.43	2.21	4.58	0.00
+6	5.01	0.00	0.00	3.73	4.87	4.46	9.08	0.00
+9	7.49	0.00	0.00	7.30	3.52	5.90	9.94	0.00
+12	9.94	0.00	0.00	12.55	0.02	5.89	9.95	0.00
max. force	10.0	20.0	10.0	15.0	20.0	6.0	10.0	10.0

Table 3.2.12e Resultant moments and moments produced by predicted muscle forces. The joint moments produced by muscle forces following the first approximation and following the optimisation procedure are shown, as well as any ligament forces required to balance joint moments. The resultant moment at joint one is held at 0.0 units while joint two is varied between resultant moments of -15.0 and +12.0 units.

	Moments				
0.0	Resultant	1st estimate	Optimisation	Ligament	difference
Joint 1	0.0	-0.06	-0.14	0.00	-0.14
Joint 2	-15.0	-14.93	-14.80	0.00	+0.20
Joint 1	0.0	0.00	-0.08	0.00	-0.08
Joint 2	-12.0	-11.95	-11.83	0.00	+0.17
Joint 1	0.0	0.00	-0.05	0.00	-0.05
Joint 2	-8.0	-7.97	-7.90	0.00	+0.10
Joint 1	0.0	0.00	-0.03	0.00	-0.03
Joint 2	-4.0	-3.98	-3.95	0.00	+0.05
Joint 1	0.0	0.00	0.00	0.00	0.00
Joint 2	0.0	0.00	0.00	0.00	0.00
Joint 1	0.0	0.00	+0.01	0.00	+0.01
Joint 2	+3.0	+2.99	+2.97	0.00	-0.03
Joint 1	0.0	0.00	+0.01	0.00	+0.01
Joint 2	+6.0	+5.97	+5.93	0.00	-0.07
Joint 1	0.0	+0.03	+0.05	0.00	+0.05
Joint 2	+9.0	+8.96	+8.92	0.00	-0.02
Joint 1	0.0	+0.04	+0.05	0.00	+0.05
Joint 2	+12.0	+11.94	+11.89	0.00	-0.11

Table 3.2.11f Muscle forces predicted following optimisation. The resultant moment at Joint 1 is held at -5.0 units while Joint 2 is varied between resultant moments of -15.0 and +12.0 units.

-5.0	Muscle							
Moment 2	1	2	3	4	5	6	7	8
-15	0.03	2.18	1.10	3.78	19.92	0.00	0.00	9.71
-12	0.00	0.79	0.41	4.43	14.02	0.00	0.00	9.65
-8	0.00	0.00	0.01	5.17	9.53	0.00	0.00	6.20
-4	0.00	0.00	0.00	6.08	5.89	0.23	0.27	2.54
0	0.92	0.00	0.00	6.23	6.42	2.13	4.10	0.00
+3	0.00	0.00	0.00	6.76	0.00	2.25	4.53	0.00
+6	0.14	0.00	0.00	5.96	0.00	3.91	9.65	0.00
+9	3.91	0.00	0.00	10.84	0.00	5.89	9.93	0.00
+12	6.41	0.00	0.00	14.96	0.00	5.88	9.91	0.00
max. force	10.0	20.0	10.0	15.0	20.0	6.0	10.0	10.0

Table 3.2.12f Resultant moments and moments produced by predicted muscle forces. The joint moments produced by muscle forces following the first approximation and following the optimisation procedure are shown, as well as any ligament forces required to balance joint moments. The resultant moment at joint one is held at -5.0 units while joint two is varied between resultant moments of -15.0 and +12.0 units.

	Moments				
-5	Resultant	1st estimate	Optimisation	Ligament	difference
Joint 1	-5.0	-5.06	-5.12	0.00	-0.12
Joint 2	-15.0	-14.93	-14.80	0.00	+0.20
Joint 1	-5.0	-5.03	-5.06	0.00	-0.06
Joint 2	-12.0	-11.95	-11.84	0.00	+0.16
Joint 1	-5.0	-5.04	-5.00	0.00	0.00
Joint 2	-8.0	-7.97	-7.86	0.00	+0.14
Joint 1	-5.0	-4.98	-4.92	0.00	+0.08
Joint 2	-4.0	-4.02	-3.99	0.00	+0.01
Joint 1	-5.0	-4.98	-4.96	0.00	+0.04
Joint 2	0.00	-0.02	-0.05	0.00	-0.05
Joint 1	-5.0	-4.98	-4.96	0.00	+0.04
Joint 2	+3.0	+2.98	+2.94	0.00	-0.06
Joint 1	-5.0	-4.99	-5.00	0.00	0.00
Joint 2	+6.0	+5.97	+5.88	0.00	-0.12
Joint 1	-5.0	-4.96	-4.95	0.00	+0.05
Joint 2	+9.0	+8.96	+8.87	0.00	-0.13
Joint 1	-5.0	-4.94	-4.92	0.00	+0.08
Joint 2	+12.0	+10.23	+10.11	+1.89	0.00

Table 3.2.11g Muscle forces predicted following optimisation. The resultant moment at Joint 1 is held at -10.0 units while Joint 2 is varied between resultant moments of -15.0 and +12.0 units.

-10.0	Muscle							
Moment 2	1	2	3	4	5	6	7	8
-15	0.00	0.30	0.16	10.33	19.77	0.00	0.00	9.67
-12	0.00	0.00	0.00	11.16	15.78	0.00	0.00	8.06
-8	0.00	0.00	0.00	12.12	11.80	0.51	0.56	5.12
-4	0.00	0.00	0.00	12.63	9.13	0.99	2.20	1.59
0	1.84	0.00	0.00	12.45	12.86	4.30	8.17	0.00
+3	0.00	0.00	0 00	13.98	0.00	3.49	3.10	0.00
+6	0.00	0.00	0 00	13.48	0.00	4.56	8.98	0.00
+9	1.40	0.00	0.00	14.97	0.00	5.88	9.91	0.00
+12	1.41	0.00	0.00	14.97	0.00	5.88	9.91	0.00
max. force	10.0	20.0	10.0	15.0	20.0	6.0	10.0	10.0

Table 3.2.12g Resultant moments and moments produced by predicted muscle forces. The joint moments produced by muscle forces following the first approximation and following the optimisation procedure are shown, as well as any ligament forces required to balance joint moments. The resultant moment at joint one is held at -10.0 units while joint two is varied between resultant moments of -15.0 and +12.0 units.

	Moments				
-10	Resultant	1st estimate	Optimisation	Ligament	difference
Joint 1	-10.0	-10.06	-10.00	0.00	0.00
Joint 2	-15.0	-14.93	-14.72	0.00	+0.28
Joint 1	-10.0	-9.95	-9.85	0. 00	+0.15
Joint 2	-12.0	-12.04	-11.92	0.00	+0.08
Joint 1	-10.0	-9.96	-9.83	0.00	+0.17
Joint 2	-8.0	-8.03	-7.98	0.00	+0.02
Joint 1	-10.0	-9.96	-9.80	0.00	+0.20
Joint 2	-4.0	-4.04	-3.98	0.00	+0.02
Joint 1	-10.0	-9.96	-9.92	0.00	+0.08
Joint 2	0.00	-0.04	-0.09	0 00	-0.09
Joint 1	-10.0	-9.96	-9.78	0.00	+0.22
Joint 2	+3.0	+2.96	+2.99	0.00	-0.01
Joint 1	-10.0	-9.97	-9.91	0.00	+0.09
Joint 2	+6.0	+5.95	+5.87	0.00	-0.13
Joint 1	-10.0	-9.95	-9.93	0.00	+0.07
Joint 2	+9.0	+7.72	+7.60	+1.40	0.00
Joint 1	-10.0	-9.94	-9.92	0.00	+0.08
Joint 2	+12.0	+7.73	+7.61	+4.39	0.00

Table 3.2.11h Muscle forces predicted following optimisation. The resultant moment at Joint 1 is held at -15.0 units while Joint 2 is varied between resultant moments of -15.0 and +12.0 units.

-15.0	Muscle							
Moment 2	1	2	3	4	5	6	7	8
-15	0.00	0.00	0.00	14.80	19.92	4.67	0.00	9.27
-12	0.00	0.00	0.00	14.78	19.83	4.73	0.00	8.59
-8	0.00	0.00	0.00	14.86	17.81	5.56	1.95	5.17
-4	0.00	0.00	0.00	14.89	17.45	5.67	4.61	0.00
0	0.10	0.00	0.00	14.96	18.26	5.84	9.88	0.00
+3	0.00	0.00	0.00	14.97	17.52	5.85	9.89	0.00
+6	0.00	0.00	0.00	14.97	17.51	5.85	9.89	0.00
+9	0.00	0.00	0.00	14.96	17.51	5.85	9.89	0.00
+12	0.00	0.00	0.00	14.97	17.51	5.85	9.89	0.00
max. force	10.0	20.0	10.0	15.0	20.0	6.0	10.0	10.0

Table 3.2.12h Resultant moments and moments produced by predicted muscle forces. The joint moments produced by muscle forces following the first approximation and following the optimisation procedure are shown, as well as any ligament forces required to balance joint moments. The resultant moment at joint one is held at -15.0 units while joint two is varied between resultant moments of -15.0 and +12.0 units.

	Moments				
-15	Resultant	1st estimate	Optimisation	Ligament	difference
Joint 1	-15.0	-14.93	-14.74	0.00	+0.26
Joint 2	-15.0	-12.59	-12.48	-2.52	0.00
Joint 1	-15.0	-14.93	-14.72	0.00	+0.28
Joint 2	-12.0	-11.94	-11.85	0.00	+0.15
Joint 1	-15.0	-14.93	-14.70	0.00	+0.30
Joint 2	-8.0	-8.00	-7.93	0.00	+0.07
Joint 1	-15.0	-14.93	-14.70	0.00	+0.30
Joint 2	-4.0	-4.05	-4.04	0.00	-0.04
Joint 1	-15.0	-14.93	-14.87	0.00	+0.13
Joint 2	0.00	-2.13	-2.21	+2.21	0.00
Joint 1	-15.0	-14.93	-14.83	0.00	+0.17
Joint 2	+3.0	-1.83	-1.88	+4.88	0.00
Joint 1	-15.0	-14.93	-14.82	0.00	+0.18
Joint 2	+6.0	-1.83	-1.87	+7.87	0.00
Joint 1	-15.0	-14.93	-14.82	0.00	+0.18
Joint 2	+9.0	-1.83	-1.87	+10.87	0.00
Joint 1	-15.0	-14.93	-14.82	0.00	-0.18
Joint 2	+12.0	-1.83	-1.87	+13.87	0.00

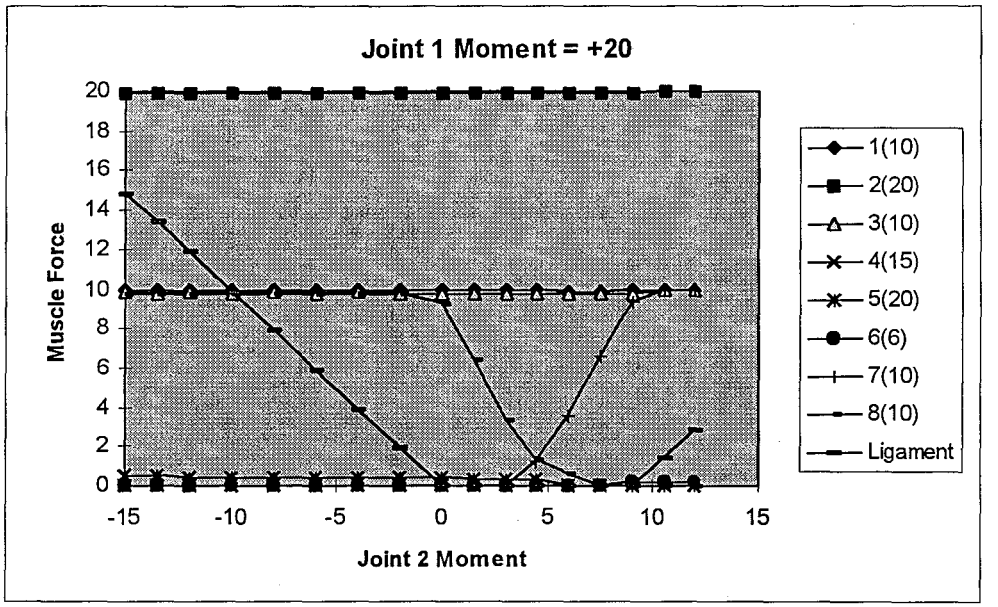

Figure 3.2.6a Muscle force prediction test example. The resultant moment at Joint 1 is held at +20 units while Joint 2 is varied between resultant moments of -15.0 and +12.0 units.

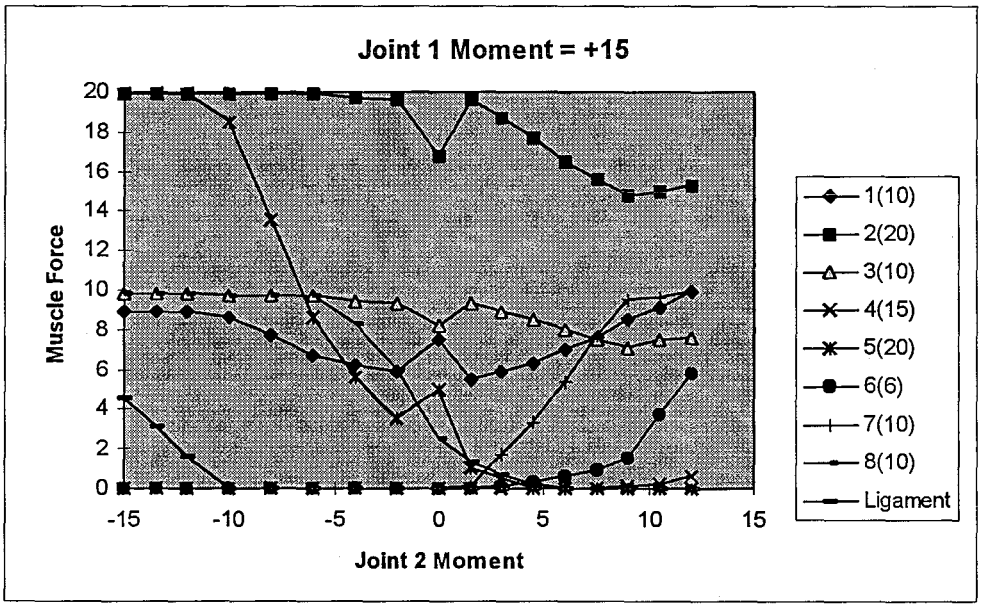

Figure 3.2.6b Muscle force prediction test example. The resultant moment at Joint 1 is held at +15 units while Joint 2 is varied between resultant moments of -15.0 and +12.0 units.

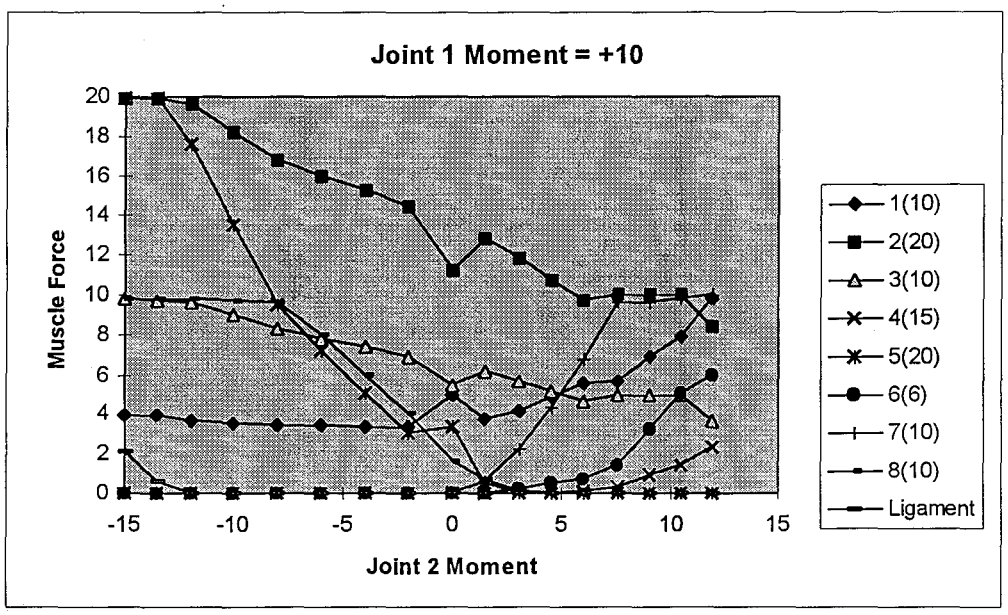

Figure 3.2.6c Muscle force prediction test example. The resultant moment at Joint 1 is held at +10 units while Joint 2 is varied between resultant moments of -15.0 and +12.0 units.

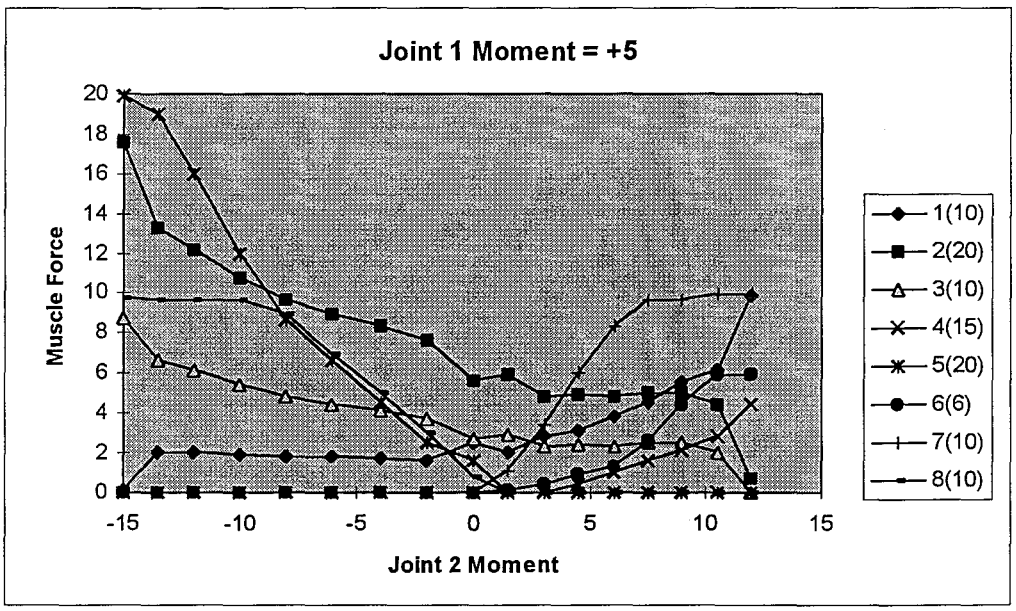

Figure 3.2.6d Muscle force prediction test example. The resultant moment at Joint 1 is held at +5 units while Joint 2 is varied between resultant moments of -15.0 and +12.0 units.

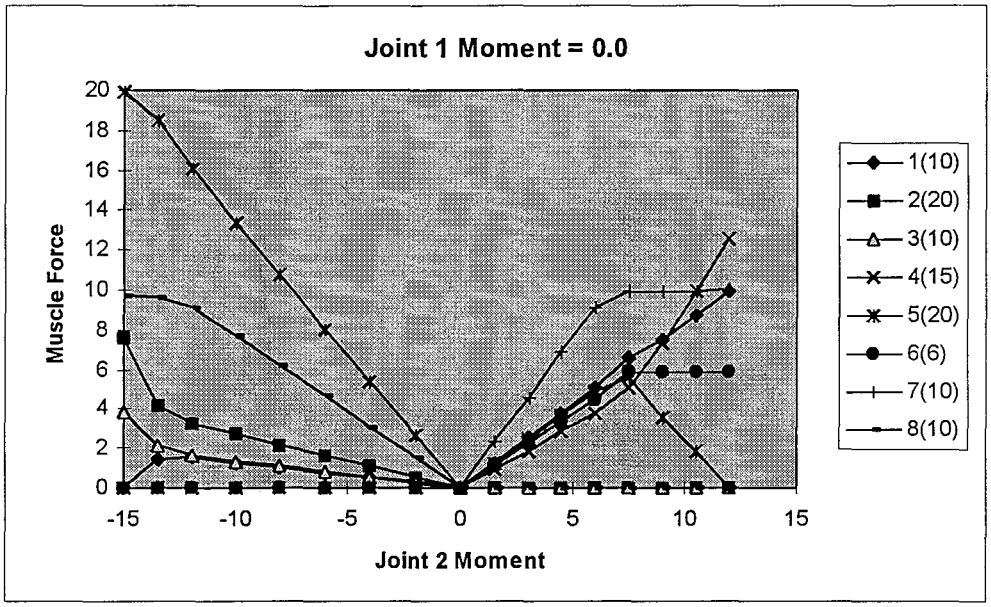

Figure 3.2.6e Muscle force prediction test example. The resultant moment at Joint 1 is held at 0.0 units while Joint 2 is varied between resultant moments of -15.0 and +12.0 units.

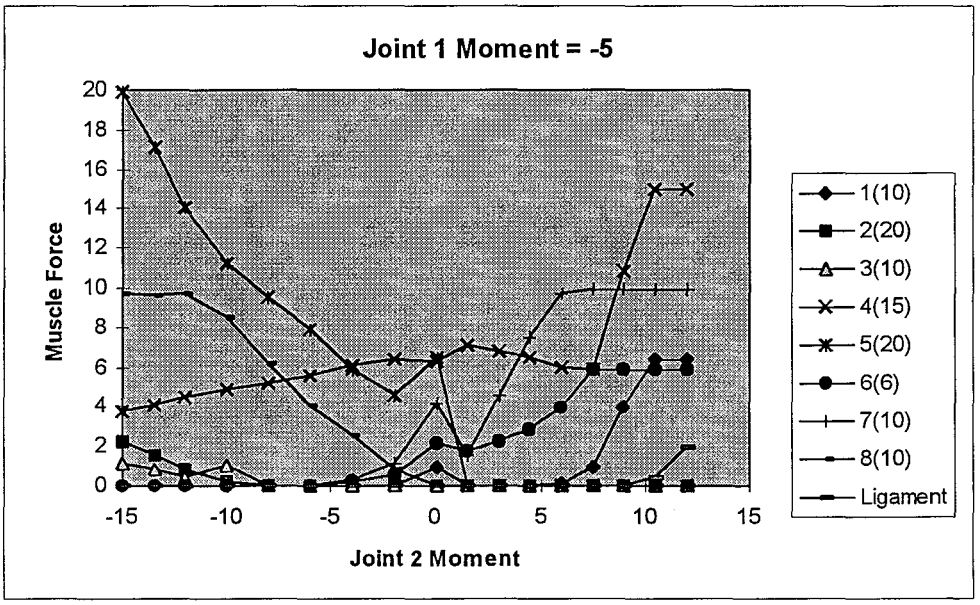

Figure 3.2.6f Muscle force prediction test example. The resultant moment at Joint 1 is held at -5 units while Joint 2 is varied between resultant moments of -15.0 and +12.0 units.

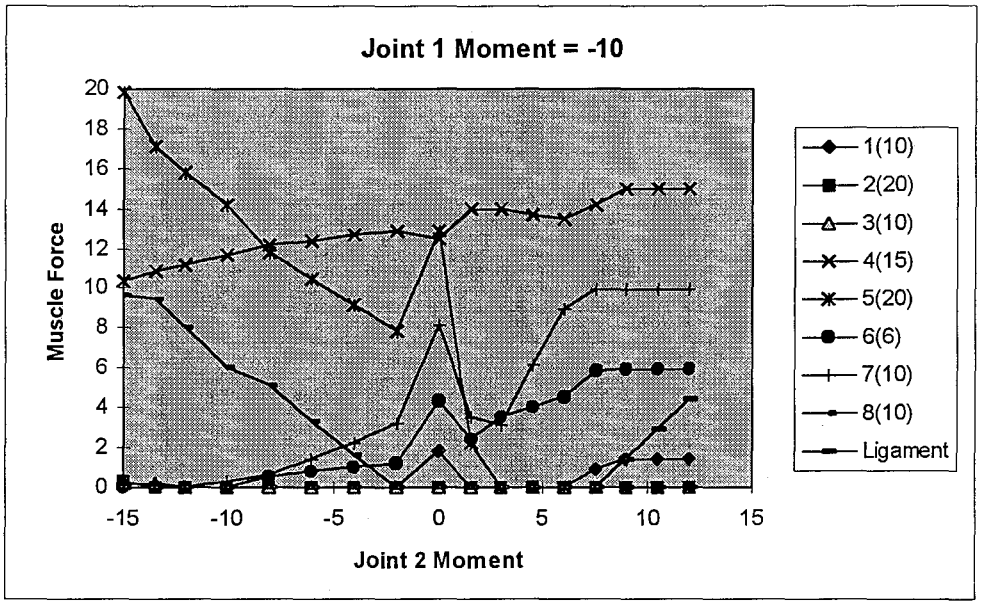

Figure 3.2.6g Muscle force prediction test example. The resultant moment at Joint 1 is held at -10 units while Joint 2 is varied between resultant moments of -15.0 and +12.0 units.

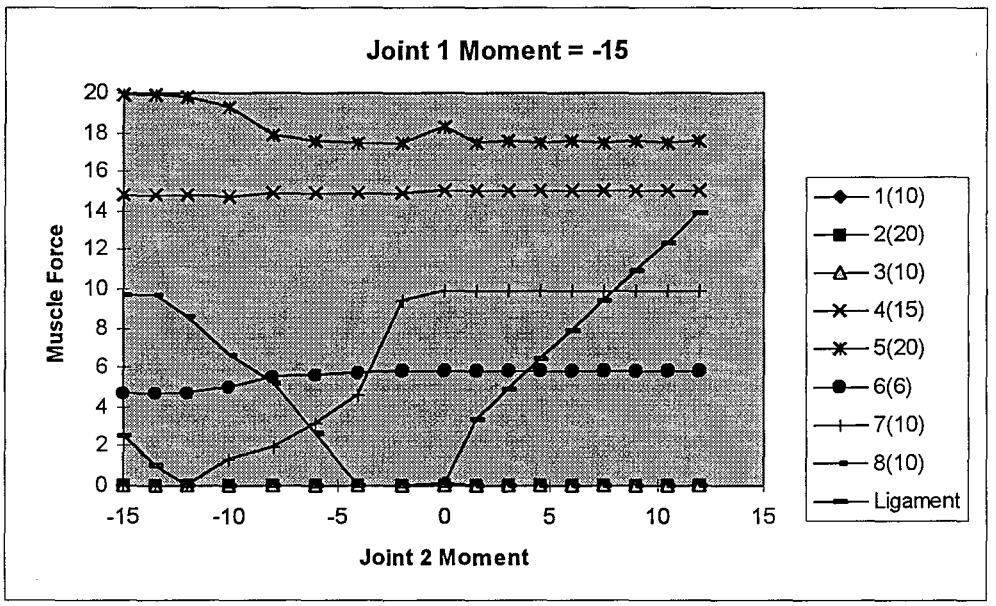

Figure 3.2.6h Muscle force prediction test example. The resultant moment at Joint 1 is held at -15 units while Joint 2 is varied between resultant moments of -15.0 and +12.0 units.

3.3 Body segments

The location and structure of each body segment is described with reference to a body-fixed Cartesian co-ordinate system embedded in each body segment. The following two sections define the body-fixed axes for each segment of the lower limb, and then give segment parameters that are used to describe the structure of each segment for the purposes of calculating resultant joint forces and resultant joint moments.

3.3.1 Subject segment axes

A body-fixed Cartesian co-ordinate system embedded in each body segment is used to describe the location of the associated segment. Segment local axes for a subject are defined from external calibration markers placed on bony landmarks of the subject. A subject calibration procedure allows the calculation of local segment axes from external calibration markers as well as the calculation of local co-ordinate data for each segment marker relative the respective segment local axes. The local co-ordinates of segment markers allows for reproduction of the segment axes during subject movements from the global positions of these external markers. The segment local axes of the subject corresponding to the respective skeletal axes are used to express reference skeletal data of segment centre of mass, inertia, joint centres and muscle co-ordinate data.

Calibration markers placed on the medial knee and medial ankle were not always visible by two cameras with the present camera set-up, with only four cameras used. In the present study the medial knee and medial ankle markers consisted of non-reflective markers placed in the centre of two reflective markers placed on a thin metal rod (Fig. 3.3.1). In subsequent sections the medial knee and medial ankle calibration markers refers to the average position calculated from two reflective markers placed either side of a non-reflective marker placed at the respective landmark.

Figure 3.3.1 Medial knee and medial ankle calibration marker. A non-reflective marker placed on the anatomical site is at the centre of two reflective markers.

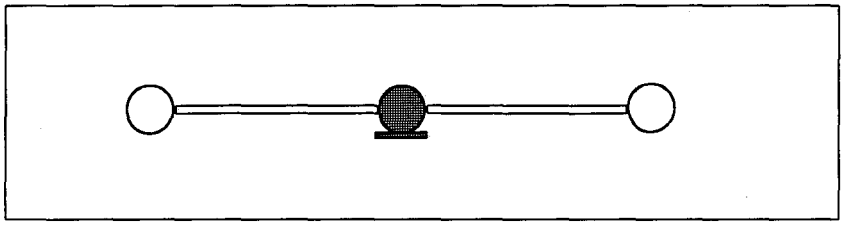

3.3.1.1 Pelvis

The pelvic segment axes are defined from the three external markers placed on the mid-PSIS, right ASIS and left ASIS positions (Appendix A). Firstly, the mid-ASIS point is calculated, and the y-axis defined as a unit vector from the mid-PSIS marker to the mid-ASIS point. A vector is then defined from the right to left ASIS markers. The pelvic z-axis is then defined as the vector cross-product of the vectors from right to left ASIS and the y-axis. With the z-axis expressed as a unit vector, the x-axis is then the cross-product of y-axis and z-axis. The origin of the pelvic local axes is found by translating the mid-ASIS point along the y-axis; a distance which will coincide with the mid-ASIS points of the skeletal axes. This translation includes skinfold thickness above the ASIS, the stand height of the external marker, and the radius of the reflective sphere (Fig 3.3.2). In the present study the axes translation was -6.7 cm.

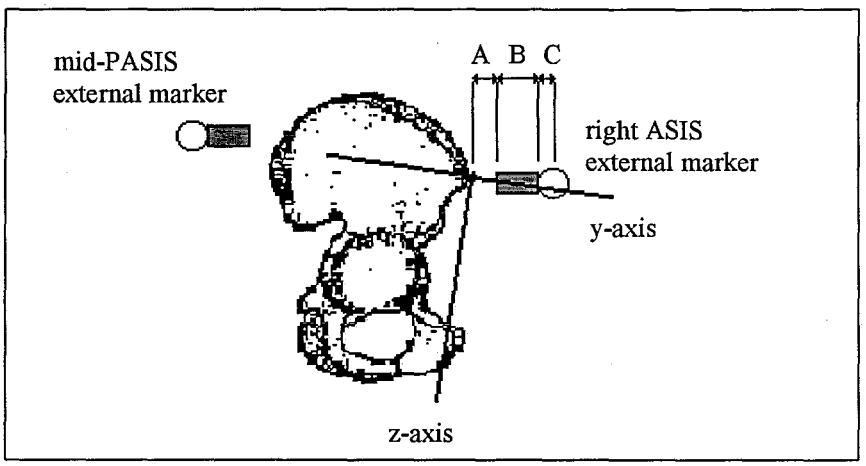

Figure 3.3.2 Pelvic local axes from external markers. Where A = skinfold, B = stand height and C = marker radius.

3.3.1.2 Thigh

The thigh segment axes are defined from two external markers placed on the medial and lateral femoral condyles and from the position of the centre of the acetabulum, as defined from the pelvis local axes (Appendix A). Firstly, the centre of the acetabulum is calculated from the position of the pelvic local axes and relative co-ordinates of the hip joint centre. In the present study the centre of the right acetabulum in the pelvis axes system was given as (-0.35xPelvicWidth) in the x-axis, (-0.383xPelvicDepth) in the y-axes and (0.413xPelvicHeight) in the z-axis (Appendix B). The midpoint of the medial and lateral condyle markers is calculated and the z-axis is defined as a unit vector from the hip joint centre to the mid-condular point. A vector is then defined from the lateral to medial femoral condyle markers for the right leg. The thigh y-axis is then defined as the vector cross-product of the z-axis and the vector from lateral to medial condyle markers of the right leg. With the y-axis expressed as a unit vector, the x-axis is then the cross-product of y-axis and z-axis. A rotation was then performed about the z-axis to account for the alignment of the condyle markers in the horizontal (transverse) plane and the medial-to-lateral direction of the segment x-axis (Fig. 3.3.3). In the present study this rotation was -25.0 degrees. The origin of the thigh axes is at the hip joint centre, or equivalently the centre of the acetabulum.

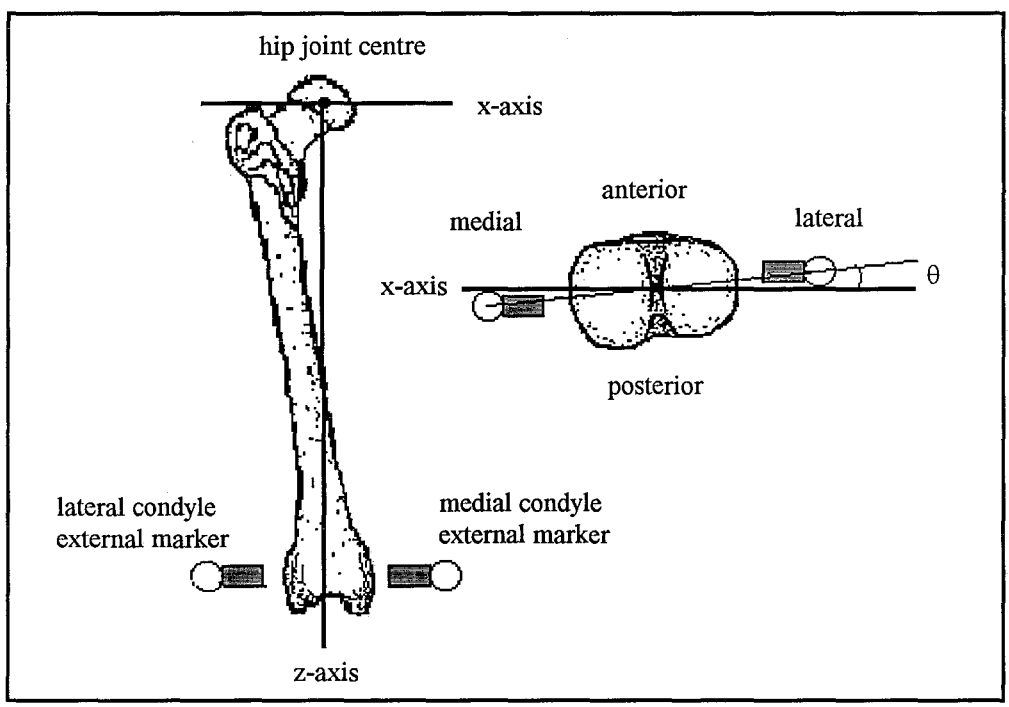

Figure 3.3.3 Thigh local axes from external markers. Where θ = angle between alignment of the condyle markers in the horizontal (transverse) plane and the segment x-axis.

3.3.1.3 Shank

The shank segment axes are defined from two external markers placed on the medial and lateral maleoli and from the position of the centre of the tibial plateau at the height of the tibiale, as defined from the thigh local axes (Appendix A). Firstly, the centre of the tibial plateau is calculated from the thigh z-axes and the distance from the origin of the thigh axes, at the hip joint centre, to the tibiale. In this study, the hip joint centre to tibiale distance is approximated by (1.041xThighLength, from de Leva, 1996), where thigh length is the distance from the Greater Trochanter to the inferior margin of lateral femoral condyle. The midpoint of the medial and lateral maleoli markers is calculated and the z-axis is define as a unit vector from the tibial plateau to the mid-maleoli point. A vector is then defined from the lateral to medial maleoli markers for the right leg. The shank y-axis is then defined as the vector cross-product of the z-axis and the vector from lateral to medial maleoli markers of the right leg. With the y-axis expressed as a unit vector, the x-axis is then the cross-product of y-axis and z-axis. A rotation was then performed about the z-axis to account for the alignment of the maleoli markers in the horizontal (transverse) plane and the true medial to lateral direction of the segment x-axis (Fig. 3.3.4). In the present study this rotation was -15.0 degrees. The origin of the shank axes is at the centre of the tibial plateau to the level of the tibiale.

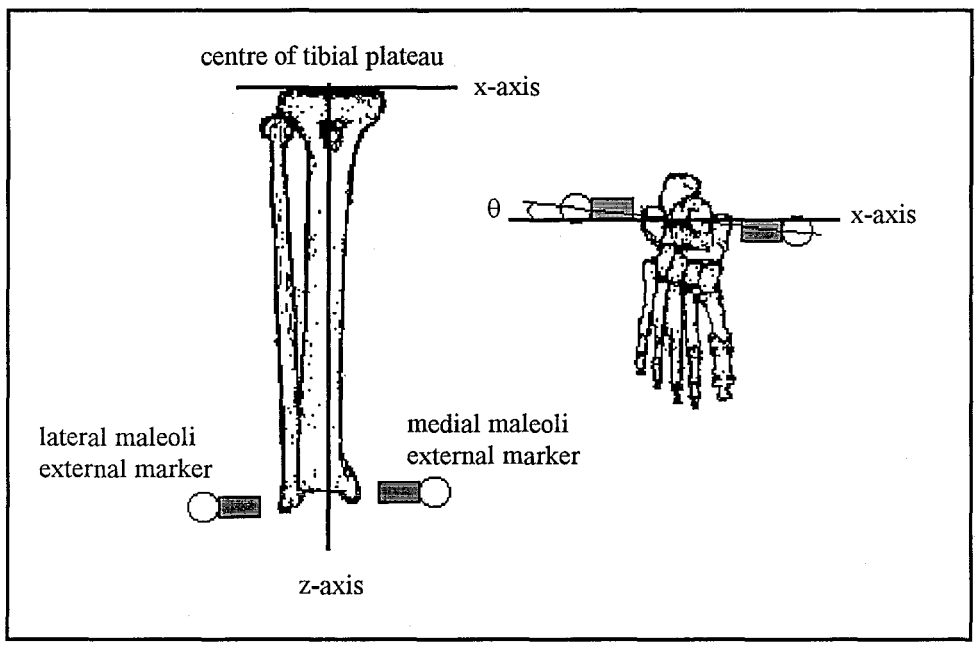

Figure 3.3.4 Shank local axes from external markers. Where θ = angle between alignment of the maleoli markers in the horizontal (transverse) plane and the segment x-axis.

3.3.1.4 Foot

The foot segment axes are defined from external markers placed on the posterior calcaneus, and 1st and 5th metatarsal heads (Appendix A). Firstly, the midpoint of the 1st and 5th metatarsal markers is calculated and the z-axis is define as a unit vector from the posterior calcaneus marker to the mid-metatarsal point. A vector is then defined from the 5th to the 1st metatarsal markers for the right leg. The foot y-axis is then defined as the vector cross-product of the z-axis and the vector from 1st to 2nd metatarsal markers of the right leg. With the y-axis expressed as a unit vector, the x-axis is then the cross-product of y-axis and z-axis. In the present study the 5th metatarsal marker was placed superior to this point to avoid being hit by the contra-lateral leg, while the 1st metatarsal marker was placed lateral to this point. Three rotation were then performed about the x, y, and z axes to account for the alignment of the 1st and 2nd maleoli markers in the horizontal (transverse) plane foot and the true medial-to-lateral direction of the segment x-axis, as well as the shift laterally of the mid-metatarsal point (Fig 3.3.5). In the present study the rotations were 10 degrees about the x-axis, 5.0 degrees about the y-axis and -10.0 about the z-axis. The origin of the foot local axes is found by translating the posterior calcaneus marker along the z-axis a distance which will coincide with the posterior calcaneus point of the skeletal axes. This translation includes skinfold thickness above the posterior calcaneus, the stand height of the external marker, and the radius of the reflective sphere (Fig 3.3.5). In the present study the axes translation was +1.3 cm.

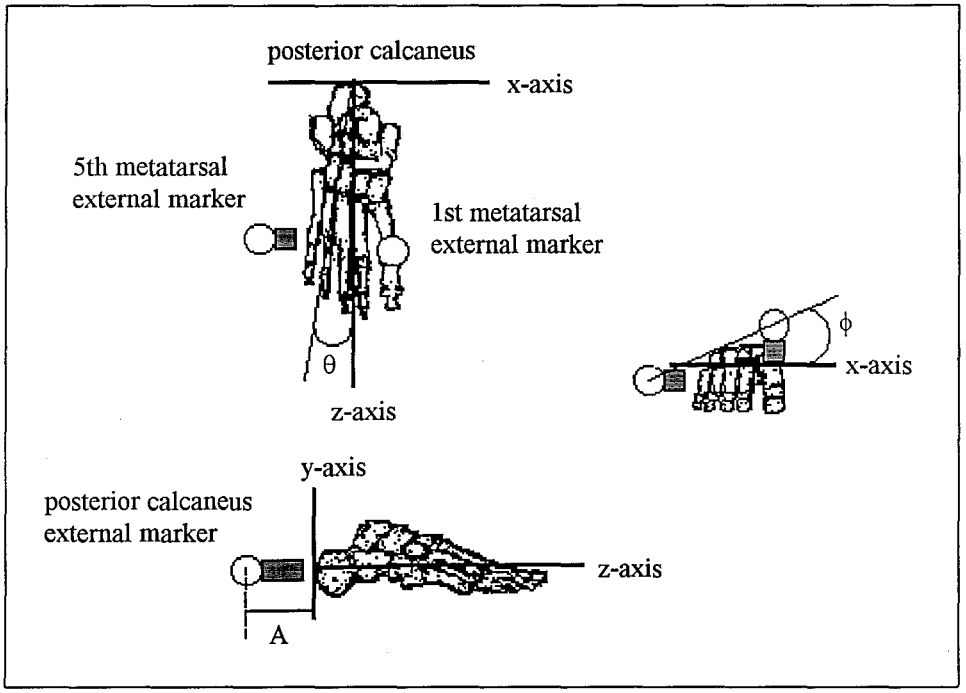

Figure 3.3.5 Foot local axes from external markers. Where A = offset between posterior calcaneus external marker and posterior calcaneus, θ = angle between mid-metatarsal from external markers and the segment z-axis, ϕ = angle between alignment of the maleoli markers in the horizontal (transverse) plane of the foot and the segment x-axis.

3.3.2 Segment Parameters

A set of segment parameters are used to descibe each segment. For the purpose of calculating resultant joint moments, mass, centre of mass, inertia and joint centres of each segment need to be described.

3.3.2.1 Segment mass

Segment masses for the pelvis, thigh, shank and foot were taken from de Leva (1996). Each respective segment mass was expressed relative to total body mass, and is presented in Appendix B.

3.3.2.2 Segment centre of mass

A description of the derivation and normalised co-ordinates for the pelvis, thigh, shank and foot centre of mass used in the present study are presented.

Pelvis centre of mass location was adapted from Hatze (1980), who described the centre of mass location relative to a pelvic axes with origin in the mid horizontal cross section at the height of the umbilicus. Due to the asymmetry about the coronal plane, the axes were rotated about the mediolateral axes to coincide with the principal axes of the pelvis. Using pelvic axes and centre of mass location as described by Hatze (1980), the centre of mass location relative to the present skeletal axes system was estimated and expressed relative to normative data on width, depth and length for the male and female pelvis given by de Leva (1996). A description of the pelvic axes is given in Section 3.3.1.1. Relative to the pelvic axes the normalised co-ordinates of the pelvic centre of mass were (0.0, -0.450, 0.048) for the female pelvis and (0.0, -0.450, 0.079) for the male pelvis, and are expressed relative to pelvic width, pelvis depth and pelvis height respectively (Appendix B).

Segment centre of mass locations for the thigh, shank and foot were adapted from de Leva (1996). The author expressed standard centre of mass locations with respect to bony distances that are not always possible to measure directly on live subjects. Using standard anthropometric data also presented by the author, absolute centre of mass location were calculated for the male and female populations refered to in the article. Then, again using standard anthropometric data as presented by de Leva (1996), relative centre of mass location were calculated for male and female populations with respect to anthropometric measures between bony landmarks used in the present study. A description of the thigh, shank and foot axes are given in Sections 3.3.1.2 - 3.3.1.4 respectively. Relative to the thigh axes, the normalised co-ordinates of the thigh centre of mass were (0.0, 0.0, 0.334) for the female thigh and (0.0, 0.0, 0.382) for the male thigh ,and expressed relative to thigh width, thigh width and thigh length respectively (Appendix B). The normalised co-ordinates of the shank centre of mass relative to the shank axes were (0.0, 0.0, 0.402) for the female shank, and (0.0, 0.0, 0.405) for the male shank, and expressed relative to shank width, shank width and shank length respectively (Appendix B). The normalised co-ordinates of the foot centre of mass relative to the foot axes were (0.0, 0.0, 0.513) for the female foot, and (0.0, 0.0, 0.564) for the

male foot, and expressed relative to foot width, foot width and foot length respectively (Appendix B).

3.3.2.3 Segment inertia

Segment radii of gyration data were adapted from de Leva (1996) for the three anatomical axes of each segment. The author expressed radii of gyration values with respect to bony distances that are not always possible to measure directly on live subjects. As with centre of mass locations, absolute radii of gyration values were calculated for the male and female populations refered to in the article, using standard anthropometric data presented by the author. Then, again using standard anthropometric data presented by de Leva (1996), relative radii of gyration values were calculated for male and female populations with respect to anthropometric measures between bony landmarks used in the present study. In the present study, products of inertia were ignored due to lack of data and the assumption that products of inertia will be small due to the approximate alignment of the body-fixed axes with segment principal axes. A description of the pelvis, thigh, shank and foot axes are given in Sections 3.3.1.1 - 3.3.1.4 respectively. The normalised radii of gyration relative to the pelvic axes were (2.425, 1.323, 2.136) for the female pelvis, and (4.001, 2.261, 3.399) for the male pelvis. The three co-ordinates are expressed relative to pelvic depth and height, pelvic width and height, and pelvic width and depth respectively (Appendix B). The normalised radii of gyration relative to the thigh axes were (4.659, 4.723, 11.349) for the female thigh, and (4.235, 4.235, 10.497) for the male thigh. The three co-ordinates are expressed relative to thigh width and length, thigh width and length and thigh width squared respectively (Appendix B). The normalised radii of gyration relative to the shank axes were (4.248, 4.311, 7.784) for the female shank, and (3.981, 4.077, 8.664) for the male shank. The three co-ordinates are expressed relative to shank width and length, shank width and length and shank width squared respectively (Appendix B). The normalised radii of gyration relative to the foot axes were (4.669, 5.003, 5.968) for the female foot, and (4.099, 4.301, 5.324) for the male foot. The three co-ordinates are expressed relative to foot width and length, foot width and length and foot width squared respectively (Appendix B).

3.3.2.4 Joint centre location

Joint centre locations were measured on the skeletal reference model from which muscle origin, insertion and deflection point data were also measured. The relative joint centre locations used in the present study are presented in Appendix B. A description of each joint centre is given below.

3.3.2.4.1 Hip

Hip joint centre was location at the centre of the acetabulum. A description of the pelvic axes is given in Section 3.3.1.1. The normalised co-ordinates of the right hip joint centre relative to the pelvic axes were (-0.350, -0.383, 0.413), with the three co-ordinates expressed relative to pelvic width, pelvis depth and pelvis height respectively (Appendix B). As the local thigh axes system origin was located at the centre of the acetabulum, the local thigh co-ordinates of the hip joint centre are all zero (Appendix B).

3.3.2.4.2 Knee

Knee joint centre was located at the mid-point between the centres of curvature of the posterior borders of the medial and lateral condyles of the femur. Knee joint centre was modelled as a single point which was stationary with respect to the thigh and shank local axes. A description of the thigh axes is given in Section 3.3.1.2. The normalised co-ordinates of the knee joint centre relative to the right thigh axes were (0.0, -0.197, 1.001), with the three co-ordinates expressed relative to thigh width, thigh width and thigh length respectively (Appendix B). A description of the shank axes is given in Section 3.3.1.3. The normalised co-ordinates of the knee joint centre relative to the right shank axes were (0.0, -0.217, -0.036), with the three co-ordinates expressed relative to shank width, shank width and shank length respectively (Appendix B).

3.3.2.4.3 Ankle

The ankle joint centre was located in the mid-sagittal plane of the ankle by the lateral maleoli of the ankle. The ankle joint centre was modelled as a single point which was stationary with respect to the shank and foot local axes. A description of the shank axes is given in Section

3.3.1.3. The normalised co-ordinates of the ankle joint centre relative to the right shank axes were (0.0, 0.0, 1.000), with the three co-ordinates expressed relative to shank width, shank width and shank length respectively (Appendix B). A description of the foot axes is given in Section 3.3.1.4. The normalised co-ordinates of the ankle joint centre relative to the right foot axes were (0.0, 0.474 , 0.308), with the three co-ordinates expressed relative to foot width, foot width and foot length respectively (Appendix B).

3.4 Anthropometry

Anthropometric measures are required for the scaling of segment reference data to the individual subject. For scaling reference segment masses to the subject, total body mass was used. For scaling muscle model data of individual muscle mass and tendon cross-sectional areas to the subject, segment circumferences and segment lengths were used. For scaling pelvic centre of mass location to the subject, pelvic length and depth were used, while the centre of mass of the thigh, shank and foot were scaled to segment lengths. For scaling pelvic radii of gyration to the subject, pelvic length, width and depth were used depending on the axes, while radii of gyration of the thigh, shank and foot, were scaled to segment lengths and widths. For scaling pelvic muscle co-ordinate data and joint centre locations to the subject, pelvic length, width and depth were used, and muscle co-ordinate data and joint centre locations of the thigh, shank and foot were scaled to segment lengths and widths measures.

In the present study reference data derived from different sources have been nornalised to common anthropometric segment measures. The anthropometric measures chosen being directly measurable on the subject, in addition to general body measures such as age, height and weight. The anthropometric measures and descriptions are listed in Tables 3.4.1 - Table 3.4.3.

Table 3.4.1 Segment length, width and depth measurements.

Segment Width and Length Measurements	
Pelvis width	right ASIS to left ASIS.
Pelvis depth	mid-PSIS to mid-ASIS
Pelvis length	sitting height: seat (inferior ramus of ischium) to iliac crest
Thigh width	bicondylar width, medial to lateral femoral condyles
Thigh length	G.Trochanter to inferior margin of lateral femoral condyle
Shank width	between medial and lateral maleolus.
Shank length	superior margin of medial condyle of tibia to medial maleolus
Foot width	1^{st} to 5^{th} metatarsal heads
Foot length	posterior calcaneus to 2nd metatarsal head

Table 3.4.2 Segment circumference measurements.

Segment Circumference Measurements	
pelvis	In the transverse plane at the level of the ASIS.
thigh	measured in the transverse plane at a level 2 cm. below the gluteal fold.
calf	measured in the transverse plane at the widest circumference of the calf.
foot	measured in the transverse plane (around arch of foot), at the level of the head of the 5th metatarsal.

Table 3.4.3 Skin folds.

Skin Folds	
Thigh	mid anterior thigh
Calf	medial calf

Segment lengths, widths and breadths were measured with a Harpenden Anthropometer (Holtain, U.K.), skin folds were taken with a skinfold calliper (British Indicators Ltd., England), and circumferences were taken with an anthropometric tape measure. Each measurement was taken three times by cycling through all measurements so that any single measure was not taken consecutively. The median of the three values was used as the representative measure in the movement analysis. Both right and left leg measurements were taken.

3.5 Electromyography

Electromyography produces an over all manifestation of the electrical activity in active muscle in proximity to the electrode pair (Hillstrom & Triolo, 1995). Hillstrom & Triolo (1995) recorded electrical activity in muscles whose fibres are close to the dermis using surface electrodes. However, electromyography is not suitable for small or deep muscles (Hillstrom & Triolo, 1995; Soderberg & Knutson, 1995) due to cross talk from surrounding muscles.

Electrical activity is detected by a pair of electrodes (Silver - Silver Chloride, Ag-AgCl) of 1 mm to 5 mm diameter contact area (Hillstrom & Triolo, 1995) and a spacing of 1 cm (Soderberg & Knutson, 1995). Raw EMG signals are in the order of 10 μv to 3 mv amplitude and in the range of 10 Hz to 1 KHz bandwidth and are usually pre-amplified to reduce the signal to noise ratio, with common mode rejection (Hillstrom & Triolo, 1995). The use of pre-amplifies, skin preparation usually only requires cleansing the skin with denatured alcohol (Zipp, 1982; Soderberg & Knutson, 1995). However, additional skin preparation is suggested by Zipp (1982) in the case of small electrode contact area, low amplifier input impedance, motion artefact, and electrical interference. Placing electrodes parallel to the fibres of the muscle is essential to ensure a phase delay between each electrode when receiving the same motor unit action potential. Electrodes placed perpendicular to the direction of muscle fibres may receive the same motor unit action potential at the same time and be eliminated by common mode rejection, although frequencies whose wavelengths are multiples of the electrode spacing will be partially rejected (Hillstrom & Triolo, 1995). The closer the electrode spacing, the wider the bandwidth that can be recorded, with wide electrode spacing acting like a low pass filter (Hillstrom & Triolo, 1995). Small electrodes and narrow spacing must be employed with small muscle or if high discrimination is desired between ECG and adjacent muscles (Zipp, 1982). Larger electrodes and wider separation can be used with larger muscles if more global information on the state of the muscle is desired, or if a high signal amplitude is required. An inter-electrode distance of 4-5 cm and a contact area of 50 mm^2 are recommended for medium to large muscle to be selective, representative and of sufficient amplitude (Zipp, 1982).

There is no standard electrode placement available for individual muscles. In describing EMG electrode placement, Zipp (1982) uses the convention of the 'lead line' which connects two anatomical land marks and the 'central lead point' about which electrodes are placed symmetrically on the lead line. Electrode placement is generally based on previous research and judgement (Soderberg & Knutson, 1995), although, placement of EMG electrodes should meet several requirements (Zipp, 1982):

i) Repeatability in electrode placement;
ii) Consideration of individual body dimensions; and
iii) High signal yield.

To meet these requirements, it is desirable to place electrodes such that (Zipp, 1982):

i) Positions are specified relative to anthropometrical landmarks and in relation to individual body dimensions; and
ii) Electrodes are located on the muscle bulk parallel to the direction of the muscle fibres.

In addition to these guidelines, if large movements are expected, it is recommended to attach the electrodes while the subject assumes an intermediate limb position in order to minimise the strain on the attachment (Zipp, 1982). Also placement must ensure that electrodes do not meet as the muscle shortens. Ground electrode should be placed near to the recording electrodes, preferably over an inactive site (Zipp, 1982).

The desired sampling rate for surface EMG is in the order of 500-1000 Hz, while for indwelling sample rates are in the range of 1000-2000 Hz (Soderberg & Knutson, 1995). Artefact recorded with surface EMG include electrode movement (typically below 10 Hz), mains power (either at 50 or 60 Hz), and EKG (Soderberg & Knutson, 1995). To eliminate artefacts, pre-processing the EMG signal may involve a 10 Hz high pass filter and a 50 Hz or 60 Hz notch filter, and a 500 Hz low pass anti-aliasing filter.

EMG recorded during gait are generally normalised to a percentages of the gait cycle (Soderberg & Knutson, 1995). It is also advantageous to look at several gait cycles and use an average rather than looking at just one cycle. Soderberg & Knutson (1995) suggest that three cycles should be sufficient.

Common EMG signal processing is linear envelope detection (Hillstrom & Triolo, 1995). The linear envelope consists of full wave rectification followed by a low pass filter. Generally, the lower the cut-off frequency, the smoother the result. As changes in muscle force or torque have a lower frequency than raw EMG (Hillstrom & Triolo, 1995) the linear envelope is often used to reflect muscular tension (Knutson & Soderberg, 1995).

The determination of the on-set and off-set of muscular activity can be done quantitatively by either (Soderberg & Knutson, 1995):

i) 5% of a maximum voluntary contraction, as done on a separate maximal tests; or
ii) 2-3 standard deviations above a quiet base-line value.

The signal is required to remain above this value for at least 50 ms to be considered "on", or below for 100 ms to be considered "off". Resting levels of EMG should be defined while the effected limbs are at rest, as in sitting or lying, rather than minimal during activity (Knutson & Soderberg, 1995). Reference minimum or maximum activity levels should be done with the same electrode placement as used for the trial, ideally without removing and re-attaching electrodes, and specific to the subject. However there is no collective agreement as to precise on-off determination (Soderberg & Knutson, 1995).

The relation between force and EMG amplitude is complex and is influenced by both technique and physiological factors (Knutson & Soderberg, 1995), including:

i) Size and placement of electrodes;
ii) Skin preparation;
iii) Size of muscle;
iv) Depth of muscle including adipose tissue;
v) Cross talk from and activity in adjacent muscles;
vi) Movement artefacts;
vii) Eccentric, isometric or concentric muscle action;
viii) Length-tension and force-velocity relationships;
ix) Fibre composition;
x) Muscle fatigue; and
xi) Changes in frequency spectrum of EMG.

In the present study, Blue Sensor ECG disposable electrodes, type SP-00-S (Medicotest, Denmark) were used. The electrode pair separation distance was 3 cm. Eight muscle were recorded:

- Lateral portion of Gastronemius
- Lateral portion of Soleus
- Tibialis Anterior
- Vastus Medialis
- Vastus Lateralis
- Biceps Femoris
- Rectus Femoris
- Gluteus Medius

Three ground electrodes were placed on the right ASIS, lateral femoral condyle and lateral maleolus of the ankle. The ground was common to all channels. The Rectus Femoris and Gluteus Medius ground leads were connected to the right ASIS ground electrode. The Vastus Medialis; Vastus Lateralis and Biceps Femoris ground leads were connected to the lateral femoral condyle ground electrode. Gastronemius, Soleus and Tibialis Anterior ground leads were connected to the lateral maleoli ground electrode.

The following the procedures recommended by Zipp (1982) were used to place the surface electrodes on the muscle belly's or ground positions of the leg;

i) The subject assumed a standing position;
ii) The centre of the muscle belly and the direction of the fibres were identified, as well as the site for the ground electrodes;
iii) The area was cleaned with denatured alcohol, and allowed to dry; and
iv) The electrode pair was placed in the centre of the muscle belly at a separation of 3 cm in a direction parallel with the muscle fibres.

The signal was pre-amplified at a lead distance of approximately 14 cm. from the recording electrodes. A 50 Hz notch filter was applied to each signal before sampling. The sample rate was 1000 Hz. Processing of the signal consisted of:

i) 10 Hz high pass filter;
ii) Full wave rectification; and
iii) Determination of a base line value by:

- Determing the average and standard deviation of EMG signal within every 50 ms window across the trial;
- Determining the average plus three standard deviations for each 50 ms windows across the trial;
- Ssetting the base line as the minimum of the average plus three standard deviations for each 50 ms windows across the trial;

iv) Determination of the on-set and off-set of EMG activity by:

- On-set as EMG activity remaining above the base line value for 50 ms; and
- Off-set as EMG activity remaining below the base line value for 100 ms

3.6 Subject testing protocol

Three dimensional video-based motion analysis, ground reaction force measurement and electromyographic recording were undertaken of three gait cycles and a three stepping tasks for a single subject. The three dimensional movement analysis obtaining kinematics and kinetics of the pelvis and right leg during tasks to which anatomical data and modelling methods presented in the present study can be applied to human movement.

The subject tested was female, 29 years in age, 1.66 metres in height and weighed 55.1 kg. The subject presented no gait abnormalities, leg length discrepancies, or history of gait problems. Testing was carried out in bare feet, and the subject has not been prescribed orthotics.

The video capture was carried out using Motion Analysis System (Motion Analysis Corporation, Santa Rosa, California). The system used four NEC CCD video cameras with infrared light sources to capture the motion of retro-reflective markers placed on the subject. The camera frequency was 60 Hz. Digitisation of the video images and generation of two dimensional co-ordinate data of the reflective markers for each camera view was carried out by a VP110 Video Processor (Motion Analysis Corporation).

Ground reaction force data were obtained from an AMTI (Advanced Mechanical Technology Inc., Watertown, Massachusetts) OR6-5-1000 force platform mounted in the floor. The output from which were six analog channels, three force (Fx, Fy, Fz) and three moments (Mx,

My, Mz). The signals were amplified by an AMTI SGA20 Amplifier. Collection of the force data was done by LabView data acquisition and analysis software.

Synchronisation of force and video data was done by a common switch which was activated by hand at the beginning of each gait trial. The switch placed an audio event marker on all four video recordings of the gait trial, and was used to trigger the start of the LabView analog collection system used to collect the force plate and EMG data. This event marker therefore indicated the starting point of the kinematic and kinetic analysis of each trial.

The laboratory comprised of a test area three metres long, one meter wide and 1.5 meters high, which was visible in all camera fields of view. The force platform was located towards the end of the test area, and four video cameras were placed on one side of the test area (Fig. 3.6.1). This enabled the video capture of the swing and stance phases of gait and the step task of the right lower limb.

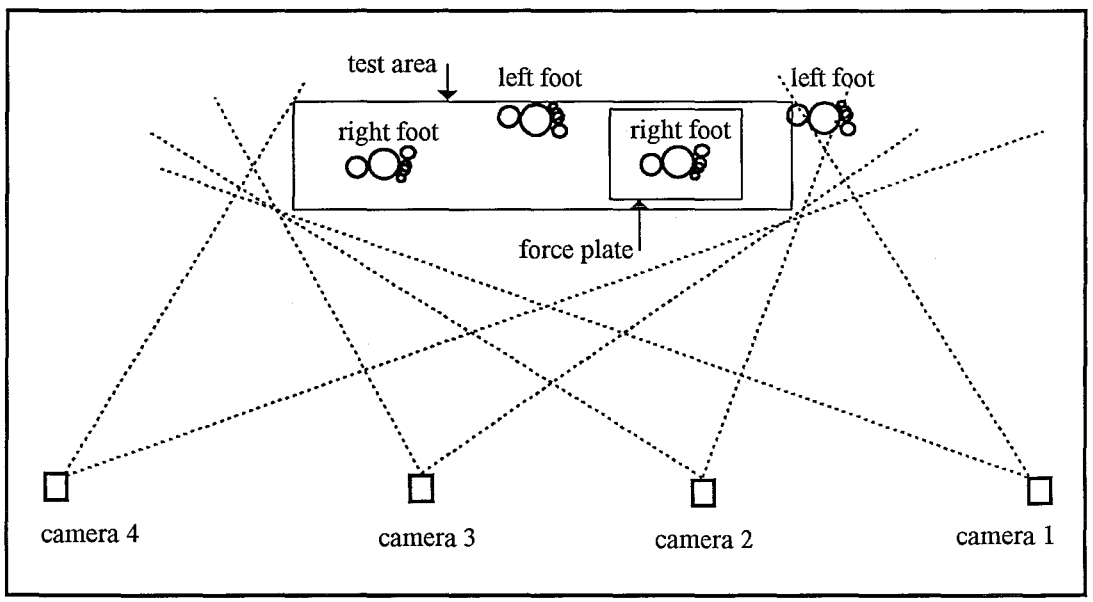

Figure 3.6.1 Test area, force platform and camera positions.

Subject preparation involved taking anthropometric measures, placement of electromyogaphic electrodes and leads, and the placement of reflective markers on the subject (Figures 3.6.2 - 3.6.4). Descriptions of the anthropometric measurements and materials used are given in Section 3.4. Both right and left legs were measured, and each measure was taken three times,

with the median value used. Descriptions of the methods and materials used in placing electrodes on the eight muscles and three ground sites are give in Section 3.5. The pre-amplifies for each electrode pair were also fixed to the subject by the use of adhesive tape. Similarly, the leads between electrodes and respective pre-amplifies and leads leaving the pre-amplifiers were fixed to the subject with adhesive tape. Finally, 30 reflective markers were placed on the subject, consisting of 10 calibration markers (Table 3.6.1) and 27 segment markers (Table 3.6.2). Marker names may appear twice if they were used as both calibration and segment markers, or are used to locate two segments. Double sided adhesive tape was used to adhere markers to the skin. To aid adhesion of the markers Skin-Prep (Smith and Nephew) protective barrier wipes were used, and this was applied to the skin and allowed to dry before the markers were placed on the skin.

Table 3.6.1 Calibration markers. These markers are used to define body-fixed axes during the subject calibration procedure.

Calibration Markers
Right ASIS
Left ASIS
mid PSIS
Medial femoral condyle
Lateral femoral condyle
Medial maleoli
Lateral maleoli
Posterior Calcaneous
1st Metatarsal head
5th Metatarsal head

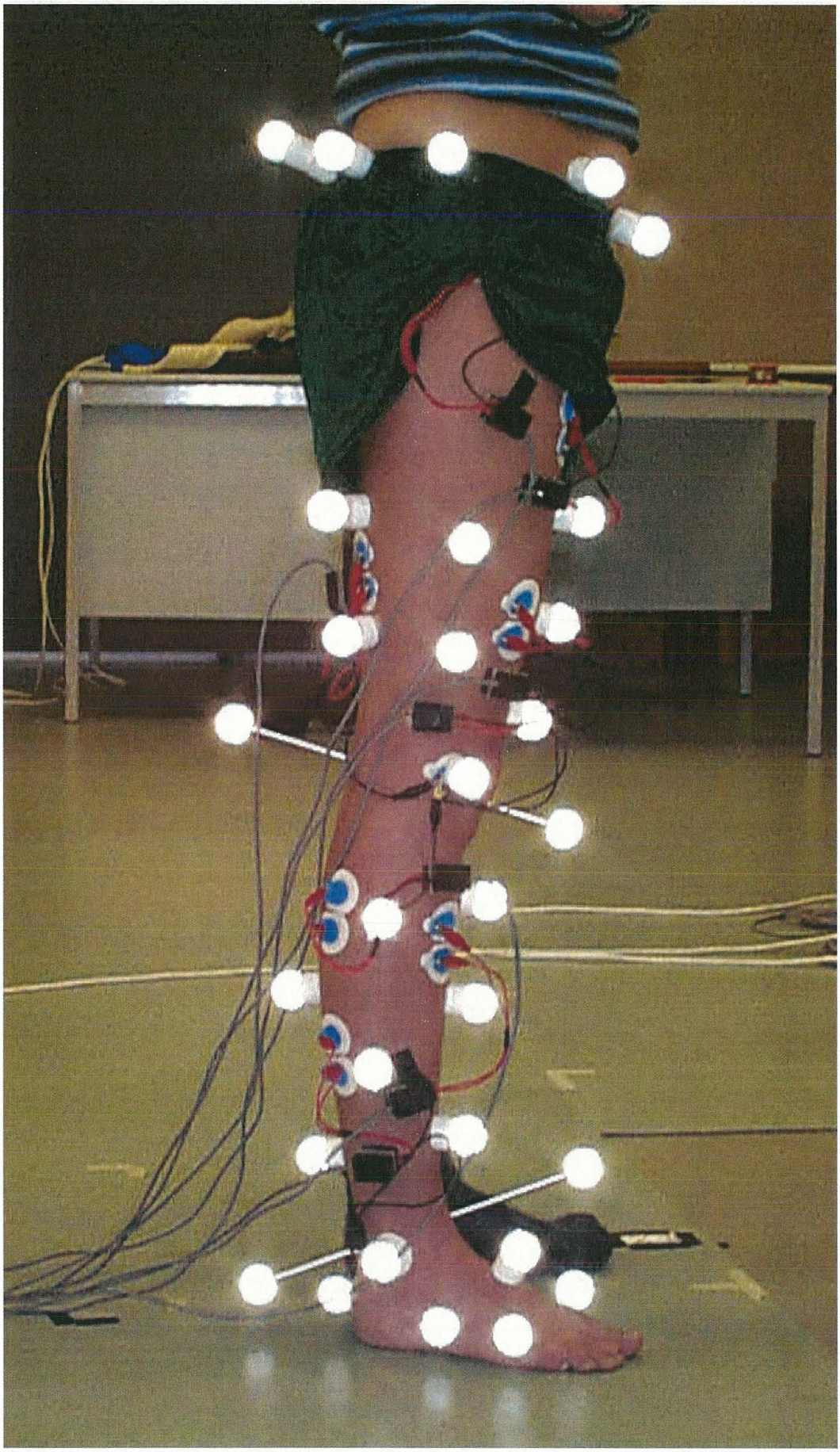

Figure 3.6.1 Subject preparation - lateral view. Shown are electromyographic electrodes, pre-amplifies and leads as well as both calibration and segment markers. Trials were performed in bare feet.

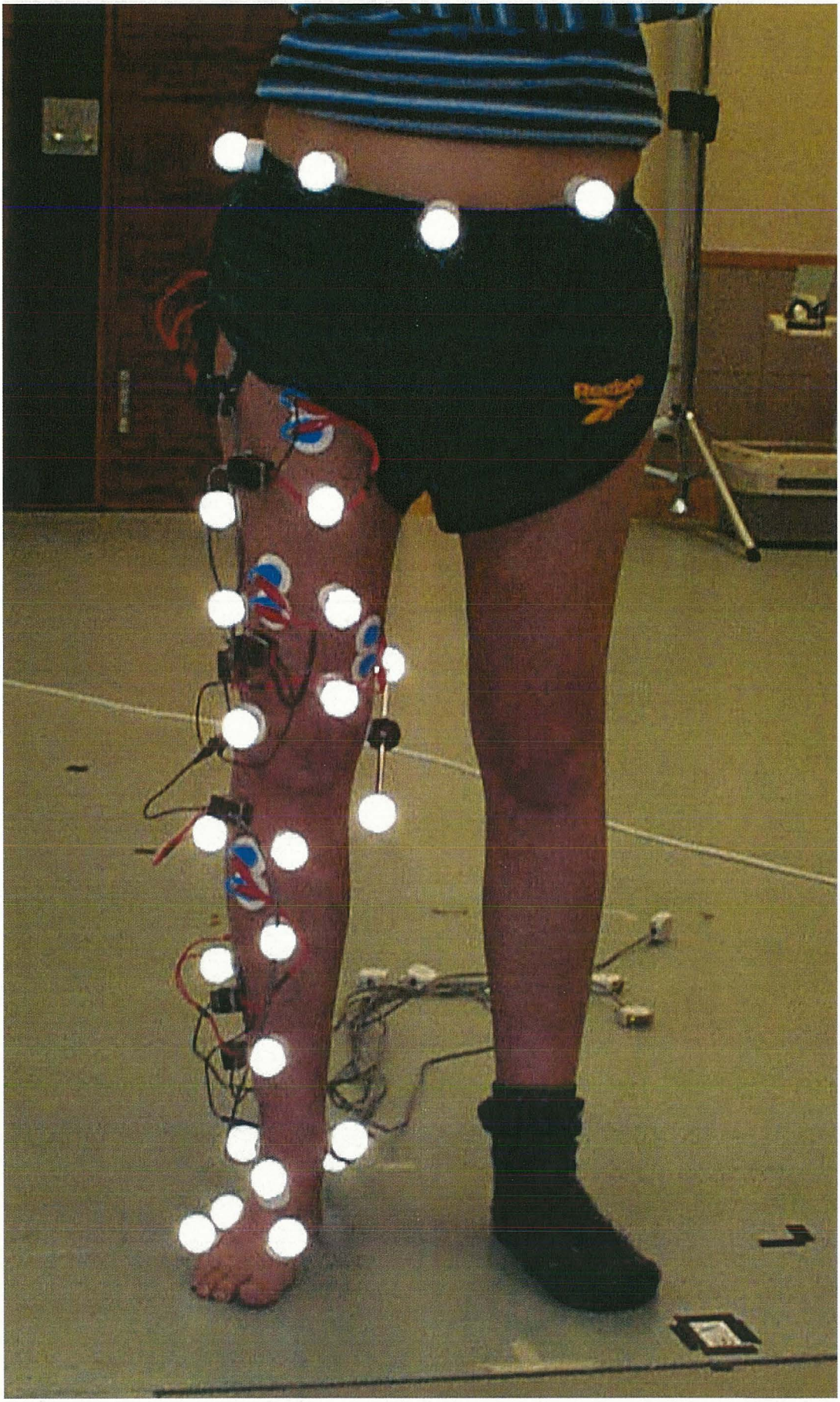

Figure 3.6.2 Subject preparation - anterior view. Shown are electromyographic electrodes, pre-amplifies and leads as well as both calibration and segment markers. Trials were performed in bare feet.

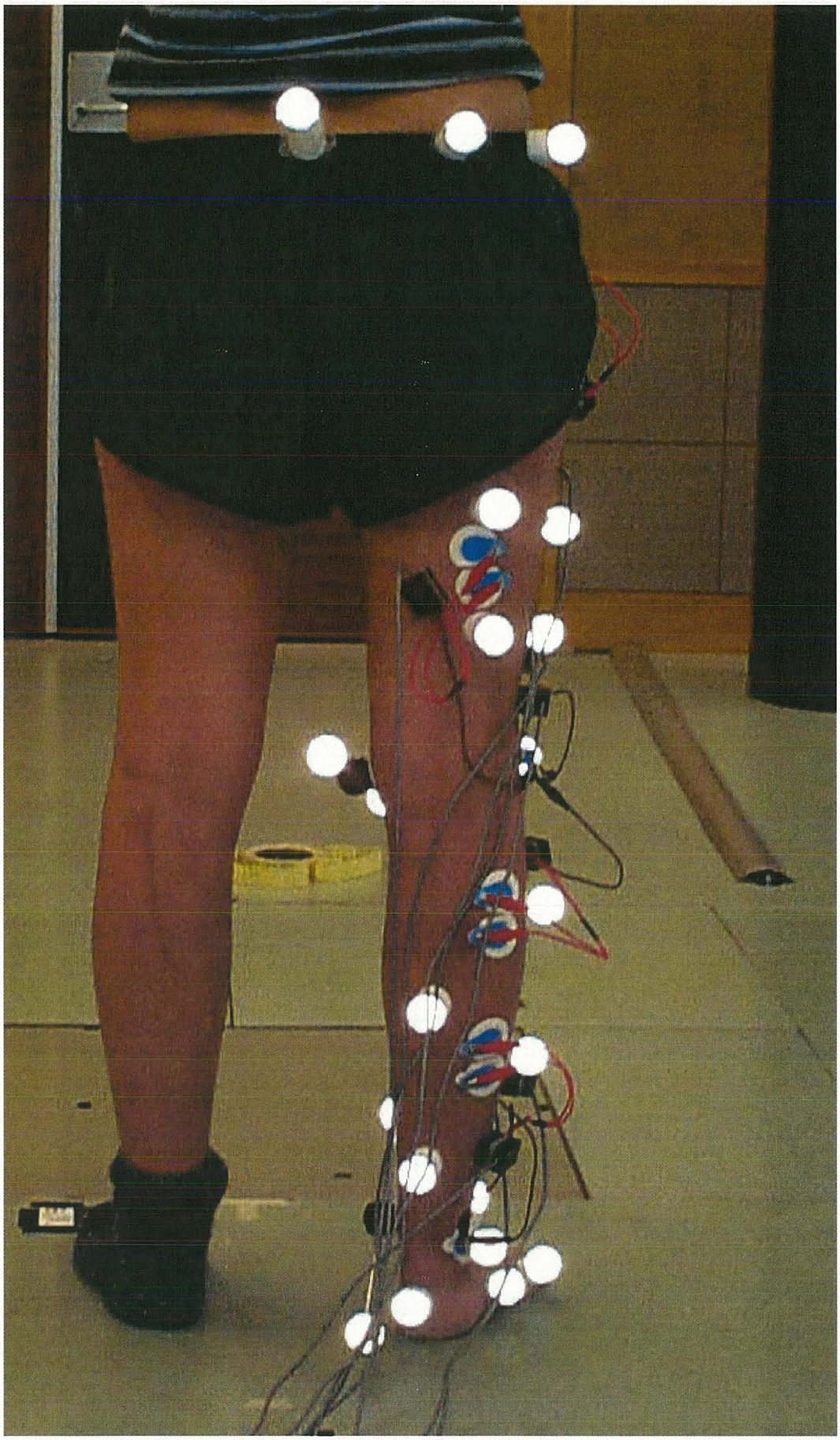

Figure 3.6.3 Subject preparation - posterior view. Shown are electromyographic electrodes, pre-amplifies and leads as well as both calibration and segment markers. Trials were performed in bare feet.

Table 3.6.2 Segment markers. These markers are used to define segment location during movement trials. The local co-ordinates of these markers, with respect to local segment axes, are obtained in the subject calibration procedure.

Segment	Marker (descriptive name)
Pelvis	Navel right ASIS right Iliac crest Posterior belt mid-PSIS
Thigh	Anterior superior thigh Anterior middle thigh Anterior inferior thigh Lateral superior thigh Lateral inferior thigh Lateral knee Posterior superior thigh Posterior inferior thigh
Shank	Anterior superior shank Anterior middle shank Anterior inferior shank Lateral superior shank Lateral inferior shank Lateral ankle Posterior superior shank Posterior inferior shank
Foot	Middle superior foot Lateral ankle Medial toe Lateral toe Posterior calcaneous Middle lateral foot

Video recording involved four stages: camera calibration, force platform location, subject calibration, and the movement (gait and step) trials. Camera calibration and force plate location were done prior to the subject testing session. Camera calibration involved collecting one second of video image of an eight point calibration frame for each camera. The calibration frame comprised of eight reflective spheres of known spatial location with respect to a laboratory (global) co-ordinate system. The size of the calibration cube was 0.75 m long, 0.5 m wide and 0.78 m high, in the global X, Y and Z directions respectively. Digitising the eight calibration points enabled DLT calibration coefficients to be calculated for each camera. The DLT transformation was orthogonalised according to Hatze (1988). The length of the area included in the walk trial in the global X direction, the direction of travel, commenced 60 cm

before the calibration cube and ended 5 cm after the cube. The height of the area included in the walk trial, in the global Z direction, was 20 cm higher than the calibration cube. Camera calibration enabled the 3D paths of all markers to be reconstructed from the four cameras over the entire area of the walk trial.

Force plate location involved collecting one second of video image of three reflective spheres placed on the force platform. The spheres were placed on the axes origin, positive 'x' and positive 'y' of the force platform. The radius of the spheres were also recorded. The reproduction of the three dimensional co-ordinates of the three force platform markers enabled a transformation matrix to the calculated which would convert centre of pressure and force vectors from the force platform local axes system to the global laboratory axes system.

Subject calibration involved collecting one second of video image of the subject while standing with all calibration and segment markers on (Tables 3.6.1 and 3.6.2). The reproduction of the three dimensional co-ordinates enabled the reproduction of segment axes (Section 3.3.1) and the calculation of co-ordinates of all segment markers with respect to local segment axes. Prior to the movement trials the medial ankle and medial knee markers were removed. The left ASIS calibration marker was left on during the trials but was seldom reproduced from two or more cameras.

The walk trials consisted of the subject walking at a slow, self-determined pace along the test area (Fig. 3.6.1), with the right foot making contact with the force platform. Video, force platform and electromyography were recorded simultaneously. After a period of familiarisation, the subject undertook three walk trials, one stride (right toe-off to right toe-off) of the right leg was recorded from each walk trial. The step trials consisted of the subject standing facing a raised platform placed on the force plate. The subject then placed the right leg on the raised platform, and at slow self determined rate, raised themselves onto the raised platform. After pausing on top of the raised platform, the subject returned to the initial standing position, again using the right leg. The left leg did not make contact with the raised platform. Video, force platform and electromyography were recorded simultaneously. After a period of familiarisation the subject undertook three step trials, one step (right toe-off the ground to right foot contact with the ground) was recorded for each step trial.

Analysis of the movement trials required obtaining digitised co-ordinate data for each segment marker, in each trial, and from each video image. Digitisation of video images, including those required for both camera and subject calibration, was achieved through the use of Motion Analysis System's video acquisition and digitisation programs. Camera calibration, the reproduction of three dimensioanl co-ordinates for subject calibration and the tracking of three dimensional paths of the movement trials were achieved via custom writen software. Likewise, the reproduction of three dimensional segment location from local segment marker co-ordinates and respective three dimensional paths of the segment markers was achieved via custom writen software.

Application of the musculoskeletal model, previously presented, to the analysis of movement trials allowed the calculation muscle model parameters to evaluate performance outcomes of the model. Muscle model parameters included acceleration of segment centre of mass, resultant joint moments, muscle lengths, muscle velocities, moment arms, muscle forces, contractile element lengths and contractile element velocities. These are presented and discussed in the following sections.

4 RESULTS

The first section presents anthropometic measures taken from the subject. The following three sections present the results from camera calibration, force platform location and subject calibration which obtained local body-fixed axes co-ordinates of segment markers. The next two sections presents comparative results of the three walk trials and comparative results of the three step trials. Results of individual trials are presented in Appendix L. The final section presents results obtained from EMG analysis.

4.1 Anthropometry

Subject descriptive data appears in Table 4.1.1. Anthropometic measurements of segment lengths, width and breadths, circumferences and skin-folds appear in Tables 4.1.2 - 4.1.4 respectively. Additional measurements taken for calibration purposes are listed in Table 4.1.5, and illustrated in Figure 4.1.1.

Table 4.1.1 Subject descriptive data.

Gender	Female
Age	29 yr.
Height	1.66 m.
Weight	55.1 kg.

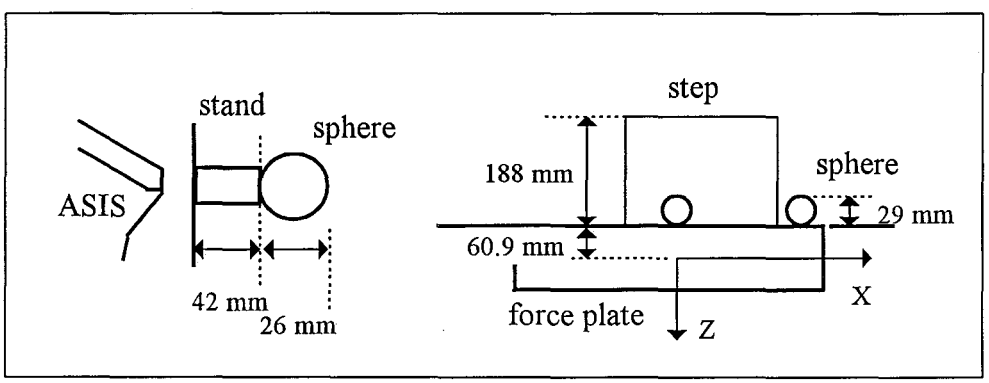

Figure 4.1.1 Additional calibration measurements.

Table 4.1.2 Subject length, width and depth measurements.

Measure	Description	Measurement (mm)			
		#1	#2	#3	Median
Pelvic Width	right ASIS to left ASIS	206.5	205	203	205
Pelvic Depth	mid-PSIS to mid-ASIS	155	154.5	155	155
Pelvic Height	Sitting height (bench top to iliac crest)	199	202	207	202
			Right		Left
Thigh Width	bicondular width (medial to lateral condyles)	#1	89		87
		#2	88.5		88
		#3	90		88
		Median	89		88
Thigh Length	Greater trochanter to inferior margin of lateral femoral condyle.	#1	409.5		396
		#2	405		392
		#3	406		394.5
		Median	406		394.5
Shank Width	Medial to lateral maleoli.	#1	64		60
		#2	63		60
		#3	63.5		60.5
		Median	63.5		60
Shank Length	Tibiale to sphyrion. (Superior margin of lateral condyle of tibia to medial maleolus)	#1	382		379.5
		#2	384		382
		#3	382		382.5
		Median	382		382
Foot Width	1^{st} to 5^{th} metatarsal heads.	#1	82.5		79
		#2	81.5		81.5
		#3	80		79
		Median	81.5		79
Foot Length	Posterior calcaneus to 2nd metatarsal head.	#1	185		184
		#2	184		184
		#3	184		183.5
		Median	184		184

Table 4.1.3 Subject circumference measurements.

Circumference	Description	Measurement (cm)			
		#1	#2	#3	Median
Pelvic	In the transverse plane at the level of ASIS	81.0	81.4	81.8	81.4
			Right		Left
Thigh	In the transverse plane at a level 2 cm below the gluteal fold.	#1	53.4		53
		#2	53.4		53.5
		#3	52.4		53.1
		Median	53.4		53.1
Shank	In the transverse plane at the widest circumference of the calf	#1	33.2		33
		#2	33		32.8
		#3	33.1		32.9
		Median	33.1		32.9
Foot	In the transverse plane at at the level the head of the 5th metatarsal.	#1	22.1		22.6
		#2	22		21.8
		#3	22.1		22.7
		Median	22.1		21.8

Table 4.1.4 Subject skin-fold measurements.

Skin-fold	Description	Measurement (mm)		
			Right	Left
Thigh	mid anterior thigh	#1	26	28
		#2	25.5	26
		#3	26	28.5
		Median	26	28
Shank	medial calf at the widest circumference of the calf	#1	16.5	18
		#2	16.5	18.5
		#3	16.5	18
		Median	16.5	18

Table 4.1.5 Additional calibration measurements.

ASIS markers	
stand height	42 mm
sphere diameter	26 mm
Post.Calcaneus marker	
stand height	0 mm
sphere diameter	26 mm
Force plate	
origin to plate surface	60.9 mm
sphere diameter	29 mm
step height	188 mm

Subject specific segment centre of mass and joint locations are listed in Table 4.1.6. Subject specific segment mass and radii of gyration are listed in Table 4.1.7. Co-ordinate locations, masses, radii of gyration have been obtained by multiplying normalised reference data in Appendix B by the subject anthopometric measures listed above. Lean thigh and shank circumferences are shown in Table 4.1.8, as calculated from respective circumference and skin-fold measurement listed above.

Table 4.1.6 Segment centre of mass and joint location. Locations are found by using segment measures in Table 4.1.2 and normalised co-ordinates of Appendix B.

Segment	Point	Co-ordinate* (m)		
		X	Y	Z
Pelvis	centre of mass	0	-0.0698	0.0097
	L5-S1 joint centre	0	-0.0969	-0.0149
	hip joint centre	-0.0718	-0.0594	0.0834
Thigh	centre of mass	0	0	0.1356
	hip joint centre	0	0	0
	knee joint centre	0	-0.0175	0.4064
Shank	centre of mass	0	0	0.1536
	knee joint centre	0	-0.0138	-0.0138
	ankle joint centre	0	0	0.3820
Foot	centre of mass	0	0	0.0944
	ankle joint centre	0	0.0386	0.0567

* relative to local axes as described in Appendix A.

Table 4.1.7 Segment mass and radii of gyration. Values were found using segment measures in Table 4.1.2 and normalised co-ordinates of Appendix B.

Segment	Mass (kg)		Radii of gyration* (m)		
			X	Y	Z
Pelvis	6.89		0.0759	0.0548	0.0679
Thigh	8.15	right	0.1683	0.1707	0.0899
		left	0.1617	0.1640	0.0879
Shank	2.64	right	0.1030	0.1046	0.0314
		left	0.0974	0.0988	0.0280
Foot	0.72	right	0.0700	0.0750	0.0396
		left	0.0679	0.0727	0.0372

* relative to local axes (Appendix A)

Table 4.1.8 Segment lean circumference. Lean circumference is circumference minus Pi*skin-fold.

Segment	Lean Circumference (cm)	
	Right	Left
Thigh	45.2	44.3
Shank	27.9	27.3

4.2 Camera calibration

The laboratory co-ordinates of the eight calibration cube markers are listed in Table 4.2.1 and the camera co-ordinates of the eight respective markers are listed in Table 4.2.2.

Table 4.2.1 Laboratory co-ordinates of camera calibration cube markers.

Calibration Marker	Laboratory (global) Co-ordinate (m)		
	X	Y	Z
1	0.0000	0.0000	0.0369
2	0.7483	0.0000	0.0368
3	0.7500	0.5024	0.0378
4	0.0006	0.5004	0.0372
5	-0.0004	0.0005	0.7863
6	0.7480	-0.0007	0.7876
7	0.7481	0.4500	0.7877
8	-0.0004	0.5012	0.7871

Table 4.2.2 Camera co-ordinates of eight calibration cube markers.

Marker	Camera 1		Camera 2		Camera 3		Camera 4	
	X	Y	X	Y	X	Y	X	Y
1	79.14	79.43	109.00	93.29	111.92	73.22	140.11	68.23
2	155.44	66.38	183.13	89.81	187.84	69.70	203.00	77.81
3	181.00	79.22	180.50	105.81	175.00	75.41	169.00	86.29
4	110.07	89.29	115.00	108.34	107.27	79.19	109.44	78.38
5	78.84	162.62	108.59	163.81	116.59	149.81	140.73	153.60
6	157.35	159.59	186.41	161.34	192.58	144.34	204.69	154.47
7	183.15	162.08	184.18	170.55	179.66	142.67	170.08	155.92
8	110.66	164.34	115.00	172.41	111.50	147.00	109.20	155.00

Identifying the eight calibration points on the calibration cube yielded the following calibration results. The linearized DLT calibration parameters for each camera are listed in Table 4.2.3. The lab point standard error's (LPSE) and conjugate point error (CPE) for each camera are listed in Table 4.2.4 and Table 4.2.5 respectively. The camera perspective centres, found during the calibration procedure from the intersection of perspective lines, are listed in Table 4.2.6. Finally the normalisation curve for lab point error and angle for two point identified in two cameras is listed in Table 4.2.7.

Table 4.2.3 DLT parameters for each camera.

parameter	Camera 1	Camera 2	Camera 3	Camera 4
1	79.709	94.768	106.010	114.421
2	86.551	38.602	16.515	-36.621
3	-2.984	-7.654	6.222	-2.420
4	79.166	108.959	111.583	140.069
5	-26.467	-5.850	-3.364	24.580
6	40.626	56.296	30.287	38.177
7	105.478	82.920	101.279	110.034
8	75.234	89.660	69.612	63.078
9	-0.141	-0.019	0.025	0.150
10	-0.227	0.235	0.241	0.229
11	-0.035	-0.069	-0.003	-0.024

Table 4.2.4 LPSE for three dimensional points produced from three and four camera points.

Cameras	LPSE (m)	
	mean	std.dev.
4	0.0007	0.0003
3	0.0009	0.0005

Table 4.2.5 CPE for each camera.

Camera	CPE*	
	mean	std.dev.
1	0.229	0.104
2	0.210	0.122
3	0.215	0.122
4	0.170	0.100

* camera digitised units (256x256)

Table 4.2.6 Camera perspective centres.

Camera	Laboratory (global) Co-ordinates (m)		
	X	Y	Z
1	2.1857	-2.8948	0.9502
2	0.5099	-3.7737	1.5167
3	-0.4453	-4.0948	0.5224
4	-2.1264	-2.8779	0.8912

Table 4.2.7 Normalisation curve of lab point error from two camera co-ordinates.

Coefficient	value
c0	0.0256
c1	-0.0210
c2	0.0066
minimum = 0.0089 at 1.591 radians	

Curve = c0 + c1*radians + c2*radians*radians.
Where radians is the angle formed by camera perspective centre, lab point and the second camera perspective centre.

4.3 Force plate calibration

Three dimensional co-ordinates of three reflective spheres placed on the plate surface at the plate axes origin, positive 'x' and positive 'y' directions are shown in Table 4.3.1 as reproduced from the four camera views.

Table 4.3.1 Force platform axes location.

Marker	Laboratory (global) Co-ordinates (m)		
	X	Y	Z
+ve X	0.209	0.071	0.004
origin	0.508	0.069	0.005
+ve Y	0.505	0.517	0.004
Z axes translation		0.075 m	
Z axes plate surface		-0.061 m	

4.4 Subject calibration

A graphical reproduction of the plotted calibration markers and segment markers for the post-trial subject calibration is presented in Fig. 4.4.1.

Figure 4.4.1 Markers used in subject calibration.

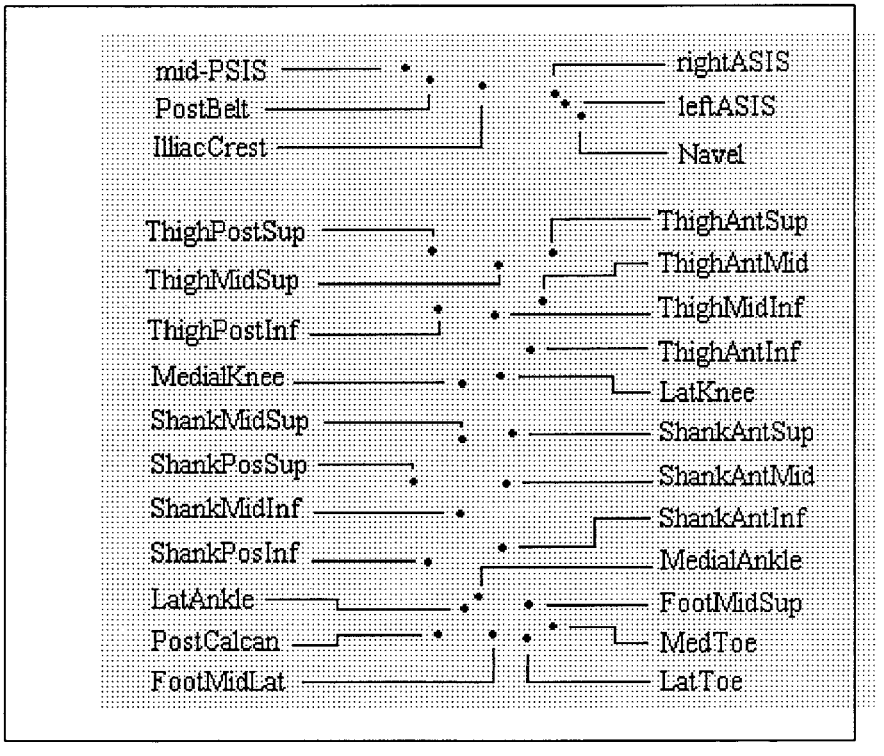

The reproduced three dimensional co-ordinates of the pre-trial and post-trial subject calibrations are presented in Table 4.4.1 and Table 4.4.2 respectively. Local segment axes origin and unit vectors with respect to global space of the pre-trial and post-trial subject calibrations, defined from three dimensional laboratory positions of calibration markers for the respective segment, are presented in Table 4.4.3 and Table 4.4.4 respectively. Local axes co-ordinates of segment markers from the pre-trial and post-trial subject calibrations are presented in Table 4.4.5 and Table 4.4.6. The differences between local axes co-ordinates of the segment markers for the pre-trial and post-trial subject calibrations are presented in Table 4.4.7. Reference muscle lengths calculated from the reference segment positions of the pre-trial and post-trial subject calibrations are presented in Table 4.4.8 and Table 4.4.9. The reference segment positions were subject standing, as used for segment calibration.

Table 4.4.1 Laboratory points reproduced for pre-trial subject calibration.

Marker	Lab (global) Co-ordinate (m)			Cameras and Camera point				
	X	Y	Z	total	1	2	3	4
mid-PSIS	-0.2122	-0.0989	0.9617	3	-	1	26	1
PostBelt	-0.1841	-0.2199	0.9467	3	-	30	1	2
IlliacCrest	-0.1054	-0.2987	0.9437	4	1	3	2	3
r.ASIS	0.0244	-0.2473	0.9332	4	2	4	3	4
l.ASIS	0.0660	-0.0286	0.9171	2	3	2	-	-
Navel	0.0820	-0.1650	0.8928	3	4	5	4	-
ThighPostSup	-0.1926	-0.2530	0.6729	4	5	6	5	5
ThighAntSup	0.0147	-0.2377	0.6627	4	6	7	6	6
ThighMidSup	-0.0878	-0.3076	0.6472	4	7	8	7	7
ThighAntMid	-0.0033	-0.2199	0.5790	3	9	9	10	-
ThighPostInf	-0.1825	-0.2518	0.5755	4	22	10	8	8
ThighMidInf	-0.0984	-0.3001	0.5633	4	8	11	9	9
ThighAntInf	-0.0237	-0.2180	0.5009	4	10	13	12	11
#1MedialKnee	-0.2600	-0.1288	0.4937	3	-	12	11	10
LateralKnee	-0.0889	-0.2877	0.4637	4	11	14	13	12
#2MedialKnee	0.0015	-0.1831	0.4058	4	12	15	14	13
ShankAntSup	-0.0672	-0.2478	0.3588	4	14	16	16	14
ShankMidSup	-0.1604	-0.3004	0.3553	4	13	17	15	15
ShankPostSup	-0.2288	-0.2159	0.2844	3	-	18	17	16
ShankAntMid	-0.0812	-0.2533	0.2760	4	15	19	18	17
ShankMidInf	-0.1687	-0.2928	0.2333	4	16	20	19	18
ShankAntInf	-0.0899	-0.2558	0.1701	4	17	22	20	19
ShankPostInf	-0.2116	-0.2134	0.1478	3	-	21	21	21
#1MedAnkle	0.0119	-0.1964	0.1266	4	18	23	22	20
FootSuperior	-0.0466	-0.2564	0.0734	4	20	25	24	22
LateralAnkle	-0.1612	-0.2666	0.0683	4	19	26	23	23
MedialToe	0.0003	-0.2386	0.0371	4	21	27	27	26
#2MedAnkle	-0.2530	-0.1697	0.0291	3	-	24	25	24
PostCalc	-0.1996	-0.2194	0.0283	3	-	31	30	25
LateralToe	-0.0559	-0.3077	0.0198	4	24	29	29	28
FootMidLat	-0.1122	-0.2793	0.0192	4	23	28	28	27

Error*2.0, Close = 0.0388 m

Table 4.4.2 Laboratory points reproduced for post-trial subject calibration.

Marker	Lab (global) Co-ordinate (m)			Cameras and Camera points				
	X	Y	Z	total	1	2	3	4
mid-PSIS	-0.2663	0.0371	0.9741	3	-	31	1	1
PostBelt	-0.2251	-0.0753	0.9534	4	1	1	2	2
IlliacCrest	-0.1406	-0.1467	0.9432	4	21	3	3	3
r.ASIS	-0.0178	-0.0840	0.9327	4	2	4	4	4
l.ASIS	-0.0010	0.1284	0.9146	2	3	30	-	-
Navel	0.0250	0.0011	0.8928	3	4	5	5	-
ThighPostSup	-0.2246	-0.1088	0.6669	4	5	7	6	5
ThighAntSup	-0.0205	-0.0654	0.6651	3	6	6	7	-
ThighMidSup	-0.1129	-0.1465	0.6449	4	7	8	8	6
ThighAntMid	-0.0379	-0.0441	0.5838	3	8	9	10	-
ThighPostInf	-0.2118	-0.1093	0.5696	4	9	10	9	7
ThighMidInf	-0.1201	-0.1373	0.5618	4	10	11	11	8
ThighAntInf	-0.0589	-0.0386	0.5028	3	11	29	13	-
#1MedialKnee	-0.3121	-0.0067	0.4693	4	12	12	12	9
LateralKnee	-0.1073	-0.1162	0.4610	4	13	13	14	10
#2MedialKnee	-0.0354	0.0128	0.4244	3	14	14	15	-
ShankAntSup	-0.0898	-0.0689	0.3606	3	15	15	17	-
ShankMidSup	-0.1723	-0.1423	0.3507	4	16	16	16	11
ShankPostSup	-0.2533	-0.0700	0.2818	4	17	17	18	12
ShankAntMid	-0.0983	-0.0786	0.2762	4	18	18	19	13
ShankMidInf	-0.1778	-0.1269	0.2270	4	19	19	20	14
ShankAntInf	-0.1056	-0.0763	0.1708	4	20	20	21	15
ShankPostInf	-0.2307	-0.0524	0.1464	4	23	21	22	17
#1MedAnkle	-0.0085	-0.0013	0.1265	4	22	22	23	16
FootSuperior	-0.0625	-0.0601	0.0738	4	24	24	24	18
LateralAnkle	-0.1693	-0.0961	0.0688	4	28	25	26	19
#2MedAnkle	-0.2841	-0.0098	0.0511	4	29	23	25	20
MedialToe	-0.0211	-0.0365	0.0391	4	25	26	27	22
PostCalc	-0.2127	-0.0346	0.0255	3	0	2	28	23
FootMidLat	-0.1239	-0.1049	0.0243	4	26	27	29	21
LateralToe	-0.0658	-0.1152	0.0184	3	27	28	30	-

Error*2.0, Close = 0.0388 m

Table 4.4.3 Local segment axes origin and unit vectors with respect to global space for the pre-trial subject calibration.

Segment	Description	Laboratory (global) Co-ordinate (m)		
		X	Y	Z
Pelvis	Origin	-0.020	-0.128	0.934
	X unit vector	0.141	0.988	-0.066
	Y unit vector	0.979	-0.149	-0.139
	Z unit vector	-0.147	-0.045	-0.988
Thigh	Origin	-0.101	-0.194	0.865
	X unit vector	0.140	0.988	-0.071
	Y unit vector	0.990	-0141	-0.010
	Z unit vector	-0.020	-0.069	-0.997
Shank	Origin	-0.109	-0.223	0.443
	X unit vector	0.180	0.984	-0.021
	Y unit vector	0.980	-0.181	-0.082
	Z unit vector	-0.085	-0.006	-0.996
Foot	Origin	-0.187	-0.223	0.028
	X unit vector	0.187	0.981	0.048
	Y unit vector	0.139	-0.074	0.987
	Z unit vector	0.972	-0.178	-0.151

Table 4.4.4 Local segment axes origin and unit vectors with respect to global space for the post-trial subject calibration.

Segment	Description	Laboratory (global) Co-ordinate (m)		
		X	Y	Z
Pelvis	Origin	-0.075	0.026	0.937
	X unit vector	0.043	0.996	-0.078
	Y unit vector	0.980	-0.057	-0.192
	Z unit vector	-0.196	-0.068	-0.978
Thigh	Origin	-0.153	-0.048	0.872
	X unit vector	-0.073	0.997	-0.023
	Y unit vector	0.997	0.074	0.027
	Z unit vector	0.029	-0.021	-0.999
Shank	Origin	-0.140	-0.057	0.450
	X unit vector	-0.023	1.000	0.017
	Y unit vector	0.999	0.024	-0.046
	Z unit vector	-0.047	0.016	-0.999
Foot	Origin	-0.200	-0.038	0.026
	X unit vector	0.122	0.990	0.068
	Y unit vector	0.122	-0.083	0.989
	Z unit vector	0.985	-0.112	-0.130

Table 4.4.5 Segment marker local co-ordinates, pre-trial subject calibration.

Segment	Point	Local Axes Co-ordinate (m)		
		X	Y	Z
Pelvis	mid-PSIS	0.000	-0.196	0.000
	PostBelt	-0.115	-0.148	0.016
	IlliacCrest	-0.181	-0.059	0.011
	r.ASIS	-0.111	0.062	0.000
	l.ASIS	0.111	0.072	0.000
	Navel	-0.019	0.112	0.028
Thigh	ThighPostSup	-0.058	-0.080	0.198
	ThighAntSup	-0.013	0.123	0.202
	ThighMidSup	-0.095	0.031	0.225
	ThighAntMid	0.008	0.103	0.285
	ThighPostInf	-0.048	-0.070	0.294
	ThighMidInf	-0.083	0.021	0.308
	ThighAntInf	0.013	0.084	0.363
	LateralKnee	-0.063	0.029	0.406
Shank	ShankAntSup	-0.015	0.053	0.081
	ShankMidSup	-0.084	-0.029	0.093
	ShankPostSup	-0.011	-0.105	0.169
	ShankAntMid	-0.021	0.047	0.165
	ShankMidInf	-0.075	-0.028	0.215
	ShankAntInf	-0.023	0.048	0.271
	ShankPostInf	-0.003	-0.078	0.303
	LateralAnkle	-0.045	-0.012	0.378
Foot	FootSuperior	-0.004	0.067	0.136
	LateralAnkle	-0.036	0.046	0.027
	MedialToe	0.020	0.036	0.184
	PostCalc	0.001	-0.002	-0.013
	LateralToe	-0.059	0.016	0.144
	FootMidLat	-0.041	0.006	0.084

Table 4.4.6 Segment marker local co-ordinates, post-trial subject calibration.

Segment	Point	Local Axes Co-ordinate (m)		
		X	Y	Z
Pelvis	mid-PSIS	0.000	-0.195	0.000
	PostBelt	-0.109	-0.144	0.020
	IlliacCrest	-0.175	-0.056	0.018
	r.ASIS	-0.107	0.063	0.000
	l.ASIS	0.107	0.071	0.000
	Navel	-0.017	0.108	0.025
Thigh	ThighPostSup	-0.051	-0.082	0.204
	ThighAntSup	-0.022	0.125	0.211
	ThighMidSup	-0.096	0.026	0.230
	ThighAntMid	0.002	0.107	0.291
	ThighPostInf	-0.050	-0.072	0.302
	ThighMidInf	-0.084	0.017	0.313
	ThighAntInf	0.011	0.084	0.371
	LateralKnee	-0.062	0.029	0.413
Shank	ShankAntSup	-0.015	0.054	0.086
	ShankMidSup	-0.087	-0.029	0.099
	ShankPostSup	-0.014	-0.105	0.173
	ShankAntMid	-0.026	0.050	0.171
	ShankMidInf	-0.073	-0.029	0.223
	ShankAntInf	-0.025	0.047	0.276
	ShankPostInf	0.001	-0.076	0.307
	LateralAnkle	-0.045	-0.012	0.381
Foot	FootSuperior	-0.002	0.066	0.132
	LateralAnkle	-0.051	0.051	0.031
	MedialToe	0.024	0.035	0.173
	PostCalc	0.001	-0.002	-0.013
	LateralToe	-0.061	0.015	0.142
	FootMidLat	-0.057	0.013	0.083

Table 4.4.7 Differences between pre-trial and post-trial subject calibration of local segment marker co-ordinates.

Segment	Point	Pre and Post subject calibration Differences in Local Axes Co-ordinates (m)		
		dX	dY	dZ
Pelvis	mid-PSIS	0.000	+0.001	0.000
	PostBelt	+0.006	+0.004	+0.004
	IlliacCrest	+0.006	+0.003	+0.007
	r.ASIS	+0.004	+0.001	0.000
	l.ASIS	-0.004	-0.001	0.000
	Navel	+0.002	-0.004	-0.003
Thigh	ThighPostSup	+0.007	-0.002	+0.006
	ThighAntSup	-0.009	0.002	+0.009
	ThighMidSup	-0.001	-0.005	+0.005
	ThighAntMid	-0.006	+0.004	+0.006
	ThighPostInf	-0.002	-0.002	+0.008
	ThighMidInf	-0.001	-0.004	+0.005
	ThighAntInf	-0.002	0.000	+0.008
	LateralKnee	+0.001	0.000	+0.007
Shank	ShankAntSup	0.000	0.001	+0.005
	ShankMidSup	-0.003	0.000	+0.006
	ShankPostSup	-0.003	0.000	+0.004
	ShankAntMid	-0.005	+0.003	+0.006
	ShankMidInf	+0.002	-0.001	+0.008
	ShankAntInf	-0.002	-0.001	+0.005
	ShankPostInf	+0.004	+0.002	+0.004
	LateralAnkle	0.000	0.000	+0.003
Foot	FootSuperior	+0.002	-0.001	-0.004
	LateralAnkle	-0.015	+0.005	+0.004
	MedialToe	+0.004	-0.001	-0.011
	PostCalc	0.000	0.000	0.000
	LateralToe	-0.002	-0.001	-0.002
	FootMidLat	-0.016	+0.007	-0.001

Table 4.4.8 Reference muscle lengths, pre-trial subject calibration.

Muscle	Length (m)
Psoas_Major	0.307
Iliacus	0.193
Gremellus_Superior	0.099
Gremellus_Inferior	0.094
Obturator_Externus	0.114
Obturator_Internus	0.163
Piriformis	0.136
Quadratus_Femoris	0.074
Pectineus	0.137
Adductor_Longus	0.210
Adductor_Magnus(ant)	0.113
Adductor_Magnus(mid)	0.188
Adductor_Magnus(inf)	0.319
Adductor_Brevis	0.152
Gluteus_Minimus(ant)	0.096
Gluteus_Minimus(pos)	0.127
Gluteus_Medius(ant)	0.115
Gluteus_Medius(mid)	0.134
Gluteus_Medius(pos)	0.142
Gluteus_Maximus(ant)	0.205
Gluteus_Maximus(mid)	0.205
Gluteus_Maximus(pos)	0.211
Tensor_Fascia_Lata	0.531
Semimembranosis	0.412
Semitendinosus	0.465
Gracilis	0.456
Satorius	0.570
Rectus_Femorus	0.555
Biceps_Femorus(long)	0.423
Biceps_Femorus(short)	0.242
Vastus_Lateralis	0.289
Vastus_Intermedius	0.330
Vastus_Medialis	0.311
Popliteus	0.085
Gastrocnemius(lateral)	0.444
Gastrocnemius(medial)	0.450
Plantaris	0.447
Soleus(lateral)	0.299
Soleus(medial)	0.319
Tibialis_Anterior	0.343
Tibialis_Posterior	0.352
Peroneus_Longus	0.395
Peroneus_Brevis	0.225
Peroneus_Tertius	0.158
Ext_Digit_Longus	0.403
Ext_Halluc_Longus	0.278
Flex_Digit_Longus	0.437
Flex_Halluc_Longus	0.342

Table 4.4.9 Reference muscle lengths, post-trial subject calibration.

Muscle	Length (m)
Psoas_Major	0.303
Iliacus	0.189
Gremellus_Superior	0.103
Gremellus_Inferior	0.096
Obturator_Externus	0.111
Obturator_Internus	0.167
Piriformis	0.142
Quadratus_Femoris	0.072
Pectineus	0.130
Adductor_Longus	0.199
Adductor_Magnus(ant)	0.105
Adductor_Magnus(mid)	0.183
Adductor_Magnus(inf)	0.318
Adductor_Brevis	0.143
Gluteus_Minimus(ant)	0.095
Gluteus_Minimus(pos)	0.130
Gluteus_Medius(ant)	0.115
Gluteus_Medius(mid)	0.140
Gluteus_Medius(pos)	0.151
Gluteus_Maximus(ant)	0.214
Gluteus_Maximus(mid)	0.214
Gluteus_Maximus(pos)	0.221
Tensor_Fascia_Lata	0.528
Semimembranosis	0.414
Semitendinosus	0.468
Gracilis	0.449
Satorius	0.569
Rectus_Femorus	0.558
Biceps_Femorus(long)	0.426
Biceps_Femorus(short)	0.242
Vastus_Lateralis	0.289
Vastus_Intermedius	0.330
Vastus_Medialis	0.312
Popliteus	0.085
Gastrocnemius(lateral)	0.451
Gastrocnemius(medial)	0.456
Plantaris	0.454
Soleus(lateral)	0.306
Soleus(medial)	0.325
Tibialis_Anterior	0.353
Tibialis_Posterior	0.365
Peroneus_Longus	0.399
Peroneus_Brevis	0.227
Peroneus_Tertius	0.166
Ext_Digit_Longus	0.411
Ext_Halluc_Longus	0.288
Flex_Digit_Longus	0.449
Flex_Halluc_Longus	0.353

4.5 Walk trials: comparative

The following graphs compare results from the three walk trials. The data from each walk trial has been normalised using the occurrences of the first toe-off, heel strike and second toe-off events. First toe-off occurs at frame zero, heel strike at frame 31 and second toe-off at frame 80. As swing and stance phases varied slightly in duration between walk trials, normalisation effectively equated the respective time intervals between first toe-off, heel-strike and second toe-off.

Variables which did not require a knowledge of ground reactions forces at the foot, were analysed from the first to last frames from which the three dimensional segment locations could be reproduced from video images. Results from the first ten and last ten frames analysed were eliminated from each trial, due to the requirement of previous data points in smoothing and differentiation procedures to obtain accurate position, velocity and acceleration data. As such, Cardan rotations, centre of mass acceleration, muscle lengths, and muscle velocities were obtained over the entire trial. Variables which required a knowledge of the ground reaction forces were analysed from first toe-off to second toe-off of the walk. As such, resultant joint moments, muscle forces, and contractile element lengths and velocities were analysed within this period. For all results presented, first toe-off is taken as frame zero. The frames over which segment marker were visible for each trial, are presented in Tables 4.5.1, 4.5.3 and 4.5.5, while frames used for kinematic and kinetic analyses for each trial, are presented in Tables 4.5.2, 4.5.4 and 4.5.6.

Comparative results of the relative Cardan rotations between the pelvis, thigh, shank and foot are presented in Figures 4.5.1 - 4.5.9. The three rotations X, Y' and Z" correspond to segment flexion-extension, abduction-adduction and internal-external rotation. Comparative centre of mass acceleration of the pelvis, hip, shank and foot for the three walk trials are presented in Figures 4.5.10 - 4.5.21. Comparative resultant joint moments about the hip, knee and ankle joints of the three walk trials are presented in Figures 4.5.22 - 4.5.30.

Table 4.5.1 First walk trial - frames in which paths were repoduced. Parentheses indicating when path started or ended within the frames that were analysed.

PATH	Frames
Navel	8-**109**
rightASIS	8-158
IlliacCrest	8-158
PostBelt	8-158
Mid-PSIS	8-158
ThighAntSup	8-150
ThighAntMid	8-154
ThighAntInf	8-151
ThighMidSup	8-158
ThighMidInf	8-158
ThighPosSup	8-158
ThighPosInf	8-158
LatKnee	8-158
ShankAntSup	8-158
ShankAntMid	8-158
ShankAntInf	8-158
ShankMidSup	8-158
ShankMidInf	8-158
ShankPosSup	8-158
ShankPosInf	8-158
LatAnkle	8-158
FootDorsal	8-158
MedToe	8-**136**
LatToe	8-158
FootMidLat	8-158
PostCalcan	**22-154**

Table 4.5.2 Event occurrences and frames analysed for first walk trial.

	Subject first visable	Toe Off (on-off)	Heel Strike (off-on)	Toe Off (on-off)	Subject last visable
Frame	8	59-60	89-90	134-135	158
Kinematics	18----------148				
Kinetics	60----------148				

Table 4.5.3 Second walk trial - frames in which paths were reproduced. Parentheses indicating when path started or ended within the frames that were analysed.

PATH	Frames
Navel	16-**137**
rightASIS	16-164
IlliacCrest	16-164
PostBelt	16-164
Mid-PSIS	16-164
ThighAntSup	16-164
ThighAntMid	16-164
ThighAntInf	16-164
ThighMidSup	16-164
ThighMidInf	16-164
ThighPosSup	16-164
ThighPosInf	16-164
LatKnee	16-164
ShankAntSup	16-164
ShankAntMid	16-164
ShankAntInf	16-164
ShankMidSup	16-164
ShankMidInf	16-164
ShankPosSup	17-164
ShankPosInf	16-164
LatAnkle	16-164
FootDorsal	16-164
MedToe	16-164
LatToe	16-164
FootMidLat	16-164
PostCalcan	**31**-163

Table 4.5.4 Event markers and frames analysed for second walk trial.

	Subject first visable	Toe Off (on-off)	Heel Strike (off-on)	Toe Off (on-off)	Subject last visable
Frame	16	77-78	106-107	154-155	164
Kinematics	26----------154				
Kinetics	78----------154				

Table 4.5.5 Third walk trial - frames in which paths were reproduced. Parentheses indicating when path started or ended within the frames that were analysed.

PATH	Frames
Navel	1-**92**
rightASIS	1-152
IlliacCrest	1-152
PostBelt	1-152
Mid-PSIS	**31**-152
ThighAntSup	1-152
ThighAntMid	1-144
ThighAntInf	1-147
ThighMidSup	1-152
ThighMidInf	1-152
ThighPosSup	1-152
ThighPosInf	1-152
LatKnee	1-152
ShankAntSup	1-152
ShankAntMid	1-152
ShankAntInf	1-152
ShankMidSup	1-152
ShankMidInf	1-152
ShankPosSup	7-152
ShankPosInf	1-152
LatAnkle	1-152
FootDorsal	1-**132**
MedToe	1-**50, 79-124**
LatToe	1-152
FootMidLat	1-152
PostCalcan	1-152

Table 4.5.6 Event markers and frames analysed for third walk trial.

	Subject first visable	Toe Off (on-off)	Heel Strike (off-on)	Toe Off (on-off)	Subject last visable
Frame	1	48-49	78-79	128-129	152
Kinematics	11----------142				
Kinetics	49----------142				

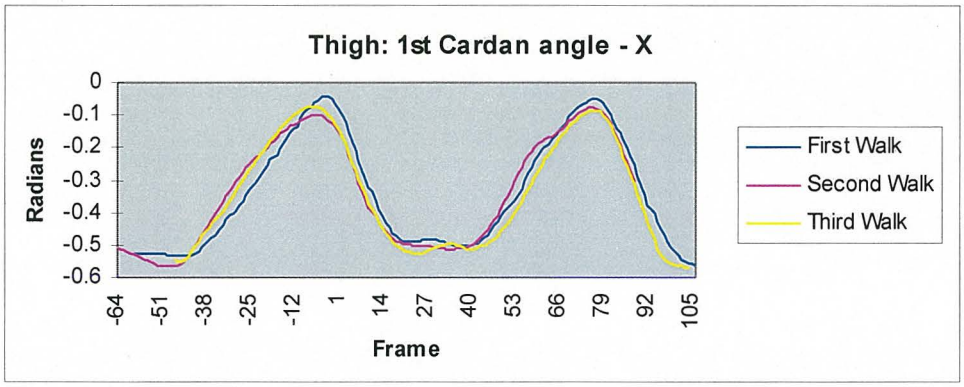

Figure 4.5.1 Walk trials 1st Cardan rotation of the thigh. The rotation corresponding to flexion-extension of the thigh relative to the pelvis.

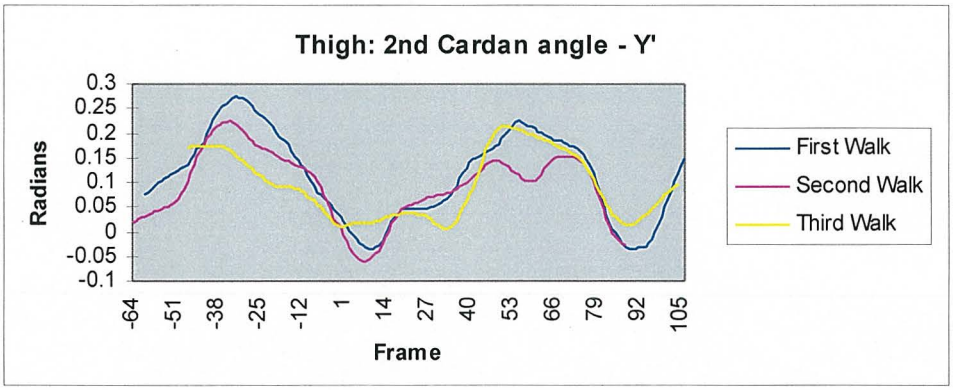

Figure 4.5.2 Walk trials 2nd Cardan rotation of the thigh. The rotation corresponding to adduction-abduction of the thigh relative to the pelvis.

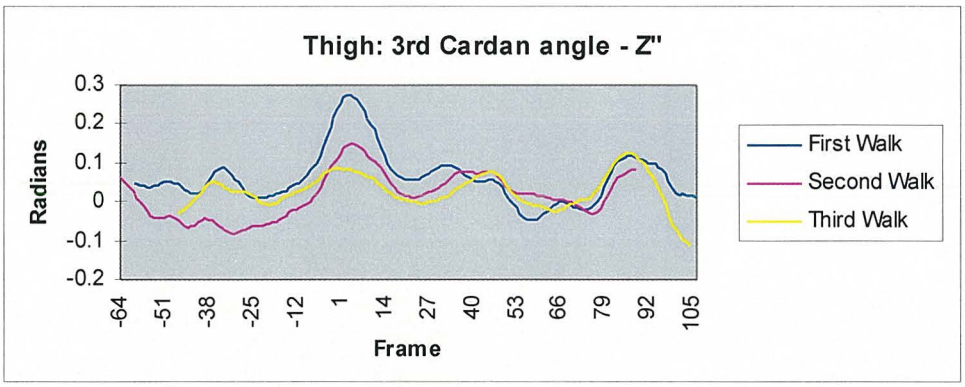

Figure 4.5.3 Walk trials 3rd Cardan rotation of the thigh. Corresponding to internal-external rotation of the thigh relative to the pelvis.

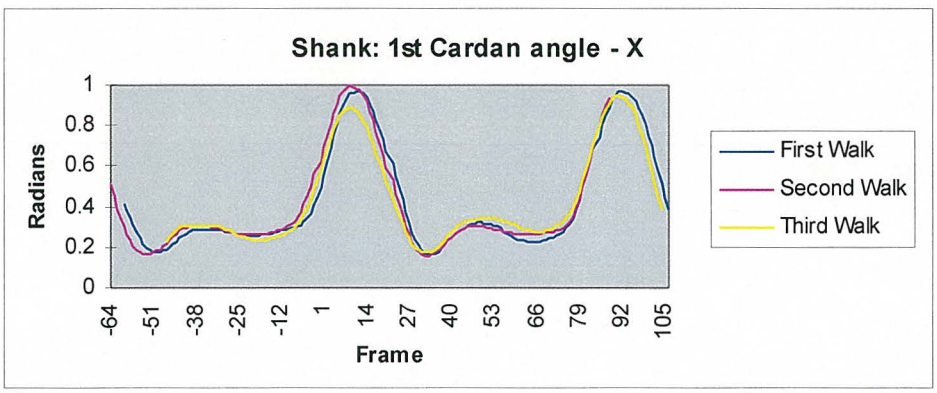

Figure 4.5.4 Walk trials 1st Cardan rotation of the shank. The rotation corresponding to flexion-extension of the shank relative to the thigh.

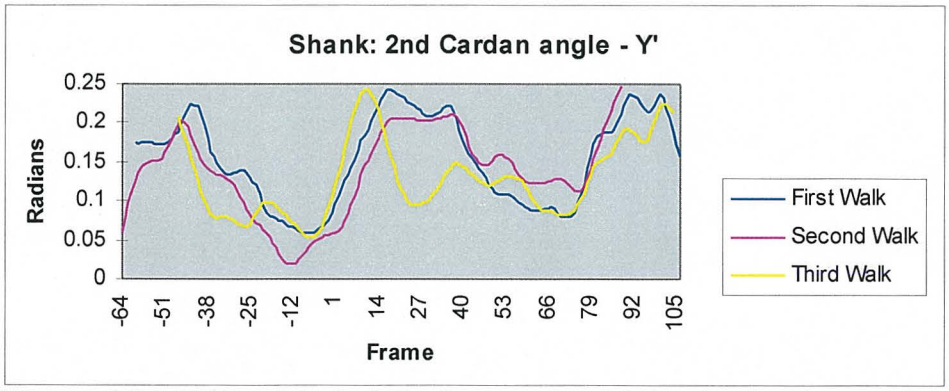

Figure 4.5.5 Walk trials 2nd Cardan rotation of the shank. The rotation corresponding to adduction-abduction of the shank relative to the thigh.

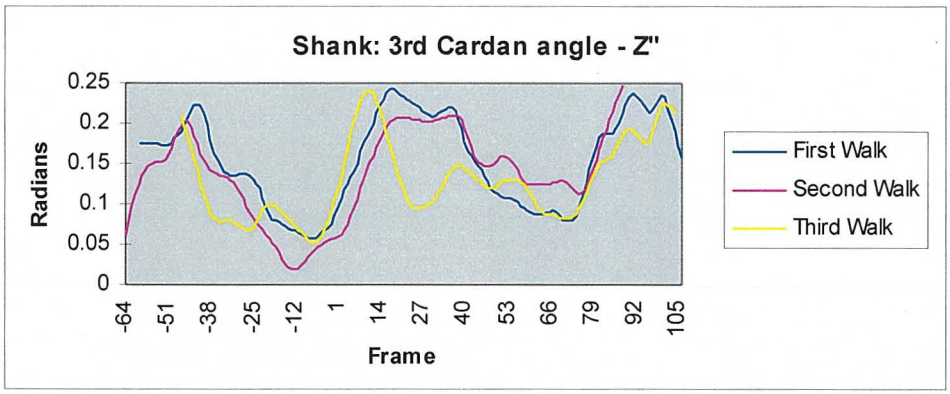

Figure 4.5.6 Walk trials 3rd Cardan rotation of the shank. Corresponding to internal-external rotation of the shank relative to the thigh.

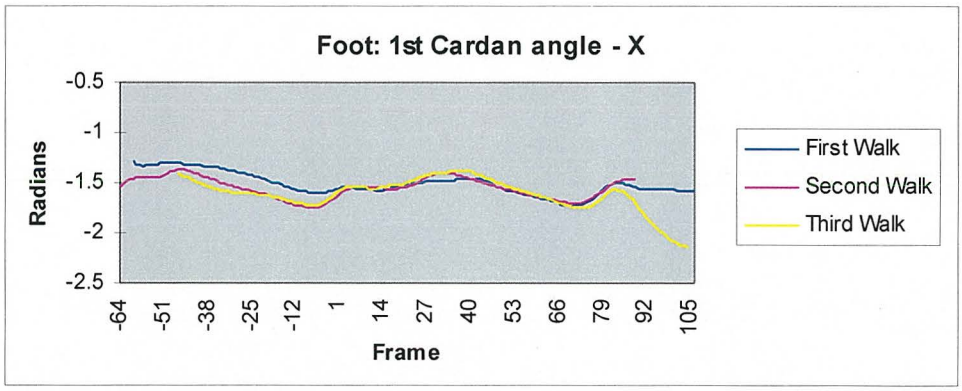

Figure 4.5.7 Walk trials 1st Cardan rotation of the foot. The rotation corresponding to flexion-extension of the foot relative to the shank.

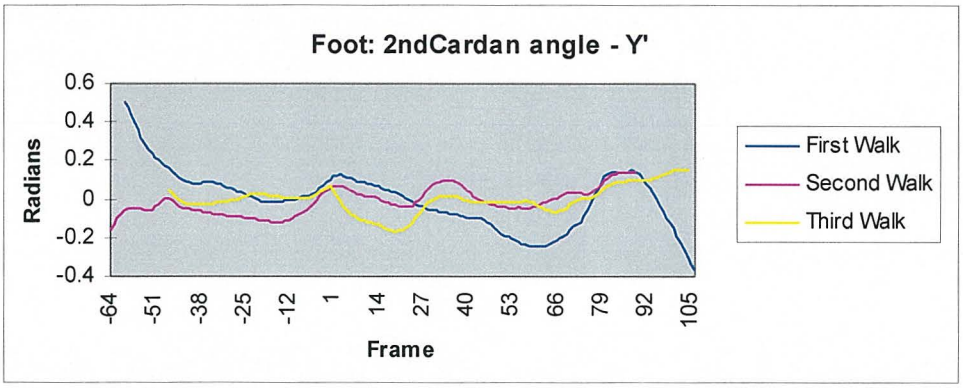

Figure 4.5.8 Walk trials 2nd Cardan rotation of the foot. The rotation corresponding to adduction-abduction of the foot relative to the shank.

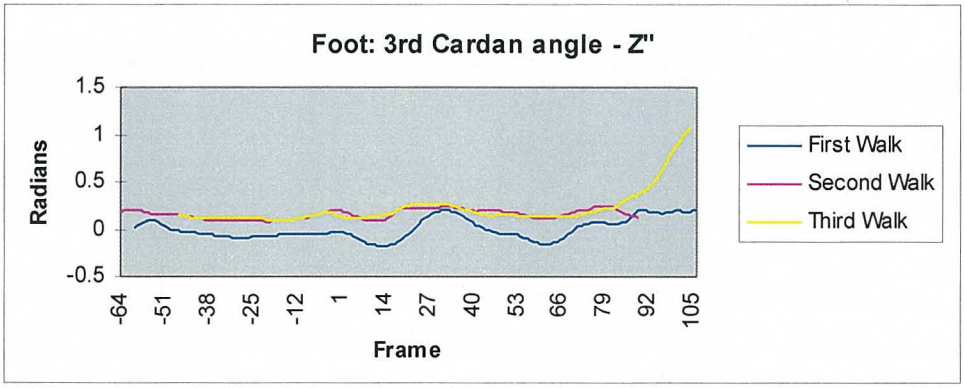

Figure 4.5.9 Walk trials 3rd Cardan rotation of the foot. Corresponding to internal-external rotation of the foot relative to the shank.

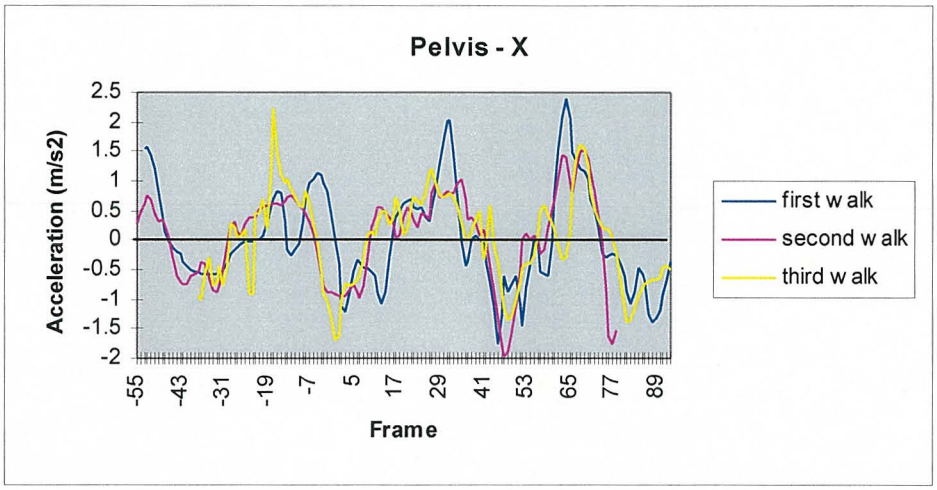

Figure 4.5.10 Walk trials - pelvis centre of mass acceleration in global x axis.

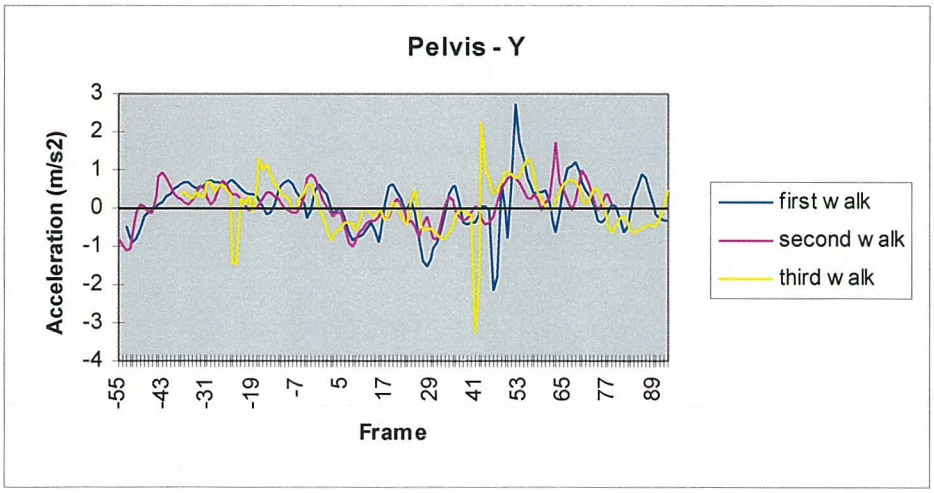

Figure 4.5.11 Walk trials - pelvis centre of mass acceleration in global y axis.

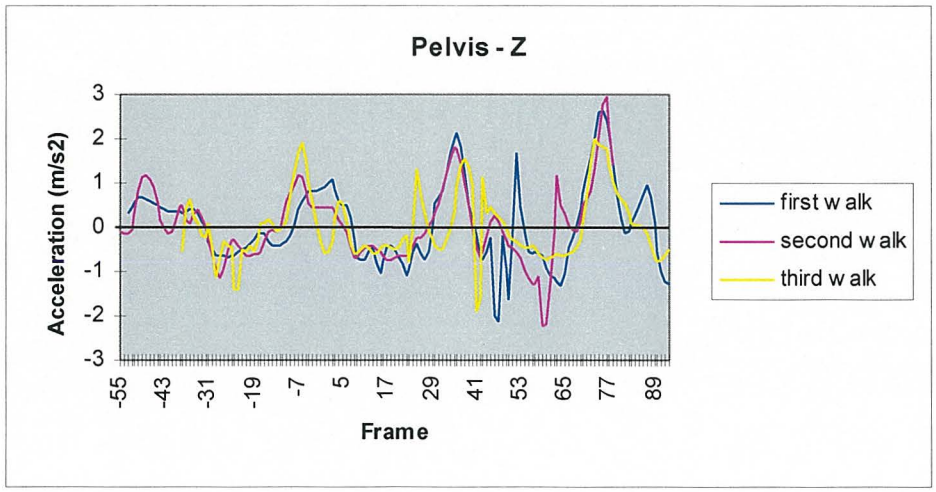

Figure 4.5.12 Walk trials - pelvis centre of mass acceleration in global z axis.

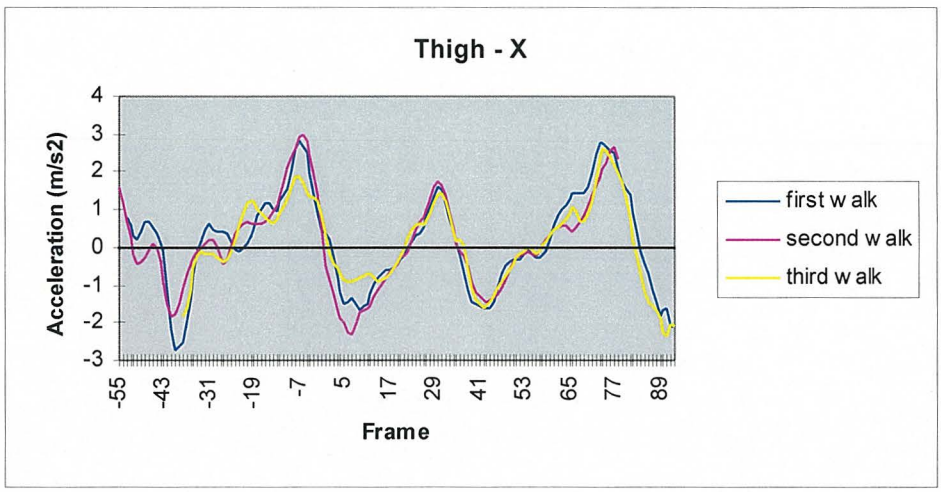

Figure 4.5.13 Walk trials - thigh centre of mass acceleration in global x axis.

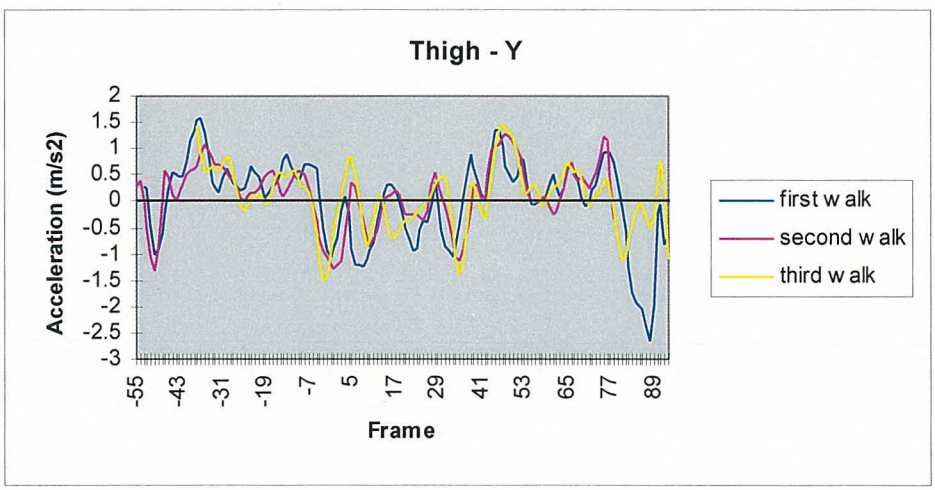

Figure 4.5.14 Walk trials - thigh centre of mass acceleration in global y axis.

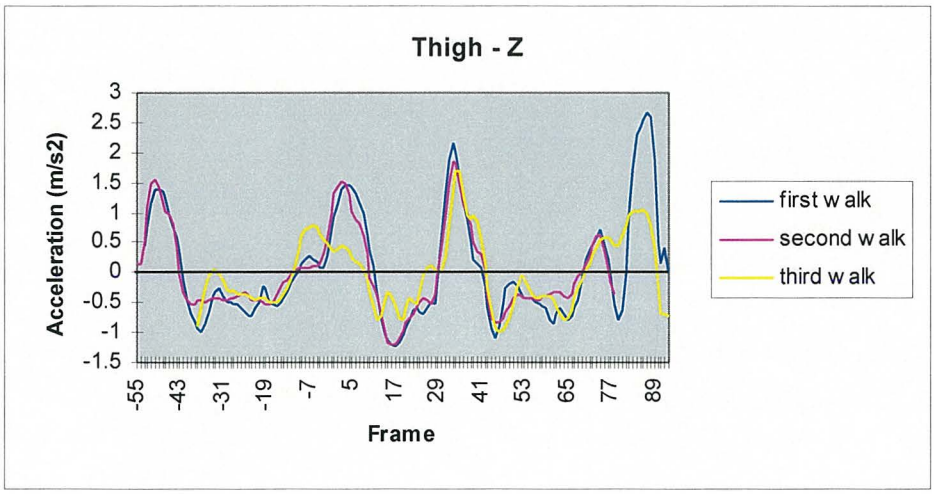

Figure 4.5.15 Walk trials - thigh centre of mass acceleration in global z axis.

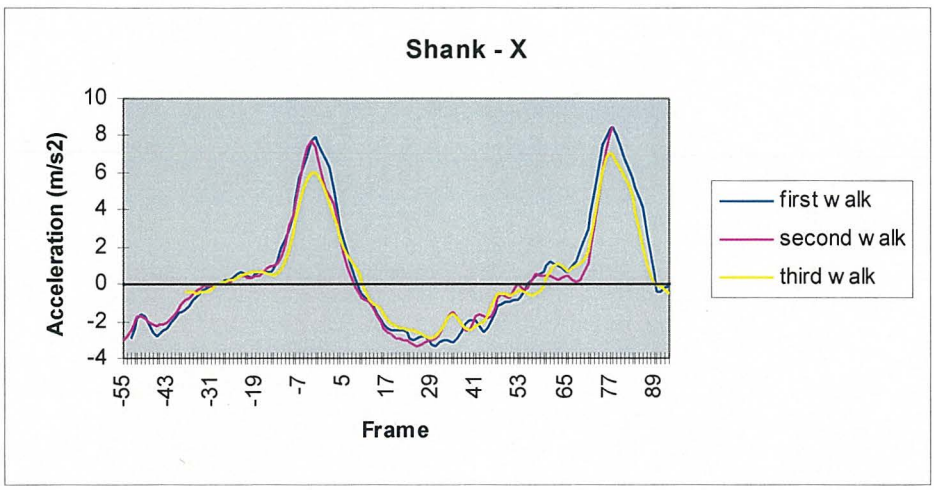

Figure 4.5.16 Walk trials - shank centre of mass acceleration in global x axis.

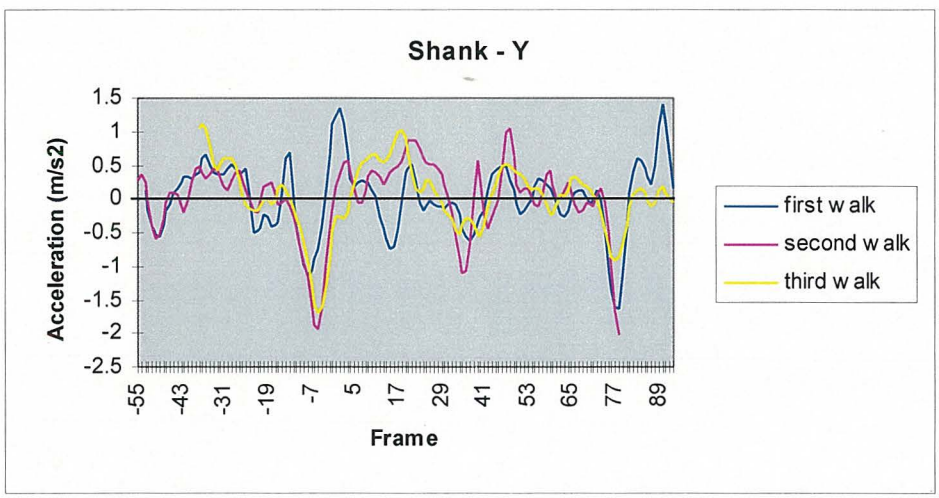

Figure 4.5.17 Walk trials - shank centre of mass acceleration in global y axis.

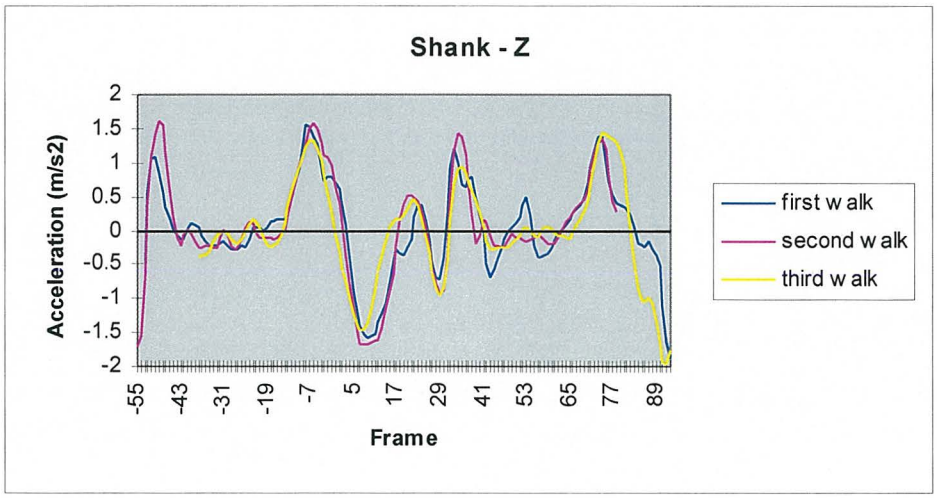

Figure 4.5.18 Walk trials - shank centre of mass acceleration in global z axis.

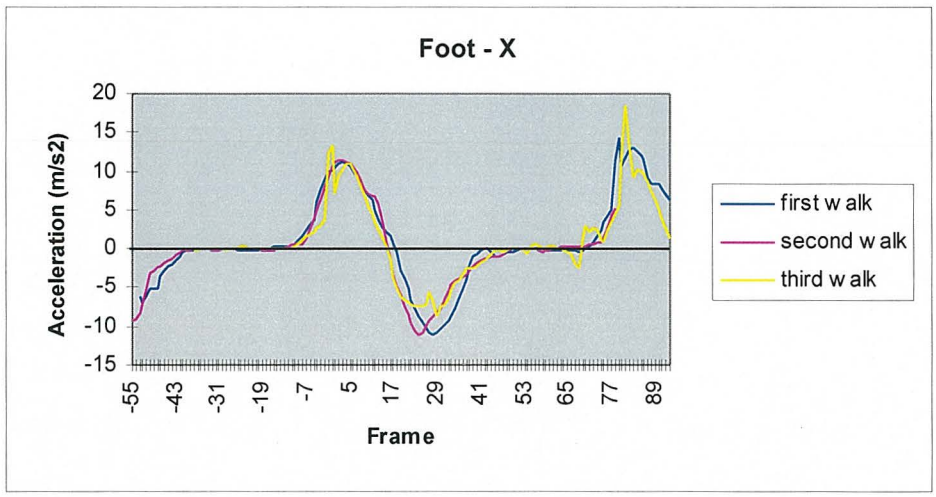

Figure 4.5.19 Walk trials - foot centre of mass acceleration in global x axis.

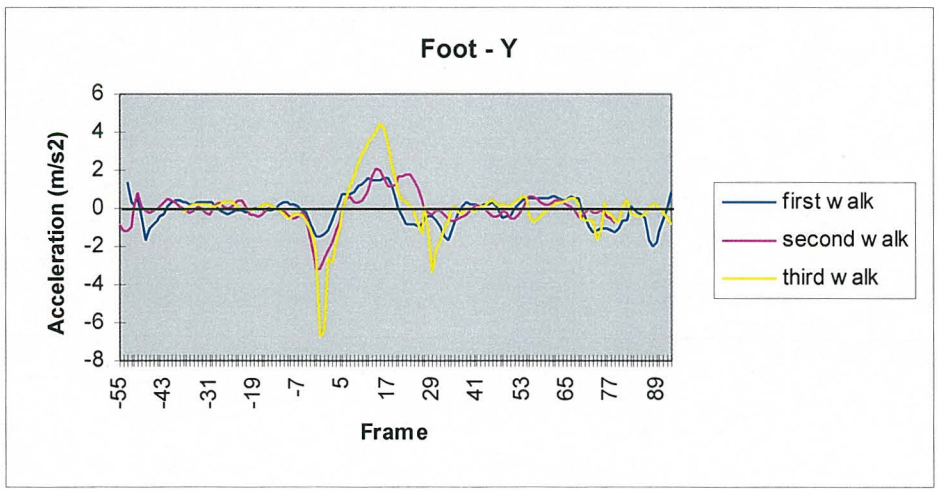

Figure 4.5.20 Walk trials - foot centre of mass acceleration in global y axis.

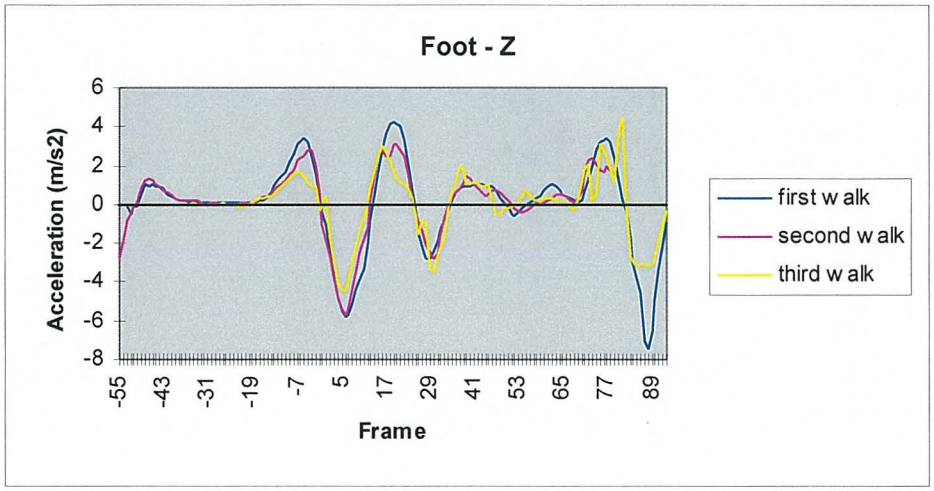

Figure 4.5.21 Walk trials - foot centre of mass acceleration in global z axis.

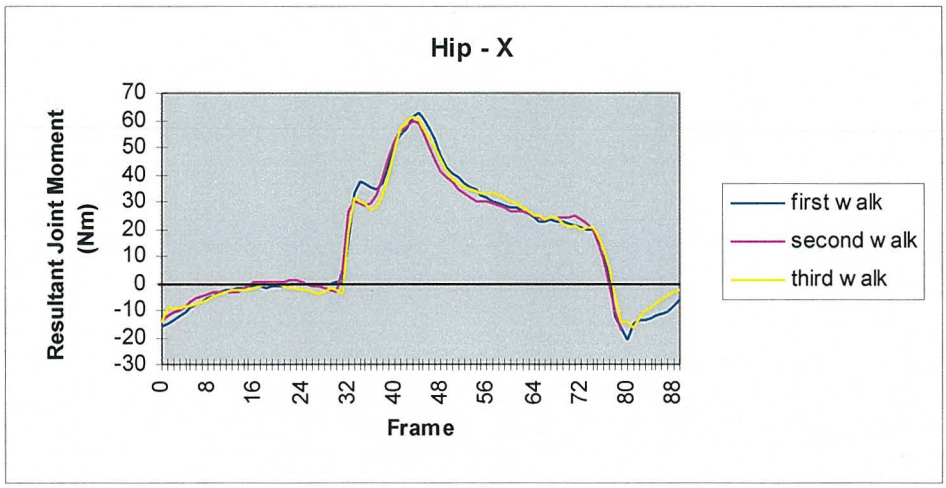

Figure 4.5.22 Walk trials - resultant joint moments about hip x axis.

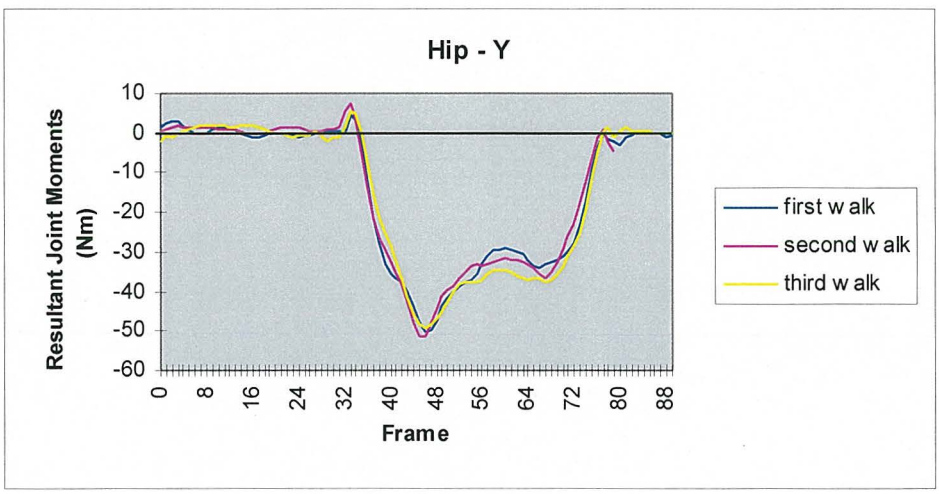

Figure 4.5.23 Walk trials - resultant joint moments about hip y axis.

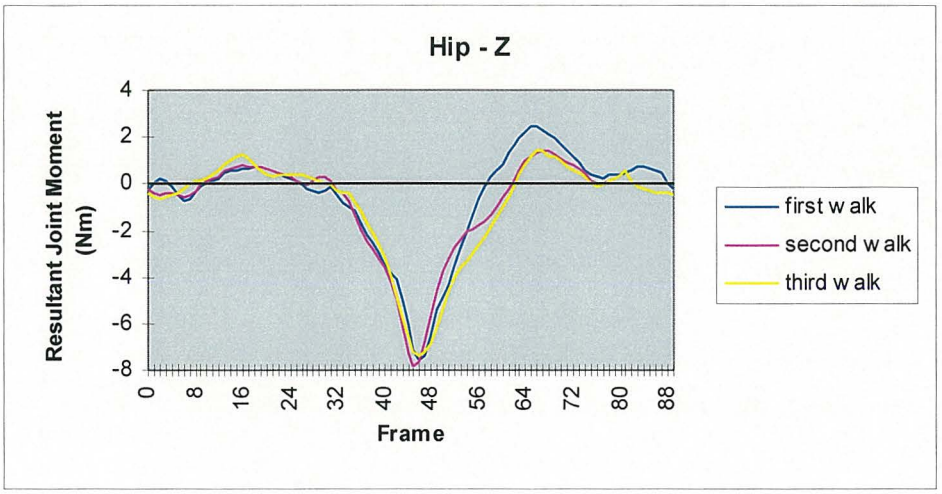

Figure 4.5.24 Walk trials - resultant joint moments about hip z axis.

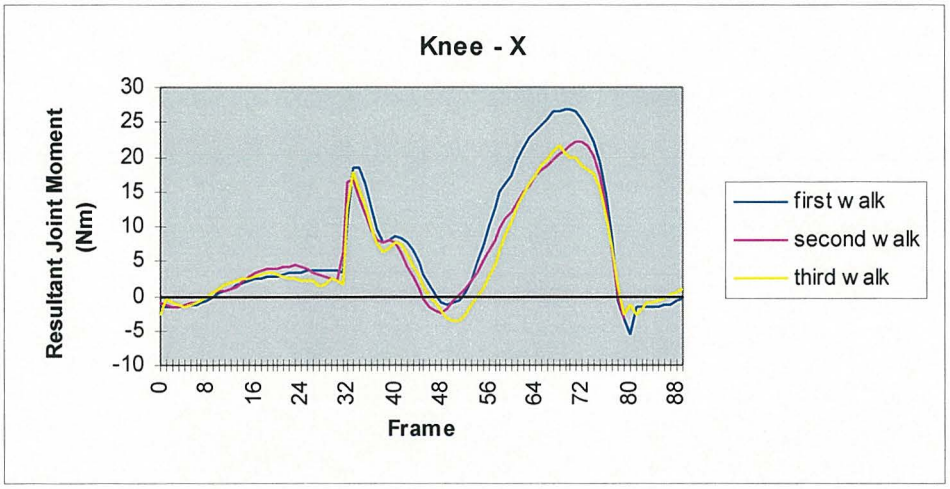

Figure 4.5.25 Walk trials - resultant joint moments about knee x axis.

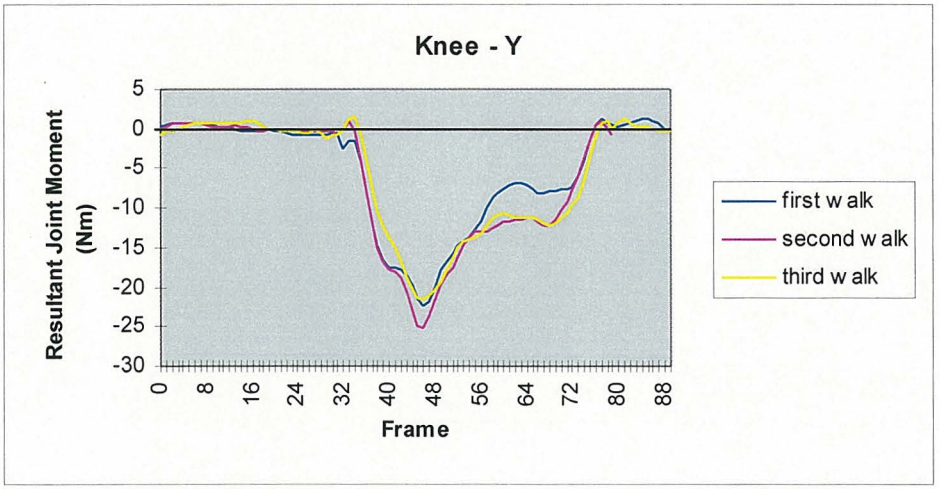

Figure 4.5.26 Walk trials - resultant joint moments about knee y axis.

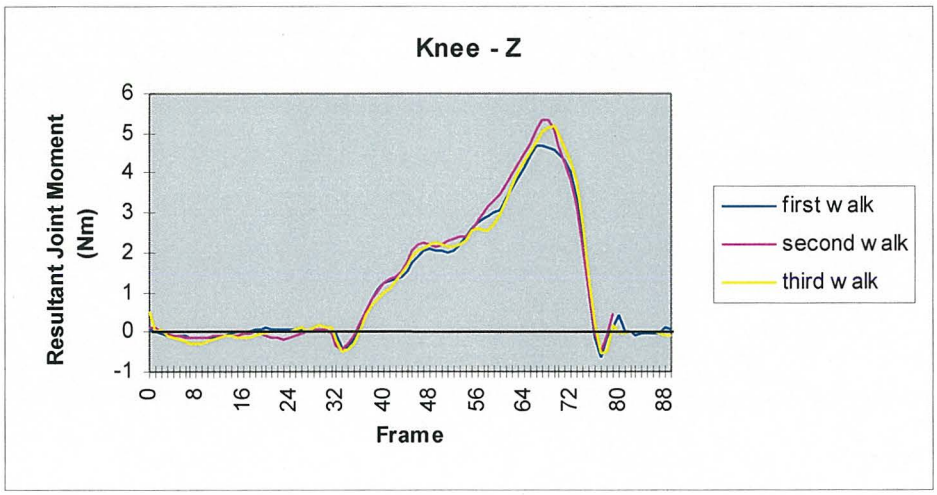

Figure 4.5.27 Walk trials - resultant joint moments about knee z axis.

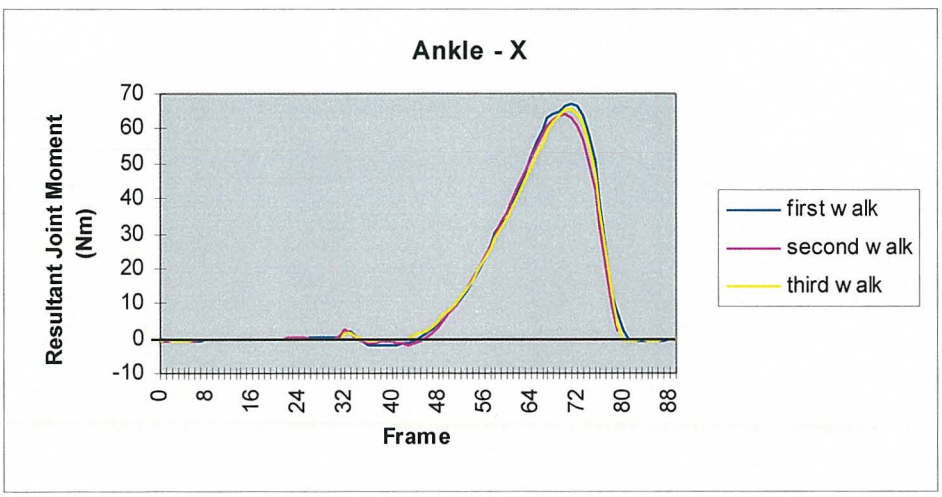

Figure 4.5.28 Walk trials - resultant joint moments about ankle x axis.

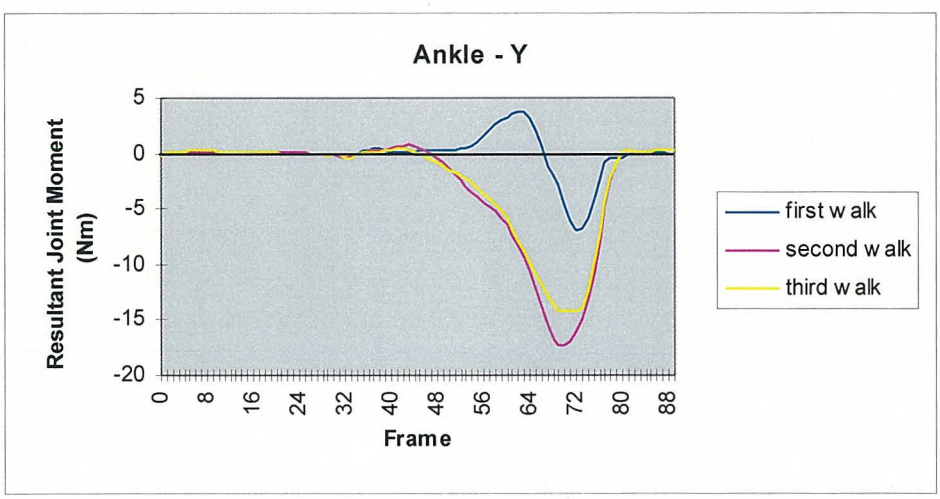

Figure 4.5.29 Walk trials - resultant joint moments about ankle y axis.

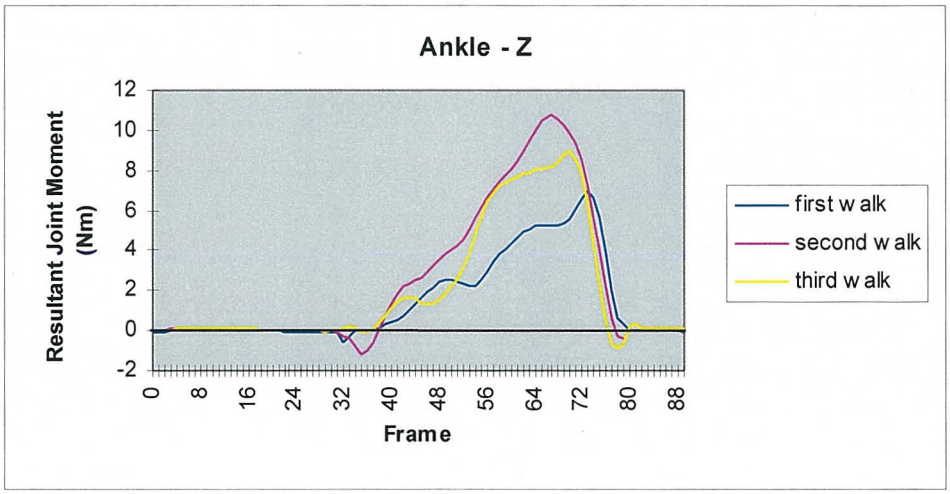

Figure 4.5.30 Walk trials - resultant joint moments about ankle z axis.

Fifteen muscles were chosen to compare predicted muscle forces across the three walking trials as presented in Figures 4.5.31 - 4.5.45. Comparative moment arms for the 48 modelled muscles during the three walk trials are presented from Figure 4.5.46 to 4.5.103.

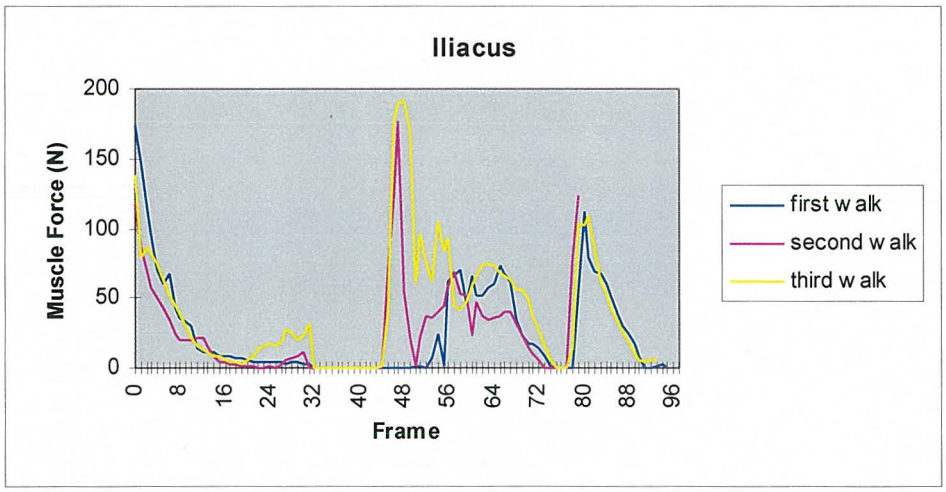

Figure 4.5.31 Walk trials - Iliacus predicted muscle forces.

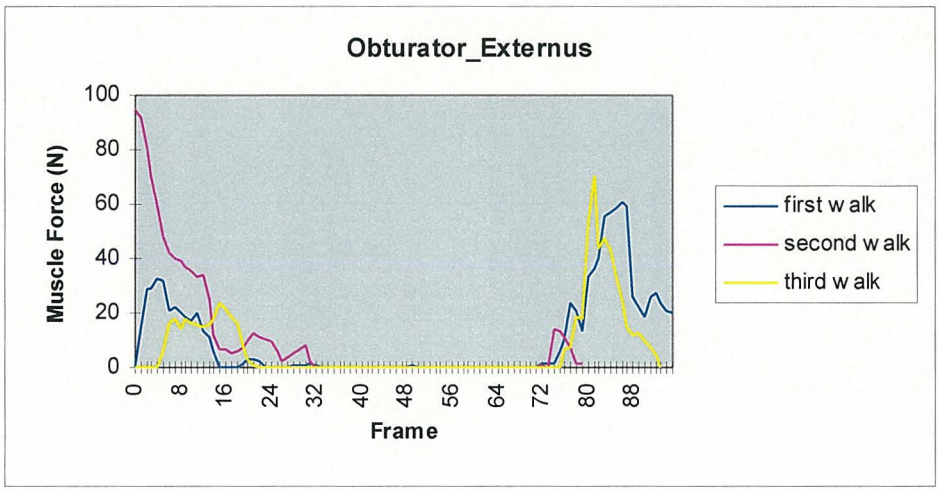

Figure 4.5.32 Walk trials - Obturator Externus predicted muscle forces.

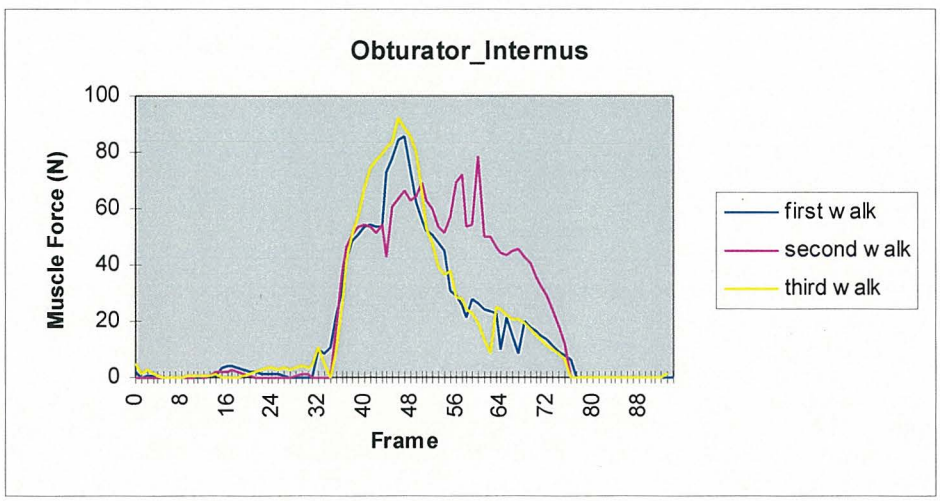

Figure 4.5.33 Walk trials - Obturator Internus predicted muscle forces.

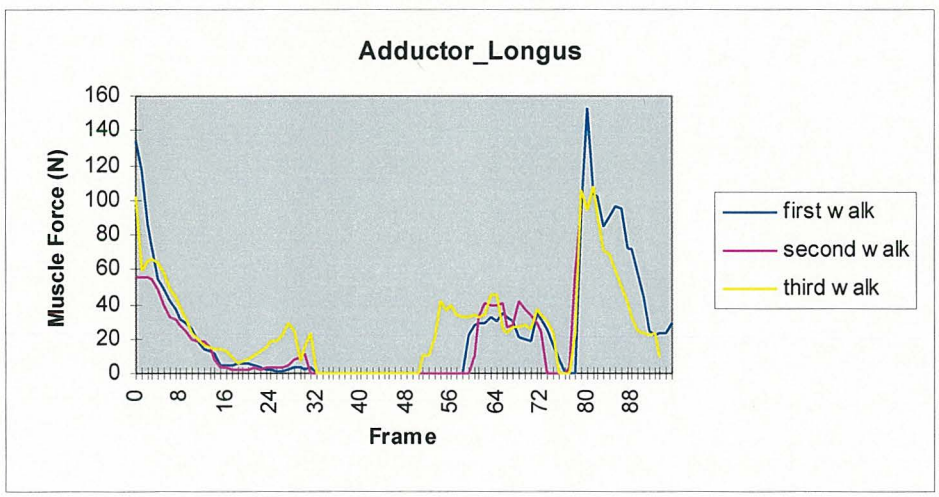

Figure 4.5.34 Walk trials - Adductor Longus predicted muscle forces.

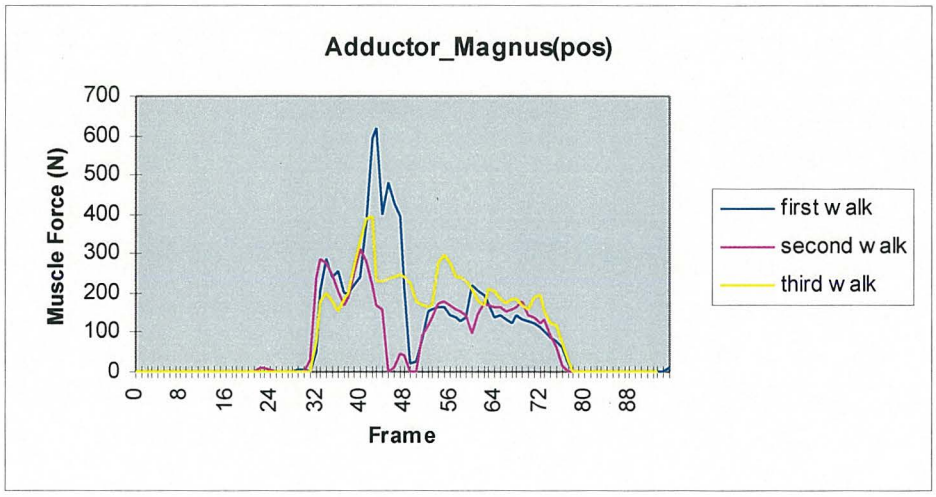

Figure 4.5.35 Walk trials - Adductor Magnus(pos) predicted muscle forces.

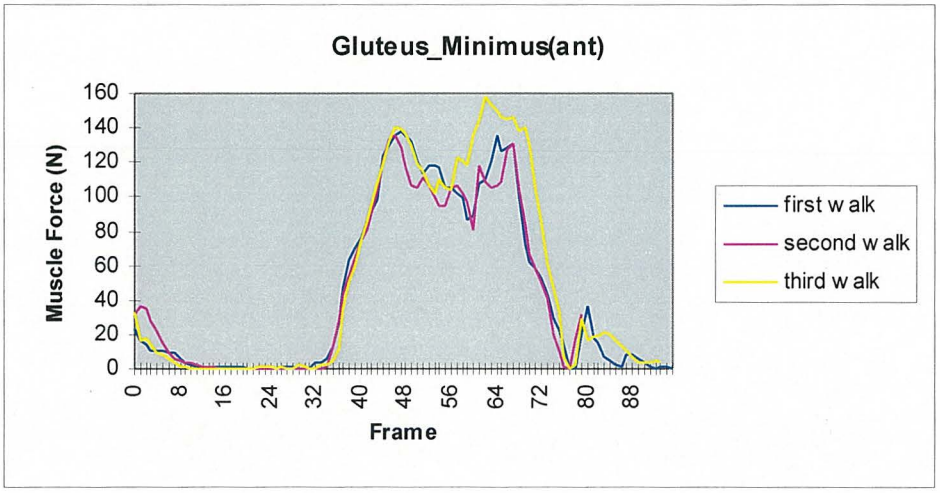

Figure 4.5.36 Walk trials - Gluteus Minimus(ant) predicted muscle forces.

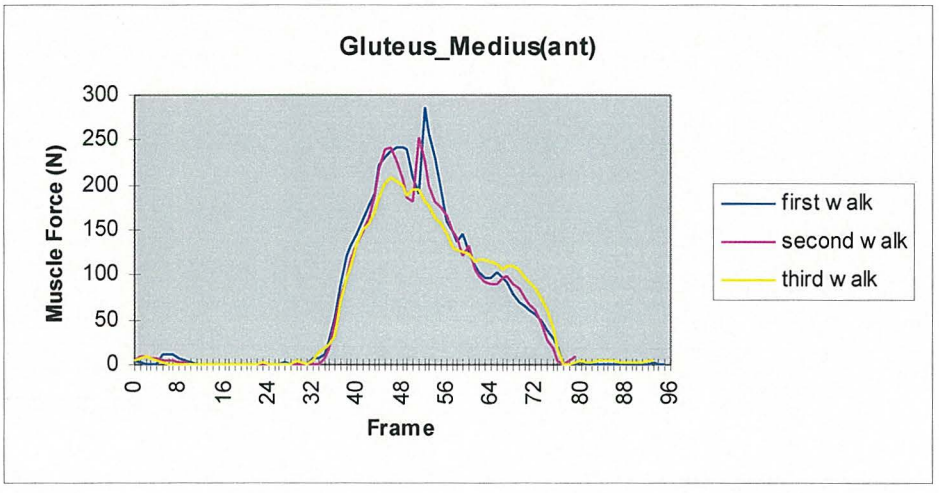

Figure 4.5.37 Walk trials - Gluteus Medius(ant) predicted muscle forces.

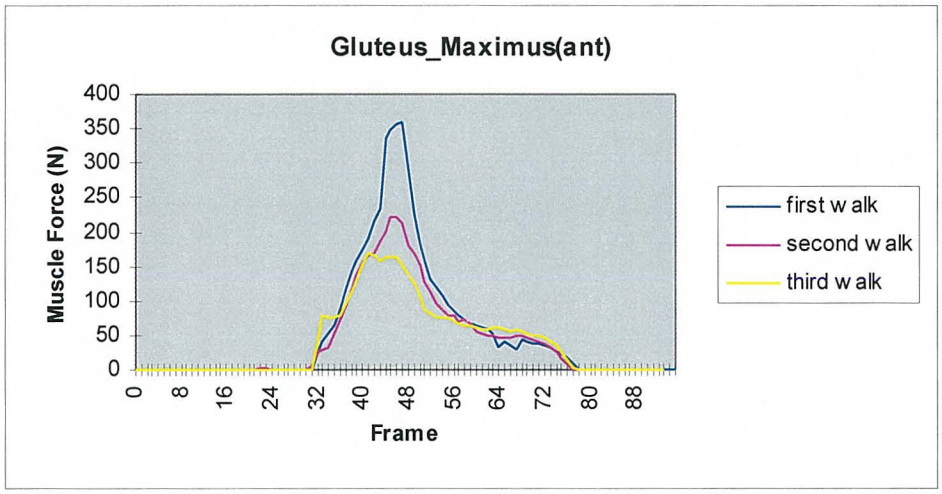

Figure 4.5.38 Walk trials - Gluteus Maximus(ant) predicted muscle forces.

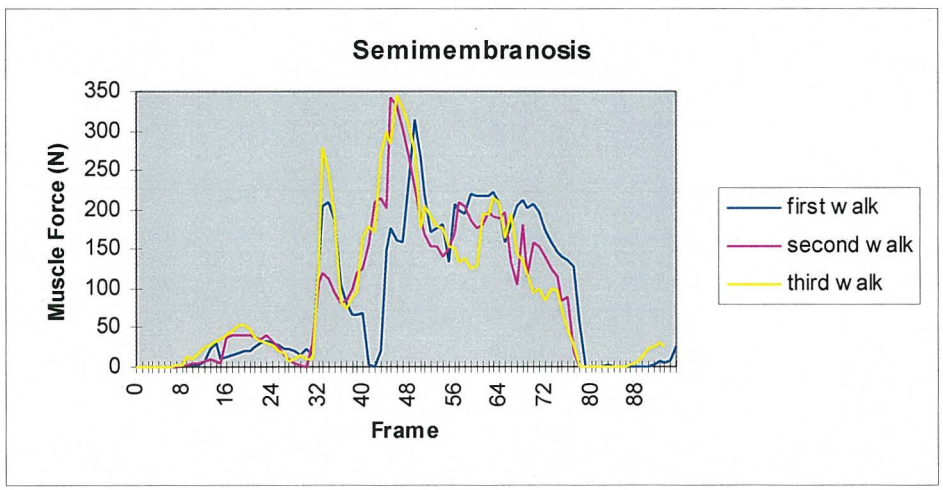

Figure 4.8.39 Walk trials - Semimembranosis predicted muscle forces.

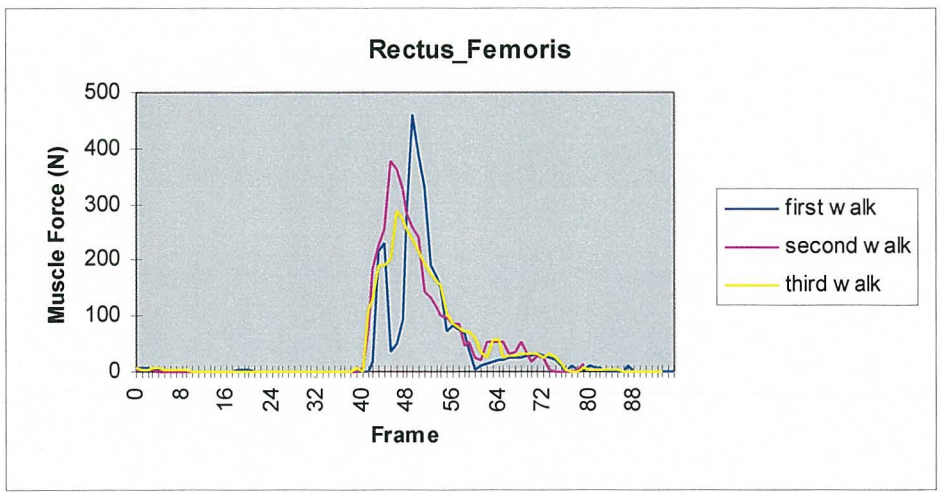

Figure 4.8.40 Walk trials - Rectus Femoris predicted muscle forces.

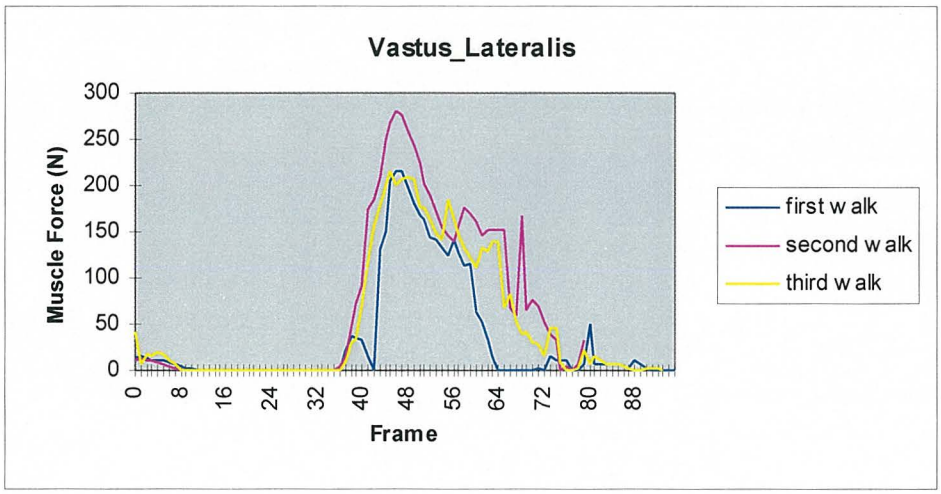

Figure 4.5.41 Walk trials - Vastus Lateralis predicted muscle forces.

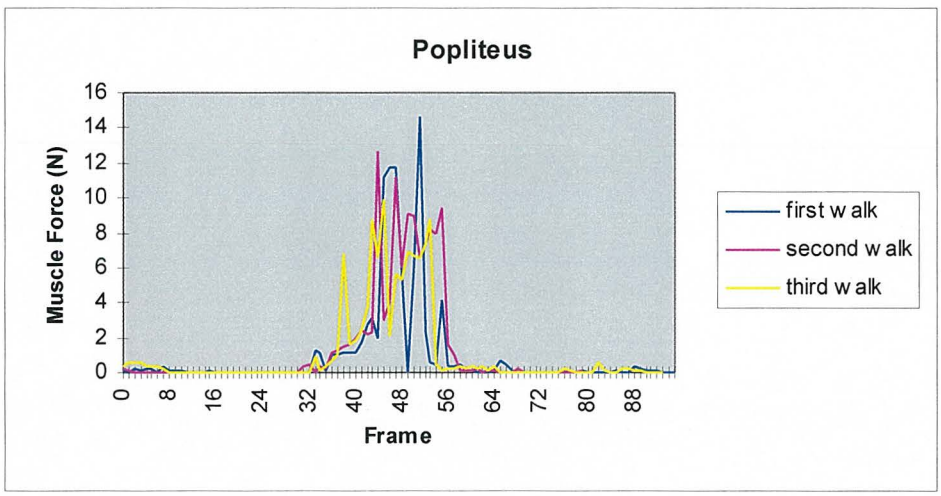

Figure 4.5.42 Walk trials - Popliteus predicted muscle forces.

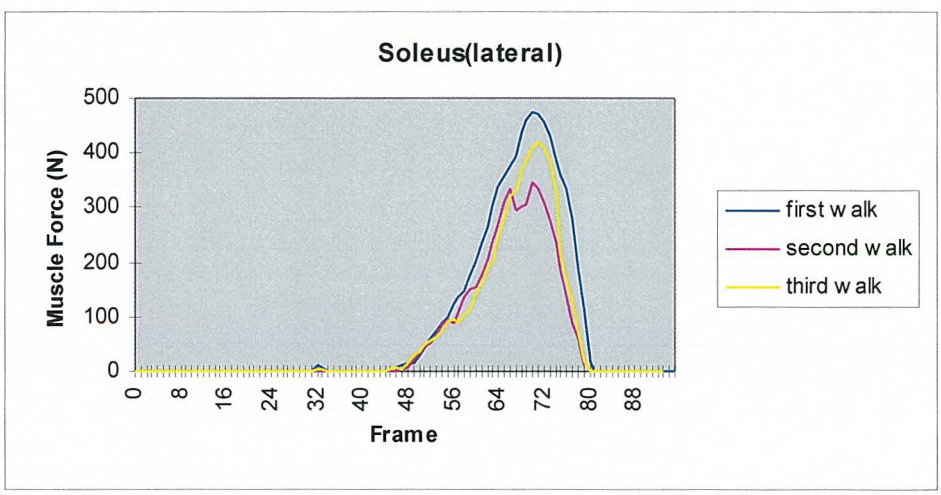

Figure 4.5.43 Walk trials - Soleus(lateral) predicted muscle forces.

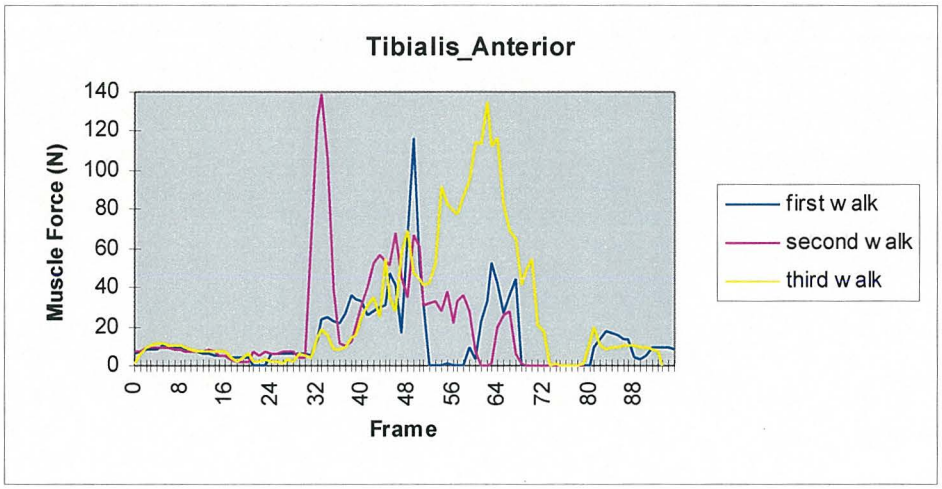

Figure 4.5.44 Walk trials - Tibialis Anterior predicted muscle forces.

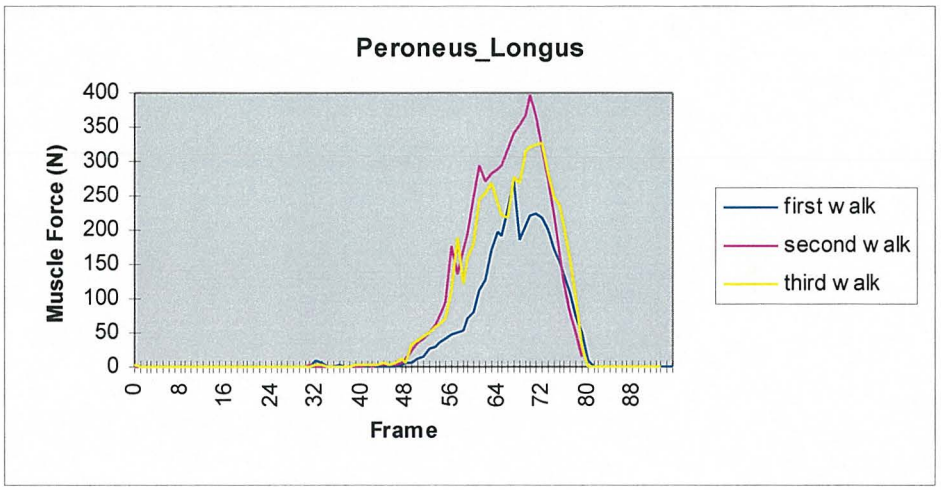

Figure 4.5.45 Walk trials - Peroneus Longus predicted muscle forces.

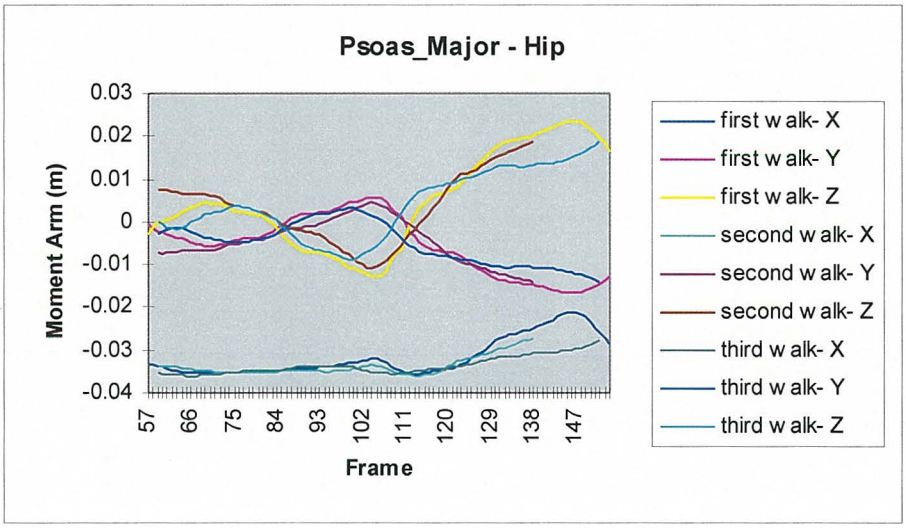

Figure 4.5.46 Walk trials - Psoas major, hip moment arms.

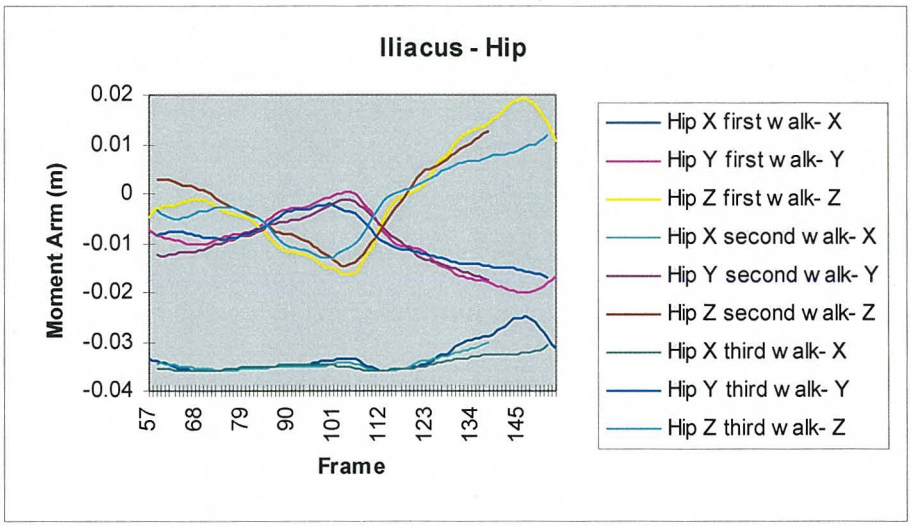

Figure 4.5.47 Walk trials - Iliacus, hip moment arms.

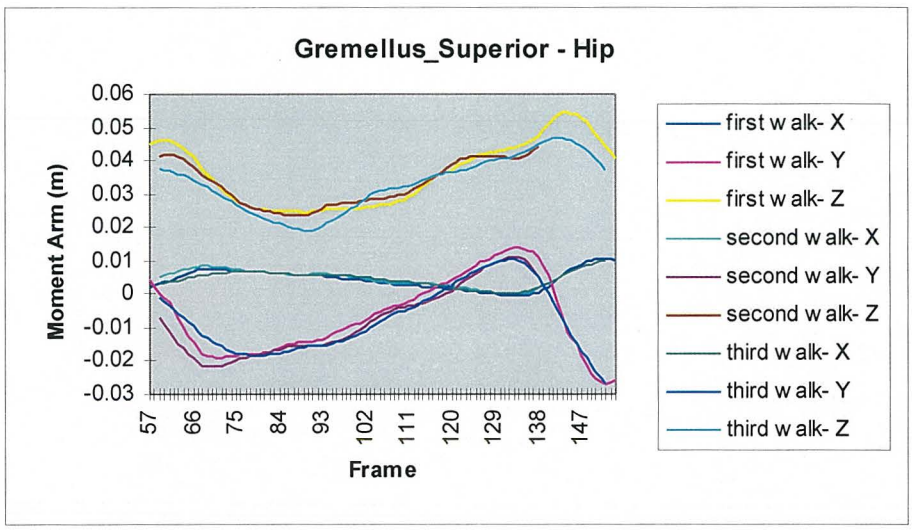

Figure 4.5.48 Walk trials - Gremellus Superior, hip moment arms.

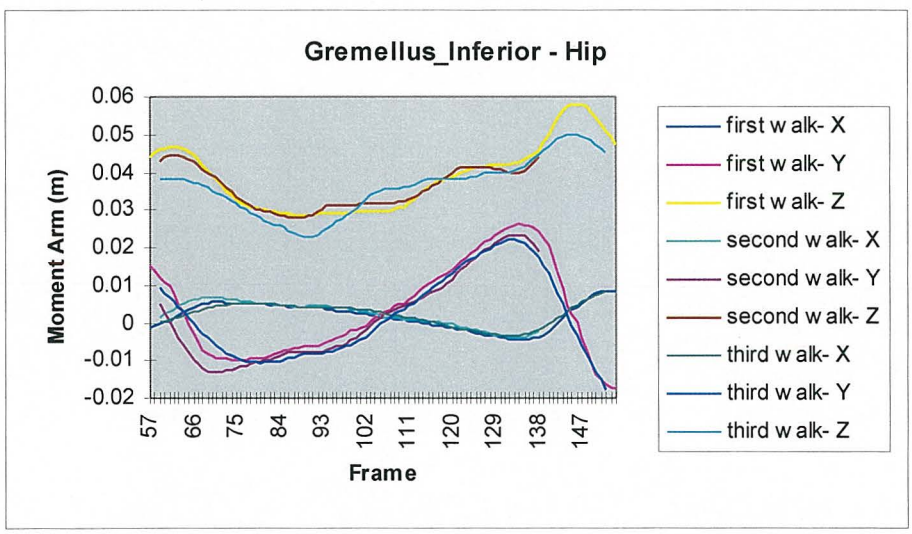

Figure 4.5.49 Walk trials - Gremellus Inferior,hip moment arms.

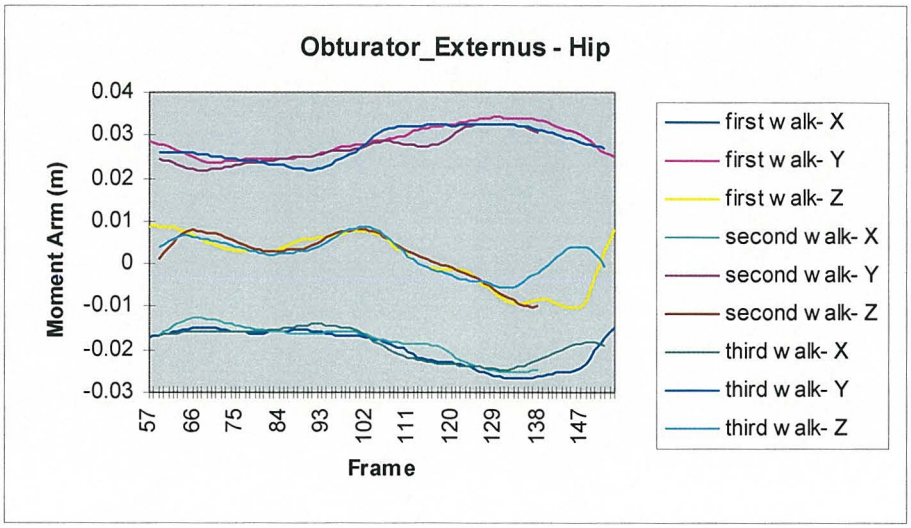

Figure 4.5.50 Walk trials - Obturator Externus,hip moment arms.

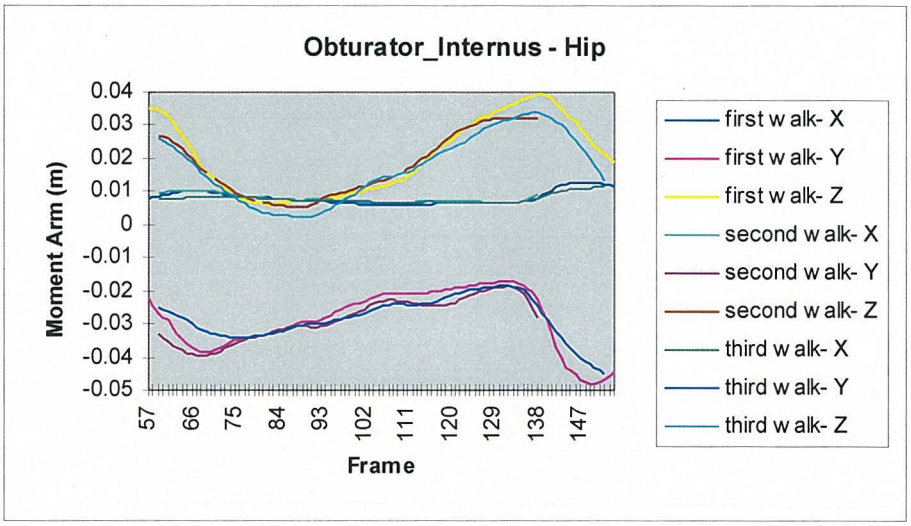

Figure 4.5.51 Walk trials - Obturator Internus, hip moment arms.

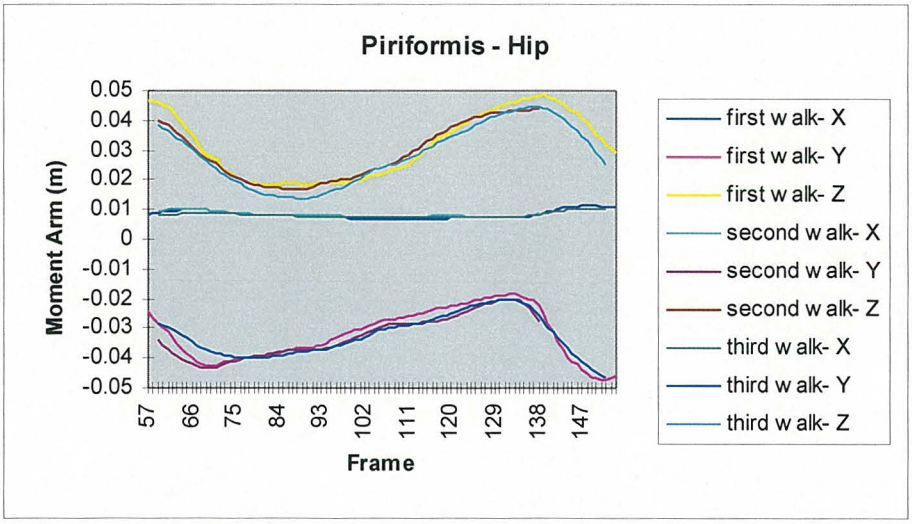

Figure 4.5.52 Walk trials - Piriformis, hip moment arms.

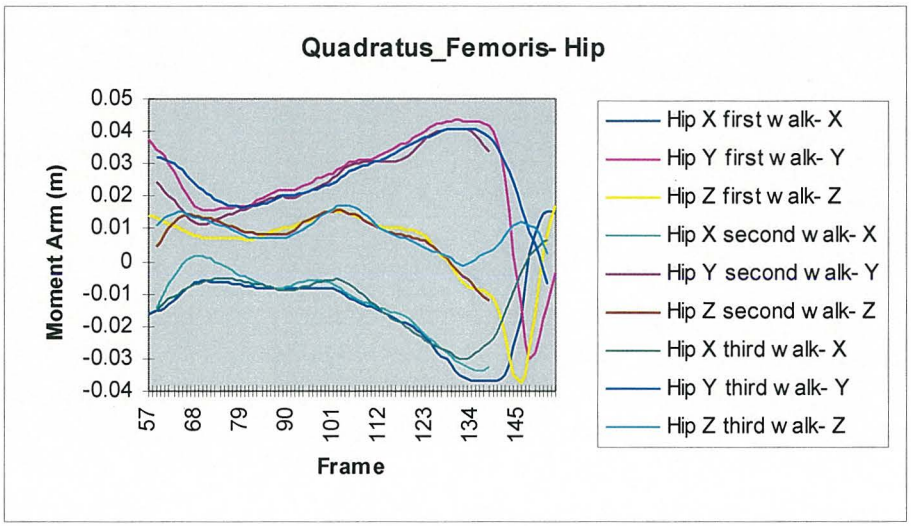

Figure 4.5.53 Walk trials - Quadratus Femoris, hip moment arms.

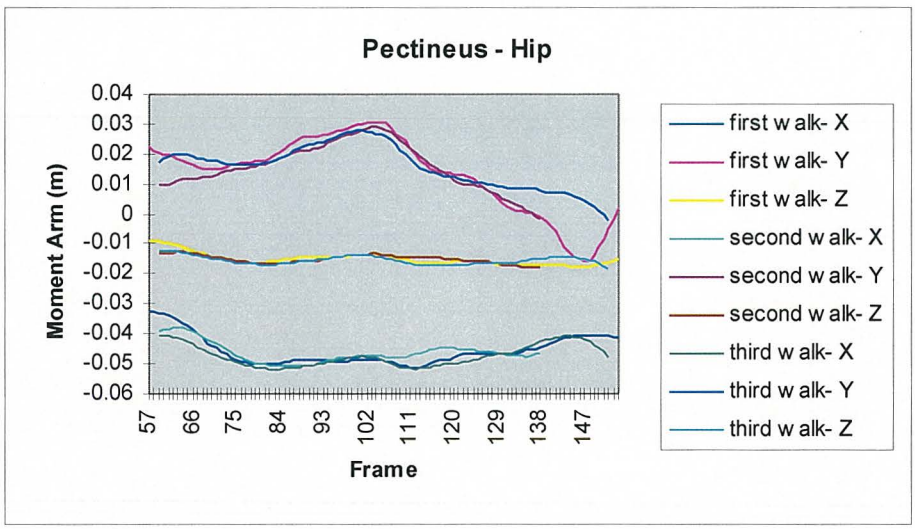

Figure 4.5.54 Walk trials - Pectineus, hip moment arms.

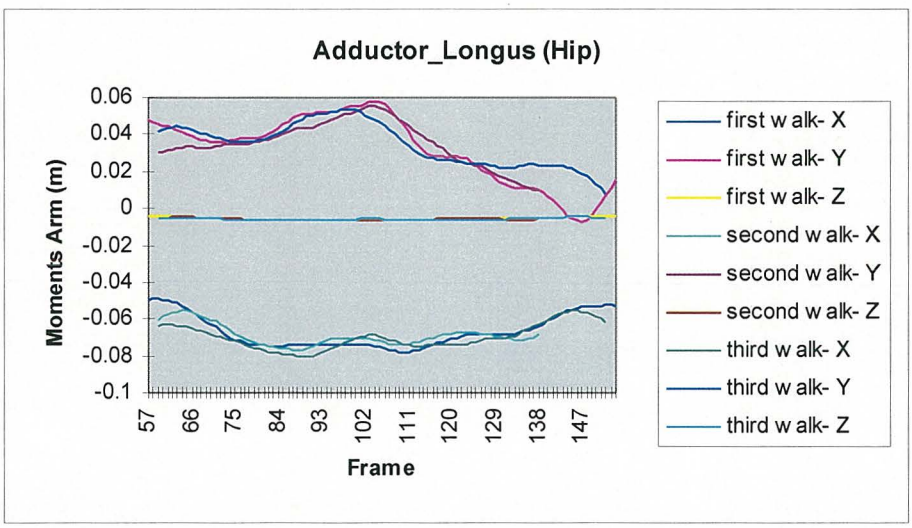

Figure 4.5.55 Walk trials - Adductor Longus, hip moment arms.

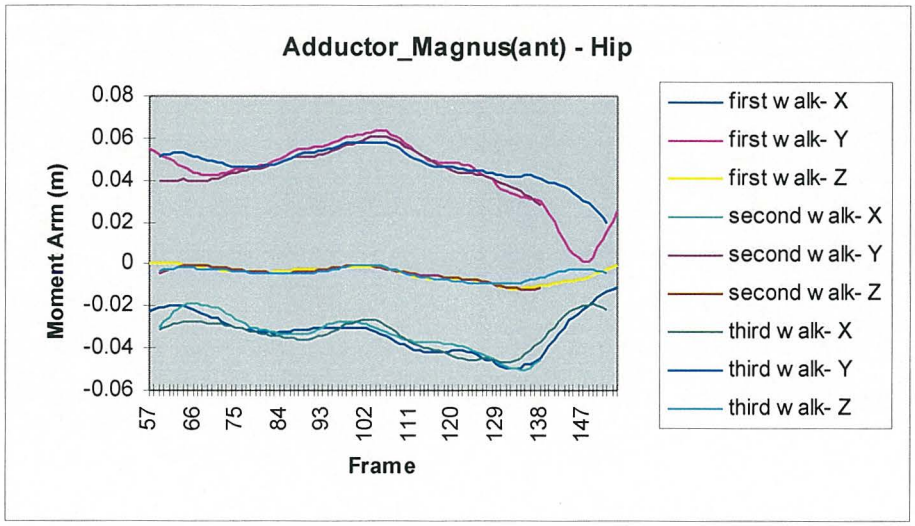

Figure 4.5.56 Walk trials - Adductor Magnus(ant), hip moment arms.

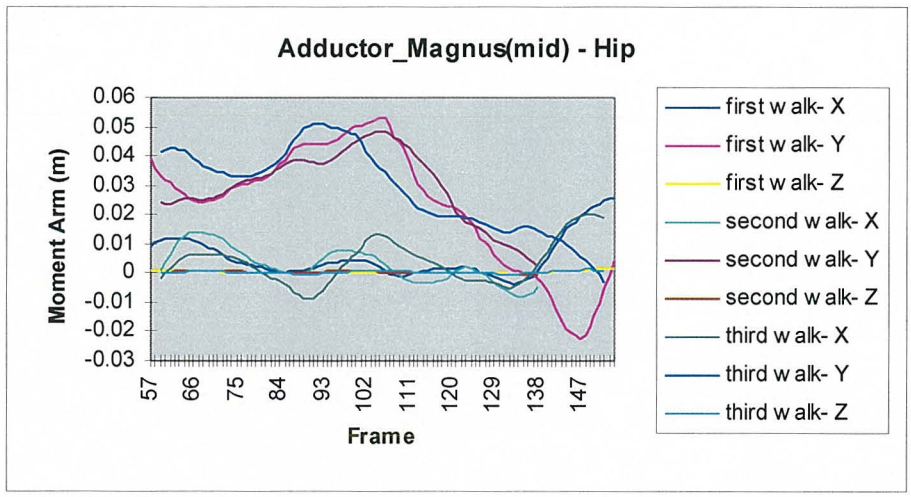

Figure 4.5.57 Walk trials - Adductor Magnus(mid), hip moment arms.

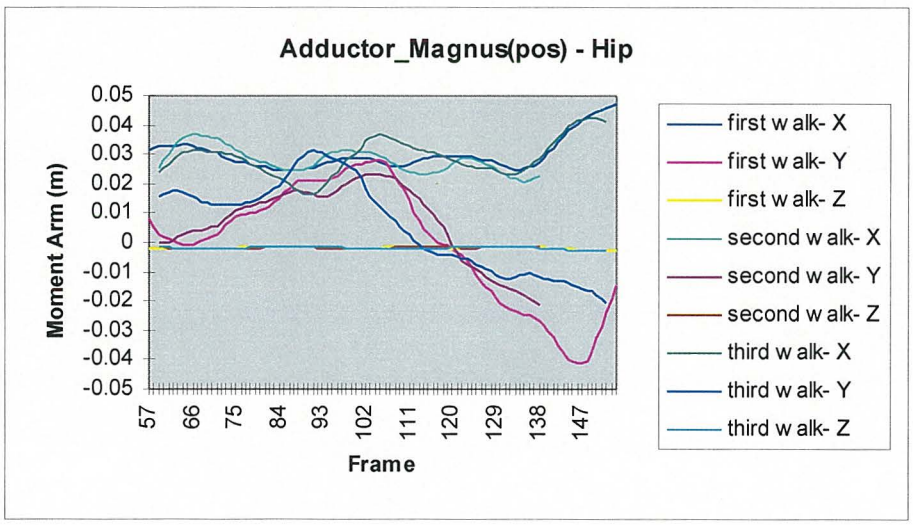

Figure 4.5.58 Walk trials - Adductor Magnus(pos), hip moment arms.

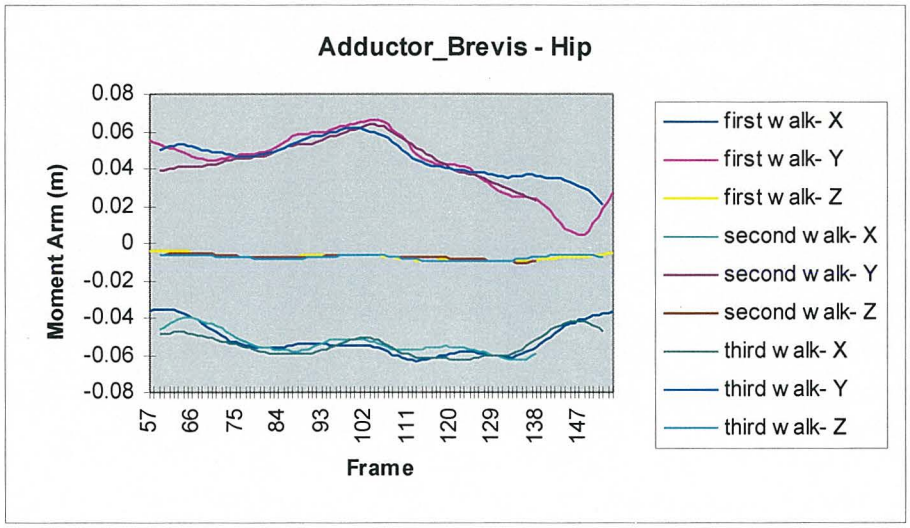

Figure 4.5.59 Walk trials - Adductor Brevis, hip moment arms.

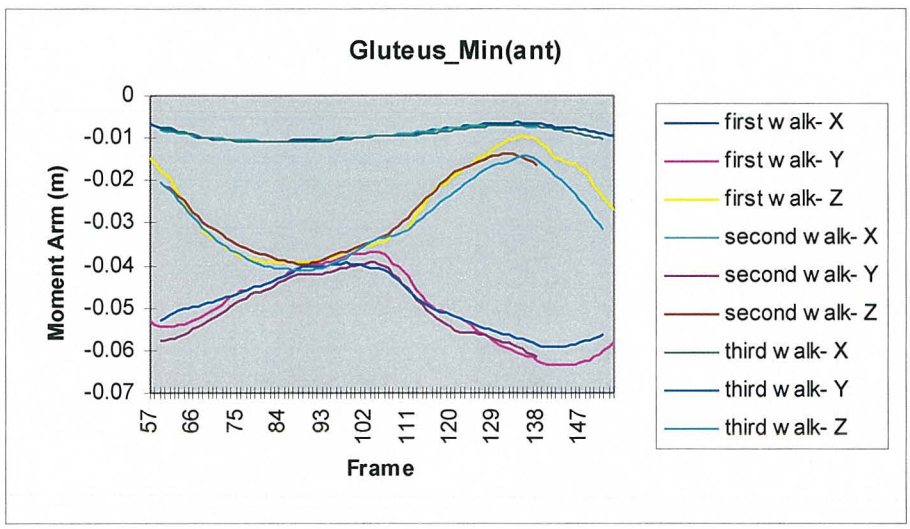

Figure 4.5.60 Walk trials - Gluteus Minimus(ant), hip moment arms.

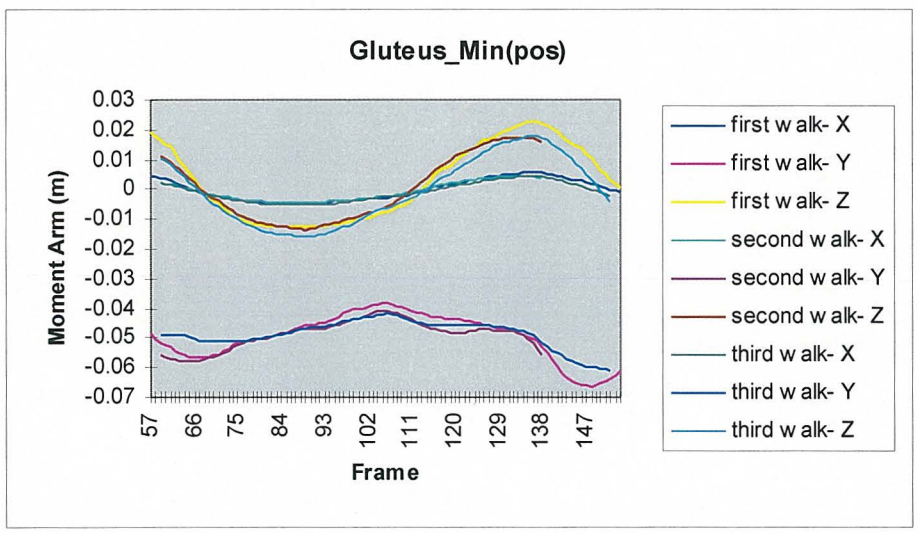

Figure 4.5.61 Walk trials - Gluteus Minimus(post), hip moment arms.

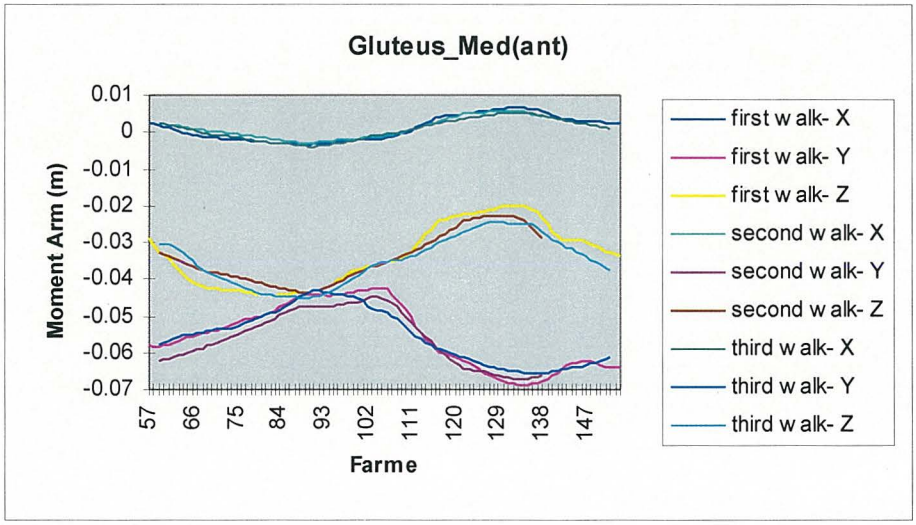

Figure 4.5.62 Walk trials - Gluteus Medius(ant) hip moment arms.

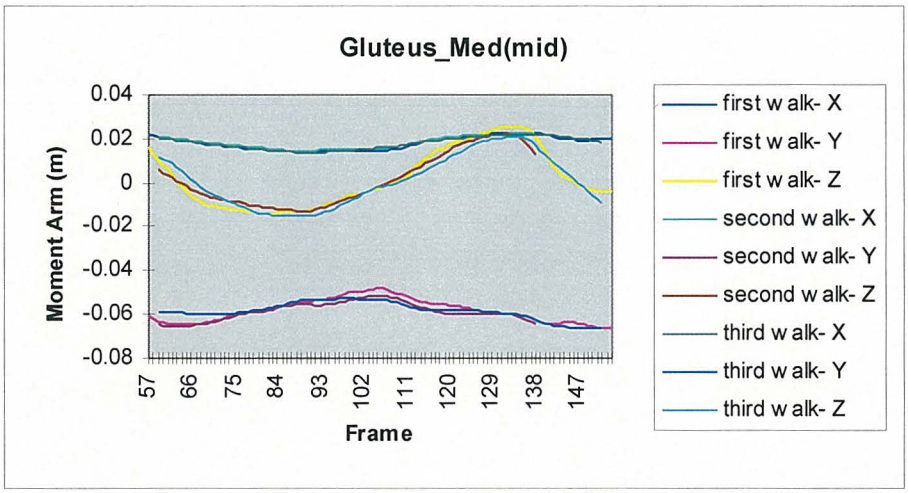

Figure 4.5.63 Walk trials - Gluteus Medius(mid) hip moment arms.

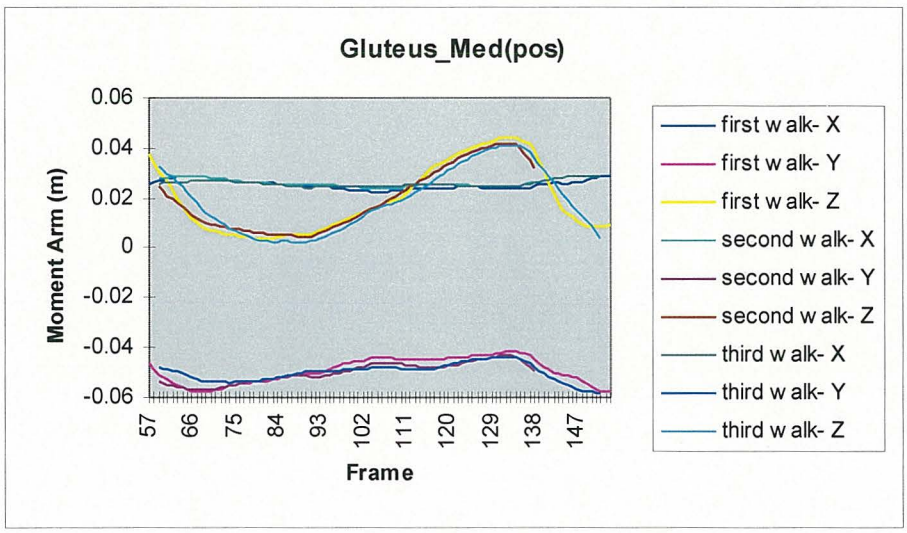

Figure 4.5.64 Walk trials - Gluteus Medius(post), hip moment arms.

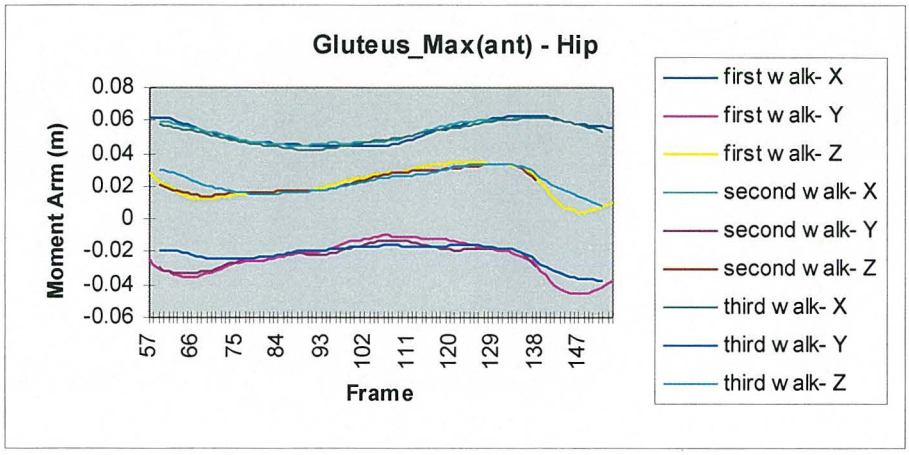

Figure 4.5.65 Walk trials - Gluteus Maximus(ant), hip moment arms.

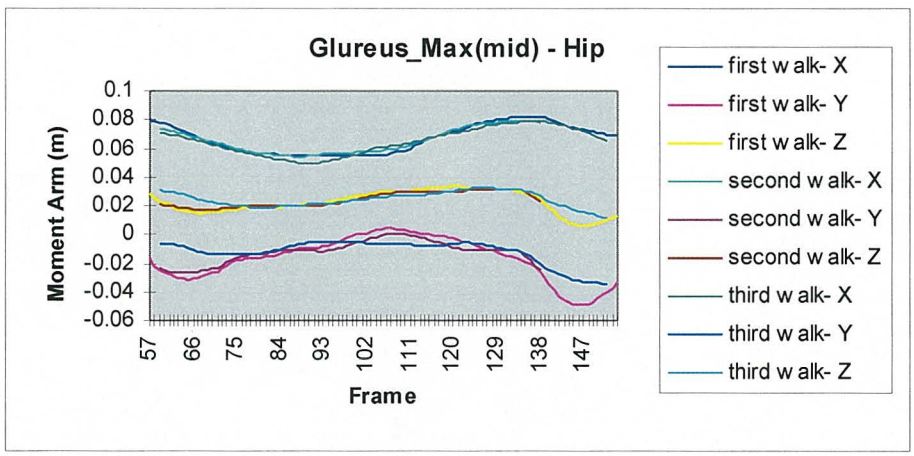

Figure 4.5.66 Walk trials - Gluteus Maximus(mid), hip moment arms.

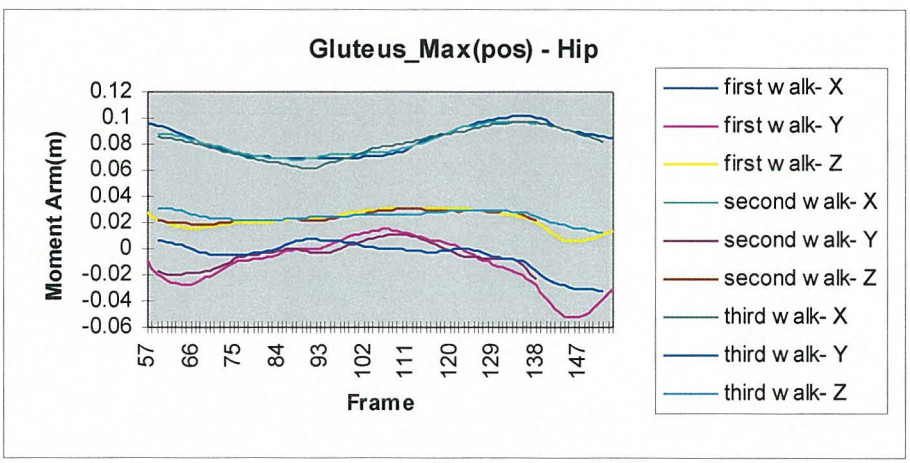

Figure 4.5.67 Walk trials - Gluteus Maximus(post), hip moment arms.

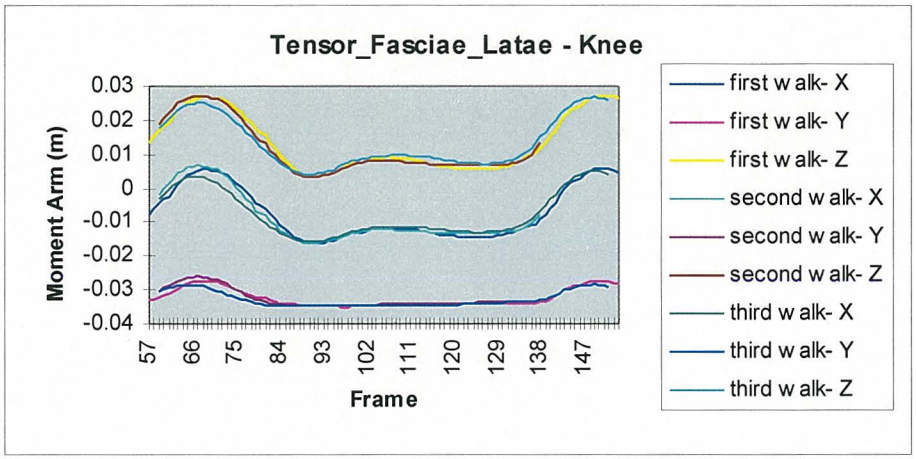

Figure 4.5.68 Walk trials - Tensor Fasciae Latae, knee moment arms.

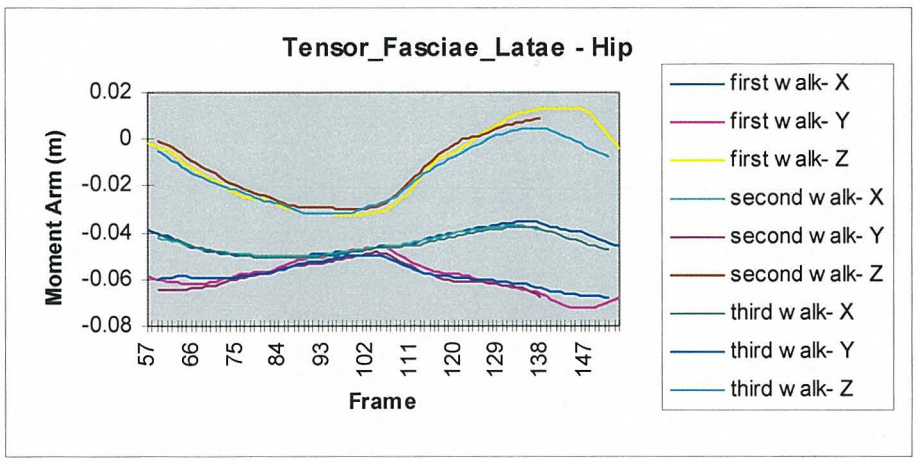

Figure 4.5.69 Walk trials - Tensor Fasciae Latae, hip moment arms.

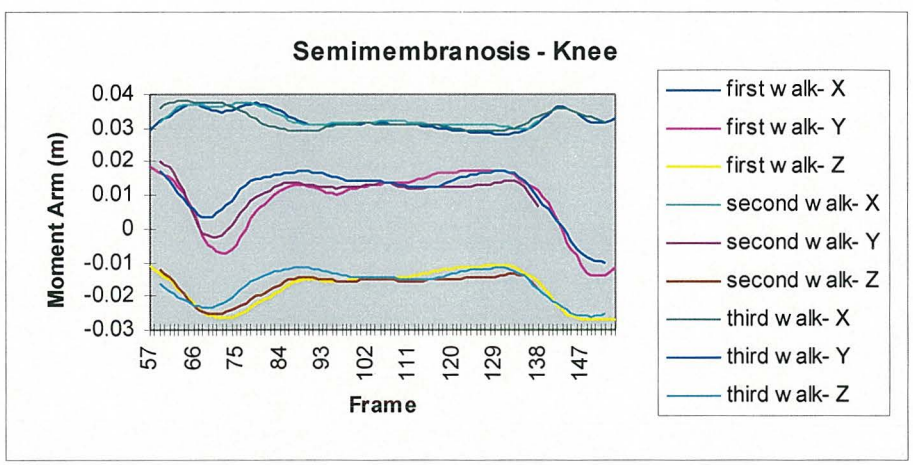

Figure 4.5.70 Walk trials - Semimembranosis, knee moment arms.

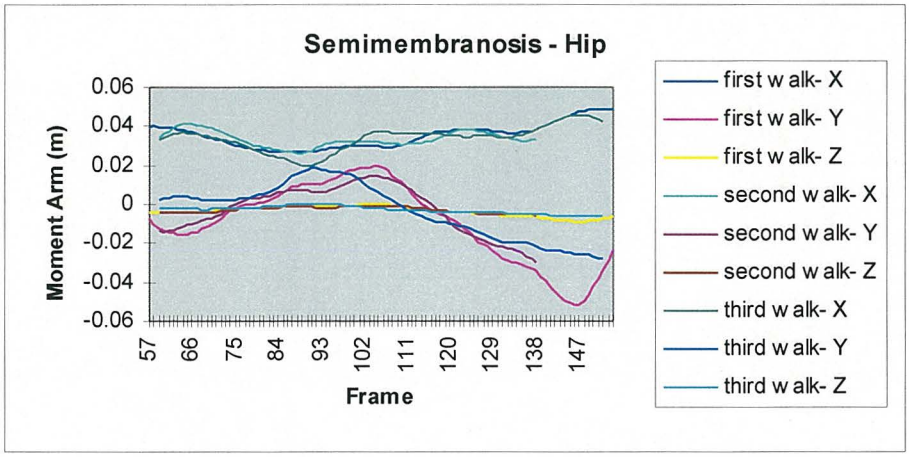

Figure 4.5.71 Walk trials - Semimembranosis, hip moment arms.

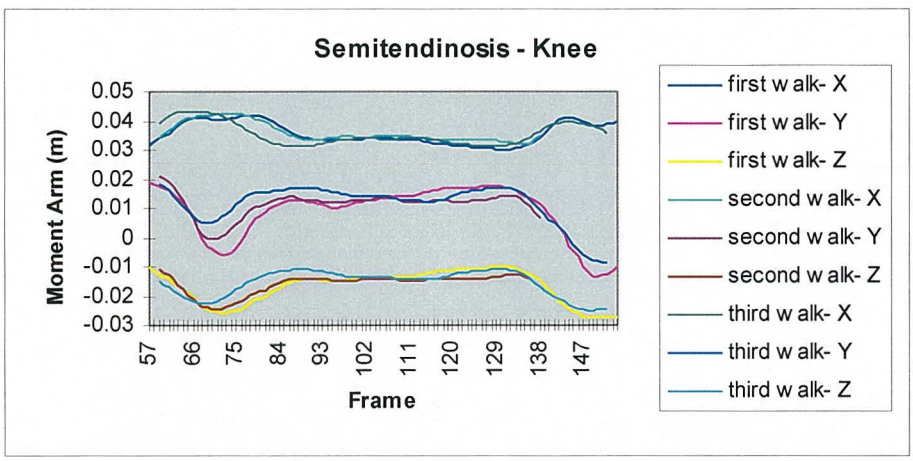

Figure 4.5.72 Walk trials - Semitendinosus, knee moment arms.

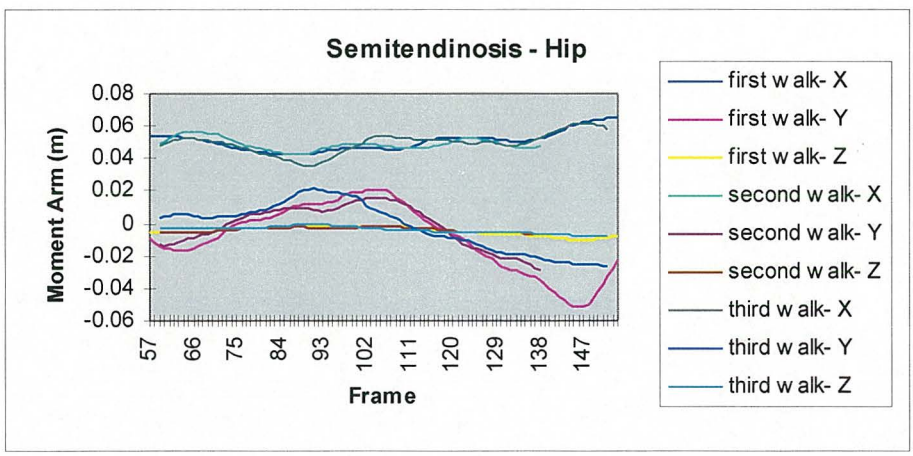

Figure 4.5.73 Walk trials - Semitendinosus, hip moment arms.

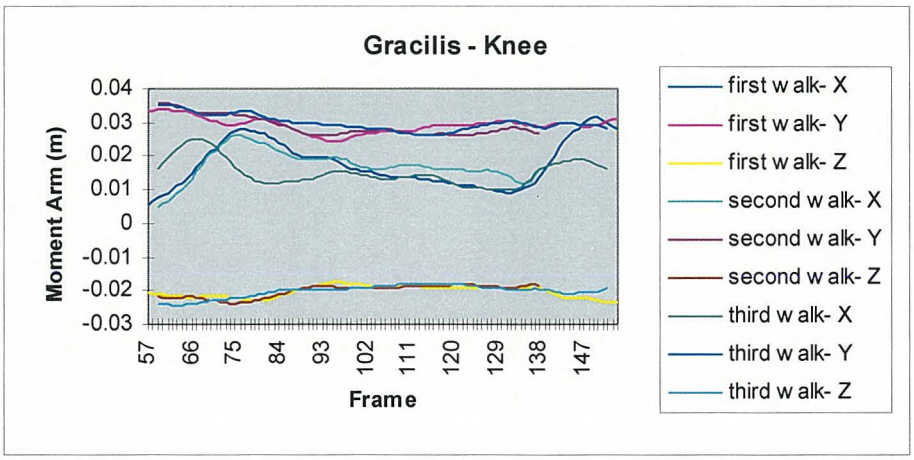

Figure 4.5.74 Walk trials - Gracilis, knee moment arms.

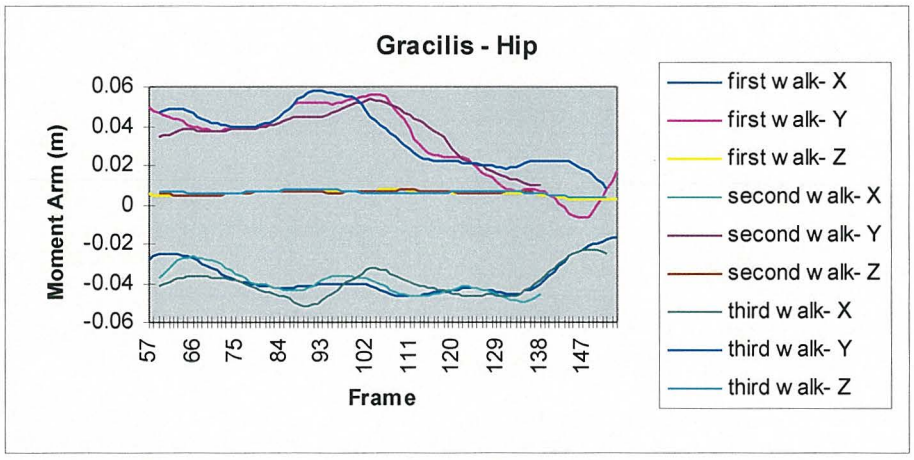

Figure 4.5.75 Walk trials - Gracilis, hip moment arms.

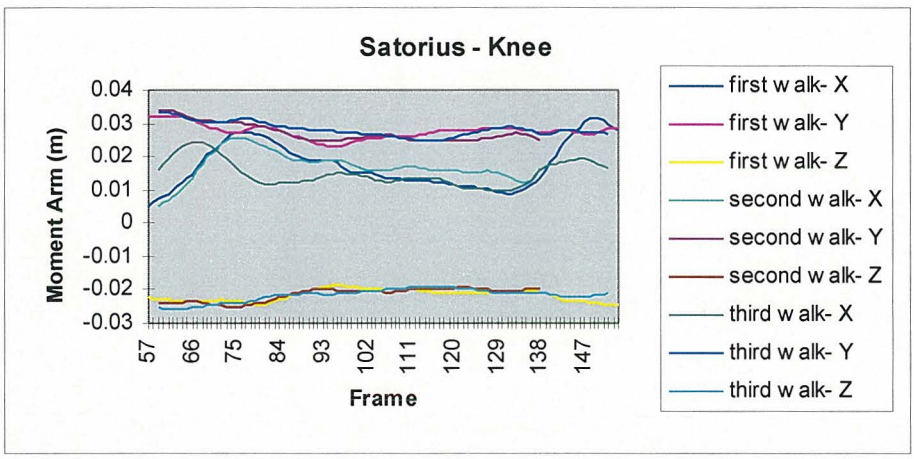

Figure 4.5.76 Walk trials - Satorius, knee moment arms.

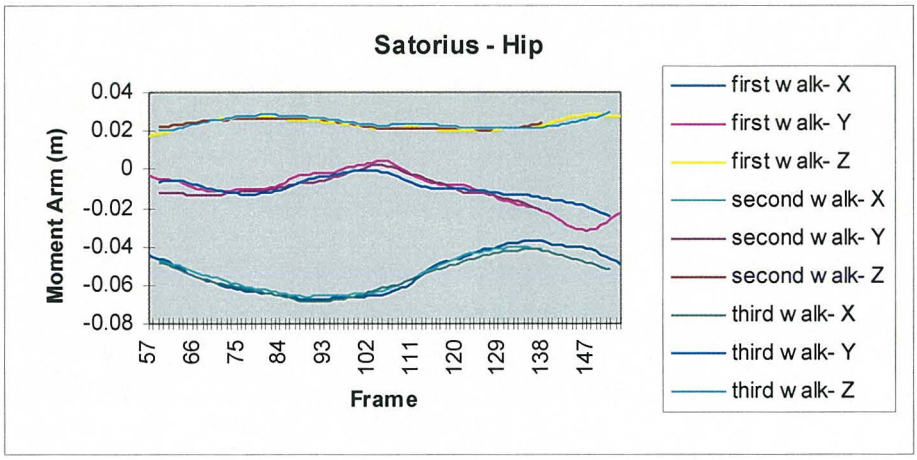

Figure 4.5.77 Walk trials - Satorius, hip moment arms.

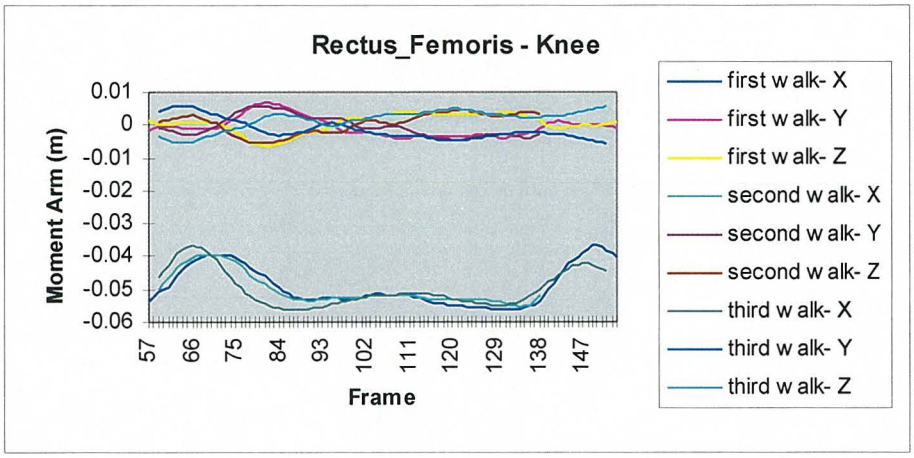

Figure 4.5.78 Walk trials - Rectus Femoris, knee moment arms.

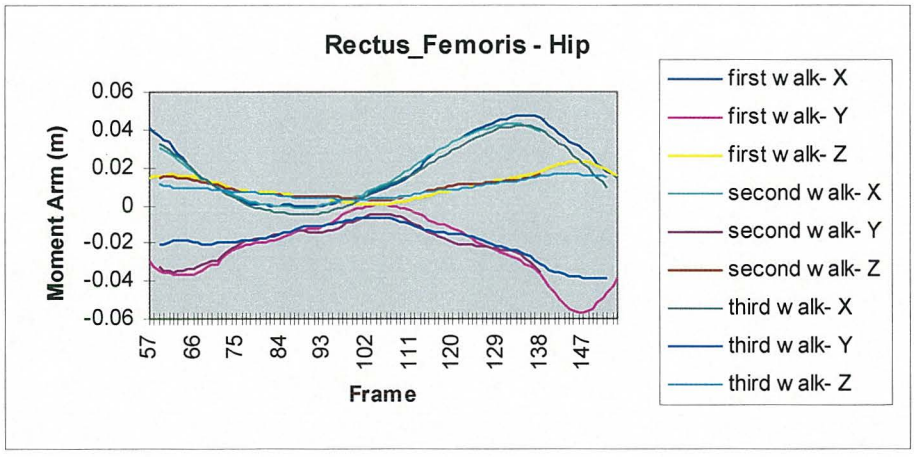

Figure 4.5.79 Walk trials - Rectus Femoris, hip moment arms.

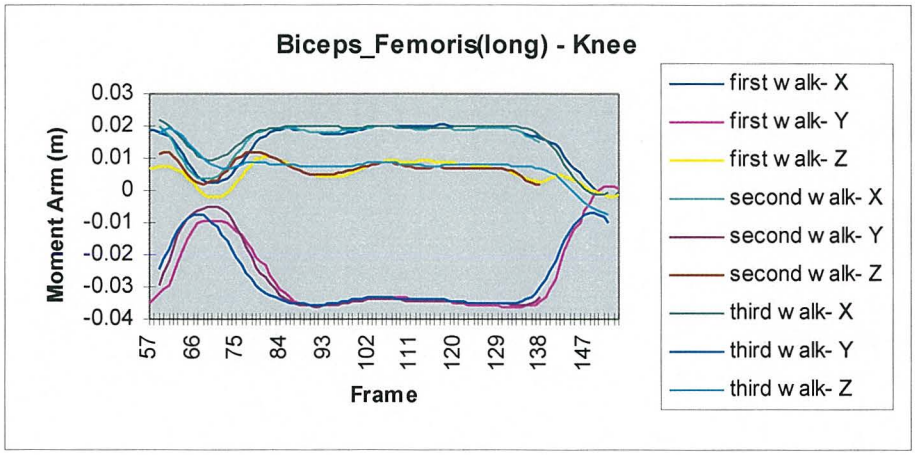

Figure 4.5.80 Walk trials - Biceps Femoris(long), knee moment arms.

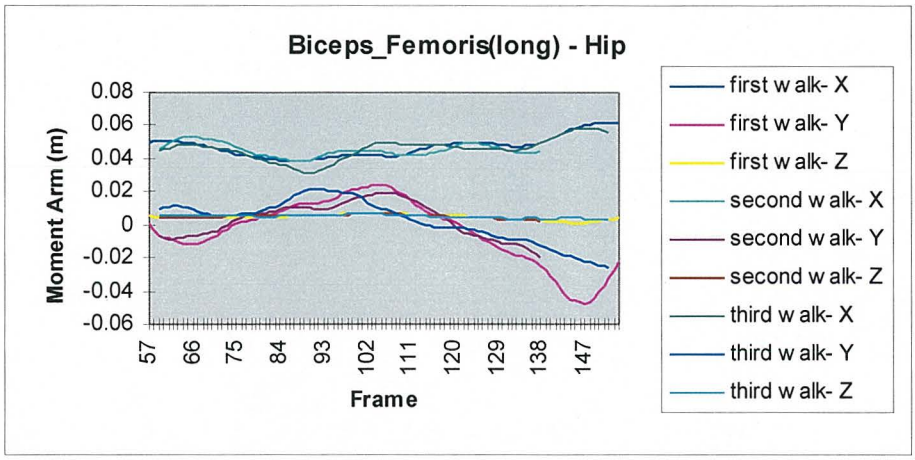

Figure 4.5.81 Walk trials - Biceps Femoris(long), hip moment arms.

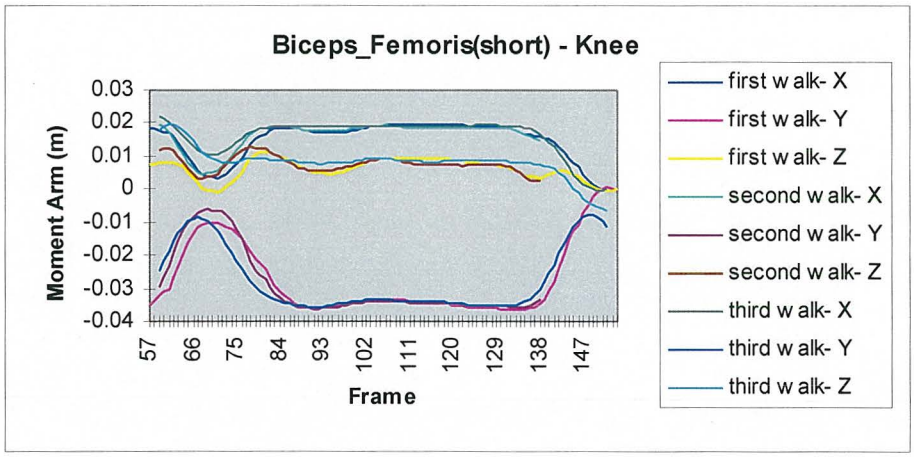

Figure 4.5.82 Walk trials - Biceps Femoris(short), knee moment arms.

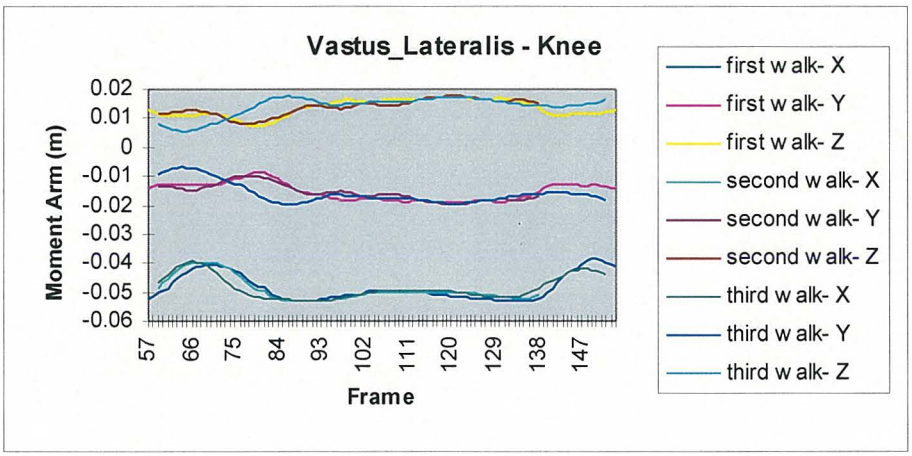

Figure 4.5.83 Walk trials - Vastus Lateralis, knee moment arms.

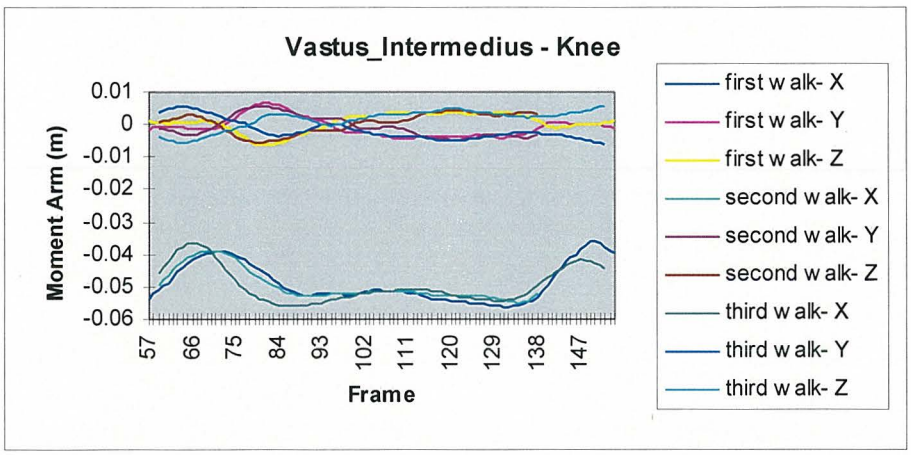

Figure 4.5.84 Walk trials - Vastus Intermedius, knee moment arms.

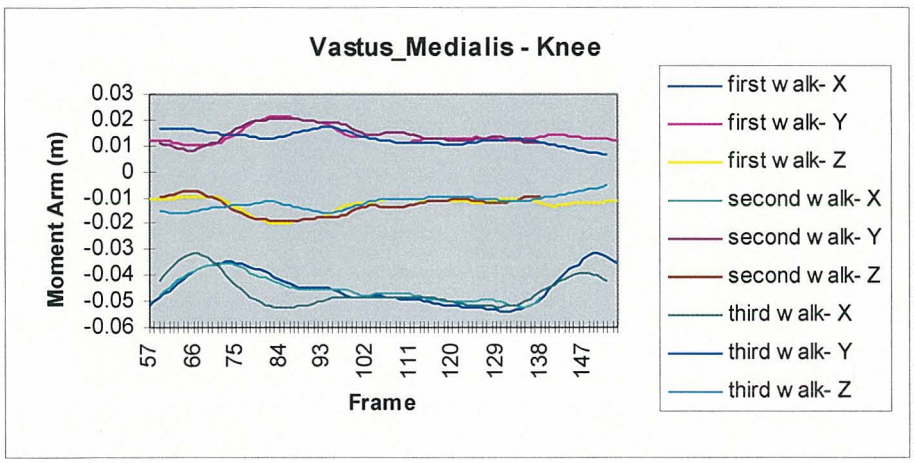

Figure 4.5.85 Walk trials - Vastus Medialis, knee moment arms.

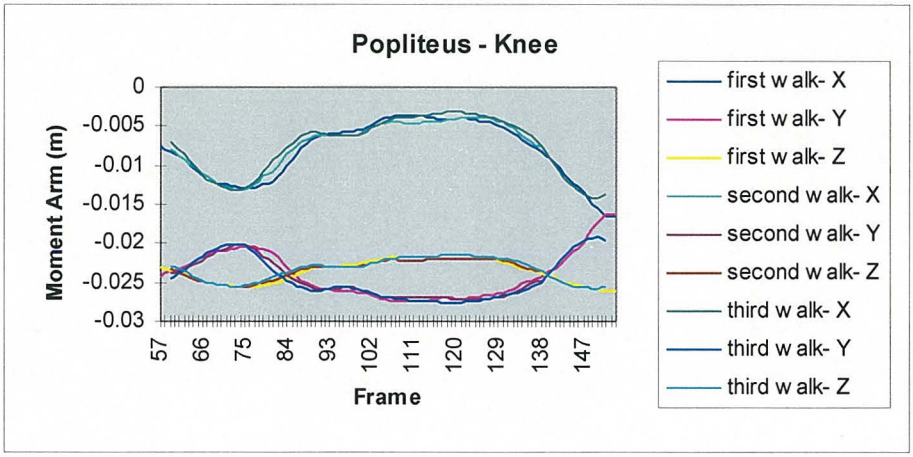

Figure 4.5.86 Walk trials - Popliteus, knee moment arms.

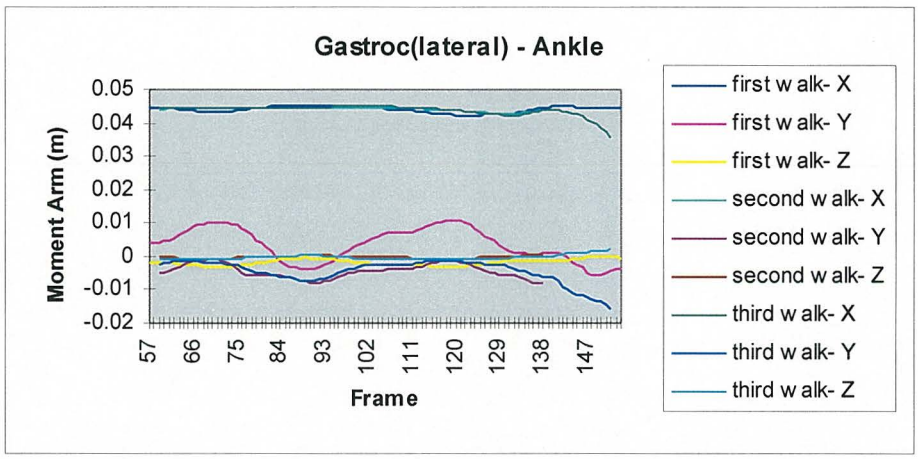

Figure 4.5.87 Walk trials - Gastrocnemius(lat), ankle moment arms.

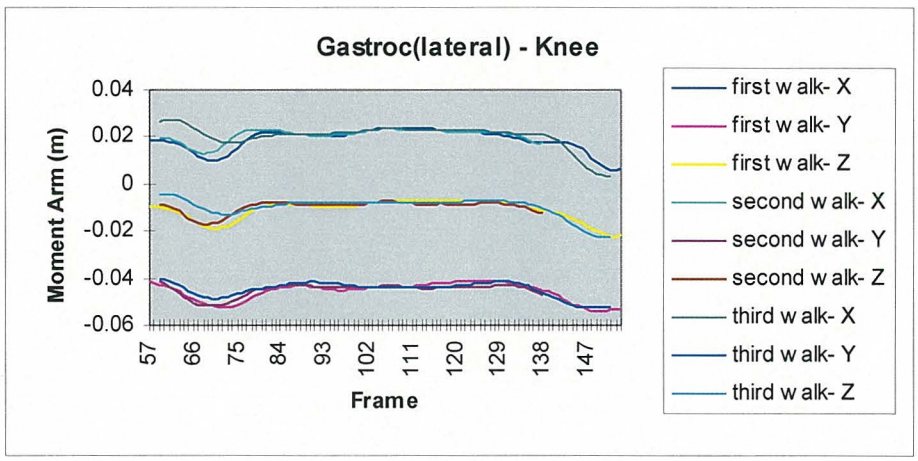

Figure 4.5.88 Walk trials - Gastrocnemius(lat), knee moment arms.

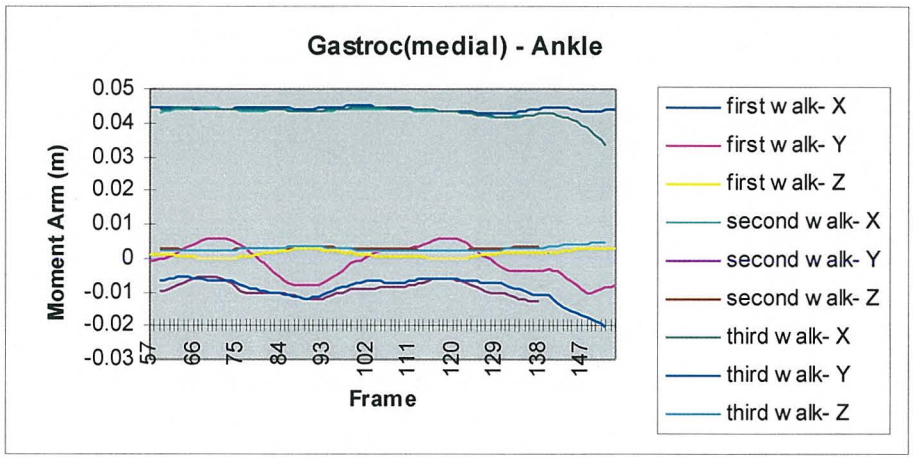

Figure 4.5.89 Walk trials - Gastrocnemius(med), ankle moment arms.

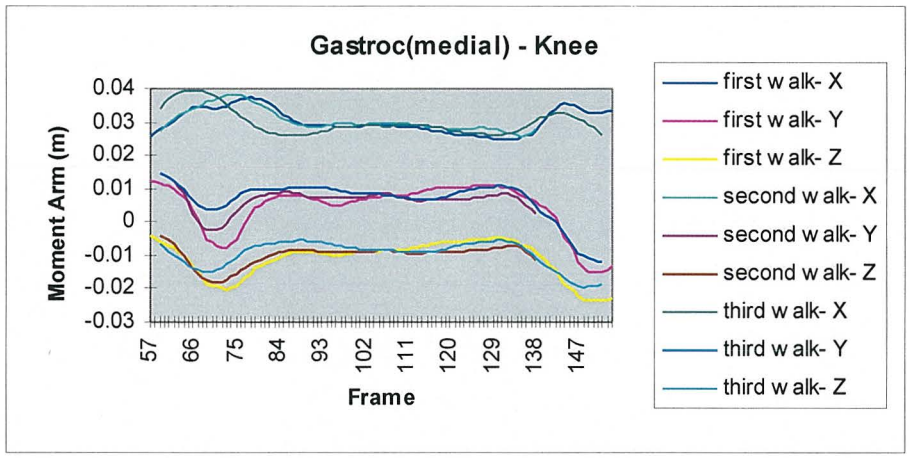

Figure 4.5.90 Walk trials - Gastrocnemius(med), knee moment arms.

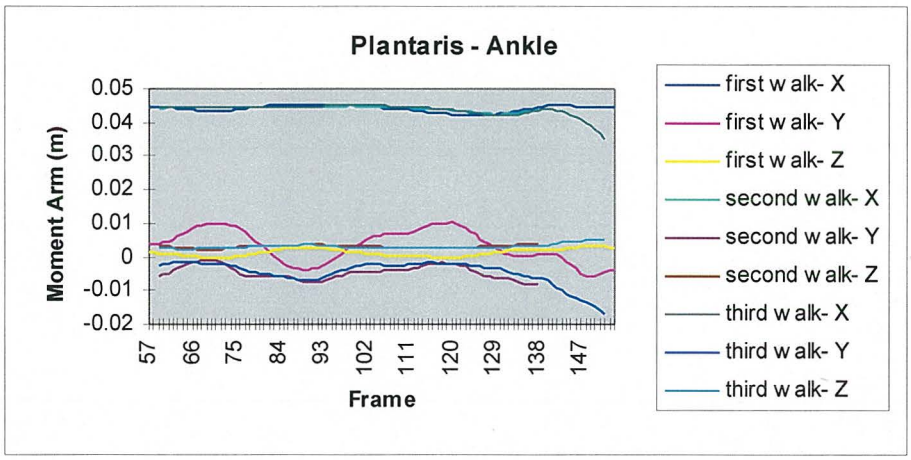

Figure 4.5.91 Walk trials - Plantaris, ankle moment arms.

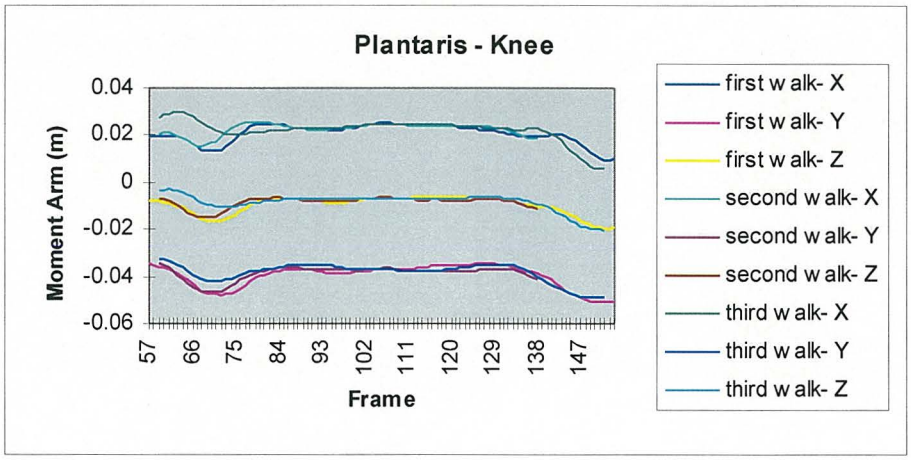

Figure 4.5.92 Walk trials - Plantaris, knee moment arms.

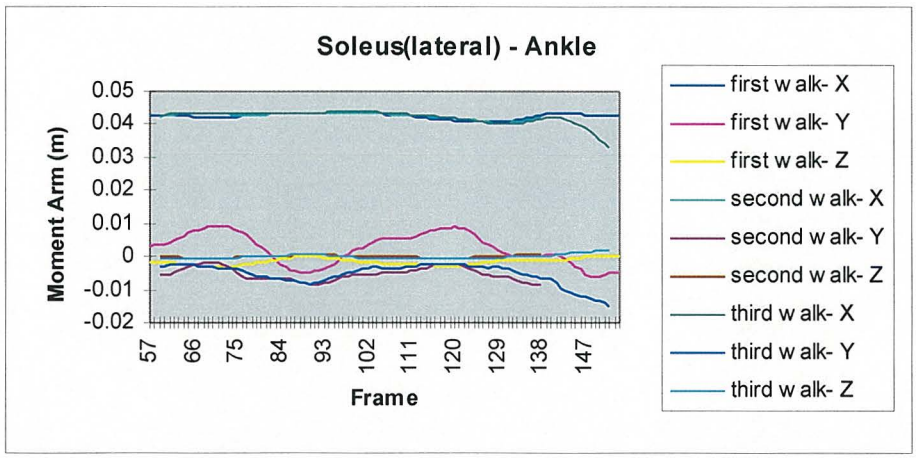

Figure 4.5.93 Walk trials - Soleus(lat), ankle moment arms.

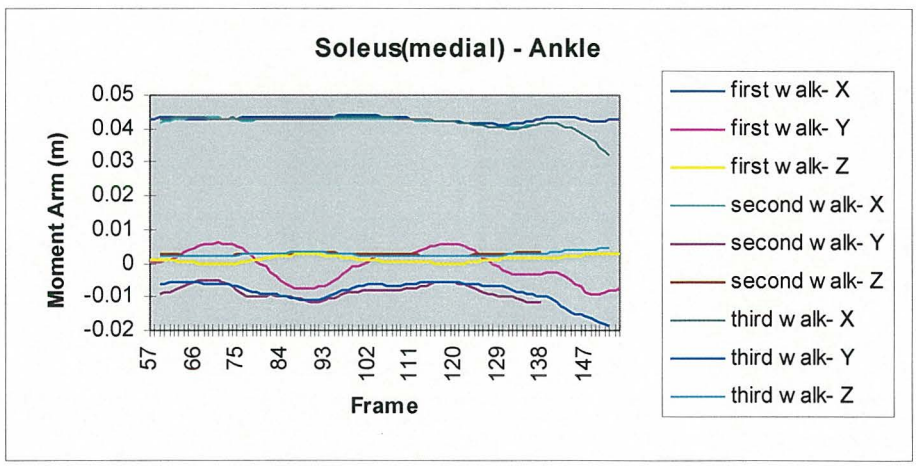

Figure 4.5.94 Walk trials - Soleus(med), ankle moment arms.

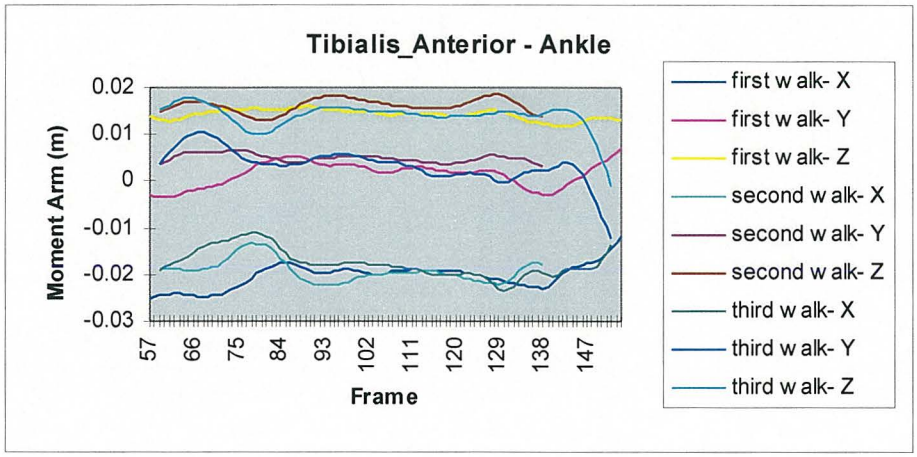

Figure 4.5.95 Walk trials - Tibialis Anterior, ankle moment arms.

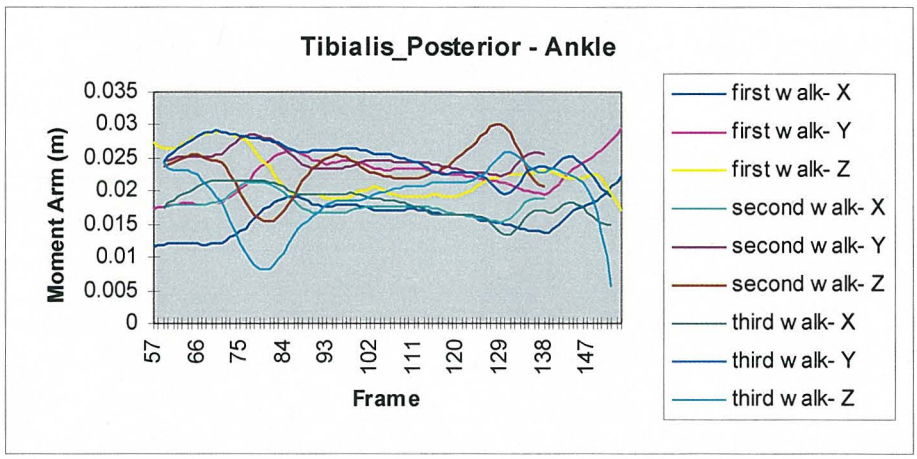

Figure 4.5.96 Walk trials - Tibialis Posterior, ankle moment arms.

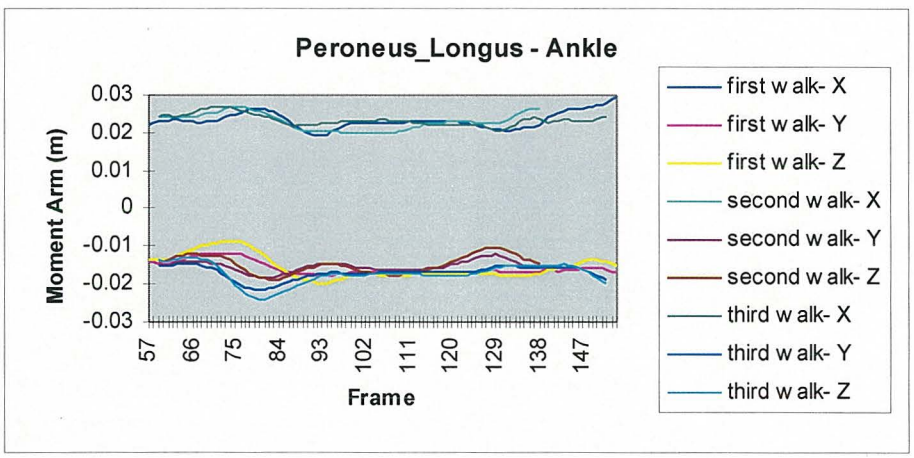

Figure 4.5.97 Walk trials - Peroneus Longus, ankle moment arms.

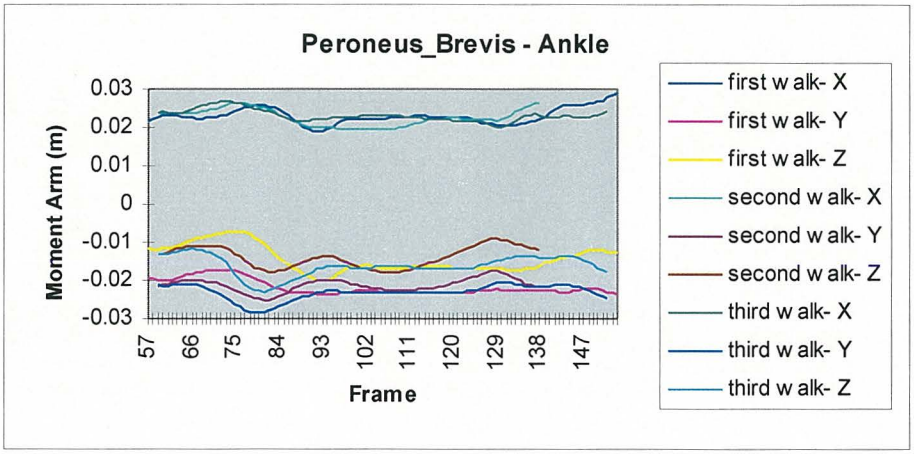

Figure 4.5.98 Walk trials - Peroneus Brevis, ankle moment arms.

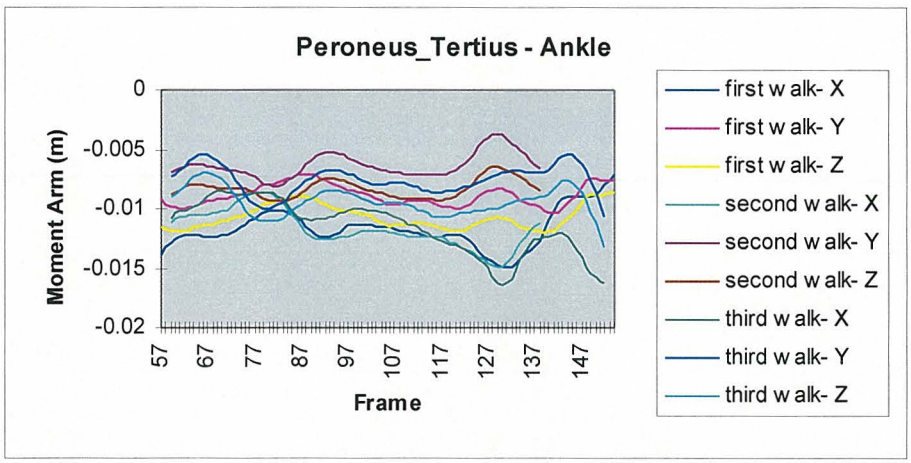

Figure 4.5.99 Walk trials - Peroneus Tertius, ankle moment arms.

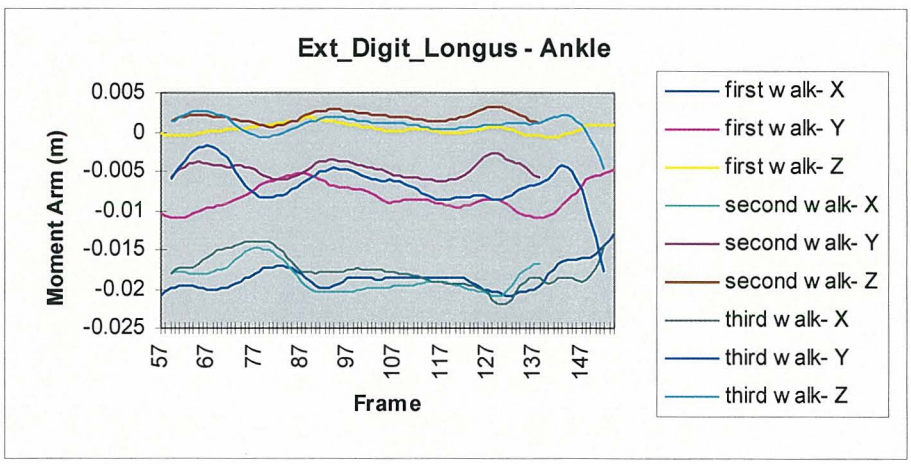

Figure 4.5.100 Walk trials - Ext.Digitorum Longus, ankle moment arms.

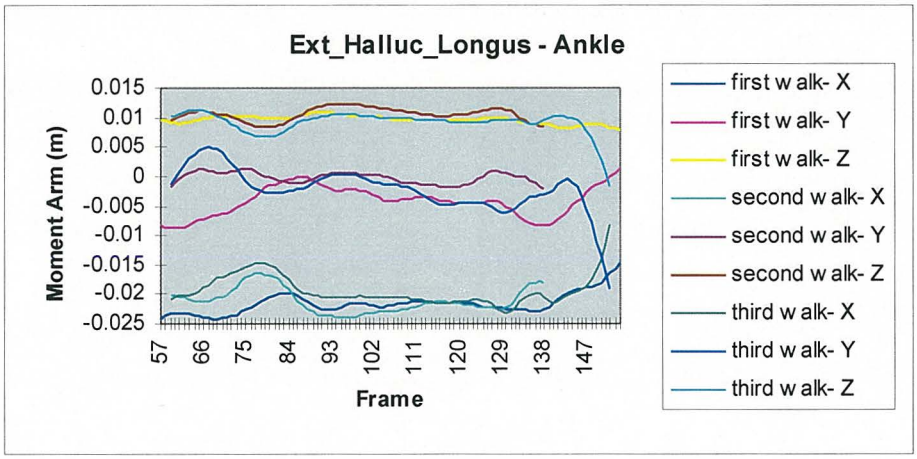

Figure 4.5.101 Walk trials - Ext.Hallucis Longus, ankle moment arms.

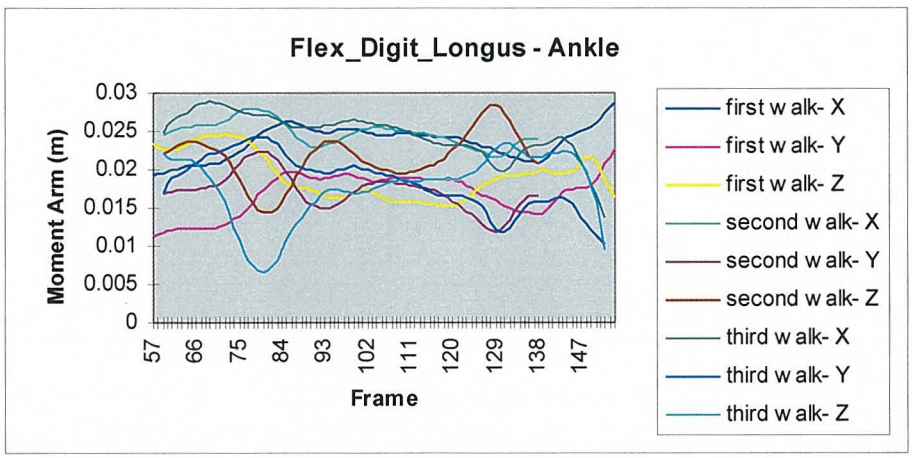

Figure 4.5.102 Walk trials - Flex.Digitorum Longus, ankle moment arms.

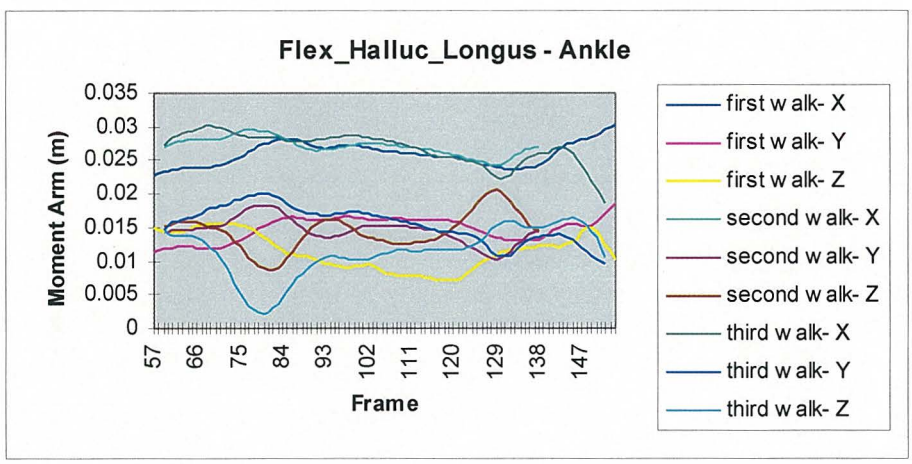

Figure 4.5.103 Walk trials - Flex.Hallucis Longus, ankle moment arms.

4.6 Step trials: comparative

The following graphs compare results from the three step trials. The data from each step trial has been normalised using the occurrences of the floor toe-off, step contact, step toe-off and floor contact events. Floor toe-off occurs at frame zero, step contact occurs at frame 52, step toe-off at frame 216 and floor contact at frame 270. As leg raise, step contact (comprising body rise, one legged stance and body lowering) and leg return phases varied in duration between step trials, normalisation effectively equated the respective time intervals between floor toe-off, step contact, step toe-off and floor contact.

Variables which did not require a knowledge of ground reactions forces at the foot, were analysed from the first to last frames from which the three dimensional segment locations could be reproduced from video images. Results from the first ten and last ten frames analysed were eliminated from each trial, due to the requirement of previous data points in smoothing and differentiation procedures to obtain accurate position, velocity and acceleration data. As such, Cardan rotations, centre of mass acceleration, muscle lengths, and muscle velocities were obtained over the entire trial. Variables which required a knowledge of the ground reaction forces were analysed from floor toe-off to ground contact at completion of the step. As such, resultant joint moments, muscle forces, and contractile element lengths and velocities were analysed within this period. For all results presented, floor toe-off is taken as frame zero. The frames over which segment marker were visible for each trial, are presented in Tables 4.6.1, 4.6.3 and 4.6.5, while frames used for kinematics and kinetic analyses for each trial, are presented in Tables 4.6.2, 4.6.4 and 4.6.6.

Comparative results of the relative Cardan rotations between the pelvis, thigh, shank and foot are presented in Figures 4.6.1 - 4.6.9. The three rotations X, Y' and Z" correspond to segment flexion-extension, abduction-adduction and internal-external rotation. Comparative centre of mass accelerations of the pelvis, hip, shank and foot of the three step trials are presented in Figures 4.6.10 - 4.6.21. Comparative resultant joint moments about the hip, knee and ankle joints of the three step trials are presented in Figures 4.6.22 - 4.12.30.

Table 4.6.1 First step trial - frames in which paths were reproduced. Parentheses indicating when path started or ended within the frames that were analysed.

PATH	Frames
Navel	1-**282**
rightASIS	1-300
IlliacCrest	1-300
PostBelt	1-300
Mid-PSIS	1-300
ThighAntSup	1-300
ThighAntMid	1-300
ThighAntInf	1-300
ThighMidSup	1-300
ThighMidInf	1-300
ThighPosSup	1-300
ThighPosInf	1-300
LatKnee	1-300
ShankAntSup	1-300
ShankAntMid	1-300
ShankAntInf	1-300
ShankMidSup	1-300
ShankMidInf	1-300
ShankPosSup	1-300
ShankPosInf	1-300
LatAnkle	1-300
FootDorsal	1-300
MedToe	1-300
LatToe	1-**284**
FootMidLat	1-300
PostCalcan	1-300

Table 4.6.2 Event markers and frames analysed for first step trial.

	First Frame	Floor Toe-Off (on-off)	Step Contact (off-on)	Step Toe-Off (on-off)	Floor Contact (off-on)	Last Frame
Frame	1	46-47	93-94	231-232	280-281	300
Kinematics	11----------290					
Kinetics	47----------280					

Table 4.6.3 Second step trial - frames in which paths were reproduced. Parentheses indicating when path started or ended within the frames that were analysed.

PATH	Frames
Navel	1-300
rightASIS	1-300
IlliacCrest	1-300
PostBelt	1-300
Mid-PSIS	1-300
ThighAntSup	1-300
ThighAntMid	1-300
ThighAntInf	1-300
ThighMidSup	1-300
ThighMidInf	1-300
ThighPosSup	1-300
ThighPosInf	1-300
LatKnee	1-300
ShankAntSup	1-300
ShankAntMid	1-300
ShankAntInf	1-300
ShankMidSup	1-300
ShankMidInf	1-300
ShankPosSup	1-300
ShankPosInf	1-300
LatAnkle	1-300
FootDorsal	1-300
MedToe	1-300
LatToe	1-300
FootMidLat	1-300
PostCalcan	1-300

Table 4.6.4 Event markers and frames analysed for second step trial.

	First Frame	Floor Toe-Off (on-off)	Step Contact (off-on)	Step Toe-Off (on-off)	Floor Contact (off-on)	Last Frame
Frame	1	43-44	95-96	259-260	-	300
Kinematics	11----------290					
Kinetics	44----------290					

Table 4.6.5 Third step trial - frames in which paths were reproduced. Parentheses indicating when path started or ended within the frames that were analysed.

PATH	Frames
Navel	4-300
rightASIS	4-300
IlliacCrest	4-**285**
PostBelt	4-300
Mid-PSIS	4-300
ThighAntSup	4-300
ThighAntMid	4-300
ThighAntInf	4-300
ThighMidSup	4-300
ThighMidInf	4-300
ThighPosSup	4-300
ThighPosInf	4-300
LatKnee	4-300
ShankAntSup	4-300
ShankAntMid	4-300
ShankAntInf	4-300
ShankMidSup	4-300
ShankMidInf	4-300
ShankPosSup	4-300
ShankPosInf	4-300
LatAnkle	4-300
FootDorsal	4-300
MedToe	4-**167**
LatToe	4-**238**
FootMidLat	4-300
PostCalcan	4-300

Table 4.6.6 Event markers and frames analysed for third step trial.

	First Frame	Floor Toe-Off (on-off)	Step Contact (off-on)	Step Toe-Off (on-off)	Floor Contact (off-on)	Last Frame
Frame	4	52-53	100-101	228-229	279-180	300
Kinematics	14----------290					
Kinetics	53----------279					

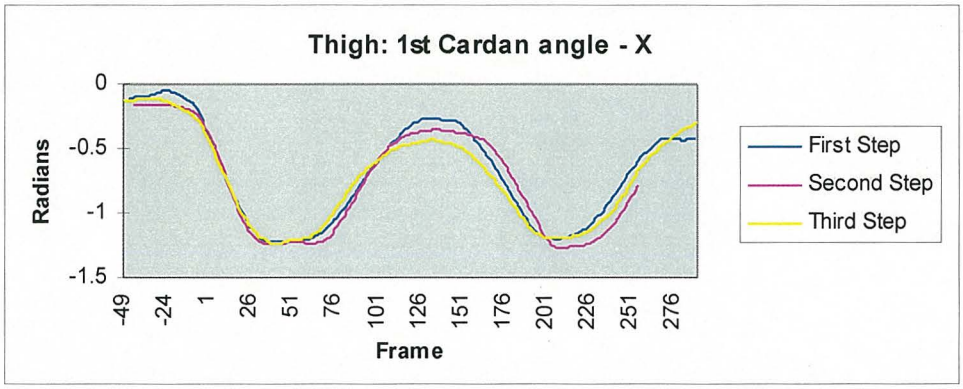

Figure 4.6.1 Step trials 1st Cardan rotation of the thigh. The rotation corresponding to flexion-extension of the thigh relative to the pelvis.

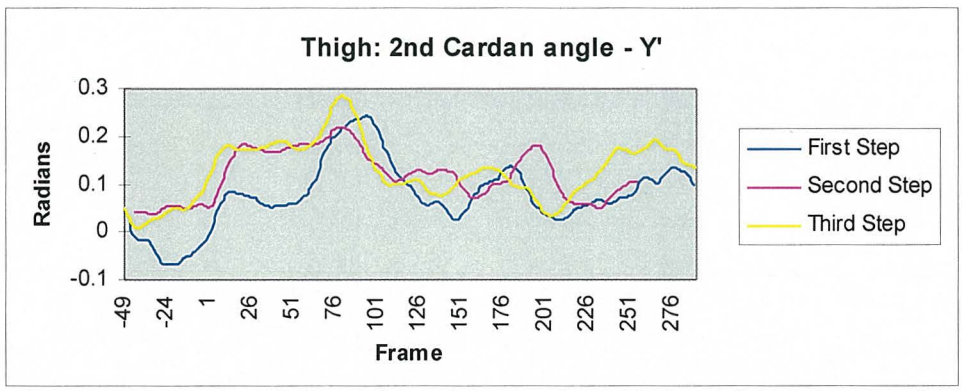

Figure 4.6.2 Step trials 2nd Cardan rotation of the thigh. The rotation corresponding to adduction-abduction of the thigh relative to the pelvis.

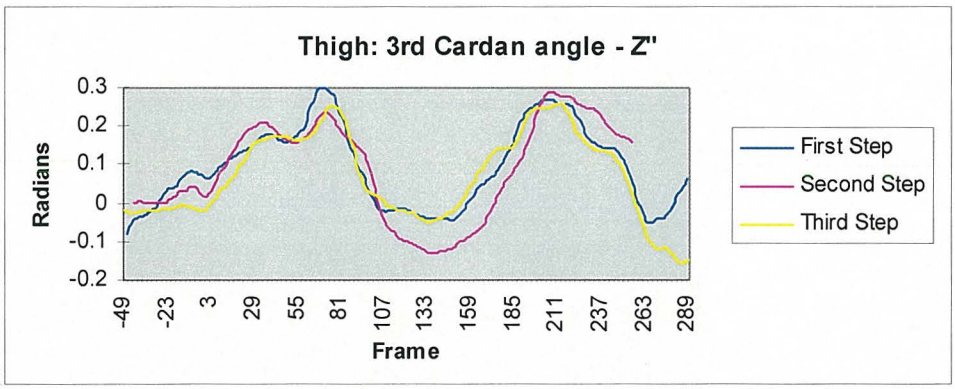

Figure 4.6.3 Step trials 3rd Cardan rotation of the thigh. Corresponding to internal-external rotation of the thigh relative to the pelvis.

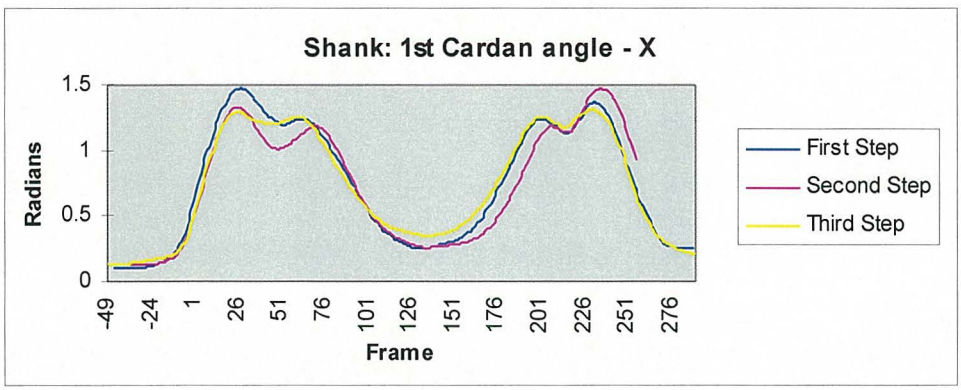

Figure 4.6.4 Step trials 1st Cardan rotation of the shank. The rotation corresponding to flexion-extension of the shank relative to the thigh.

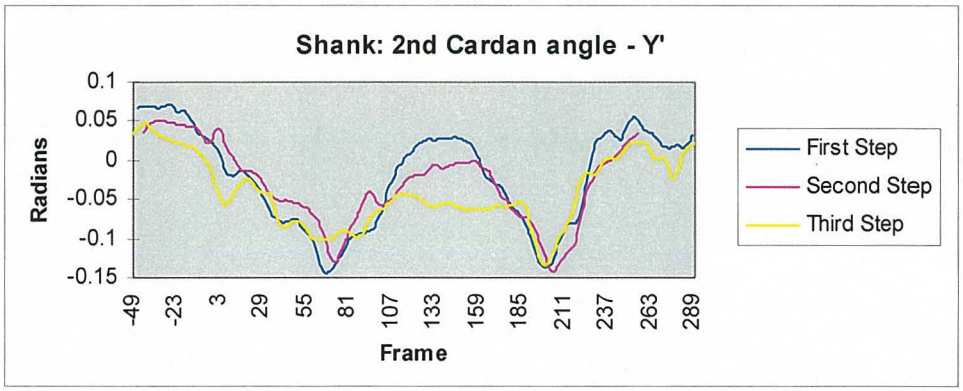

Figure 4.6.5 Step trials 2nd Cardan rotation of the shank. The rotation corresponding to adduction-abduction of the shank relative to the thigh.

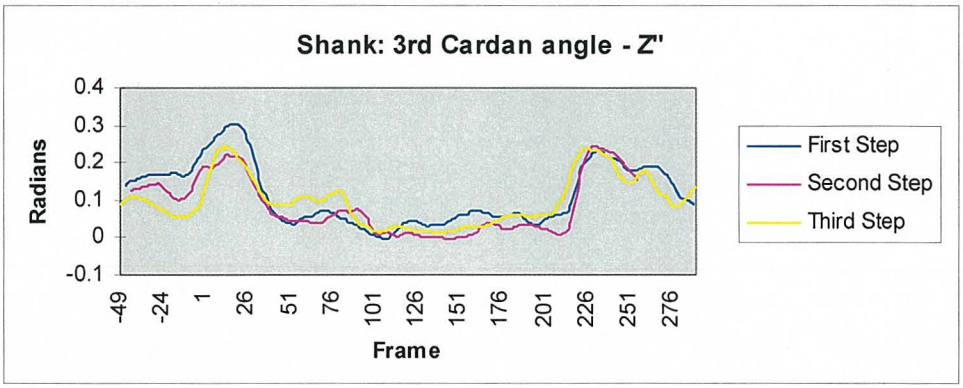

Figure 4.6.6 Step trials 3rd Cardan rotation of the shank. Corresponding to internal-external rotation of the shank relative to the thigh.

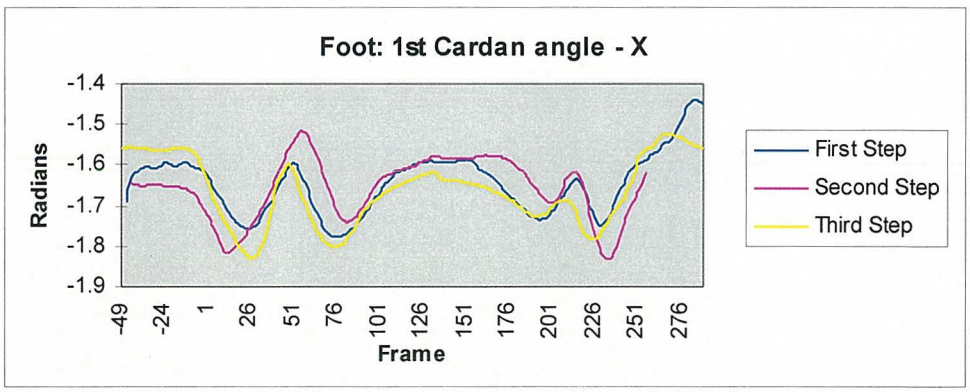

Figure 4.6.7 Step trials 1st Cardan rotation of the foot. The rotation corresponding to flexion-extension of the foot relative to the shank.

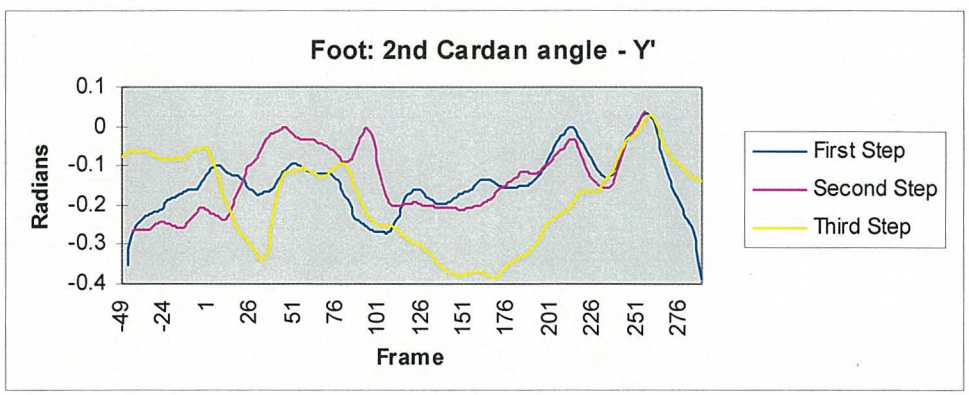

Figure 4.6.8 Step trials 2nd Cardan rotation of the foot. The rotation corresponding to adduction-abduction of the foot relative to the shank.

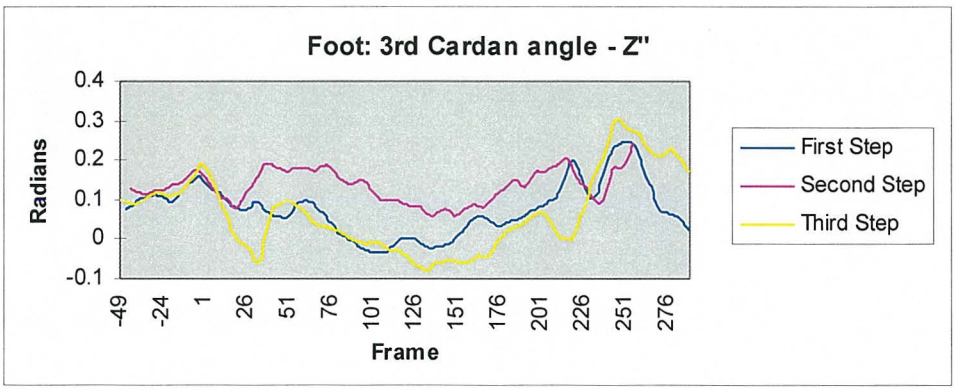

Figure 4.6.9 Step trials 3rd Cardan rotation of the foot. Corresponding to internal-external rotation of the foot relative to the shank.

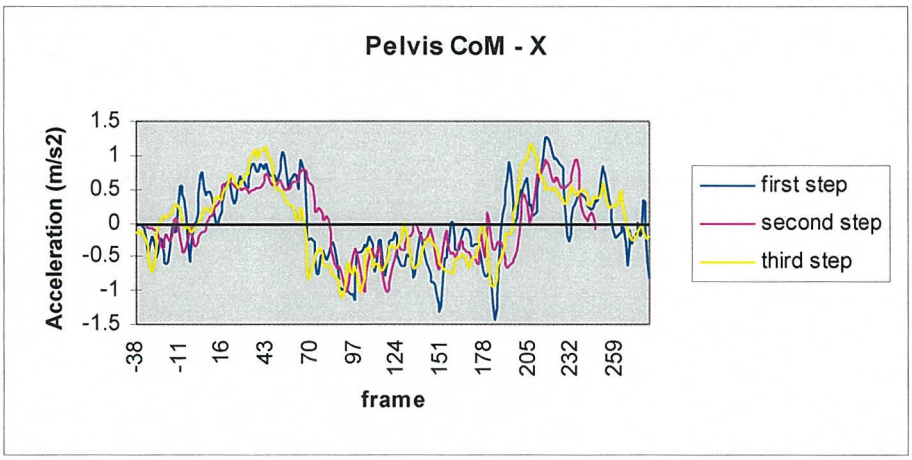

Figure 4.6.10 Step trials - pelvis centre of mass acceleration in global x axis.

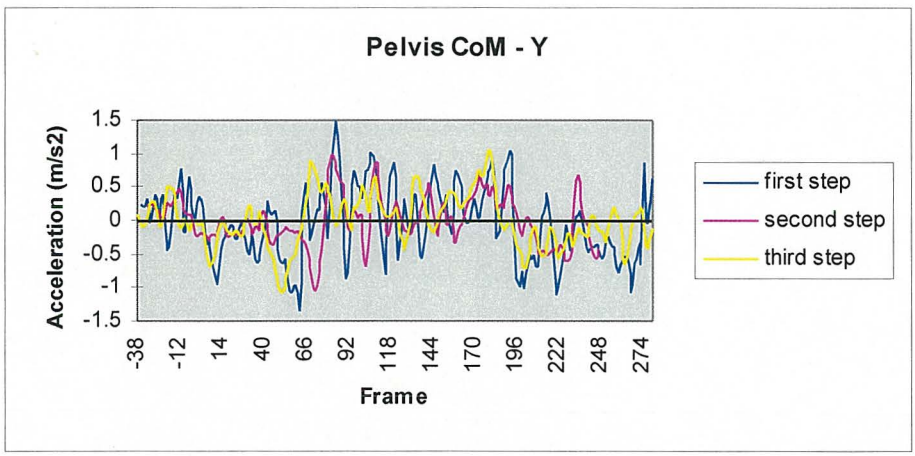

Figure 4.6.11 Step trials - pelvis centre of mass acceleration in global y axis.

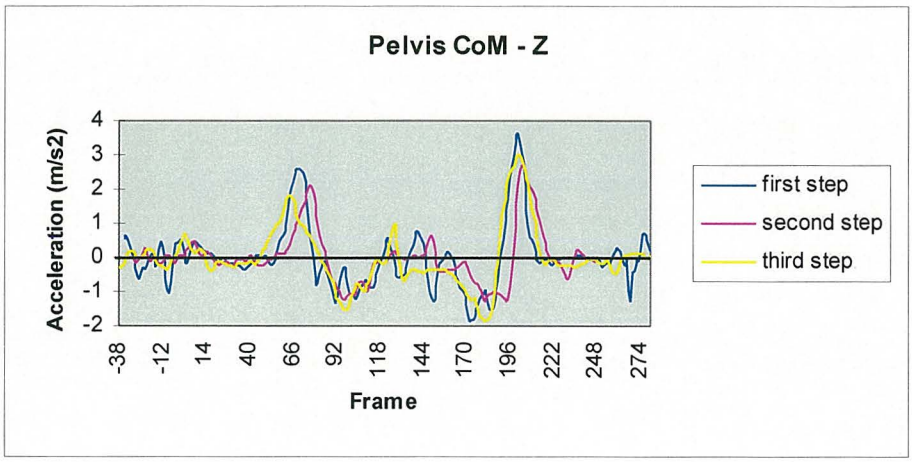

Figure 4.6.12 Step trials - pelvis centre of mass acceleration in global z axis

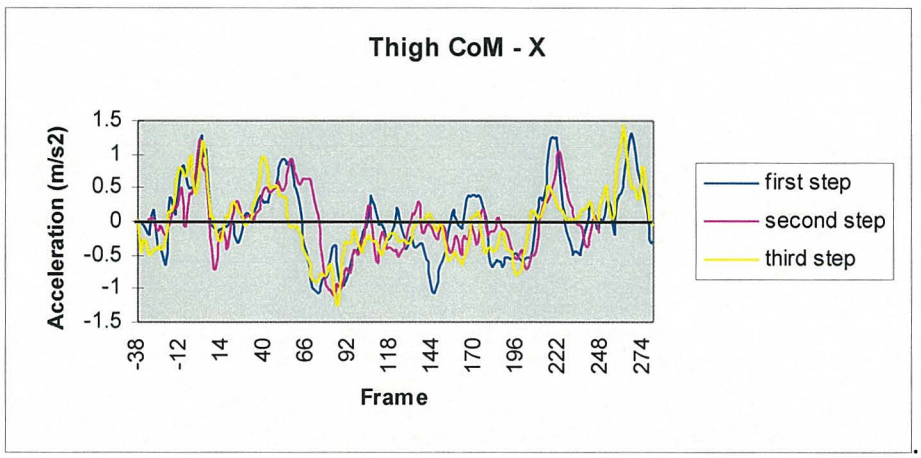

Figure 4.6.13 Step trials - thigh centre of mass acceleration in global x axis.

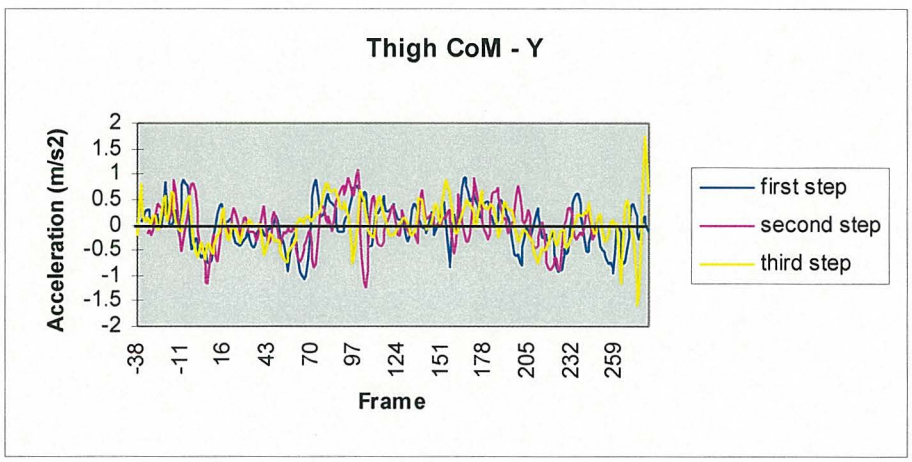

Figure 4.6.14 Step trials - thigh centre of mass acceleration in global y axis.

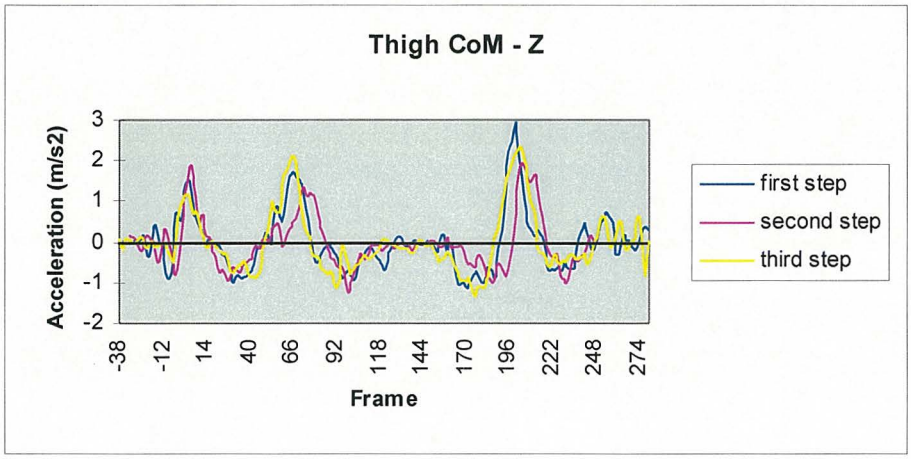

Figure 4.6.15 Step trials - thigh centre of mass acceleration in global z axis.

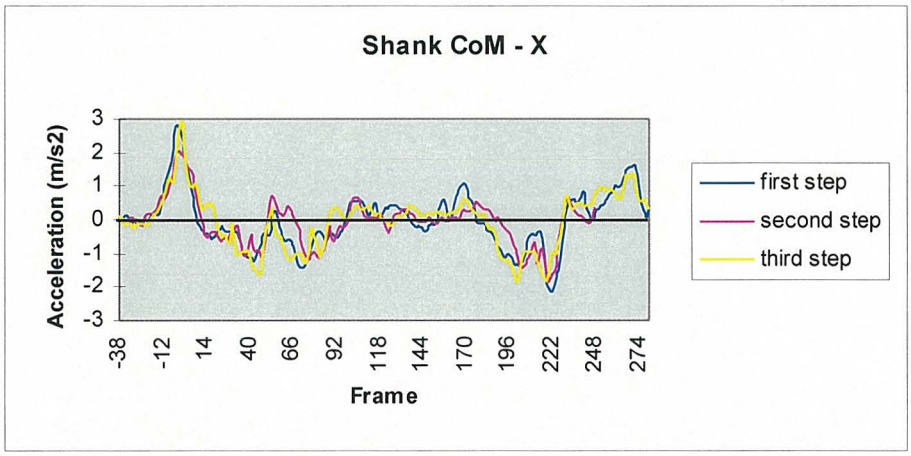

Figure 4.6.16 Step trials - shank centre of mass acceleration in global x axis.

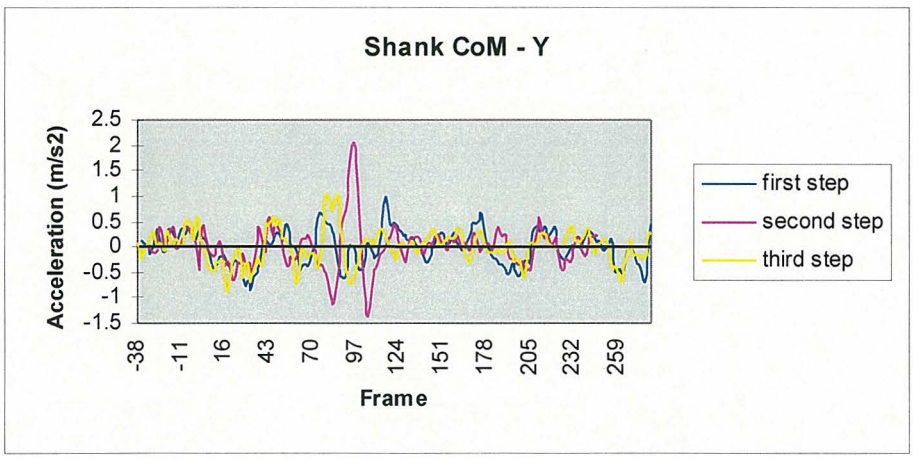

Figure 4.6.17 Step trials - shank centre of mass acceleration in global y axis.

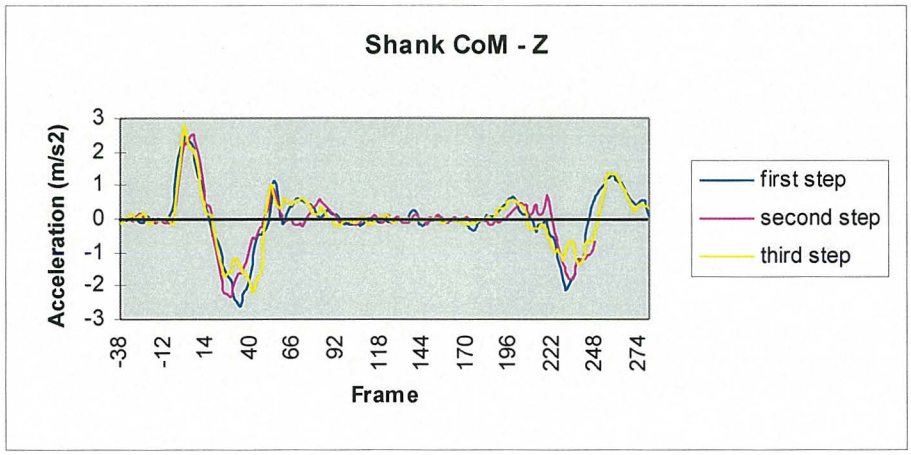

Figure 4.6.18 Step trials - shank centre of mass acceleration in global z axis.

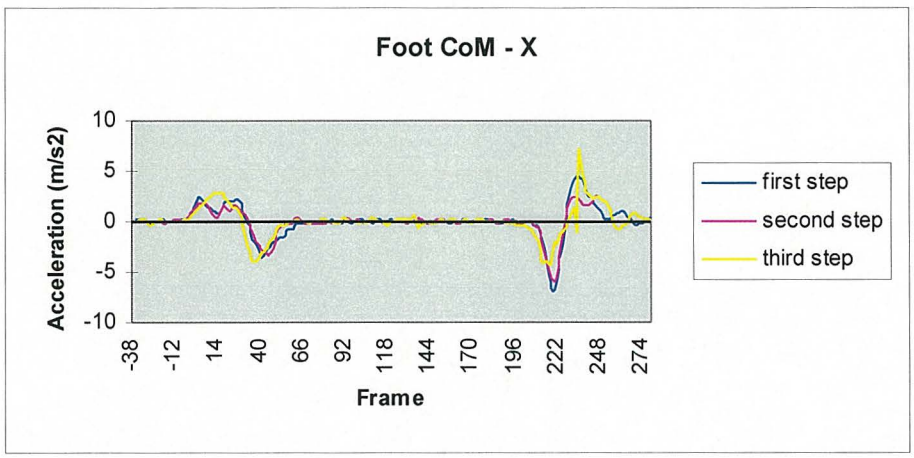

Figure 4.6.19 Step trials - foot centre of mass acceleration in global x axis.

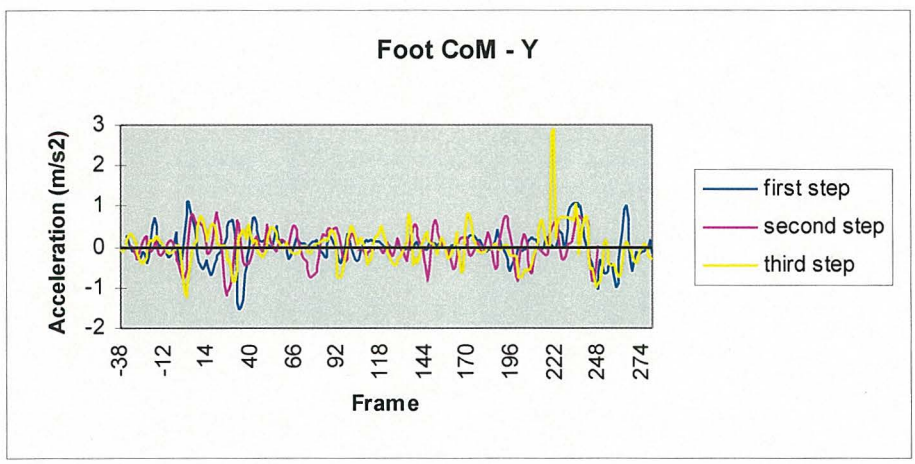

Figure 4.6.20 Step trials - foot centre of mass acceleration in global y axis.

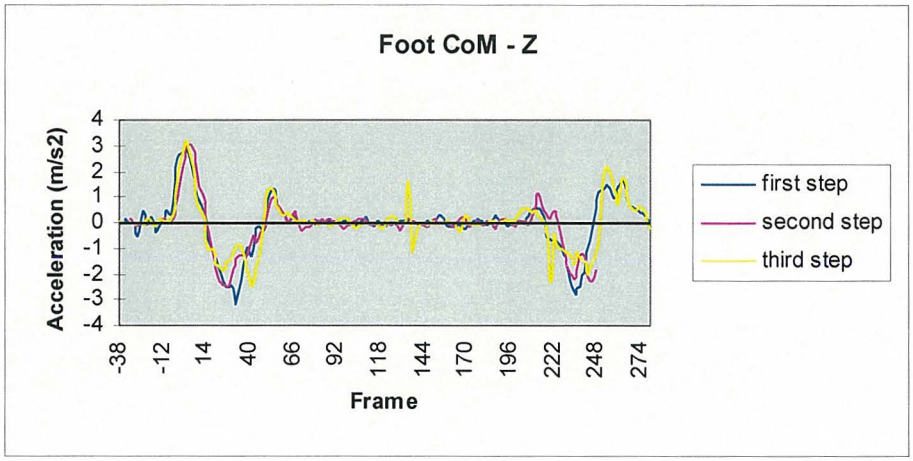

Figure 4.6.21 Step trials - foot centre of mass acceleration in global z axis.

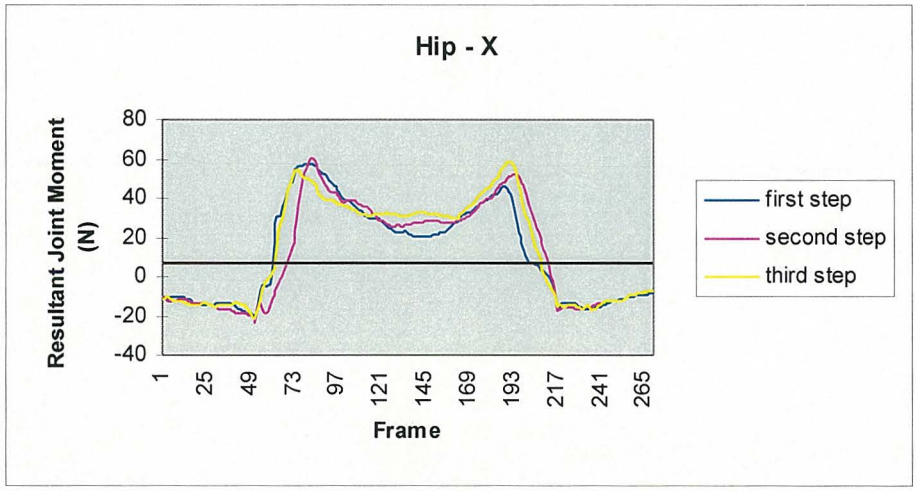

Figure 4.6.22 Step trials - resultant joint moments about hip x axis.

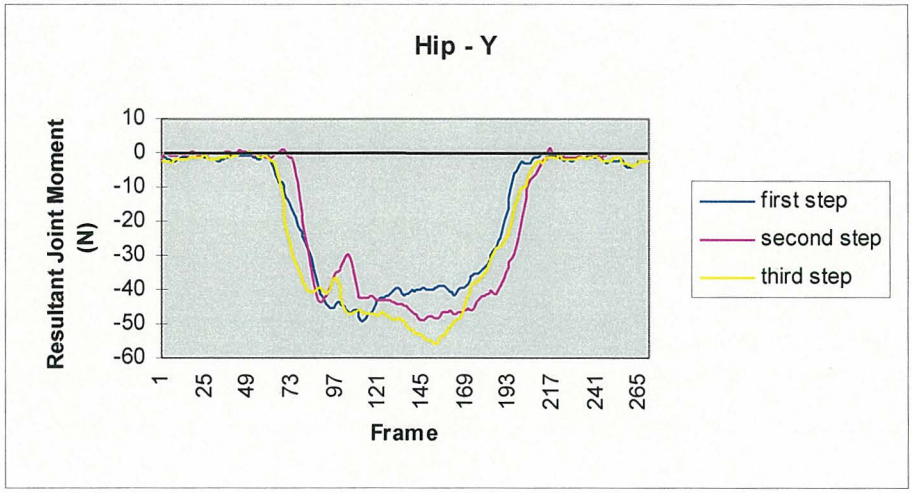

Figure 4.6.23 Step trials - resultant joint moments about hip y axis.

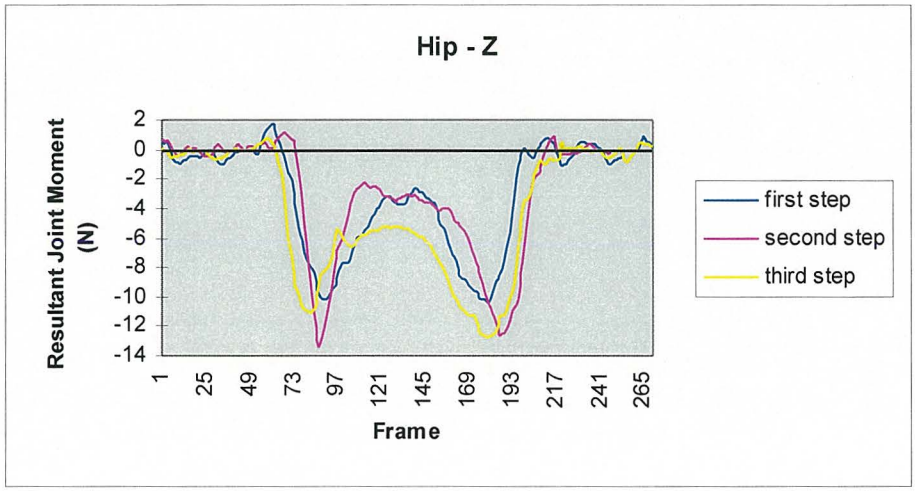

Figure 4.6.24 Step trials - resultant joint moments about hip z axis.

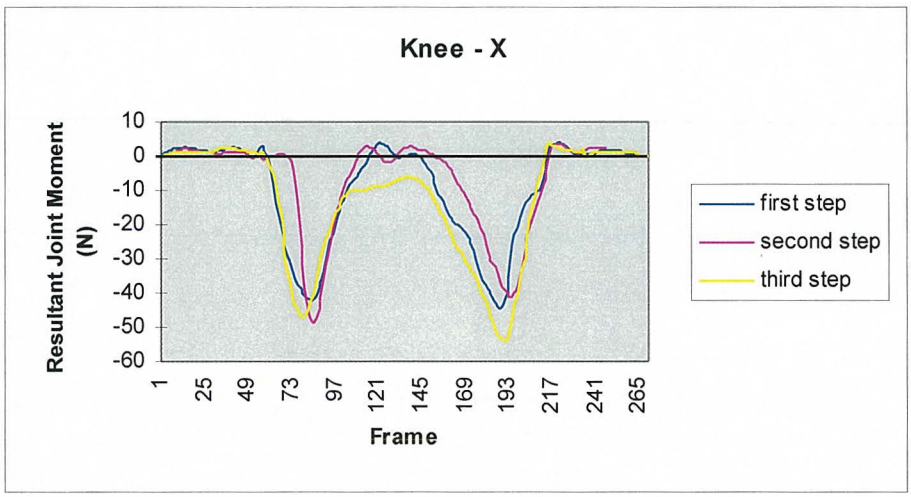

Figure 4.6.25 Step trials - resultant joint moments about knee x axis.

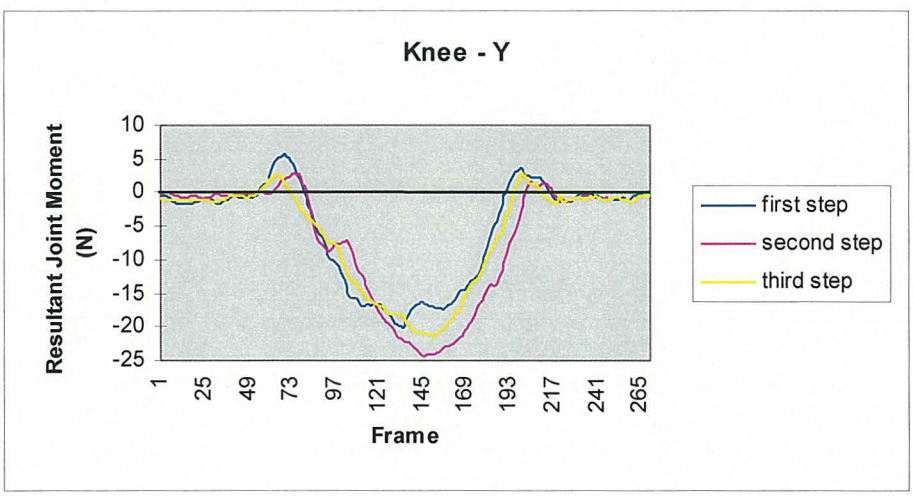

Figure 4.6.26 Step trials - resultant joint moments about knee y axis.

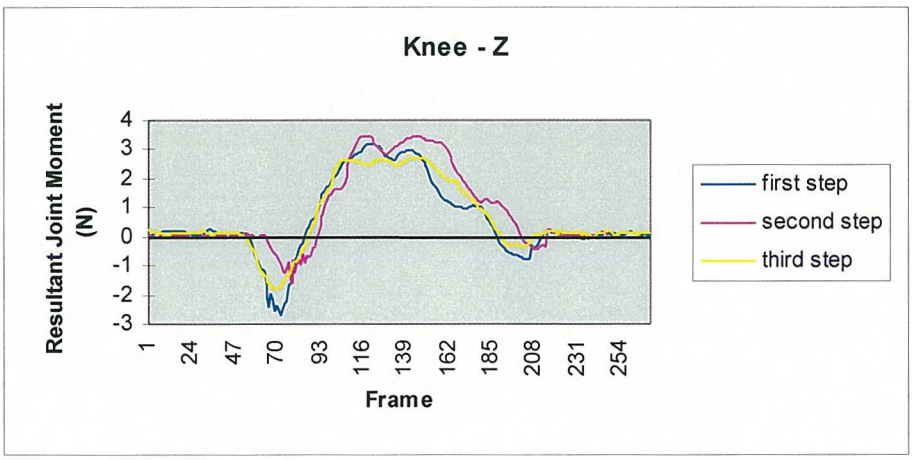

Figure 4.6.27 Step trials - resultant joint moments about knee z axis.

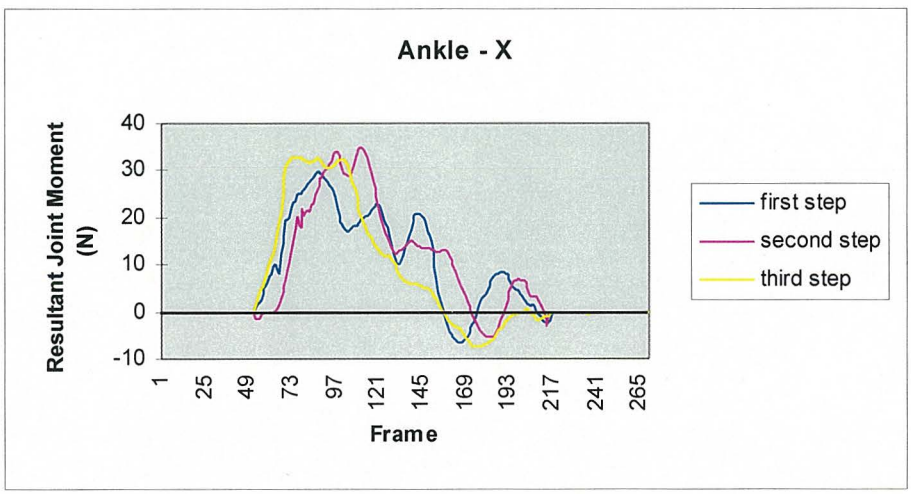

Figure 4.6.28 Step trials - resultant joint moments about ankle x axis.

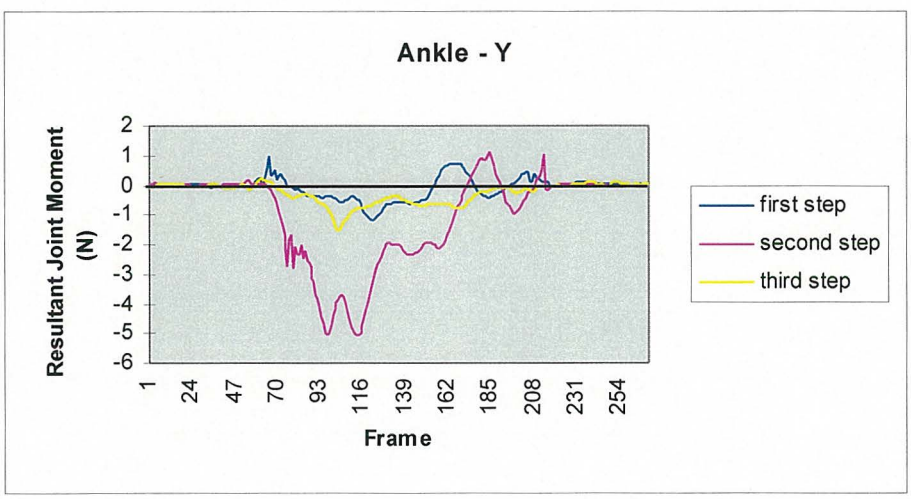

Figure 4.6.29 Step trials - resultant joint moments about ankle y axis.

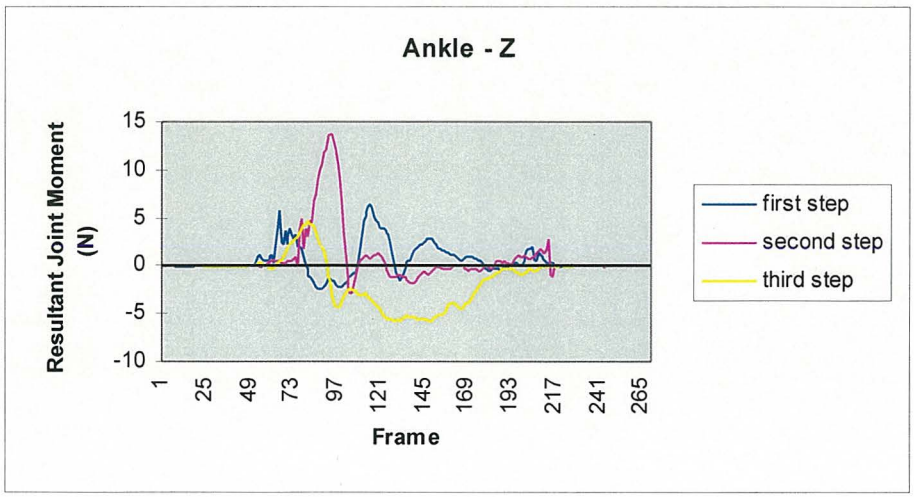

Figure 4.6.30 Step trials - resultant joint moments about ankle z axis.

Fifteen muscles were chosen and predicted muscle forces were compared across the three step trials as presented in Figures 4.6.31 - 4.6.45. Comparative moment arms for the 48 modelled muscles during the three step trials are presented from Figure 4.6.46 to 4.6.103.

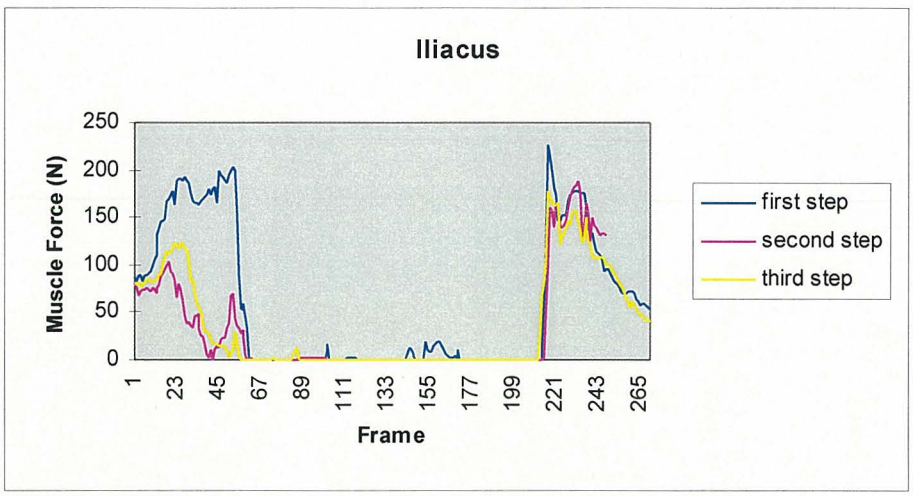

Figure 4.6.31 Step trials - Iliacus predicted muscle forces.

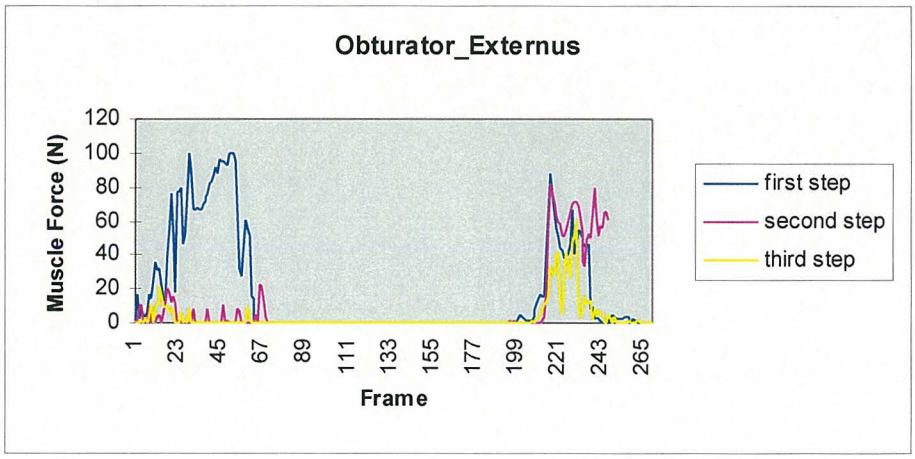

Figure 4.6.32 Step trials - Obturator Externus predicted muscle forces.

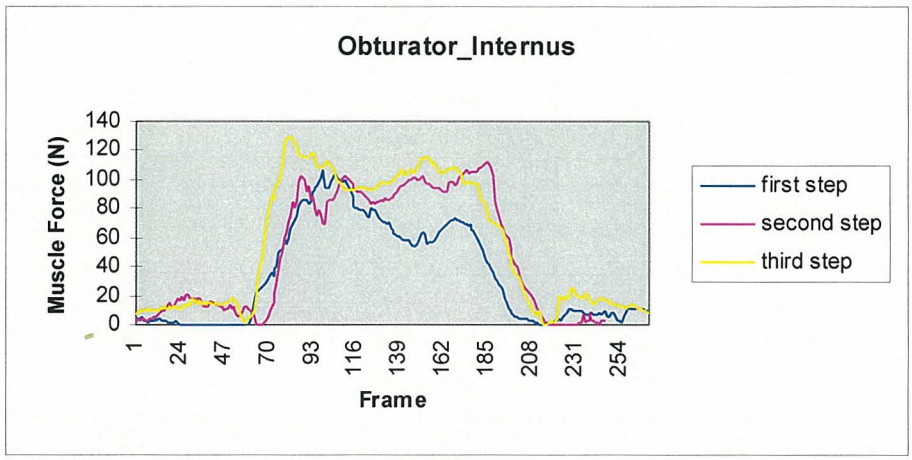

Figure 4.6.33 Step trials - Obturator Internus predicted muscle forces.

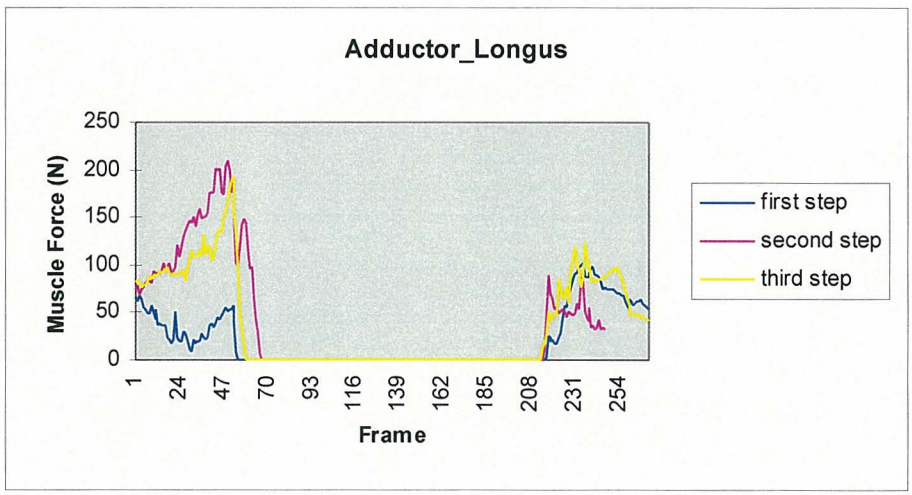

Figure 4.6.34 Step trials - Adductor Longus predicted muscle forces.

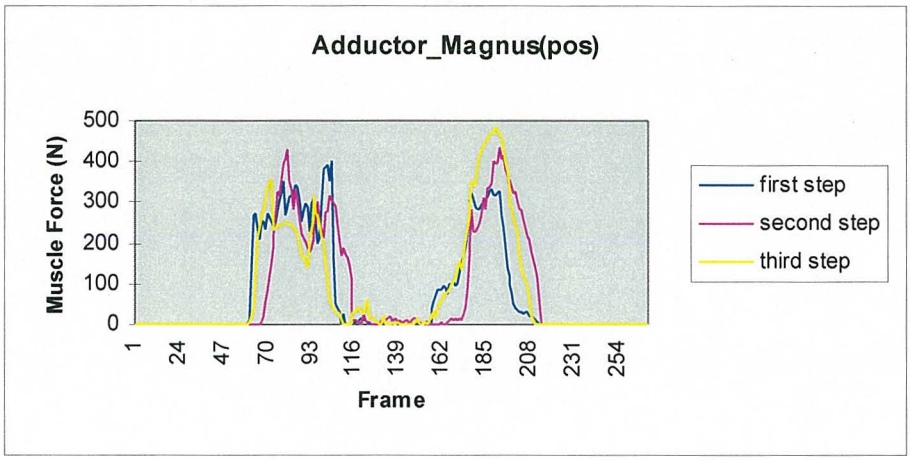

Figure 4.6.35 Step trials - Adductor Magnus(pos) predicted muscle forces.

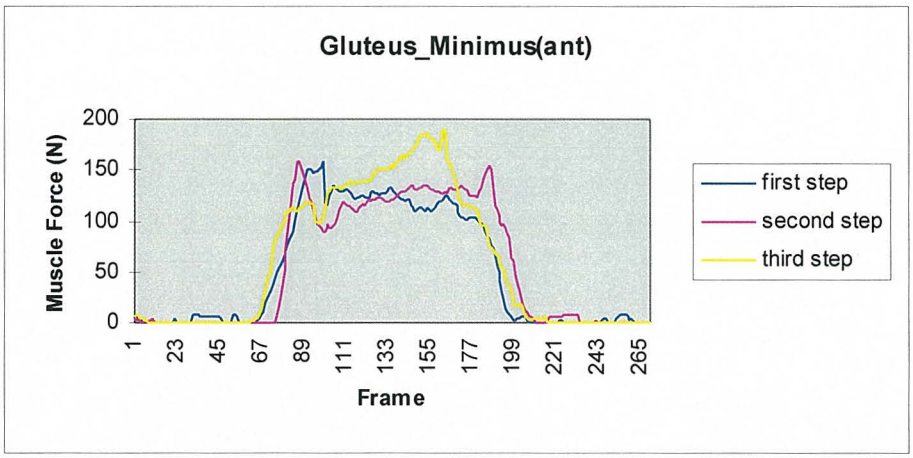

Figure 4.6.36 Step trials - Gluteus Minimus(ant) predicted muscle forces.

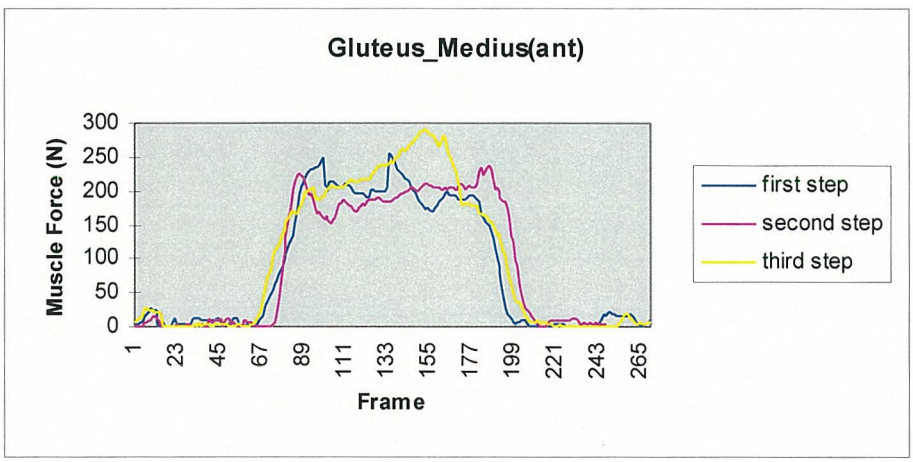

Figure 4.6.37 Step trials - Gluteus Medius(ant) predicted muscle forces.

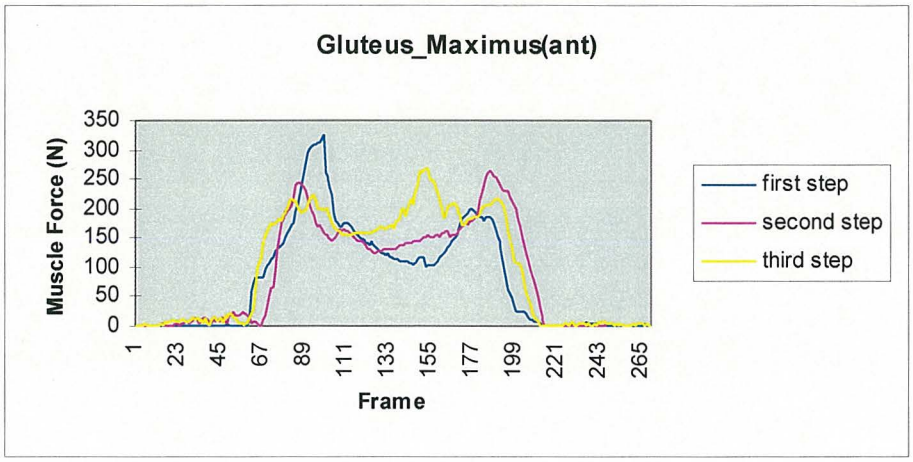

Figure 4.6.38 Step trials - Gluteus Maximus(ant) predicted muscle forces.

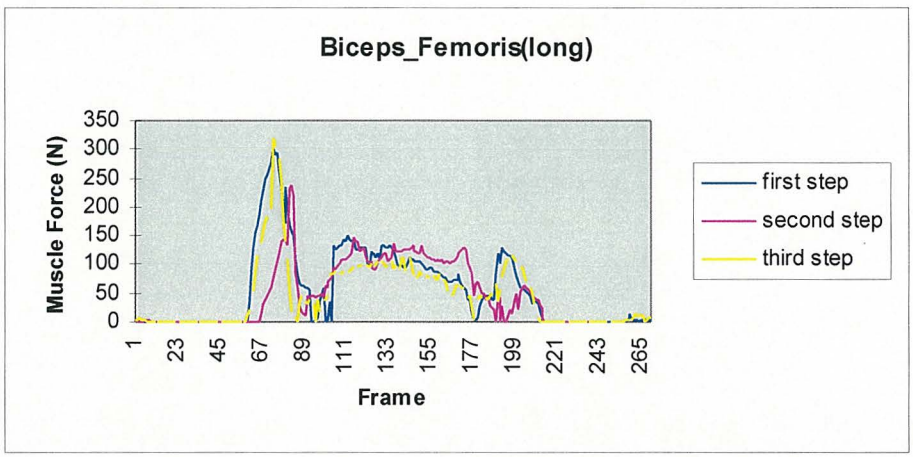

Figure 4.6.39 Step trials - Biceps Femoris(long) predicted muscle forces.

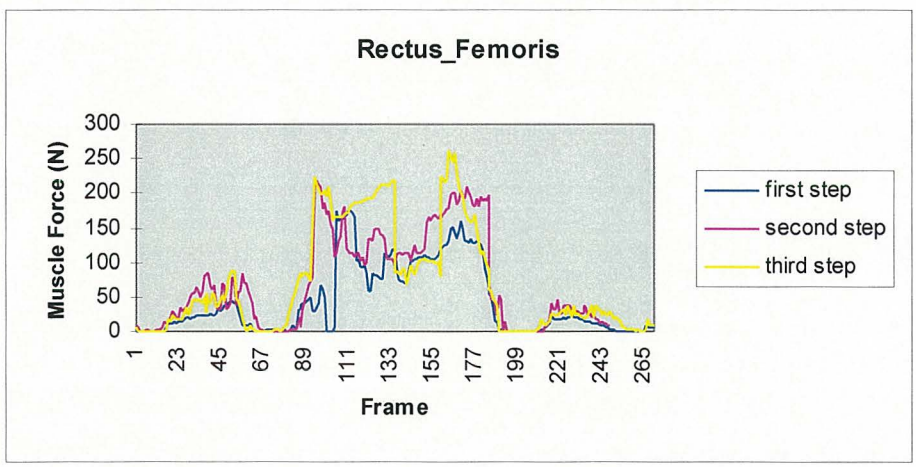

Figure 4.6.40 Step trials - Rectus Femoris predicted muscle forces.

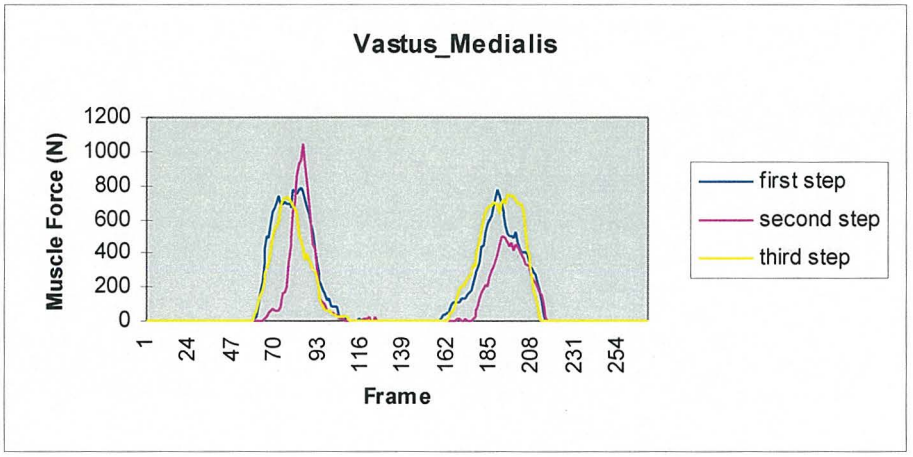

Figure 4.6.41 Step trials - Vastus Medialis predicted muscle forces.

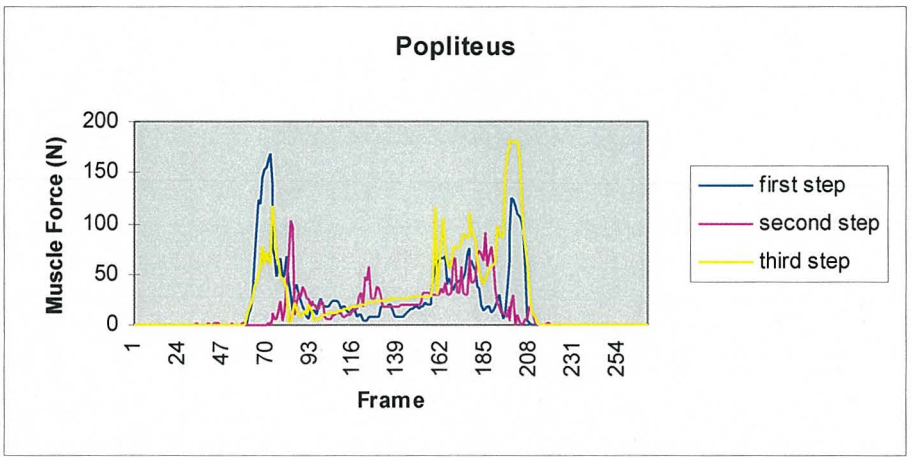

Figure 4.6.42 Step trials - Popliteus predicted muscle forces.

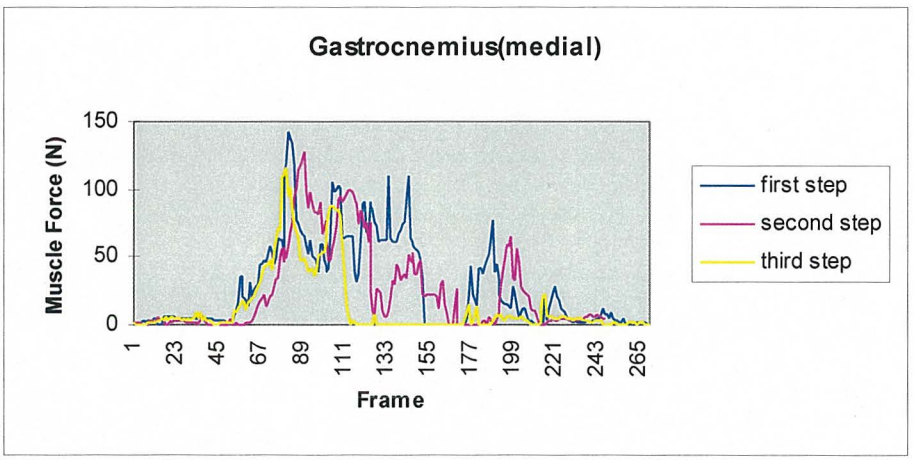

Figure 4.6.43 Step trials - Gastrocnemius(medial) predicted muscle forces.

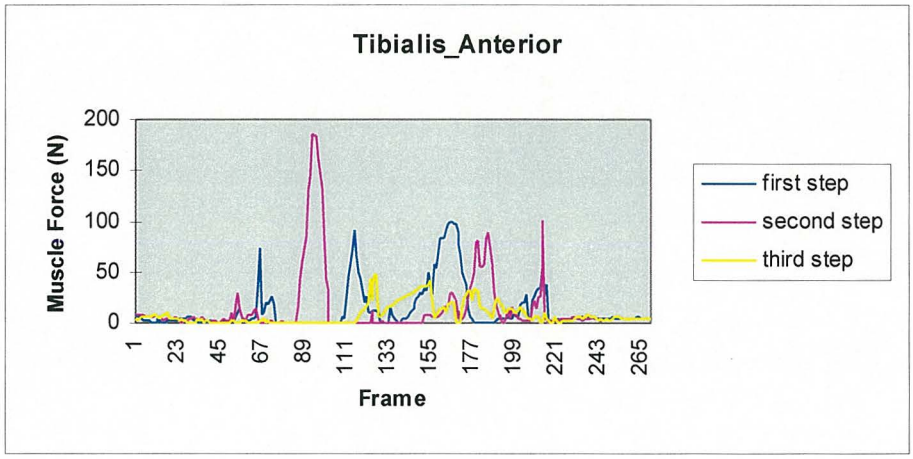

Figure 4.6.44 Step trials - Tibialis Anterior predicted muscle forces.

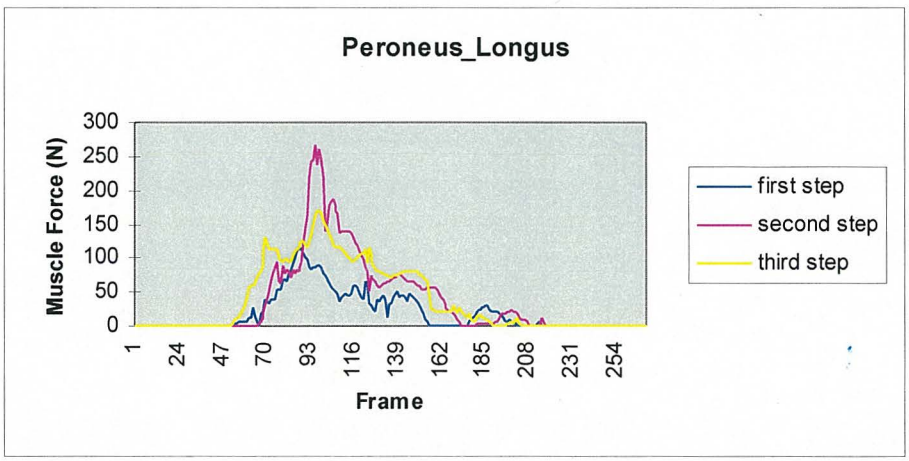

Figure 4.6.45 Step trials - Peroneus Longus predicted muscle forces.

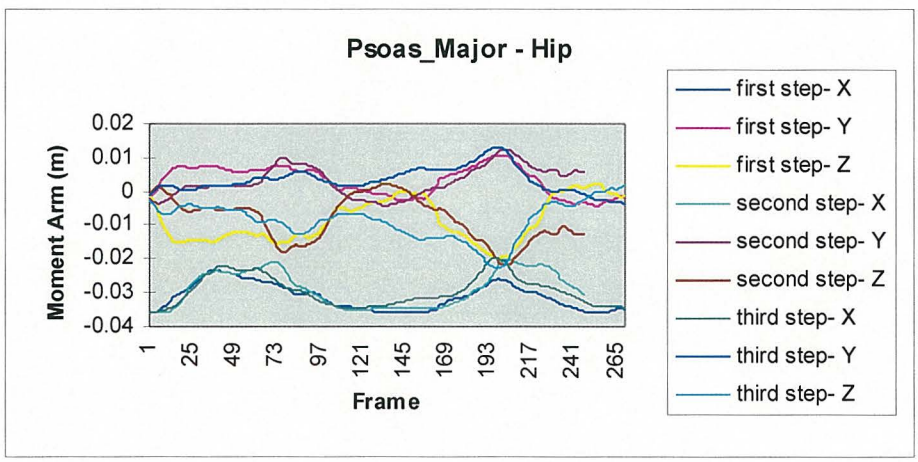

Figure 4.6.46 Step trials - Psoas major, hip moment arms.

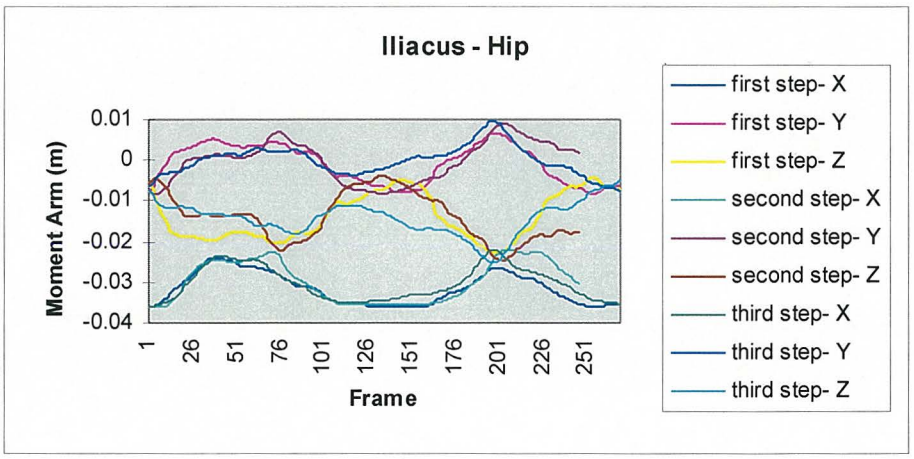

Figure 4.6.47 Step trials - Iliacus, hip moment arms.

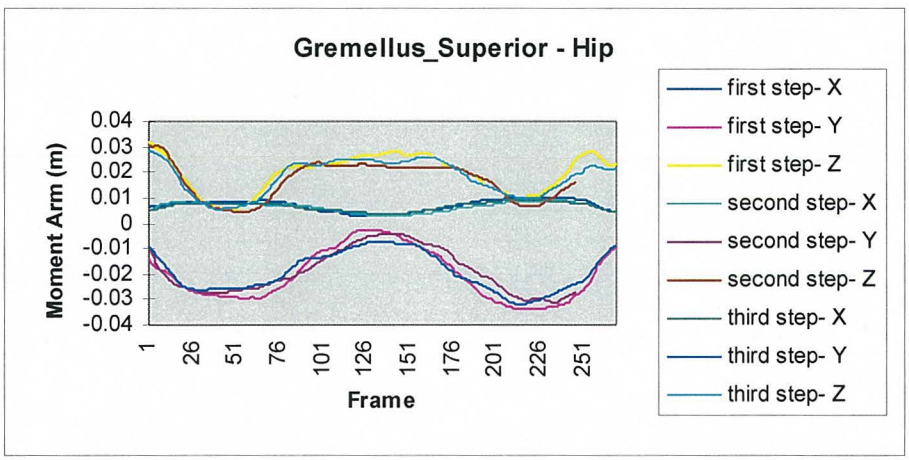

Figure 4.6.48 Step trials - Gremellus Superior, hip moment arms.

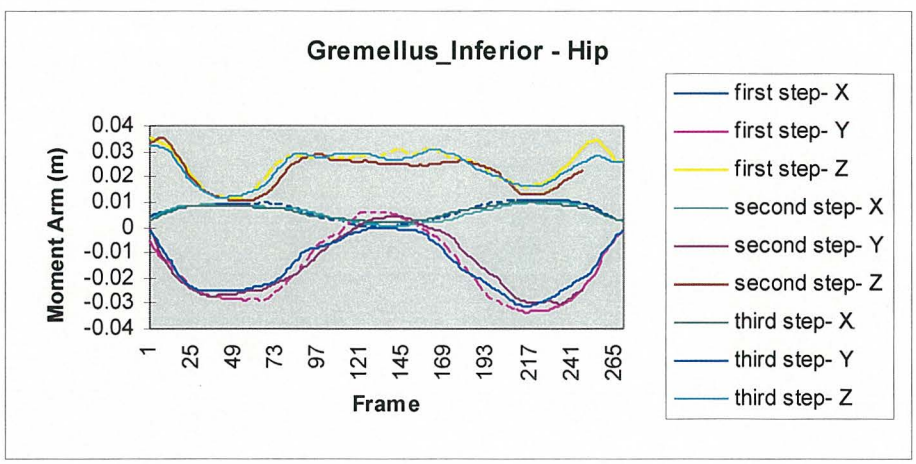

Figure 4.6.49 Step trials - Gremellus Inferior,hip moment arms.

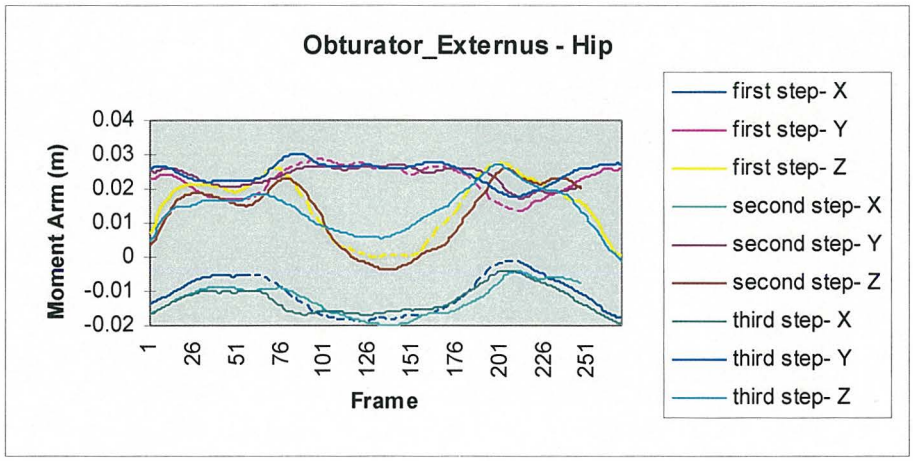

Figure 4.6.50 Step trials - Obturator Externus,hip moment arms.

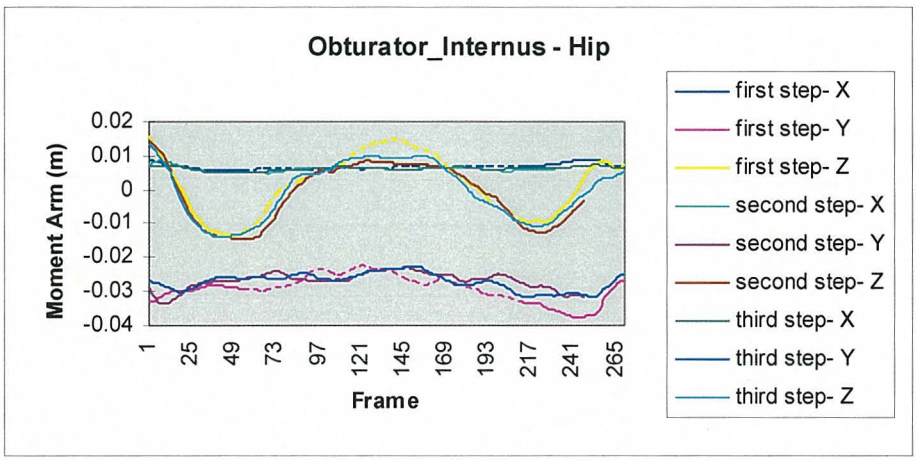

Figure 4.6.51 Step trials - Obturator Internus, hip moment arms.

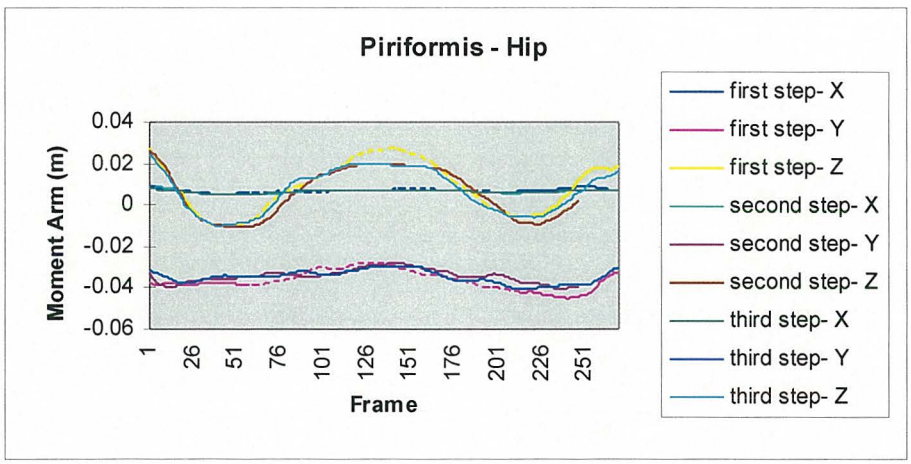

Figure 4.6.52 Step trials - Piriformis, hip moment arms.

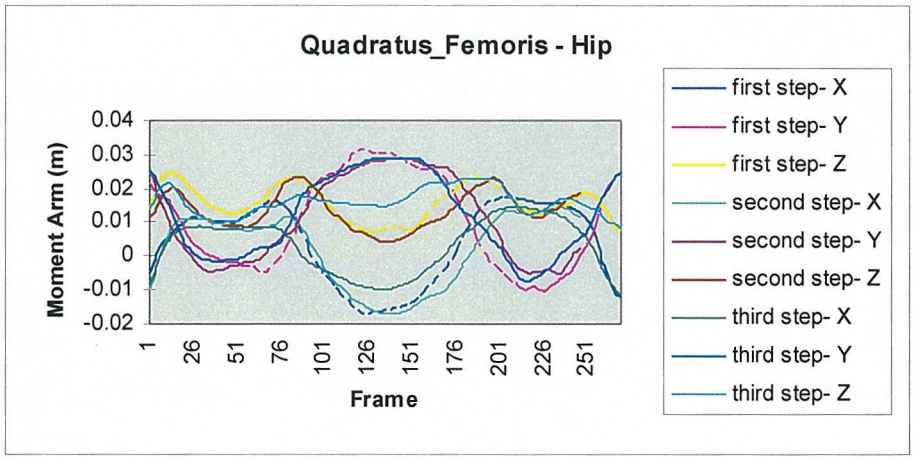

Figure 4.6.53 Step trials - Quadratus Femoris, hip moment arms.

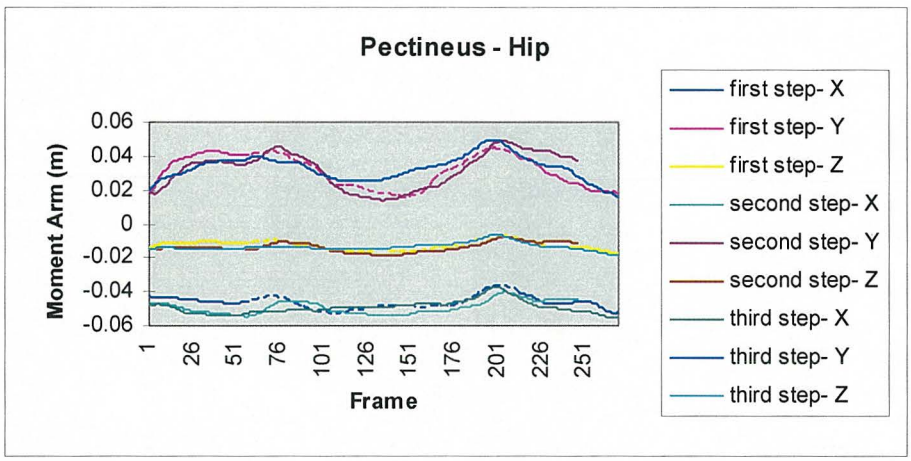

Figure 4.6.54 Step trials - Pectineus, hip moment arms.

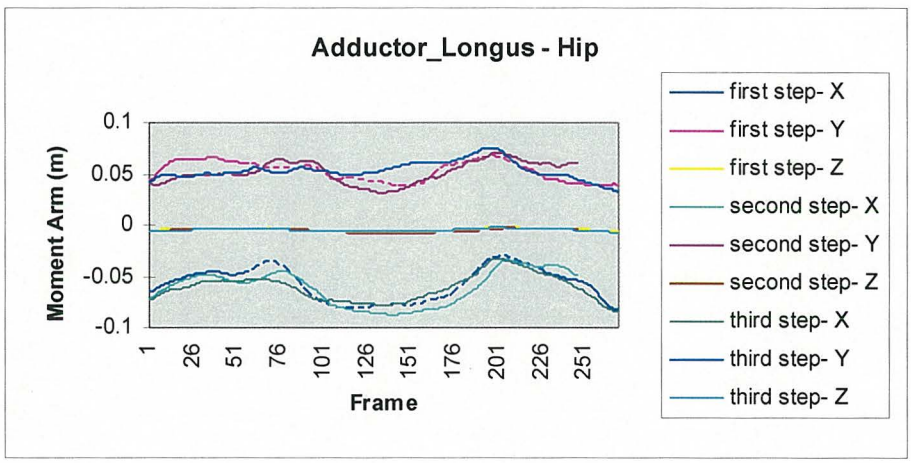

Figure 4.6.55 Step trials - Adductor Longus, hip moment arms.

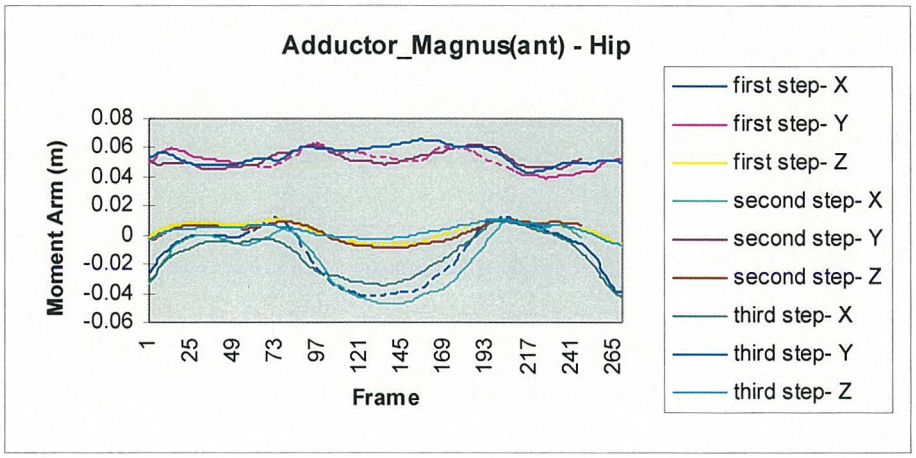

Figure 4.6.56 Step trials - Adductor Magnus(ant), hip moment arms.

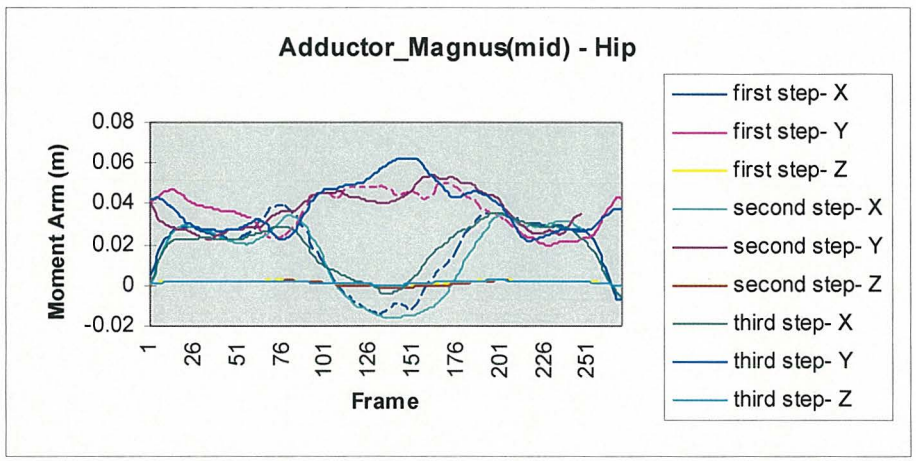

Figure 4.6.57 Step trials - Adductor Magnus(mid), hip moment arms.

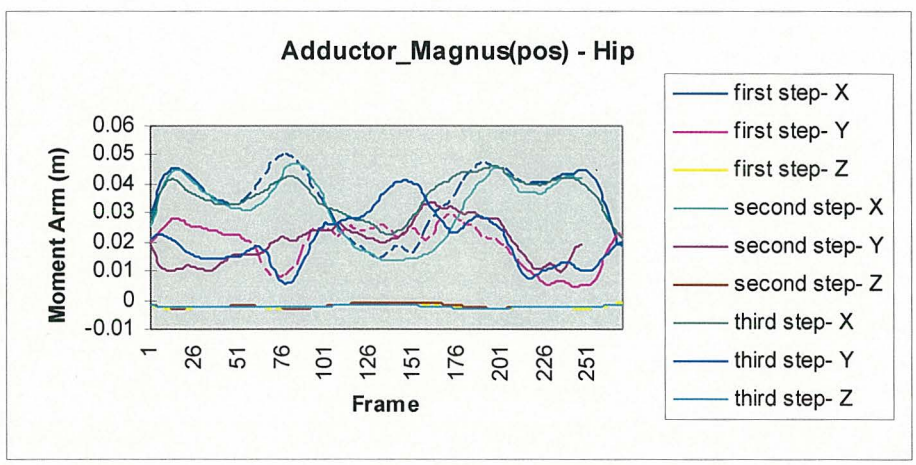

Figure 4.6.58 Step trials - Adductor Magnus(pos), hip moment arms.

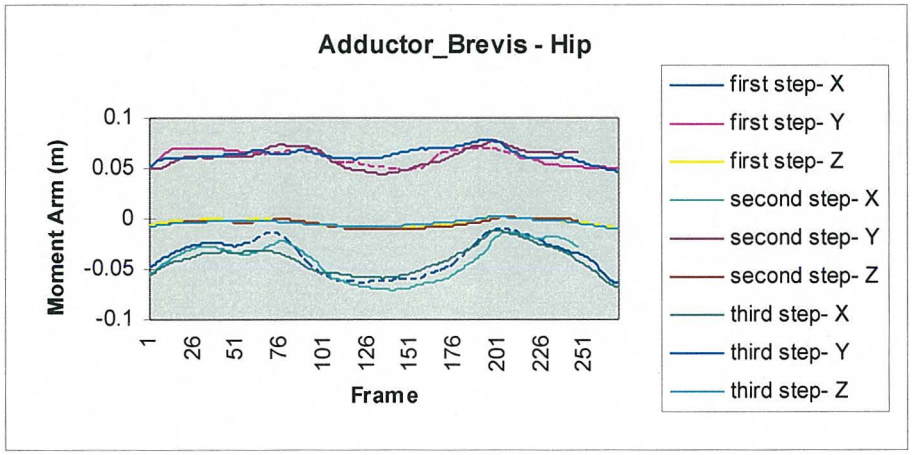

Figure 4.6.59 Step trials - Adductor Brevis, hip moment arms.

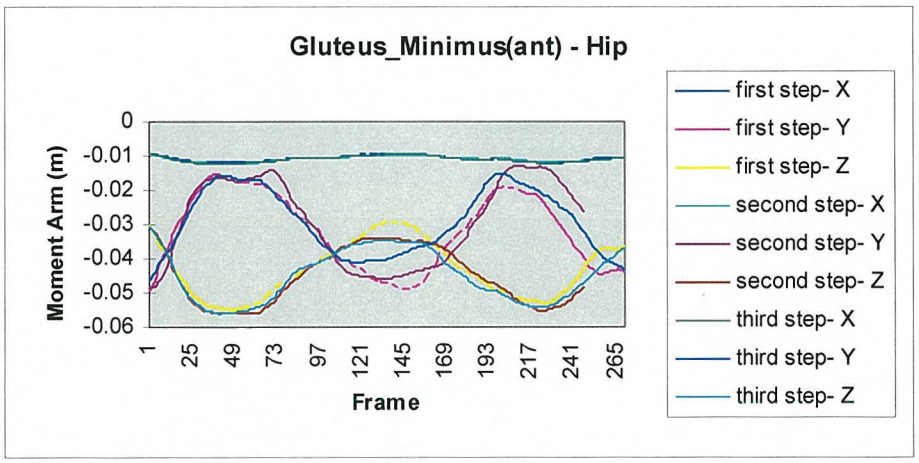

Figure 4.6.60 Step trials - Gluteus Minimus(ant), hip moment arms.

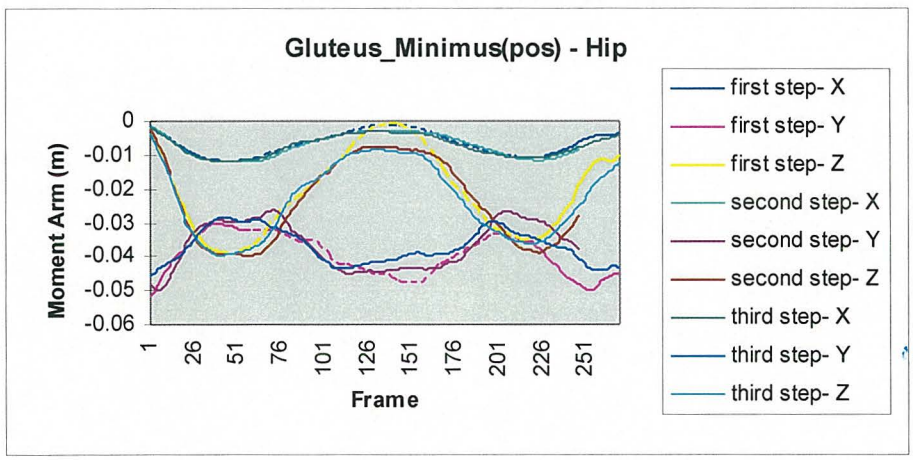

Figure 4.6.61 Step trials - Gluteus Minimus(post), hip moment arms.

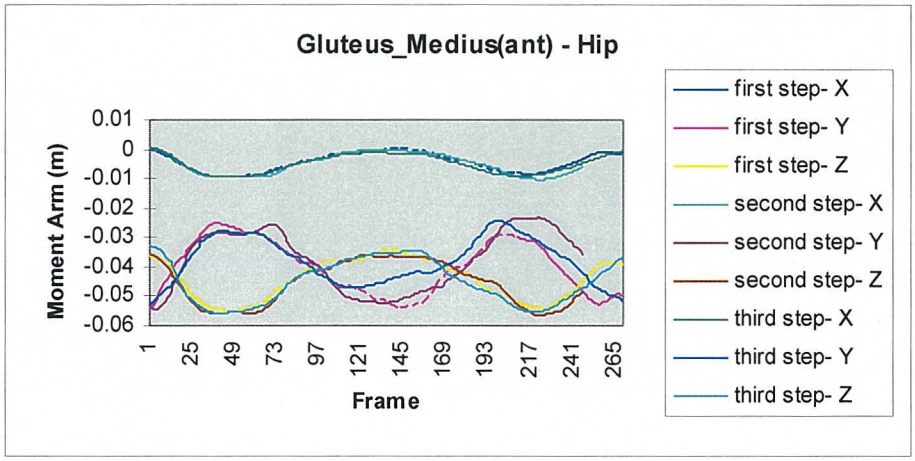

Figure 4.6.62 Step trials - Gluteus Medius(ant) hip moment arms.

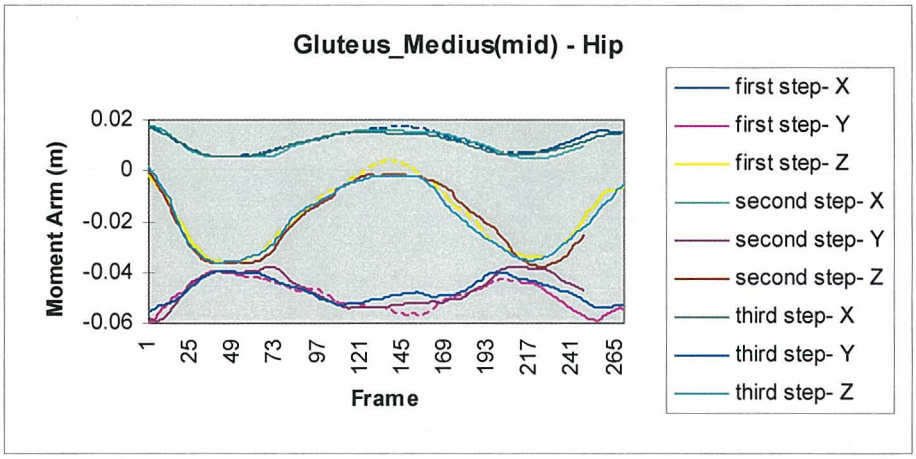

Figure 4.6.63 Step trials - Gluteus Medius(mid) hip moment arms.

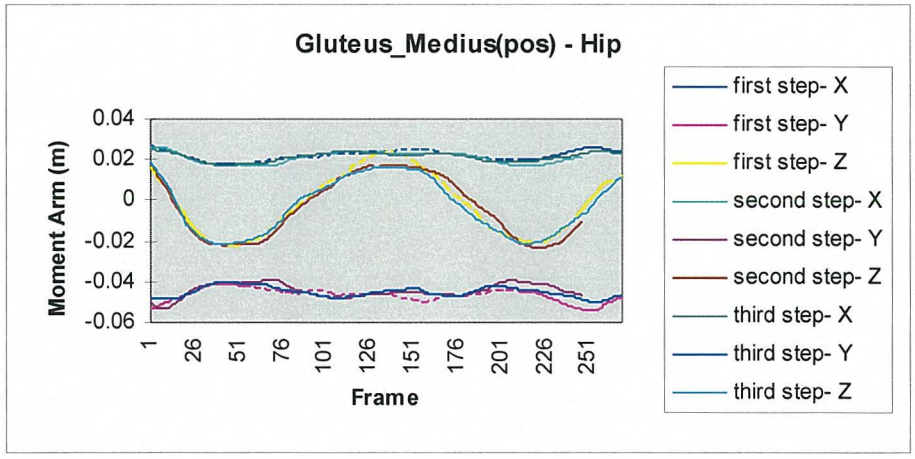

Figure 4.6.64 Step trials - Gluteus Medius(post), hip moment arms.

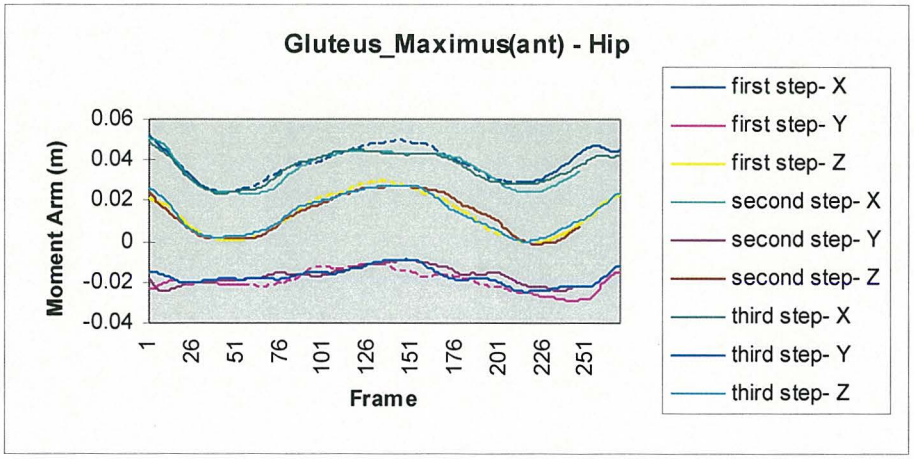

Figure 4.6.65 Step trials - Gluteus Maximus(ant), hip moment arms.

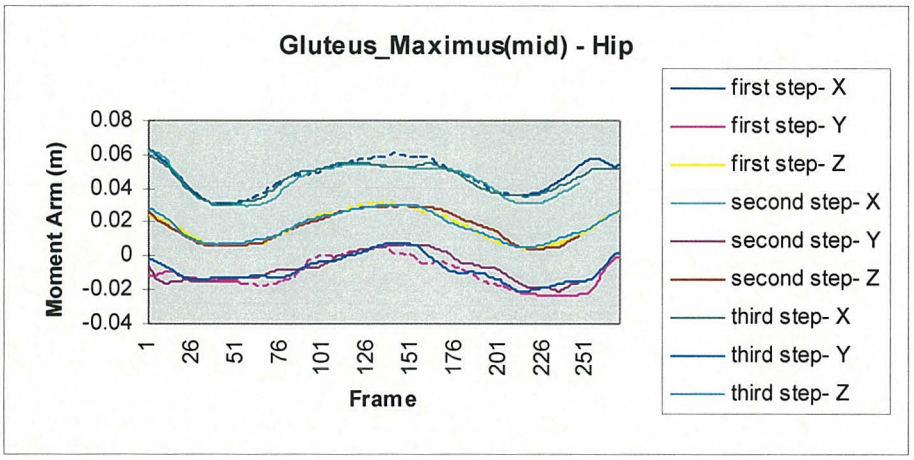

Figure 4.6.66 Step trials - Gluteus Maximus(mid), hip moment arms.

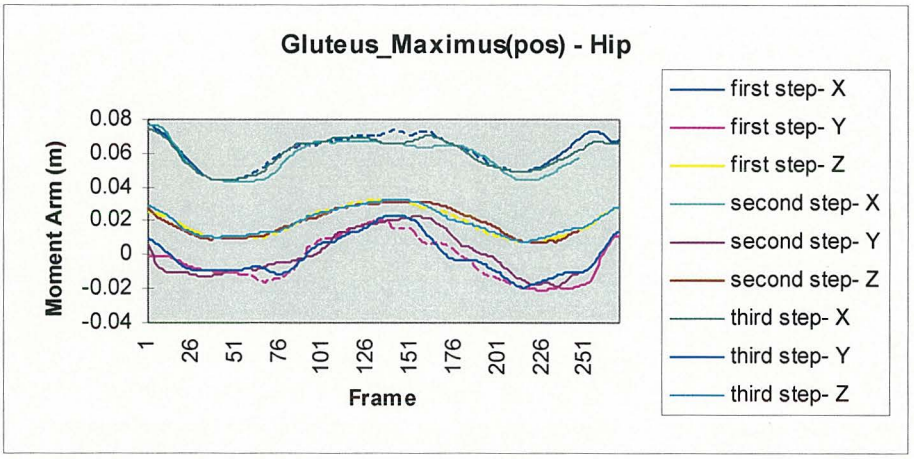

Figure 4.6.67 Step trials - Gluteus Maximus(post), hip moment arms.

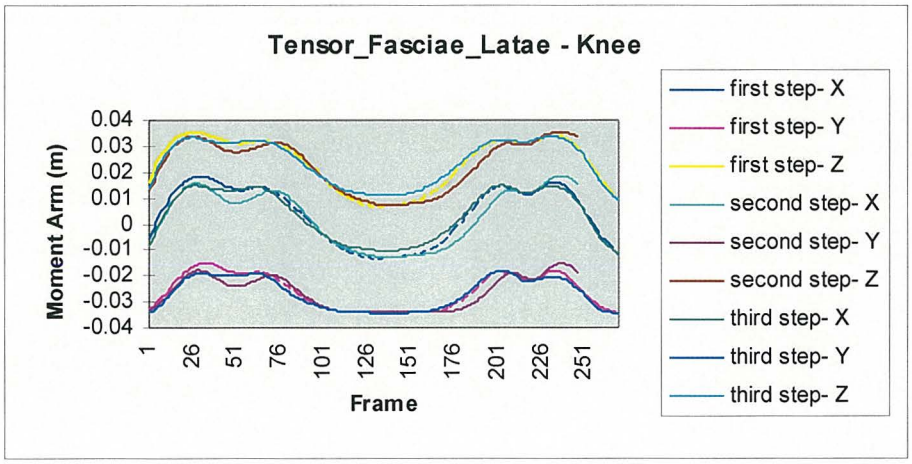

Figure 4.6.68 Step trials - Tensor Fasciae Latae, knee moment arms.

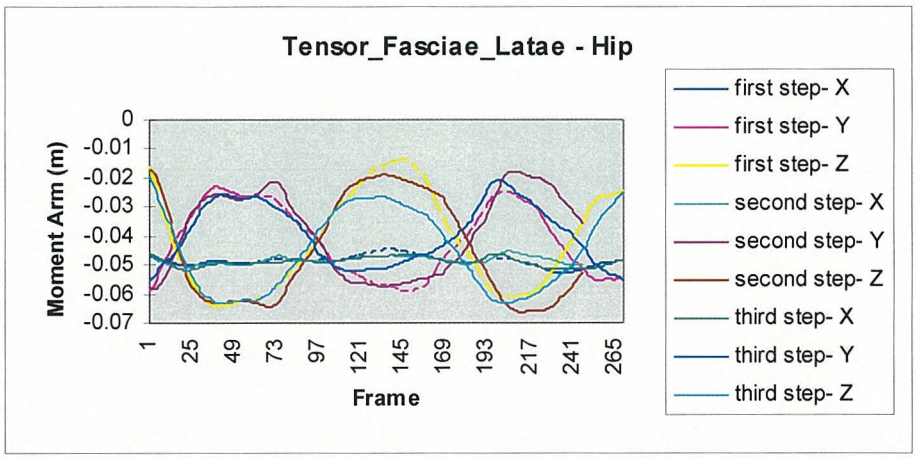

Figure 4.6.69 Step trials - Tensor Fasciae Latae, hip moment arms.

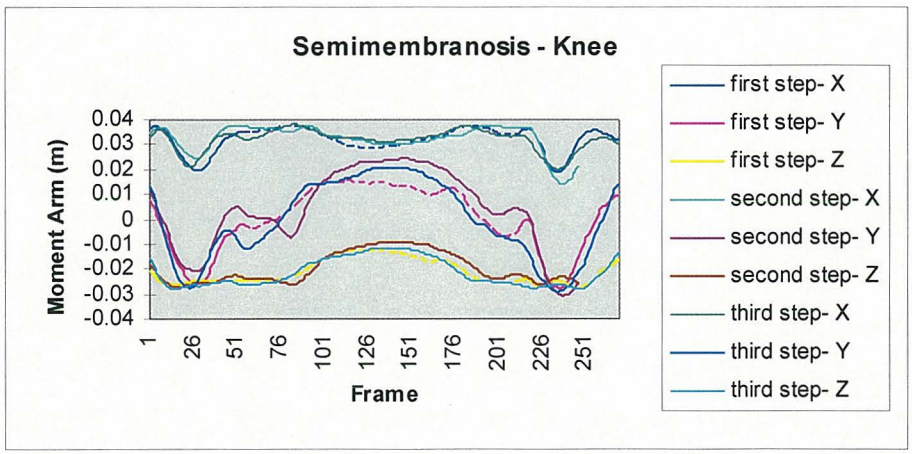

Figure 4.6.70 Step trials - Semimembranosis, knee moment arms.

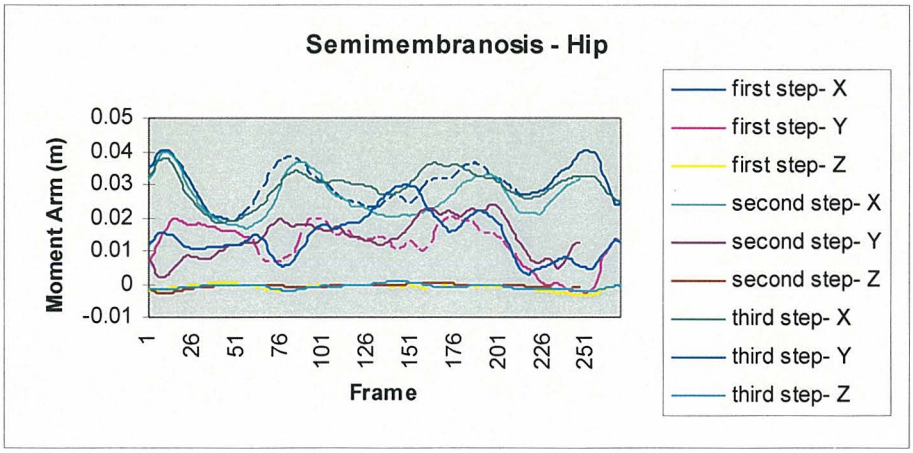

Figure 4.6.71 Step trials - Semimembranosis, hip moment arms.

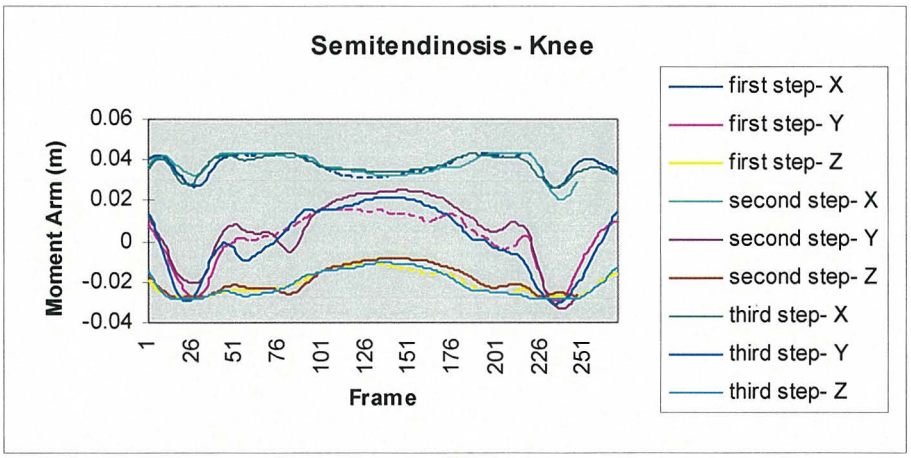

Figure 4.6.72 Step trials - Semitendinosus, knee moment arms.

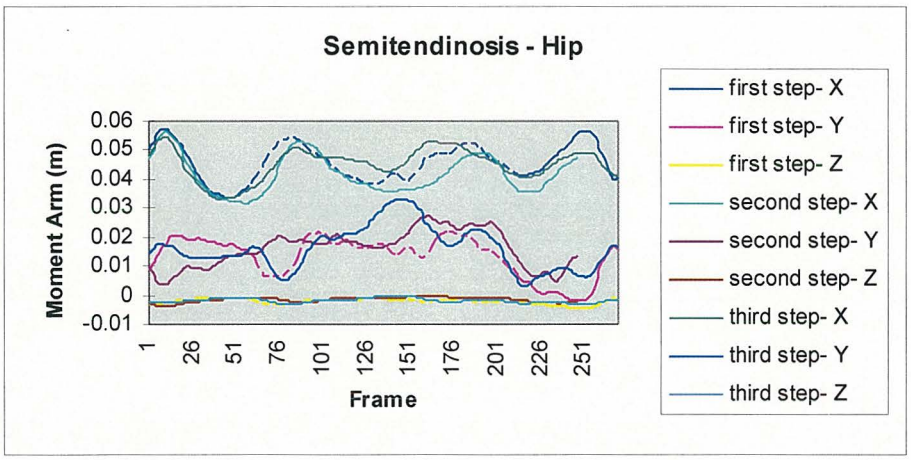

Figure 4.6.73 Step trials - Semitendinosus, hip moment arms.

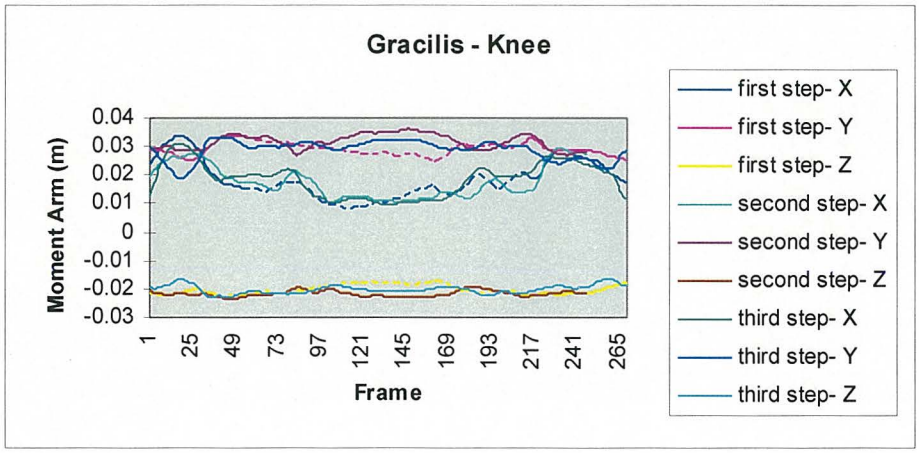

Figure 4.6.74 Step trials - Gracilis, knee moment arms.

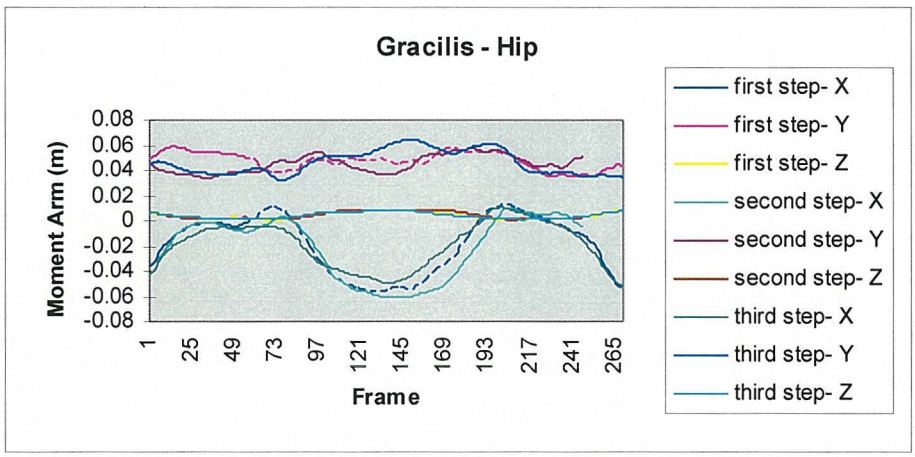

Figure 4.6.75 Step trials - Gracilis, hip moment arms.

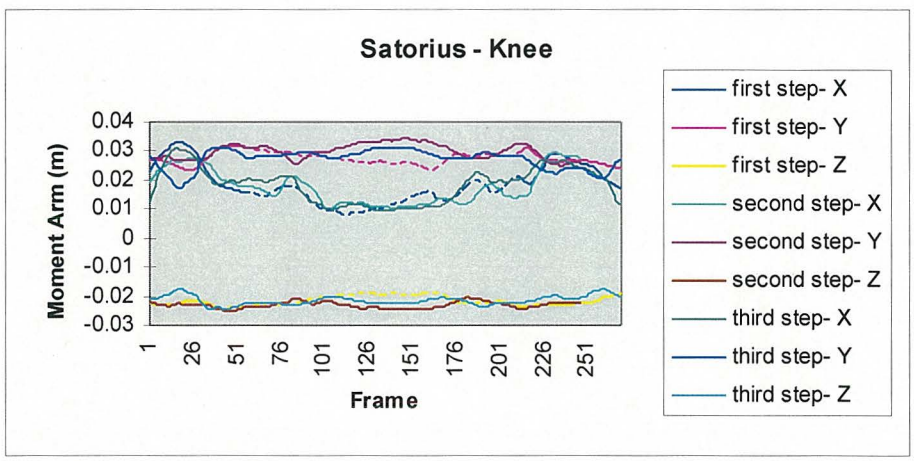

Figure 4.6.76 Step trials - Satorius, knee moment arms.

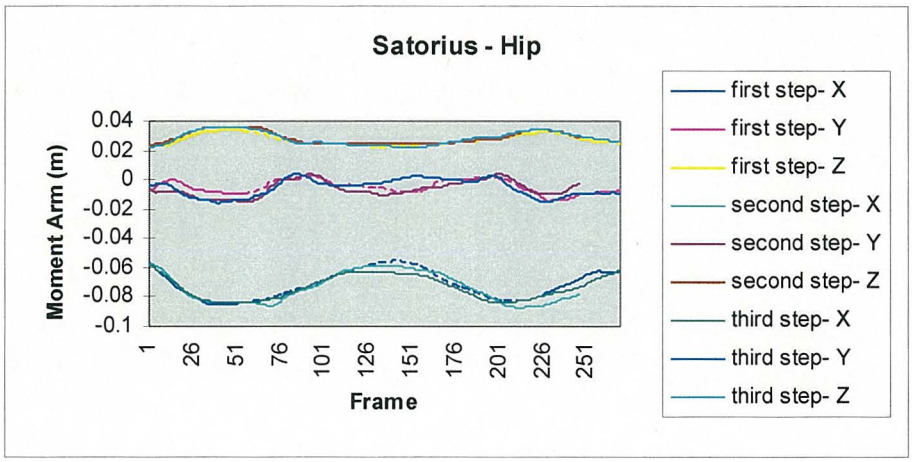

Figure 4.6.77 Step trials - Satorius, hip moment arms.

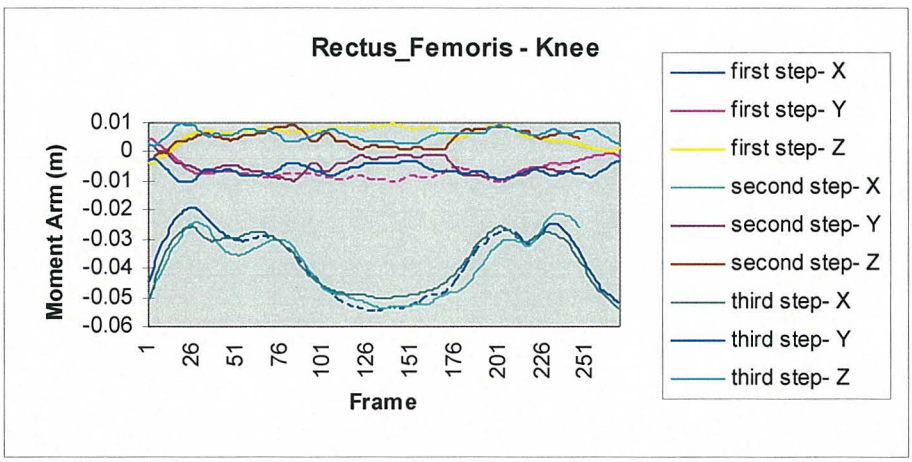

Figure 4.6.78 Step trials - Rectus Femoris, knee moment arms.

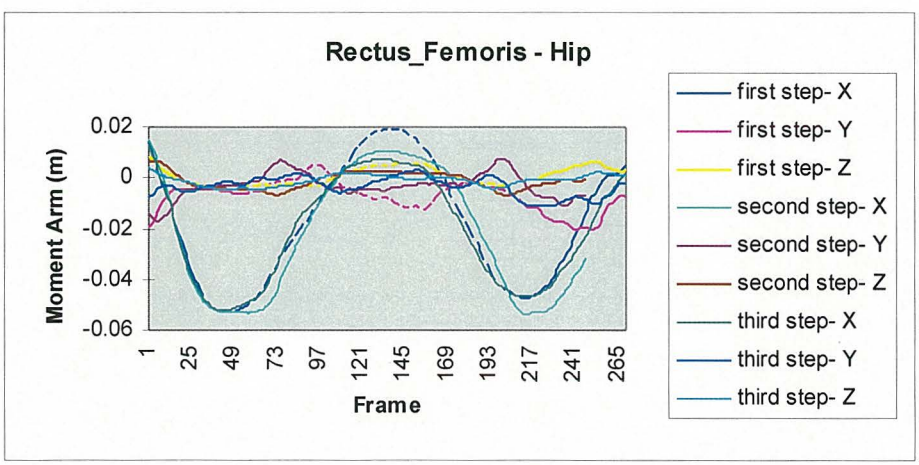

Figure 4.6.79 Step trials - Rectus Femoris, hip moment arms.

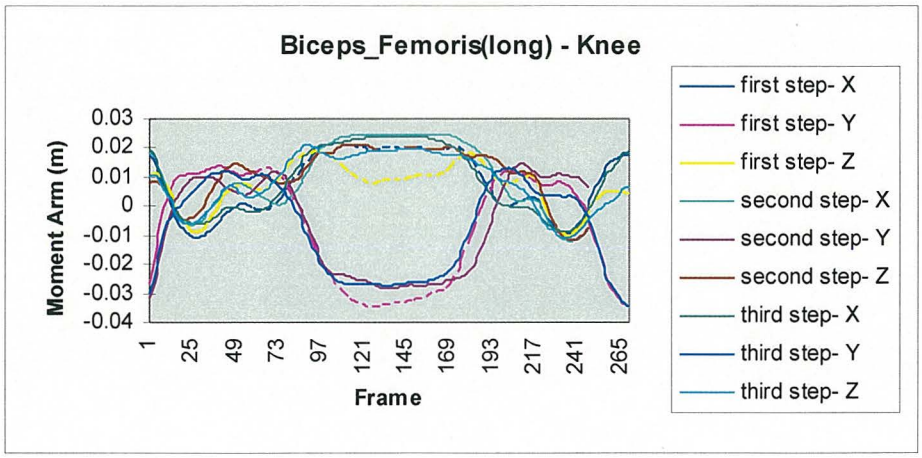

Figure 4.6.80 Step trials - Biceps Femoris(long), knee moment arms.

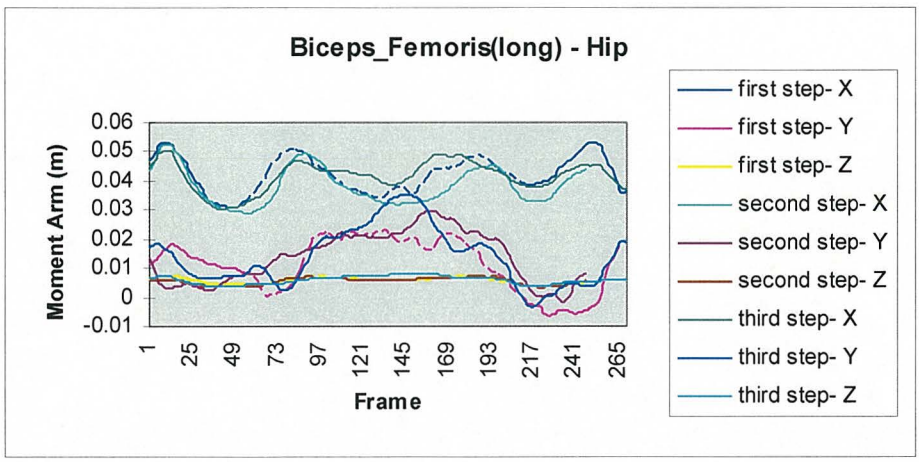

Figure 4.6.81 Step trials - Biceps Femoris(long), hip moment arms.

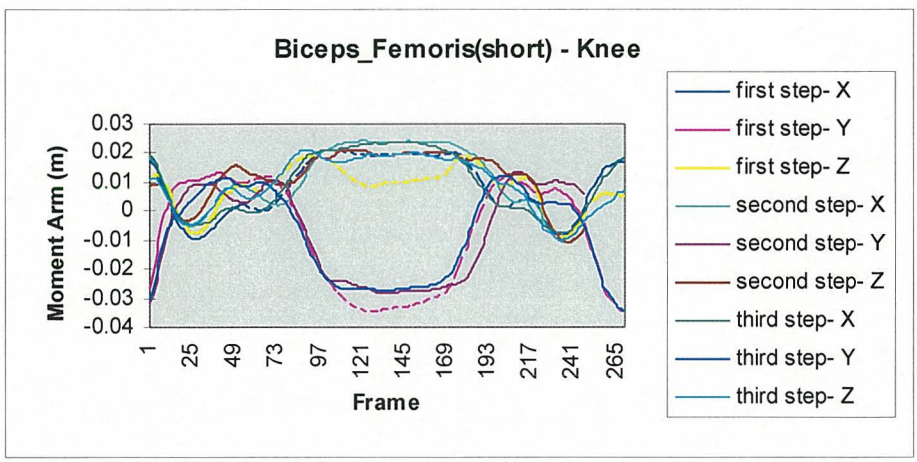

Figure 4.6.82 Step trials - Biceps Femoris(short), knee moment arms.

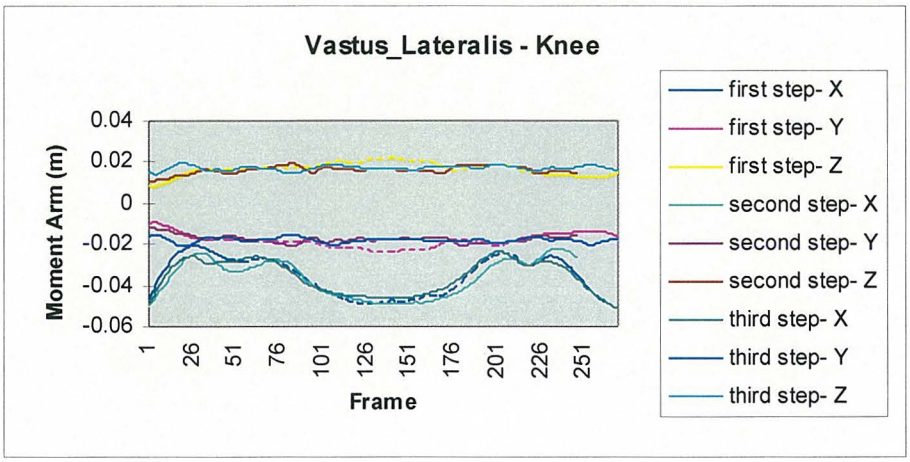

Figure 4.6.83 Step trials - Vastus Lateralis, knee moment arms.

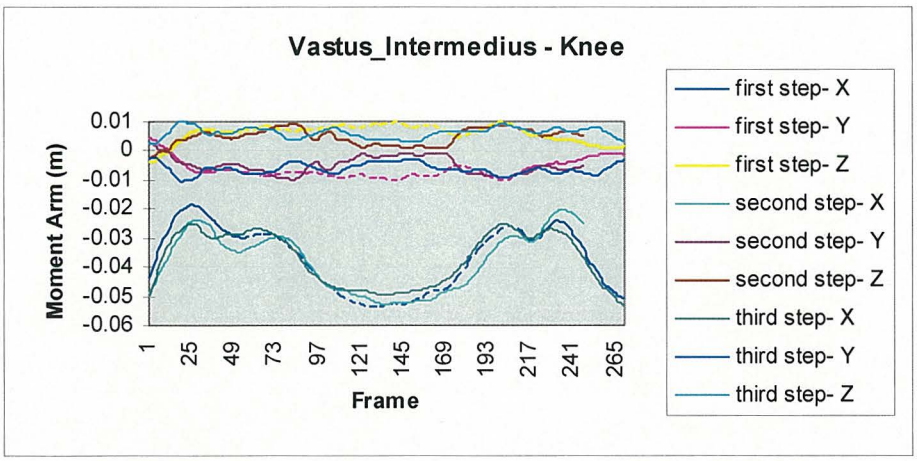

Figure 4.6.84 Step trials - Vastus Intermedius, knee moment arms.

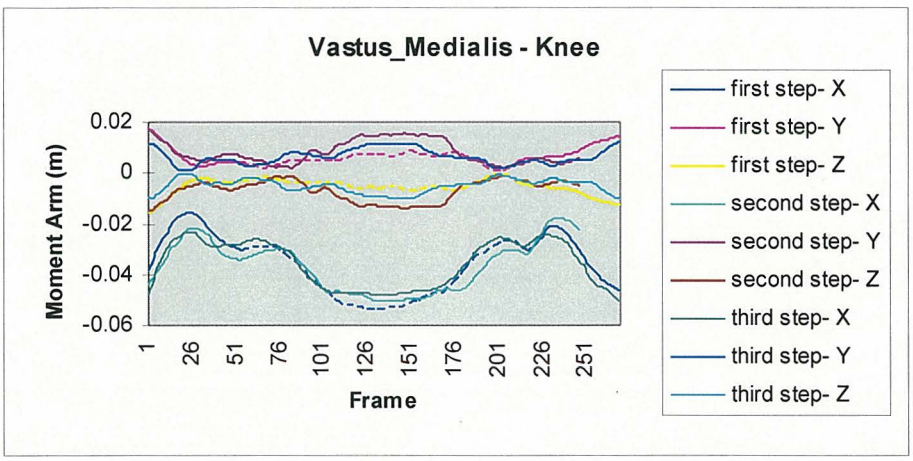

Figure 4.6.85 Step trials - Vastus Medialis, knee moment arms.

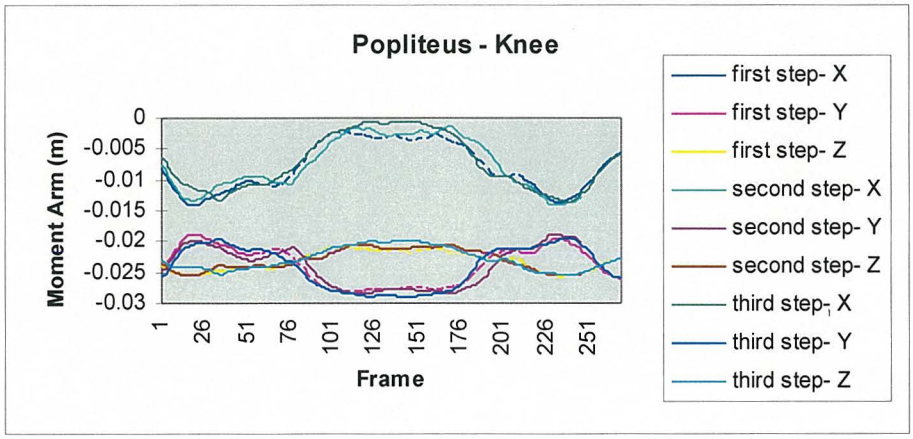

Figure 4.6.86 Step trials - Popliteus, knee moment arms.

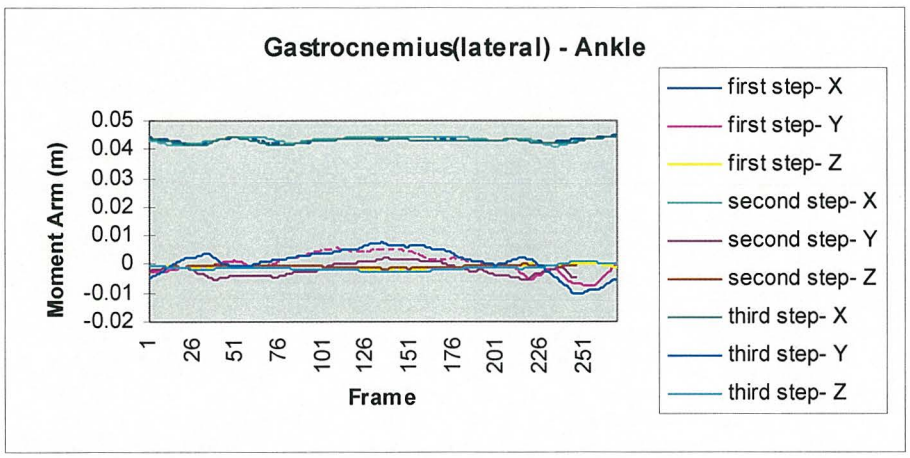

Figure 4.6.87 Step trials - Gastrocnemius(lat), ankle moment arms.

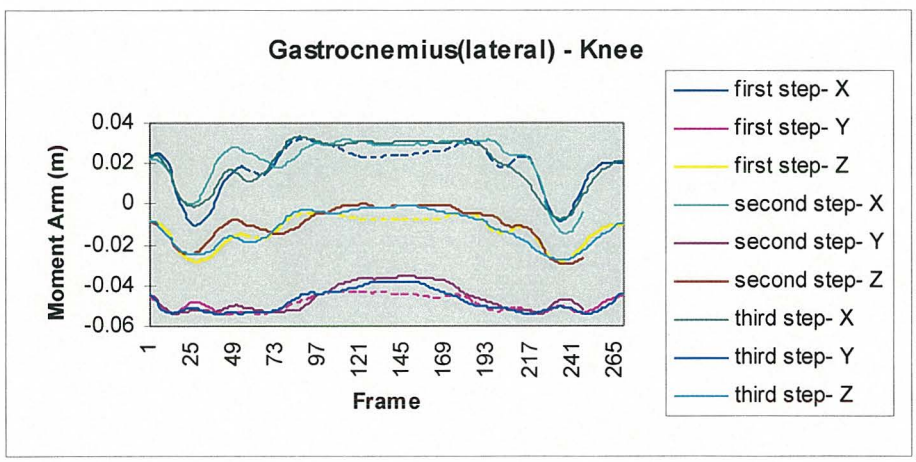

Figure 4.6.88 Step trials - Gastrocnemius(lat), knee moment arms.

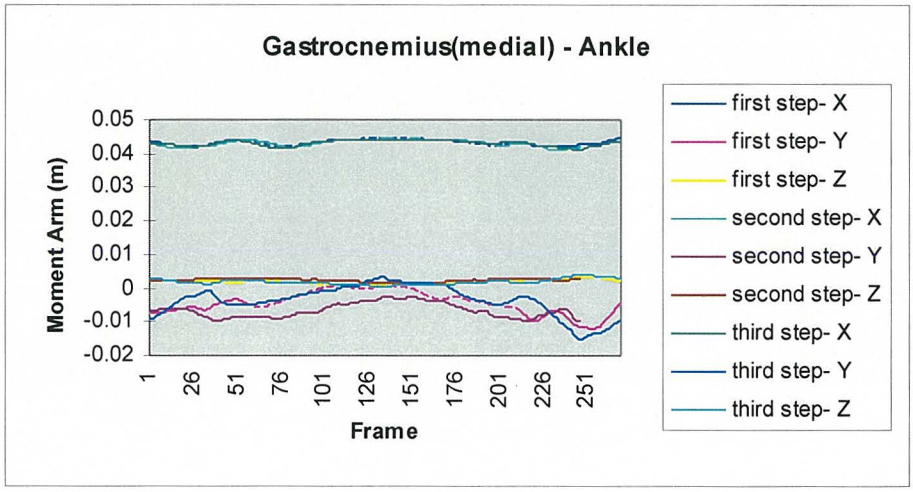

Figure 4.6.89 Step trials - Gastrocnemius(med), ankle moment arms.

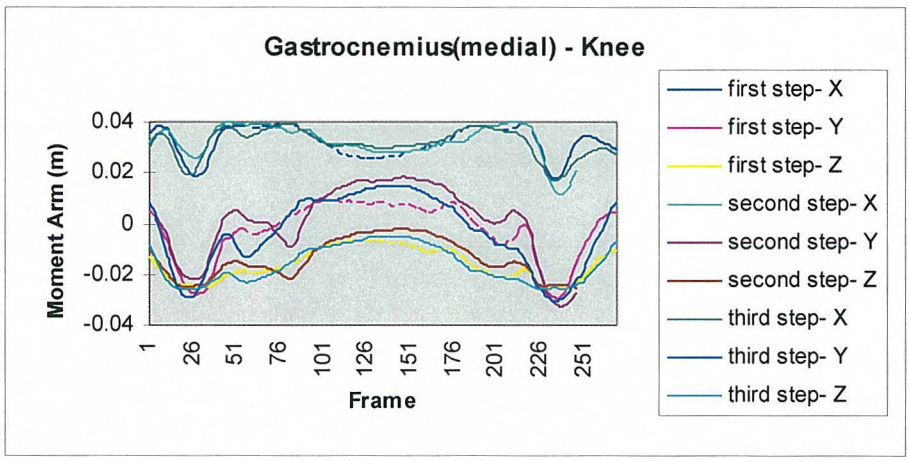

Figure 4.6.90 Step trials - Gastrocnemius(med), knee moment arms.

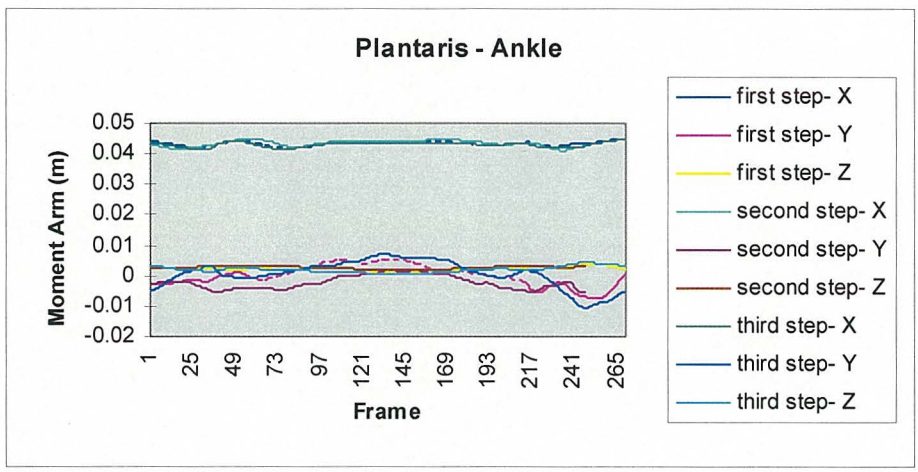

Figure 4.6.91 Step trials - Plantaris, ankle moment arms.

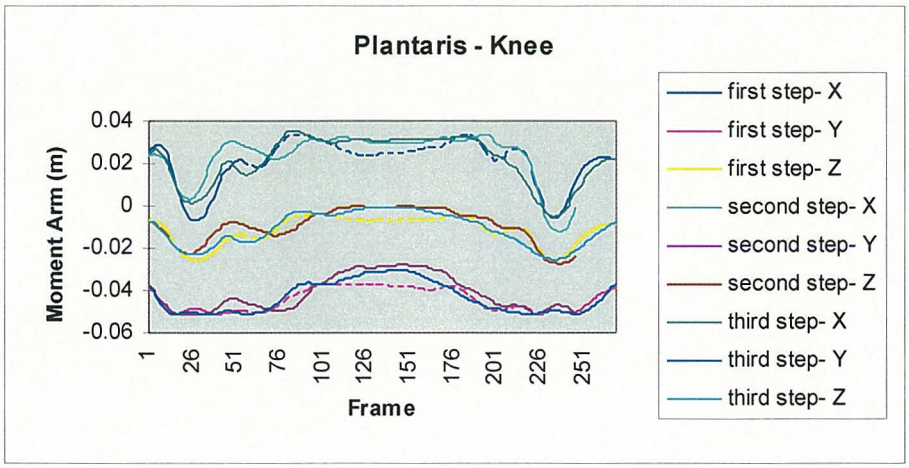

Figure 4.6.92 Step trials - Plantaris, knee moment arms.

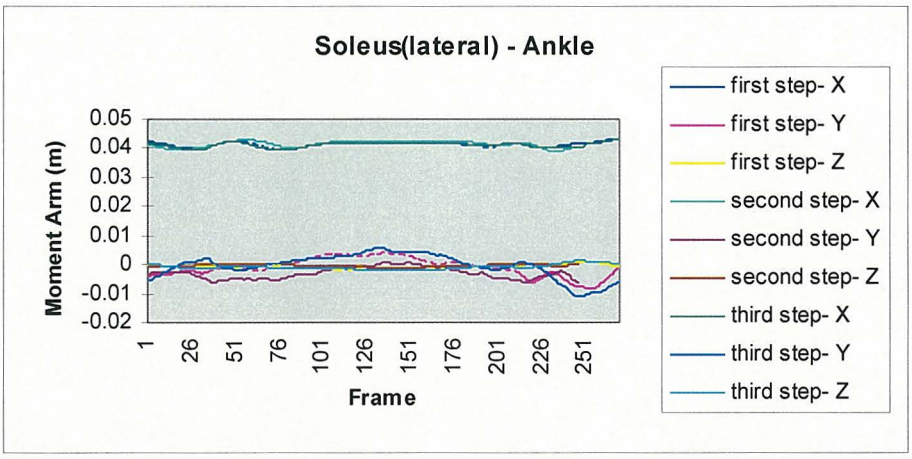

Figure 4.6.93 Step trials - Soleus(lat), ankle moment arms.

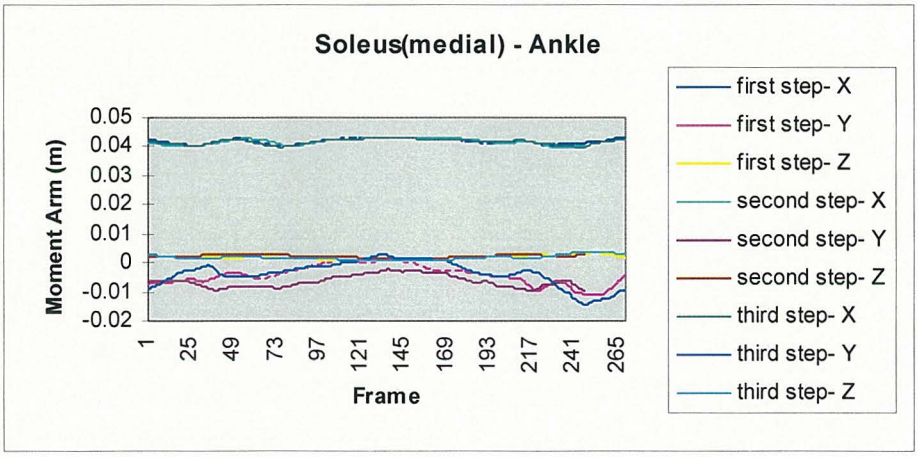

Figure 4.6.94 Step trials - Soleus(med), ankle moment arms.

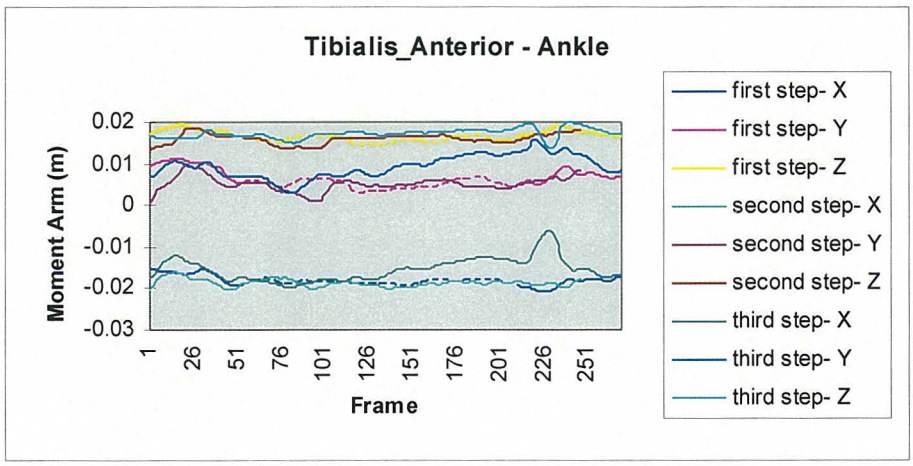

Figure 4.6.95 Step trials - Tibialis Anterior, ankle moment arms.

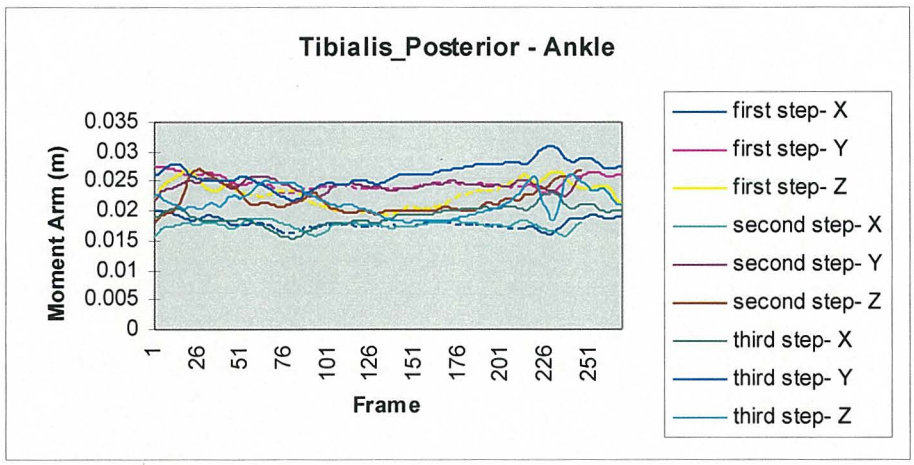

Figure 4.6.96 Step trials - Tibialis Posterior, ankle moment arms.

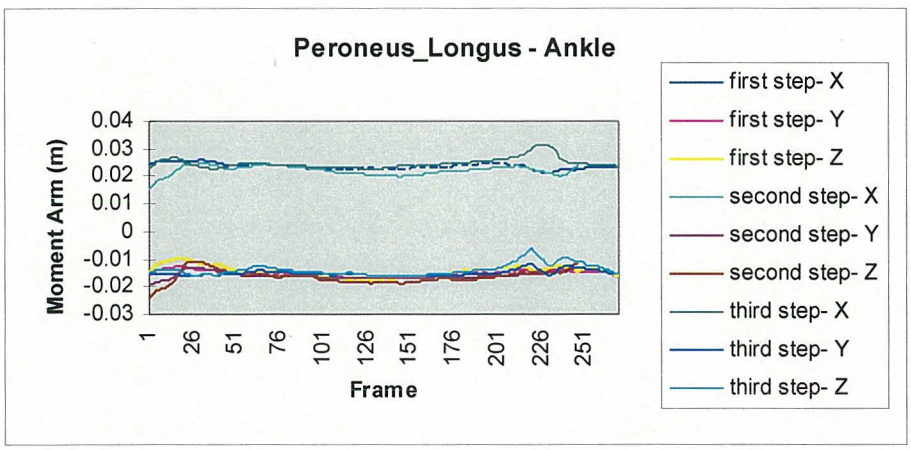

Figure 4.6.97 Step trials - Peroneus Longus, ankle moment arms.

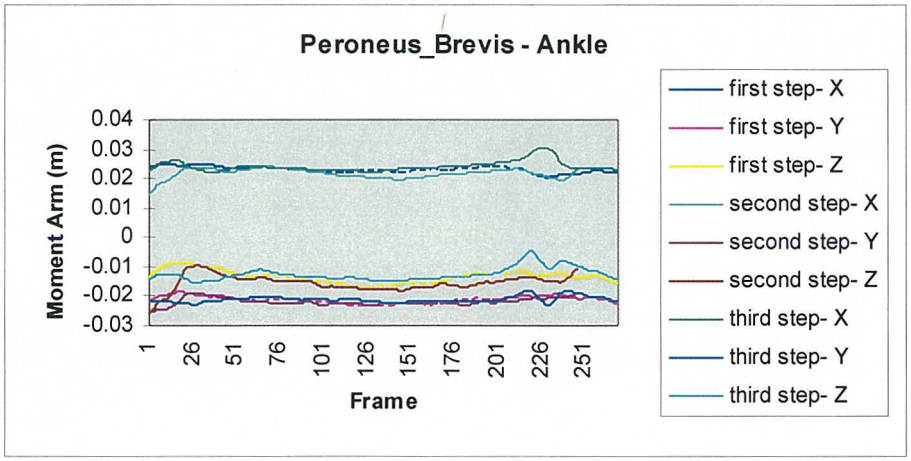

Figure 4.6.98 Step trials - Peroneus Brevis, ankle moment arms.

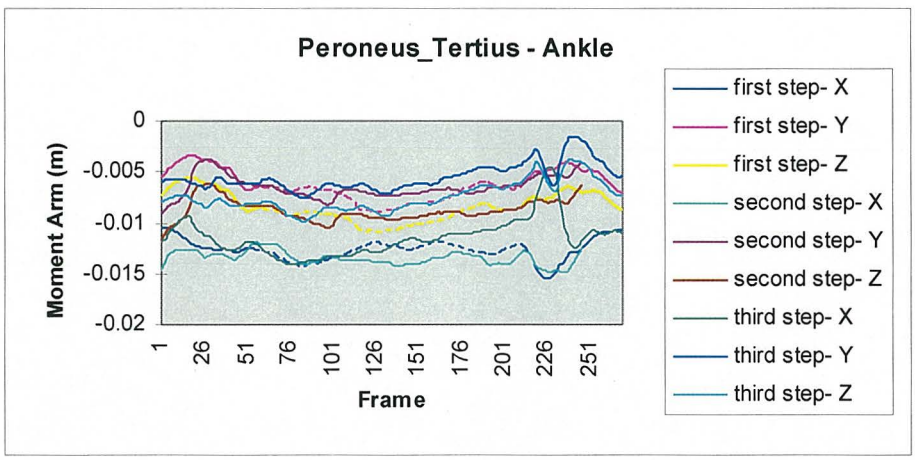

Figure 4.6.99 Step trials - Peroneus Tertius, ankle moment arms.

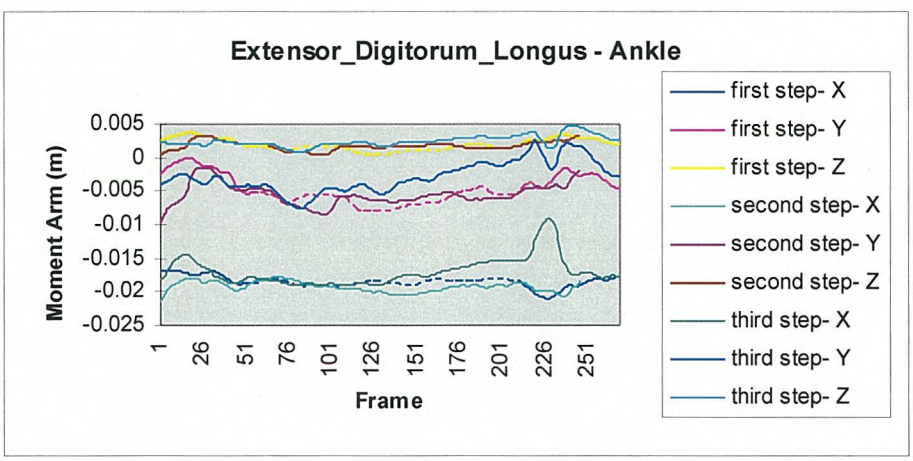

Figure 4.6.100 Step trials - Ext.Digitorum Longus, ankle moment arms.

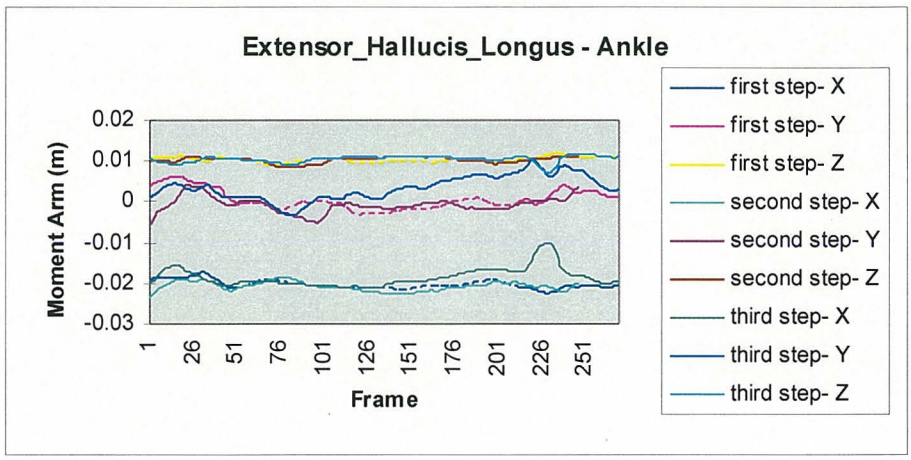

Figure 4.6.101 Step trials - Ext.Hallucis Longus, ankle moment arms.

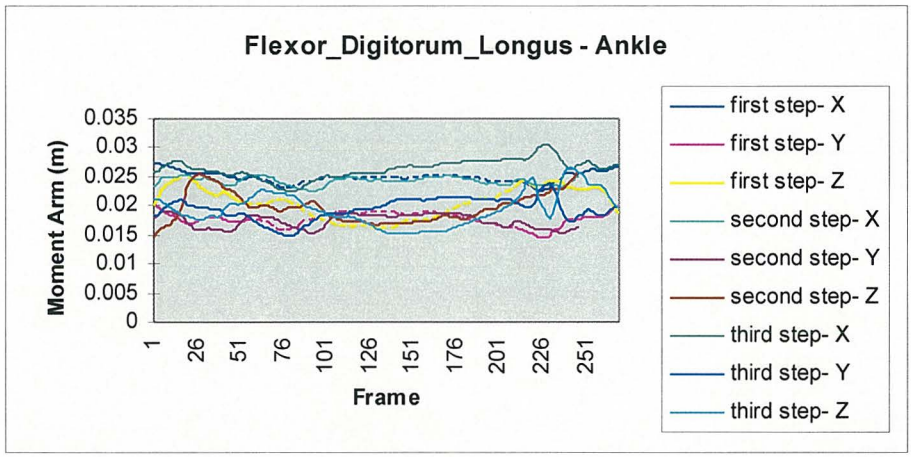

Figure 4.6.102 Step trials - Flex.Digitorum Longus, ankle moment arms.

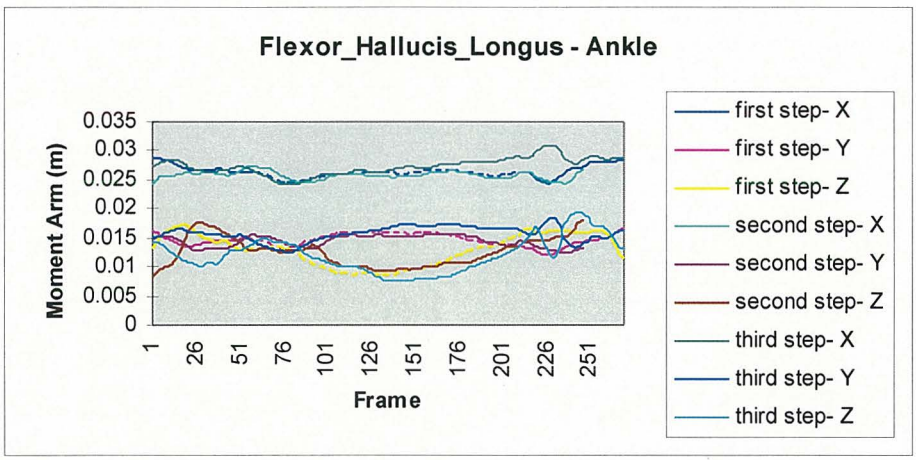

Figure 4.6.103 Step trials - Flex.Hallucis Longus, ankle moment arms.

4.7 Electromyography

Results of electromyography (EMG) analysis for eight muscle of the lower limb during the walk and step trials are presented. For each muscle recorded the EMG signal following filtering and following full wave rectification are presented. A Butterworth digital filter was used for all EMG signals, with a band-pass of 30-450 Hz. The threshold value was the largest sum of mean signal plus three standard deviations calculated from all 50 ms windows of the full wave rectified EMG signal. For all EMG signals an on-set occurred if the full wave rectified EMG signal was above the threshold for 50 ms while on offset occurred if the full wave rectified EMG signal was below the threshold for 100 ms.

For the walk trials, results for both filtered and full wave rectified EMG for the eight muscle of the lower limb, are presented in Figures 4.7.1 - 4.7.48. Displayed with the filtered EMG results for the walk trials are toe-off and heel strike occurrences, while for the step trials the floor and step toe-off as well as step and ground contact occurrences are displayed. Displayed with the results of full wave rectified EMG are calculated on-sets and offset of electrical activity for each trial. On-sets and offset of electrical activity are also presented in tabular form for each walk trial in Tables 3.7.1 - 3.7.3, along with the base-line signal used in their calculation and the RMS for the electrical signal during each interval between on-sets and offset.

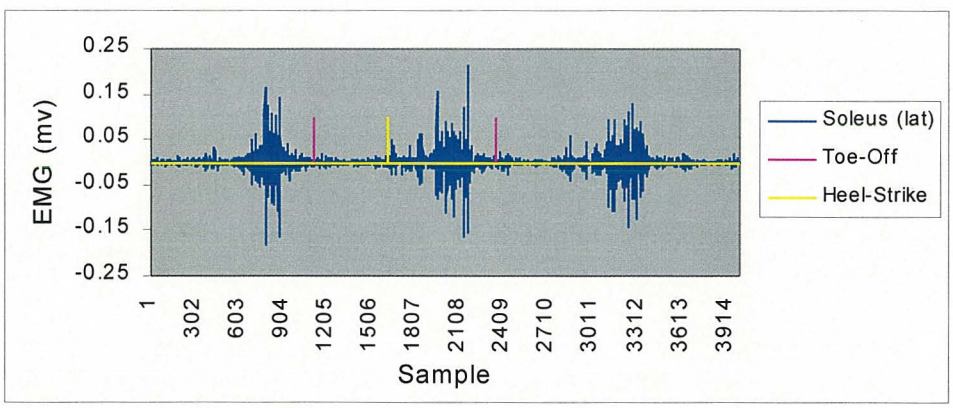

Figure 4.7.1 First walk trial - Soleus (lat) electromyography.

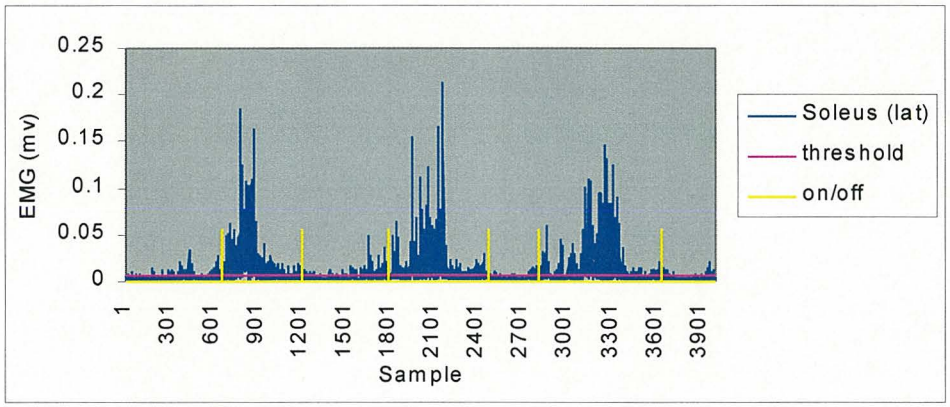

Figure 4.7.2 First walk trial - Soleus (lat) electromyography on/offsets.

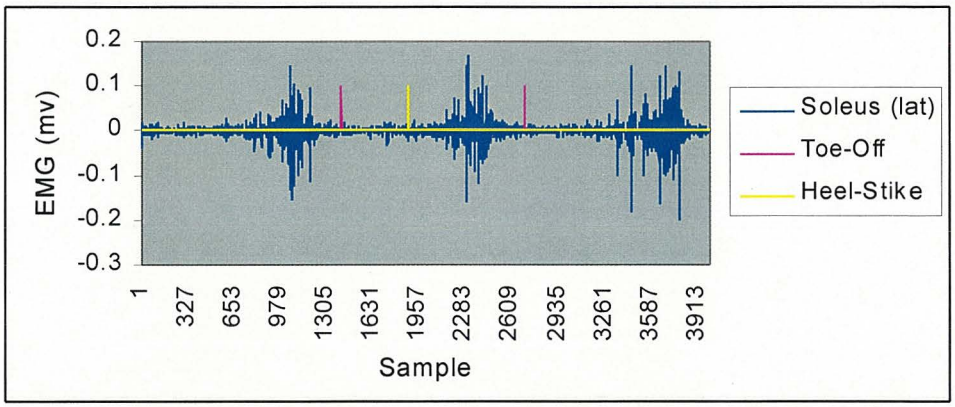

Figure 4.7.3 Second walk trial - Soleus (lat) electromyography.

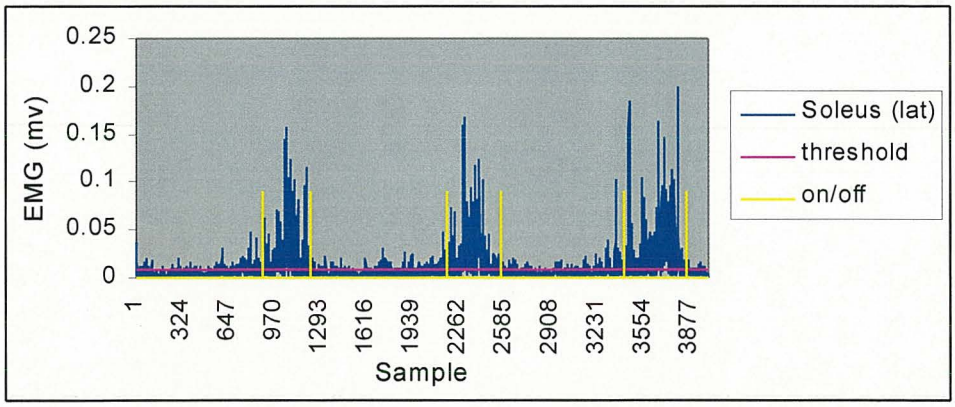

Figure 4.7.4 Second walk trial - Soleus (lat) electromyography on/offsets.

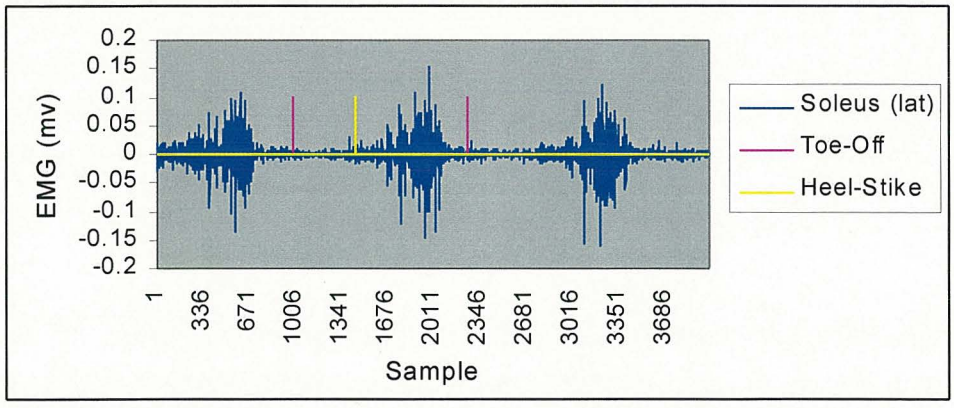

Figure 4.7.5 Third walk trial - Soleus (lat) electromyography.

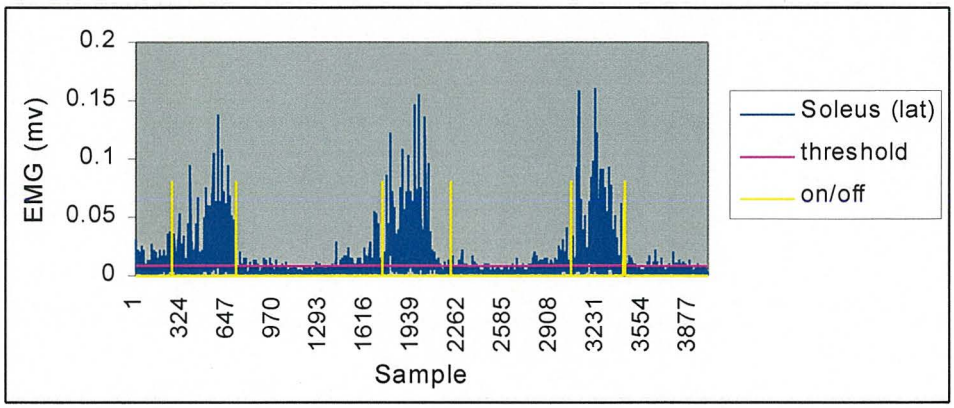

Figure 4.7.6 Third walk trial - Soleus (lat) electromyography on/offsets.

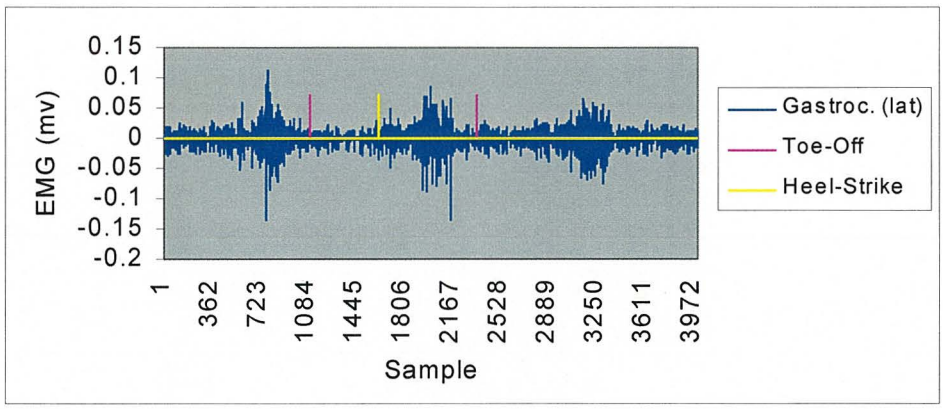

Figure 4.7.7 First walk trial - Gastrocnemius (lat) electromyography.

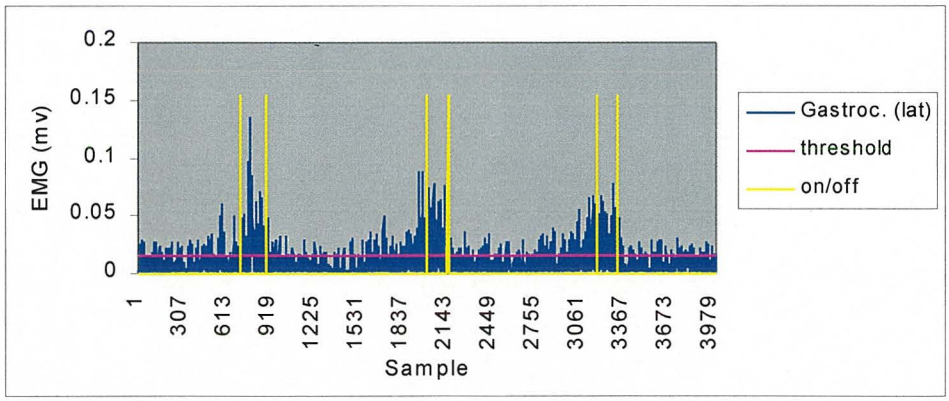

Figure 4.7.8 First walk trial - Gastrocnemius (lat) electromyography on/offsets.

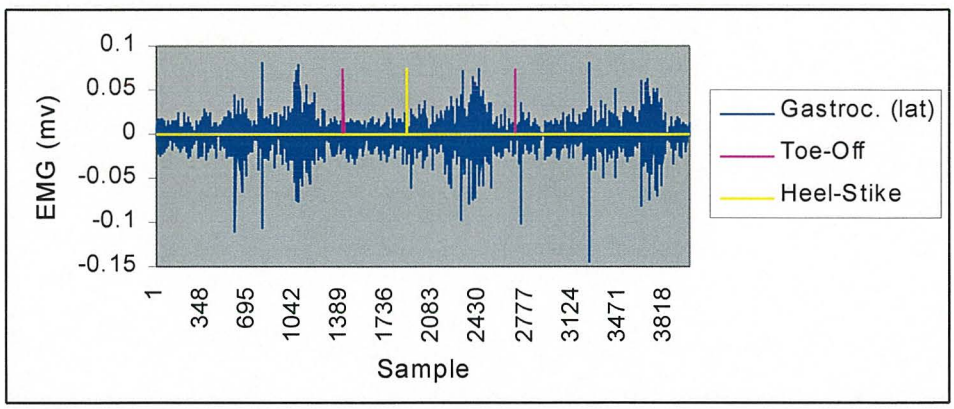

Figure 4.7.9 Second walk trial - Gastrocnemius (lat) electromyography.

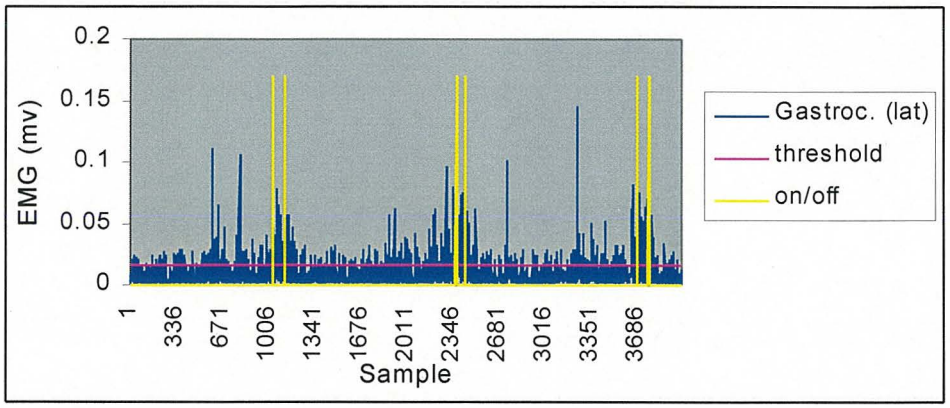

Figure 4.7.10 Second walk trial - Gastrocnemius (lat) electromyography on/offsets.

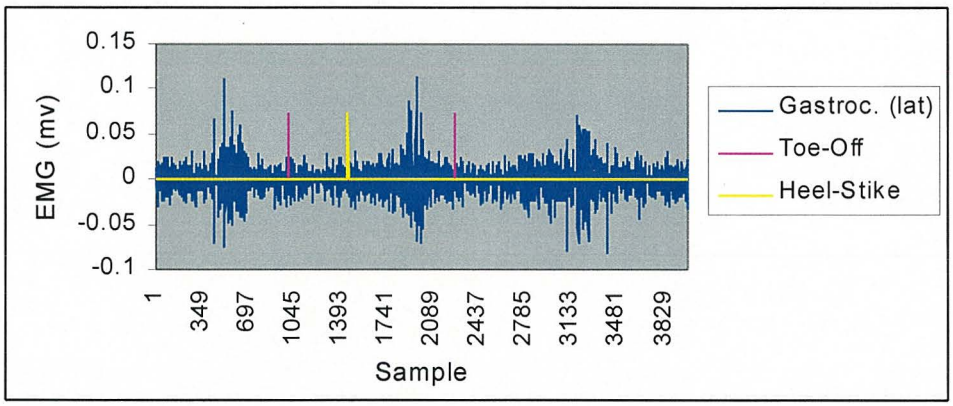

Figure 4.7.11 Third walk trial - Gastrocnemius (lat) electromyography.

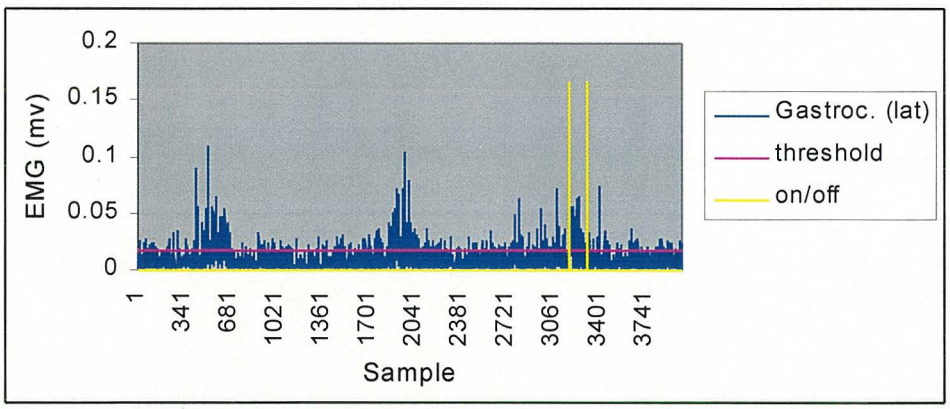

Figure 4.7.12 Third walk trial - Gastrocnemius (lat) electromyography on/offsets.

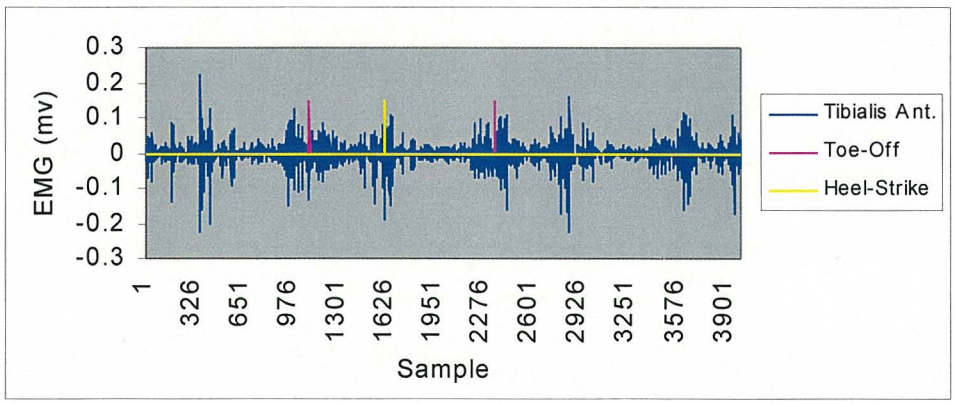

Figure 4.7.13 First walk trial - Tibialis Anterior electromyography.

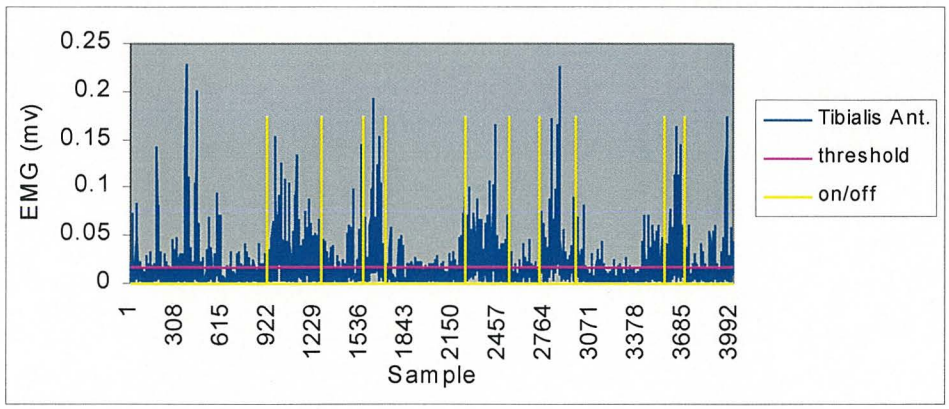

Figure 4.7.14 First walk trial - Tibialis Anterior electromyography on/offsets.

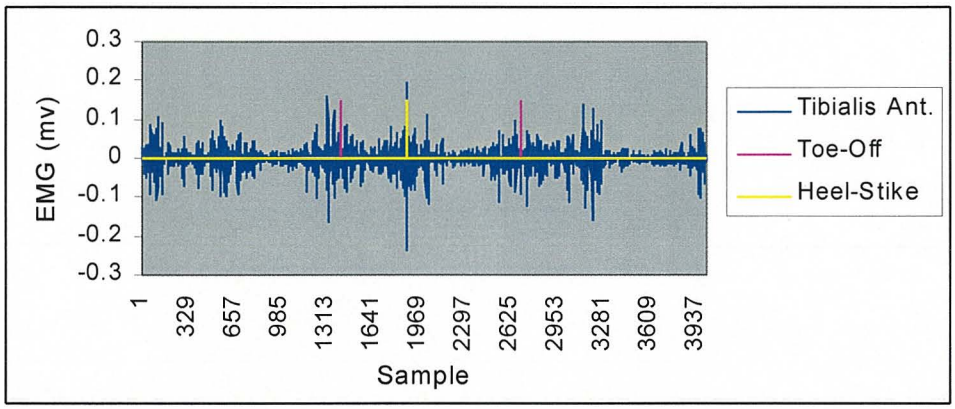

Figure 4.7.15 Second walk trial - Tibialis Anterior electromyography.

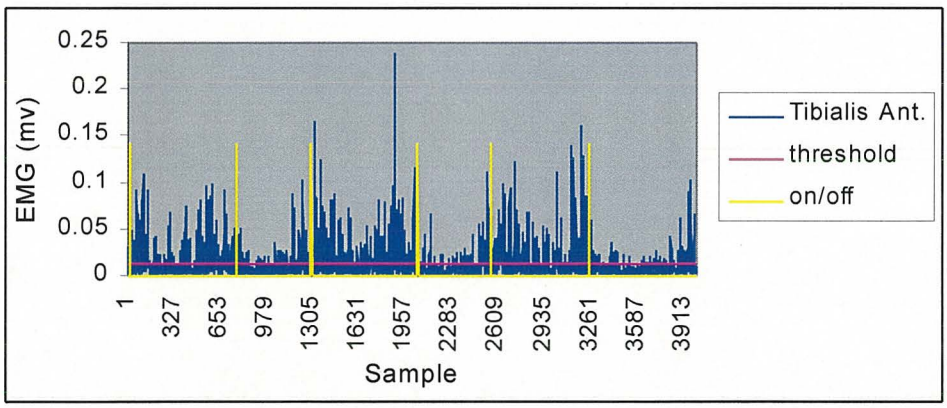

Figure 4.7.16 Second walk trial - Tibialis Anterior electromyography on/offsets.

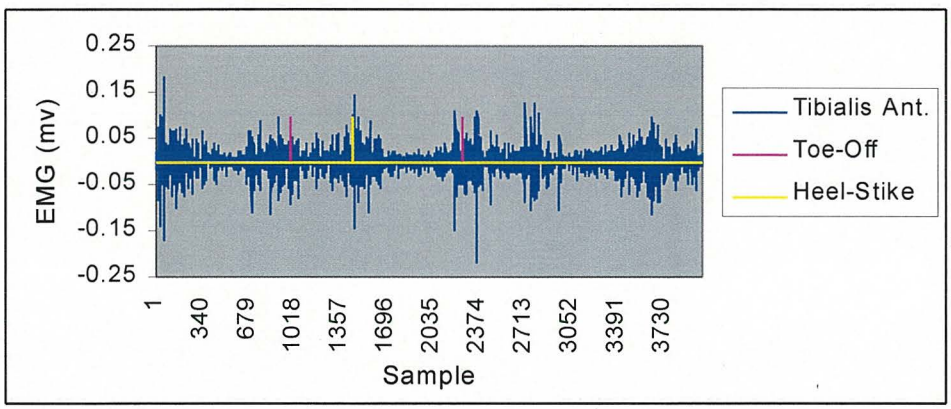

Figure 4.7.17 Third walk trial - Tibialis Anterior electromyography.

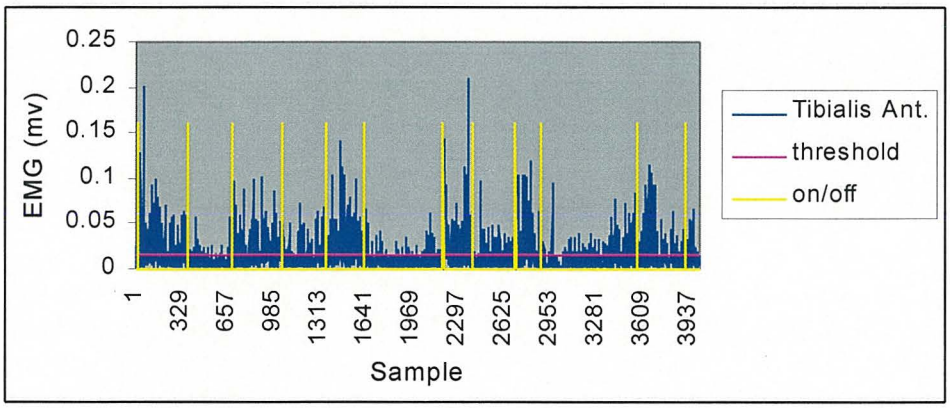

Figure 4.7.18 Third walk trial - Tibialis Anterior electromyography on/offsets.

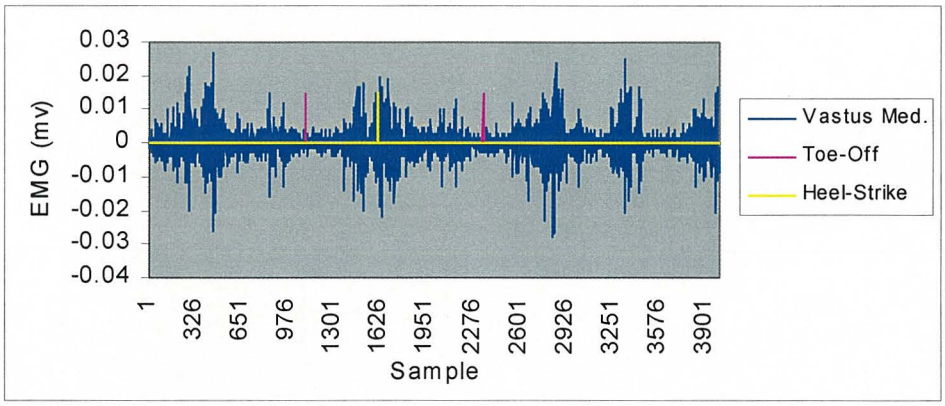

Figure 4.7.19 First walk trial - Vastus Medialis electromyography.

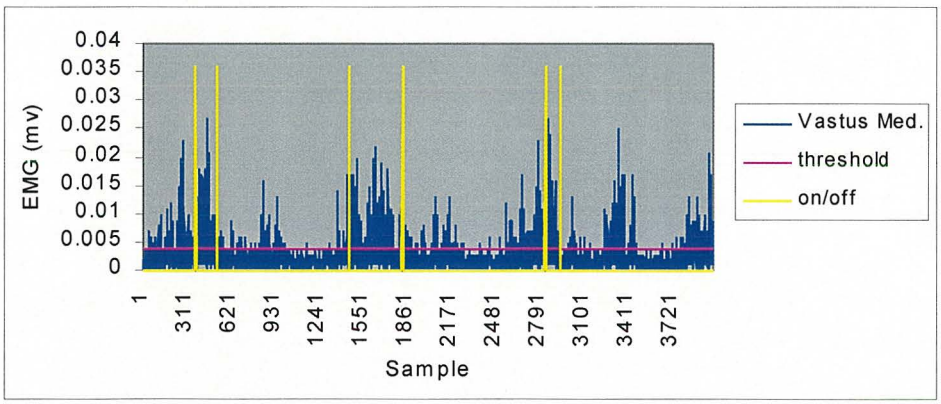

Figure 4.7.20 First walk trial - Vastus Medialis electromyography on/offsets.

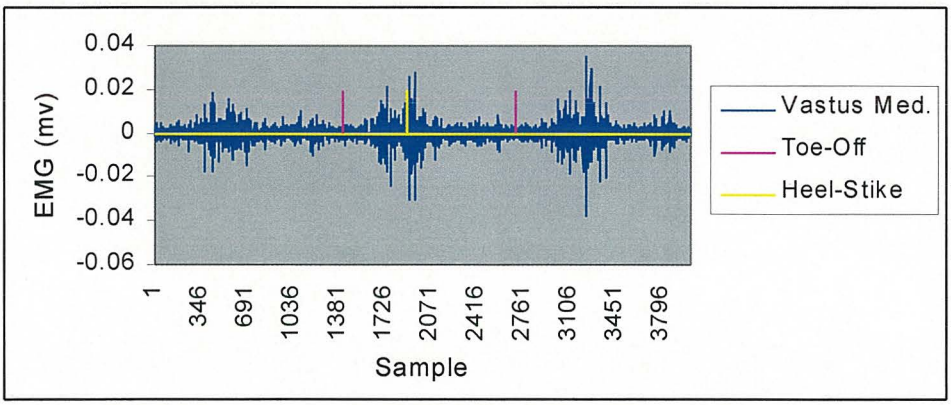

Figure 4.7.21 Second walk trial - Vastus Medialis electromyography.

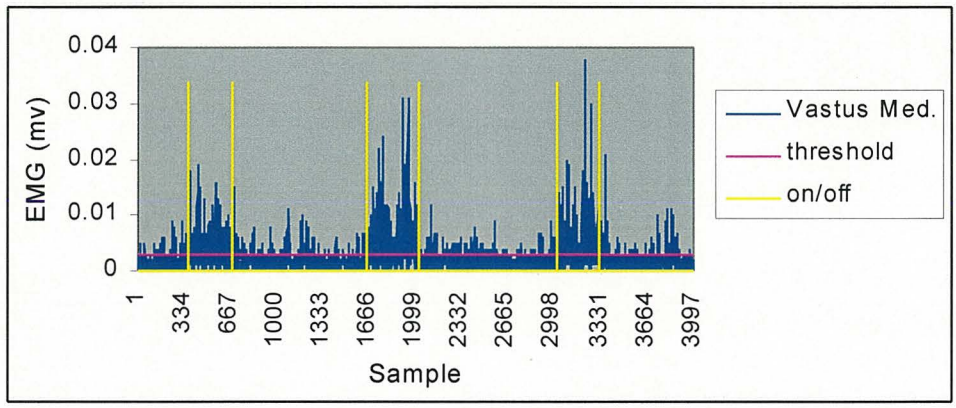

Figure 4.7.22 Second walk trial - Vastus Medialis electromyography on/offsets.

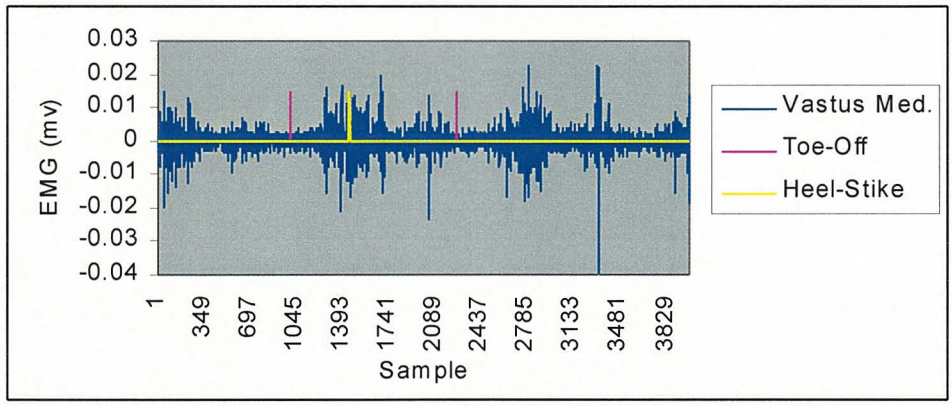

Figure 4.7.23 Third walk trial - Vastus Medialis electromyography.

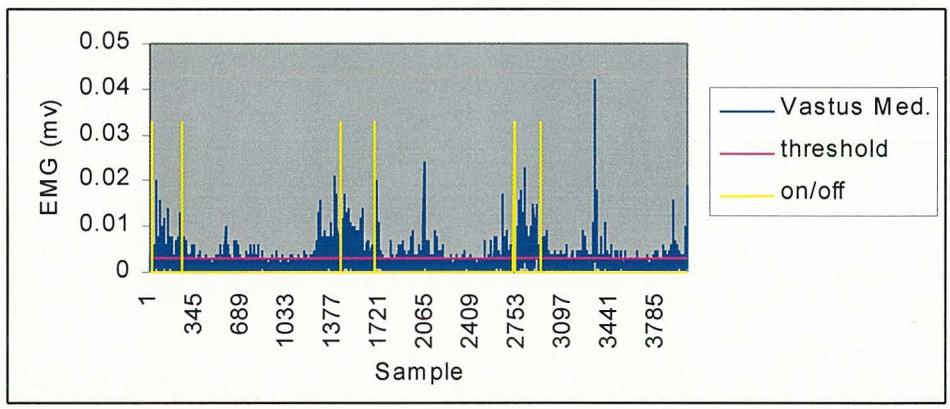

Figure 4.7.24 Third walk trial - Vastus Medialis electromyography on/offsets.

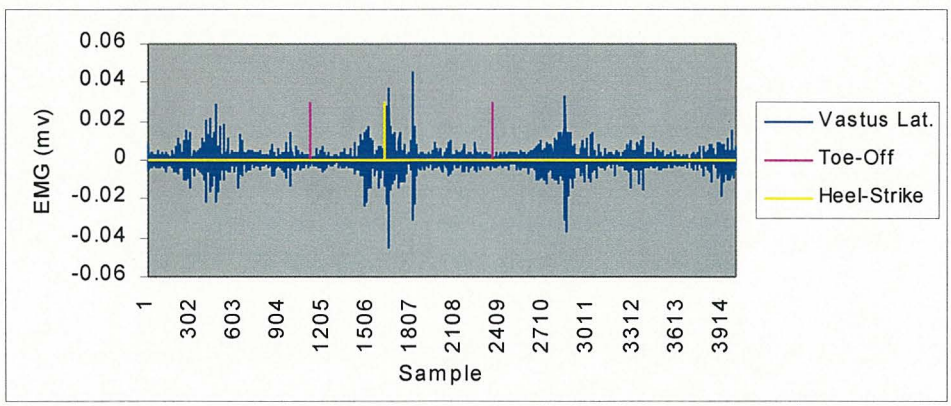

Figure 4.7.25 First walk trial - Vastus Lateralis electromyography.

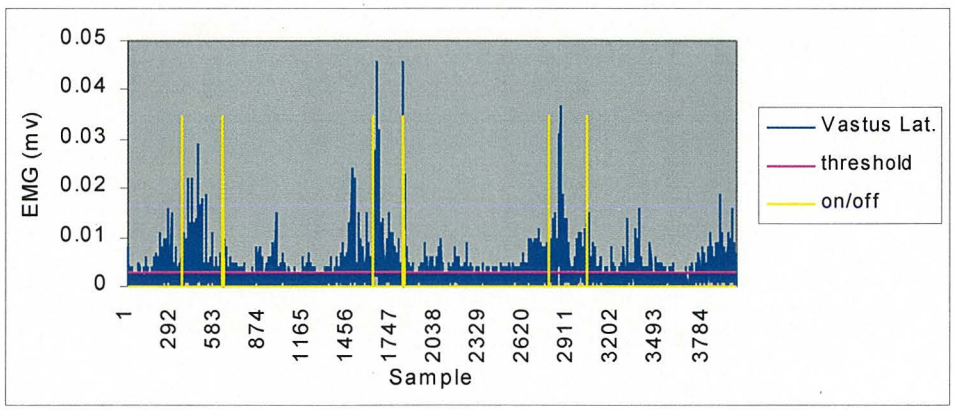

Figure 4.7.26 First walk trial - Vastus Lateralis electromyography on/offsets.

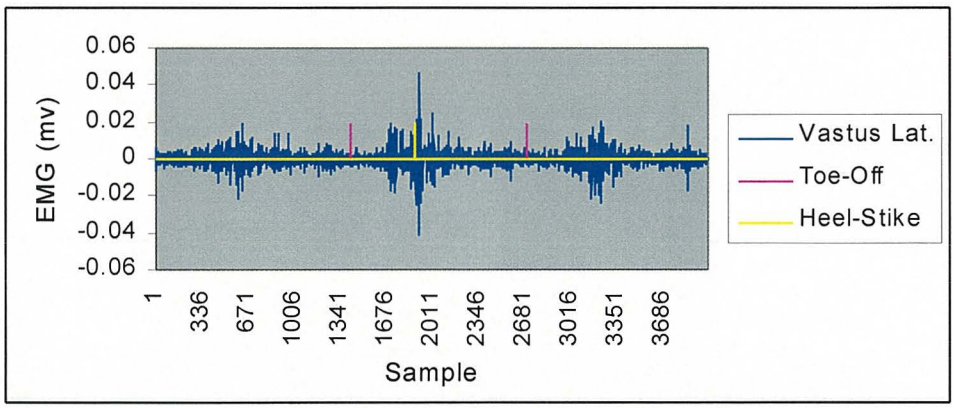

Figure 4.7.27 Second walk trial - Vastus Lateralis electromyography.

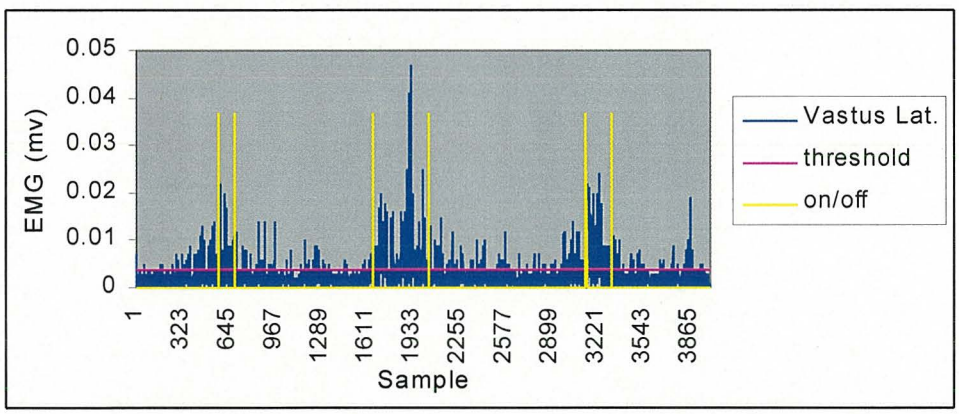

Figure 4.7.28 Second walk trial - Vastus Lateralis electromyography on/offsets.

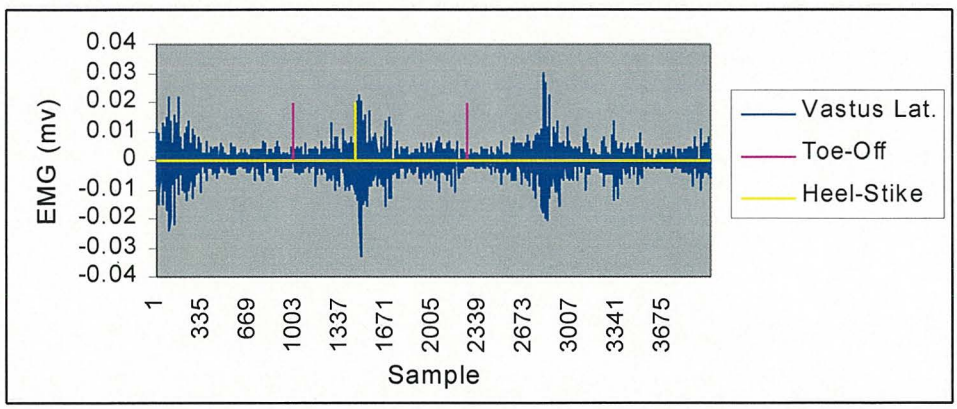

Figure 4.7.29 Third walk trial - Vastus Lateralis electromyography.

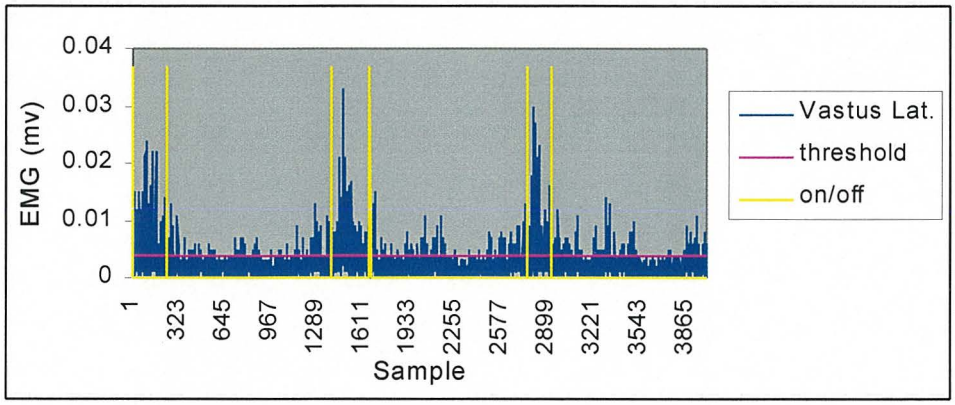

Figure 4.7.30 Third walk trial - Vastus Lateralis electromyography on/offsets.

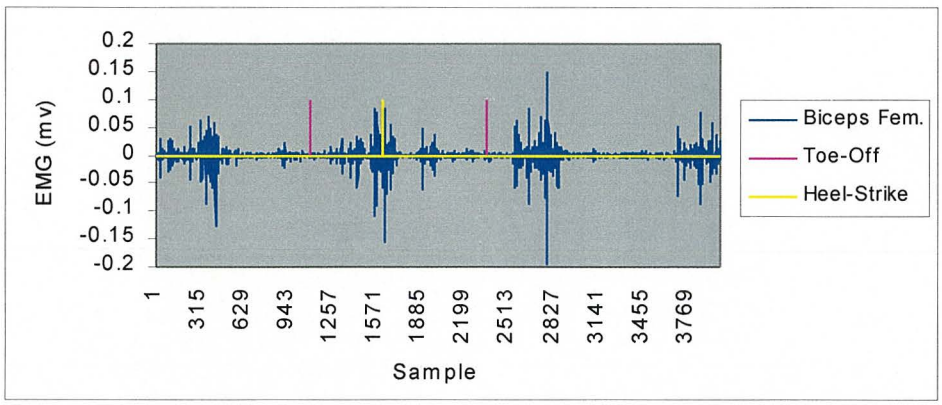

Figure 4.7.31 First walk trial - Biceps Femoris electromyography.

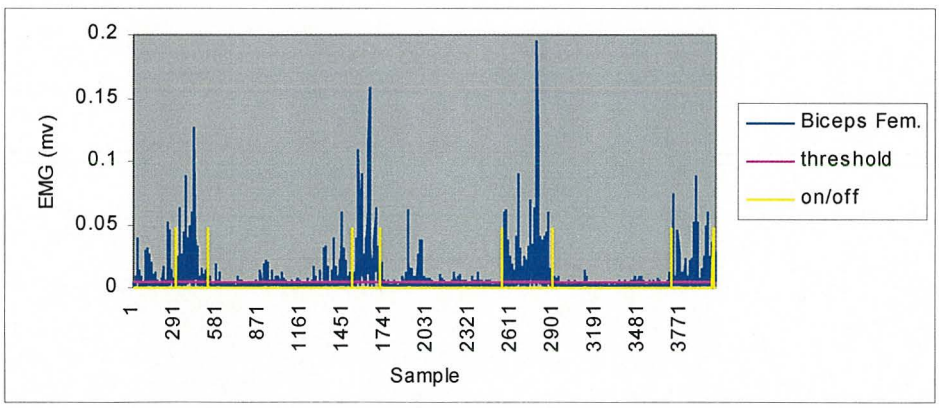

Figure 4.7.32 First walk trial - Biceps Femoris electromyography on/offsets.

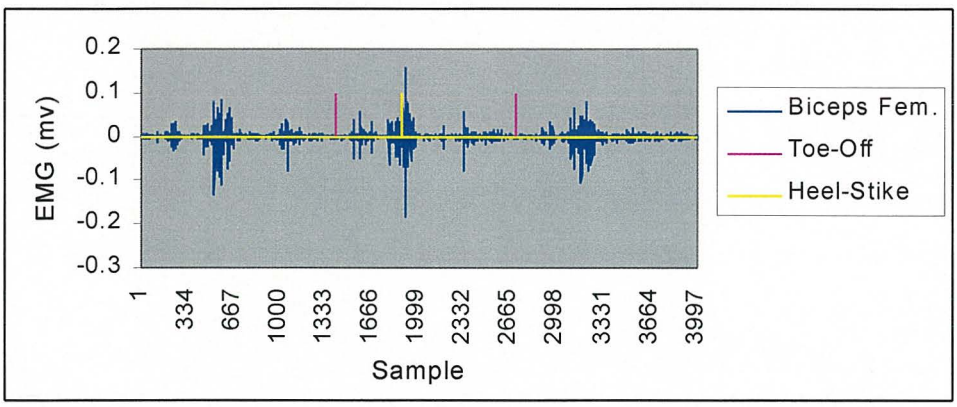

Figure 4.7.33 Second walk trial - Biceps Femoris electromyography.

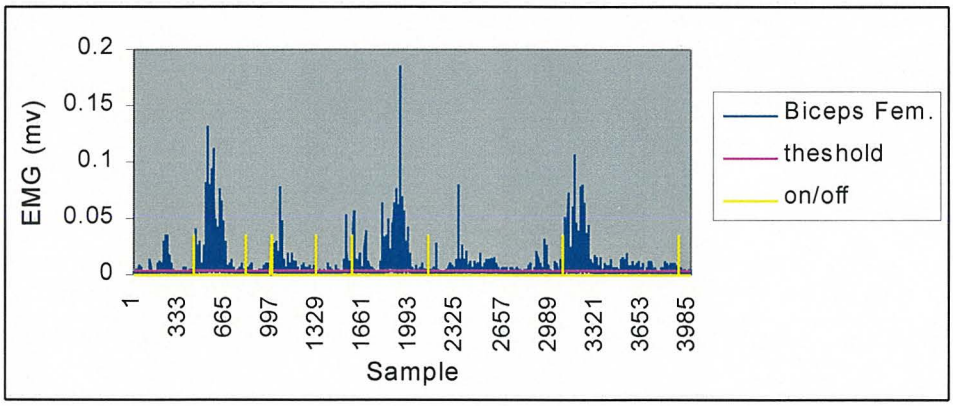

Figure 4.7.34 Second walk trial - Biceps Femoris electromyography on/offsets.

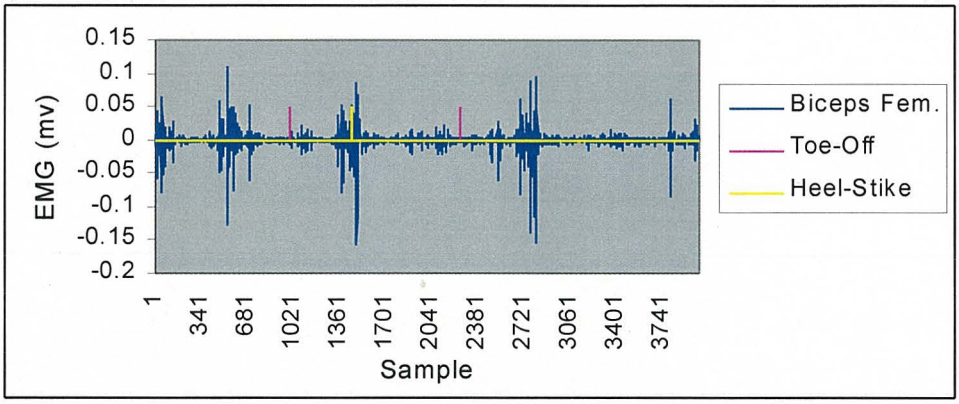

Figure 4.7.35 Third walk trial - Biceps Femoris electromyography.

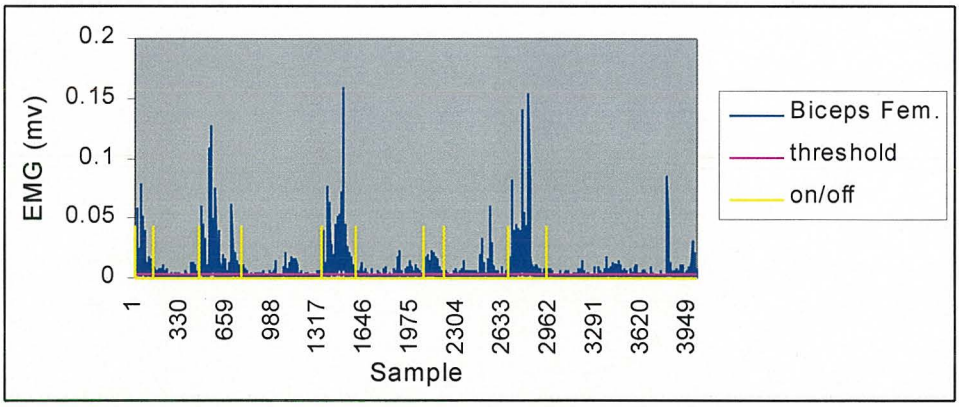

Figure 4.7.36 Third walk trial - Biceps Femoris electromyography on/offsets.

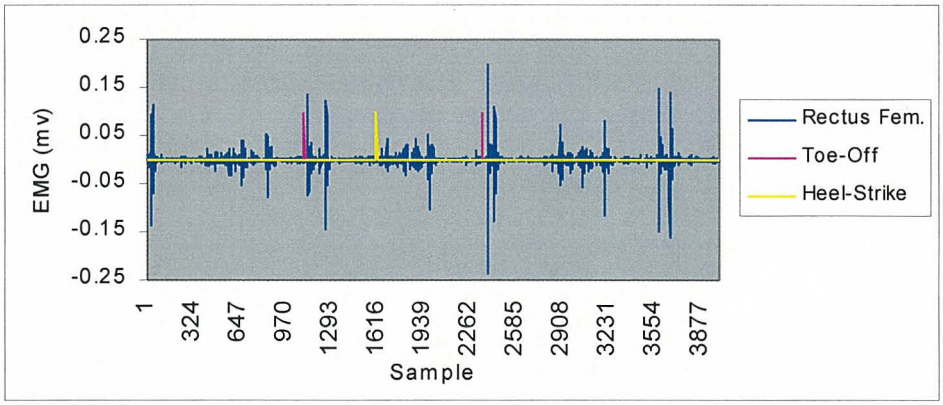

Figure 4.7.37 First walk trial - Rectus Femoris electromyography.

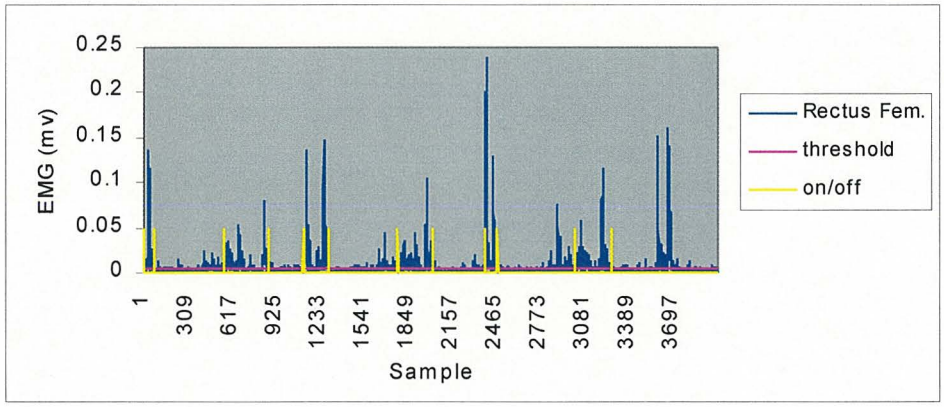

Figure 4.7.38 First walk trial - Rectus Femoris electromyography on/offsets.

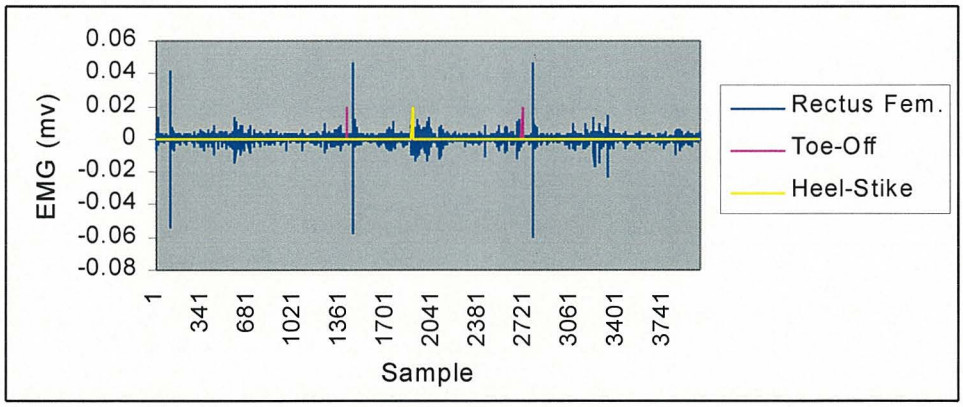

Figure 4.7.39 Second walk trial - Rectus Femoris electromyography.

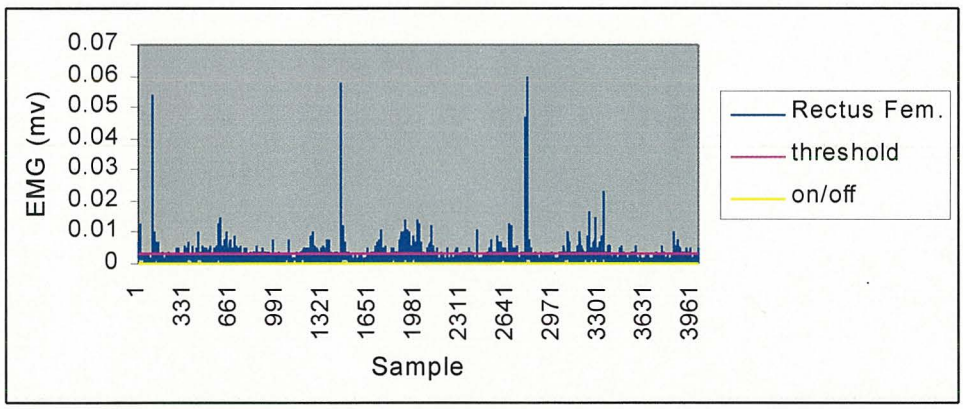

Figure 4.7.40 Second walk trial - Rectus Femoris electromyography on/offsets.

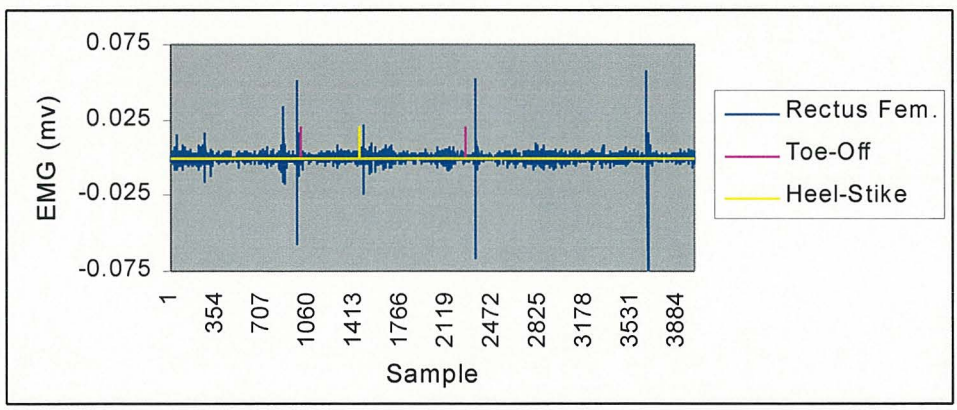

Figure 4.7.41 Third walk trial - Rectus Femoris electromyography.

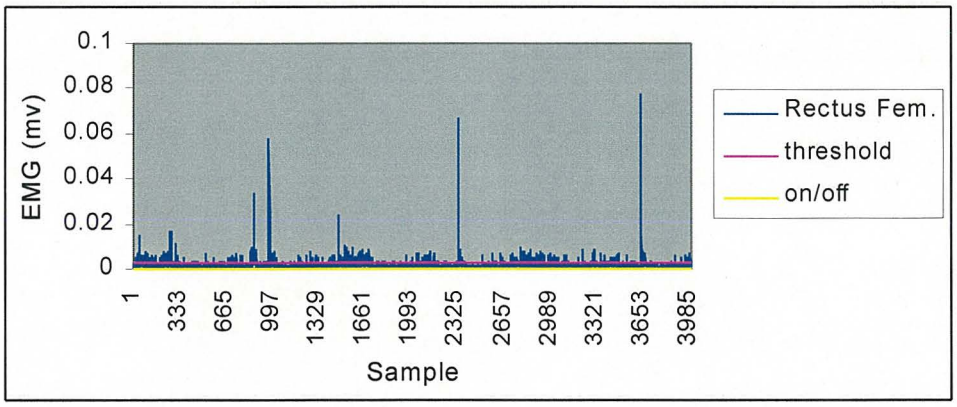

Figure 4.7.42 Third walk trial - Rectus Femoris electromyography on/offsets.

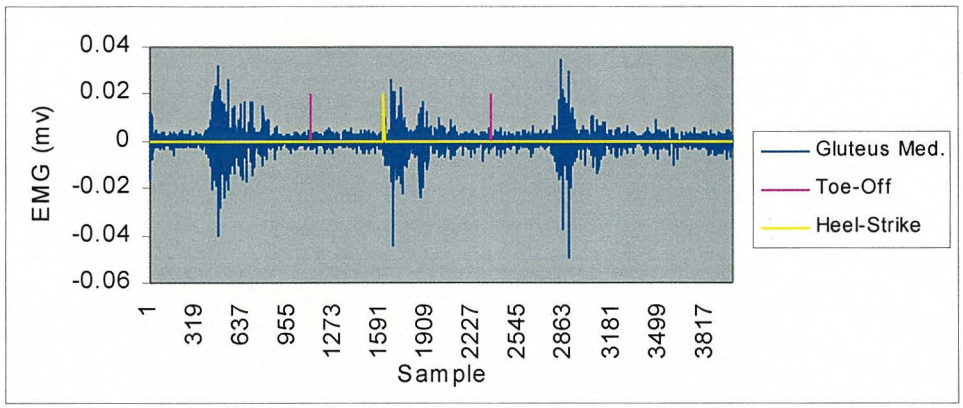

Figure 4.7.43 First walk trial - Gluteus Medius electromyography.

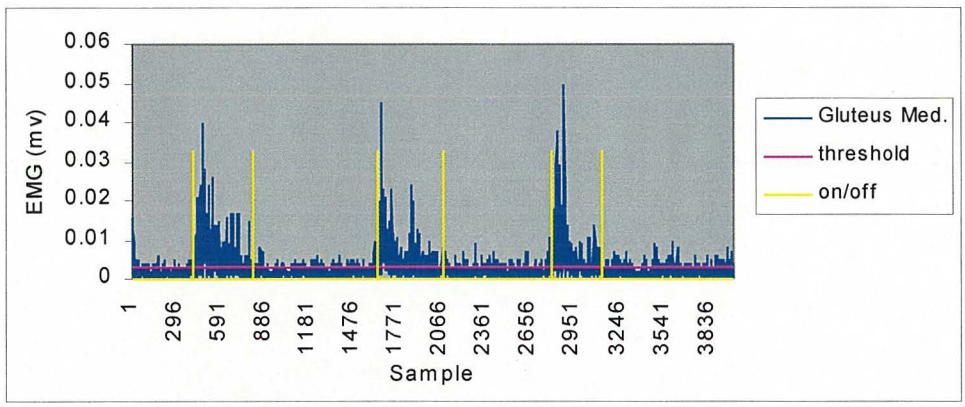

Figure 4.7.44 First walk trial - Gluteus Medius electromyography on/offsets.

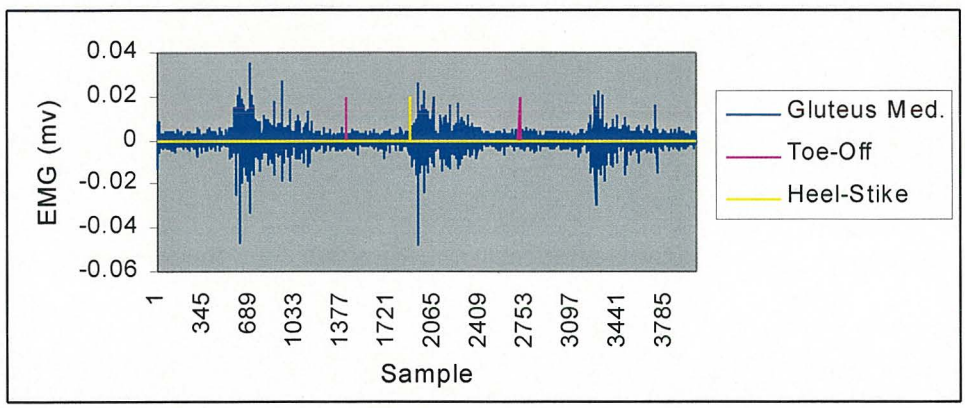

Figure 4.7.45 Second walk trial - Gluteus Medius electromyography.

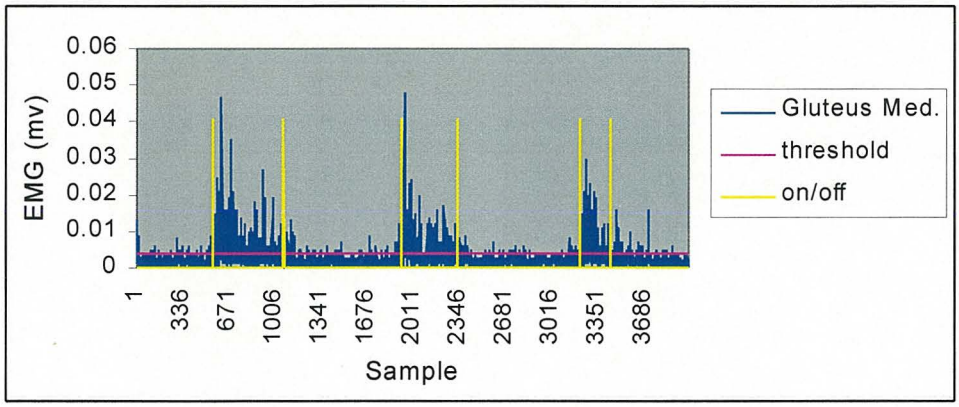

Figure 4.7.46 Second walk trial - Gluteus Medius electromyography on/offsets.

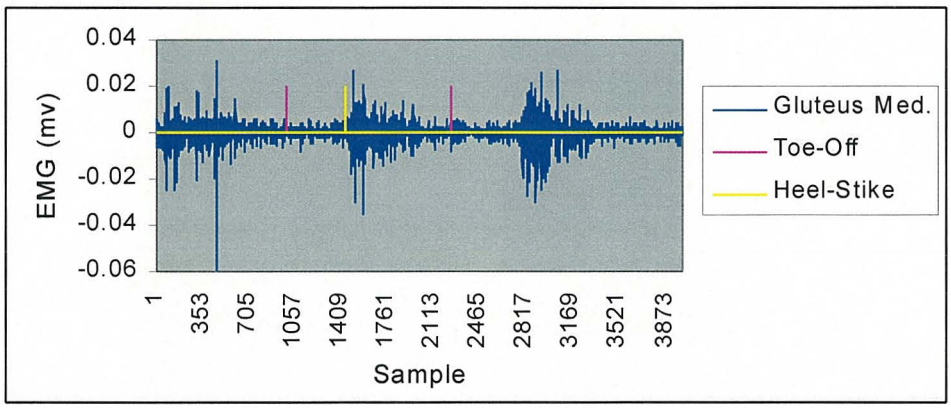

Figure 4.7.47 Third walk trial - Gluteus Medius electromyography.

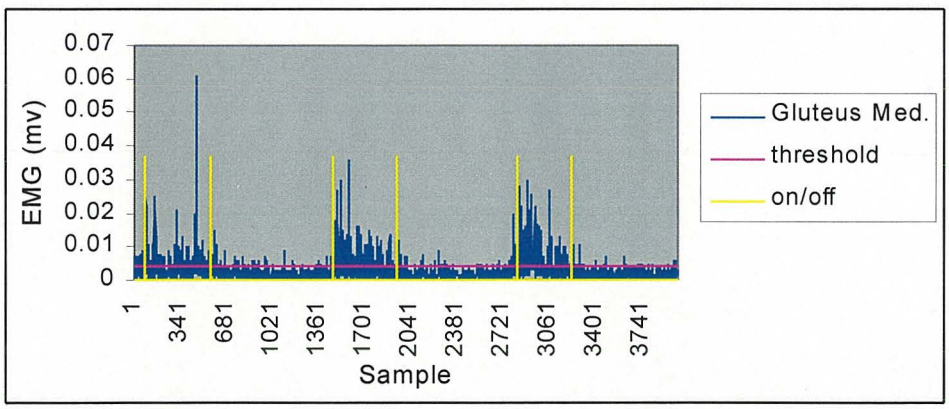

Figure 4.7.48 Third walk trial - Gluteus Medius electromyography on/offsets.

Table 4.7.1 First walk trial - electromyography on-sets and offsets.

	Electromyographic activity- first walk trial
Soleus (lateral)	
On/Off	650, 1195, 1787, 2464, 2797, 3630
RMS	0.031, 0.007, 0.028, 0.004, 0.024, 0.004
Baseline	0.0057 at 2.65 sec.
Gastrocnemius (lateral)	
On/Off	707, 893, 2001, 2146, 3176, 3325
RMS	0.012, 0.036, 0.013, 0.029, 0.015, 0.029, 0.011
Baseline	0.0154 at 1.30 sec.
Tibialis Anterior	
On/Off	907, 1272, 1550, 1688, 2230, 2517, 2722, 2960, 3549, 3682
RMS	0.028, 0.038, 0.024, 0.052, 0.015, 0.038, 0.014, 0.045, 0.017, 0.049, 0.026
Baseline	0.0174 at 3.15 sec.
Vastus Medialis	
On/Off	372, 518, 1449, 1823, 2824, 2927
RMS	0.005, 0.008, 0.003, 0.007, 0.004, 0.009, 0.004
Baseline	0.0036 at 1.15 sec.
Vastus Lateralis	
On/Off	351, 625, 1604, 1815, 2768, 3026
RMS	0.004, 0.007, 0.004, 0.010, 0.003, 0.008, 0.003
Baseline	0.0035 at 1.25 sec.
Biceps Femoris	
On/Off	292, 513, 1501, 1701, 2535, 2881, 3698, 3980
RMS	0.010, 0.023, 0.006, 0.031, 0.006, 0.027,0.003, 0.019, 0.013
Baseline	0.0047 at 3.25 sec.
Rectus Femoris	
On/Off	1, 73, 556, 871, 1111, 1282, 1768, 2007, 2381, 2468, 3002, 3258
RMS	0.040, 0.005, 0.014, 0.004, 0.031, 0.006, 0.017, 0.004, 0.058, 0.008, 0.018, 0.018
Baseline	0.0048 at 2.25 sec.
Gluteus Medius	
On/Off	401, 808, 1632, 2075, 2791, 3133
RMS	0.002, 0.009, 0.002, 0.007, 0.002, 0.008, 0.002
Baseline	0.0033 at 3.35 sec.

Table 4.7.2 Second walk trial - electromyography on-sets and offsets.

	Electromyographic activity- second walk trial
Soleus (lateral)	
On/Off	887, 1223, 2177, 2534, 3409, 3844
RMS	0.008, 0.039, 0.008, 0.037, 0.010, 0.040, 0.007
Baseline	0.0091 at 1.55 sec.
Gastrocnemius (lateral)	
On/Off	1029, 1121, 2364, 2431, 3685, 3762
RMS	0.013, 0.033, 0.015, 0.037, 0.015, 0.031, 0.013
Baseline	0.0170 at 3.95 sec.
Tibialis Anterior	
On/Off	10, 762, 1292, 2042, 2560, 3258
RMS	0.015, 0.026, 0.017, 0.035, 0.017, 0.032, 0.015
Baseline	0.0142 at 3.55 sec.
Vastus Medialis	
On/Off	364, 679, 1651, 2022, 3014, 3328
RMS	0.002, 0.005, 0.003, 0.008, 0.002, 0.008, 0.003
Baseline	0.0034 at 3.90 sec.
Vastus Lateralis	
On/Off	575, 680, 1652, 2036, 3140, 3312
RMS	0.003, 0.007, 0.003, 0.008, 0.003, 0.008 , 0.003
Baseline	0.0037 at 1.10 sec.
Biceps Femoris	
On/Off	434, 802, 985, 1304, 1563, 2120, 3085, 3908
RMS	0.006, 0.024, 0.004, 0.010, 0.007, 0.021, 0.007, 0.013, 0.003
Baseline	0.0036 at 0.30 sec.
Rectus Femoris	
On/Off	-
RMS	-
Baseline	0.0032 at 3.65 sec.
Gluteus Medius	
On/Off	553, 1069, 1915, 2324, 3217, 3430
RMS	0.008, 0.003, 0.007, 0.002, 0.008, 0.003
Baseline	0.0041 at 1.50 sec.

Table 4.7.3 Third walk trial - electromyography on-sets and offsets.

	Electromyographic activity- third walk trial
Soleus (lateral)	
On/Off	255, 697, 1723, 2202, 3045, 3419
RMS	0.030, 0.008, 0.032, 0.007, 0.036, 0.006
Baseline	0.0081 a 1.05 sec.
Gastrocnemius (lateral)	
On/Off	3170, 3302
RMS	0.014, 0.029, 0.012
Baseline	0.0167 at 1.20 sec.
Tibialis Anterior	
On/Off	11, 370, 685, 1038, 1356, 1628, 2185, 2390, 2698, 2871, 3557, 3897
RMS	0.012, 0.038, 0.013, 0.030, 0.020, 0.036, 0.014, 0.041, 0.018, 0.038, 0.019, 0.028, 0.020
Baseline	0.0162 at 3.00 sec.
Vastus Medialis	
On/Off	13, 232, 1418, 1670, 2710, 2913
RMS	0.004, 0.005, 0.003, 0.005, 0.003, 0.007, 0.004
Baseline	0.0033 at 0.95 sec.
Vastus Lateralis	
On/Off	1, 242, 1380, 1657, 2755, 2918
RMS	0.000, 0.007, 0.003, 0.007, 0.003, 0.008, 0.003
Baseline	0.0037 at 3.55 sec.
Biceps Femoris	
On/Off	1, 134, 460, 762, 1326, 1571, 2058, 2204, 2652, 2927
RMS	0.001, 0.020, 0.003, 0.019, 0.004, 0.027, 0.004, 0.008, 0.006, 0.025, 0.006
Baseline	0.0043 at 0.30 sec.
Rectus Femoris	
On/Off	-
RMS	-
Baseline	0.0027 at 2.45 sec.
Gluteus Medius	
On/Off	67, 565, 1464, 1929, 2814, 3212
RMS	0.003, 0.007, 0.003, 0.007, 0.003, 0.008, 0.002
Baseline	0.0037 at 2.35 sec.

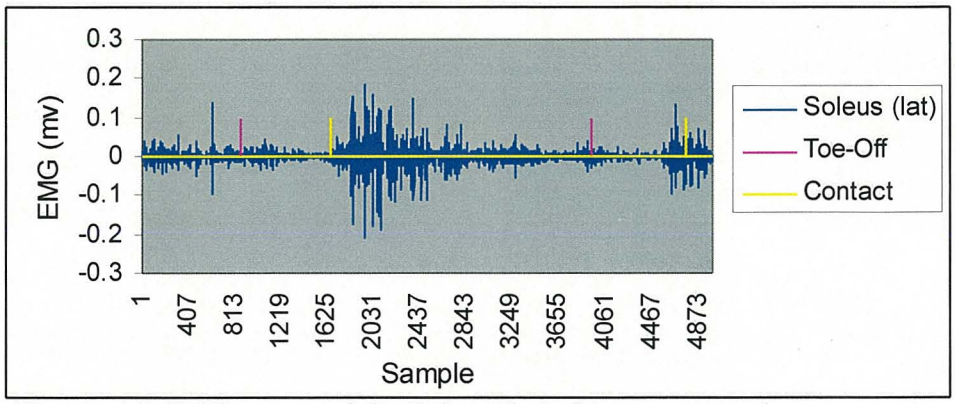

Figure 4.7.49 First step trial - Soleus (lat) electromyography.

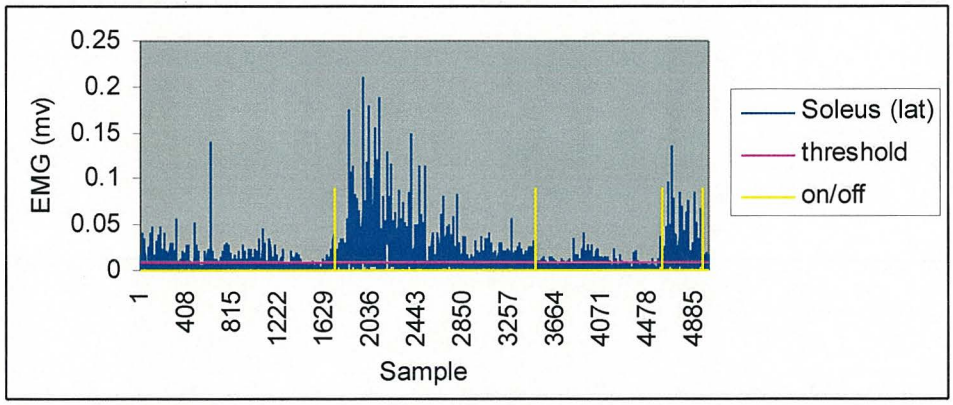

Figure 4.7.50 First step trial - Soleus (lat) electromyography on/offsets.

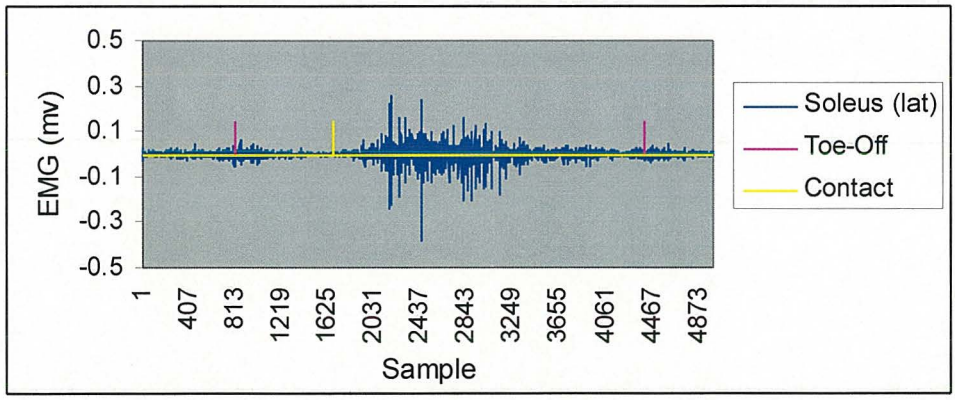

Figure 4.7.51 Second step trial - Soleus (lat) electromyography.

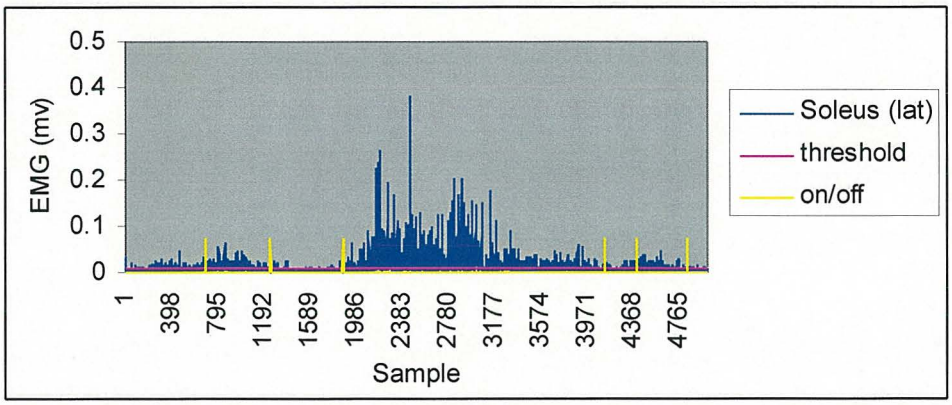

Figure 4.7.52 Second step trial - Soleus (lat) electromyography on/off-sets.

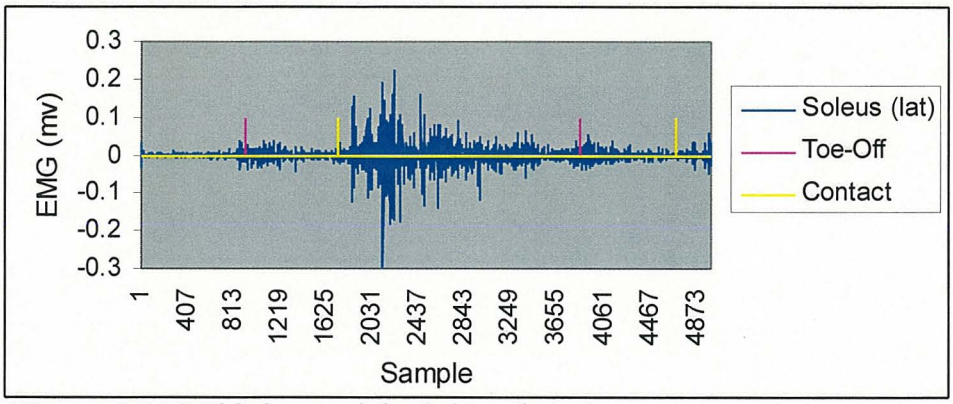

Figure 4.7.53 Third step trial - Soleus (lat) electromyography.

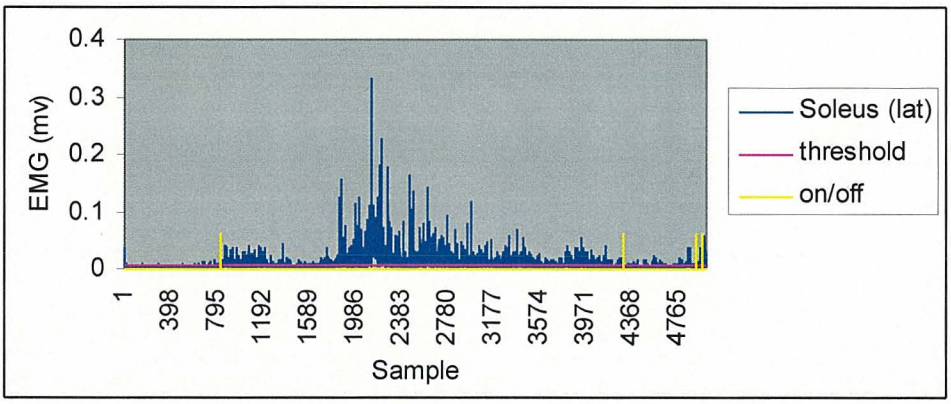

Figure 4.7.54 Third step trial - Soleus (lat) electromyography on/off-sets.

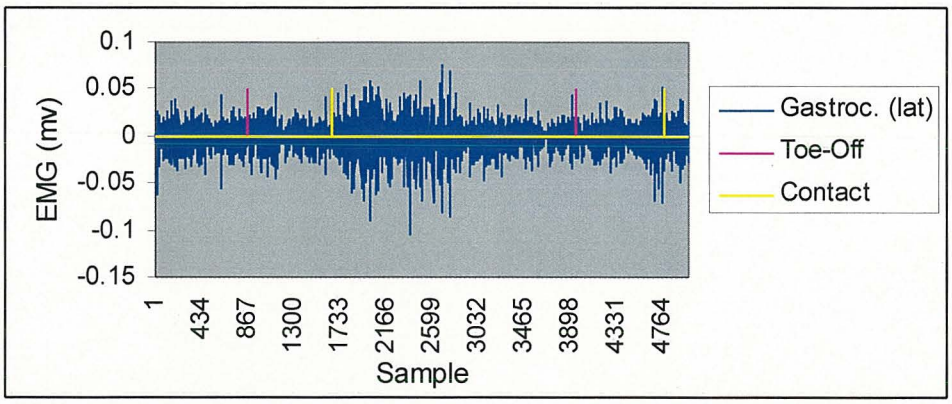

Figure 4.7.55 First step trial - Gastrocnemius (lat) electromyography.

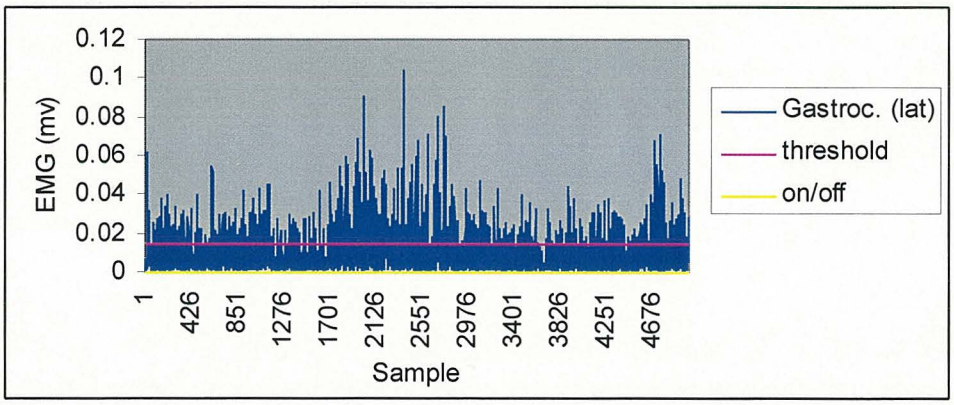

Figure 4.7.56 First step trial - Gastrocnemius (lat) electromyography on/offsets.

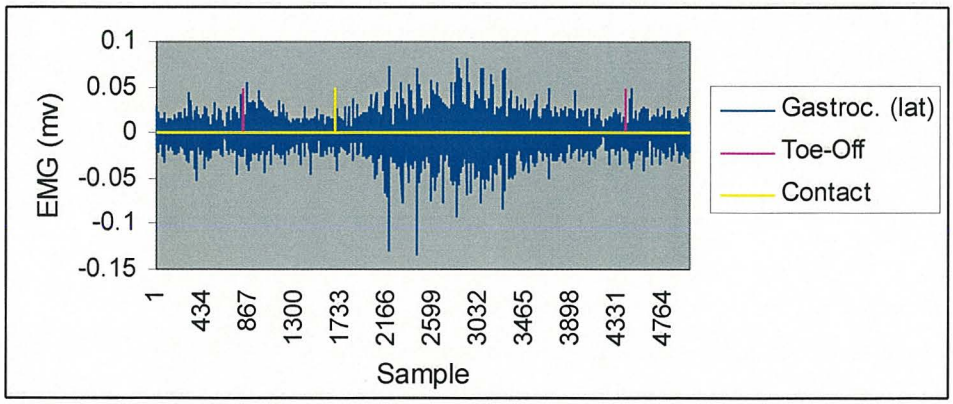

Figure 4.7.57 Second step trial - Gastrocnemius (lat) electromyography.

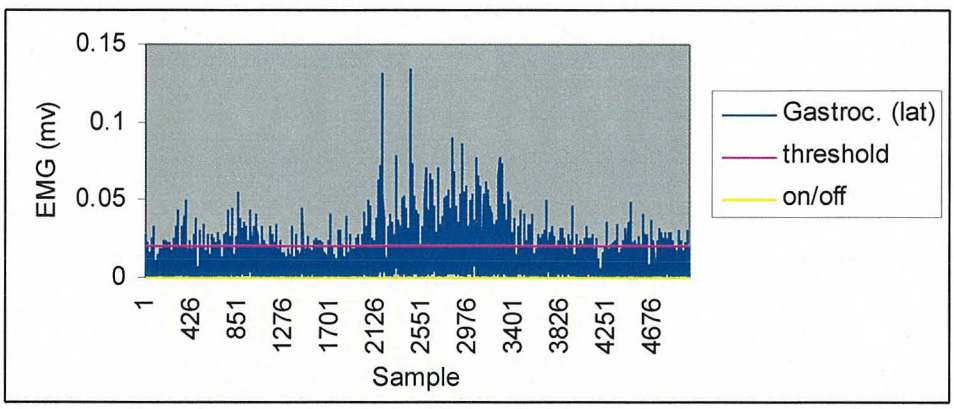

Figure 4.7.58 Second step trial - Gastrocnemius (lat) electromyography on/offsets.

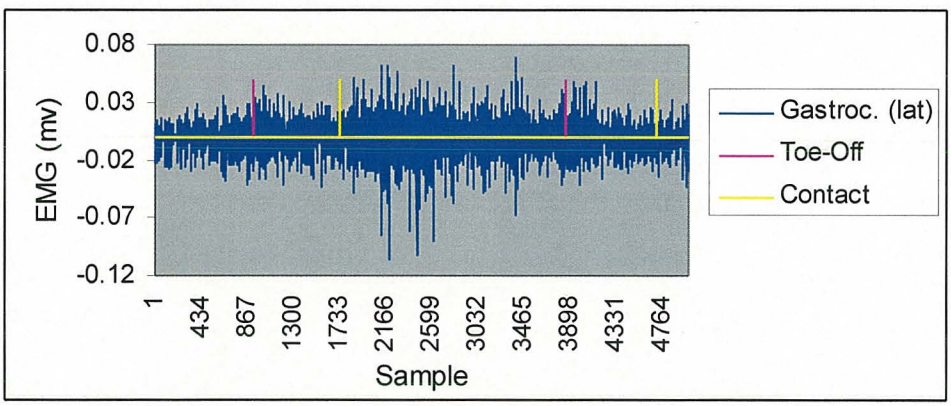

Figure 4.7.59 Third step trial - Gastrocnemius (lat) electromyography.

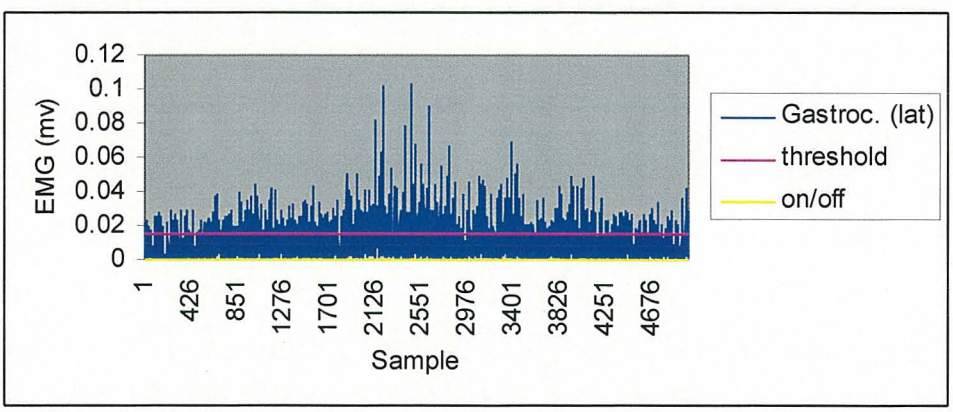

Figure 4.7.60 Third step trial - Gastrocnemius (lat) electromyography on/offsets.

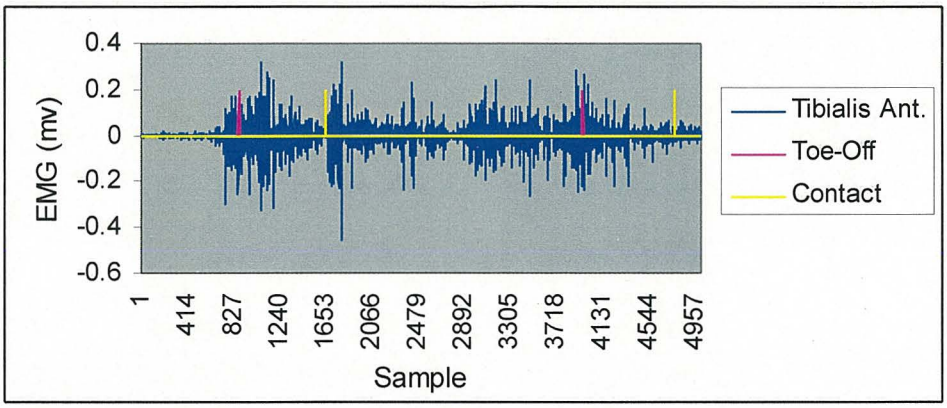

Figure 4.7.61 First step trial - Tibialis Anterior electromyography.

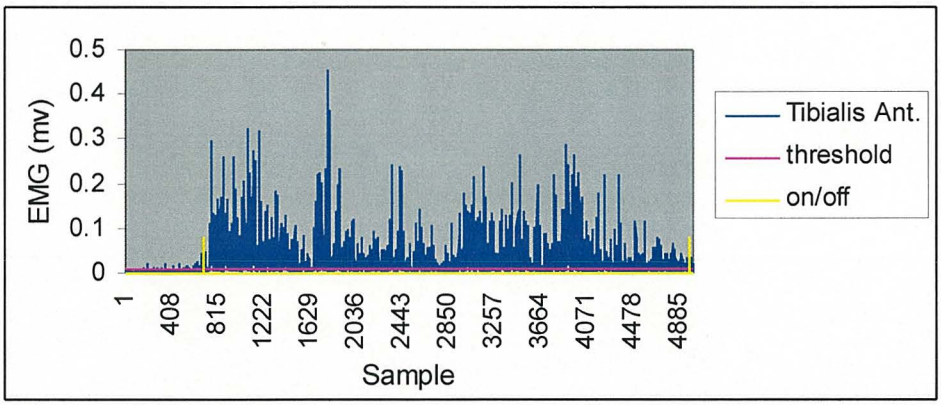

Figure 4.7.62 First step trial - Tibialis Anterior electromyography on/offsets.

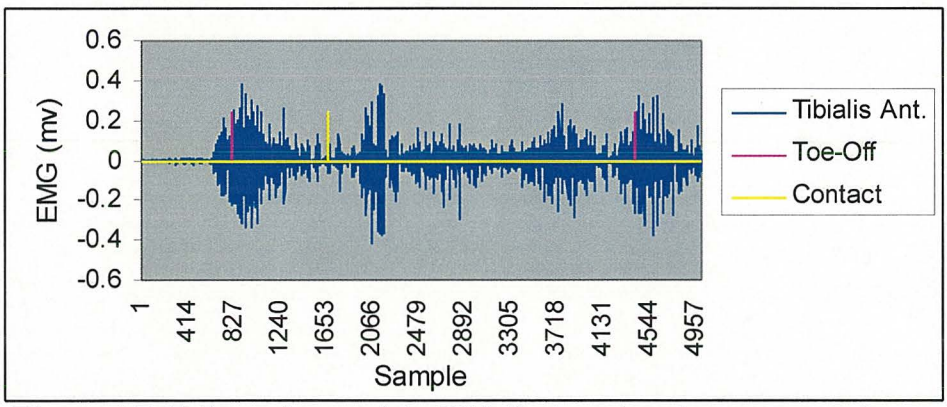

Figure 4.7.63 Second step trial - Tibialis Anterior electromyography.

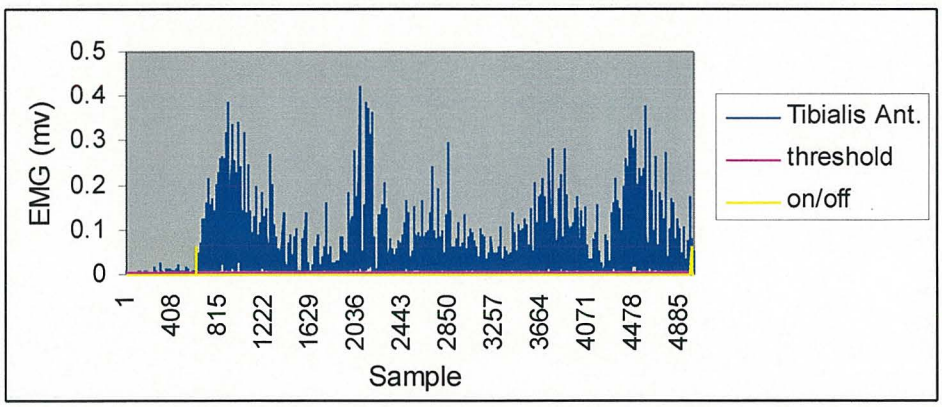

Figure 4.7.64 Second step trial - Tibialis Anterior electromyography on/offsets.

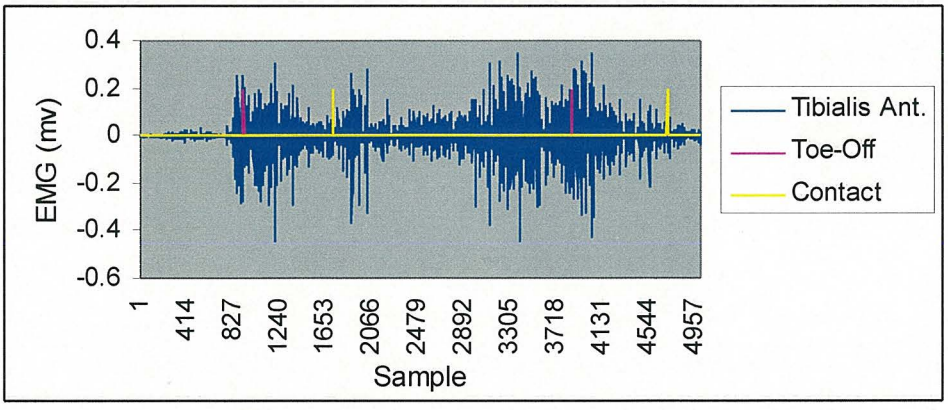

Figure 4.7.65 Third step trial - Tibialis Anterior electromyography.

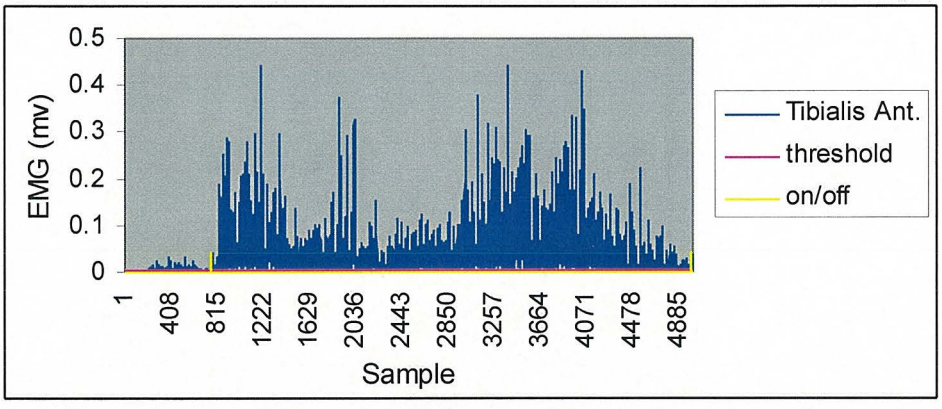

Figure 4.7.66 Third step trial - Tibialis Anterior electromyography on/offsets.

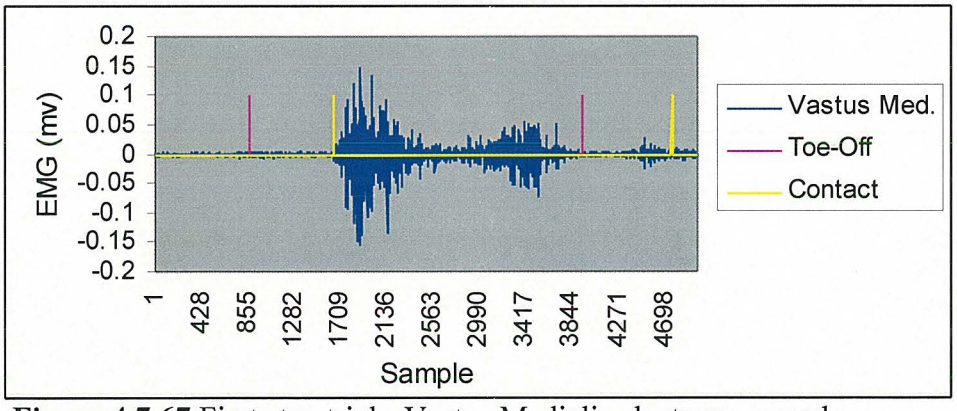

Figure 4.7.67 First step trial - Vastus Medialis electromyography.

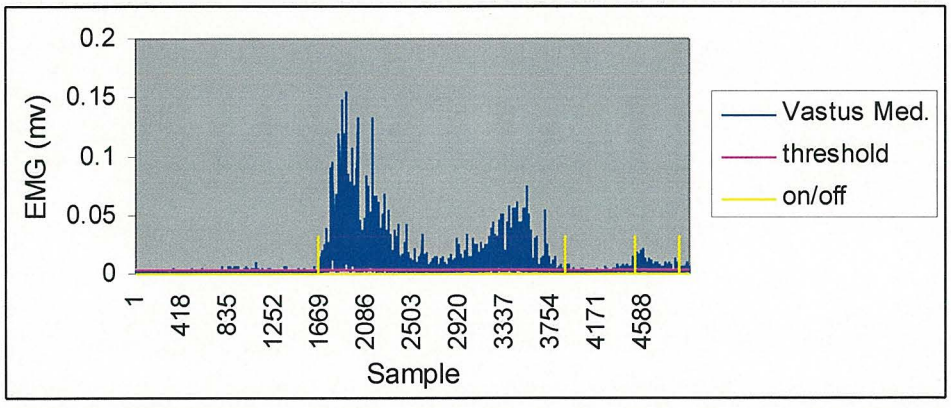

Figure 4.7.68 First step trial - Vastus Medialis electromyography on/offsets.

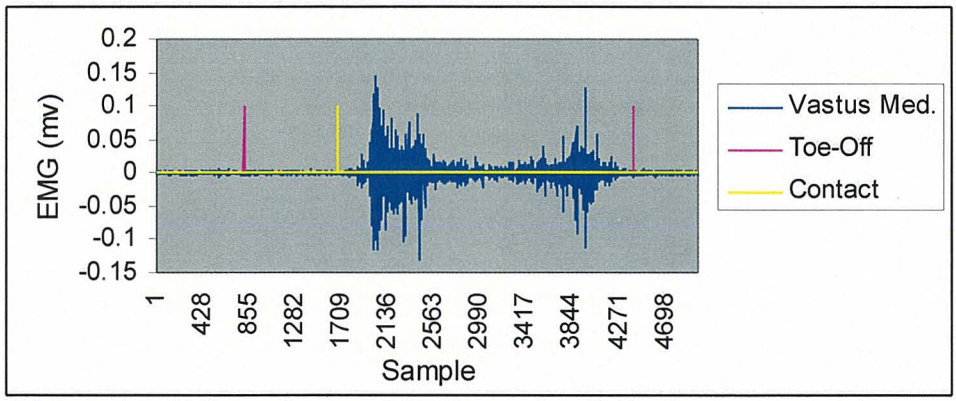

Figure 4.7.69 Second step trial - Vastus Medialis electromyography.

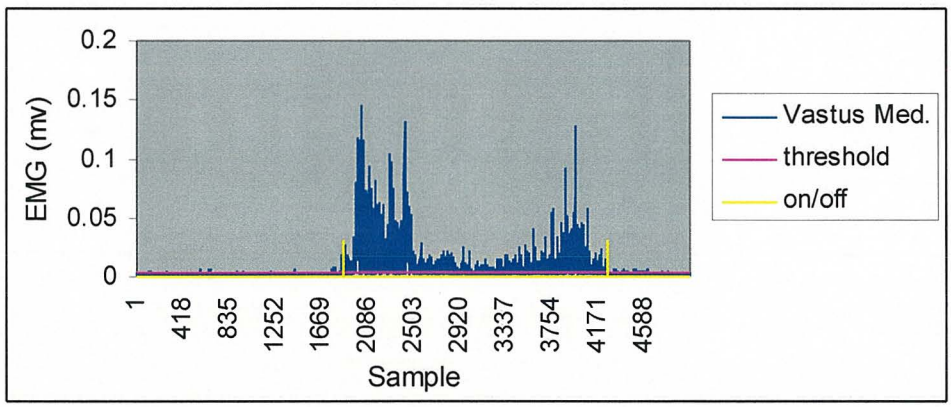

Figure 4.7.70 Second step trial - Vastus Medialis electromyography on/offsets.

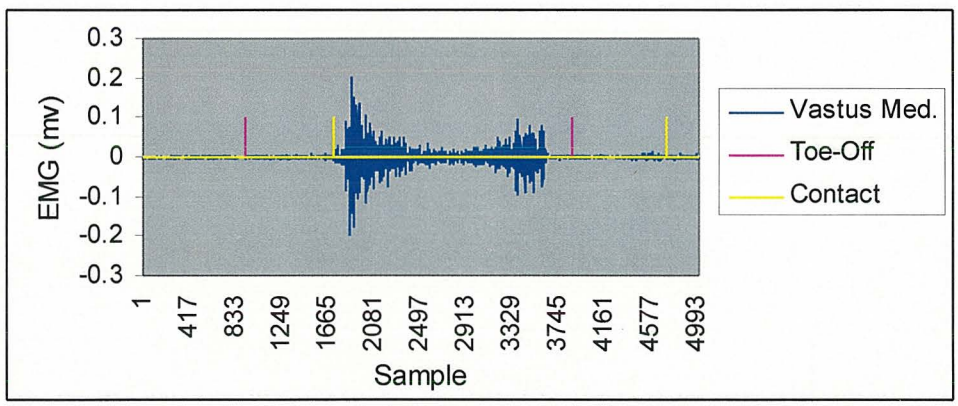

Figure 4.7.71 Third step trial - Vastus Medialis electromyography.

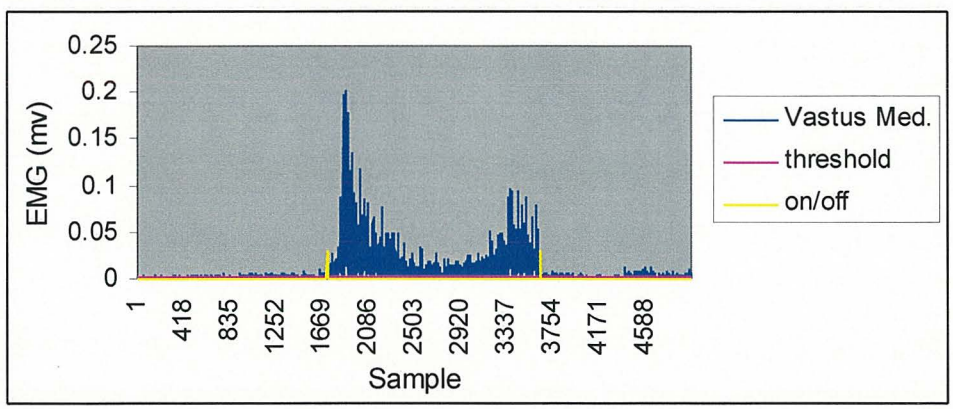

Figure 4.7.72 Third step trial - Vastus Medialis electromyography on/offsets.

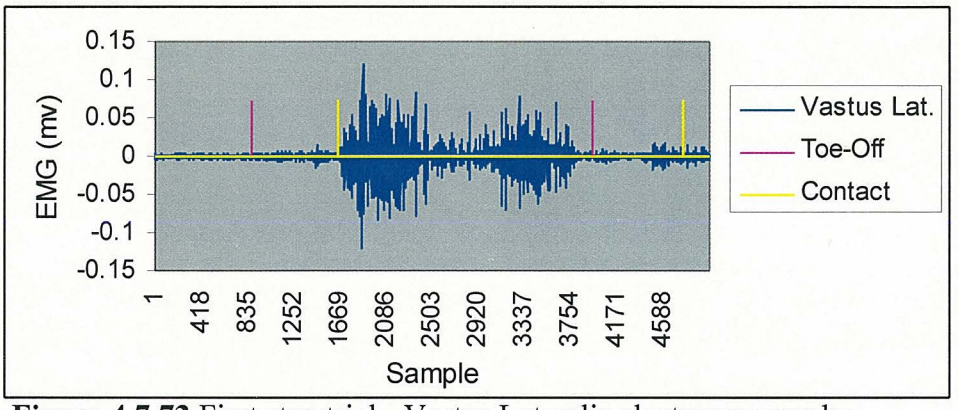

Figure 4.7.73 First step trial - Vastus Lateralis electromyography.

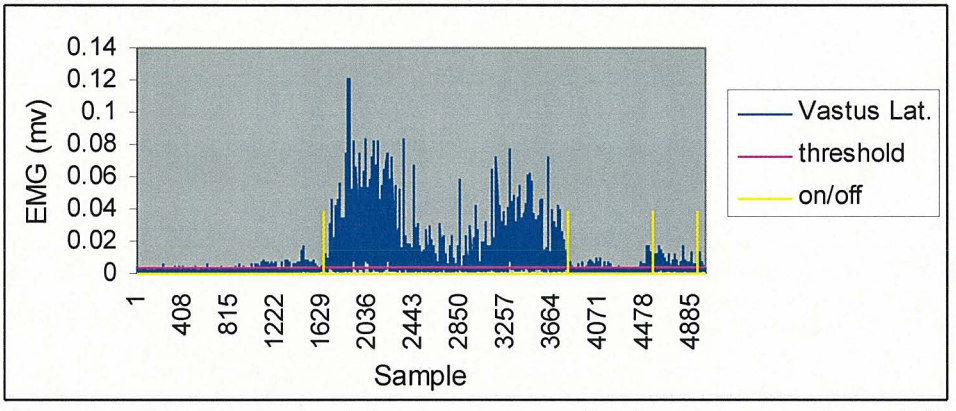

Figure 4.7.74 First step trial - Vastus Lateralis electromyography on/offsets.

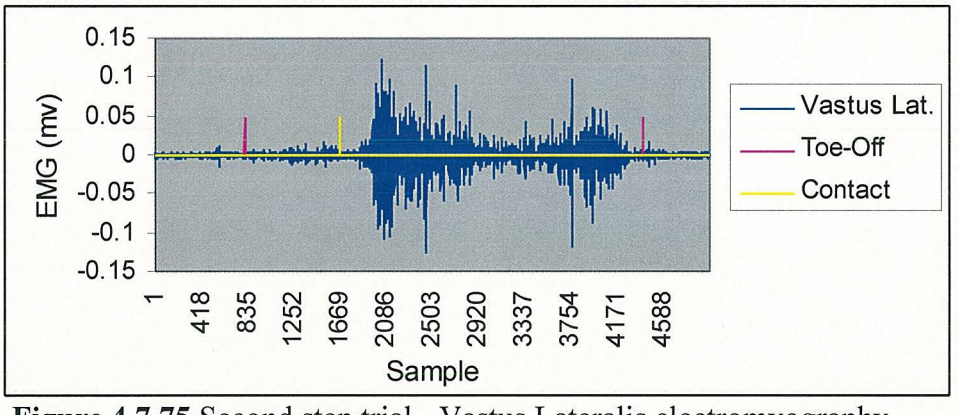

Figure 4.7.75 Second step trial - Vastus Lateralis electromyography.

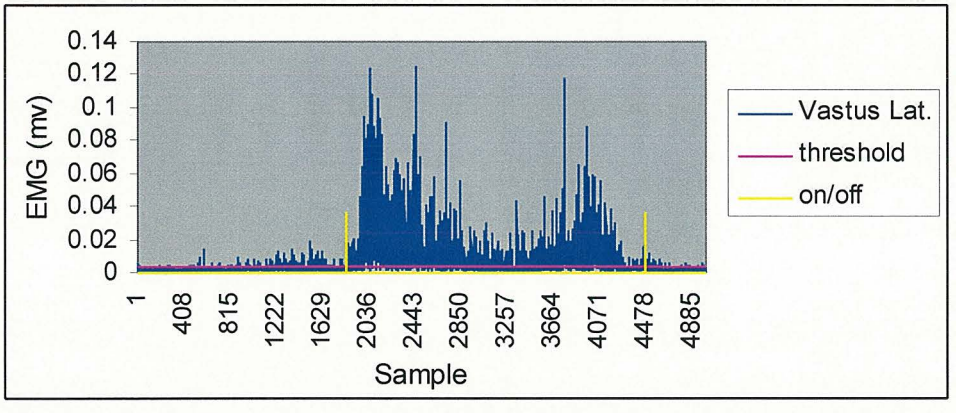

Figure 4.7.76 Second step trial - Vastus Lateralis electromyography on/offsets.

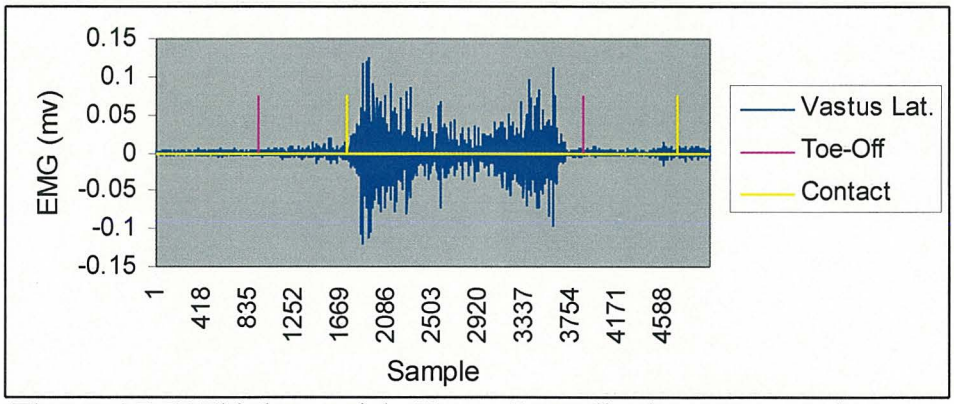

Figure 4.7.77 Third step trial - Vastus Lateralis electromyography.

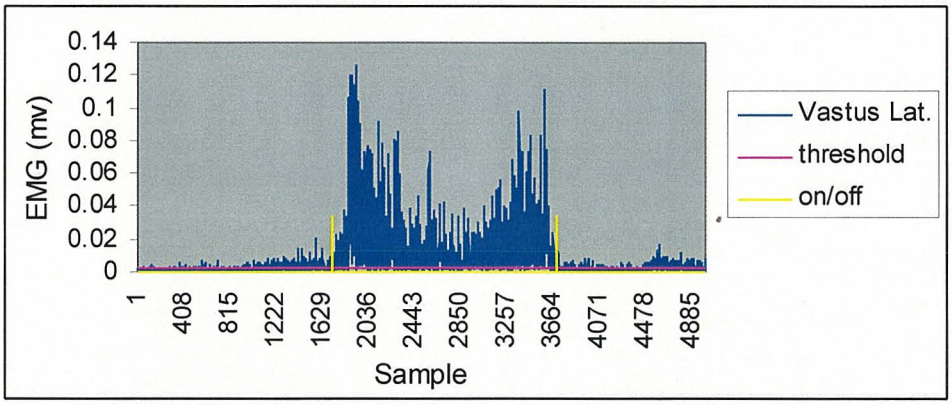

Figure 4.7.78 Third step trial - Vastus Lateralis electromyography on/offsets.

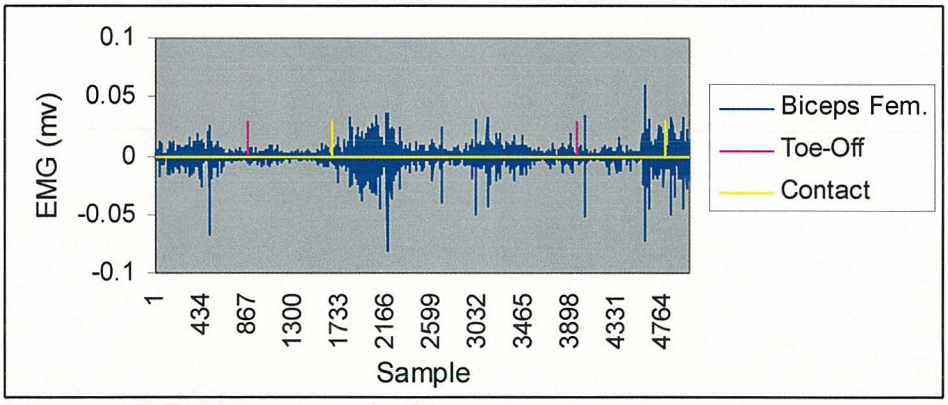

Figure 4.7.79 First step trial - Biceps Femoris electromyography.

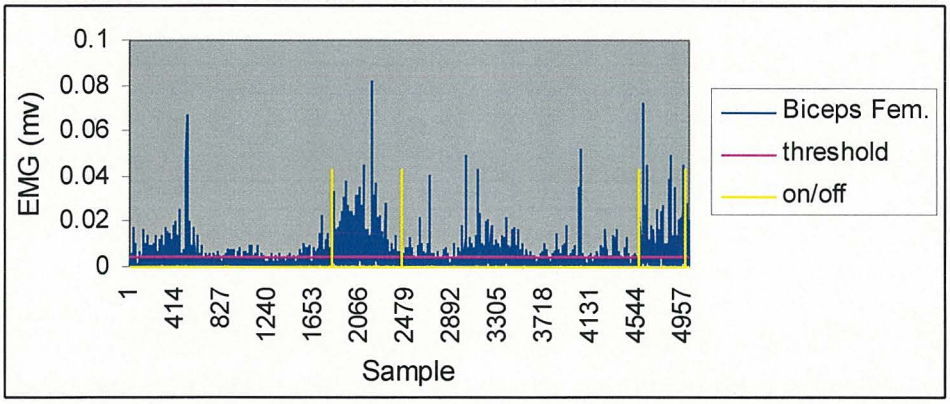

Figure 4.7.80 First step trial - Biceps Femoris electromyography on/offsets.

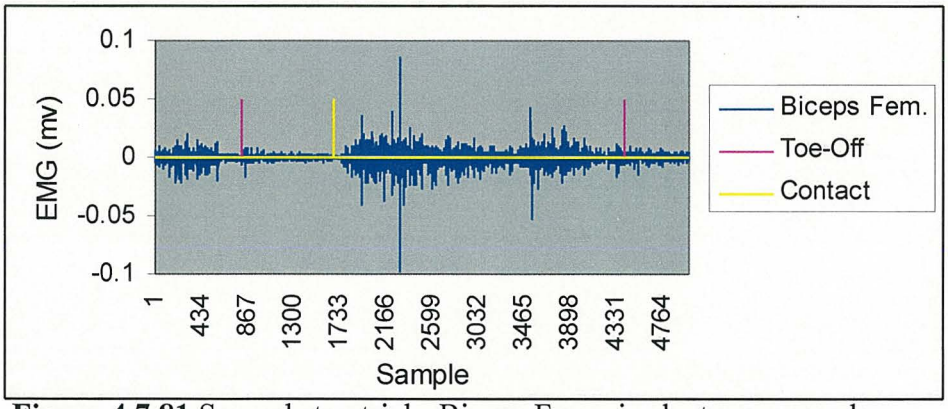

Figure 4.7.81 Second step trial - Biceps Femoris electromyography.

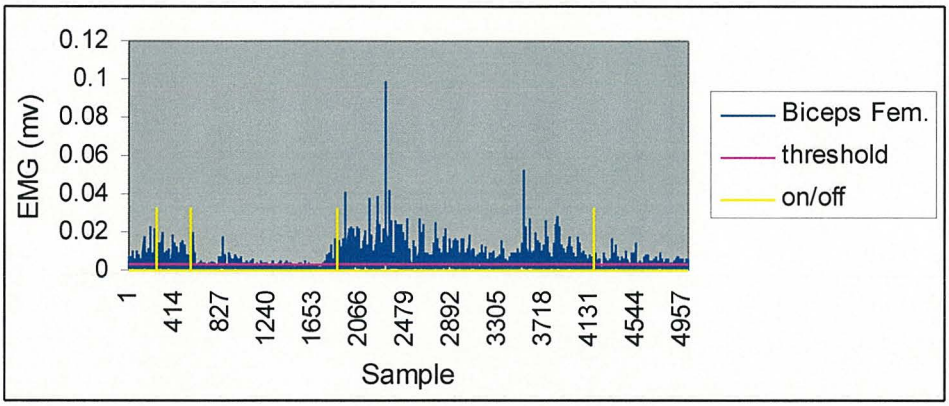

Figure 4.7.82 Second step trial - Biceps Femoris electromyography on/offsets.

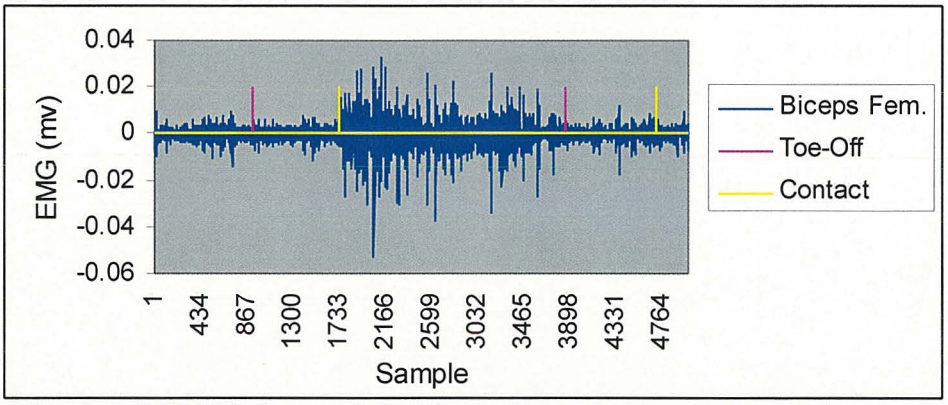

Figure 4.7.83 Third step trial - Biceps Femoris electromyography.

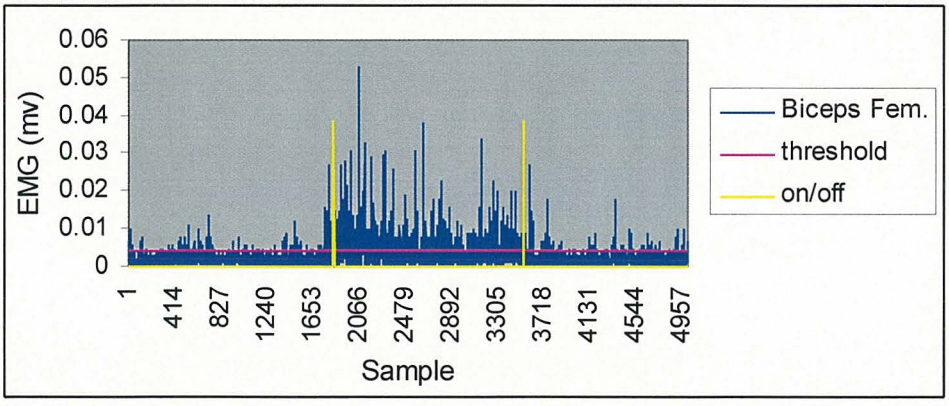

Figure 4.7.84 Third step trial - Biceps Femoris electromyography on/offsets.

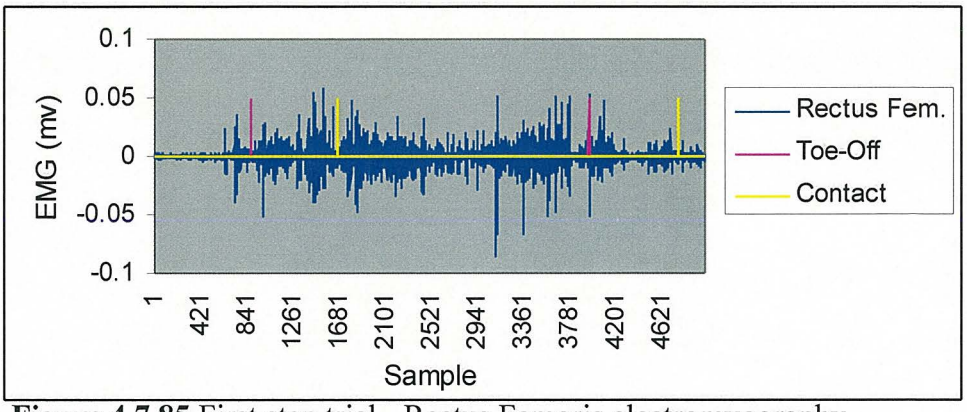

Figure 4.7.85 First step trial - Rectus Femoris electromyography.

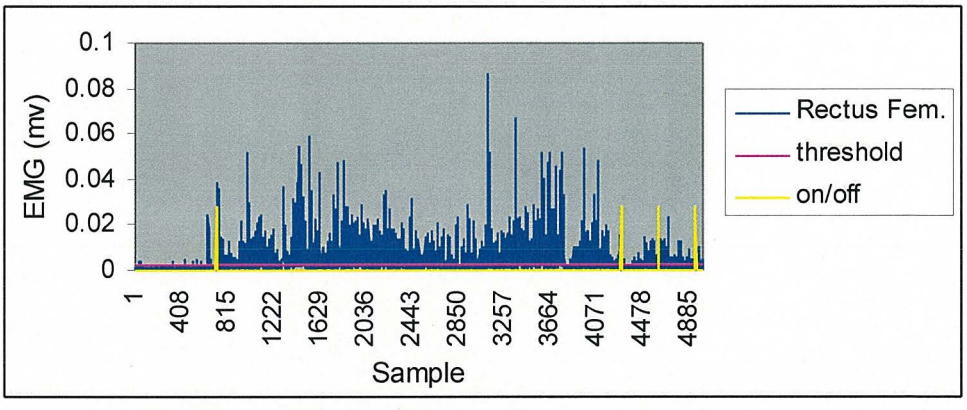

Figure 4.7.86 First step trial - Rectus Femoris electromyography on/offsets.

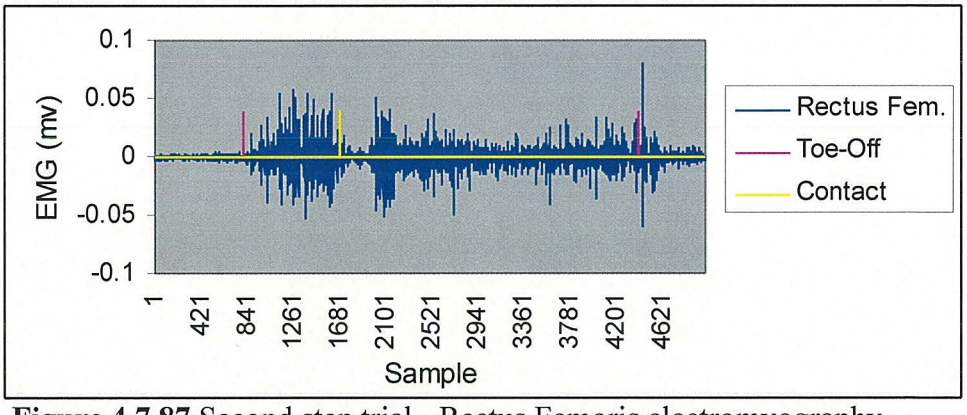

Figure 4.7.87 Second step trial - Rectus Femoris electromyography.

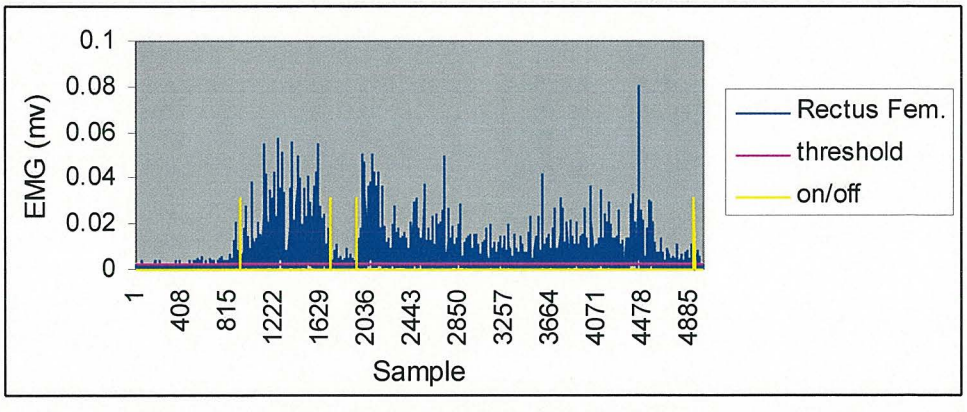

Figure 4.7.88 Second step trial - Rectus Femoris electromyography on/offsets.

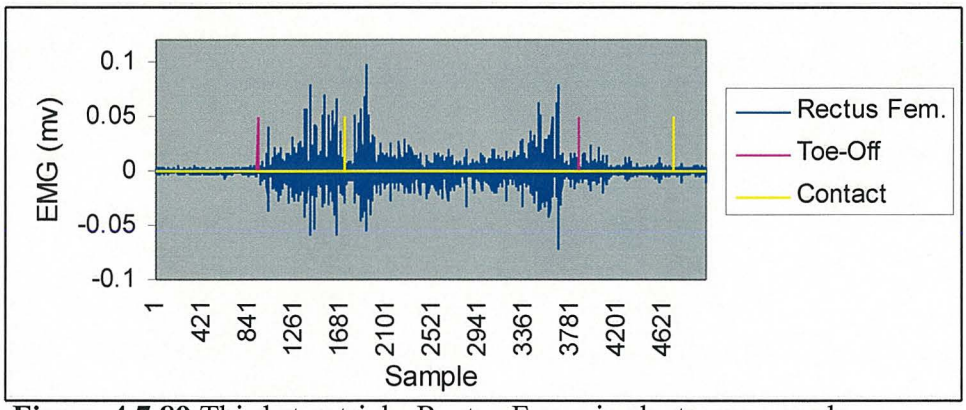

Figure 4.7.89 Third step trial - Rectus Femoris electromyography.

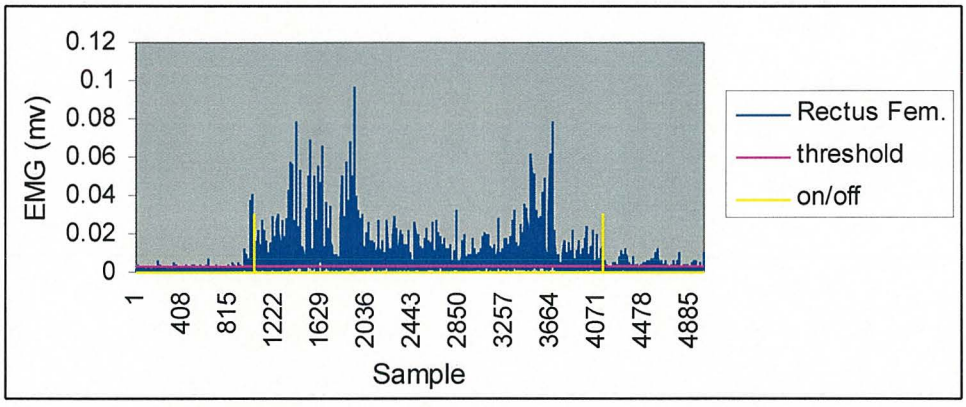

Figure 4.7.90 Third step trial - Rectus Femoris electromyography on/offsets.

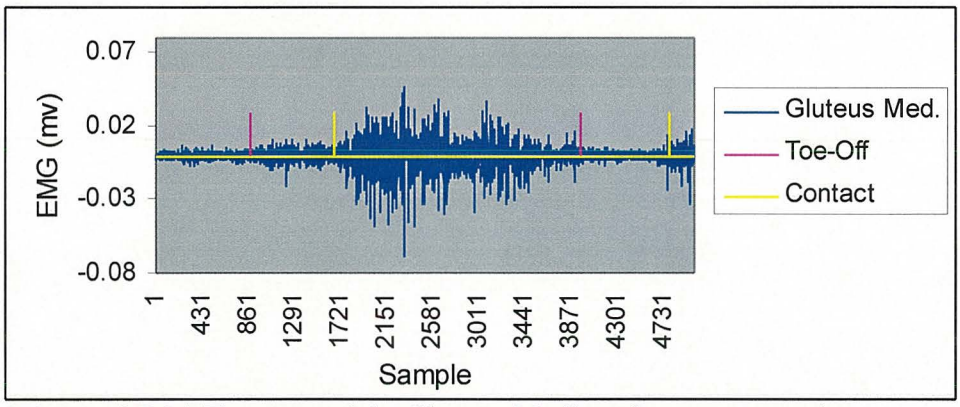

Figure 4.7.91 First step trial - Gluteus Medius electromyography.

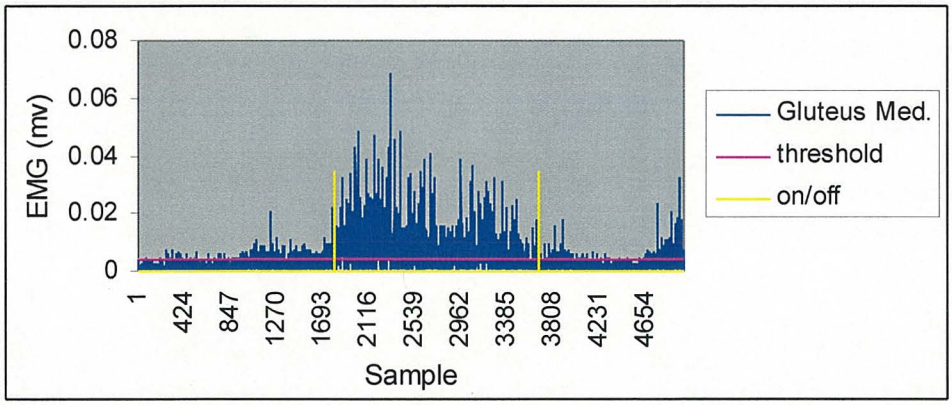

Figure 4.7.92 First step trial - Gluteus Medius electromyography on/offsets.

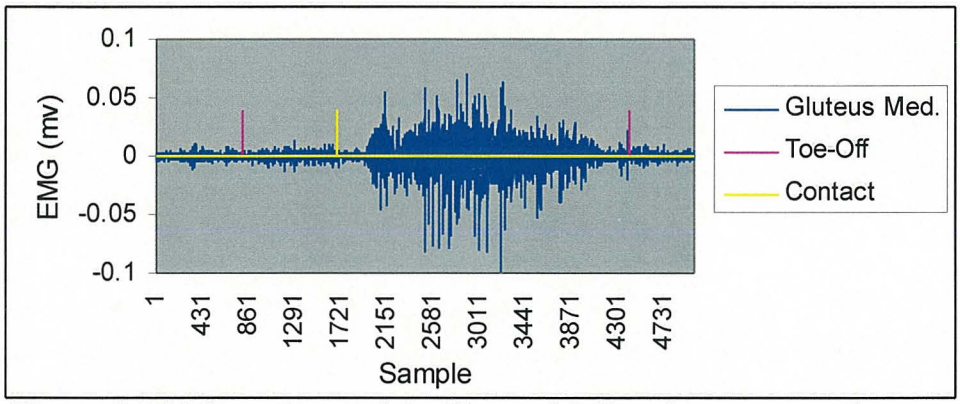

Figure 4.7.93 Second step trial - Gluteus Medius electromyography.

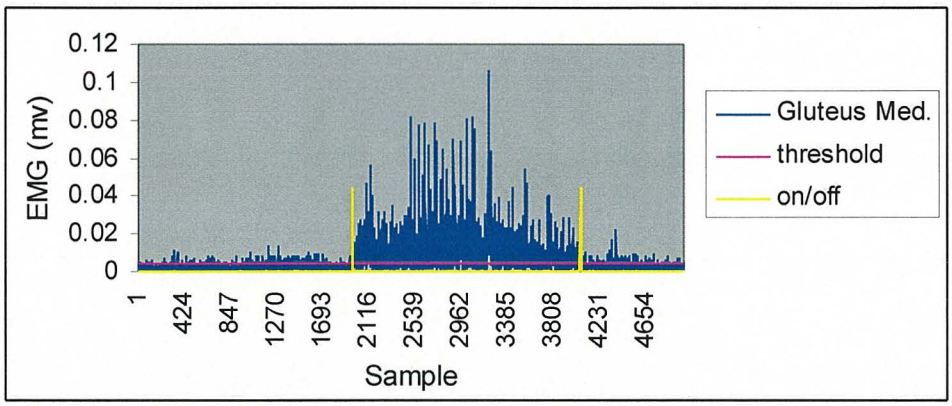

Figure 4.7.94 Second step trial - Gluteus Medius electromyography on/offsets.

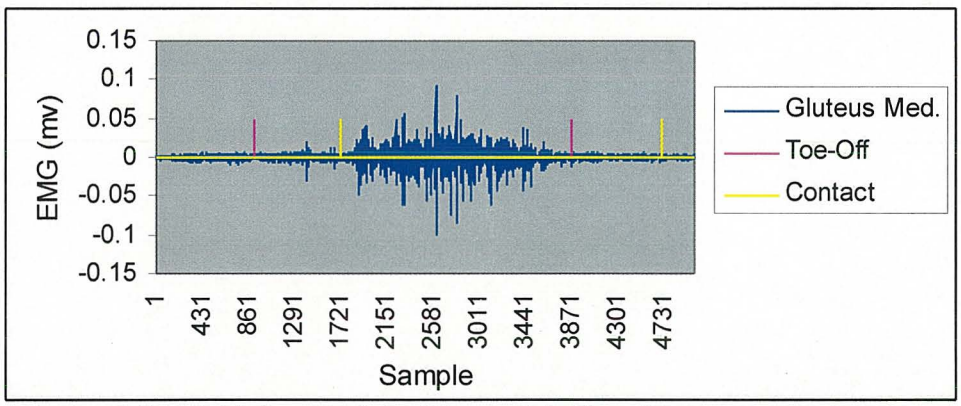

Figure 4.7.95 Third step trial - Gluteus Medius electromyography.

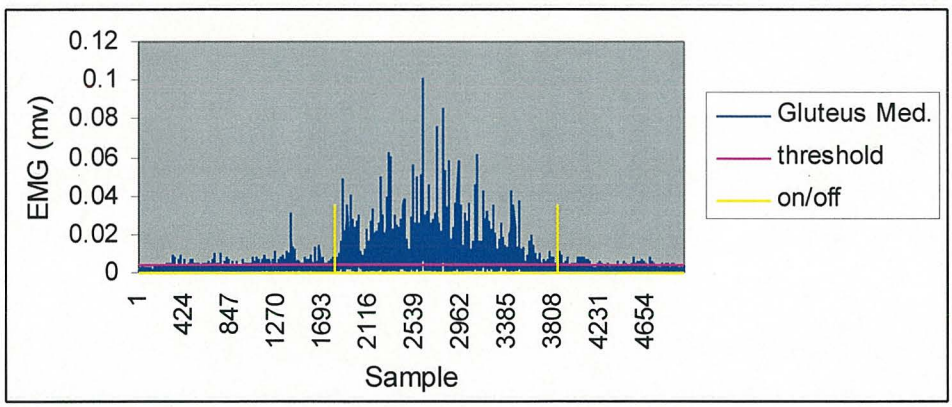

Figure 4.7.96 Third step trial - Gluteus Medius electromyography on/offsets.

Table 4.7.4 First step trial - electromyography on-sets and offsets.

	Electromyographic activity- first step trial
Soleus (lateral)	
On/Off	1714, 3474, 4600, 4943
RMS	0.012, 0.031, 0.008, 0.028, 0.013
Baseline	0.0089 at 1.50 sec.
Gastrocnemius (lateral)	
On/Off	-
RMS	-
Baseline	0.0155 at 3.65 sec.
Tibialis Anterior	
On/Off	681, 4963
RMS	0.007, 0.055, 0.016
Baseline	0.0083 at 0.10 sec.
Vastus Medialis	
On/Off	1651, 3870, 4511, 4916
RMS	0.002, 0.024, 0.003, 0.006, 0.003
Baseline	0.0032 at 0.60 sec.
Vastus Lateralis	
On/Off	1641, 3795, 4541, 4929
RMS	0.003, 0.021, 0.003, 0.005, 0.004
Baseline	0.0039 at 0.10 sec.
Biceps Femoris	
On/Off	1806, 2441, 4559, 4968
RMS	0.005, 0.012, 0.005, 0.013, 0.012
Baseline	0.0043 at 4.05 sec.
Rectus Femoris	
On/Off	716, 4286, 4606, 4939
RMS	0.002, 0.011, 0.004, 0.005, 0.003
Baseline	0.0028 at 0.35 sec.
Gluteus Medius	
On/Off	1804, 3673
RMS	0.003, 0.012, 0.004
Baseline	0.0036 at 0.15 sec.

Table 4.7.5 Second step trial - electromyography on-sets and offsets.

	Electromyographic activity- second step trial
Soleus (lateral)	
On/Off	696, 1248, 1870, 4121, 4403, 4832
RMS	0.009, 0.015, 0.006, 0.039, 0.009, 0.012, 0.006
Baseline	0.0074 at 1.50 sec.
Gastrocnemius (lateral)	
On/Off	-
RMS	-
Baseline	0.0206 at 4.15 sec.
Tibialis Anterior	
On/Off	612, 4975
RMS	0.005, 0.073, 0.036
Baseline	0.0061 at 0.05 sec.
Vastus Medials	
On/Off	1872, 4263
RMS	0.002, 0.021, 0.002
Baseline	0.0031 at 0.15 sec.
Vastus Lateralis	
On/Off	1836, 4466
RMS	0.003, 0.020, 0.002
Baseline	0.0037, 0.35 sec.
Biceps Femoris	
On/Off	249, 548, 1869, 4160
RMS	0.005, 0.006, 0.003, 0.009, 0.003
Baseline	0.0033 at 1.70 sec.
Rectus Femoris	
On/Off	926, 1720, 1937, 4920
RMS	0.002, 0.015, 0.003, 0.009, 0.003
Baseline	0.0032 at 0.10 sec.
Gluteus Medius	
On/Off	1966, 4055
RMS	0.003, 0.017, 0.004
Baseline	0.0045 at 0.15 sec.

Table 4.7.6 Third step trial - electromyography on-sets and offsets.

	Electromyographic activity- third step trial
Soleus (lateral)	
On/Off	824, 4296, 4921, 4972
RMS	0.004, 0.026, 0.007, 0.013, 0.024
Baseline	0.0063 at 0.20 sec.
Gastrocnemius (lateral)	
On/Off	-
RMS	-
Baseline	0.0145 at 0.45 sec.
Tibialis Anterior	
On/Off	759, 4980
RMS	0.007, 0.70, 0.020
Baseline	0.0044 at 0.10 sec.
Vastus Medialis	
On/Off	1712, 3645
RMS	0.002, 0.027, 0.003
Baseline	0.0030 at 0.85 sec.
Vastus Lateralis	
On/Off	1708, 3693
RMS	0.003, 0.025, 0.003
Baseline	0.0034 at 0.00 sec.
Biceps Femoris	
On/Off	1836, 3529
RMS	0.003 , 0.007 , 0.003
Baseline	0.0040 at 0.20 sec.
Rectus Femoris	
On/Off	1039, 4111
RMS	0.003, 0.012, 0.003
Baseline	0.0031 at 0.25 sec
Gluteus Medius	
On/Off	1808, 3838
RMS	0.003, 0.015, 0.002
Baseline	0.0036 at 0.05 sec.

5 DISCUSSION

The discussion chapter consists of five sections. The first deals with the accuracy of three dimensional segment locations in the present study and the influence of the number of markers per segment on the accuracy of derived musculoskeletal parameters. This was done using the three walk trials and instances where changes occurred in the number of markers used to reproduce segment three dimensional location and the continuity of derived parameters. The next section discusses the muscle model which includes limitations in the muscle-tendon local co-ordinate data used to define muscle-tendon paths over a range of joint motions, the use of muscle parameter optimisation to define force-length relationships over a range of joint motions, and the integration of muscle force-length force-velocity relationships in the present study. The third section discusses the optimisation procedure including the cost function used, obtaining initial muscle force estimates and the influence on muscle force prediction. The results of the movement trials are then discussed. This includes the accuracy of segment centre of mass acceleration, the accuracy and validity of muscle moment arms derived from the present musculo-skeletal model, and muscle forces predicted in comparison to electromyographic recordings. Throughout the discussion, limitations and inaccuracies in the methods are presented along with possible changes and corrections, which leads to the final section concerning future research arising from the present study.

5.1 Three dimensional segment location

The accuracy of reproducing three dimensional segment position is essential in determining segment acceleration, moment arms and muscle forces. As reported in previous research (Carman, 1996) when reproducing the three dimensional location of a single point from video-graphic analysis, a significant improvement can be made with the use of three cameras as opposed to just two. No significant difference in accuracy was seen between three and four cameras, however a small but significant improvement was seen when using five compared to three cameras. When using two cameras the accuracy was dependent on the angle between camera perspective centres and the three dimensional point, with the minimum error occurring at 90 degrees. The error approached infinity at 0 and 180 degrees. Furthermore, the minimum error at 90 degrees and the rate at which the error increases as camera angle moved away from 90 degrees was dependent on the accuracy of the photogrammetric system. When using three or more cameras a least squares approach was adopted to determine three dimensional

location and the dependency on camera angle was eliminated. This is of significance to the present study which relies on the accuracy of three dimensional segment location which in turn are reproduced from the three dimensional location of external points located on each segment. In this study, tracking three dimensional paths displayed small step discontinuities where the tracked point alternated between being visible in either three or two cameras. The sections comprising the path were continuous but were displaced from each other due to a jump in three dimensional location which occurred between the least squares point and a point derived from two cameras. The greater errors in reproducing a path with two cameras also produced greater variability in the path.

Similar errors to those seen when reproducing three dimensional point location resulting from changes in the number of cameras were also seen in the reproduction of three dimensional segment location of the pelvis and foot, where there were changes in the number of markers used to determined segment location during the movement trial. This was due to markers being obscured from the view of cameras during the trials and therefore unable to be reproduced in three dimensional space. The influence of marker numbers on segment accuracy and derived measures is now discussed.

5.1.1 Pelvis and foot segment location

Significant oscillations in the centre of mass acceleration occurred which corresponded to frames at which there was a change in the number of segment markers use to reproduce pelvis and foot three dimensional location. This would indicate a significant shift in segment location due to the change in segment marker numbers, and that the use of lesser number of markers was not sufficient to reproduce segment location and acceleration when compared to the accuracy of the greater number of markers. In this section results are presented for the first walk trial to demonstrate the findings, however, the same observation could be made and conclusions drawn from the second and third walk trials.

In the walking trials not all markers of the pelvis were visible in a least two cameras for the whole step cycle. For the first walk trial the three dimensional location of the navel marker was not reproduced from frames 110 to 158 (Table 4.5.1). Hence for the first walk trial, the pelvis location was reproduced from five markers from frames 8 to 109, while from frames 110 to 158, the pelvic location was reproduced from four markers (Table 5.1.1).

Table 5.1.1 First walk trial - markers used to reproduce segment location.

Segment	Markers per segment*
Pelvis	8----------(**5**)----------109:110---------(**4**)--------158
Thigh	8----------(**8**)----------158
Shank	8----------(**8**)----------158
Foot	8---(**5**)---22:23---------(**6**)---------136:137----- (**5**)-----158

*The number of markers are indicated by bold type in brackets, plain type indicate frames.

In the three walk trials, not all markers of the foot were visible in at least two cameras for the whole step cycle. For the first walk trial the three dimensional location of the medial toe marker was not reproduced from frames 137 to 158, and the posterior calcaneus was not reproduced from frames 8 to 21 (Table 4.5.1). Therefore for the first walk trial, from frames 8 to 21 the foot was reproduces from five markers, from frames 22 to 136 the foot was reproduced from six markers and from frames 137 to 158 the foot was reproduced from five markers (Table 5.1.1). Changes in the number of markers the foot was reproduced from occurred at frames 22 and 136.

In the first walk trial significant oscillations in the pelvis centre of mass acceleration (Figures 4.5.10 - 4.5.12, and Appendix L) were seen at frame 109 in the global y-axis (± 2.5 m/s^2) and z-axis (± 2.0 m/s^2). In the global x-axis no significant errors in centre of mass accelerations could be seen at frame 109. In the first walk trial significant oscillations in the foot centre of mass acceleration (Figures 4.5.19 - 4.5.21, Appendix L) were seen in the global x-axis at frame 133 (± 2.0 m/s^2). In the global y-axis, significant errors in the foot centre of mass acceleration were seen at frame 22 (± 1.0 m/s^2).

Significant spikes in muscle velocities were seen corresponding to frames at which a changes occurred in the number of segment markers used to reproduce pelvis and foot three dimensional location. However, not all frames where segment marker numbers changed produced sharp spikes in velocity data and not all muscles attaching to the respective segment were effected. The effect of shifts in the pelvis or foot location on muscles may depend on the orientation of the muscle and the magnitude and direction of the shift in segment location.

Contractile element velocities predicted by the muscle model were also effected due to the dependency on muscle velocity as well as contractile element force.

For the first walk trial Adductor Longus, Adductor Brevis, Adductor Magnus (ant) and Pectineus displayed distinct spikes in muscle velocities at frame 109 (Appendix L). Quadratus Femoris, Gluteus Minimus (ant) showed deviations in muscle velocities at frame 109 (Appendix L). Peroneus Longus, Peroneus Brevis showed distinct spikes in muscle velocities at frame 136.

For the three walk trials, no errors in the form of sharp oscillations were seen in the resultant joint moments of the hip (Figures 4.5.22 - 4.5.24) and ankle (Figure 4.5.28 - 4.5.30) corresponding to frames where changes occurred in the number of markers used to determine segment location. Therefore, in the present study involving slow movements of the lower limb, errors seen in segment location that resulted in significant oscillation in segment acceleration were not significant in the determined resultant joint moments. Similarly, for the first walk trial no significant shifts occurred in muscle lengths (Appendix L), muscle fibre and contractile element lengths (Appendix L), or muscle moment arms (Figures 4.5.46 - 4.5.103) corresponding to frames where changes in segment marker numbers occurred.

In the present study the experimental set-up used was not sufficient to accurately reproduce the locations of the pelvis and foot consistently during the movements analysed, as indicated by segment centre of mass acceleration and muscle velocities. This was due to insufficient markers on the pelvis (five) and insufficient cameras to record the movement of all the markers on the pelvis and foot during the entire movement. With the limitation of four cameras, which were placed on one side of the subject, the contra-lateral ASIS marker was seldom visible in two cameras in both the walk and step trials. The navel marker was only reproduced in the first half of the walk trials while the PSIS markers was only reproduced in the second half, as the subject progressed through the test area. Similarly for the foot, the medial toe was visible in two cameras for the first half of the walk trials and the posterior calcaneus was only reproduced in the second half the walk trials. As a result of the present study, in order to accurately reproduce the three dimensional location of the pelvis and foot it is necessary to increase the numbers of markers on the pelvis to at least six, as this segment is subject to movement artefact. This will allow the reproduction of a contra-lateral ASIS marker on the pelvis as well as navel, PSIS, medial toe and posterior calcaneus during the entire trial. The

possible placement of the cameras would be to the front and rear of the subject on the contra-lateral side compared to the present four camera set-up. However, the current experimental set-up and achieved accuracy was sufficient to obtain resultant joint moments in slow walking, as shown by the insensitivity of these measures to errors in segment accelerations and segment inertial forces. This may not be the case in other activities involving larger segment inertial forces and small external forces. The current experimental set-up and achieved accuracy is not sufficient to determine muscle contraction dynamics which rely on muscle contractile element velocity to determine muscle maximum dynamic forces, as muscle contractile element velocity was significantly effected by the accuracy of segment location in the present study.

5.1.2 Thigh and shank segment location

In the three walk trials the thigh and shank were reproduced from all eight segment markers for the entire gait cycle analysed: frames 18 to 148 for the first walk trial (Table 4.5.1 and 4.5.2), frames 26 to 154 for the second walk trial (Tables 4.5.3 and 4.5.4), and frames 11 to 142 for the third walk trial (Tables 4.5.5 - 4.5.6).

In the present study the locations of the thigh and shank were reproduced consistently in the three walk trials with eight markers on the respective segments and four cameras position on the ipsi-lateral side of the subject. This was reflected in segment centre of mass acceleration (Figures 4.5.13 - 4.5.18) and muscle velocities of the first walk trial (Appendix L). It is not known whether more than eight markers would increase the accuracy beyond the present study. However, additional cameras may increase accuracy by allowing anterior and posterior markers of the thigh and shank to be viewed and reproduced by three cameras instead of two, thereby increasing the accuracy of the three dimensional points used to calculate three dimensional segment location.

5.2 Muscle model

A discussion of the three areas which have been developed to improve the application of the muscle modelling to the force prediction in the analysis of three dimensional movement are now presented. These are: (i) muscle model co-ordinate data used to describe muscle-tendon path during a range of joint angles; (ii) muscle parameter optimisation to range of muscle lengths; and (iii) integration of the force-length and force-velocity relationships.

5.2.1 Muscle model: muscle co-ordinate data

In order to describe muscle-tendon lengths and moment arms during a range of joint motion of the ankle, knee and hip, local segment co-ordinate data are presented describing muscle origins, insertions and deflection points for 48 muscle elements of the lower limb. It was considered that a larger number of deflection points defined around a joint capsule, bony prominence or retinaculum would more accurately represent the muscle-tendon path. However, if these deflection points are expressed as segment-fixed local co-ordinates, then with changes in joint angle, points defining different segments may coincide, cross adjacent points or move into adjacent segments. Hence, with fixed local co-ordinates describing deflection points, there are limitations placed on where they may be defined in order to best describe muscle-tendon paths for a range of joint angles. Therefore, limitations were placed on the number of deflection points that may be used to describe a muscle-tendon path when applied to a range of joint angles. Equally, the muscle co-ordinate data presented are only valid within a given range of joint angles measured from the standing anatomical position (Section 3.1.1). Therefore, limitations to the range of motion at which the present co-ordinate data can describe muscle path resulted from:

a) Two deflection points of a single muscle-tendon complex, both defined relative to adjacent segments, that come in close proximity to one another with changes in joint angle. If the moment arm is calculated from the vector joining the two deflection points, then the vector represents the line of action of the muscle-tendon complex with respect to the joint centre. Ideally, with changing joint angle the deflection points would move apart or together but would not meet resulting in an overlap in muscle tendon paths. In the non-ideal case, with the inclusion of errors in three dimensional segment locations, erroneous and erratic moment arms would result if two deflection points move in close proximity to each other. In this situation, the length of the muscle-tendon would be affected to a lesser extent, due to the small distances between the deflection points. However, large variations in the direction of the vector joining the two points, and consequently moment arms, would result.

b) The use of a fixed local co-ordinate to identify deflection points means that with changing joint angle, the point is fixed and cannot change due movement of the muscle relative to the underlying bone. A deflection point may therefore meet surrounding

bone or other tissue as the joint angle changes. This also introduces error when segment rotations may cause a change in the position of the muscle or tendon relative to the underlying bone due to movement of the surrounding soft-tissue structures.

c) The line joining origin, insertion and deflection points meeting or passing through a joint capsule or bone. The true path of the tendon would be expected to pass around such structures, and therefore, at these joint angles, the muscle tendon length and moment arm would be underestimated.

The following limitations to joint range of motion resulting from the fixed local positions of muscle-tendon defection points were encountered in the present study:

a) Hip flexion was limited by Psoas and Iliacus deflection points on the femur, located anterior to the femoral head, rising up to meet the Psoas and Iliacus deflection point on the pelvis. By moving Psoas and Iliacus deflection point along the z-axis of the Femur inferior to its present location, would result in an increase in hip flexion. By manipulating the present muscle model, it is estimated that an inferior relocation of this deflection point of approximately 1.5 cm would increase the range of hip flexion of the present muscle model to 90 degrees.

b) Hip extension from the anatomical position was limited by the line joining Psoas and Iliacus deflection points of the femur and pelvis passing inside the joint capsule. Hip extension was also limited by, in order of priority, Obturator Externus, Obturator Internus, Gremellus Superior, Gremellus Inferior, and to a lesser extent Piriformis muscle lines passing through the posterior margin of the rim of the acetabulum and the joint capsule. By moving Psoas and Iliacus deflection point more anteriorly on the pelvis, and the deflection point on the femur more anteriorly, an increase in hip extension would result. It is estimated that an anterior shift of approximately 0.5 cm. in both the femur and pelvis deflection points of Psoas and Iliacus and introducing a deflection point for Obturator Externus, Obturator Internus, Gremellus Superior, Gremellus Inferior, and Piriformis at the posterior margin of the rim of the acetabulum would increase hip extension in the present model to 35 degrees.

c) Hip adduction was limited by Psoas and Iliacus deflection point on the femur moving into the bone of the pelvis at the superior ramus of the pubis. By moving Psoas and Iliacus deflection point on the Femur inferiorly and anteriorly to its present location, an increase in hip flexion would result.

d) Hip abduction was limited by the insertion points of Gluteus Medius (ant) and to a lesser extent Gluteus Medius (mid) on the femur rising up to meet their respective deflection points on the pelvis. By moving the both Gluteus Medius (ant) and Gluteus Medius (mid) deflection points on the pelvis more superiorly, an increase in hip abduction would result. The line of the Obturator Externus moving into the hip joint capsule also limited hip abduction. It is estimated that a superior shift of approximately 1.0 cm and 0.5 cm to the pelvis deflection points of Gluteus Medius (ant) and Gluteus Medius (pos) respectively, and introduction of a deflection point for Obturator Externus at the posterior margin of the rim of the acetabulum, would increase hip abduction in the present model to 45 degrees.

e) Hip internal rotation was limited by, in order of priority, the lines of Obturator Externus, Obturator Internus, Gremellus Superior, Gremellus Inferior, and to a lesser extent, Piriformus muscles passing through the hip joint capsule. Hip internal rotation was also limited by the deflection points of Psoas and Iliacus on the femur moving into the bone of the pelvis at the superior ramus of the pubis. Moving the deflection points of Psoas and Iliacus inferior to it present location would increase hip flexion. It is estimated that an inferior shift of approximately 1.5 cm in the femur deflection points of Psoas and Iliacus and introducing a deflection points for Obturator Externus, Obturator Internus, Gremellus Superior, Gremellus Inferior, and Piriformis at the posterior margin of the rim of the acetabulum would increase hip internal rotation in the present model to 35 degrees.

f) Knee flexion was limited by Semimembranosus, Semitendinosus, Biceps Femoris (long), and Biceps Femoris (short) deflection points on the shank meeting their respective deflection points on the femur. By moving Semimembranosus, Semitendinosus, Biceps Femoris (long), and Biceps Femoris (short) deflection points on the femur superior and moving Biceps Femoris (long) and Biceps Femoris (short) deflection points on the shank inferiorly and posteriorly, an increase in knee flexion

would result. Knee flexion is limited to a lesser extent by Gastrocnemius (lat), Gastrocnemius (med) and Plantaris deflection points on the shank meeting their respective deflection points on the femur. By moving Gastocnemius (lat), Gastrocnemius (med) and Plantaris deflection points on the femur more anteriorly, an increase in knee flexion would result. It is estimated that a superior shift of approximately 1.5 cm in Semimembranosus, Semitendinosus, Biceps Femoris (long) and Biceps Femoris (short) deflection points on the shank, an inferior and posterior shift of approximately 0.5 cm and 1.0 cm respectively in the shank deflection point of Biceps Femoris (long) and Biceps Femoris (short), and an anterior shift of approximately 0.5 cm of Gastocnemius (lat), Gastrocnemius (med) and Plantaris deflection points on the femur, would increase knee flexion in the present model to 110 degrees.

g) Knee internal and external rotation with knee flexion was limited by Semimembranosus, Semitendinosus, Biceps Femoris (long), and Biceps Femoris (short) deflection points on the shank meeting their respective deflection points on the femur. As with knee flexion, by moving the Semimembranosus, Semitendinosus, Biceps Femoris (long) and Biceps Femoris (short) deflection points on the femur more superioly, and by moving Biceps Femoris (long) and Biceps Femoris (short) deflection points on the shank more inferiorly and posteriorly, an increase in knee internal and external rotation would result.

In the present model of muscle-tendon paths, limits placed on the range of motion of hip external rotation, knee extension and movements of the ankle were due to physical joint constraints of the skeletal model rather than muscle origin, insertion and deflection points limiting the range of motion.

When analysing muscle moment arms over the step and walk trials, moment arms in the anatomical position were as expected when compared to previous research, however, some moment arms showed inconsistencies towards the end ranges of motion within the walk and step trials. See section 5.4.2 for a detailed discussion of muscle moment arm results and the errors involved in reproducing moment arms from segment motion. To reduce errors associated with the relative motion of segment fixed points used to define muscle-tendon paths, and to ensure that the muscle-tendon co-ordinate data could adequately describe

moment arms in walking and stepping trials, the muscle-tendon co-ordinate data were reviewed. This was achieved by going back to the skeletal model and suggesting changes in location of deflection point data so as to increase the range of motion over which moment arms could be defined and at the same time not adversely effect moment arms in the anatomical position.

The following changes are recommended to the muscle co-ordinate data presented in the present study to increase the range of joint angles over which the co-ordinate data is valid in describing muscle-tendon lengths and moment arms. The results of the changes are an estimated increase of 20 degrees in joint ranges of motion for hip flexion and knee flexion, an increase of 10 degrees in internal and external rotation at 90 degrees knee flexion, and an increase in 10 degrees in hip extension, hip adduction and hip abduction over those presented in Section 3.1.1. Possible magnitudes of the changes in location are expressed in brackets:

a) Moving Psoas and Iliacus deflection points on the femur inferiorly (1.5 cm) and anteriorly (0.5 cm);
b) Moving Psoas and Iliacus deflection points anteriorly on the pelvis (0.5 cm);
c) Introducing deflection points on the posterior margin of the rim of the acetabulum for Obturator Externus, Obturator Internus, Gremellus Superior, Gremellus Inferior, and Piriformis muscles;
d) Moving Gluteus Medius (ant) and Gluteus Medius (mid) deflection points superiorly on the pelvis (1.0 cm and 0.5 cm respectively);
e) Moving Semimembranosus, Semitendinosus, Biceps Femoris (long), and Biceps Femoris (short) deflection points superiorly on the femur (1.5 cm);
f) Moving Biceps Femoris (long) and Biceps Femoris (short) deflection points on the shank inferiorly (0.5 cm) and posteriorly (1.0 cm); and
g) Moving Gastrocnemius (lat) and Plantaris deflection points of the femur anteriorly (0.5 cm).

With the possible exception of Quadratus Femoris and Soleus muscles, all other muscle elements modelled in the present study required three or more points expressed relative to local fixed segment axes to adequately describe muscle-tendon path and moment arms for a range of joint angles.

5.2.2 Muscle model: parameter optimisation

In the present study a muscle model comprising a fibre length, a contractile element length, a fibre series elastic component length, pennation angle, muscle belly length, and tendon length was used to represent a muscle or muscle element. The muscle model reference fibre length and reference pennation angle are defined at the reference muscle length, which was taken at the standing anatomical position for the lower limb musculature. Reference belly length was used to determine the changes in muscle belly lengths for the muscle model. For any given movement, a range of muscle lengths can be determined and expressed as a maximum and minimum change in muscle belly length from the reference belly length in the reference body position. The muscle model also describes a force-length relationship which has a unique maximum and minimum fibre length determined by the optimal fibre length of the muscle model. Muscle model parameter optimisation ensures that the muscle model parameters of reference fibre length and pennation angle can describe a maximum and minimum change in muscle belly lengths that includes the changes in muscle belly length determined for the movement. The model must also ensure the optimal fibre length can also describe a maximum and minimum fibre length that includes the fibre lengths required of the maximum and minimum changes in belly length of the movement trial. The maximum and minimum belly lengths obtained from the movement trial establish the minimum required changes of length, however reference fibre lengths and pennation angles or optimal fibre lengths may well describe a range of muscle belly lengths greater than those required for the current movement trial.

Muscle model fibre length, pennation angle, series elastic component, and contractile element length represent the structure and function of the whole muscle and as such, represent the function of all muscle fibres of that muscle. The muscle model parameters of reference fibre length, pennation angle, belly length, and optimal fibre length are modified during the optimisation procedure to describe estimated length and force characteristic of the whole muscle. Therefore, fibre length, pennation angle and optimal fibre length produced in the present study do not represent an individual muscle fibre. Similarly, following muscle parameter optimisation, muscle reference belly length may no longer represent the anatomical belly length for the respective muscle as it may be lengthened to accommodate changes in reference pennation angle and reference fibre length. However, this fact does not alter the function of the model as the changes in muscle belly length from the reference belly length are

used to calculate new pennation angles and fibre lengths relative to the reference fibre length and reference pennation angle. Muscle belly length is calculated from muscle length and tendon length. In the present study optimisation of muscle model parameters does not alter tendon slack length as scaled from reference skeletal data.

Muscle model parameter optimisation involves solving a set of simultaneously equations to arrive at a reference fibre length, reference pennation angle, reference belly length, optimal fibre length and optimal isometric force. These equations describe the relationship between the maximum and minimum fibre lengths and pennation angles derived from the changes in belly length of the movement trial, and the maximum and minimum fibre lengths determined from the optimal fibre length. Three assumptions were made in the muscle parameter optimisation routine which introduced three equations and one conditional statement into the set of simultaneous equations.

1) The first assumption was that muscles were able produce a contractile element force at the maximum and minimum belly lengths and corresponding segment positions determined from the range of motion of each movement trial. The optimisation procedure produces an optimal fibre length which describes a force-length relationship between a maximum and minimum fibre length. A constant 15% was added to the measured maximum and minimum changes in belly length, as determined from the movement trial, to ensure the maximum and minimum fibre length at which force can be generated, as described by the force-length relationship, encompassed the fibre lengths of the movement trial. The value of 15% was made on visual observation, so that the maximum fibre lengths of the movement trial would avoid the asymptotic region of force-length profile at larger fibre lengths. An increase of 15% would result in the maximum fibre lengths of the actual movement trial falling at the start of the asymptotic region (Section 3.1.3). This introduced two equations to the iterative procedure that increased the respective changes in muscle belly length determined from the movement trial.

2) The second assumption was that the maximum and minimum fibre length derived from the optimal fibre length equally spanned the maximum and minimum fibre lengths derived from the changes in muscle belly length of the movement trial, see Fig. 3.1.4. This introduced one equation to the iterative procedure relating maximum and

minimum fibre lengths determined from the changes in muscle belly length of the movement trial to optimal fibre length.

3) The third assumption was that the maximum allowable pennation angle was 40 degrees. This prevented the pennation angle of the muscle model from approaching or going beyond 45 degrees producing zero tendon force or negative tendon forces in the muscle model. This introduced a condition into the iteration equations and, if this condition was met, the reference pennation angle and reference fibre length were changed and the iteration repeated.

The assumption that the maximum and minimum fibre lengths derived from the optimal fibre length and force velocity equation should equally span the required fibre lengths of the movement was supported by Hawkins & Bey (1997) who, in measuring the force-length properties and range of lengths at which the rat Tibialis Anterior operates *in vivo*, found that during movements involving a normal range of motion, the Tibialis Anterior operated within the optimal region of its force-length relationship. However the authors noted that similar studies on different muscle and different animals produced varying results, with muscles operating in different regions of the force-length curve. Therefore, with respect to the present study, it would be more appropriate to use the maximum range of joint motions and resulting changes in muscle belly length in the optimisation of muscle model parameters. This would describe a more realistic optimal fibre length and force-length relationship for the muscle length presented in the movement trial.

Due to the highly non-linear nature of the equations, an iterative procedure was used where, with the same number of equations as unknowns and each muscle model parameter given by a separate equation, each parameter estimate was sequentially improved by cycling though each equation and solved in turn based on an improved parameter estimate. The cycling continued until the magnitude of the change in parameters fell below a criterion value and convergence was achieved. With an appropriate ordering of equations and a starting estimate involving muscle model parameters that do not vary to a large extent from the initial values, convergence was achieved.

Prior to implementing the iterative procedure, the three dimensional segment locations for the movement trial would need to be calculated and the muscle model co-ordinate data of origins,

insertions and deflection points applied to establish maximum and minimum muscle lengths for the movement trial. In addition reference muscle model parameters would also need to be determined by scaling reference data to the reference muscle lengths of subject. The reference muscle lengths were determined by the three dimensional segment locations while in the reference position. From the reference muscle model data for the subject and from the muscle lengths derived from the movement trial, the following are known:

i) Reference muscle-tendon length at current joint angles and segment positions;
ii) Maximum and minimum muscle-tendon lengths for each movement trial;
iii) Tendon slack length; and
iv) Reference muscle belly length.

The changes in belly length required by the muscle model are determined from the muscle lengths of the movement trial, as well as the maximum and minimum tendon lengths. From these, the extended changes in muscle belly length are calculated to ensure contractile forces at full range of motion are also known. To start the optimisation procedure, the maximum tendon length under optimal isometric force is first approximated by tendon slack length. Then, from equation 3.1.1:

a) the positive or maximum required change in belly length is given from the maximum muscle length, tendon slack length and reference belly length;
b) the negative or minimum required change in belly length is given from the minimum muscle length, maximum tendon length and reference belly length;
c) extended maximum change in muscle belly length is given by the maximum required change in belly length plus 15% of the difference between maximum and minimum required changes in muscle belly lengths; and
d) extended minimum change in muscle belly length is given by the minimum required change in belly length minus 15% of the difference between maximum and minimum required changes muscle belly lengths.

In the case of a non-pennate muscle, the fibre length is given directly from the muscle belly length and the pennation angle is always zero, leaving only the reference fibre length to be determined. Then, from equation 3.1.3:

e) maximum and minimum fibre lengths are given directly from the maximum and minimum extended changes in belly lengths and reference belly length;
f) minimum optimal fibre length required is given from the difference between maximum and minimum fibre lengths;
g) optimal fibre length is given from the sum of maximum and minimum fibre lengths;
h) if the optimal fibre length is less than the minimum required optimal fibre length then the optimal fibre length is set to the minimum required optimal fibre length;
i) maximum and minimum fibre lengths are given from the optimal fibre length;
j) reference fibre length is given from the maximum fibre length and maximum extended change in belly length;
k) reference belly length is given directly from the reference fibre length; and
l) reference muscle-tendon length is given from the reference belly length and tendon slack length.

In the case of the pennate muscle, changes in muscle belly length from the reference muscle belly length are used to calculate new pennation angles relative to the reference pennation angle and reference fibre length. With the new pennation angle, a new fibre length is calculated. In order to determine reference pennation angle, reference fibre length and reference muscle belly length, an iterative procedure is required due to their inter-dependency. To start the iterative procedure, reference fibre length, reference pennation angle and reference muscle belly length determined from skeletal reference data are used. Then, from equation 3.1.14:

e) if reference muscle belly length is less than reference fibre length multiplied by the sine of reference pennation angle, then the reference muscle belly length is set equal to the reference fibre length multiplied by the sine of the reference pennation angle. Reference muscle-tendon length is set equal to the sum of the reference muscle belly length and tendon slack length;
f) maximum pennation angle is given from the maximum extended change in belly length;
g) minimum pennation angle is given from the minimum extended change in belly length;
h) maximum fibre length is given from the maximum pennation angle;
i) minimum fibre length is given from the minimum pennation angle;

j) if the pennation angle at minimum change in belly length is less than 40 degrees, then the reference pennation angle is decreased and the reference fibre length is increased and the iteration procedure is repeated from e);

k) minimum optimal fibre length required is given from the difference between maximum and minimum fibre lengths;

l) optimal fibre length is given from the sum of the maximum and minimum fibre lengths;

m) if the optimal fibre length is less than the minimum required optimal fibre length, then the reference fibre length is increased, and the iteration procedure is repeated from e);

n) minimum possible muscle model fibre length is given from the reference fibre length and reference pennation angle;

o) absolute minimum fibre length of the force length relationship is given by the optimal fibre length;

p) if the absolute minimum fibre length is less then the minimum model fibre length, then the reference pennation angle is decreased and the reference fibre length is increased, and the iteration procedure is repeated from e);

q) minimum absolute pennation angle of the force length relationship is given from the absolute minimum fibre length of the force-length relationship;

r) if the absolute minimum pennation angle of the force-length relationship is less than 40 degrees, then the reference pennation angle is decreased and the reference fibre length is increased, and the iteration procedure is repeated from e);

s) while there is a change in reference fibre length or reference pennation angle, the iteration procedure is repeated from e).

The result of both the pennate and non-pennate procedures provide the reference muscle-tendon length, reference belly length, reference fibre length, reference pennation angle, and optimal fibre length. For both the pennate and non-pennate muscles, the reference series elastic component length, contractile element length, physiological cross section area, and maximum isometric force at the reference muscle-tendon length can be calculated (equations 3.2.15 - 3.1.18). The fibre length resulting from the maximum isometric force at the current muscle-tendon length is then calculated followed by the optimal isometric force (equations 3.1.19-3.1.24). For the pennate muscle, knowledge of the optimal isometric force, optimal fibre length and resulting pennation angle allows calculation of the maximum tendon length

(equations 3.1.25 - 3.1.26). For the non-pennate muscle, the maximum tendon length is given directly from the optimum isometric force (equation 3.1.26).

To conclude the optimisation procedure, the minimum change in muscle belly length is re-calculated from the minimum muscle length, reference muscle belly length and new maximum tendon length and then compared to the extended minimum muscle belly length used in the optimisation procedure. For the first iteration, the tendon slack length was used as an estimation of the maximum tendon length. In the event that the minimum change in muscle belly length was greater than the extended minimum muscle belly length, then both the maximum and minimum changes in belly length were increased and the optimisation procedure repeated. This situation may occur in muscles with small fibre lengths and changes in muscle belly length compared to the length of the tendon. From Section 3.1.3, the following can be described:

t) a new minimum change in muscle belly length is given from the minimum muscle length, maximum tendon length and reference muscle belly length;
u) if the new minimum change in belly length is less than the extended minimum change in muscle belly length, then the minimum and maximum changes in belly length as calculated from the movement trial are increased and the optimisation procedure repeated from c).

If, in the course of the procedures, reference muscle-tendon length is increased from the originally calculated value at the reference segment positions, then the quantity added is stored for the respective muscle element. Whenever the muscle-tendon length is subsequently calculated from segment positions, the muscle-tendon length is increased if required prior to the use of the optimised reference muscle model parameters and muscle model in predicting muscle force.

In the present study, muscle model parameter optimisation was successful for all applications of the equations, including a muscle model test example (Section 3.1.6) and in modelling 48 muscle elements of the lower limb during walking and stepping tasks (Appendix F). In the muscle model test example (Section 3.1.6), muscle model parameter optimisation was presented for both a pennate and non-pennate muscle example. The two muscles were considered to have the same reference muscle-tendon length, tendon slack length and

reference muscle belly length, and both muscles were optimised to the same changes in muscle belly length. However, the pennate muscle had a smaller reference fibre length and muscle mass than the non-pennate muscle example (Table 3.1.4). In the non-pennate muscle example, the required maximum and minimum fibre lengths were the same as the maximum and minimum changes in muscle belly length. Also, in the non-pennate example, the optimal fibre length calculated was greater than the minimum optimal fibre length required to span the range of fibre lengths. Therefore, this optimal fibre length was used without alterations to the reference fibre length (Table 3.1.5). The geometric relationship between reference fibre length, maximum and minimum belly lengths, optimal fibre length, and maximum and minimum fibre lengths calculated from the optimal fibre length are presented in Fig. 3.1.7.

For the pennate muscle, a smaller reference fibre length resulted in a reduction in the both the maximum and minimum muscle fibre lengths produced by the maximum and minimum changes in muscle belly length (Table 3.1.5). As a consequence, the optimal fibre length, calculated as a function of the sum of maximum and minimum muscle fibre lengths, was also reduced. In the pennate muscle, the minimum optimal fibre length required to span the range of muscle fibre lengths was slightly reduced due to the angle of pennation. However, the required changes in muscle belly length were the same for the pennate and non-pennate muscle examples. Also, in the pennate example, reference muscle fibre length was increased and reference pennation angle reduced to increase the sum of the maximum and minimum fibre lengths produced by the changes in muscle belly length. This also increased the optimal fibre length.

In the present example the iterations would have proceeded until the maximum and minimum fibre length described by the optimal fibre length included the maximum and minimum fibre lengths produced from the changes in muscle belly length, the reference muscle fibre length, and reference pennation angle. The geometric relationship between reference fibre length, reference pennation angle, maximum and minimum muscle belly lengths, optimal fibre length, maximum and minimum fibre lengths, and corresponding muscle belly length calculated from the optimal fibre length are presented in Fig. 3.1.8.

For both the pennate and non-pennate examples, the reference muscle-tendon length, reference muscle belly length and tendon slack lengths were unaltered by the optimisation procedure. The optimal fibre length of the non-pennate muscle producing a larger range of muscle fibre lengths than required by the changes in muscle belly lengths. Conversely, in the pennate

muscle, the range of muscle fibre lengths has been increased by the optimisation procedure to just cover that required by the changes in muscle belly lengths. In the present examples the larger optimal muscle fibre length and consequently larger range of muscle fibres of the non-pennate muscle has resulted in a smaller optimal isometric force than in the pennate muscle example. This was due to the increased range of fibre lengths described by the force-length relationship of the non-pennate muscle and resulted in the reference fibre length being closer to the optimal fibre length than in the pennate muscle example, where the reference fibre length was closer to the maximum fibre length. Therefore, a smaller optimal isometric force is calculated from the reference isometric force in the non-pennate muscle example.

In modelling 48 muscle elements of the lower limb during the walking and stepping trials, the muscle model parameter optimisation was employed for each muscle element for the ranges of muscle belly lengths produced from each trial. The results of the muscle parameter optimisation for each muscle element of the first walk trial are presented in Appendix F, and includes:

i) pre-optimisation reference muscle model parameters;
ii) maximum and minimum muscle lengths from the movement trial;
iii) maximum and minimum changes in belly length for the movement trial;
iv) the extended maximum and minimum changes in belly length;
v) optimised reference muscle model parameters;
vi) optimal fibre length, reference series elastic component length, reference contractile element length, physiological cross sectional area, maximum reference isometric force, and optimal isometric force;
vii) the absolute maximum and minimum muscle lengths determined from optimal fibre length;
viii) the maximum isometric force and corresponding muscle fibre lengths, pennation angle, muscle belly length, and tendon length for a range of muscle lengths between the absolute maximum and minimum muscle lengths; and
ix) the number of iterations of the optimisation procedure is also given.

For the majority of muscles modelled in the lower limb during walking and stepping, muscle model parameter optimisation did not change the reference muscle model parameters (Table 5.2.1). In this situation, the force-length relationship defined from the optimal fibre length

included the maximum and minimum fibre lengths determined for the movement trial from the changes in muscle belly lengths, reference muscle fibre lengths and reference pennation angles. In addition the condition placed on the maximum pennation was satisfied. However, muscle model parameter optimisation was still necessary to determine optimal fibre lengths and optimal isometric force.

Whether the reference muscle parameters were altered depended on the relationship between reference fibre length, reference pennation angle and the changes in muscle belly length required of the movement. For non-pennate muscles, the muscle model parameters were left unchanged for muscles with proportionally larger fibre lengths in comparison to the changes in muscle belly lengths (Table 5.2.1). For non-pennate muscles with small muscle fibre lengths in proportion to the changes in muscle belly length, the optimisation procedure increased reference muscle fibre length, thereby increasing the optimal fibre length. In so doing, this increased the maximum and minimum fibre lengths in the force-length curve to include the required changes in muscle belly length. This can be seen in comparing the optimisation results for Obturator Externus, Obturator Internus and Quadratus Femoris (Table 5.2.2) with other non-pennate muscles (Table 5.2.1).

For pennate muscles, the need to change muscle model parameters was also dependent on the ratio between muscle fibre length and changes in muscle belly length, in addition to the condition placed on the maximum pennation angle at minimum change in belly length. Pennation angle also influenced the maximum and minimum fibre lengths resulting from the changes in belly length as well as the force in the direction of the tendon and tendon length. If the optimal fibre length was less than the minimum required optimal fibre length in the pennate muscle, then the reference muscle fibre length was increased while pennation angle remained the same. This had the effect of increasing the sum of the maximum and minimum fibre lengths, determined from the changes in muscle belly length, and increasing the optimal fibre length. This can be seen in Semimembranosus, Biceps Femoris (long), Peroneus Brevis, Peroneus Tertius, Extensor Hallucis Longus, Extensor Digitorum Longus, and Rectus Femoris (Table 5.2.2 and Table 5.2.3). If the minimum change in belly length in the pennate muscle was producing an invalid pennation angle (greater than 40 degrees in the present study), pennation angle was reduced and the reference fibre length increased. This reduced the pennation angle at minimum change in muscle belly length and can be seen in Vastus Medialis,

Tibialis Posterior, Peroneus Longus, Flexor Digitorum Longus, Flexor Hallucis Longus, and Soleus muscles (Table 5.2.2 and Table 5.2.3).

The optimisation procedure was repeated when the stretch in tendon length under optimal isometric force was greater than the amount by with the changes in belly length were extended to avoid zero muscle forces at maximum and minimum muscle lengths of the movement trial. This circumstance necessitated an increase in the changes in belly length as measured from the movement trial and the optimisation procedure being repeated. The optimisation procedure was repeated for those muscles with relatively small fibre lengths and relatively small changes in muscle belly length and proportionally large tendon lengths. This can be seen in the optimisation results of Rectus Femoris, Gastrocnemius (lat) and Soleus (Table 5.2.3). Large maximum isometric forces and small pennation angles also influence the force in the tendon and tendon stretch. This is seen in comparing the optimisation results of Extensor Digitorum Longus and Extensor Hallucis Longus (Table 5.2.2 and Table 5.2.3), where, with similar fibre lengths, changes in belly length, and tendon lengths, the greater optimal isometric force of the former produced sufficient tendon stretch for the optimisation routine to increase the required changes in belly length and repeat the procedure. A muscle such as the Tensor Fasciae Latae (Table 5.2.1), despite small changes in belly length and long tendon length, possessed sufficient fibre length so that additional increases in the required muscle belly length due to tendon stretch could be achieved with the existing fibre length and pennation angle. The inter-relationship between fibre length, changes in belly length and pennation angle, and the response of the optimisation procedure, is also demonstrated by Plantaris and Gastrocnemius. With similar changes in belly lengths, pennation angles and tendon lengths, Plantaris had a sufficient fibre length so that alterations in muscle model parameters were not required (Table 5.2.1). However, Gastrocnemius (med) possessed a relatively small fibre length, which the optimisation procedure increased, as well as decreasing pennation angle to achieve the required changes in belly length. Gastrocnemius (lat) also possessed a relatively small fibre length. However, with a lower optimal isometric force but small pennation angle, the tendon stretch required an increase in the belly length and the optimisation was repeated (Table 5.2.3). The end result for the three muscles were very similar fibre lengths (0.0908 m, 0.0889 m and 0.0859 m) and pennation angles (0.087, 0.191 and 0.157) respectively.

Table 5.2.1 Muscle elements where muscle model parameter optimisation did not alter model parameters.

Muscle	Fibre length (m)	-ΔBelly (m)	+ΔBelly (m)	Pennation (radians)	Tendon length (m)
Psoas Major	0.2422	-0.0086	0.0261	0.00	0.0605
Iliacus	0.1887	-0.0063	0.0232	0.00	0.00
Gremellus Sup.	0.0926	-0.0296	0.0324	0.00	0.0103
Gremellus Inf.	0.0868	-0.0313	0.0304	0.00	0.0097
Piriformus	0.1066	-0.0238	0.0331	0.00	0.0355
Pectineus	0.1298	-0.0145	0.0217	0.00	0.00
Adductor Long.	0.1993	-0.0253	0.0219	0.00	0.00
Add.Mag. (ant)	0.1051	-0.0206	0.0350	0.00	0.00
Add.Mag. (mid)	0.1833	-0.0133	0.0437	0.00	0.00
Add.Mag. (pos)	0.2385	-0.0127	0.0492	0.00	0.0795
Adductor Brev.	0.1427	-0.0241	0.0282	0.00	0.00
Glut.Min. (ant)	0.0760	-0.0083	0.0288	0.00	0.0190
Glut.Min. (pos)	0.1041	-0.0135	0.0316	0.00	0.0260
Glut.Med. (ant)	0.0980	-0.0119	0.0275	0.00	0.0173
Glut.Med. (mid)	0.1188	-0.0164	0.0319	0.00	0.0210
Glut.Med. (pos)	0.1281	-0.0208	0.0334	0.00	0.0226
Glut.Max. (ant)	0.1924	-0.0229	0.0405	0.00	0.0214
Glut.Max. (mid)	0.1928	-0.0248	0.0447	0.00	0.0214
Glut.Max. (pos)	0.1988	-0.0264	0.0493	0.00	0.0221
Tensor Fasciae L.	0.0793	-0.0168	0.0190	0.00	0.4491
Semitendinosus	0.2809	-0.0207	0.0405	0.00	0.1873
Gracilis	0.2693	-0.0171	0.0279	0.00	0.1795
Satorius	0.4549	-0.0133	0.0213	0.00	0.1137
BicepFem.(short)	0.1087	-0.0215	0.0043	0.00	0.1328
Vastus Lateralis	0.0543	-0.0025	0.0341	0.349	0.0578
Vastus Intermed.	0.0585	-0.0030	0.0360	0.175	0.0826
Popliteus	0.0680	-0.0044	0.0142	0.00	0.0170
Plantaris	0.0908	-0.0485	0.0117	0.087	0.3631
Tibialis Anterior	0.0735	-0.0232	0.0186	0.175	0.2826

Results are for the first walk trial.

Table 5.2.2 Muscle elements where muscle model parameter optimisation altered model parameters with one pass through the optimisation procedure.

Muscle	Fibre length (m)		-ΔBelly (m)	+ΔBelly (m)	Pennation (radians)		Tendon (m)
	pre	post			pre	post	
Obturator Ext.	0.0720	0.1090	-0.0528	0.0213	0.00	0.00	0.0388
Obturator Int.	0.0667	0.0698	-0.0248	0.0356	0.00	0.00	0.1001
Quadratus Fem.	0.0720	0.0956	-0.0407	0.0308	0.00	0.00	0.00
Semimembran.	0.0397	0.0582	-0.0232	0.0365	0.262	0.262	0.1448
Bicep.Fem.(long)	0.0622	0.0684	-0.0295	0.0408	0.262	0.262	0.1916
Vastus Medialis	0.0617	0.0678	-0.0018	0.0348	0.436	0.393	0.0623
Gastroc. (med)	0.0552	0.0889	-0.0494	0.0178	0.262	0.191	0.2964
Tibialis Posterior	0.0288	0.0748	-0.0334	0.0264	0.349	0.229	0.2189
Peroneus Longus	0.0348	0.0677	-0.0330	0.0248	0.175	0.141	0.3196
Peroneus Brevis	0.0476	0.0634	-0.0285	0.0242	0.175	0.175	0.2040
Peroneus Tertius	0.0331	0.0401	-0.0153	0.0187	0.175	0.175	0.0911
Ext.Halluc.Long.	0.0345	0.0460	-0.0200	0.0184	0.175	0.175	0.2446
Flex.Digit.Long.	0.0381	0.0558	-0.0238	0.0247	0.349	0.283	0.2916
Flex.Halluc.Long	0.0318	0.0619	-0.0276	0.0247	0.349	0.229	0.2295

Results are for the first walk trial.

Table 5.2.3 Muscle elements where muscle model parameter optimisation altered model parameters with more than one pass though the optimisation procedure.

Muscle	Fibre length (m)		-ΔBelly (m)	+ΔBelly (m)	Pennation (radians)		Tendon (m)
	pre	post			pre	post	
Rectus Femoris	0.0570	0.0689	-0.0080	0.0621	0.262	0.262	0.2234
Gastrocnem. (lat)	0.0587	0.0859	-0.0500	0.0115	0.175	0.157	0.2934
Soleus (lat)	0.0316	0.0900	-0.0306	0.0165	0.262	0.212	0.2451
Soleus (med)	0.0335	0.1156	-0.0275	0.0165	0.262	0.212	0.2600
Ext.Digit.Longus	0.0494	0.0597	-0.0229	0.0184	0.262	0.262	0.3291

Results are for the first walk trial.

The muscle parameter optimisation equations and methods presented proved to be robust in allowing muscle model parameters to be determined which complied with the force-length relationship and range of muscle length measured for movement trials, whether the muscle was pennate or non-pennate, under varying relationships between reference fibre lengths, reference pennation angles and required changes in muscle belly length, and under varying relationships between muscle fibre lengths, changes in muscle belly length, optimal isometric force, pennation angles, and tendon lengths.

The present muscle model parameter optimisation procedure does not ensure that the maximum muscle forces attained from the muscle model are accurate predictions of a subject's maximum muscle forces. In the present study, maximum isometric forces at the reference muscle length are predicted from reference fibre length, muscle mass, muscle density, and muscle-specific tension. Reference muscle fibre length, mass and density are used to predict physiological cross sectional area. Physiological cross sectional area and muscle specific-tension is then used to predict muscle maximum isometric force at the reference length. The accuracy of predicted maximum muscle forces in the present study will therefore be largely determined by the accuracy and validity of individual muscle mass and reference fibre length estimations. The maximum optimal isometric force that was predicted in the current muscle model was dependent on the optimal fibre length, the reference fibre length and the reference isometric force. The further the reference fibre length was positioned from the optimal fibre length along the force-length curve, the greater the predicted optimal isometric force. In the current muscle model parameter optimisation procedure, a muscle with a relatively large change in muscle belly length in the movement trial, as measured from the reference muscle position, will result in a greater optimal fibre length, producing a greater range of fibre lengths described by the force-length relationship. Range of motion from the reference position and maximum isometric forces predicted at the reference position will influence the optimal isometric force predicted. The closer the reference position is to the limits of the range of motion, the greater the optimal isometric force, while the closer the reference position was to 0.344 times the range of fibre lengths, the closer the optimal isometric force will be to the reference isometric force. In determining range of motion and subsequent changes in muscle belly length from the reference position in the optimisation procedure presented, it is therefore advantageous to use to the subject's full range of motion and not just the range of motion utilised in the movement trial. This will ensure a more realistic optimal fibre length and force-length curve describing maximum isometric forces for the muscle lengths used in the movement trial.

5.2.3 Muscle model: force-length and force-velocity relationship

The dependency of fibre length, pennation angle, contractile element length, fibre series elastic component, muscle belly length, and tendon length in the production of muscle force was accounted for by the solution of simultaneous equations. Due to the highly non-linear nature of the equations, an iterative procedure was used where, with the same number of equations as

unknowns, and each muscle model parameter given by a separate equation, each parameter estimate was sequentially improved by cycling though the equations and solving it in turn based on the current parameter estimates. The cycling continued until the magnitude of the change in parameters fell below a criterion value. Convergence was achieved with an appropriate ordering of equations and a starting estimate involving muscle model parameters that did not vary to a large extent from the initial values.

Prior to implementing of the iteration procedure in the analysis of human movement, muscle parameter optimisation was carried out to establish reference muscle model parameters and optimal fibre lengths based on the changes in muscle belly lengths measured for the movement trial. From scaling the reference muscle model data to the subject, and from the results of muscle model parameter optimisation, the following are known:

i) muscle length at current joint angles and segment positions;
ii) tendon slack length;
iii) tendon cross sectional area;
iv) percent SO, FO, FG fibre types;
v) reference belly length;
vi) reference pennation angle;
vii) reference fibre length;
viii) reference series elastic component length;
ix) optimal fibre length;
x) maximum isometric force at optimal fibre length; and
xi) contractile element length at a previous instant in time for calculating contractile element velocity at the current instant in time.

In the case of a non-pennate muscle, fibre length is given directly from the muscle belly length and the force in the direction of the tendon is the same as the contractile element force. In the isometric case for the non-pennate muscle, three equations result that relate tendon length, fibre length and isometric force. To start the iteration procedure, tendon length was first approximated by tendon slack length, and then, from equation 3.1.30:

a) muscle fibre length is given from tendon length and known muscle length;
b) maximum isometric muscle force is given from muscle fibre length;

c) tendon length is given from maximum isometric muscle force; and

d) the iteration is then repeated.

In the dynamic case for the non-pennate muscle, the contractile element length and velocity need to be determined by introducing equations for the fibre series elastic component. In addition, the maximum force of the three fibre types (slow oxidative (SO), fast oxidative (FO) and fast glycolitic (FG)) vary for the same contractile element velocity, requiring the maximum force to be calculated for each fibre type. To start the iteration procedure, tendon length was first approximated by the tendon slack length and fibre series elastic component length was first approximated by the reference fibre series elastic component length. Then, from equation 3.1.34:

a) muscle fibre length is given from tendon length and known muscle length;
b) contractile element length is given from fibre length and fibre series elastic component length;
c) contractile element velocity is given by contractile element length and known previous contractile element length;
d) maximum isometric muscle force is given from muscle fibre length;
e) maximum isometric force in each fibre type is given from maximum isometric muscle force and known proportions of each fibre type;
f) maximum force in each fibre type is given by maximum isometric force in each fibre type and velocity of the contractile elements;
g) maximum muscle force is given from the sum of maximum forces in each fibre type;
h) tendon length is given from maximum muscle force;
i) fibre series elastic component length is given by maximum muscle force; and
j) the iteration is then repeated.

In the case of a pennate muscle, changes in muscle belly length from the reference belly length are used to calculate the new pennation angle relative to the reference pennation angle. With the new pennation angle, a new fibre length is calculated. In addition, the force in the direction of the tendon is also given by the pennation angle. In the isometric case for the pennate muscle, tendon length is first approximated by tendon slack length. Then, from equation 3.1.29:

a) change in muscle belly length is given from the tendon length as well as known muscle length and reference belly length;
b) pennation angle is given from the change in muscle belly length;
c) muscle fibre length is given from the pennation angle;
d) maximum isometric contractile element force is given from muscle fibre length;
e) tendon length is given from the maximum isometric contractile element force and pennation angle; and
f) the iteration is then repeated.

In the dynamic case for the pennate muscle, the contractile element length and velocity need to be determined as well as the maximum force of the three different fibre types (SO, FO, GG) relative to the contractile element velocity. To start the iteration procedure, tendon length is first approximated by the tendon slack length and the fibre series elastic component length is first approximated by the reference fibre series elastic component length. Then, from equation 3.1.33:

a) change in muscle belly length is given from the tendon length as well as the known muscle length and reference belly length;
b) pennation angle is given from the change in muscle belly length;
c) muscle fibre length is given from the pennation angle;
d) contractile element length is given from the fibre length and fibre series elastic component length;
e) contractile element velocity is given by the contractile element length and known previous contractile element length;
f) maximum isometric contractile element force is given from the muscle fibre length;
g) maximum isometric contractile element force in each fibre type is given from the maximum isometric contractile element force and known proportions of each fibre type;
h) maximum contractile element force in each fibre type is given by the maximum isometric force in each fibre type and velocity of the contractile elements;
i) maximum contractile element force is given from the sum of maximum forces in each fibre type;
j) tendon length is given from the maximum contractile element force and pennation angle;

k) fibre series elastic component length is given by the maximum contractile element force; and

l) the iteration is then repeated.

A modification of the above equations was used in the muscle parameter optimisation routine, and since maximum isometric contractile element force was known along with reference muscle model parameters, the problem was to determine fibre lengths, pennation angles and tendon lengths subject to this force. Muscle-tendon length was known, and in the non-pennate muscle, the length of the tendon was given directly from the contractile element force, and the length of the muscle fibre was given directly from the length of the tendon and the length of the muscle. Pennation angle was zero. In the pennate muscle case, an iterative procedure resulted, with the pennation angle at first being approximated by the reference pennation angle. Then, from equation 3.1.20.

a) tendon length is given by the pennation angle and known contractile element force;

b) change in muscle belly length is given from the tendon length as well as known muscle length and reference belly length; and

c) pennation angle is given from the change in belly length.

In the present study, convergence was achieved for all applications of the equations, including muscle model test example (Section 3.1.6) and in modelling 48 muscle elements of the lower limb during walking and stepping trials. In modelling 48 muscle elements of the lower limb during walking and stepping trials, the iterative procedures were employed to predict maximum muscle forces given the current muscle length and contraction dynamics. Maximum muscle forces were used to (i) establish the maximum moment generating capacity of muscles for obtaining first estimates of muscle forces; (ii) establish the muscle force limit for the optimisation procedure from previous activation levels; and (iii) establish current excitation values given current predicted muscle forces. For the first walk trial, the maximum dynamic muscle force predictions for the 48 muscle elements for frame 120 of the stance phase of the walking trial are given in Appendix G. This presents for each muscle element, the current muscle length, previous contractile element velocity, optimal fibre length and optimal isometric force from the muscle parameter optimisation, the number of iterations used to arrive at the maximum dynamic force, the resultant fibre length, contractile element velocity, maximum force in each fibre type, the total contractile element force, the force in the direction of the

tendon, and the pennation angle. The iterative procedures were also employed to give muscle model parameters, primarily muscle contractile element length for the current muscle force and length, which were used for calculating contractile element velocities at the next instant in time. Muscle fibre lengths, contractile element lengths and contractile element velocities for each muscle element, based on the instantaneous muscle lengths and predicted muscle forces, are presented for the first walk trial and for the first step trial in Appendix L.

The iterative equations presented proved to be robust in that convergence was achieved whether the problem:

i) was to determine maximum force for a given muscle length or to determine the model parameters (for example, pennation angle, fibre length) for a given muscle force and length;
ii) applied to pennate or non-pennate muscles;
iii) applied to all muscle lengths as determined from the optimal fibre length and corresponding pennation angle;
iv) applied to isometric, eccentric or concentric contraction.

However, prior to the application of the iteration procedures to implement force-length and force-velocity relationships in muscle models, the muscle model parameters needed to be optimised to the changes in muscle belly lengths of the movement trial. This ensured that the force-length relationship was valid for all fibre lengths that resulted from the movement. In the model presented, it should be noted that contractile element force-velocity relationship used produced a maximum velocity of contraction of approximately 0.3 m/s and that the muscle will still produce a force.

5.2.3.1 Response of muscle model to varying contractile conditions

The response of the muscle model and iteration procedures in predicting maximum dynamic forces and resultant muscle model parameters in varying muscle lengths and velocities are presented in the muscle model test example (Section 3.1.6) and in the results from the first walk trial.

The relationship between individual muscle model parameters at varying maximum isometric forces showed consistency in predicted muscle model parameters at varying muscle lengths. For a given muscle length, force in the direction of the tendon determines tendon length, which, in turn, increases pennation angle and reduces muscle fibre length. Changes in muscle fibre length also change contractile element forces and influence force in the direction of the tendon and ultimately influence tendon length. In the muscle model test example, muscle belly length, tendon length, fibre length, and pennation angle are presented for a pennate and non-pennate muscle example following maximum isometric contractions at reference muscle lengths (Table 3.1.6), at optimal fibre lengths (Table 3.1.7) and following maximum isometric contractions at 11 muscle lengths spread over the range of possible muscle length of the non-pennate (Table 3.1.9, and Figures. 3.1.11 and 3.1.12) and pennate (Table 6.1.10, and Figures 3.1.13 - 3.1.15) muscle examples. Results also show the changes in the tendon length due to changing maximum isometric force in the direction of the tendon. In the non-pennate muscle, a non-linear relationship is displayed between muscle fibre length and muscle length, demonstrating the small changes in fibre length due to tendon stretch. A non-linear relationship was also displayed between muscle fibre length and muscle length for the pennate muscles due to the angle of pennation and tendon stretch. Small reductions in the force in the direction of the tendon due to changing pennation angles can be seen for the pennate muscle when compared to the non-pennate muscle at different muscle lengths. The response of the muscle model and iterative procedures to predicting maximum isometric forces is also presented in Appendix F. Here, the maximum isometric contractile element force over the range of possible muscle lengths are presented for each muscle of the first walk trial, along with corresponding fibre lengths, pennation angles, muscle belly lengths, and tendon lengths. The number of iterations required to achieve convergence to the maximum isometric force and related model parameters is also given.

The relationship between forces in the individual fibre types at varying maximum dynamic forces shows consistency in the prediction of muscle forces at varying muscle velocities. In the present model, under maximum isometric force each fibre type contributes force in proportion to its percentage distribution within the muscle. With increasing velocities of contractile element shortening, the maximum force in the SO fibres diminishes more rapidly than in the FO and FG fibres, thereby changing the relative contributions to maximum force at a given contractile element velocity, as predicted by the force-velocity relationship (Pierrynowski & Morrison, 1985b). This results in FO and FG fibres being able to produce force at higher

maximum velocities of shortening than the SO fibres. In the muscle model test example (Section 3.1.6), force in the SO and FG fibres, and force in the direction of the tendon, are presented for the pennate and non-pennate muscle examples at a constant muscle length (0.25 m) and fibre composition (50/50) but at varying muscle velocities (Table 3.1.11, Figures 3.1.16 and 3.1.17). Also presented in the muscle model test example (Section 3.1.6) is the force in the direction of the tendon for the pennate and non-pennate muscle examples at a constant muscle length (0.25 m) but varying fibre composition and varying muscle contractile element velocities (Table 3.1.12, Figures 3.1.18 and 3.1.19). In both cases, the velocities range from 1.3 m/s eccentric to 0.15 m/s concentric. Results show the influence of SO and FG fibre distribution and velocity of the contractile elements on maximum predicted force. As previously mentioned, in the present muscle model, the maximum velocity at which SO fibres produce force is considerably less than that of the FG and FO fibres. The distribution of SO, FG and FO fibre in the present muscle model also influence the maximum contractile element force at different velocities of contractile element shortening. A higher proportion of FO and FG fibres results in greater contractile element force for a given contractile element velocity of shortening.

The present model and iterative procedures predict a positive linear relationship between the maximum contractile element velocity of shortening at which the muscle can produce force and muscle length for both the pennate and non-pennate examples (Fig. 3.1.22). The model produced an increase in the maximum contractile element velocity of shortening with an increase in muscle fibre length. In the muscle model test example (Section 3.1.6), force in the direction of the tendon is presented for the pennate and non-pennate muscle examples at varying muscle lengths and muscle contractile element velocities, but with a consistent fibre composition (50/50) (Table 3.1.13, Figures 3.1.20 and 3.1.21). The muscle contractile element velocities ranged from 1.3 m/s eccentric to 0.15 m/s concentric. For varying muscle lengths, for both pennate and non-pennate muscles, the present muscle model predicted greater maximum contractile element velocities of shortening for longer muscle lengths, despite the isometric force varying. In addition, for a muscle at different lengths with similar isometric force (that is, on different sides of the force-length curve), the results showed that the larger muscle and fibre lengths produced greater maximum contractile element velocities of shortening. If the linear relationship between maximum velocity of shortening and muscle length (Fig. 3.1.22) is extrapolated to the muscle length corresponding to zero maximum velocity of shortening then:

a) for the non-pennate muscle, this muscle length is equal to the tendon slack length with an effective muscle fibre length of zero; and
b) for the pennate muscle, this muscle length is equal to the tendon slack length plus the reference belly length minus the proportion of the reference fibre length in the direction of the tendon.

Hence, the effective fibre length in the direction of the tendon is zero. For the non-pennate muscle, this would suggest that the model predicts a greater maximum contractile element velocity of shortening as fibre length increases, but would theoretically reduce to zero when muscle fibre length reduces to zero. For the pennate muscle, the angle of pennation also influences the predicted velocity of contractile element shortening, reducing to zero when the pennation angle of the muscle model reaches 90 degrees and the muscle model belly length and fibre length can not reduce further. The linear relationship predicted is not in agreement with finding of Herzog (1996), which would suggest that the speed of unloaded shortening was similar within a range of fibre lengths. The method by which force-length and force-velocity relationships should be combined and the dynamic responses on muscle fibres is still unknown (Herzog, 1996). Therefore, further application is needed of the present study on the implementation of the force-velocity relationship and the dynamic response of the present model to changes in optimal fibre length and changes in muscle length.

5.2.3.2 Implementing force-velocity relationships in movement trials

Maximum dynamic force is calculated for each muscle to determine maximum and minimum force limits from previous excitation levels for the respective muscles. In the calculation of maximum dynamic muscle forces in the movement trials, muscle contractile element velocity was calculated, but was subsequently set to zero in the iterative equations for determining maximum force for the current contractile conditions. All other variables in the analysis process remained unaltered, hence substituting maximum isometric force for the contractile elements for the maximum dynamic force of the contractile elements. The reason for this is that the contractile element velocities calculated (Appendix L) were larger than those modelled by the present force-velocity equations, which resulted in the maximum contractile element forces approaching zero when the instantaneous contractile element length was shortening. The maximum contractile element forces calculated for the current fibre lengths and

contractile element velocities for the 48 muscle elements for a representative frame (frame 120) of the stance phase of the first walk trial are presented in Appendix G. Also presented are the maximum contractile element forces calculated for the current fibre length, but substituting zero for the contractile element velocity for the 48 muscle elements modelled. Table 5.2.4. presents a comparison of the maximum muscle forces predicted for frame 120 using the current contractile element velocity or zero contractile element velocity for those muscles whose contractile element were shortening (concentric) in the first walk trial. The significantly reduced maximum contractile element force found when contractile elements were shortening reduced the muscle force limits calculated from previous activation levels. This therefore reduced the maximum moments that could be generated about each degree freedom and altered the predicted muscle forces (see Appendix G for an example of muscle force prediction for frame 120 of the first walk trial with and without the use of contractile element velocities). A comparison of muscle forces predicted for frame 120 using the current contractile element velocity or zero contractile element velocity are presented in Table 5.2.5 for a selection of muscle in the first walk trial.

Due to the slow movements analysed in the present study, the maximum concentric force of the contractile elements would be expected to be close to the maximum isometric force. The use of maximum isometric forces in the optimisation procedure was not considered to have a substantial effect on the predicted forces due to the slow movement patterns and sub-maximal forces expected in the slow walking and stepping trials in an active and healthy subject.

As a result of the present study, it is considered necessary to either adjust the parameters describing the force-velocity relationship in the current application of these equations or to scale a reference force-velocity curve to the maximum contractile element velocities expected in the application of the present muscle model. This is to avoid the model predicting unreasonably small maximum muscle force estimates when the instantaneous contractile element length is shortening.

Table 5.2.4 Maximum contractile element force, including contractile element velocity or assuming isometric contraction.

Muscle	CE velocity (m/s)	Maximum muscle CE force (N)		
		Dynamic	Isometric	Optimal
Iliacus	-0.618	60.4	584.1	662.7
Obturator Externus	-0.021	145.2	199.2	265.3
Quadratus Femoris	-0.016	122.8	162.5	176.1
Adductor Magnus(pos)	-0.555	132.6	935.4	983.8
Gluteus Minimus(pos)	-0.463	11.2	200.5	215.2
Gluteus Medius(pos)	-0.504	19.9	292.5	311.6
Gluteus Maximus(ant)	-0.838	22.7	438.8	466.3
Tensor Fasciae Latae	-0.679	0.0	237.8	239.1
Semimembranosus	-0.014	1504.9	2077.0	2225.5
Semitendinosus	-0.356	89.5	301.8	326.0
Rectus Femoris	-0.016	1122.3	1472.8	1476.8
Gastrocnemius(lat)	-0.183	47.7	357.8	810.1
Gastrocnemius(med)	-0.344	39.6	663.6	1301.0
Tibialis Posterior	-0.220	47.8	427.7	691.5
Peroneus Longus	-0.119	98.7	612.6	708.7
Peroneus Brevis	-0.116	95.2	457.1	502.7
Peroneus Tertius	-0.040	55.9	140.8	142.4
Ext. Digit..Longus	-0.028	340.6	560.5	636.6
Ext. Halluc. Longus	-0.027	145.9	309.3	318.4
Flex. Halluc. Longus	-0.191	41.0	350.4	514.4

Table 5.2.5 Predicted muscle force, including contractile element velocity or assuming isometric contraction. Muscles listed changed at least 30N between the two conditions

Muscle	Muscle Force (N)	
	Dynamic	Isometric (N)
Iliacus**	15.0	164.8
Adductor Magnus(pos)**	0.0	53.3
Gluteus Minimus(ant)	234.8	157.9
Gluteus Minimus(pos)**	1.7	48.3
Gluteus Medius(ant)	245.2	187.7
Gluteus Medius(pos)**	0.0	33.0
Gluteus Maximus(ant)**	0.0	63.7
Gluteus Maximus(mid)	95.7	64.5
Tensor Fasciae Latae**	0.0	37.4
Biceps Femoris(short)	163.6	112.7
Biceps Femoris(long)	360.3	225.2
Gastrocnemius(lat)**	0.0	58.5
Gastrocnemius(med)**	18.0	197.6
Soleus (lat)	595.4	352.9
Soleus(med)	574.3	310.0
Tibialis Posterior**	20.5	120.3
Peroneus Longus**	33.3	90.1
Peroneus Brevis**	36.3	75.8
Flex.Digit. Longus	92.2	49.8
Flex. Halluc. Longus**	19.7	110.0

** the contractile element instantaneous length was shortening.

5.3 Muscle force optimisation

A cost function was proposed based on the minimisation of the sum of squared muscle stress, and incorporated soft constraints on both maximum and minimum muscle forces. The rationale for this was that a more realistic muscle force distribution would result at minimum muscle forces when compared to the cost function of Siemienski (1992) in which soft constraints were placed on the maximum muscle forces. A more realistic muscle force distribution would also result at both maximum and minimum muscle forces when compared to the minimisation of the sum of squared muscle stress without soft constraints. The rationale for the use of a cost function with maximum and minimum soft constraints also lies in reducing the computational effort of the optimisation procedure. Upper and lower limits on muscle forces for each muscle were obtained from previous excitation levels and muscle excitation dynamics. Incorporating these constraints into the cost function results in the unconstrained minimisation of the cost

function. Minimisation was achieved by starting at an initial estimation of muscle forces, which were required to meet the equipolance equation describing resultant joint moments and, at the same time, be a good approximation at the minimum solution. With the use of a gradient projection algorithm, the initial muscle force estimates are improved towards the minimum of the cost function.

The application of the cost function and optimisation procedure has been demonstrated on a test example involving a simple joint with four muscles (Section 3.2.1). Results show the validity on the approach where, like the cost function of Siemienski (1992), all muscle forces reached their respective maximum values at the maximum resultant joint moment. With the minimum muscle force limits included in the present cost function, unconstrained minimisation of the cost function resulted in all muscles reaching their respective minimum values at the corresponding minimum resultant joint moment. The cost function presented also places mathematical bounds on the muscle forces that can be used in the initial muscle forces estimates which are used as the starting point for the minimisation procedure. Outside of these boundaries, the cost function cannot be defined. For each muscle, the maximum boundary force is the same as the maximum force limit used within the cost function. Conversely, the minimum force boundary is the minimum force limit used within the cost function less the difference between the maximum and minimum force limits used within the cost function (Section 3.2.1). In the cost function example, the minimum force limit for the four muscles was less than half the respective maximum force limits, such that all muscle force values between zero and the respective maximum muscle force lay within the bounds of the cost function and could be used in the initial estimate, so long as the resultant joint moments were met. In the application of the cost function to the prediction of forces in the lower limb, the activation levels from the previous frame determined the upper and lower activation levels for the current frame. This in turn, knowing the maximum contractile element force for the current contraction dynamics, determined the maximum and minimum muscle force limits.

In the analysis of slow walking and step trials, the pre-activation levels and resulting muscle force limits for two frames, one in the swing and the other in the stance phase, are presented in Appendix G. In the analysis of slow walking and step trials, both with low muscle forces in comparison to predicted maximum muscle forces, the pre-activation levels of the SO fibres varied between zero and one but were generally below 0.5. The pre-activation levels of the FO fibre type rarely rose above zero and the pre-activation levels of the FG fibre type were zero.

With the parameters describing the activation dynamics in the present study, all pre-activity levels of the SO, FO and FG fibre types between zero and one resulted in a maximum activation levels for the single frame for all fibre types. Therefore, the maximum force limit was always equal to the maximum muscle force predicted from the contraction dynamics. Again, with the parameters describing the activation dynamics in the present study, the minimum activation levels for the current frame for the SO fibre varied between zero and 0.8 but were generally below 0.3, while the minimum activation levels of the FO fibres were generally zero or close to zero, and the minimum activity levels for the FG fibres were zero. Therefore, the minimum muscle force limit was always below half of the maximum muscle force limit. Hence, all muscle forces between zero and the maximum force predicted for the contraction dynamics lay within the bounds of the cost function and could be used in the muscle force initial estimate in arriving at the resultant joint moments as described by the equipolance equations. From the initial muscle force estimates, the optimisation procedure would, in an iterative process, adjust the muscle force estimates to arrive at the minimum of the cost function given the constraints on muscle forces.

The validity of the optimisation procedure was demonstrated on a test example involving eight muscles in a simple two joint system (Section 3.2.3). Optimisation was carried out at varying resultant joint moments. The range of resultant moments tested for each joint was determined by summing all the positive and negative maximum moments produced by each muscle for a respective joint, giving a range of +20 Nm to -15 Nm for the first joint and +12 Nm to -15 Nm for the second joint. Not all combinations of moments could be met by muscle forces alone due to the action of two-joint muscles included in the model. In the determination of muscle force initial estimates, moments were balanced by non-muscle forces (ligament and bone contact forces) if convergence could not be achieved at the required joint moments. Minimisation of the cost function would then adjust muscle forces, maintaining the resultant joint moment as produced by the muscle forces of the first estimate. The initial muscle forces and resultant joint moments, the non-muscular moments assigned in arriving at the first estimates, the predicted muscle forces and the resultant joint moments following optimisation, and the difference between the joint moments resulting from the optimisation routine and the required resultant joint moments, are presented in the test example (Section 3.2.3). Results show the routine for obtaining initial muscle force estimates was successful in providing muscle forces and non-muscular forces which met the resultant joint moments, and when used as a starting point to minimising the cost function, converged to a solution that was achieved

while maintaining resultant joint moments. This example also demonstrated a continuity in predicted muscle forces and non-muscle forces between varying resultant joint moments in that no discontinuities occurred in muscle forces and all forces predicted agreed with expected values.

The results of the optimisation procedure in predicting 48 muscle element forces of the lower limb are presented for two frames of the first walk trial in Appendix G - one frame in the swings phase (frame 80) and the other in the stance phase (frame 120). In this more complex application of the optimisation procedures, the following limitations were encountered:

i) The first problem is to arrive at the resultant joint moments that need to be balanced by muscle forces. In the present musculo-skeletal model, the ankle and knee joints were modelled as simple ball and socket joints by a single point about which resultant joint moments were balanced by muscle forces. Bone contact and ligament forces also play a role in balancing resultant joint moments. The muscle moment generating capacity about the anterior-posterior axes of the knee and ankle are relatively small in comparison to the medio-lateral axes. Therefore, small increases in the moments that are required to be balanced by muscles about the anterior-posterior axes will result in relatively large increases in predicted muscle forces. In the present study, more accurate models of the knee and ankle joints are needed to determine the contribution of bone contact and ligament forces to resultant joint moments. It would also be expected that in activities of high muscle force, the accuracy of joint models and the resulting moments required of muscle force will become more critical in achieving convergence to initial muscle force estimates and the validity of the muscle forces predicted.

ii) The procedure for obtaining the initial muscle force estimates was only partially successful in predicting forces in 48 muscles of the lower limb. This can be attributed to either the ability to converge to the resultant joint moment in all situations, or being unable to produce a reasonable approximation for the global minimum of the cost function. In predicting initial muscle force estimates, an iterative procedure was used in which each iteration reduced the differences between current and required joint moments based on the moment generating capacity of each muscle about the respective degrees of freedom. The procedure initially converged to within

approximately 5% of the required joint moments, however, often convergence was not fully met with further iterations producing little or no improvements. This was due to small changes in muscle force affecting the moments produced at other degrees of freedom and other muscle forces. The result was often a cyclic shifting of muscle forces between sets of muscles where one set of changes would be offset by following changes with no net gain in convergence. In determining initial muscle force estimates the iteration procedure often balanced resultant joint moments about the longitudinal and anterior-posterior axes of the ankle and knee by ligament forces when close to the required resultant joint moments in order to achieve convergence. The lack of convergence, and the need to include ligament forces, is expected to be a function of the iteration procedure used and the highly indeterminate nature of the problem (with 48 muscles and 9 degrees of freedom) as well as the need to balance resultant joint moments at the knee and ankle by purely muscle forces. In the present analysis of walking and stepping trials, the iterative procedure was arbitrarily stopped at 50 iterations. If convergence had not been achieved by this time, further iterations tended to provide little or no improvement.

In balancing resultant joint moments of the lower limb a control strategy that has been used is to only balance by muscle forces, degrees of freedom that have significant movement and moment generating capacity (Buchanan & Schreeve, 1996; Glitsch & Baumann, 1997). This approach assumes that our control systems does not actively balance degrees of freedom possessing small rotations and moment generating capacity, leaving these moments to be balanced by bone and ligaments forces. Hence, in modelling the lower limb, abduction/adduction and internal/external moments at the knee and ankle joints are effectively ignored in the equipollence equations. This approach however does not actively check the muscle moments about these ignored degrees of freedom or attempt to reduce the difference between moments produced by muscles and the required resultant joint moments. In the present approach, the optimisation procedure initially attempts to balance all degrees of freedom about the knee and ankle joints by muscular forces. The present model of the knee and ankle joint did not include joint contact and ligament forces in the equipollence equations. As the procedure progressed towards attaining an initial muscle force estimate, those degrees of freedom at the ankle and knee about which we have a relatively small moment generating capacity, were often removed so as to achieve convergence. This

approach, although not always balancing all degrees of freedom at least reduces the differences between muscular and resultant joint moments about those degrees of freedom that have reduced moment generating capacity.

Despite the problems encountered in achieving the desired level of convergence in the walking and stepping examples, the predicted muscle forces were consistent over the trials. The problem in achieving the required level of convergence was not present in the test example involving only 8 muscles and two degrees of freedom. In the optimisation approach of the present study, an improved method is needed to obtain initial muscle force estimates, either by modifying the current procedure or adopting alternatives such as the reductionism approach of Pierrynowski & Morrison (1985b).

iii) Minimisation of the cost function, although successful in reducing the cost function from the initial estimates and maintaining joint moments, did not change muscle force estimates significantly from the initial estimated values. Therefore, in predicting muscle forces of the lower limb involving 48 muscle elements and 9 degrees of freedom, the solution of the optimisation procedure was largely determined by the initial muscle force estimates. This was due to two main factors:

a) A number of muscle elements have an initial muscle force close to or at zero force. The optimisation procedure calculates small changes in each muscle force, the magnitude of which is determined by the step size, which would progress the cost function toward a minimum solution while maintaining the joint moments. The current solution to optimisation procedure was already limited by boundary conditions where no muscle force could be less than zero. For the optimisation procedure to proceed toward a minimum in this situation, negative muscle forces would result. In the present optimisation procedure, small negative muscle forces were allowed within a criteria value to permit the optimisation procedure to continue. At the conclusion of the minimisation procedure, the small negative muscle forces were set to zero. For this reason, the joint moments resulting from the initial muscle estimates may vary slightly from the joint moments calculated from the optimised muscle forces of the lower limb. From the muscle force optimisation results presented of the first walk trial (Appendix G), only two iterations proceeded for the swing phase

(frame 80) due to the changes in force falling below the criterion value. The maximum change in force for the last iteration was 0.058 N with a limit of 0.322 N, while the largest negative force was -0.122 N with a limit of -0.643N. Furthermore, only three iterations proceeded for the stance phase (frame 120) due to the changes in force being below the criterion value. The maximum change in force for the last iteration was 1.762 N with a limit of 1.766 N, while the largest negative force was -0.775 N with a limit of -3.532 N.

b) A local minimum is reached within a few iterations of the first approximation. From the muscle force optimisation results presented for the first walk trial (Appendix G), three iterations proceeded for the stance phase (frame 120) due to the changes in force falling below the criterion value. The cost function was initially -47.807, and following the three iterations was -47.814, -47.821 and -47.827 respectively. The diminishing changes in the cost function suggest a local minimum was achieved, however, the convergence to a global minimum is not known. Caution must therefore be made in reaching a solution in a complex system as there are likely to exist a large number of local minima to the optimisation problem. This can lead to the possibility that different solutions may be obtained for muscle forces from different optimisation approaches that may be a local or global minimum.

The results of the present study show that procedures developed on simple examples would work on more complex problems that involve a larger numbers of muscles in a highly complex and indeterminate problem. The results of the optimisation procedure, including obtaining first estimates of muscle forces, are not known for higher resultant joint moments in the analysis of the lower limb, where the muscle forces are closer to maximum values. This is despite the optimisation procedure being shown to work on the entire range of resultant joint moments due to all possible muscle forces in the test example (Section 3.2.3). In the analysis of movements of the lower limb with greater forces, muscle pre-activation states will be higher, resulting in higher minimum muscle force limits due to activation dynamics. As a consequence, bounds are likely to be placed on the range of values that can be used in obtaining an initial muscle force estimate as determined by the maximum and minimum boundary values that can be used in the cost function. With high relative muscle forces, the validity of the maximum

muscle force prediction, as well as the validity of the excitation dynamics, will also be more critical in determining upper and lower excitation values. It is also expected that improved models of the knee and ankle joints would be needed, along with higher resultant joint moments, and the contribution of ligament and bone forces would become more critical in estimating the moments that are required to be balanced by muscle forces.

To summarise the results of the optimisation approach, a procedure was presented which successfully predicted individual muscle forces for simplified test examples. The first test example showed the validity of the presented cost function, involving soft maximum and minimum constraints, in predicting a realistic distribution of muscle forces between maximum and minimum resultant joint moments. The second test example showed the validity of the procedures used to obtain an initial muscle force estimate which met the equipollence equations, and to minimise the cost function presented to arrive at individual muscle forces. In the application of the procedures to predicting individual muscle forces of the lower limb in walking and stepping trials, consistency in predicted muscle forces was achieved across the trials. However, several limitations were encountered due to the highly complex and indeterminate nature of the problem. The procedure for determining initial muscle force estimates had difficulties in converging to the desired degree of accuracy at the resultant joint moments. The minimisation of the cost function was achieved without significant changes in the initial muscle force estimates making the results of the optimisation procedure largely dependent on the initial muscle force estimates. The limitations highlighted the need to improve the modelling the knee and ankle joints to determining moments that are required to be balanced by muscular forces. Equally, there is a need to improve methods for determining initial muscle force estimates which meet the required joint moments and are sufficiently close to the minimum solution to achieve convergence.

Despite the accepted use of optimisation procedures to determine individual muscle forces in order to overcome the indeterminacy of the musculo-skeletal system, questions still remain as to the appropriateness of the optimisation procedure and the use of a cost function. These questions need to be considered when interpreting the predicted muscle forces, and include:

i) the use of one cost function when many different competing strategies may exist. The strategies and the priority of those strategies in muscular recruitment may vary depending on the goal of the movement, as in achieving speed or accuracy;

ii) The appropriateness of minimising stress or energy expenditure. In analysing the execution of a single task, is there a high priority or even a need to minimise a variable that the body can adapt to in the long term, such as muscle stress or energy expenditure? With repeated execution of the task, the body has the ability to adapt to the demands and so decrease, in the long term, muscle stress and energy expenditure for the task. In contrast, structures such as ligaments and articular cartilage are relatively poor at accommodating certain loading situations such as repeated loading and shear forces respectively and, coupled with a poor blood supply and poor ability to repair, suggest criteria which protects these structures worthy of consideration. In addition, during tasks that involve low levels of muscular output, could there be a strategy of higher priority than stress or fatigue?

iii) The relative insensitivity of the cost function used (for example, force, stress, normalised force, and fatigue). These cost functions are all dependent on the physiological cross section area and moment arms predicted for each muscle. The equipolance equations, involving resultant joint moments, moment arms and muscle forces, must still be solved regardless of the cost function.

iv) Minimising a function based on stress or energy expenditure does not favour co-contraction. Therefore, the optimisation is not applicable if considerable co-contraction is known to exists (Raikova, 1999), such as in unfamiliar tasks, movement requiring accuracy, or in movement involving pain or pathological conditions.

v) The appropriateness of introducing mathematical constraints or methods to overcome shortcomings in the optimisation procedure, such as in the use of squared or cubed terms in the sum of stress or normalised force as opposed to just stress or normalised stress.

5.4 Movement trials

Segment centres of mass acceleration, moment arms and predicted muscle forces were subject to the largest errors in predicted values. In the following section, these three variables are discussed in relation to the methodologies used in the present study. Firstly, the errors seen in segment centres of mass acceleration are discussed with respect to the accuracy of segment location. Then the accuracy of predicted moment arms are discussed, including the straight-line representation of muscle-tendon path, the location of body-fixed axes from external markers, and the accuracy of segment location. Finally, predicted muscle forces of the step and walk trials are discussed in comparison to recorded EMG and predicted moment arms.

5.4.1 Segment centre of mass acceleration

The acceleration of segment centre of mass for the pelvis, thigh, shank and foot in the three global directions were consistent across the three walk trials (Figures 4.5.10 - 4.5.21) and three step trials (Figures 4.6.10 - 4.5.21), indicating the repeatability of the walk and step movement patterns in the present subject. Overlaying centre of mass accelerations from the three trials also indicates the underlying pattern and contribution of errors within the acceleration data. In the present study however, errors in centres of mass accretion are not true indicators of segment accuracy of the thigh, shank and foot. The location of the centre of mass of the thigh, shank and foot were on the respective longitudinal axes, hence segment location errors about the longitudinal axis, potentially the largest errors, will not be present in the acceleration data for these segments. The acceleration of the centre of mass does however, indicate a high level of accuracy in the predicted three dimensional location of each segment axis origin and rotations about the medio-lateral and anterior-posterior axes. The largest variation in segment centre of mass accelerations across different trials was seen in the pelvis. This was due to the pelvis being subject to relatively large skin movement artefacts, being reproduced from the fewest number of external markers, and the centre of mass not being located on a segment axis.

The present study demonstrates the need to analyse more than one trial to ascertain whether small changes in acceleration are artefact due to random measurement error or, in fact, repeatable occurrences. Analysing more than one trial, and the magnitude of variations that occur consistently and repeatedly with in the data, can give an indication of the accuracy of the

data. However, systematic error may also produce consistent and repeatable artefact within the measured data. In the case of segment position and acceleration, a consistent movement artefact or oscillation in soft tissue, and hence derived segment location, may occur during movement such as at heel strike. This would produce a small but consistent oscillation in position and acceleration of the segment that would be measurable across repeated trials. The use of multiple external markers placed around the segment will help reduce this systematic error, however it will not remove it entirely. Therefore, in observing consistent and repeated occurrences in data, such as oscillations in position or acceleration, consideration of systematic motion artefact needs to be considered.

5.4.2 Muscle moment arms

Muscle moment arms are discussed in relation to the step task, which involved going from a standing position to one leg support on the elevated platform, and then returning to the standing position on the floor. Changing moment arms during the step task are a function of the combined rotations about the three axes of each segment rather than resulting from individual axis rotations under controlled movements. Therefore, in comparing moment arms during the step task with moment arms of previous research (Jensen & Davy, 1975; Nemeth & Ohlsen, 1985; Spoor, et.al. 1990; Rugg, et.al. 1990; Spoor & Leeuwen 1992; Delp, et.al. 1999) consideration must be given to the combined effect of segment rotations in the present study. The segment rotations during the three repetitions of the step task were consistent between trials. A brief description of the rotations and approximate angles for the three repetitions of the step task follows:

> For the step task, the initial mean standing thigh angle about the medio-lateral axis was 7 degrees of flexion, which increased to 69 degrees of flexion when placing the foot on the step. On ascent of the step, thigh flexion angle reduced to 22 degrees on standing. The mean initial standing thigh angle about the anterior-posterior axis was 2 degrees of adduction, which increased to 10 degrees of adduction when placing the foot on the step. On ascent of the step, thigh adduction angle reduced to 6 degrees. The initial mean standing thigh angle about the longitudinal axis was 1 degree of internal rotation, which changed to 10 degrees of external rotation when placing the foot on the step. On ascent of the step, longitudinal axis rotation initially increased to 14 degrees of external rotation before reducing to 3 degrees of internal rotation.

The initial mean standing shank angle about the medio-lateral axis was 9 degrees of flexion. This increased to a peak of 80 degrees flexion before reducing to 69 degrees of flexion when placing the foot on the step. On ascent of the step, thigh flexion angle initially increased before reducing to 17 degrees on standing. The initial mean standing shank angle about the anterior-posterior axis was 3 degrees of adduction, which changed to 4 degrees of abduction when placing the foot on the step. On ascent of the step, thigh anterior posterior angle initially increased to 7 degrees of abduction before reducing to zero degrees abduction on standing. The initial standing shank angle about the longitudinal axis was 7 degrees of external rotation. This increased to a peak of 14 degrees of external rotation before reducing to 4 degrees when placing the foot on the step. On ascent of the step longitudinal axis rotation reduced slightly to 2 degrees of external rotation.

The initial mean standing foot angle about the medio-lateral axis was zero degrees of flexion, where 92 degrees is taken as the neutral foot position. This increased to a peak of 11 degrees dorsi-flexion before returning to the neutral position when placing the foot on the step. On ascent of the step, foot dorsi-flexion angle increased to 9 degrees before returning to the neutral position on standing. The initial mean standing foot angle about the anterior-posterior axis was 9 degrees of abduction, which reduced to 6 degrees of abduction when placing the foot on the step. On ascent of the step, foot abduction increased to 12 degrees. The initial mean standing foot angle about the longitudinal axis was 7 degree of external rotation. This increased slightly to 10 degrees before returning to 7 degrees of external rotation when placing the foot on the step. On ascent of the step, longitudinal axis rotation reduced to zero degrees on standing.

Muscle moment arms were extremely sensitive to measurement error and modelling methods and consequently, moment arms showed large relative errors which significantly affected the ability to predict individual muscles forces. Errors in moment arms result from:

i) The ability to accurately locate body-fixed axes from external markers. Body-fixed axes are required to coincide with the reference skeletal axes from which co-ordinate data describing muscle-tendon paths and joint centres are derived. Errors in alignment

between the body-fixed axes and the underlying subject skeleton result in differences in the predicted joint centre of rotation and the actual centre of rotation, causing points describing muscle-tendon paths and joint centres to move;

ii) The location of points used to describe muscle-tendon paths and the joint ranges of motion. When the muscle-tendon points were close, and when the errors in three dimensional segment location were large, the errors in moment arms were also great;

iii) The use of straight or curved lines to define muscle-tendon paths. In the present study, use of straight lines underestimated moment arms in situations where tendons wrapped around joint capsules;

iv) The method used to define joint centres. Moment arms of knee extensors showed a sudden decrease when approaching full extension and consequently, an anterior shift in the joint centre of rotation. Similarly, moment arms of knee flexors showed a sudden decrease in moment arms when approaching 90 degrees flexion and consequently, a posterior shift in the joint centre of rotation. These may not be adequately represented with a fixed centre of rotation; and

v) Accuracy of three dimensional segment location. Large errors in segment location resulted in more variability in the predicted moment arms between repeated trials, as well as the model's sensitivity to above-mentioned errors.

Several of the above factors, which contribute to errors in moment arms that have particular relevance to the present study, are discussed in more detail:

5.4.2.1 Errors due to straight line model of muscle tendon paths

Jenson & Davy (1975) found that the straight line approach underestimated moment arms by 1 to12% compared to the centroid line approach. The authors also found that the moment arm components of about each axes can vary considerably more. The centroid line approach uses cross-sectional slices to define the path of the muscle centroid (Jenson & Davy, 1975; Dostal & Andrews, 1981) and the latter autors cited several disadvantages of the centroid line approach:

i) It requires large amounts of data to represent a muscle in one joint configuration;

ii) Difficulty in defining a transverse centroid for a broad muscle or insertion;

iii) It is not valid for when the join configuration changes; and

iv) Muscles under tension may follow a more direct cause from origin to insertion.

In the present model, muscle-tendon paths have been represented by origin, insertion and deflection points interconnected by straight lines. The number of points defining tendon paths around a joint has been limited to enable the tendon path to be defined for a range of joint motions (see Section 5.2.1). In calculating moment arms where tendons wrap around joint capsules, bone or retinacula under-estimations of moment arms are expected due to the movement of the deflection points around the centre of rotation. This would lead to a reduction in moment arms as the line joining the deflection points moves closer to the joint centre (Fig. 5.4.1). Muscles crossing the knee joint affected would include Semimembranosus, Semitendinosus, Biceps Femoris (long and short heads), Vastus Lateralis, Vastus Intermedius, Vastus Medialis, Rectus Femoris, Gastrocnemius (medial and lateral), Plantaris, and Popliteus. The same limitation needs to be considered for the muscle of the hip joint, for example Iliopsoas, and for the ankle joint, for example, the extensors (Tibialis Anterior, Extensor Digitorum Longus, Extensor Hallucis Longus, and Peroneus Brevis) where retinaculae influence tendon path. To overcome this limitation, both curved and straight-line path segments may need to be included to adequately represent the path of muscle-tendon complexes around joints and to determine muscle lengths and moment arms from the origin, insertion and deflection points defined for the present study.

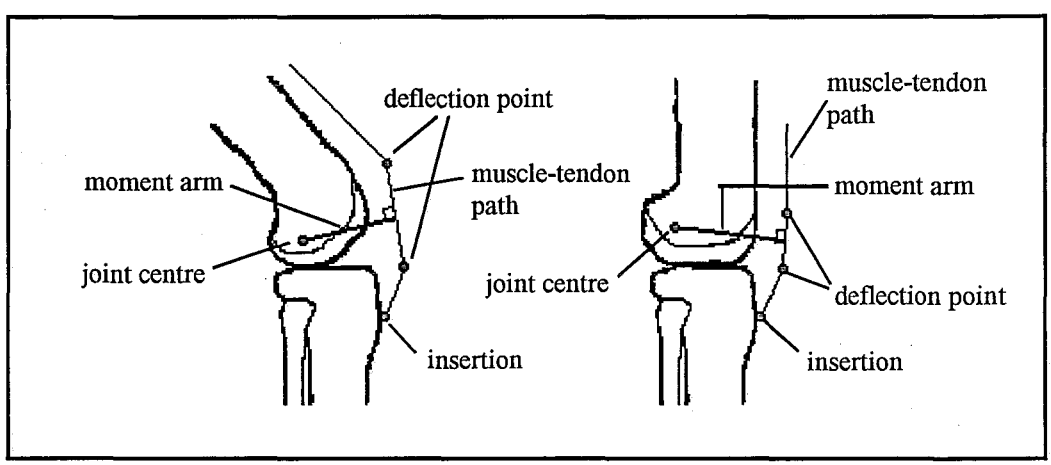

Figure 5.4.1 Changing magnitude of vastus moment arm of a straight line muscle-tendon model with fixed local points of origin, insertion and deflection points due to changing joint angle.

5.4.2.2 Errors due to accuracy of segment location

The consistency in muscle moment arms between different trials of the same movement are comparable with other measures such as acceleration of segment centres of mass, Cardan rotations and muscle lengths. This would indicate that the main source of errors seen in determining moment arms in the present study resulted from the present methods used to define the moment arm rather than the accuracy of segment location. This is demonstrated in later sections, where the location of muscle point co-ordinates and their changing relationship with the joint centre with changing joint angles result in large errors in some moment arms.

5.4.2.3 Errors due to location of body fixed axes from external markers

The location of the shank axes origin does not vary significantly with respect to the local thigh axes during the step trials (Figs. 5.4.2 - 5.4.4). The step tasks produce 80 degrees of knee flexion and a possible 5 mm inferior and 4 mm posterior relative displacement of the shank origin. These changes are of the same magnitude as the errors in locating the relative position of the shank with respect to the thigh. In the current model of the knee joint, 80 degrees of rotation about the medio-lateral axes, defined by a fixed point relative to the thigh and shank axes, would be expected to produce a significant posterior displacement of the shank relative to the thigh (Fig. 5.4.5). The relatively constant shank axes origin with respect to the thigh is likely to have resulted from errors originating from the calibration procedure in defining local axes from external markers. In the calibration procedure, the thigh axes origin was located at the hip joint centre, as defined from the pelvic axis system. The thigh z-axis (longitudinal) was defined by the axis origin and the mid-point of the medial and lateral femoral condyles. The shank axes origin was located in the middle of the tibial plateau, which in the present study, was located along the thigh z-axis at a distance of 104.1% of the thigh length, measured between the greater trochanter and the inferior border of the lateral femoral condyle. The thigh length was also scaled to the z-axis co-ordinate data of the thigh. For the present subject, the shank axes origin was located at (0.0 m, 0.0 m, 0.423 m) relative to the thigh axes and the knee joint centre was (0.0 m, -0.014 m, -0.014 m) relative to the shank axes system. An error in defining the local shank axes system for the subject from external markers by 1.4 cm superior and 1.4 cm posterior would place the shank axes origin at a position estimated to be the joint centre of rotation. Hence the positions of the muscle co-ordinate data and predicted joint centre, which are expressed relative to the shank axes, would also be translated by the

same amount in relation to the underlying segment. These errors could result from two situations:

i) When scaling anatomical data to the subject, the ratio between thigh length and the distance from hip joint centre to tibial plateau (shank axes origin) may vary from skeletal reference data (104.1%) to that of the subject. However, variation in the points used to measure thigh length on the skeletal reference from the thigh length measured on the subject are more likely to contribute to the error in longitudinal position of the shank axes origin. A 1.4 cm difference can easily occur if measuring from the inferior, most lateral or superior margins of the greater trochanter. Any difference in the measured thigh length would shift the shank axes origin along the superior-inferior direction of the thigh z-axis relative to the underlying skeletal system of the subject when scaling the reference data to the subject;

ii) When locating the middle of the tibial plateau from external markers placed on the femoral condyles, the mid-point may not coincide with the centre of the tibial plateau. Thus, differences in the mid-point of the femoral condyle markers and the expected direction of the thigh z-axis would shift the shank axes anteriorly, posteriorly, medially, or laterally relative to the model and consequently, relative to the underlying bone. In the present application, if the mid-point of the markers was 1.4 cm posterior to that expected by the model, then thigh z-axis would pass through the knee joint centre and the shank axes origin moved accordingly.

In the standing position, the correctly located shank axes and translated shank axes (1.4 cm posterior and 1.4 cm superior) with respect to the lower limb model would produce similar results. Differences in measured thigh length would result in scaling the thigh z-axis and muscle co-ordinate data, as well as a shift in the shank axes. A posterior shift in shank axes would produce a slight variation in predicted knee angle and accompanying changes in moment arms between the two situations in the standing position. However, as the subject flexes the knee, the motion of the shank axes, as defined from external markers, and consequently moment arms, would vary considerably between the correctly located shank axes and one displaced both superiorly and posteriorly. In the ideal case, as the subject flexes the knee, the predicted shank axes would rotate about the predicted knee joint centre and the moment arms would be predicted by the points describing muscle-tendon path within a range

of angles (Figs. 5.4.5 and 5.4.6). With the displaced shank axes described previously, the shank axes would rotate about the shank axes origin as the knee flexes, producing erroneous motions of the points describing muscle-tendon paths and knee joint centre, which would result in erroneous moment arms (Figs. 5.4.5 and 5.4.7). Inaccuracies would increase with increasing knee flexion, and with the present muscle model (Figs. 5.4.5 and 5.4.7), moment arms would change rapidly and become meaningless beyond 75 degrees flexion.

In the present study, if measurement error resulted in both a posterior and anterior shift of the shank axes of approximately 1.4 cm when defining the shank axes from external markers, then moment arms calculated with respect to the knee joint would also be inaccurate, except near the full extended anatomical position, where rotations are minimal. This is expected in the present study, where the shank axes origin remains relatively stationary relative to the thigh during knee flexion.

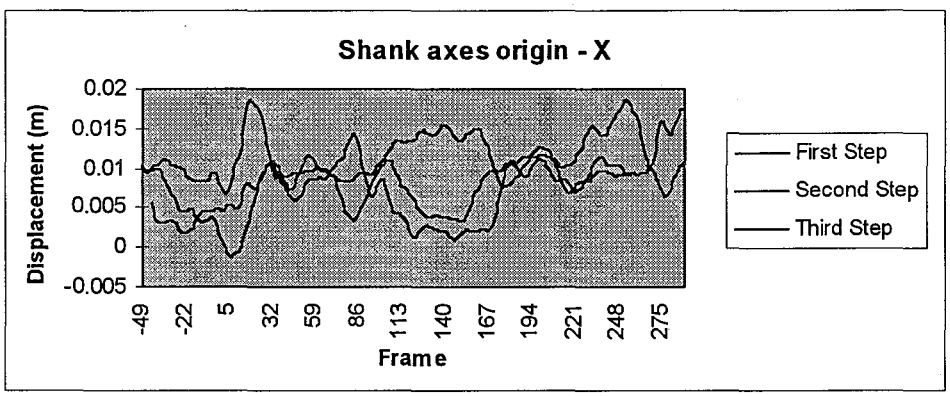

Figure 5.4.2 Step trials: location of shank axes origin along thigh x-axis.

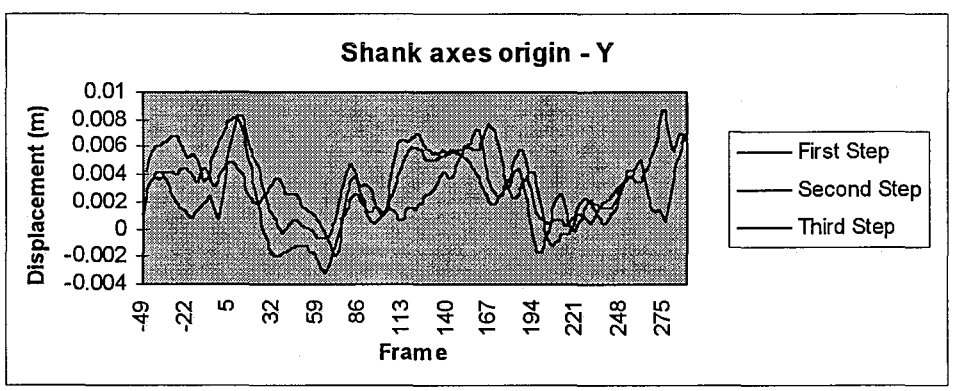

Figure 5.4.3 Step trials: location of shank axes origin along thigh y-axis.

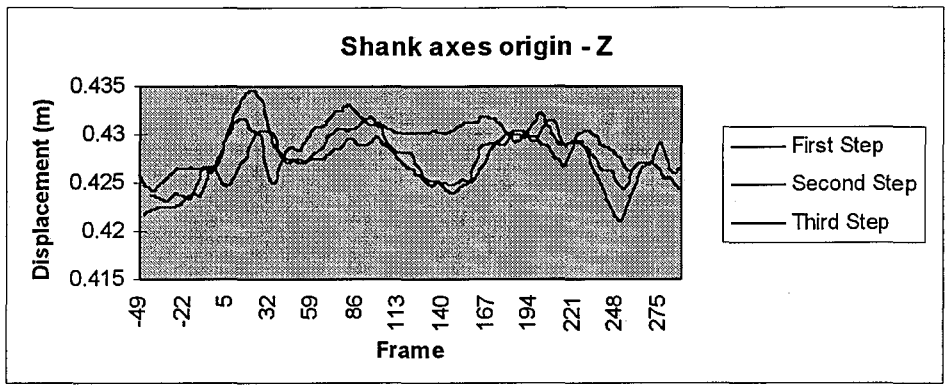

Figure 5.4.4 Step trials: location of shank axes origin along thigh z-axis.

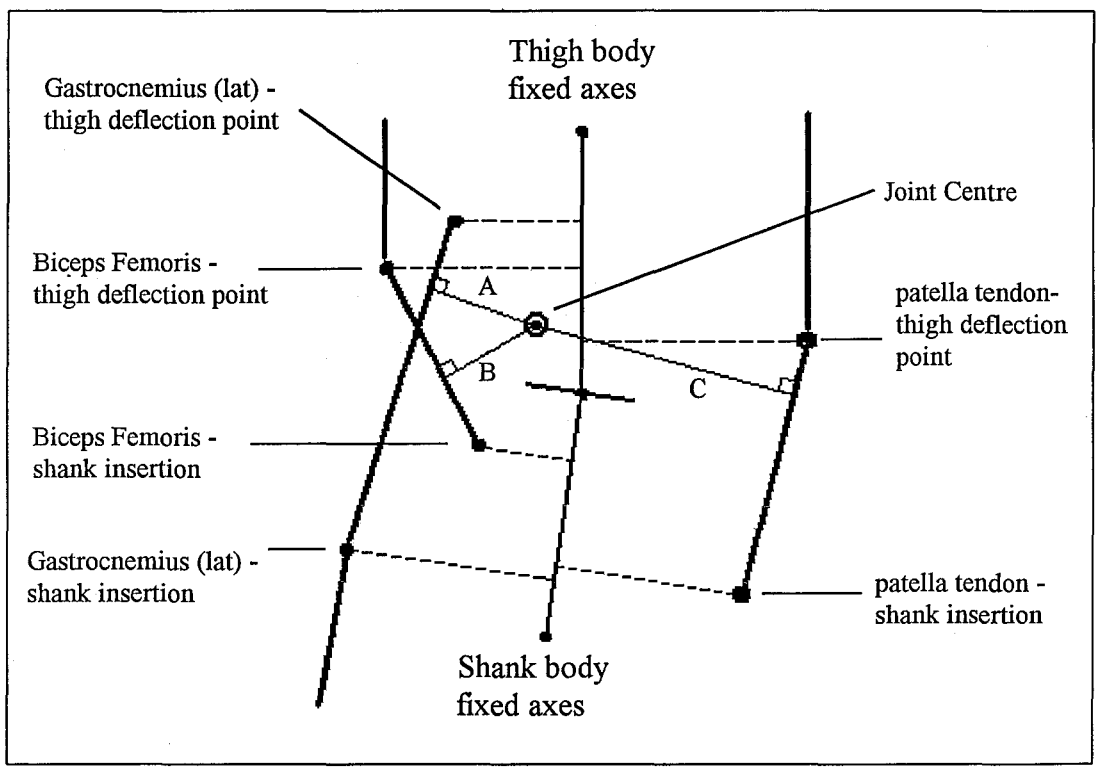

Figure 5.4.5 Moment arms of Biceps Femoris, Gastrocnemius (lateral) and patella tendon in standing position. Moment arms are A = Gastrocnemius (lateral), B = Biceps Femoris and C = patella tendon.

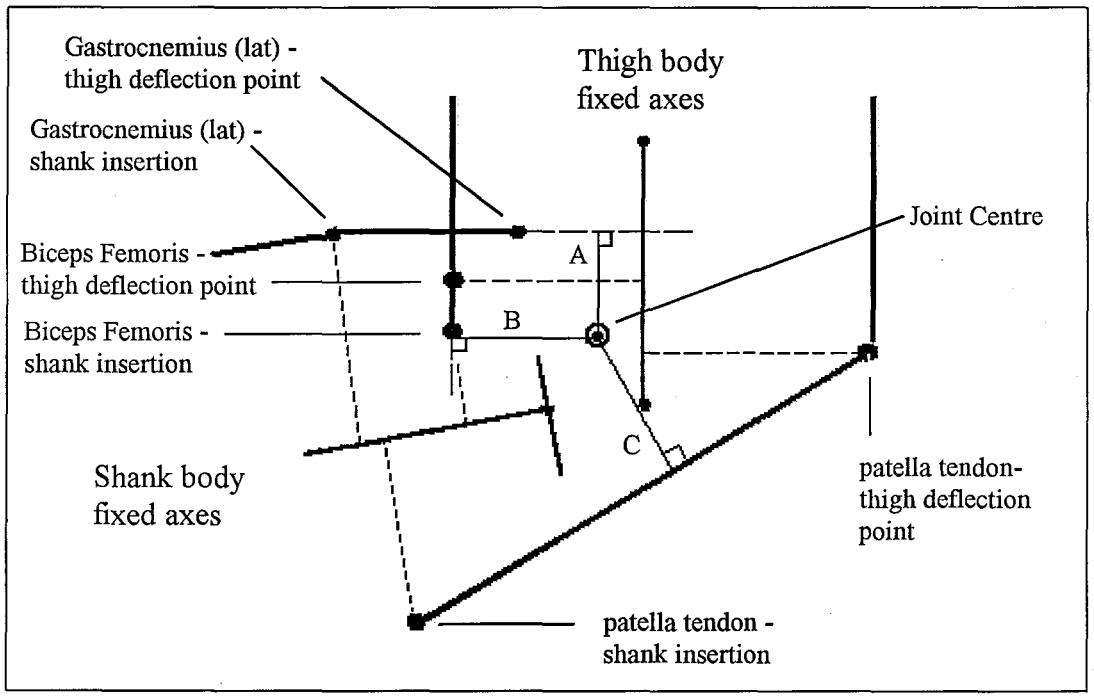

Figure 5.4.6 Moment arms of Biceps Femoris, Gastrocnemius (lateral) and Patella Tendon at 80 degrees shank flexion. Moment arms are A = Gastrocnemius (lateral), B = Biceps Femoris and C = patella tendon.

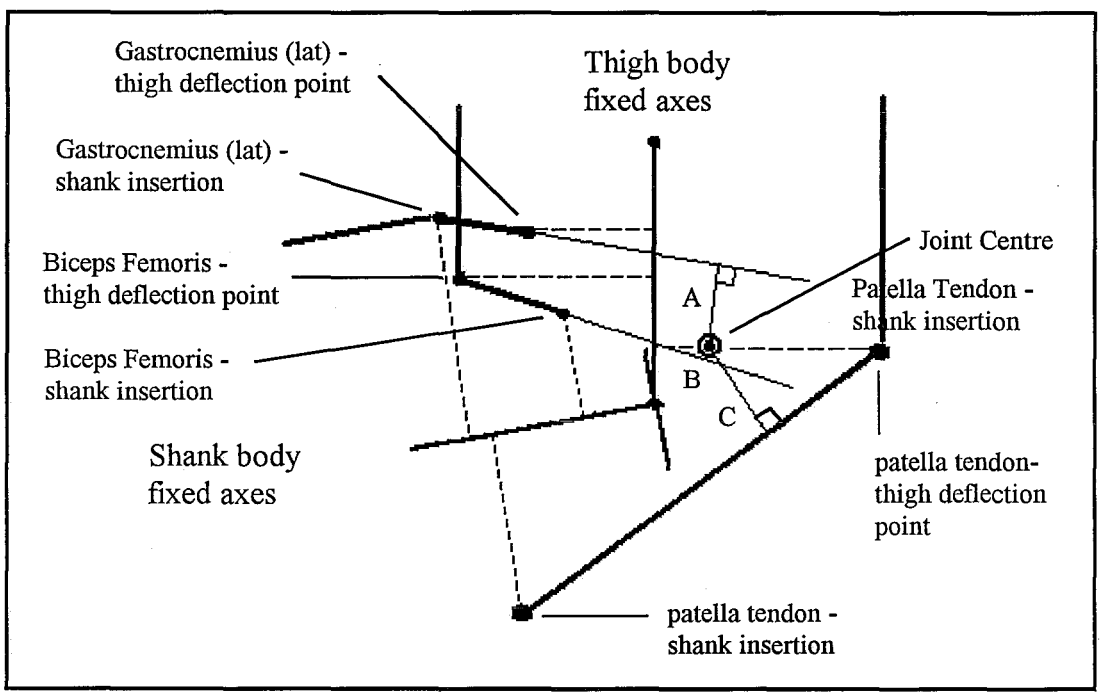

Figure 5.4.7 Moment arms of Biceps Femoris, Gastrocnemius (lateral) and Patella Tendon at 80 degrees shank flexion with rotation occuring at shank segment axes origin. Moment arms are A = Gastrocnemius (lateral), B = Biceps Femoris and C = patella tendon.

5.4.2.4 Step trial moment arms

Moment arms produced for the step trial are compared with those obtained in previous studies in relation to segment rotations, location of local points describing muscle-tendon path, and possible sources of error moment arm calculation.

Semitendinosus, Semimembranosus and Biceps Femoris moment arms (Figures 4.6.72, 4.6.70 and 4.6.80) about the medio-lateral axis of the knee in the extended position are in agreement with MRI measured moment arms obtained by Spoor & Leeuwen (1992). In the present study, moment arms in the standing position about the medio-lateral, anterior-posterior and longitudinal axes were 35 mm (extension), 10 mm (adduction) and -20 mm (internal) for Semimembranosus, 37 mm (extension), 10 mm (adduction) and -20 mm (internal) for Semitendinosus, and 18 mm (extension), -30 mm (abduction) and 10 mm (external) for Biceps Femoris. Spoor & Leeuwen (1992) measured moment arms about the medio-lateral axis of the knee at angles between 10 and 80 degrees flexion, obtaining moment arms between 35 mm and 40 mm for Semimembranosus, an increase in Semitendinosus moment arm from 35 mm to 55 mm and an increase in Biceps Femoris moment arm from 15 to 25 mm. The present study produced a decrease in knee extensor moment arms between 7 degrees and 80 degrees flexion, with Semitendinosus reducing from 37 mm to 28 mm, Semimembranosus reducing from 35 mm to 23 mm, and Biceps Femoris showing the largest decreases in moment arms, reducing from 18 mm to -7 mm. The large decreases in moment arms, especially between 75 and 80 degrees flexion, the greater errors in Biceps Femoris moment arm and the close agreement of the changes in moment arms to the pattern of knee flexion (Fig. 4.12.4), are consistent with a posterior and inferior displacement of the shank axes origin and the observed stationary displacement of the shank axes origin relative to the thigh local axes (see Section 5.4.5.2).

Vastus Lateralis, Vastus Medialis, Vastus Intermedius and Rectus Femoris moment arms (Figures 4.6.83, 4.6.85, 4.6.84, and 4.6.78) about the medio-lateral axis of the knee in the extended position are in agreement with the MRI measured moment arms of Rectus Femoris obtained by Spoor & Leeuwen (1992) and Duda et. al. (1996). In the present study, moment arms in the standing position about the medio-lateral, anterior-posterior and longitudinal axes were -48 mm (extension), -10 mm (abduction), 10 mm (external) for Vastus Lateralis, -48 mm (extension), 15 mm (adduction), -12 mm (internal) for Vastus Medialis, and -48 mm

(extension), 0 mm, and 0 mm for Vastus Intermedius and Rectus Femoris. Spoor & Leeuwen (1992) measured moment arms about the medio-lateral axis of the knee at angles between 10 and 80 degrees flexion, and produced a steady decrease in Rectus Femoris moment arm from -43 mm to -27 mm. The present study produced a decrease in knee extensor moment arms between 7 degrees and 80 degrees flexion, with the four muscles reducing from -48 mm to -25 mm. Despite the apparent agreement in moment arms about the medio-lateral axis with knee flexion, the present moment arms cannot be considered accurate. This inaccuracy is due to the expected errors in shank axes alignment, which altered locations of the knee joint centre and insertion points, and underestimated moment arms with increasing angles of knee flexion (Fig. 4.5.7). Duda et. al. (1996), using cadaver measurements and the straight-line approach, obtained overall moment arms in the anatomical position of 42 mm, 43 mm, 43 mm and 46 mm for Vastus Lateralis, Vastus Medialis, Vastus Intermedius and Rectus Femoris at the knee respectively. This compares with 50 mm, 52 mm, 48 mm and 48 mm for the same four muscles respectively in the standing position in the present study.

Spoor & Leeuwen (1992), utilising the tendon travel approach to measure moment arms, demonstrated a decrease in moments arms about the medio-lateral axis of the hamstring group when moving from 75 to 95 degrees of flexion. This indicates a posterior shift in the functional centre of rotation with respect to these muscles when approaching full flexion. Likewise for Rectus Femoris, Spoor & Leeuwen (1992) showed decreases in moments arms about the medio-lateral axis in moving from 30 to 5 degrees flexion. This indicated an anterior shift in the functional centre of rotation when approaching full extension for this muscle. The present method of defining moment arms by using a fixed knee joint centre of rotation would not predict a decrease in moment arms that may occur when approaching full extension or flexion for Rectus Femoris or hamstring muscle respectively. The apparent shifts in joint centre measured for the hamstring muscles were not present in Satorius, Gracilis or Gastronnemius moment arms when measured using the tendon travel approach (Spoor & Leeuwen, 1992). The apparent shifts in joint centre of rotation may be the result of the experimental process in obtaining joint movements from cadaver specimens, where the congruity of the joint may produce apparent shifts in moment arms as measured for Rectus Femoris and hamstring muscles.

Tensor Fasciae Latae moment arms (Fig. 4.6.68) about the medio-lateral axis of the knee are in agreement with the moment arms obtained by Spoor & Leeuwen (1992) and Duda et. al.

(1996). In the present study, moment arms in the standing position were -8 mm (extension), -33 mm (abduction), and 15 mm (external). Spoor & Leeuwen (1992), using the tendon travel approach, found an increase in moment arm about the medio-lateral axis from 2 mm (flexion) to 22 mm (flexion) in moving from 5 degrees to 35 degrees flexion followed by a decrease in moment arm to 17 mm (flexion) at 90 degrees flexion. The present study produced a decrease in moment arm to zero (extension) before increasing to 15 mm (flexion) when the knee angle changed from 7 degrees to 80 degrees flexion. The difference was due to the location of the insertion of the iliotibial tract. In the extended knee of the present study, the insertion is located slightly anterior to the predicted knee joint centre as opposed to slightly posterior in the study of Spoor & Leeuwen (1992). In both studies, the insertion moves in a posterior direction relative to the knee joint centre as the knee flexes. Duda et. al. (1996), from cadaver measurements using the straight-line approach, obtained a moment arm in the anatomical position of 32 mm for Tensor Fasciae Latae at the knee, which compares favourably with 37 mm in the present study.

Sartorius and Gracilis moments arms (Figures 4.6.74 and 4.6.76)about the medio-lateral axis of the knee are in agreement with MRI measured moment arms of Spoor & Leeuwen (1992). In the present study, moment arms about the medio-lateral, anterio-posterior and longitudinal axes were 20 mm (flexion), 25 mm (adduction) and -22 mm (internal) respectively for both muscles. The present study produced an increase in both Sartorius and Gracilis moment arms about the medio-lateral axis (20 mm to 32 mm, flexion) when moving from 7 degrees and 80 degrees flexion. Spoor & Leeuwen (1992), produced a slight increase in moment arms about the medio-lateral axis of both the Sartorius (28 mm to 32 mm, flexion) and Gracilis (34 mm to 40 mm, flexion) between 10 and 80 degrees flexion. As with the other muscles of the knee, the agreement in moment arms does not support the accuracy of predicted moment arms at the knee joint of the present study, with the exception of full extension. These differences are due to the expected errors in shank axes alignment, which would alter the relative movements of the knee joint centre and insertion points with knee flexion (Fig. 5.4.7). In correcting the present model, the alignment of the shank axes is such that the knee joint centre is stationary with respect to the thigh (Fig. 5.4.6). Sartorius and Gracilis moment arms in the present study would then be expected to decrease for the full range of flexion approaching zero at 80 degrees flexion. A 5 mm posterior and 20 mm anterior shift in the Sartorius and Gracilis thigh deflection points from the present location at the knee would correct this. The moment arms of these two muscles would then be expected to increase slightly from 20 mm in changing

from 7 degrees to 45 degrees flexion, followed by a slight decrease in changing from 45 degrees to 80 degrees extension. Duda et. al. (1996) obtained overall moment arms in the anatomical position of 21 mm and 23 mm for the Satorius and Gracilis respectively at the knee) from cadaver measurements using the straight-line approach. This is less than found the present study (39 mm for the both the Satorius and Gracilis muscles), and less than that obtained by Spoor & Leeuwen (1992).

Gastrocnemius moment arms (Figures 4.6.88 and 4.6.90) about the medio-lateral axis of the knee in the fully extended position are in agreement with moment arms of Spoor et. al. (1990) and Spoor & Leeuwen (1992). In the present study, the moment arms in the standing position about the medio-lateral, anterior-posterior, longitudinal axis were 32 mm (flexion), 7 mm (adduction) and -12 mm (internal) for Gastrocnemius Medialis and 23 mm (flexion), -45 mm (abduction) and -10 mm (internal) for Gastrocnemius Lateralis. The small adduction moment arm and internal rotation moment of Gastrocnemius Medialis in the standing position is likely to be due to the thigh deflection point being located to close to the mid-line of the thigh. Therefore in the muscle co-ordinate data presented in Appendix B, a medial shift of is recommended of approximately 5-7 mm along the medio-lateral axis the thigh of the thigh deflection point of the medial muscle. Spoor et. al. (1990) found a decrease in Gastrocnemius moment arms from 32 mm to 22 mm and 32 mm to 12 mm for the medial and lateral muscles respectively between 5 degrees and 75 degrees flexion. While Spoor & Leeuwen (1992) showed a constant moment arm of Gastrocnemius Medialis (17 mm) and a slight decrease in Gastrocnemius Lateralis moment arm (20 mm to 13 mm) in moving from 10 degrees to 80 degrees flexion. The present study produced a decrease in Gastrocnemius moment arms between 7 degrees and 80 degrees flexion, with Gastrocnemius Medialis reducing from 32 mm to 20 mm and Gastrocnemius Lateralis reducing from 23 mm to -3 mm. As mentioned with the hamstring muscles, the larger decreases in moment arms, especially between 75 and 80 degrees flexion, are associated with the greater error in Gastrocnemius Lateralis moment arm. The close agreement in the changes in moment arms with the pattern of knee flexion (Fig. 4.12.4) are consistent with the posterior and inferior displacement of the shank axes relative to the underlying bone (see Section 5.4.5.2). Duda et. al. (1996) obtained overall moment arms in the anatomical position of 23 mm and 30 mm for the Gastrocnemius Medialis and Gastrocnemius Lateralis at the knee respectively. This is smaller than the 35 mm and 52 mm predicted for the medial and lateral muscles respectively for the present study.

The Achilles tendon moment arms (Gastrocnemius, Soleus and Plantaris, Figures 4.6.87, 4.6.89, 4.6.91, 4.6.93 and 4.9.94) about the medio-lateral axis of the ankle are in agreement with moment arms reported by Rugg et. al. (1990) and Spoor et. al. (1990). The present study produced a decrease in moment arms (45 mm to 40 mm) when changing from the anatomical position (92 degrees) to 11 degrees of dorsi flexion. Spoor et. al. (1990), using the tendon travel approach, found a decrease in Achilles tendon moment arm (50 mm to 45 mm) when changing from the neutral position (90 degrees) to 20 degrees dorsi flexion. In measurements from MRI, Rugg et. al. (1990) also found a decrease in Achilles tendon moment arm (53 mm to 50 mm) when going from the neutral position (111 degrees) to 11 degrees dorsi flexion.

Tibialis Anterior, Extensor Digitorum Longus, Extensor Hallucis Longus, and Peronius Tertius moment arms (Figures 4.6.95, 4.6.100, 4.6.101 and 4.6.99) about the medio-lateral axis of the ankle are in agreement with Spoor et. al. (1990). In the present study, the moment arms in the standing position about the medio-lateral axis were -20 mm, -20 mm, -23 mm and -13 mm for the four muscles respectively. The present study produced a decrease in moment arms about the medio-lateral axis to -15 mm, -17 mm, -18 mm, and -11 mm respectively, when changing from the anatomical position to 11 degrees of dorsi flexion with 4 degrees of external rotation. Spoor et. al. (1990), using the tendon travel approach, produced moment arms in the neutral position about the medio-lateral axes of -40 mm, -42 mm, -44 mm, and -38 mm for the four muscles respectively. They also found a decrease in moment arms to -13 mm, -15 mm, -15 mm, and -15 mm for the four respective muscles when changing from the neutral position to 20 degrees dorsi flexion. It was suggested the decrease in dorsi flexion moment arms during dorsi flexion may be caused by the retinacula, and perhaps to a lesser extent, an anterior displacement of the flexion axis. In contrast, Rugg et. al. (1990) and Maganaris (2000) both found an increases in Tibialis Anterior moment arm (45 mm to 50 mm and 35 mm to 45 mm, respectively) in going from the neutral position to 11 degrees and 15 degrees dorsi flexion, respectively.

The contradiction in the changes in moment arms with dorsi flexion between the present study, Spoor et. al. (1990) and the studies of Rugg et. al. (1990) and Maganaris (2000) highlight the sensitivity of moment arms to the methods used in moment arm calculation. Different points of reference for the line of action of the Tibialis Anterior change the moment arm with changes in joint angle (Fig. 5.4.8). With a fixed ankle joint centre and shank deflection point, there exists a joint angle which will result in the largest moment arm for a given foot deflection point (Fig.

5.4.8). Conversely, when defining the tendon line of action or the foot deflection point at a set reference ankle position, the location of the foot deflection point may produce an increase in moment arm with dorsi flexion and a decrease in moment arm with plantar flexion. Similarly, the relative position of the point may produce a decrease in moment arm with dorsi flexion and an initial increase followed by decrease in moment arm with plantar flexion when moving from the reference position (Fig. 5.4.8).

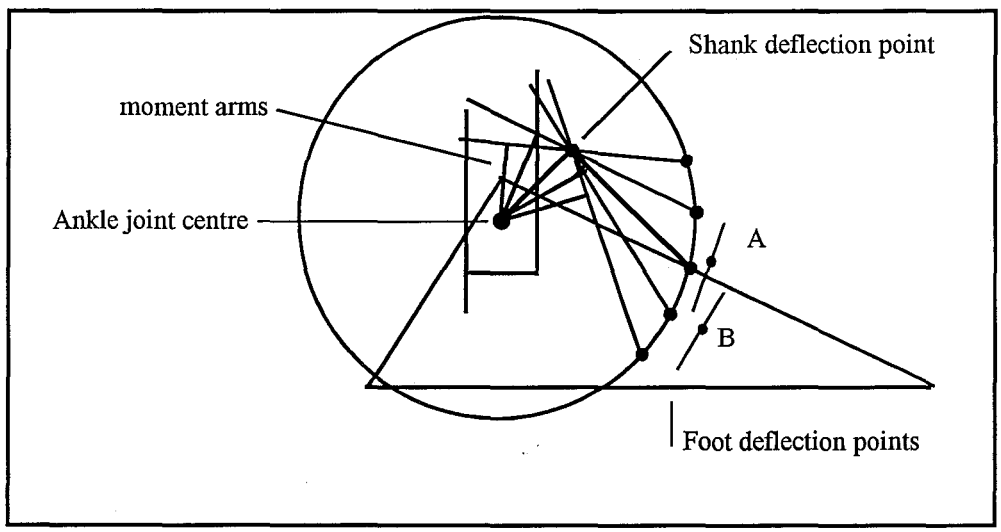

Figure 5.4.8 Changes in moment arms with changing joint angle. Arc A produces a decrease in moment arm with dorsi flexion and an initial increase followed by decrease in moment arm with plantar flexion when moving from the mid-point of A. Arc B produces an increase in moment arm with dorsi flexion and a decrease in moment arm with plantar flexion when moving from the mid-point of B.

In the standing position, Tibialis Posterior, Flexor Digitorum Longus and Flexor Hallucis Longus moment arms about the medio-lateral axis of the ankle are in agreement with Spoor et. al. (1990). In the present study, the moment arms in the standing position about the medio-lateral axis were 18 mm, 27 mm, and 28 mm for the three muscles respectively. The present study produced a decrease in moment arms about the medio-lateral axis to 15 mm, 23 mm and 24 mm respectively, when changing from the anatomical position to 11 degrees of dorsi flexion with 4 degrees of external rotation. Spoor et. al. (1990) produced moment arms in the neutral position about the medio-lateral axes of 10 mm, 15 mm, and 26 mm for the three muscle respectively and found an increase in moment arms to 18 mm, 21 mm, and 32 mm for the three respective muscles when changing from the neutral position to 20 degrees dorsi flexion. They also found a decrease in moment arms to 2 mm, 10 mm, and 15 mm for the three

respective muscles when going from the neutral position to 30 degrees plantar flexion. The difference in moment arms with dorsi flexion may result from the relative positions of the deflection points and ankle joint centre. To produce an increase in moment arms with dorsi flexion and a decrease with plantar flexion, the deflection point on the foot for the Tibialis Posterior, Flexor Digitorum Longus and Flexor Hallucis Longus would need to be moved approximately 10 mm posteriorly along the foot z-axis from the location presented in Appendix B (Figure 5.4.9).

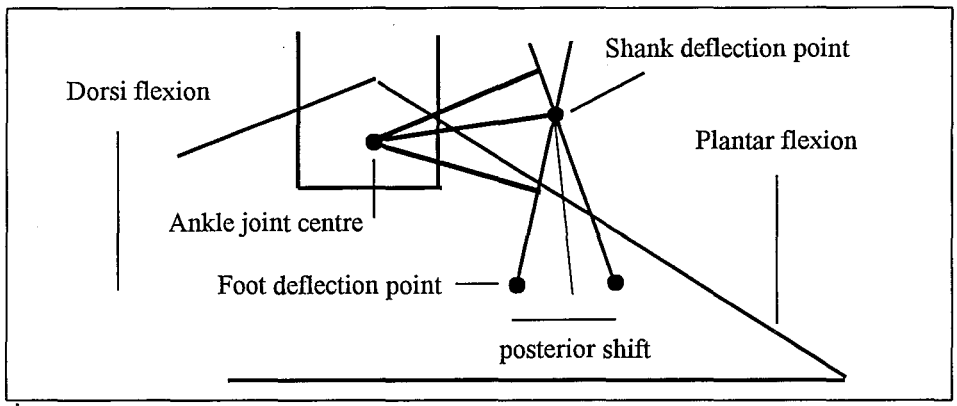

Figure 5.4.9 Posterior shift in foot deflection point of Tibialis Posterior. The posterior shift will result in an increase in moment arm with dorsi flexion and a decrease in moment arm with plantar flexion.

Peronius Longus and Peronius Brevis moment arms (Figures 4.6.97 and 4.6.98) about the medio-lateral axis of the ankle are in agreement with Spoor et. al. (1990). The present study produced an increase in moment arms (21 mm to 25 mm and 22 mm to 25 mm, respectively) when moving from the standing position to 11 degrees of dorsi flexion with 4 degrees of external rotation. Spoor et. al. (1990) found an increase in moment arms (14 mm to 16 mm, and 10 mm to 16 mm. respectively) when changing from the neutral position to 20 degrees dorsi flexion, and in plantar flexion, found a small initial decrease in moment arms (2 mm) when going from the neutral position to 10 degrees plantar flexion. Thereafter, Peroneus Longus and Peroneus Tertius showed an increase in moment arms (12 mm to 20 mm and 8 mm to 20 mm, respectively) when changing from 10 degrees to 30 degrees plantar flexion.

The shorter moment arms produced in the present study for Tibialis Anterior, Extensor Hallucis Longus, Extensor Digitorum Longus, and Peroneus Brevis, and longer moment arms of Tibialis Posterior, Peroneus Longus, Peroneus Brevis, may have resulted from the ankle

joint centre being defined more superiorly in the present study than in the studies that used the MRI-defined joint centre or the functional joint centres of the tendon travel approach (Fig. 5.4.10). This may be due to scaling reference data to the subject, based on external measurements. In the present study, the Achilles tendon and Flexor Hallucis Longus moment arm would not be affected to the same extent by a superior shift in the ankle joint centre due to the more inferior-superior line of action of these muscle at the ankle joint (Fig. 5.4.10). In the present study, Flexor Digitorum Longus was defined with a line of action at the ankle joint similar to that of Flexor Hallucis Longus. However, Flexor Digitorum Longus moment arm was considerably longer than that obtained by Spoor et. al. (1990). This may have been due to the deflection point on the foot being defined too posterior - a move of 10 mm anteriorly along the foot z-axis from the data presented in Appendix B would place the deflection point between the Tibialis Posterior and Flexor Hallucis Longus deflection points and, in so doing, reduce the moment arm.

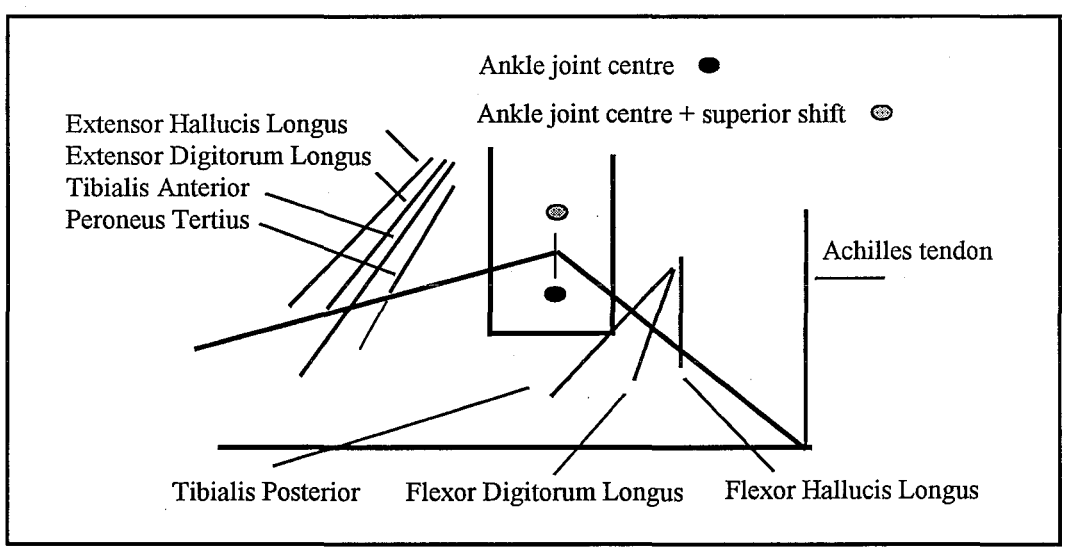

Figure 5.4.10 Sagittal plane line of action of the muscles crossing the ankle joint

Gluteus Maximus moment arms (Figures 4.6.65, 4.6.66 and 4.6.67) are in agreement with Delp, et. al. (1999) and Nemeth & Ohlsen (1985). The present study produced moment arms in the standing position (6 degrees flexion) about the medio-lateral thigh axis of 50 mm (extension), 60 mm (extension) and 75 mm (extension) for Gluteus Maximus (ant), Gluteus Maximus (mid) and Gluteus Maximus (pos) respectively. Moment arms in the standing position about the anterior-posterior thigh axis were -10 mm (abduction), 5 mm (adduction) and 15 mm (adduction) for the three respective muscle elements. Moment arms in the standing

position about the longitudinal thigh axis were 25 mm (external), 27 mm (external) and 30 mm (external) for the three respective muscle elements. When changing from the standing position to 70 degrees flexion, with 10 degrees of adduction and 10 degrees of external rotation, moment arms about the medio-lateral axis reduced to 25 mm (extension), 30 mm (extension) and 45 mm (extension) for the anterior, middle and posterior elements respectively. The moment arms about the longitudinal axis also reduced to zero (external), 5 mm (external) and 10 mm (external) for the anterior, middle and posterior elements respectively. Conversely, the moment arms about the anterior-posterior axis increased to -25 mm (abduction) for the anterior element, while the middle and posterior elements reduced to zero (adduction) before increasing to -20 mm (abduction) and -15 mm (abduction) respectively. Delp et. al. (1999) obtained moment arms in the anatomical position about the longitudinal axis of 23 mm (external), 28 mm (external) and 16 (external) for Gluteus Maximus (ant), Gluteus Maximus (mid) and Gluteus Maximus (pos) elements respectively. With 90 degrees of hip flexion, the Gluteus Maximus (ant) and Gluteus Maximus (mid) moment arms decreased to zero (external) before increasing to -40 mm and -7 mm (internal) respectively, while the Gluteus Maximus (pos) moment arm decreased to 7 mm (external). Nemeth & Ohlsen (1985) produced Gluteus Maximus moment arms about the medio-lateral axis of the hip from radiographic images of 81 mm and 75 mm (extension) for males and females respectively in the standing position. With 90 degrees hip flexion, Gluteus Maximus moment arms decreased to 33 mm and 31 mm (extension) for males and females respectively.

Gluteus Medius moment arms (Figures 4.6.62, 4.6.63 and 4.6.64) are in agreement with the data presented by Jenson & Davy (1975), Dostal & Andrews (1981), and Delp et. al. (1999). The present study produced moment arms in the standing position (6 degrees flexion) about the medio-lateral thigh axis of 0 mm (extension), 18 mm (extension) and 25 mm (extension) for the Gluteus Medius (ant), Gluteus Medius (mid), and Gluteus Medius (pos) respectively. Moment arms in the standing position about the anterior-posterior thigh axis were -55 mm (abduction), -60 mm (abduction) and -55 mm (abduction) for the three respective muscle elements. Moment arms in the standing position about the longitudinal thigh axis were -35 mm (internal), 0 mm (internal) and 20 mm (external) for the three respective muscle elements. When changing from the standing position to 70 degrees flexion with 10 degrees of adduction and 10 degrees of external rotation, moment arms about the medio-lateral axis of the anterior element increased to -10 mm (flexion), while the middle and posterior elements reduced to 5 mm (extension) and 18 mm (extension) respectively. The moment arms about the longitudinal

axis of the anterior and middle elements increased to -55 mm (internal) and -35 mm (internal) respectively, while the posterior element reduced to 0 mm (external) before increasing to -20 mm (internal). The moment arms about the anterior-posterior axis reduced to -25 mm (abduction), -40 mm (abduction) and -40 mm (abduction) for the anterior, middle and posterior elements respectively. Dostal & Andrews (1981) obtained moment arms of 10 mm (extension), -65 mm (abduction) and -25 mm (internal rotation) about the thigh axes in the anatomical position from cadaver measurements using the straight-line muscle representations. With 15 degrees of extension, the first moment arm increased to 20 mm (extension), the second moment arm increased to -70 mm (abduction), and the third moment arm reduced to -5 mm (internal rotation). With 90 degrees flexion, the first moment arm initial reduced to zero before increasing to -25 mm (flexion), the second moment arm reduced to zero (abduction), while the third moment arm increased to -65 mm (internal rotation). Delp et. al. (1999), using the tendon travel approach, obtained moment arms in the anatomical position about the longitudinal axis of -7 mm (internal), 15 mm (external) and 41 mm (external) for the Gluteus Medius (ant), Gluteus Medius (mid) and Gluteus Medius (pos) elements respectively. With 90 degrees of hip flexion, the Gluteus Medius (ant) moment arm increased to -58 mm (internal). While the Gluteus Medius (mid) and Gluteus Medius (post) moment arms both decreased to zero before increasing to -47 mm (internal) and -22 mm (internal) respectively. The larger external moment produced about the longitudinal axis in the anatomical position of Delp et. al. (1999) may result from muscle element origins being defined more posterior on the pelvis than in the present study. Jenson & Davy (1975), from cadavers using the muscle centroid approach, obtained moment arms in the anatomical position of 4 mm (extension), -45 mm (abduction) and 23 mm (external rotation) about the thigh axes respectively. Conversely, Duda et. al. (1996), from cadaver measurements using the straight-line muscle representation, obtained an overall moment arm in the anatomical position of 43 mm, which compares with an overall moment in the standing position of 65 mm, 62 mm, and 64 mm for the anterior, middle and posterior muscle elements respectively.

Moment arms of Semimembranosus, Semitendinosus, and Biceps Femoris (long) (Figures 4.6.71, 4.6.73 and 4.6.81) are in agreement with Nemeth & Ohlsen (1985) and Duda et. al. (1996). The present study produced moment arms in the standing position about the medio-lateral thigh axis of 35 mm (extension), 50 mm (extension) and 45 mm (extension) for Semimembranosus, Semitendinosus, and Biceps Femoris (long) respectively. Moment arms in the standing position about the anterior-posterior thigh axis were 10 mm (adduction), 10 mm

(adduction) and 12 mm (adduction) for the three respective muscles. Moment arms in the standing position about the longitudinal thigh axis were -2 mm (internal), -2 mm (internal) and 7 mm (external) for the three respective muscles. When changing from the standing position to 70 degrees flexion with 10 degrees of adduction and 10 degrees of external rotation, moment arms about the medio-lateral axis initially increased by 8 mm at approximately 35 degrees flexion before reducing to 20 mm (extension), 35 mm (extension) and 30 mm (extension) respectively. The moment arms about the longitudinal axis of the anterior and middle elements reduced to 0 mm (internal), 0 mm (internal) and 5 mm (external) for the three muscles respectively. From radiographic images, Nemeth & Ohlsen (1985) predicted hamstring moment arms about the medio-lateral axis of the hip of 68 mm and 61 mm extension for males and females respectively in the standing position. With hip flexion, the hamstring moment arm increased to 80 mm for males and 70 mm for females at 35 - 40 degrees flexion. Thereafter, hamstring moment arm decreased to 48 mm for males and 40 mm for females at 90 degrees flexion. Duda et. al. (1996) obtained overall moment arms at the hip in the anatomical position of 38 mm, 44 mm and 43 mm for Semimembranosus, Semitendinosus and Biceps Femoris (long) respectively. This compares with an overall moment in the standing position of 36 mm, 51 mm, and 47 mm for the Semimembranosus, Semitendinosus and Biceps Femoris (long) muscles respectively.

Adductor Magnus moment arms (Figures 4.6.56, 4.6.57 and 4.6.58) are in agreement with Nemeth & Ohlsen (1985), while the moment arms of the anterior, middle and posterior elements in the anatomical position are in agreement with Duda et. al. (1996). The present study produced moment arms in the standing position about the medio-lateral thigh axis of -35 mm (flexion), 0 mm (extension) and 25 mm (extension) for the Adductor Magnus (ant), Adductor Magnus (mid), and Adductor Magnus (pos) respectively. Moment arms in the standing position about the anterior-posterior thigh axis were 55 mm (adduction), 40 mm (adduction) and 20 mm (adduction) for the three respective muscle elements. Moment arms in the standing position about the longitudinal thigh axis were 0 mm (internal), 0 mm (internal) and -2 mm (internal) for the three respective muscle elements. When changing from the standing position to 70 degrees flexion with 10 degrees of adduction and 10 degrees of external rotation, moment arms about the medio-lateral axis of the anterior element reduced to 0 mm (flexion), while the middle and posterior elements initially increased to 30 mm (extension) and 45 mm (extension) respectively at 46 degrees flexion before reducing to 25 mm (extension) and 35 mm (extension) respectively. The moment arms about the longitudinal

axis increased to 10 mm (external), 2 mm (external), and -4 mm (internal) of the anterior, middle and posterior elements respectively while the moment arms about the anterior-posterior axis reduced to 50 mm (adduction), 25 mm (abduction) and 15 mm (abduction) for the anterior, middle and posterior elements respectively. From radiographic images, Nemeth & Ohlsen (1985) predicted Adductor Magnus moment arms about the medio-lateral axis of the hip of 15 mm and 24 mm extension for males and females respectively in the standing position. With hip flexion, Adductor Magnus moment arms increased to 62 mm for males and 60 mm for females at 75 degrees flexion. Thereafter, Adductor Magnus moment arms decreased by 1 mm for males and 3 mm for females at 90 degrees flexion. Duda et. al. (1996) obtained overall moment arms in the anatomical position of 73 mm 65 mm and 51 mm for the Adductor Magnus (ant), Adductor Magnus (mid) and Adductor Magnus (pos) and at the hip respectively which compares with an overall moment in the standing position of 65 mm, 40 mm, and 32 mm for the Adductor Magnus (ant), Adductor Magnus (mid) and Adductor Magnus (pos) elements respectively.

Gluteus Minimus moment arms (Figures 4.6.60 and 4.6.61) in the present study are in agreement with Delp et. al. (1999), with moment arms in the standing position about the medio-lateral thigh axis of -10 mm (flexion) and -2 mm (flexion) for the Gluteus Minimus (ant) and Gluteus Minimus (pos) respectively. Moment arms in the standing position about the anterior-posterior thigh axis were -48 mm (abduction) and -48 mm (abduction) for the two respective muscle elements. Moment arms in the standing position about the longitudinal thigh axis were -32 mm (internal) and -2 mm (internal) for the two respective muscle elements. When changing from the standing position to 70 degrees flexion with 10 degrees of adduction and 10 degrees of external rotation, moment arms about the medio-lateral axis increased to -12 mm (flexion) and -12 mm (flexion) for the anterior and posterior elements respectively. The moment arms about the longitudinal axis increased to -55 mm (internal) and -40 mm (internal) for the anterior and middle elements respectively while the moment arms about the anterior-posterior axis reduced to -15 mm (abduction) and -30 mm (abduction) for the anterior and posterior elements respectively. Delp et. al. (1999) obtained moment arms in the anatomical position about the longitudinal axis of -18 mm (internal) and 30 mm (external) for the Gluteus Minimus (ant) and Gluteus Minimus (pos) elements respectively. With 90 degrees of hip flexion, the Gluteus Minimus (ant) moment arm increased to -35 mm (internal) while the Gluteus Minimus (post) moment arm decreased to zero before increasing to -26 mm (internal). The greater external moment of the posterior muscle element about the longitudinal axes

possibly resulted from the origin of this muscle element being placed more posteriorly on the pelvis in the study of Delp et. al. (1999) than in the present study.

Psoas Major and Iliacus moment arms (Figures 4.6.46 and 4.6.47) are in agreement with Delp et al. (1999) in the anatomical position, however an increase in the internal moment arm about the longitudinal axis was seen in the present study compared with little change in moments about the longitudinal axes of Delp et al. (1999). This was due to the deflection point on the anterior of the hip joint capsule being fixed relative to the thigh, and with external rotation, the deflection point moved externally instead of sliding over the joint capsule. An alternative method is needed to define this deflection point, and could possibly be a curved line from the deflection point on the pelvis to insertion on the thigh in the sagittal plane of the pelvis. The present study produced moment arms in the standing position about the medio-lateral thigh axis of -36 mm (flexion) and -36 mm (flexion) for the Psoas Major and Iliacus respectively. Moment arms in the standing position about the anterior-posterior thigh axis were -2 mm (abduction) and -8 mm (abduction) for the two respective muscles, and about the longitudinal thigh axis, were -2 mm (internal) and -8 mm (internal) for the two respective muscles. When changing from the standing position to 70 degrees flexion with 10 degrees of adduction and 10 degrees of external rotatio, moment arms about the medio-lateral axis reduced to -22 mm (flexion) and -24 mm (flexion) for the Psoas and Iliacus respectively. The moment arms about the longitudinal axis increased to -15 mm (internal) and -20 mm (internal) for the two muscles respectively while the moment arms about the anterior-posterior axis reduced to zero abduction before increasing to 8 mm (adduction) and 5 mm (adduction) for the two muscles respectively. Delp et. al. (1999), from function evaluations of moment arms using the tendon travel approach, obtained moment arms about the longitudinal axis of -2 mm (internal) for the Iliopsoas in the anatomical position, and with 90 degrees of hip flexion, the moment arm decreased to zero before increasing to 4 mm (external).

Piriformus moment arms (Fig. 4.6.52) are in agreement with Delp et. al. (1999). The present study produced moment arms in the standing position about the medio-lateral thigh axis of 9 mm (extension), the anterior-posterior thigh axis of -35 mm (abduction) and the longitudinal thigh axis of 25 mm (external). When changing from the standing position to 70 degrees flexion with 10 degrees of adduction and 10 degrees of external rotation, moment arms about the medio-lateral axis reduced to 5 mm (extension). The moment arms about the longitudinal axis reduced to zero (external) before increasing to -10 mm (internal). Delp et. al. (1999)

obtained moment arms about the longitudinal axis of 29 mm (external) for the Piriformus in the anatomical position, and with 90 degrees of hip flexion, the moment arm decreased to zero before increasing to -14 mm (internal).

Quadratus Femoris moment arms (Fig. 4.6.53) are in agreement with Delp et. al. (1999), however a reduction in moments was seen about the longitudinal axis at hip flexion angles above 60 degrees in the present study. The present study produced moment arms in the standing position about the medio-lateral thigh axis of -8 mm (flexion), the anterior-posterior thigh axis of 25 mm (adduction) and the longitudinal thigh axis of 15 mm (external). When moving from the standing position to 70 degrees flexion with 10 degrees of adduction and 10 degrees of external rotation, moment arms about the medio-lateral axis reduced to zero (flexion) before increasing to 10 mm (extension). The moment arms about the longitudinal axis initially increased to 22 mm (external) before reducing to 10 mm (external) and the moment arms about the anterior-posterior axis reduced to zero (adduction). Delp et. al (1999) obtained moment arms in the anatomical position about the longitudinal axis of 22 mm (external), and at 90 degrees of hip flexion, they found an increase in moment arm to 27 mm (external). The differences in moments about the longitudinal axes at hip flexion angles above 60 degrees may be due to external rotation of the thigh in the step trials which increases with thigh flexion angle. This may bring the line of action of the Quadratus Femoris closer to the line of the longitudinal axes the thigh. Duda et. al. (1996) obtained an overall moment arm in the anatomical position of 45 mm which compares with 30 mm for the moment arm in the standing position of the Quadratus Femoris in the present study.

Obturator Internus moment arms (Figure 4.6.51) are in agreement with Delp et. al. (1999), however greater reductions in the longitudinal moments with hip flexion were seen in the present study. The present study produced moment arms in the standing position about the medio-lateral thigh axis of 8 mm (extension), the anterior-posterior thigh axis of -30 mm (abduction) and the longitudinal thigh axis of 15 mm (external). When changing from the standing position to 70 degrees flexion with 10 degrees of adduction and 10 degrees of external rotation, moment arms about the medio-lateral axis reduced to 5 mm (extension). The moment arms about the longitudinal axis reduced to zero (external) before increasing to -15 mm (internal). Delp et. al. (1999) obtained moment arms in the anatomical position about the longitudinal axis of 30 mm (external), and with 90 degrees of hip flexion, the moment arm decreased to 7 mm (external). The greater reduction in moment about the longitudinal axis,

also seen in the Quadratus Femoris, may be due to the increasing external rotation of the thigh which occurs with hip flexion in the step trials. Duda et. al. (1996) obtained an overall moment arm in the anatomical position of 30 mm, which compares with 34 mm for the moment arm in the standing position of the Obturator Internus in the present study.

Obturator Externus moment arms (Figure 4.6.52) are in agreement with Delp et. al. (1999). The present study produced moment arms in the standing position about the medio-lateral thigh axis of -15 mm (flexion), the anterior-posterior thigh axis of 25 mm (adduction) and the longitudinal thigh axis of 5 mm (external). When changing from the standing position to 70 degrees flexion with 10 degrees of adduction and 10 degrees of external rotation, moment arms about the medio-lateral axis reduced to -8 mm (flexion), while the moment arms about the longitudinal axis increased to 20 mm (external) and the moment arms about the anterior-posterior axis reduced to 17 mm (adduction). Delp et. al. (1999) obtained moment arms in the anatomical position about the longitudinal axis of 14 mm (external), which with 90 degrees of hip flexion, the increased to 26 mm (external). Conversely, Duda et. al. (1996) obtained an overall moment arm in the anatomical position of 31 mm, which compares favourably with 30 mm for the moment arm in the standing position of the Obturator Externus in the present study.

Satorius moment arms (Fig. 4.6.77) are in agreement with Jenson & Davy (1975) and Duda et. al. (1996). The present study produced moment arms in the standing position about the medio-lateral thigh axis of -60 mm (flexion), the anterior-posterior high axis of -5 mm (abduction) and the longitudinal thigh axis of 25 mm (external). When changing from the standing position to 70 degrees flexion with 10 degrees of adduction and 10 degrees of external rotation, moment arms about the medio-lateral axis increased to -85 mm (flexion). The moment arms about the longitudinal axis increased to 35 mm (external) and the moment arms about the anterior-posterior axis initially reduced to zero (abduction) before increasing to -10 mm (abduction). Jenson & Davy (1975) obtained moment arms in the anatomical position of -48 mm (flexion), -29 mm (abduction) and 12 mm (external rotation) about the thigh axes, while Duda et. al. (1996) obtained an overall moment arm in the anatomical position of 63 mm at the hip. An improvement in the abduction moment arm of the present study, when compared to that of Jenson & Davy (1975), may be made by moving the deflection point on the thigh laterally from +30 mm to +10 mm on the local thigh x-axis compared to the muscle co-ordinate data as presented in Appendix B.

The present study has shown the sensitivity of moment arms to measurement errors in the three dimensional analysis of human movement. Therefore, improvements in accuracy of moment arms predicted for a range of joint motions in the present study can be made by:

i) Improving the location of body-fixed axes defined from external markers for individual subjects. A possible solution may be to carry out a pre-analysis of simple movements or of the trial itself to determine moment arms and the relative positions of joint centres with respect to the local axes of the proximal segment. This would enable adjustments to the location of the body-fixed axes, as defined from external markers, to produce consistency between the skeletal model and the movements of the skeletal system of the subject, ensuring that the relative motion of joint centres and moment arms were in agreement with expected values. Hence, if the joint centre is modelled as a fixed point, then it would remain stationary with respect to the proximal segment. In the present study, this was necessary for the shank local axis system, but should also have been implemented for the hip and ankle joint centres to account for measurement errors and to achieve a functional joint centre;

ii) Improving the accuracy of the pelvis and foot three dimensional locations in the present study, which could be achieved by the use of an adequate number of markers per segment and a greater camera numbers to reproduce the three dimensional motion;

iii) Improvements can be made in the representation of muscle-tendon paths of the present study to include the use of straight and curved line segments and to improve the muscle co-ordinate data as suggested in the Discussion;

iv) More research is needed to validate the moment arms reported in the present study, and includes comparing moment arms produced in controlled subject movements to expected values and to previous research data. However, little information is presently available on the moments produced by the muscles of the lower limb about all three axes of the thigh, shank and foot for a range of hip, knee and ankle displacements.

5.4.3 Muscle forces

In this section, predicted muscle forces are compared to EMG data simultaneously recorded for selected muscles. Predicted muscle forces were consistent over the three walk trials and consistent over the three step trials. Therefore, in the following discussion, predicted force refers to the mean of three trials unless otherwise stated. Similarly the electromyographic data (EMG) were consistent over the three walk trials and the three step trials, and therefore EMG also refers to the mean of the three trails.

5.4.3.1 Walk Trials

The predicted Soleus and Gastrocnemius forces (Fig. 4.5.43 and Appendix L) showed no significant magnitude during the swing phase of the gait cycle. A small peak in force, primarily in the Gastrocnemius (med), muscle occurred at heel strike, followed by relative small forces until at 30% of the stance phase. At this stage of the gait cycle, the predicted force rose sharply, reaching a peak at 80% of the stance phase, and then falling rapidly to zero at toe-off. Soleus (lat) consistently reached the highest force values while Gastrocnemius (lat) consistently produced the lowest maximum force. Soleus (med) and Gastrocnmeius (med) showed similar maximum force values. This was supported by EMG recordings, where the Soleus (lat) and Gastrocnemius (med) showed minimal electrical activity during the swing phase. Electrical activity increased at heel strike reaching an on-set level at 30% of the stance phase for the Soleus (lat) which then diminished to an offset level at toe-off. EMG of the Gastrocnemius Lateralis showed high levels of resting electrical activity in relation to maximum activity, achieving the on-set and offset values for only the peak electrical activities. For Gastrocnemius Lateralis, the peak activity occurred at 70% of the stance phase. Soleus and Gastrocnemius predicted muscle forces and EMG patterns are in agreement with Winter (1991), Collins (1995), and Glitsch & Baumann (1997).

The predicted Tibialis Posterior, Peroneus Longus, Peroneus Brevis, Flexor Digitorum Longus, and Flexor Hallucis Longus forces (Fig. 4.5.45 and Appendix L) showed no significant magnitude during the swing phase. All muscles produced small increases in force shortly after heel strike, before rising sharply at 30% of the stance phase, to reach a peak force at 80% of stance phase and then falling rapidly to zero at toe-off. Peroneus Longus consistently reached the highest maximum force and Flexor Digitorum Longus consistently

produced the lowest in maximum force. Tibialis Posterior, Peroneus Brevis and Flexor Hallucis Longus muscles reached similar predicted force values. These findings ae in agreement with the Peroneus Longus, and Peroneus Brevis EMG patterns reported by Winter (1991).

The predicted Tibialis Anterior, Peroneus Tertius, Extensor Digitorum Longus and Extensor Hallucis Longus forces (Fig. 4.5.44 and Appendix L) all showed similar patterns across the three walk trials prior to and including toe-off and during the swing phase. No significant forces were predicted in these muscles immediately prior to toe-off, while small but consistent forces occurred at toe-off and for the duration of the swing phase. During the stance phase, an increase in muscle force was predicted for all four muscles, but considerably less than that of the extensor muscles and showing no distinct pattern across the three trials. Within a given trial, these muscles showed similar patterns, with the predicted force for Tibialis Anterior and Extensor Digitorum consistently being higher than that of Extensor Hallucis Longus and Peroneus Tertius. The predicted muscle force of Tibialis Anterior was only supported by EMG recordings during the swing phase, while the activity predicted during the stance phase was not supported by EMG data. EMG of Tibialis Anterior showed electrical activity centred at both toe-off and heel-strike, although some electrical activity was also seen during mid-swing. This was considered sufficient in the second walk trial for the muscle to be considered as remaining active for the duration of the swing phase. The EMG finding of that study are in agreement with Winter (1991) and Collins (1995) who found EMG activity during the swing phase which increased to a peak at heel strike. The authors reported little EMG activity during the middle and late stance phase.

The predicted Vastus Lateralis, Vastus Medialis and Vastus Intermedius forces (Fig. 4.5.41 and Appendix L) all produced a small peak in force at toe-off which gradually diminished to zero by 30% of the swing phase. Zero force was predicted for the rest of the swing phase and at heel-strike. Shortly after heel-strike, at 10% of the stance phase, the predicted Vastus Lateralis force climbed sharply to a peak at 30% of the stance phase, upon which it declined steadily to approach zero force prior to toe-off. The pattern of predicted Vastus Lateralis force was similar to that of the Rectus Femoris, but became active earlier following heel-strike, reached a lower peak force, and remained active longer during the stance phase. Vastus Intermedius also showed a brief period of predicted force at 40% of the stance phase. The muscle forces predicted for the vasti muscles were poorly supported by EMG, with the

majority of predicted force seen in Vastus Lateralis and little force in Vastus Medialis. In addition Vastus Lateralis became active after heel strike, whereas EMG suggested both medial and lateral muscles should be active prior to heel strike. EMG recordings of Vastus Lateralis and Vastus Medialis showed similar periods of electrical activity centred about heel-strike, with an on-set in activity at 80% of swing phase and offset at 20% of the stance phase. A second period of electrical activity was seen for both the Vastus Lateralis and Vastus Medialis at mid to late stance phase but was insufficient to produce the criteria of on-set of activity. The predicted vastus muscle forces and EMG patterns are in agreement with Winter (1991), Collins (1995), and Glitsch & Baumann (1997). The authors reporting EMG activity centred at heel strike and a small activity centred at toe-off, similarly to the present study, Collins (1995), and Glitsch & Baumann (1997) failed to predict forces for these muscle prior to heel strike.

The predicted Rectus Femoris force (Fig. 4.5.40 and Appendix L) showed negligible forces at toe-off which remained low until 30% of the swing phase, where they decreased to zero and remained at zero for the rest of the swing phase, including heel strike. Following heel-strike, from between 20% and 60% of the stance phase, the predicted muscle force climbed sharply to a peak at 30% of the stance phase and then declined rapidly. For the remainder of the stance phase, small muscle forces were predicted which, by 90% of the stance phase, became negligible. EMG recordings of Rectus Femoris supported the pattern of predicted Rectus Femoris force except for the small muscle forces that were predicted in the second half of the stance phase. EMG of the Rectus Femoris during the first walk trial showed an on-set of activity at toe-off which lasted until 30% of the swing phase. A second on-set of activity occurred after heel strike at 20% of the stance phase and lasted until 50% of the stance phase. However, the EMG signals were insufficient to determine on-sets and offsets for the second and third walk trials. Rectus Femoris EMG patterns are in agreement with Winter (1991) who reported a major burst of following heel srike and a minor burst following toe-off.

The predicted Semimembranosus, Semitendinosus and Biceps Femoris forces (Fig. 4.5.39 and Appendix L) were all zero at toe-off and during the initial swing phase. At 30% of the swing phase, the predicted force for Semimembranosus and Biceps Femoris (short) increased to produce a small force at mid-swing decreasing towards heel strike. All three muscle showed a sharp increase in force at heel strike, reaching a peak at 30% of the stance phase, which continued, although decreasing slightly, for the duration of the stance phase. For the three

walk trials, Semimembranosus, Biceps Femoris (short) and Biceps Femoris (long) had consistently higher predicted muscle forces than Semitendinosus. All predicted muscle forces dropped to zero at toe-off. EMG activity of Biceps Femoris supported the small forces predicted at mid-swing and the large forces predicted at heel strike and early stance. However, the EMG recordings would suggest the onset of large muscle forces should occur prior to heel strike as well as a fall in activity during the stance phase followed by a small and brief rise at mid-stance. This is contradictory to the continued muscle force currently predicted during the stance phase. EMG shows a small period of activity at mid-swing but this was not sufficiently large to qualify as an on-set of activity. EMG also showed the predominant muscle activity was centred at heel strike with an on-set occurring at 80% of the swing phase and an offset at 20% of stance phase. A third period of electrical activity was seen at mid-stance phase, but was only of significant magnitude to produce an on-set in the third walking trial. Biceps Femoris EMG is in agreement with EMG reported by Winter (1991), Collins (1995), and Glitsch & Baumann (1997), who reported EMG activity for this muscle from late swing to early stance with a peek in activity at heel strike.

The predicted Gluteus Maximus force (Fig. 4.5.38 and Appendix L) demonstrated a rapid increase in force at heel strike, which reached a maximum at 30% of the stance phase, and thereafter decreased, at first rapidly, to reach zero force at toe-off. At toe-off, and for the duration of the swing phase, no force was predicted for Gluteus Maximus. The predicted forces in the anterior element of the muscle tended to be slightly higher than those predicted for the middle and posterior elements. Gluteus Maximus predicted force from middle stance to toe-off is not supported by EMG of Winter (1991) and Collins (1995), who reported activity for this muscle from late swing to early stance with a peek in activity at heel strike. Similar to vastus and hamstring muscles the present study did not predict Gluteus Maximus force prior to heel strike.

The predicted Gluteus Medius, Gluteus Minimus and Tensor Fasciae Latae force (Figures 4.5.37, 4.5.36 and Appendix L) demonstrated a very small rise in force at toe-off, which approached zero again by 30% of the swing phase. For the remainder of the swing phase, all muscles were close to zero force. At heel strike, predicted forces in all muscle groups increased rapidly to a peak at 30% of the stance phase, after which they steadily decreased to zero at toe-off. Gluteus Medius produced a similar force pattern to those predicted for Gluteus Maximus, while Gluteus Minimus and Tensor Fasciae Latae demonstrated

successively less force. EMG recordings supported the force profile predicted for the Gluteus Medius, which saw a significant on-set of activity at heel strike followed by a steady decrease in electrical activity, and reached an offset level at 60% of the stance phase. Gluteus Medius predicted muscle forces and EMG patterns are in agreement with Winter (1991), Collins (1995). These authors reported little Gluteus Medius electrical activity during swing phase and a peak at heel strike which decreased during the stance phase.

The predicted Adductor Magnus (pos) force (Fig. 4.5.35 and Appendix L) produced a rapid rise in force at heel strike, which was maintained during the initial stages of the stance phase before decreased rapidly at 40% of the stance phase. Muscle force increased again after 40% of the stance phase to reach a second lesser peak, which decreased gradually until just prior to toe-off. After toe-off, the predicted force rapidly reduced to zero. At toe-off and for the duration of the swing phase no force was predicted for the Adductor Magnus (pos).

The predicted Adductor Longus, Adductor Brevis and Pectineus forces (Fig. 4.5.34 and Appendix L) produced a rapid rise in force immediately prior to toe-off (at 90% of the stance phase) to reach a peak at toe-off. Thereafter, the predicted force decreased steadily to reach zero force at heel strike. No force was predicted for these muscles from heel strike until 40% of the stance phase, where forces rose to a lesser peak, were maintained before decreasing to zero prior to toe-off. The predicted force patterns of these muscles were similar to those predicted for Iliacus and Psoas. The predicted Adductor Longus muscle forces at toe-off are in agreement with EMG recordings for this muscle made by Winter (1991). However these author also reported a peak in EMG at heel strike which was not predicted by the present study. No EMG activity were recorded for these muscles for the present study.

The predicted Obturator Internus and Piriformus forces (Fig. 4.5.33 and Appendix L) showed minimal force during toe-off and the swing phase. At heel strike, the predicted forces increased rapidly to reach a peak at 30% of the stance phase. Muscle forces then declined steadily over the stance phase to reach zero at toe-off. In contrast, the predicted Obturator Externus and Quadratus Femoris force (Fig. 4.5.32 and Appendix L) were low during the stance phase, but rose immediately prior to toe-off to reach a peak immediately following toe-off at 10% of the swing phase. Thereafter, the predicted force declined steadily during the swing phase to reach zero force at heel strike. From heel strike to 90% of the stance phase, the predicted forces for both Obturator Externus and Quadratus Femoris were zero. Throughout

the gait cycle, Obturator Externus had a consistently higher predicted force than Quadratus Femoris..

The predicted Iliacus and Psoas forces (Fig. 4.5.31 and Appendix L) showed a rapid rise immediately prior to toe-off (at 90% of the stance phase) to reach a peak at toe-off. Thereafter, the predicted forces decreased steadily to reach zero force at heel strike. No force was predicted for these muscles from heel strike until 30% of the stance phase, where the forces rose to a lesser peak and were maintained during the remainder of the stance phase before decreasing to zero prior to toe-off. The force patterns of these muscles were similar to those of the Adductor Longus, Adductor Brevis and Pectineus muscles.

5.4.3.2 Step Trials

The step trial is discussed with respect to four events and three respective periods. The events in sequence are:

1) First toe-off, when the foot leaves the ground;
2) Step contact, when the foot makes contact with the step;
3) Second toe-off, when the foot leaves the step; and
4) Ground contact, when the foot again makes contact with the ground.

The three phases in the stepping cycle are:

1) leg raise, where the leg is raised from the ground to the step;
2) stepping, during which the body is raised onto the step, pauses and is then lowered to the ground; and
3) leg return, where the leg is lowered from the step to the ground.

The predicted Soleus (lat), Soleus (med) and Gastrocnemius (med) forces (Fig. 4.6.43 and Appendix L) all demonstrated a rise in force at step contact, reached a peak at 20% of the stepping phase, and then steadily decrease to zero force at 60% of the stepping phase. A second lesser peak of short duration occurred at 80% of the stepping phase, but returned to zero force by the second toe-off event. The predicted Gastrocnemius (lat) force showed a

delayed increase in force at 20% of the stepping phase that was maintained until 80% of the stepping phase. From there it decreased to zero force by the second toe-off event. Both Gastrocnemius muscles also demonstrated small forces after the first and second toe-off. The predicted Soleus (lat) force was supported by EMG, which showed an on-set of activity at first toe-off which continues until 50% of the leg raise phase. The predominant electrical activity occurred at step contact and continued until 80% of the stepping phase. A third period of muscle activity occurred at second toe-off which continued until 50% of the leg return. EMG of Gastrocnemius (lat) showed high levels of resting electrical activity in relation to maximum activity, but failed to producing on-sets in electrical activity for the three step trials.

The predicted Tibialis Posterior, Peroneus Longus, Peroneus Brevis, Flexor Digitorum Longus, and Flexor Hallucis Longus forces (Fig. 4.6.45 and Appendix L) demonstrated no significant force during the leg raise and leg return phases. All muscles produced a sharp rise in forces at step contact that peaked at 20% of the stepping phase, which steadily declined to zero at 70% of the stepping phase. This was followed by a second small rise in muscle forces at 80% of the stepping phase which quickly returned to zero force by the second toe-off event.

The predicted Tibialis Anterior, Peroneus Tertius, Extensor Digitorum Longus, and Extensor Hallucis Longus forces (Fig. 4.6.41 and Appendix L) all demonstrated similar patterns in the three step trials for the leg raise, first contact and up to 20% of the stepping phase. Small but consistent forces were predicted during leg raise, with a small peak in forces immediately preceding and following first contact. This was again followed by small but consistent forces for the initial period of the stepping phase. These muscle also showed similar patterns in the three step trials for the last 20% of the stepping phase, second toe-off and for the leg return phase. In the final period of the stepping phase, a rise in predicted forces was seen to a peak at second toe-off, followed by small but consistent forces for the leg return phase. During the middle of the stepping phase, brief periods of muscle force were predicted for all four muscles but varied between trials in their occurrence and showed no consistent pattern across the three trials. The occurrence of predicted force, as well as the peaks force from first toe-off to 20% of the stepping phase and from 80% of the stepping phase to ground contact was supported by EMG recordings of Tibialis Anterior. However, during the middle of the stepping phase, the occurrence of discrete bursts of muscle force were not supported by EMG activity, which suggested continuous activity. EMG of Tibialis Anterior showed an on-set of activity prior to first toe-off which continued for the duration of the step task. Within the task, several peaks of

electrical activity could be seen occurring after first toe-off at 20% of the leg raise, after step contact at 10% of the stepping phase, at 80% of the stepping phase, and following second toe-off at 10% of the leg return.

The predicted Vastus Lateralis, Vastus Intermedius and Vastus Medialis forces (Fig. 4.6.41 and Appendix L) demonstrated sharp increases in magnitude at first contact, reaching a peak at 10% of the stepping phase. The predicted force steadily declined to a minimum in the middle of the stepping phase before rising to a second peak at 80% of the stepping phase, before again decreasing to zero at second toe-off. The peak forces were greatest for Vastus Medialis and smallest for Vastus Lateralis. The minimal forces at mid-stepping phase saw a reversal of the order, with Vastus Lateralis showing the greatest force and Vastus Medialis showing zero force. The predicted forces of Vastus Lareralis and Vastus Medialis are supported by EMG, with the exception of Vastus Medialis in the middle of the stepping phase where the subject is supported on one leg. In this position, the predicted Vastus Medialis force was zero while Vastus Lateralis continued to exert force. EMG of the Vastus Lateralis and Vastus Medialis showed an on-set of activity at step contact which continued until 90% of the stepping phase. Within the stepping phase, peak activities occurred at 10% and 80% of this phase, which corresponded with raising and lowering of the body. A relatively small amount of electrical activity occurred for the two vastus muscles at ground contact, which was only of sufficient magnitude to cause an on-set of activity in the first step trial.

The predicted Semimembranosus, Semitendinosus, Biceps Femoris (long), and Biceps Femoris (short) forces (Fig. 4.6.39 and Appendix L) demonstrated a sharp increase in force at step contact which peaked at 10% of the stepping phase before falling sharply approaching zero force at 20% of the stepping phase. Predicted force immediately rose again to a lower level that was maintained until 80% of the stepping phase. It again quickly returned to zero force before immediately rising to a further peak which returned to zero force by the second toe-off event. For these muscles, no force was predicted in the leg raise and leg return phases, except for a brief and small forces predicted for the Biceps Femoris (short) in the first trial in the middle of the leg return phase. The Biceps Femoris (long) and Biceps Femoris (short) muscles had consistently higher predicted forces than Semimembranosus and Semitendinosus. Predicted muscle forces for the Biceps Femoris are supported by EMG, where an on-set of electrical activity occurred at step contact which continued until 90% of the stepping phase. Within the stepping phase, peak activities occurred at 20% and 70% of this phase, which

corresponded to raising and lowering of the body. For the first step trial, an on-set of electrical activity also occurred at 80% of leg return and continued until after ground contact.

The predicted Rectus Femoris force (Fig. 4.6.40 and Appendix L) demonstrated a steady increase in force at 10% of the leg raise phase to reach a small peak at mid leg raise before steadily returning to zero force at toe-off. Following toe-off, at 10% of the stepping phase, a rapid rise in force was observed, reaching a peak at 20% of this phase. Predicted force fell slightly during the middle of the stepping phase before reaching a second peak at 80% of this phase and returned rapidly to zero force before second toe-off, at 90% of the stepping phase. Muscle force steadily increased at second toe-off to reach a small peak at the middle of the leg return phase, before returning to zero force just before ground contact. Predicted Rectus Femoris force was supported by EMG, where an on-set of electrical activity occurred at first toe-off which continued until 30% of the leg return phase. Within this period, peaks of activity occurred at 80% of the leg raise, at 10% of the stepping phase, and at 90% of the stepping phase.

The predicted Gluteus Maximus force (Fig. 4.6.38 and Appendix L) demonstrated a rapid increase in force at step contact to reach a peak at 20% of the stepping phase. Predicted forces were reduced in the middle of the stepping phase before rising to a second peak at 80% of the phase, where they then fell rapidly to zero at second toe-off. The reduction in forces in the middle of the stepping phase was greatest for the Gluteus Maximus (mid) and Gluteus Maximus (pos), indicating the contribution of the anterior portion of this muscle in producing abduction moments at the hip while standing. The predicted Gluteus Maximus (ant) force showed a small rise in force during leg raise and during leg return. Gluteus Maximus (mid) and Gluteus Maximus (pos) showed no predicted force during the leg raise and leg return phases.

The predicted Gluteus Medius and Gluteus Minimus forces (Figures 4.6.37, 4.6.36 and Appendix L) demonstrated similar force patterns during the step trials. For both muscles, and their respective muscle elements, small forces were predicted for the duration of the leg raise and leg return phases. However, the predominant forces were predicted during the stepping phase. At step contact, a sharp rise in forces occurred to reach a peak at 20% of the stepping phase. Force was maintained in these muscle elements until 80% of this phase, when they fell rapidly to zero force by the second toe-off event. The magnitude of the predicted Gluteus Medius forces were higher than those of Gluteus Minimus. The patterns of predicted Gluteus

Medius forces were supported by EMG, where an on-set of electrical activity occurred following step contact, at 10% of the stepping phase, and continued until 90% of the stepping phase.

The predicted Adductor Longus force (Fig. 4.6.34 and Appendix L) demonstrated activity for the duration of the leg raise and leg return phases, with no muscle force predicted for the the stepping phase. The predicted Adductor Longus force was similar to that of Iliacus and Psoas, but was in contrast to Adductor Magnus (pos) (Fig. 4.6.35 and Appendix L) which demonstrated no predicted force during the leg raise and leg return phases, but a continuous force predicted for the stepping phase. In the stepping phase, two sustained peaks in force were predicted for Adductor Magnus - the first from step contact to 40% of this phase, and the second from 60% to second toe-off. No significant forces were predicted for the Adductor Magnus (ant), Adductor Magnus (mid), Adductor Brevis, or Pectineus muscles during the step tasks.

Predicted Obturator Internus and Piriformus forces (Fig. 4.6.33 and Appendix L) demonstrated small magnitudes for the duration of the leg raise and leg return phases, however the predominant forces occurred during the stepping phase. A sharp increase in force occurred at step contact, which were maintained for the duration of this phase before returning to zero at the second toe-off event. In contrast, Obturator Externus and Quadratus Femoris (Fig. 4.6.32 and Appendix L) were predicted to be active during the leg raise and leg return phases, although no forces were predicted during the stepping phase.

The predicted Iliacus and Psoas forces (Fig. 4.6.31 and Appendix L) demonstrated activity throughout the leg raise and leg return phases, with Iliacus predicted as having higher forces than Psoas. No forces were predicted for these two muscles in the stepping phase, except for a small force in Iliacus during the first step trial at 60% of the stepping phase. The predicted force pattern of these muscles was similar to that of the Adductor Longus.

5.4.3.3 Validity of muscle force prediction

The predicted forces of individual muscles were generally consistent in the occurrence and magnitude of forces during the three walk trials and three step trials. This can be seen the comparative plots of predicted muscle forces for the walk and step trials presented in Figures 4.5.31 to 4.5.45 and Figures 4.6.31 to 4.5.45 respectively, in the results section, and in the plots of muscle forces predicted for each trial in Appendix L. Muscle elements representing a single muscle were also consistent in the occurrence of predicted force for the step and walk trials. The magnitude of forces predicted in individual elements varied with changes in the moment arms. This can be clearly demonstrated in the anterior middle and posterior elements of Gluteus Maximus and Gluteus Medius, as well as the middle and posterior elements of Gluteus Medius (Appendix L). Consistency was also shown in the occurrence of force in agonist muscles between trials, which can be seen in the predicted forces for Gluteus Medius and Tensor Fasciae Latae (Appendix L).

Despite the consistency in predicted muscle forces between trials, the validity of predicted muscle force cannot be accepted in the present study until present inaccuracies are addressed. These have been discussed in previous sections and include:

i) Accuracy of the three dimensional location of pelvis and foot landmarks;
ii) Location of muscle point co-ordinates describing muscle-tendon paths;
iii) Location of body-fixed axes from external markers and the alignment of centres of rotation;
iv) The ability to predict maximum dynamic forces under current muscle contractile element velocities; and
v) The validity of moments arms calculated from joint centres and muscle-tendon co-ordinated data at varying joint angles.
vi) The ability of the optimisation procedure to distribute force in accordance to the minimum of the cost function.

Finally, the variability of muscle force prediction and moment arm calculation can be decreased by the adjustment of muscle point co-ordinates to reduce their sensitivity to error in reconstructing body fixed axes location. For example, the distribution of forces between Vastus Lateralis and Vastus Medialis during stance showed inconsistencies with expected

muscle forces, where Vastus Lateralis was predicted with relatively high forces while Vastus Intermedius had relatively low forces and Vastus Medialis practically none. However, in raising and lowering the body in the step trials, where the knee is more flexed and considerably greater forces are predicted than in either the step or walk stance phases, a reversed order of magnitude was seen in the distribution of these forces. This may be attributed to variations in moments arms which may have resulted from the alignment of the body-fixed axes of the thigh and shank during the calibration procedure. If, in the standing position, errors resulted when local axes were defined from external markers, such that the thigh axes was rotated a few degrees internally with respect to the shank axis, or the shank axes was rotated externally with respect to the thigh, then this may result in Vastus Lateral dominating extension moments of the thigh with the leg extended. In the stepping task, the knee was flexed to a greater extent and shank internally rotated from standing position, thus changing extension moment arms and producing the more even distribution of the forces seen in raising the body in the step trial. Consequently, if the moment arms were such that a more even distribution of forces in the vastus muscle were present in the standing position, then it would be expected that in raising the body in the step, when internal rotation of the shank was present, a more dominant force would be predicted in Vastus Medialis. A reduction the sensitivity of the vastus moment arms to errors in defining axes alignment could be achieved by a lateral shift of the Vastus Lateralis thigh deflection point and a medial shift of the Vastus Medialis thigh deflection point on the patella. This may also decrease the sensitivity of the model to distinguish between small changes in force distribution between the vastus muscle elements with internal or external rotation of the shank. However, due to the potential magnitudes and effect of measurement errors, the gains in reducing the variability of predicted vastus forces due to errors in axes alignment may outweight the losses in sensitivity of the model to distinguish small changes in vastus force distribution.

In comparing predicted muscle forces with electromyographic recordings and expected values, the following limitations exists in the present study:

i) The present optimisation procedure is unable to predict 'stiffening' of the joints through muscle co-contraction prior to heel-strike as suggested by EMG of Vastus Medialis, Vastus Lateralis and Biceps Femoris. Minimisation of a cost function involving the sum of muscle force or stress does not favour co-contraction when predicting muscle forces that will produce the resultant joint moments. The low

resultant joint moments prior to heel strike, and the presence of muscle co-contraction, would suggest another criterion other than minimising of force or stress is responsible for the distribution of muscle forces during this period. Another possible criterion might be to minimise the rate of change of force loading on internal structures;

ii) The reduced electrical activity in muscles of the leg during mid-stance compared to the predicted muscle forces may indicate a significant contribution from passive forces. These may include passive tension of the iliotibial tract as the pelvis drops during mid-stance, the locking of the knee joint in the fully extended leg which inhibits internal and external rotation and provides support by passive bone contact and ligament forces, and the contribution of ligament and bone contact forces at the ankle. These factors are not accounted for in the present model as it excludes passive forces of the iliotibial tract or ligament and bone contact forces at the knee and ankle joints. The muscle forces predicted for Gluteus Medius, Gluteus Minimus and Tensor Fasciae Latae in mid-stance may be overestimated due to the absence of passive forces of the iliotibial tract in the abduction moments at the hip. Similarly, the muscle forces predicted for Vastus Lateralis, Rectus Femoris and Biceps Femoris in the second half the stance phase, which were not indicated by EMG, may result from the present model balancing resultant joint moments at the knee during the mid-stance by muscle forces. Forces in the two-joint muscles would also effect the moments at the hip joint, which may also account for the forces predicted in Iliacus, Psoas, Adductor Longus, Adductor Brevis, Pectineus, and Adductor Magnus (pos) in the second half of the stance phase. The small and variable Tibialis Anterior forces predicted during mid-stance of the walk task and during weight bearing in the step task, which were not supported by EMG, may have resulted from limitations in the present model of the ankle joint. This joint was modelled as a single point without ligament or bone contact forces. Thus, in the present ankle and knee models, all moments, including those about the internal-external and abduction-adduction axes that result from the action of the extensor muscles, were balanced by muscle forces. The muscle forces predicted in the present study highlight the need for accurate models of the knee and ankle joints which accurately reflect the contribution of bone and ligament forces to resultant joint moments.

6 CONCLUSIONS

Mathematical modelling of the human musculoskeletal system enables measurement of motion and forces to gain an insight into human movement. Knowledge of muscle forces will help understand the control of movement by the central nervous system, as well as the forces placed on internal structures of the body. To successfully predict individual muscle forces, the model must accurately reflect the structure and function of the musculoskeletal system. Therefore, to predict individual muscle forces, a detailed musculo-skeletal model is required, involving anatomical data, accurate predictions of three dimensional segment locations, resultant joint moments, muscle force-length, force-velocity, and excitation characteristics, as well as a physiologically based criterion for the distribution of muscle forces. Due to the complexity of the relationships between components of this system, ignoring or failing to account for variables will increase the assumptions and limitations of the research, thereby decreasing the validity of the results and the ability to draw sound conclusions.

The aim of present study was to address the limitations in model design, anatomical data, and implementation of force-length and force velocity relationships for the purpose of improving the accuracy and validity of musculo-skeletal modelling and movement analysis.

6.1 Outcomes

To achieve the present aims, a comprehensive approach to three dimensional modelling of the musculoskeletal system of the human lower limb was developed and implemented in order to address current limitations in musculoskeletal modelling. As a result of the present study, the following were achieved:

i) Comprehensive anatomical data were presented for the three dimensional modelling of the musculoskeletal system of the lower limb. The anatomical data presented were expressed relative to a common local body-fixed axes system and normalised to a common set of anthropometric measures which were defined from palpable bony landmarks, and included:

- a method for defining local body-fixed axes from external body landmarks for four segment of the lower limb;

- segment parameters for defining mass, inertia, centre of mass, and joint centres for the four segments of the lower limb were obtained from previous literature. The data were expressed relative to local body-fixed axes and normalised to anthropometric measures;
- muscle model parameters for defining belly length, fibre length, pennation angle, mass, tendon cross sectional area, and percentage fibre type for 48 muscle elements of the lower limb were obtained from previous literature and where appropriate normalised to anthropometric measures.
- Muscle co-ordinate data was presented to define muscle origins, insertions and deflection point suitable for describing muscle and tendon paths for 48 muscle elements of the lower limb throughout a range of joint movements. The data were expressed relative to local body-fixed axes and normalised to anthropometric measures.

ii) A method was presented to optimise muscle model parameters to the changes in muscle belly lengths as measured from a movement trial for the purpose of defining a force-length relationship throughout the range of muscle fibre lengths produced by the movement trial. The optimisation procedure adjusted reference fibre length, pennation angle and belly length in accordance with the maximum and minimum changes in belly length. The procedure obtained an optimal fibre length which would define a force-length relationship for the fibre lengths of the movement trial.

iii) A method was presented for implementing the muscle model that accounted for the inter-dependence of muscle model parameters used in determining force output and the highly non-linear nature of the equations describing the muscle contraction dynamics. The method provided a solution to the equations by combing muscle model geometry, force-length and force-velocity relationships in an iterative procedure which, starting with an initial estimate for tendon length and fibre series elastic component, converged to a simultaneous solution. This allowed calculation of maximum contractile element force and model parameters for the current contraction dynamics or for a given force and muscle length using the resultant muscle model parameters.

iv) A cost function was presented which involved minimisation of the sum of squared normalised muscle forces with soft constraints on maximum and minimum muscle force. This achieved a realistic distribution of muscle forces over the range of resultant joint moments. In addition, the form of the cost function allowed for the unconstrained minimisation of the cost function, providing the initial estimates of the muscle forces were within the muscle force boundaries defined by the cost function.

v) An optimisation procedure was presented that combined the equipolance equations, muscle excitation and contraction dynamics and muscle force limits in the minimisation of the cost function. A procedure was also presented for obtaining initial muscle force estimates for the optimisation procedure that were based on the moment generating capacity of the muscles. The initial muscle force estimates were required to meet the equipolance equations and to give a reasonable approximation of the minimum of the cost function.

vi) The data and the methods presented were implemented in the three dimensional analysis of the lower limb during a walking and stepping task. The implementation produced a comprehensive description of the musculoskeletal system of the lower limb. The descriptor included relative joint rotations, acceleration of segment centres of mass, resultant joint moments, muscle moment arms, muscle lengths, muscle forces, and muscle model parameters of fibre length, pennation angle, tendon length, contractile element length, and fibre series elastic component length. Implementation of the anatomical data and methods developed in the three dimensional analysis of the lower limb allowed for validation of the procedures as well as identifying limitations and errors in the present study.

6.2 Limitations and recommendations for further study

The limitations of the present study were:

i) Significant oscillations in the acceleration of segment centre of mass occurred which corresponded to frames at which there was a change in the number of segment markers use to reproduce pelvis and foot three dimensional location. As a result, it was concluded that in the present study, the experimental set-up used was not sufficient to

accurately reproduce the locations of the pelvis and foot consistently during the movement. Additional markers on the foot and pelvis would be required, and additional cameras were also necessary to adequately reproduce the three dimensional location of these segments during movement;

ii) The accuracy of the present study was not sufficient to determine muscle and contractile element velocities. Therefore, the current experimental set-up and achieved accuracy was not sufficient to determine muscle contraction dynamics which relied on muscle contractile element velocity to determine maximum dynamic muscle forces;

iii) The muscle co-ordinate data presented were able to describe muscle-tendon lengths and moment arms in the standing position. However, with changes in joint angles, large errors in moment arms were seen for some muscles due to the sensitivity of moment arm calculation that were a result of the following errors:

- accurate location of body-fixed axes from external markers. Differences in the model joint centres of rotation and underlying skeletal segments of rotation significantly affected moment arms during joint rotation;
- the relative motion of muscle point co-ordinates and the joint centre;
- the use of straight line as opposed to curved-line tendon paths; and
- accuracy of three dimension segment location during the movement trial.

Origin and insertion points alone were not adequate to describe muscle-tendon paths and moment arms for the majority of lower limb muscles over a range of joint angles.

In the present study, it was concluded that the errors in moment arms were largely due to the inaccuracy in defining body-fixed axes from external markers and the relative motion of muscle point co-ordinates and joint centres throughout changing joint angles. A smaller influence on errors in moment arms was attributed to errors in three dimensional segment location during the movement trial, due to the consistency of predicted moment arms across trials in comparison to the large errors seen in the calculation of some moment arms with changes in joint angles. Therefore, in the present study, improvements in moment arm prediction could be made with the use of pre-trial functional evaluations of predicted centres of rotation and by improvements in defining the muscle lines of action at varying joint angles. The pre-trial function

evaluations would involve analysing simple movements and subsequently adjusting the location of body-fixed axes defined from external markers to ensure that the predicted model centre of rotation agreed with the skeletal centre of rotation. Further development is needed to improve the ability of the muscle point co-ordinates presented in this study to predict muscle lines of action at varying joint angles. As previously suggested, changes in point locations and the use of curved lines for tendon paths would both enhance the validity of the moment arms predicted by the model.

iv) Muscle model parameter optimisation to changes in muscle belly length was essential in developing the force-length muscle characteristics so they could be applied in the muscle model to a range of muscle lengths. Muscle model parameter optimisation methods presented proved to be robust, in that muscle model parameters were determined which complied with the force-length relationship and range of muscle lengths, when applied to all modelled muscles over all trials analysed in the present study.

It may be more appropriate to optimise the muscle model parameters to the range of muscle lengths determined by the end-range of motion instead of the motion within a specific trial. This would achieve a move realistic optimal fibre length and force-length relationship by considering the current change in fibre lengths within the context of an approximation of the maximum and minimum fibre lengths.

Optimisation of muscle parameters to maximum and minimum changes in muscle belly length does not ensure that the magnitude of the maximum isometric forces predicted are valid. In the present study, maximum isometric force at the reference muscle length was predicted from reference fibre length, muscle mass, muscle density, and muscle specific tension. Reference muscle fibre length, mass and density are used to predict physiological cross sectional area, which is then multiplied by muscle specific tension to give a predicted muscle maximum isometric force at the reference muscle-tendon length. The accuracy of the predicted maximum muscle forces in the present study will therefore be largely determined by the accuracy and validity of individual muscle masses and reference fibre length estimations.

v) The iterative procedures and equations presented for combining the muscle geometric model with force-length and force-velocity relationships proved to be robust in that convergence and consistent results were achieved, whether the problem was:

- to determine maximum force for a given muscle length or to determine the model parameters (for example, pennation angle, fibre length) for a given muscle force and length;
- applied to pennate or non-pennate muscles;
- applied to all muscle lengths as determined from the optimal fibre length and corresponding pennation angle;
- applied to all muscle forces up to the optimal isometric muscle force; or
- applied to isometric, eccentric or concentric muscle contractions.

In the isometric case, the approach showed consistency in the predicted muscle model parameters at varying muscle lengths and corresponding maximum isometric forces. The validity of the maximum forces predicted by the force-length relationship depended on the optimal fibre length, obtained from the optimisation of the muscle model parameters to the measured changes in belly length, and the estimations of PCSA.

In the dynamic case, the approach also showed consistency in the prediction of forces in SO, FG and FO fibre types at varying muscle contraction velocities. With increasing maximum velocities of contractile element shortening, the maximum force in the SO fibres diminished more rapidly than in the FO and FG fibres, thereby changing the relative contributions to maximum force at a given muscle contraction velocity. The FO and FG fibres were therefore able to produce force at a higher maximum velocity of shortening than the SO fibres. The maximum contractile element force for a given contractile element velocity of shortening was directly dependent on the proportion of FO and FG fibres. In the present model, an iterative procedure for obtaining force length and force velocity relationships predicted a positive linear relationship between muscle length and the maximum contractile element velocity of shortening at which force can be produced, where the maximum contractile velocity of shortening increased with muscle fibre length. The linear relationship predicted was not in agreement with the finding of Herzog (1996), which would suggest that the speed of

unloaded shortening was similar within a range of fibre lengths. However, the method by which force-length and force-velocity relationships should be combined, and the dynamic response of muscle fibres, is still unknown (Herzog, 1996). Further research is therefore needed on the implementation of the force-velocity relationship and the dynamic response of the muscle model developed in the present study to accommodate changes in optimal fibre length and changes in muscle length.

When applying the model to the analysis of human movement, the contractile element velocities calculated were larger than those modelled by the present force-velocity equations, which resulted in the maximum contractile element forces approaching zero when the instantaneous contractile element length was shortening. In the present application of the force-velocity relationships, there is a need to scale a normalised force-velocity curve to the maximum contractile element velocities.

vi) A cost function was proposed based in the minimisation of the sum of squared muscle stress, and incorporating soft constraints on both maximum and minimum muscle forces. Validity of the optimisation approach, including cost function, initial muscle force estimate and minimisation routine, was demonstrated on test examples involving both a simple one-joint, four-muscle system, and a two-joint, eight-muscle system. In both cases, the model produced the expected distribution of muscle forces between maximum and minimum resultant joint moments. In applying the optimisation approach to predicting forces in 48 muscle elements of the lower limb in walking and stepping trials, consistent muscle forces were achieved across all trials. The optimisation procedure, with few exceptions, produced muscle forces in agreement with EMG and previous research. However, due to the highly complex and indeterminate nature of the problem, two limitations were encountered when applying the optimisation procedures to the model of the lower limb:

- the iterative procedure for determining initial muscle force estimates had difficulty in converging to the resultant joint moments with the desired degree of accuracy; and
- minimisation of the cost function, although successful in reducing the cost function from the initial estimates and maintaining joint moments, did not change muscle forces significantly from their initial estimated values. This

made the results of the optimisation procedure largely dependent on the initial muscle force estimates.

vii) In the application of the optimisation procedures to the model of the lower limb, the following improvements are proposed to overcome inaccuracies in the present musculoskeletal model:

- increased accuracy of the pelvis and foot three dimensional locations;
- improve the validity of the knee and ankle joint models used in determining moments that are required to be balanced by muscular forces. In the present model, bone contact and ligament forces were not included in the equipolance equations. With the inclusion of ligament and bone contact forces, a reduction in the moments about the medio-lateral and longitudinal axes that are to be balanced by muscle forcest is expected. This would increase in the ability of the iterative procedure used to obtain initial muscle force estimates to converge to the resultant joint moments with the required accuracy as well as reduce the muscle forces predicted by the optimisation procedure;
- improved location of muscle point co-ordinates as well as the use of straight and curved line segments to describe muscle-tendon paths;
- improved location of body-fixed axes from external markers and the subsequent alignment of centres of rotation;
- improved ability to predict maximum dynamic forces under current muscle contractile element velocities, which includes implementation of force-velocity relationship and validity of the muscle model parameters to predict maximum isometric and dynamic muscle forces; and
- improved methods for determining initial muscle force estimates which meet the required joint moments and are sufficiently close to the minimum solution to achieve convergence to a global minimum.

The performance of the optimisation procedures in the analysis of movements involving higher muscle forces is not known. In this situation, the accurate prediction of maximum muscle forces, modelling of joint passive forces, and excitation dynamics becomes more critical. With an increase in muscle forces, there will also be an increase in the minimum muscle limits for each frame as determined from the excitation dynamics. Higher minimum muscle force within the cost function will impose

boundary conditions on the muscle forces used in the cost function which must be satisfied by the initial muscle force estimates. Higher minimum muscle force limits may also affect the ability of the optimisation procedure to meet the resultant joint moments and the continuity of predicted muscle forces.

These limitations and sources of inaccuracies should be addressed in future studies to improve the validity of the moment arms, muscle forces and muscle model parameters predicted in the present approach to the modelling of the musculoskeletal system.

The results of the present study show that procedures developed on simple examples are not assured of working on more complex problems that involve a larger numbers of muscles in a highly complex and indeterminate system. In order to validate procedures intended for the analysis of the musculoskeletal system, there is a need to apply them to the analysis of actual human movements and compare the results to experimental data.

6.3 Conclusion

The present study highlights the complexity of developing a valid model of the musculoskeletal system. Limitations in the model design, and inaccuracies in data used in any phase of the modelling process, will effect the accuracy and validity of the results of the musculoskeletal model. Methods have been presented and implemented in an attempt to improve the accuracy and validity of a musculoskeletal model of the lower limb. It is hoped this model will provide a basis for further research into the three dimensional modelling of the musculoskeletal system, including further research into anatomical data describing joint centres and muscle-tendon paths, more information on modelling muscle excitation contraction dynamics, and refinement of the optimisation approach to predicting individual muscle forces in human movement.

Previous models have tended not to address the complexity of the musculo-skeletal system through failing to simultaneously addressing the combined effects of anatomical design and constraints, muscle mechanics, and modelling techniques. The present model attempts to achieve this aim, and while it succeeds in many respects, its succeeds most in identifying the complexity of the process and proposing methods to achieve greater success.

7 REFERENCES

Andrews, J.G. (1984) On the specification of joint configuration and motions. *Journal of Biomechanics*, 13, 989-1006.

Andriacchi, T.P. & Strickland, A.B. (1985) Gait analysis as a tool to assess joint kinetics. In Berme, N., Engin, A.E. and Correia da Silva, K.M. (Eds.) *Biomechanics of Normal and Pathological Human Articulating Joints*. Martinus Nijhoff Publishers, Boston.

Agur, A.M.R., Lee, M.J. and Anderson, J.E. eds. (1991) *Grant's Atlas of Anatomy*, 9th ed. Baltimore, Williams & Wilkins.

Audu, M.L. & Davy, D.T. (1985) The influence og muscle model complexity in musculoskeletal motion modelling. *Journal of Biomechanical Engineering*, 107, 147-156.

Baratta, R.V., Solomonow, M., Best, R., Zembo, M. and D'Ambrosia, R. (1995) Architecture based force-velocity models of load-moving skeletal muscles. *Clinical Biomechanics*, 10, 149-155.

Baratta, R.V., Solomonow, M., Nguyen, G. and D'Ambrosia, A. (2000) Characterisation of load-length-velocity relationships of nine different skeletal muscles, *Journal of Biomechanics*, 33, 381-385.

Basmajian, J.V. & De Luca, C.J. (1985) *Muscles Alive : their functions revealed by electromyography*. 5th Ed. Williams & Wilkins, Baltimore.

Bell, A.L., Brand, R.A. and Pedersen, D.R. (1989) Prediction of hip joint centre location from external landmarks. *Human Movement Science*, 8, 3-16.

Bell, A.L., Pedersen, D.R. and Brand, R.A. (1990) A comparison of the accuracy of several hip centre location prediction methods. *Journal of Biomechanics*, 23(6), 617-621.

Bergmann, G., Graichen, F. and Rohlmann, A. (1993) Hip joint loading during walking and running, measured in two patients. *Journal of Biomechanics*, 26, 969-990.

Bergmann, G., Kniggendorf, H., Graichen, F. and Rohlmann, A. (1995) Influence of shoe and heel strike on the loading of the hip joint. *Journal of Biomechanics*, 28, 817-827.

Blankevoort, L. Huiskes, R. and de Lange, A. (1990) Helical axis of passive joint motions. *Journal of Biomechanics*, 23, 1219-1229.

Bogert, A.J. van den (1994) Analysis and simulation of mechanical loads on the musculoskeletal system: a methodological overview. *Exercise and Sports Science Reviews*, 22, 23-51.

Brand, R.A. & Crowinshield, R.D. (1981) Comment on criteria patient evaluation. *Journal of Biomechanics*, 14(9), 655.

Brand, R.A., Crowninshield, R.D., Wittstock, C.E., Pederson, D.R., Clark, C.R. and van Krieken, F.M. (1982) A model of lower extremity muscular anatomy. *Journal of Biomedical Engineering*, 104, 304-310.

Brand, R.A., Pedersen, D.R. and Friederich, J.A. (1986) The sensitivity of muscle force predictions to changes in physiological cross-sectional area. *Journal of Biomechanics*, 19, 589-596.

Brand, R.A. & Yack, H.J. (1996) Effects of leg length discrepancies on the forces at the hip joint. *Clinical Orthopaedics and Related Research*, 333, 172-180.

Buchanan, T.S. & Shreeve, D.A. (1996) An evaluation of optimisation techniques for the prediction of muscle activation patterns during isometric tasks. *Journal of Biomechanical Engineering*, 118, 565-574.

Burton, P. (1984) Computer oriented analytical dynamics of machinery. In Haug, E.J. (Ed.) *Computer Aided Analysis and Optimization of Mechanical System Dynamics*. Springer-Verlag, Germany, 41-87.

Cappozzo, A. (1983) Considerations in clinical gait evaluation. *Journal of Biomechanics*, 16(4), 302.

Cappozzo, A. (1985) Experimental techniques, data acquisition and reduction. In Berme, N., Engin, A.E. and Correia da Silva, K.M. (Eds.) *Biomechanics of Normal and Pathological Human Articulating Joints*. Martinus Nijhoff Publishers, Boston.

Cappozzo, A., Figura, F., Marchetti, M. and Pedotti, A. (1976) The interplay of muscular and external forces in human ambulation. *Journal of Biomechanics*, 9(1), 36-43.

Carman, A.B. (1996) The development and validation of conjugate imaging techniques in the automated reproduction of three dimensional co-ordinates from multiple camera images. Thesis. M.Sc., University of Wollongong, Australia.

Chaffin, D.B. & Andersson, G.B.J. (1991) *Occupational biomechanics*. New York, Wiley.

Challis, J. (1995) A procedure for determining rigid body transformation parameters. *Journal of Biomechanics*, 28(6), 733-737.

Chao E.Y.S. (1980) Justification of triaxial goniometer for the measurement of joint rotation. *Journal of Biomechanics*,13(12), 989-1006

Chase, M.A. (1984) Methods and experience in computer aided design of large-displacement mechanical systems. In Haug, E.J. (Ed.) *Computer Aided Analysis and Optimization of Mechanical System Dynamics*. Springer-Verlag, Germany, 233-259.

Collins, J. J. (1995) The redundant nature of locomotor laws. *Journal of Biomechanics*. 28, 251-267.

Crowninshield, R.D., Johnston, R.C., Andrews, J.G. and Brand, R.A. (1978) A biomechanical investigation of the human hip. *Journal of Biomechanics*, 11(1), 75-86.

Crowninshield, R.D. & Brand, R.A. (1981) A physiologically based criterion of muscle force prediction in locomotion. *Journal of Biomechanics*, 14(11), 793-801.

Cutts, A. & Seedhom, B. B. (1993) Validity of cadaveric data for muscle physiological cross-sectional area ratios: a comparative study of cadaveric and in-vivo data in human thigh muscles. *Clinical Biomechanics*, 8:156-162.

Dainis A. (1980) Whole body and segment centre of mass determination from kinematic data. *Journal of Biomechanics*,13(8), 647-652.

Davis, R.D. (1988) Clinical Gait Analysis. *IEEE Engineering in Medicine and Biology*, September, 35-40.

Davy, D. T. & Audu M. L. (1987) A dynamic optimisation technique for predicting muscle forces in the swing phase of gait. *Journal of Biomechanics*, 20:187-201.

De Leva, P. (1996a) Adjustments to Zatsiorsky-Seluyanov's segment inertia parameters. *Journal of Biomechanics*, 29(9), 1223-1230.

De Leva, P. (1996b) Joint centre longitudinal positions computed from a selected subset of Chandler's data. *Journal of Biomechanics*, 29(9), 1231-1233.

Delp, S.L., Arnold, A.S., Speers, R.A. and Moore, C.A. (1996) Hamstring and psoas lengths during normal and crouch gait: implications for muscle tendon surgery. *Journal of Orthopaedic Research*, 14, 144-151.

Delp, S.L., Hess, W.E., Hungerford, D.S., Jones, L.C. (1999) Variation of rotation moment arms with hip flexion. *Journal of Biomechanics*, 32, 493-501.

Delp, S.L., Komattu, A.V. and Wixson, R.L. (1994) Superior displacement of the hip in total joint replacement: effects of prosthetic neck length, neck-stem angle, and anteversion angle on the moment-generating capacity of the muscles. *Journal of Orthopaedic Research*, 12, 860-870.

Delp, S.L. & Maloney, W. (1993) Effects of hip centre location on the moment-generating capacity of the muscles. *Journal of Biomechanics*, 26, 485-499.

Delp, S.L. & Zajac, F.E. (1992) Force- and moment-generating capacity of lower extremity muscles before and after tendon lengthening. *Clinical Orthopaedics and Related Research*, 284, 247-259.

Dostal, W.F. & Andrews, J.G. (1981) A three dimensional biomechanical model of hip musculature. *Journal of Biomechanics*, 14(11), 803-812.

Duda, G.N., Brand, D., Freitag, S., Lierse, W. and Schneider, E. (1996) Variability of femoral muscle attachments. *Journal of Biomechanics*, 29(9), 1185-1190.

Duda, G.N., Schneider, E. and Chao, E.Y.S. (1997) Internal forces and moments in the femur during walking. *Journal of Biomechanics*, 30, 933-941.

Dul, J., Townsend, M. A., Shiavi, R. and Johnson, G. E. (1984a) Muscular Synergism - I. On criteria for load sharing between synergistic muscles. *Journal of Biomechanics*, 17, 663-673.

Dul, J., Johnson, G. E., Shiavi, R., and Townsend, M. A. (1984b) Muscular Synergism - II. A minimum-fatique criterion for load sharing between synergistic muscles. *Journal of Biomechanics*, 17, 675-684.

Enoka, R.M. (1988) *Neuromechanical basis of kinesiology*. Human Kinetics Publishers, Champaign, Illinois.

Engin, A. (1980) On the biomechanics of the shoulder complex. *Journal of Biomechanics*, 13, 575-590.

Fioretti, S., Leo, T. and Maurizi, M. (1991) Usefulness of instantaneous helical axis in functional movement evaluation. In *XIII International Congress on Biomechanics: Book of Abstracts*, (pp.347-348), Eds Marshal, R.N., Wood, G.A., Elliott, B.C., Ackland, T.R., McNair, P.J., The University of Western Australia, Perth, Austalia.

FitzHugh, R. (1977) A model of optimal voluntary muscular control. *Journal of Mathematical Biology*, 4, 203-236.

Forcinito, M., Epstein, M. & Herzog, W. (1998) Can a rheological muscle model predict force depression/enhancement?. *Journal of Biomechanics*, 31, 1093-1099.

Free, S.A. & Delp, S.L. (1996) Trochanter transfer in total hip replacement: effects on the moment arms and force-generating capacities of the hip abductors. *Journal of Othopaedic Research*, 14, 245-250.

Gage, J.R. (1991) *Gait analysis in cerebral palsy*. London, Mac Keith Press.

Gage, J.R. & Coop, S.E. (1995) Clinical gait analysis: application to management of cerebral palsy. In Allard, P., Stokes, I.A. & Blanchi, J. (Eds.) *Three Dimensional Analysis of Human Movement*, Champaign, Illinois, Human Kinetics Publishers, 349-362.

Gore, D.R., Murray, M.P., Gardner, G.M. and Sepic, S.B. (1977) Roentgenographic measurements after Muller total hip replacement. *Journal of Bone and Joint Surgery*, 59A, 948.

Gottlieb, G.L. (1996) Muscle compliance: implications for the control of movement. *Exercise and Sports Science Reviews*, 14, 1-34.

Greene, W.B. & Heckman, J.D. Eds. (1994) *The Clinincal Measurment of Joint Motion*, American Academy of Orthopaedic Surgeons, Rosemont, Illinois, USA.

Grood, E.S. & Suntay, W.J. (1983) A joint coordinate system for the clinical description of three dimensional motions: application to the knee. *Journal of Biomechanical Engineering*, 105 (May), 136-144.

Hatze, H. (1977) A myocybernetic control model of skeletal muscle. *Biological Cybernetics*, 25, 103-119.

Hatze, H. (1980) A mathematical model for the computational determination of parameter values of anthropomorphic segments. *Journal of Biomechanics*,13(10), 833-843.

Hatze, H. (1988) High-precision three-dimensional photogrametric calibration and object space reconstruction using a modified DLT-approach. *Journal of Biomechanics*, 21(7), 533-538.

Hampton, S.J., Andriacchi, T.P. and Galante, J.O. (1980) Three Dimensional Stress Analysis of the Femoral Stem in Total Hip Prosthesis. *Journal of Biomechanics*, 13(5), 443-448.

Hardt, D.E. (1978) Determining muscle forces in the leg during normal walking - an application and evaluation of optimisation methods. *Journal of Biomechanical Engineering*, 100, 72-78.

Hawkins, D. & Bey, M. (1997) Muscle and tendon force-length properties and their interaction in vivo. *Journal of Biomechanics*, 30, 63-70.

Hay, J.G & Reid, J.G. (1988) *Anatomy Mechanics and Human Motion*, 2nd ed. Prentice-Hall Inc., Englewood Cliffs, New Jersey, USA.

Heckman, C.J. & Sandercock, T.G. (1996) From motor unit to whole muscle properties during locomotor movements. *Exersice and Sports Science Reviews*, 24, 109-133.

Herzog, W. (1985) Determination of muscle model parameters using an optimisation technique. In Jonsson, B. (Ed) *International Series on Biomechanics: Biomechanics X-B*, Champaign, Illinois, Human Kinetics, 1175-1179.

Herzog, W. (1987) Individual muscle force estimations using a non-linear optimal design. *Journal of Neuroscience Methods*, 21, 167-179.

Herzog, W. (1996) Force-sharing among synergistic muscles: theoretical considerations and experimental approaches. *Exercise and Sports Science Reviews*, 24:173-202.

Herzog, W. & Binding, P. (1994) Mathematically indeterminate systems. In Nigg, B.M. & Herzog, W. (Eds.) *Biomechanics of the Musculo-skeletal System*. Wiley & Sons, Chichester, England, 472-486.

Herzog, W. & Leonard, T.R. (1991) Validation of optimisation models that estimate the forces exerted by synergistic muscles. *Journal of Biomechanics*, 24(Suppl.1), 31-39.

Hill, A.V. (1938) The heat of shortening and the dynamic constants of muscles. *Proceedings of the Society of London*, 126, 136-195.

Hillstrom & Triolo (1995) EMG Theory. In Craik, R.L. & Oatis, C.A. (Eds) *Gait Analysis: Theory and Application*, St.Louis, Mosby.

Hoeltzel, D.A, Walt, M.J., Kyle, R.F. and Simons, F.D. (1989) The effects of femoral head size on the deformation of ultrahigh molecular weight polyethylene acetabular cups. *Journal of Biomechanics*, 22(11), 1163-1173.

Hof, A.L. & Berg, Jw. van den (1981) EMG to force processing - 1 An electrical analogue of the Hill muscle model. *Journal of Biomechanics*, 14, 747-758.

Huiskes, R. & Boeklagen, R. (1989) Mathematical shape optimization of hip prosthesis design. *Journal of Biomechanics*, 22(9), 793-804.

Huiskes, R. & Chao, E.Y.S. (1983) A survey of finite element methods in orthopaedic biomechanics: the first decade. *Journal of Biomechanics*, 16(6), 385-409.

Hussain, M. (1977) *Measurement of spatial motion using analytical photogrammetric system.* University Microfilms, Michigan.

Inkster, R.G. (1964) Osteology. In Romanes, G.J. (Ed.) *Cunningham's Textbook of Anatomy.*10th Ed., Oxford University Press, London.

Jacob, H.A.C. & Huggler, A.H. (1980) An investigation into biomechanical causes of prothesis stem loosening within the proximal end of the human femur. *Journal of Biomechanics*, 13(2), 159-173.

Jensen, R.H. & Davy, D.T. (1975) An investigation of muscle lines of action about the hip: a centroid line approach vs the straight line approach. *Journal of Biomechanics*, 8(2), 103-110.

Johnston, R.C., Brand, R.A. and Crowninshield, R.D. (1979) Reconstruction of the hip: A mathematical approach to determine optimum geomtric relationships. *Journal of Bone and Joint Surgery*, 61A, 639.

Keating, T.J. (1977) *Analytical Photogrammetry from digitized image densities.* University Microfilms, Michigan.

Knutson & Solderburg (1995) EMG Use and Interpritation. In Craik, R.L. & Oatis, C.A. (Eds) *Gait Analysis: Theory and Application*, Mosby, St.Louis.

Kotzar, G.M., Davy, D.T., Berilla, J. and Goldberg, V.M. (1995) Torsional loads in the early postoperative period following total hip replacement. *Journal of Othopaedic Research*, 13, 945-955.

Kreighbaum, E. & Barthels, K.M. (1990) *Biomechanics : A qualitative approach for studying human movement.* 3rd. Ed., Macmillian Publishing Company, New York.

Leardini, A., Cappozzo, A., Catani, F., Toksvig-Larsen, S., Petitto, A., Sforza, V., Cassanelli, G. and Giannini, S. (1999) Validation of a functional method for the estimation of hip joint centre location. *Journal of Biomechanics*, 32, 99-103.

Lew, W. D. & Lewis, J. L. (1977) An anthropometric scaling method with application to the knee joint. *Journal of Biomechanics*, 10, 171-181.

Lockhart, R.D., Hamilton, G.F. and Fyfe, F.W. (1965) *Anatomy of the Human Body*, 2nd Ed. Faber and Faber, London.

Loeb, G.E. & Gans, C. (1986) *Electromyography for Experimentalists.* University of Chicago Press, Chicago.

Lucchetti, L., Cappozzo, A., Cappello, A. and Della Croce, U. (1998) Skin movement artefact assessment and compensation in the estimation of knee-joint kinematics. *Journal of Biomechanics*, 31, 977-984.

Maganaris, C. (2000) In vivo measurement-based estimations of the moment arm in the human tibialis anterior muscle-tendon unit. *Journal of Biomechanics*, 33, 375-379.

Marieb, E.N. & Mallett, J. (1992) *Human Anatomy*. Redwood City, California, Benjamin & Cummings Publishers.

McGee, R.J., Koozeekanani, S.H., Weimer, F.C. and Rahmani, S. (1979) Dynamic modelling of human locomotion. *In Proceedings of Joint Automatic Control Conference*. American Institute of Chemical Engineers, New York.

Miller, N.R., Shapiro, R. and McLaughlin, T.M. (1980) A technique for obtaining spatial kinematic parameters of segments of biomechanical systems from cinematographic data. *Journal of Biomechanics*,13(7), 535-548.

Mulier, J.C. (1985) Clinical aspects of human articulating joints. In Berme, N., Engin, A.E. and Correia da Silva, K.M. (Eds.) *Biomechanics of Normal and Pathological Human Articulating Joints*. Martinus Nijhoff Publishers, Boston.

National Advisory Committee on Core Health and Disability Support Services (1992) *Hip and Knee Joint Replacements*. NACCHDSS, Wellington.

Nemeth, G. & Ohlsen, H. (1985) In vivo moment arm lengths for hip extensor muscles at different angles of hip flexion. *Journal of Biomechanics*, 18(2), 129-140.

Nigg, B.M. (1894) Mechanics. In Nigg, B.M. & Herzog, W. (Eds) *Biomechanics of the Musculo-skeletal System*. John Wiley & Sons, Chichester, England, 36-46.

Olney, S. J. & Winter, D.A. (1985) Predictions of knee and ankle moments of force in walking from EMG and kinematic data. *Journal of Biomechanics*, 18, 9-20.

Paul, J.P. & Berme, N. (1985) Significance of mathematical modelling. In Berme, N., Engin, A.E. and Correia da Silva, K.M. (Eds.) *Biomechanics of Normal and Pathological Human Articulating Joints*. Martinus Nijhoff Publishers, Boston.

Palastanga, N., Field, D. and Soames, R. (1989) *Anatomy and Human Movement: structure and function*. Heinemann Medical Books, Oxford.

Pedotti, A., Krishnan, V.V. and Stark, L. (1978) Optimisation of muscle force sequencing in human locomotion. *Mathematical Biosciences*, 38, 57-76.

Pedersen, D.P., Brand, R.A. and Davy, D.T. (1997) Pelvic muscle and acetabular contact forces during gait. *Journal of Biomechanics*, 30, 959-65.

Pierrynowski, M. R. (1995) Analytical representation of muscle lines of action and geometry. In Allard, P., Stokes, I. A. & Blanchi, J. P. (Eds) *Three Dimensioal Analysis of Human Movement*. Human Kinetics Publishers, Champaign, Illinois, 215-156.

Pierrynowski, M.R. & Morrison, J.B. (1985a) Estimating the muscle forces generated in the human lower extemity when walking: A physiological solution. *Mathematical Biosciences*, 75, 43-68.

Pierrynowski, M.R. & Morrison, J.B. (1985b) A physiological model for the evaluation of muscular forces in human locomotion: theoretical aspects. *Mathematical Biosciences*, 75, 69-101.

Press,W.H., Teukolsky, S.A., Vetterling,W.T. and Flannery, B.P. (1992) *Numerical Recipes in C, The Art of Scientific Computing*. 2nd Ed., Cambridge University Press, New York.

Prilutsky, B.I., Herzog, W. and Allinger, T.A. (1997) Forces of individual cat ankle extensor muscles during locomotion predicted by using static optimisation. *Journal of Biomechanics*, 30(10), 1025-1033.

Raikova, R. (1999) About weight factors in the non-linear objective functions used for solving indeterminate problems in biomechanics. *Journal of Biomechanics*, 32, 689-694.

Rasch, P.J. & Burke, R.K. (1978) *Kinesiology and Applied Anatomy*, 6th Ed. Philadelphia: Lea & Febiger.

Reinschmidt, C., van den Bogert, A.J., Nigg, B.M., Lundberg, A. and Murphy, N. (1997) Effect of skin movement on the analysis of skeletal knee joint motion during running. *Journal of Biomechanics*, 30(7), 729-732.

Rohrle, H., Scholten, R., Sigolotto, C., Sollbach,W. and Kellner H. (1984) Joint forces in the human pelvis-leg skeleton during walking. *Journal of Biomechanics*, 17(6), 409-424.

Romanes, G.J. ed. (1972) *Cunningham's Text Book of Anatomy*. 11th ed., London, Oxford University Press.

Rugg, S.G., Gregor, R.J.,Mandelbaum, B.R. and Chiu, L. (1990) In vivo moment arm calculations at the ankle using magnetic resonance imaging (MRI). *Journal of Biomechanics*, 23(5), 495-501.

Sale, D.G. (1987) Influence of exercise and training on motor unit activation. In K.B. Pandolf (Ed.), *Exercise and Sports Science Reviews*, 15, 95-151.

Schiehlen, W.O. (1984) Computer generation of equations of motion. In Haug, E.J. (Ed.) *Computer Aided Analysis and Optimization of Mechanical System Dynamics*. Springer-Verlag, Germany, 183-215.

Seidel, G.K., Marchinda, D.M., Dijkers, M. and Soutas-Little, R.W. (1995) Hip joint centre from palpable bony land marks - a cadaver study. *Journal of Biomechanics*, 28(8), 995-998.

Seireg, A. & Arvikar, R.J. (1973) A mathematical model for evaluation of forces in lower extremities of the musculo-skeletal system. *Journal of Biomechanics*, 6, 313-326.

Seireg, A. & Arvikar, R.J. (1975) The prediction of muscular load sharing and joint forces in the lower extremities during walking. *Journal of Biomechanics*, 8(2), 89-102.

Seireg, A. & Arvikar, R. (1989) *Biomechanical Analysis of the Musculoskeletal Structure for Medicine and Sports*. Hemisphere Publishing Corporation, New York.

Shapiro, R. (1978) The direct linear transformation method for three dimensional cinematography. *Research Quarterly*, 49(2), 197-205.

Shih, Chun-Hsiung, Du, Yuan-Kuen, Lin, Yang-Hua and Wu, Chi-Chuan (1994) Muscular recovery around the hip after total hip arthroplasty. *Clinical Orthopaedics and Related Research*, 302, 15-120.

Siemienski, A. (1992) Soft saturation, an idea for load sharing between muscles. application to the study of human locomotion. In: Cappozzo, A., Marchetti, M. and Tosi, V. (Eds.) *Biolocomotion: a century of research using moving pictures*. pp.293-303, Promograph, Italy.

Small, C.F., Bryant, J.T. and Pichora, D.R. (1982) Rationalisation of kinetic descriptions for three dimensional hand and finger motion. *Journal of Biomedical Engineering*. 14 (March), 133-141.

Soderberg, G.L. (1986) *Kinesiology : Application to Pathological Motion*. Baltimore, Williams & Wilkins.

Soderberg & Knutson (1995) EMG Methodology. In Craik, R.L. & Oatis, C.A. (Eds) *Gait Analysis: Theory and Application*, St.Louis, Mosby.

Spoor, C.W. & van Leeuwen, J.L. (1992) Knee muscle moment arms from MRI and from tendon travel. *Journal of Biomechanics*, 25(2), 201-206.

Spoor, C.W., van Leeuwen, J.L., Meskers, C.G.M., Titulaer, A.F. and Huson, A. (1990) Estimation of instantanious moment arms of lower leg muscles. *Journal of Biomechanics*, 23(12), 1247-1259.

Sprigings, E.J., Burko, D.B. and Watson, L.G. (1987) An evaluation of three segmental methods used to predict the location of the total body cg for human airbourne movements. *Journal of Human Movement Sciences*. 13, 57-68.

Stauffer, D.C. & Strauss, A.M (1976) An estimate of damage on the contact surfaces of total hip prosthesis due to walking. *Journal of Biomechanics*, 9(11), 711-721.

Tortora, G.L. & Anagnostakos, N.P. (1987) *Principles of Anatomy and Physiology*, 5th. Ed. Harper and Row, New York, USA.

Townsend, M.A. (1981) Dymanics and coordination of torso motions in human locomotion. *Journal of Biomechanics*, 14(11), 727-738.

Vasavada, A.N., Delp, S.L., Maloney, W.J., Schurman, D.J. and Zajac, F.E. (1994) Compensating for changes in muscle length in total hip arthroplasty: effectson the moment generating capacity of muscles. *Clinical Orthopaedics and Related Research*, 302, 121-133.

Wehage, R.A. (1984) Quaternions and euler parameters - a brief exposition. In Haug, E.J. (Ed.) *Computer Aided Analysis and Optimization of Mechanical System Dynamics*. Springer-Verlag, Germany, 147-180.

Wells, D.A. (1967) *Schaum's outline of theory and problems in Lagrangian dynamics: with a treatment of Euler equations of motion, Hamilton's equations and Hamilton's principle.* Schaum Publishing Company, New York.

Williams, P.L. & Bannister, L.H. eds. (1995) *Gray's Anatomy*, 38th ed. Edinburgh, New York, Churchill Livingston.

Winter, D.A. (1990) *Biomechanics and Motor Control of Human Movement*, 2nd ed. John Wiley & Sons, New York.

Woltring, H.J. & Huiskes, R. (1990) Stereophotogrammetry. In Berme, N. & Cappozzo, A. (Eds.) *Biomechanics of Human Movement : Applications in Rehabilitation, Sports and Ergonomics.* Bertec Corporation, Worthington, Ohio.

Wood, G.A. (1982) Data smoothing and differentiation procedures in biomechanics. *Exercise and Sports Science Reviews*, 10, 308-362.

Wu, J.Z. & Herzog, W. (1999) Modelling concentric contraction of muscle using an improved cross-bridge model. *Journal of Biomechanics*, 32, 837-848.

Yeadon, M.R. (1990a) The simulation of aerial movement- I. The determination of orientation angles from film data. *Journal of Biomechanics*, 23(1), 59-66.

Yeadon, M.R. (1990b) The simulation of aerial movement- III. The determination of the angular momentum of the human body. *Journal of Biomechanics*, 23(1), 75-83.

Zatsiorsky, V.M. (1998) *Kinematics of Human Movement.* Human Kinetics, Chanmpaign, Illinois, USA.

Zatsiorsky, V., Seluyanov, V. and Chugunova, L. (1990) In vivo body segment inertial parameters determination using a gammer-Scanner method. In Berme, N. & Cappozzo, A. (Eds.) *Biomechanics of Human Movement : Applications in Rehabilitation, Sports and Ergonomics.* Bertec Corporation, Worthington, Ohio.

Zajac, F.E. & Gordon, M.E. (1989) Determining muscle's force and action in multi-articular movements. *Exersice and Sports Sciences Reviews*, 17, 187-230.

Zipp, P. (1982) Recomendations for the standardization of lead positions in surface electoromyography. *European Journal of Applied Physiology*, 50, 41-54.